PLANT PROTEASES

EDITED BY: Mercedes Diaz-Mendoza, Juan Guiamet and Frank Van Breusegem

PUBLISHED IN: Frontiers in Plant Science

frontiers Research Topics

frontiers

ISSN 1664-8714
ISBN 978-2-88963-399-9
DOI 10.3389/978-2-88963-399-9

About Frontiers

Frontiers is more than just an open-access publisher of scholarly articles: it is a pioneering approach to the world of academia, radically improving the way scholarly research is managed. The grand vision of Frontiers is a world where all people have an equal opportunity to seek, share and generate knowledge. Frontiers provides immediate and permanent online open access to all its publications, but this alone is not enough to realize our grand goals.

Frontiers Journal Series

The Frontiers Journal Series is a multi-tier and interdisciplinary set of open-access, online journals, promising a paradigm shift from the current review, selection and dissemination processes in academic publishing. All Frontiers journals are driven by researchers for researchers; therefore, they constitute a service to the scholarly community. At the same time, the Frontiers Journal Series operates on a revolutionary invention, the tiered publishing system, initially addressing specific communities of scholars, and gradually climbing up to broader public understanding, thus serving the interests of the lay society, too.

Dedication to Quality

Each Frontiers article is a landmark of the highest quality, thanks to genuinely collaborative interactions between authors and review editors, who include some of the world's best academicians. Research must be certified by peers before entering a stream of knowledge that may eventually reach the public - and shape society; therefore, Frontiers only applies the most rigorous and unbiased reviews.
Frontiers revolutionizes research publishing by freely delivering the most outstanding research, evaluated with no bias from both the academic and social point of view. By applying the most advanced information technologies, Frontiers is catapulting scholarly publishing into a new generation.

What are Frontiers Research Topics?

Frontiers Research Topics are very popular trademarks of the Frontiers Journals Series: they are collections of at least ten articles, all centered on a particular subject. With their unique mix of varied contributions from Original Research to Review Articles, Frontiers Research Topics unify the most influential researchers, the latest key findings and historical advances in a hot research area! Find out more on how to host your own Frontiers Research Topic or contribute to one as an author by contacting the Frontiers Editorial Office: researchtopics@frontiersin.org

PLANT PROTEASES

Topic Editors:
Mercedes Diaz-Mendoza, SEIPASA S.A., Center for Plant Biotechnology and Genomics, Spain
Juan Guiamet, National University of La Plata, Argentina
Frank Van Breusegem, Ghent University, Belgium

Plant proteases are involved in most aspects of plant physiology and development, playing key roles in the generation of signaling molecules and as regulators of essential cellular processes such as cell division and metabolism. They take part in important pathways like protein turnover by the degradation of misfolded proteins and the ubiquitin-proteasome pathway, and they are responsible for post-translational modifications of proteins by proteolysis at highly specific sites. Proteases are also implicated in a great variety of environmentally controlled processes, including mobilization of storage proteins during seed germination, development of seedlings, senescence, programmed cell death and defense mechanisms against pests and pathogens.

However, in spite of their importance, little is known about the functions and mode of actions of specific plant proteases. This Research Topic collects contributions covering diverse aspects of plant proteases research.

Citation: Diaz-Mendoza, M., Guiamet, J., Van Breusegem, F., eds. (2020). Plant Proteases. Lausanne: Frontiers Media SA. doi: 10.3389/978-2-88963-399-9

Table of Contents

frontiers in Plant Science

ORIGINAL RESEARCH
published: 11 January 2019
doi: 10.3389/fpls.2018.01998

A New Role for SAG12 Cysteine Protease in Roots of *Arabidopsis thaliana*

Maxence James[1], Céline Masclaux-Daubresse[2], Anne Marmagne[2], Marianne Azzopardi[2], Philippe Laîné[1], Didier Goux[3], Philippe Etienne[1]*† and Jacques Trouverie[1]†*

[1] INRA, UNICAEN, UMR 950 EVA, SFR Normandie Végétal (FED4277), Normandie Université, Caen, France, [2] INRA, CNRS, Institut Jean-Pierre Bourgin, AgroParisTech, Université Paris-Saclay, Versailles, France, [3] CMABIO3, SF 4206 ICORE, Normandie Université, Caen, France

Senescence associated gene (SAG) 12, which encodes a cysteine protease is considered to be important in nitrogen (N) allocation to *Arabidopsis thaliana* seeds. A decrease in the yield and N content of the seeds was observed in the Arabidopsis SAG12 knockout mutants (*sag12*) relative to the wild type (Col0) under limited nitrogen nutrition. However, leaf senescence was similar in both lines. To test whether SAG12 is involved in N remobilization from organs other than the leaves, we tested whether root N could be used in N mobilization to the seeds. Root architecture, N uptake capacity and 15N partitioning were compared in the wild type and *sag12* under either high nitrogen (HN) or low nitrogen (LN) conditions. No differences in root architecture or root N uptake capacity were observed between the lines under HN or LN. However, under LN conditions, there was an accumulation of ^{15}N in the *sag12* roots compared to the wild type with lower allocation of ^{15}N to the seeds. This was accompanied by an increase in root N protein contents and a significant decrease in root cysteine protease activity. SAG12 is expressed in the root stele of the plants at the reproductive stage, particularly under conditions of LN nutrition. Taken together, these results suggest a new role for SAG12. This cysteine protease plays a crucial role in root N remobilization that ensures seed filling and sustains yields when nitrogen availability is low.

Keywords: cysteine protease activity, N remobilization, reproductive stage, roots, SAG12, N uptake

OPEN ACCESS

Edited by:
Mercedes Diaz-Mendoza, Centro de Biotecnología y Genómica de Plantas (CBGP), Spain

Reviewed by:
Christine Helen Foyer, University of Leeds, United Kingdom
Kris Vissenberg, University of Antwerp, Belgium

****Correspondence:***
Maxence James
maxence.james@unicaen.fr
Philippe Etienne
philippe.etienne@unicaen.fr

† These authors have contributed equally to this work

Specialty section:
This article was submitted to Plant Physiology, a section of the journal Frontiers in Plant Science

Received: *05 October 2018*
Accepted: *24 December 2018*
Published: *11 January 2019*

Citation:
James M, Masclaux-Daubresse C, Marmagne A, Azzopardi M, Laîné P, Goux D, Etienne P and Trouverie J (2019) A New Role for SAG12 Cysteine Protease in Roots of Arabidopsis thaliana. Front. Plant Sci. 9:1998. doi: 10.3389/fpls.2018.01998

INTRODUCTION

Many field crop species are high nitrogen (N) demanding plants. In the context of switching to a sustainable agricultural model, a reduction in inorganic nitrogen inputs is required. To reach this goal, it is necessary to deepen the knowledge of the physiological mechanisms related to N management in plants. Among them, senescence metabolism is essential as it allows the redistribution of nutrients from the source organs to the sink organs (Peoples and Dalling, 1988; Masclaux et al., 2000; Gregersen, 2011). In contrast to other elements such as sulfur stored, which is stored as an inorganic form in vacuoles, N is mainly stored as proteins that require some proteolysis steps to generate peptides and amino acids for remobilization to occur during senescence (Hörtensteiner and Feller, 2002; Masclaux-Daubresse et al., 2008; Tegeder and Rentsch, 2010). Such N recycling metabolism is especially important during the reproductive stage to ensure

seed N filling. Metabolic events are under the control of a large panel of transcription factors and enzymes (Kusaba et al., 2013) that are also modulated by biotic and abiotic stresses such as N deprivation (Gregersen et al., 2013; Avice and Etienne, 2014; Balazadeh et al., 2014).

Senescence, which corresponds to catabolic pathways occurring before cell death, takes place in all organs (Wojciechowska et al., 2017), but it is commonly accepted that in many plant species, leaves are the main source organs for seed filling (Masclaux-Daubresse et al., 2008). During leaf senescence, the chloroplasts, which contain more than 75% of the total N of the leaf (50% in the form of RuBisCO), are the first organelles to be degraded (Peoples and Dalling, 1988; Hörtensteiner and Feller, 2002). In contrast, the mitochondria and nucleus remain functional until cell death (Lim et al., 2007; Chrobok et al., 2016), to allow the production of energy and the expression of Senescence associated genes (SAGs) that encode proteins necessary for transport and catabolism reactions (Gan and Amasino, 1997).

Protein degradation associated with senescence requires a multitude of proteases (Guo et al., 2004). They belong to five major classes: Cysteine Proteases (CPs), Serine Proteases (SPs), Aspartate Proteases (APs), Metallo Proteases (MPs), and Threonine Proteases (TPs) (Guo et al., 2004). Their specific role in protein breakdown during leaf senescence is not well-known, and the major class overexpressed in many plant species during senescence is CPs (Guo et al., 2004; Poret et al., 2016). The SAG12 papain-like cysteine protease (Noh and Amasino, 1999a,b) is the most strongly induced CP in senescent leaves of *Brassica napus* L. and *Arabidopsis thaliana*, especially in plants cultivated under nitrogen limitation (Desclos et al., 2008; Poret et al., 2016). In addition, high SAG12 protein levels are detected in senescing leaf tissues and in fallen leaves (Desclos-Théveniau et al., 2015). For all these reasons, a major role for SAG12 in N remobilization during senescence has long been proposed. Surprisingly, no difference in the leaf senescence phenotype between Col and KO-SAG12 (*sag12*) plants has ever been observed (Otegui et al., 2005; James et al., 2018). Otegui et al. (2005) showed that a lack of SAG12 did not prevent the formation of senescence associated vacuoles (SAVs), nor was their proteolytic activity affected, suggesting that other cysteine proteases accumulated in SAVs in the senescent leaves of *Arabidopsis thaliana* (Otegui et al., 2005). More recently, James et al. (2018) confirmed the absence of a leaf senescence phenotype in *sag12*. The authors also showed that there was no difference in yield and seed N content between Col and *sag12* when cultivated under optimal N nutrition, but there was lower seed N content and yield in *sag12* when cultivated under limiting nitrogen conditions. The absence of phenotype under high nitrogen was explained by an induction of cysteine and aspartate protease activities in *sag12* that could preserve N remobilization. Nevertheless, the authors did not exclude the potential that better root N uptake in *sag12* could have maintained seed filling and plant productivity. This hypothesis is in agreement with the decrease in seed nitrogen content and yields observed in *sag12* cultivated under LN conditions. Indeed, under this particular N limitation condition, N seed filling can only be achieved by N remobilization, in spite of a possible increase in the N uptake capacity in the roots of *sag12*.

The aim of the present study was to determine whether root N uptake and/or N remobilization are involved in the preservation of seed N filling in *sag12*. Root morphology and N uptake were monitored in Col and *sag12*. Experiments using ^{15}N pulse/chase labeling were performed to investigate the distribution of ^{15}N and estimate the source and rate of remobilized nitrogen dedicated to seed filling.

MATERIALS AND METHODS

Plant Growth Conditions

Arabidopsis thaliana Columbia (Col) and *sag12* (SALK_124030) T-DNA mutants were used in this study. The KO-SAG12 SALK_124030 (*sag12*) was chosen because it was the only germplasm which was available in ABRC stock and recently characterized for some study focused on protease activities (Pružinská et al., 2017; James et al., 2018). Seeds were stratified for 48 h in 0.1% agar (Select agar, Sigma, L'Isle d'Abeau Chesnes, France) at 4°C in the dark and then sown into Eppendorf tubes (0.5 ml) filled with 0.8% agar (w/v) that had their bottoms removed. Plants were placed in a glasshouse on a tank containing 10 L of 3.75 mM NO_3^- nutrient solution during 44 days. The solutions contained 3.75 mM KNO_3, 0.5 mM $MgSO_4$, 0.25 mM KH_2PO_4, 0.2 mM EDTA.NaFe.$3H_2O$, 1.25 mM $CaCl_2$, $2H_2O$ 14 μM H_3BO_3, 5 μM $MnSO_4$, 3 μM $ZnSO_4$, 0.7 μM $CuSO_4$, 0.1 μM $CoCl_2$, and 0.1 μM Na_2MoO_4, and was renewed every week. A batch of plants was cultivated under the same conditions except that a long term ^{15}N labeling was performed (5% of atom excess, 3.75 mM $K^{15}NO_3$ during 44 days) in order to obtain homogeneous ^{15}N-labeled plants and to further appreciate the ^{15}N partitioning at harvest time (125 DAS). At 44 days after sowing (DAS) all plants were transferred to two contrasting N conditions: High Nitrogen with 3.75 mM N [HN; 1.25 mM $Ca(NO_3)_2.4H_2O$, 1.25 mM KNO_3, 0.7 μM $(NH_4)_6Mo_7O_{24}$] and Low Nitrogen with 4.2 μM N [LN; 0 mM $Ca(NO_3)_2.4H_2O$, 0 mM KNO_3, 0.7 μM $(NH_4)_6Mo_7O_{24}$]. Photosynthetic photon flux density was 110 mmol m^{-2} s^{-1} and day and night temperatures were 21 and 18°C, respectively. During the first 64 DAS, plants were cultivated with 8 h light/16 h dark photoperiod and then the reproductive stage was induced with a 16 h light/8 h dark photoperiod. Plants were harvested at the vegetative stage (64 DAS) and at the reproductive stage: 85 DAS corresponding to seed filling and 125 DAS corresponding to mature seed stage (**Supplementary Figure S1**). At each harvest time, the plant compartments present were separated, weighed and stored at −80°C for further analysis. In addition, the root and tip density was performed at 64 DAS with a flat scan (Epson expression 10000XL scanner, Suwa, Japan) coupled with Winrizho software (Regent, Sainte-Anne, QC, Canada).

Root N Uptake Capacity Analysis

Col and *sag12* plants were cultivated in HN conditions as previously described but without any ^{15}N labeling. The root N uptake analysis was performed at vegetative (64 DAS) and

reproductive stages (85 DAS) as previously described by (Lainé et al., 1993). Briefly, roots were washed twice for 1 min in a solution of $CaSO_4$ (1 mM) before immersion for 5 min in a solution of 250 μM or 2 mM $K^{15}NO_3$ (99% of atom excess) to study N uptake by the high affinity transport system (HATS) or the low affinity transport system (LATS), respectively. Then roots were rinsed twice in a solution of $CaSO_4$ (1 mM) at 4°C for 1 min to stop the N uptake. Roots and shoots were separated and weighed before ^{15}N analysis by an isotope mass ratio spectrometer (IRMS, IsoPrime GV Instruments, Manchester, United Kingdom). Uptake capacity was expressed as the total amount of ^{15}N in a whole plant per gram of dry roots per hour.

Isotopic Nitrogen Analysis

N and ^{15}N contents were quantified in the different plant compartments with an elemental analyzer (EA3000, EuroVector, Milan, Italy) coupled with an isotope mass ratio spectrometer (IsoPrime IRMS, GV Instruments, Manchester, United Kingdom).

The nitrogen quantity (***NQ***) in the sample was obtained with the following formula: $NQ = \frac{\%N \times MS}{100}$
where MS represents the dry matter of the sample.

The isotopic abundance (***A%***) was determined with the formula: $A\% = 100 \times \frac{^{15}N}{(^{15}N + ^{14}N)}$

With ^{15}N and ^{14}N representing the amount of ^{15}N and ^{14}N isotopes, respectively.

The isotopic excess (***E%***) corresponds to the difference between the isotopic abundance of sample (A%) and the N natural abundance (0.3660%): $E\% = A\% - 0.3660\%$

Finally, the isotopic excess was used to estimate the quantity of ^{15}N (μg) (***Q*^{15}*N***): $Q^{15}N = (E\% \times QN) \times 1000$.

Determination of Amino Acid Content

Ten mg of lyophilized roots were added to 400 μl of MeOH containing 0.625 nmol/μL of norvaline used as internal standard (Sigma, L'Isle d'Abeau Chesnes, France). The mix was stirred for 15 min and then 200 μl of chloroform and 400 μl of ddH_2O were added. After centrifugation (12000 rpm, 10°C, 5 min), the supernatant was recovered, evaporated and resuspended in 100 μl of ddH_2O and then filtered on a 0.2 μm membrane before derivatization using an AccQ-Tag Ultra Derivatization Kit (Waters, Guyancourt, France) following the manufacturer's protocol (Waters, Guyancourt, France). Amino acids were separated and quantified using a UPLC/PDA H-Class system (Waters, Guyancourt, France) with a BEH C18 100 mm × 2.1 mm column.

Extraction and Quantification of Soluble Proteins

Two hundred mg of frozen root leaf tissue were ground in a mortar with 250 μL of citrate-phosphate buffer (20 mM citrate, 160 mM phosphate, pH 6.8 containing 50 mg of PVPP). After centrifugation (1 h, 12,000 *g*, 4°C), the concentration of the soluble protein extract was determined in the supernatant by protein staining (Bradford, 1976) using bovine serum albumin (BSA) as standard.

Western Blot of SAG12 Protein

Twenty μg of soluble proteins were denatured by heating at 90°C for 10 min in 4x Laemmli sample buffer with β-mercaptoethanol (Laemmli, 1970). Proteins were separated on an SDS-PAGE Stainfree precast gel (4–15% acrylamide gradient; Mini-PROTEAN®, Bio-Rad, Marnes-la-Coquette, France) and transferred onto a polyvinylidene difluoride (PVDF) membrane as previously described by Desclos et al. (2008). The PVDF membrane was incubated overnight in Tris buffer saline – Tween 20 [TBST; Tris 10 mM, NaCl 150 mM, pH 8, Tween 20 0.15% (v/v)] with 3% (v/v) skimmed milk to avoid non-specific hybridization. Immunodetection of SAG12 was performed using an anti-SAG12 specific polyclonal antibody from rabbit provided by Agrisera® (AS14 2771; 1/2000 in TBST) as primary antibody and a second antibody coupled with peroxidase (1/10000 diluted in TBST, Bio-Rad®). The quantification of SAG12 was performed by the measurement of the chemiluminescence revealed with an ECL Kit (Bio-Rad®, Marnes-la-Coquette, France) using a ProXPRESS 2D proteomic imaging system (PerkinElmer, Courtaboeuf, France).

Proteolytic Activities

Proteolytic activities of cysteine proteases were determined by *in vitro* protein degradation analysis as previously described in James et al. (2018). Twenty μg of soluble proteins were incubated in a 200 μL reaction volume containing Na-acetate buffer (50 mM, pH 5.5) and 10 μg of BSA (exogenous protein used as loading control). Cysteine protease activities (CP_{act}) were obtained by the addition of 50 μM of E-64, a cysteine protease inhibitor dissolved in dimethylsufoxide (DMSO). Furthermore, 2 mM dithiothreitol (DTT) was added to this mixture and total protease activity (TP_{act}) was obtained by substituting inhibitors with an equal volume of DMSO. Then, proteins were precipitated with 1 mL of ice-cold acetone either immediately (t_0), or after incubation for 300 min (t_{300}) at 37°C under gentle agitation. After centrifugation (15 min, 16,000 *g*, 4°C), the pellet was dissolved in 2X SDS-PAGE gel loading buffer (140 mM sodium dodecyl sulfate, 200 mM Tris, 20% glycerol, 5% β-mercaptoethanol, 0.3 mM Bromophenol Blue) and heated at 90°C for 10 min. Then the soluble protein extracts were separated on a 4–15% gradient in SDS-PAGE Stainfree precast gels (Mini-PROTEAN® TGXTM Stain Free, Bio-Rad, Marnes-la-Coquette, France) and scanned under UV light with a Gel Doc™ EZ scanner (Bio-Rad, Marnes-la-Coquette, France). The proteolytic activities were quantified by monitoring degradation of four bands (95, 76, 50, and 37 kDa) corresponding to endogenous proteins (EP) as targets of proteolysis at pH 5.5. Proteolytic activities are calculated as follows:

(1) Total protease activity (TP_{act} expressed in %):

$$TP_{act} = \frac{Q_{(EP)to} - Q_{(EP)t300}}{Q_{(tot)to}} \times 100$$

(2) Cysteine protease activity (CP_{act} expressed in %):

$$CP_{act} = \frac{[Q_{(EP)to} - Q_{(EP)t300}] - [Q_{(EP)to} - Q_{(EP)t300Inhib.}]}{Q_{(tot)to}} \times 100$$

where the amount of EP ($Q_{(EP)}$) at t_0 and t_{300}, with (Inhib.) or without inhibitor, as well as the total amount of soluble proteins (Q_{tot}) at t_0 were quantified by using ImageLabTM software (Bio-Rad, Marnes-la-Coquette, France).

Extraction and Quantification of RNAs, Reverse Transcription, and PCR Analysis

Total RNAs were extracted from 200 mg of frozen leaf tissue previously ground in a mortar containing liquid nitrogen. The powder was suspended in 750 μL of extraction buffer (100 mM LiCl, 100 mM TRIS, 10 mM EDTA, 1% SDS (w/v), pH 8) and 750 μL of hot phenol (80°C, pH 4). After vortexing for 40 s and after addition of 750 μl of chloroform:isoamylalcohol (24/1, v/v), the homogenate was centrifuged (15,000 *g*, 5 min, 4°C). The supernatant was added to 750 μl of 4 M LiCl solution (w/v) and incubated overnight at 4°C. After centrifugation at 15,000 *g* for 20 min at 4°C, the pellet containing total RNAs was resuspended with 100 μL of sterile water. Then, total RNAs were purified with an RNeasy Mini Kit according to the manufacturer's protocol (Qiagen, Courtaboeuf, France). Quantification of total RNA was performed by spectrophotometry at 260 nm (BioPhotometer, Eppendorf, Le Pecq, France) before reverse transcription (RT). For RT, 1 μg of total RNAs was converted to cDNA with an iScript cDNA synthesis kit according to the manufacturer's protocol (Bio-Rad, Marnes-la-Coquette, France) before polymerase chain reaction (PCR) and quantitative PCR (qPCR) analyses.

SAG12 and 18S rRNA gene expressions were monitored by PCR using 1 μL of cDNA added to 10 μl of a PCR mix containing 250 μM dNTPs, 0.65 μM of forward and reverse primers and 0.5 μM (5 U μL^{-1}) Qbiogene Taq polymerase (MP Biomedicals, Illkirch-Graffenstaden, France). The primers were designed with primer3+ software. *SAG12 (At5g45890)*: forward: 5′-GGCAGTGGCACACCAMCCGGTTAG-3′; reverse 5′-AGAAGCMTTCATGGCAAGACCAC-3′ and *18S rRNA (NR_141642)*: forward: 5′-CGGATAACCGTAGTAATTCTAG-3′; reverse: 5′-GTACTCATTCCAATTACCAGAC-3′. PCRs were performed in a thermocycler (Applied Biosystems, Courtaboeuf, France) using the following program: 1 cycle at 95°C for 5 min, 25 and 18 cycles for Sag12 and *18S rRNA* including a denaturing step at 95°C for 30 s, a primer hybridization step at 58°C for 45 s and an amplification step at 72°C for 1 min. Each PCR reaction was finished with one cycle at 72°C for 10 min. The identity of each amplicon was checked by sequencing and BLAST analysis. PCR products were separated by electrophoresis on agarose gels (1.2% in TAE 1X with 5 μg mL^{-1} of ethidium bromide) and revealed by illumination with UV light using a Gel-Doc ^{TM} EZ Scanner (Bio-Rad, Marnes-la-Coquette, France).

Additionally, *SAG12* gene expression was monitored using RT-qPCRs analysis with 4 μl of 100× diluted RT product, 500 nM of forward and reverse primers and 1X SYBR Green PCR Master Mix (Bio-Rad, Marnes-la-Coquette, France) in a real-time thermocycler (CFX96 Real Time System, Bio-Rad, Marnes-la-Coquette, France). The program was: 95°C for 3 min followed by 40 cycles (95°C for 15 s followed by 40 s at 60°C). PCR amplifications were performed using specific primers for each housekeeping gene (*EF1-α* : forward: 5′-GCCTGGTATGGTTGTGACCT-3′; reverse: 5′-GAAGTTAGCAGCACCCTTGG-3′; *18S rRNA* : forward: 5′-CGGATAACCGTAGTAATTCTAG-3′; reverse 5′-GTACTCATTCCAATTACCAGAC-3′) and target gene *SAG12* (Forward: 5′-AAAGGAGCTGTGACCCCTATCAA-3′; reverse: 5′-CCAACAACATCCGCAGCTG-3′) as described by Kim et al. (2018). For each sample, the subsequent RT-qPCRs were performed in triplicate. The expression of the target gene in each sample was compared to the control sample (Col at the vegetative stage for each N condition) and was calculated with the delta delta Ct (ΔΔCt) method (Livak and Schmittgen, 2001).

Transgenic promoterSAG12::UIDA Construct

The SAG12 promoter (*promoterSAG12*), containing the 1–2180 bp sequence found in GenBank under the Accession No. U37336, was cloned from the pSG499 plasmid (Gan and Amasino, 1995) kindly provided by Pr. R. Amasino (University of Wisconsin-Madison, Madison, WI, United States) into the pMDC32 vector between the PmeI and AscI restriction enzyme sites, in place of the 35S promoter, giving the pMAZ01 plasmid. The pMAZ01 plasmid was fully sequenced from the RB to the Nos terminator to verify the absence of any modification especially in the SAG12 sequence. The full-length coding sequence of *UIDA* (GUS-coding gene; from 86 to 1897 of the AJ298139 accession number) was then cloned successively in the pENTR^{TM} vector (Invitrogen, Carlsbad, CA, United States), then into the pMAZ01 vector by Gateway recombination giving rise to the pMAZ02 vector containing the *promoterSAG12*::*UIDA* fusion. The correct GUS sequence was verified by sequencing.

Transgenic Arabidopsis plants carrying the *SAG12* promoter fused to the *UIDA* reporter gene were obtained by floral dipping (Clough and Bent, 1998) and eight homozygous lines of several primary transformants were selected on the basis of their hygromycin resistance and single insertion segregation rate.

GUS Staining and Observations

Based on the method of Jefferson et al. (1987), tissues from two independent *promoterSAG12::UIDA* homozygous lines were stained overnight at 37°C in 50 mM Na_3PO_4 pH 7.0, 5 mM ferricyanide, 5 mM ferrocyanide, 0.05% Triton X-100 and 5-bromo-4-chloro-3-indolyl glucuronide (1 mg mL^{-1}). Then after destaining by successive incubations in 50, 75, and 96% (v/v) ethanol, samples were kept in glycerol at 4°C before observation.

The tissues were included in low melting point agarose (5%; w/v) and cut with a vibratome (Microm 650v; Thermo Scientific; United States) before observation with a light microscope (AX70 Olympus, and Olympus SC30 camera, Japan) with the help of cellSens software.

Statistical Analysis

For all parameters, at least three biological repeats were measured ($n \geq 3$). All the data are presented as the mean ± standard error (SE). To compare Col with *sag12* data, Student's *t*-tests were performed after verifying compliance of normality with R software. Statistical significance was postulated at $p \leq 0.05$.

RESULTS

Root Architecture and N Uptake Capacity Are Not Affected in sag12

Irrespective of the N conditions (HN or LN), no significant differences were observed between Col and *sag12* for root (**Figure 1A**) and root tip (**Figure 1B**) densities. N uptake capacity was monitored by measuring the amount of ^{15}N absorbed per h and mg of root DW. In both the vegetative and reproductive stages, HATS and LATS N-uptake capacities were not different between the genotypes (**Figure 2**). LATS uptake was higher than HATS in both the vegetative and reproductive stages. Moreover, it could be noted that the N-uptake capacity related to LATS but even more to HATS was significantly lower in the reproductive than the vegetative stage.

The SAG12 Defect Affects N Allocation Under LN Conditions

The plants were labeled with ^{15}N for 44 DAS and then grown without ^{15}N until harvest at 125 DAS. The similar total ^{15}N amounts found in Col and *sag12* at the end of the ^{15}N labeling (not shown), confirmed the absence of differences between the genotypes in LATS and HATS uptake capacities at the vegetative stage. Plants were dissected into five compartments (roots, leaves, stems, pericarps, and seeds). Under HN conditions, ^{15}N was mainly found in the leaves (Col: 31.15 ± 1.96% and *sag12*: 33.28 ± 2.68%) and in the seeds (Col: 32.22 ± 1.46% and *sag12*: 30.26 ± 1.34%) of the two genotypes (**Figure 3**) and the partitioning of ^{15}N was not significantly different between Col and *sag12*. Under LN conditions, around 78% of the total ^{15}N of the plant was distributed in the roots, leaves, and seeds in both genotypes. However, the ^{15}N partitioning was significantly different in the seeds and roots of *sag12* and Col. Partitioning of ^{15}N in the seeds of *sag12* (34.35 ± 1.02%) was decreased by 6.16% compared to Col (40.51 ± 0.64%) and partitioning of ^{15}N in the roots of *sag12* (21.83 ± 0.45%) was conversely increased by 2.97% compared to Col (18.85 ± 0.50%). This then suggests a defect in ^{15}N remobilization from the roots to the seeds in *sag12*.

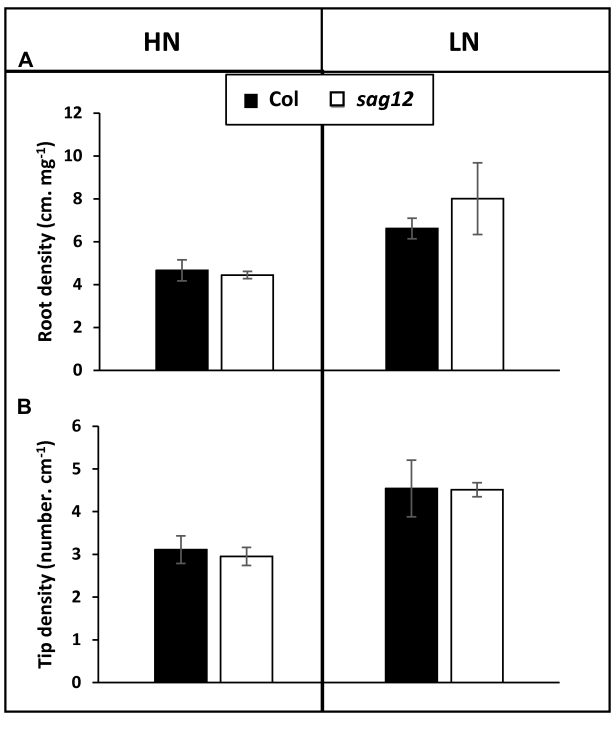

FIGURE 1 | Root architecture is similar in Col and *sag12*. Root density **(A)** and tip density **(B)** of Col (black bars) and *sag12* (white bars) plants cultivated under HN and LN conditions were determined at the vegetative stage (64 DAS). Results are presented as means ± SE (n = 3).

Protein Content Is Higher in Roots of sag12 Cultivated Under LN Condition

As expected, protein and amino acid contents were higher in both genotypes when cultivated under HN compared to LN conditions (**Figure 4**). Protein content in the roots of *sag12* and Col were similar (around 13 mg g^{-1} of DW) when plants were cultivated under HN conditions. Under LN conditions, the protein concentration was higher in the roots of *sag12* (7.87 ± 0.12 mg g^{-1} DW) than in Col (5.49 ± 0.28 mg g^{-1} DW). Interestingly irrespective of the N conditions, the amino acid contents were not significantly different between the two genotypes (**Figure 4**).

SAG12 Is Expressed in Roots at the Reproductive Stage and the Expression Is Higher Under Low Nitrogen Conditions

Low SAG12 transcripts (**Figure 5A**) and no protein (**Figure 5B**) could be detected using RT-qPCR and Western blots in the roots of Col at the vegetative stage under low and high nitrogen conditions. In contrast, high SAG12 transcripts levels (**Figure 5A**) were detected in roots of Col at the reproductive stage and especially under low nitrogen conditions. Accordingly, SAG12 protein was also detected in the roots of Col under LN conditions (**Figure 5B**). As a control, we checked that SAG12 protein and transcripts were undetectable in the roots of sag12 especially when SAG12 was detected in Col (i.e., reproductive stage and LN).

SAG12 Is Expressed in the Root Stele

In order to determine the location of SAG12 expression in the root tissues, GUS staining was performed on Arabidopsis plants transformed by the *promoterSAG12::UIDA* reporter fusion. Staining was performed at the reproductive stage, in which *SAG12* genewas previously detected, on plants cultivated under low and high N conditions. Irrespective of the N conditions, GUS staining was observed along the entire length of the root but it was located exclusively in the stele (**Figure 6**). Surprisingly, although the *SAG12* expression level was higher in the roots of LN cultivated plants (**Figure 5**), we observed that GUS staining was lower in the LN cultivated roots than in the roots of plants cultivated under HN.

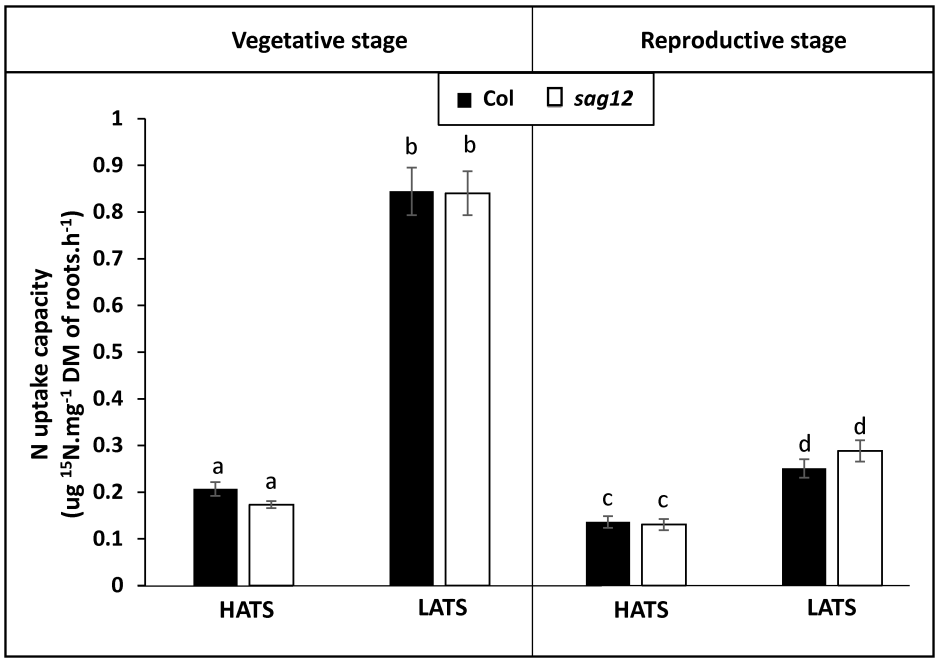

FIGURE 2 | Nitrogen uptake capacities by HATS and LATS are similar in Col and *sag12*. Col (black bars) and *sag12* (white bars) plants were harvested at the vegetative (n = 12) and reproductive stages (n = 8). N uptake capacities by high (HATS) and low (LATS) affinity transport systems are presented as means ± SE. Different letters indicate statistically significant differences according to Student's t-test ($p \leq 0.05$).

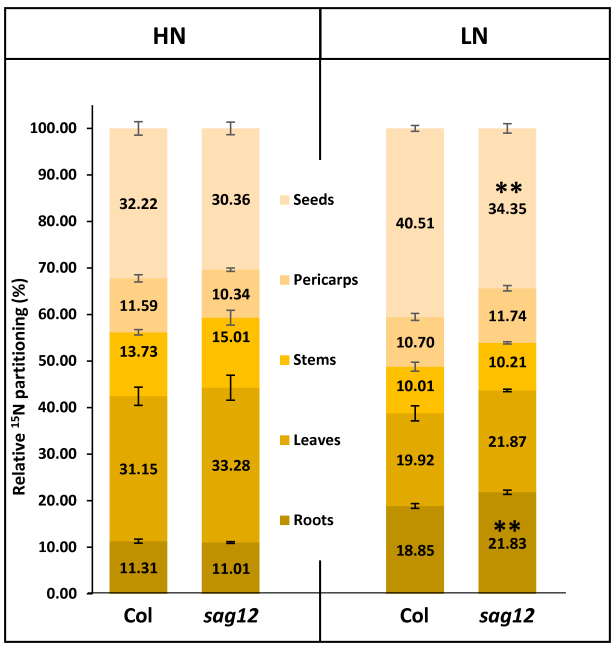

FIGURE 3 | N allocation in roots and seeds is affected in *sag12* under LN conditions. Partitioning of ^{15}N in the different plant compartments (roots, leaves, stems, pericarps, and seeds) was calculated from data obtained from plants harvested at seed maturity (125 DAS). Results are presented as means ± SE (n = 4). Significant differences between Col and *sag12* are indicated by (**$p \leq 0.01$; n = 4).

Cysteine Protease Activity Is Lower in the *sag12* Root Under LN Conditions

The total protease activity measured at the reproductive stage (at the optimum pH for SAG12 activity: pH 5.5) did not reveal any difference between Col and *sag12*, regardless of the N conditions (**Figure 7**). Similar to the total protease activity, a strong increase in cysteine protease activity was observed when plants were cultivated under LN in comparison to HN conditions (**Figure 7**). While no difference in cysteine protease activity was observed between genotypes when plants were cultivated under HN conditions, the defect in SAG12 led to a significant decrease in cysteine protease activity relative to Col when plants were cultivated under LN conditions (642.11 ± 28.04 vs. 516.88 ± 3.99% in Col and *sag12*, respectively; **Figure 7**). Such a discrepancy could be attributed to the lack of SAG12 activity.

DISCUSSION

In a recent study, James et al. (2018) have demonstrated that the absence of SAG12 in plants leads to a decrease in the production of seeds and to a lower N content in Arabidopsis seeds when cultivated under LN conditions. The absence of such a phenotype under HN conditions was explained by the increase in cysteine and aspartate protease activities, which may compensate for the SAG12 defect and sustain N remobilization during seed filling (James et al., 2018). However, although N remobilization is often considered as the major process providing

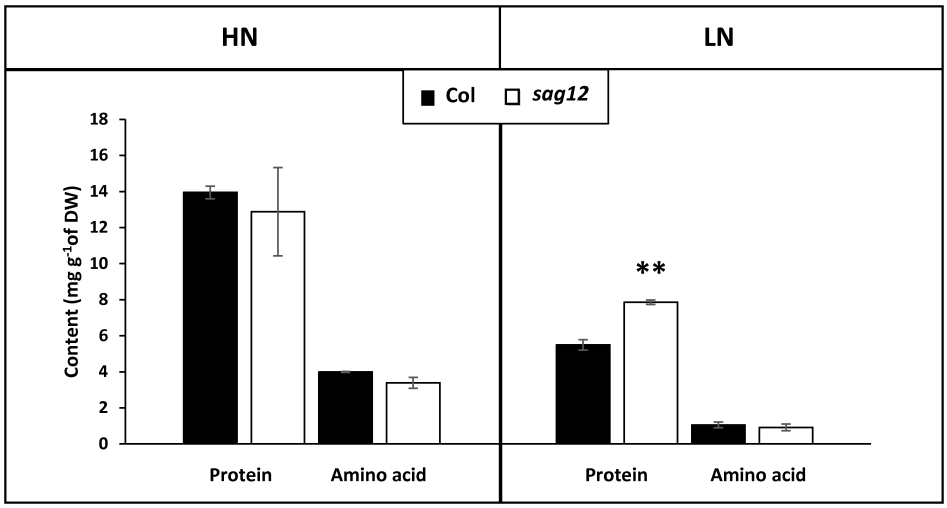

FIGURE 4 | Protein content is higher in roots of *sag12* at the reproductive stage. The roots of Col (black bars) and *sag12* (white bars) plants cultivated under high (HN) and low (LN) nitrogen conditions were harvested at the reproductive stage (85 DAS). Values are means ± SE, $n = 4$. Significant difference between Col and *sag12* (**$p \leq 0.01$; $n = 4$).

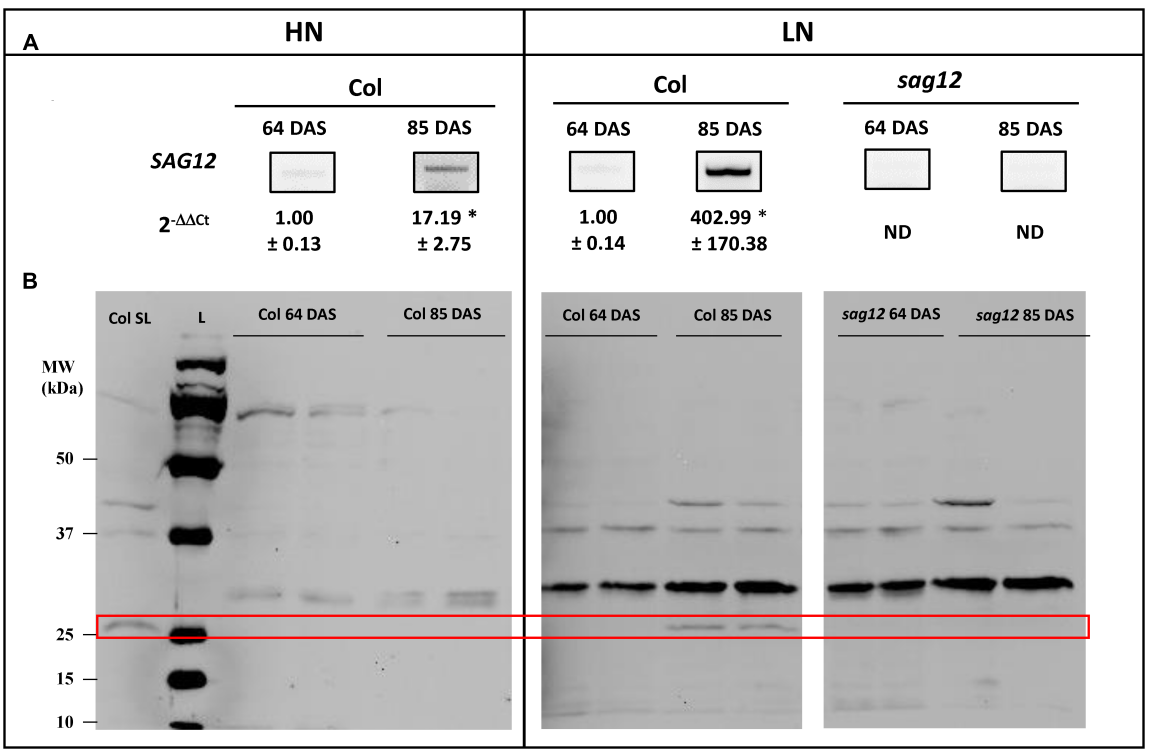

FIGURE 5 | SAG12 is expressed in roots at reproductive stage and especially under LN condition. **(A)** *SAG12* gene expression was monitored using RT-PCR and quantified using RT-qPCR for each condition (HN and LN), the expression of the *SAG12* gene at the reproductive stage (85 DAS) has been relativized with respect to the level of the *SAG12* expression in Col for the corresponding N treatment at the vegetative stage. ND, not detected. For a given nitrogen condition (HN and LN), significant difference between Col at vegetative and reproductive stage (*$p \leq 0.05$; $n = 3$). **(B)** Detection of SAG12 by Western blot using an anti-SAG12 specific polyclonal antibody provided by Agrisera® (AS142771). The red frame highlight the location of SAG12 protein. The mRNAs and soluble proteins were extracted from roots of Col and *sag12* cultivated under HN or LN conditions and harvested at vegetative (64 DAS) and reproductive (85 DAS) stages. Soluble proteins extracted from senescing leaves of Col (Col LS) were used as positive control for SAG12 expression. The molecular weights (MW; kDa) of the Precision Plus Protein Dual color Standards ladder (Bio-Rad) were indicated.

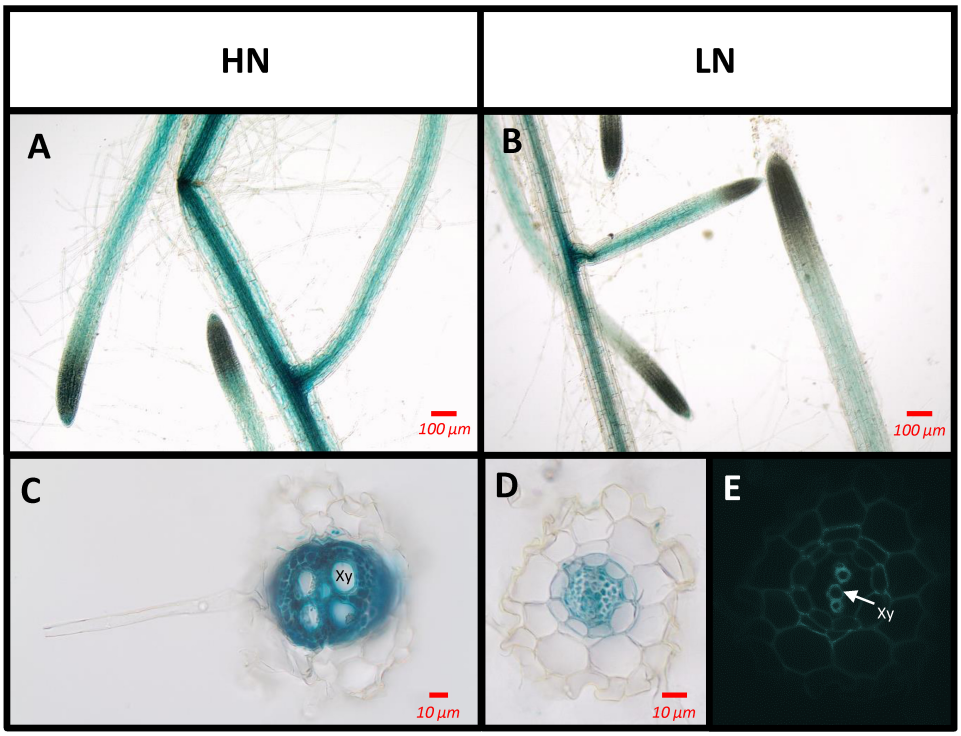

FIGURE 6 | *SAG12* is expressed in the root vascular tissues. The tissues where the SAG12 promoter was active were identified using the *promoterSAG12::UIDA* lines and GUS staining. Roots were observed using a light microscope. Transgenic lines were cultivated under HN **(A,C)** and LN **(B,D,E)** conditions and harvested at the reproductive stage. Representative pictures of the results obtained for whole root **(A,B)** and transverse root sections **(C,D)** are shown. Root section under UV excitation **(E)**. Xy, xylem tissue.

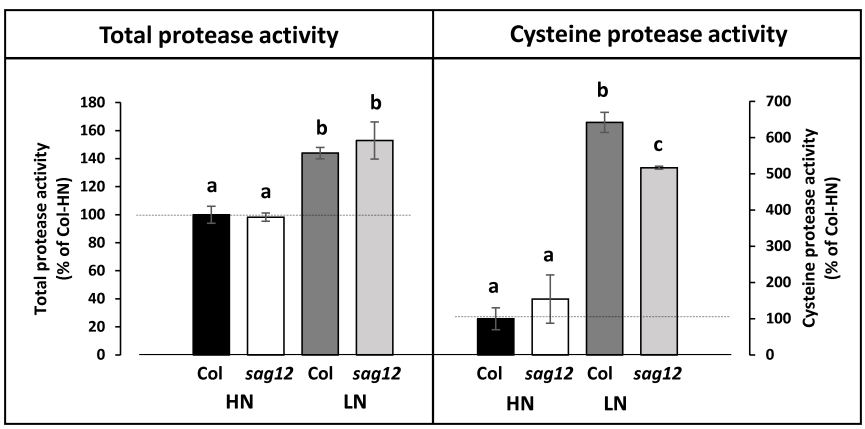

FIGURE 7 | Cysteine protease activity is decreased in roots of *sag12* under LN conditions. Soluble proteins were extracted from roots harvested at the reproductive stage (85 DAS) from Col and *sag12* plants cultivated under high (HN) or low (LN) nitrogen conditions. The cysteine and total protease activities were determined by monitoring the degradation of four endogenous proteins (95, 76, 50, 37 kDa) in the presence or the absence of the cysteine protease inhibitor E64. The protease activities are expressed as a percentage relative to the activity in the Col roots under HN conditions (100%; dot line). Values are means ± SE, $n = 3$. For a given protease activity (total or cysteine), significant differences ($p \leq 0.05$, $n = 3$) are indicated by different lower case letters.

N to the seeds (Tegeder and Masclaux-Daubresse, 2017), the assumption that a better N uptake in *sag12* could supplement the N allocation to the seeds, especially under low N, could not be excluded. Indeed, both NO_3^- uptake and root architecture are known to be regulated depending on the internal N status of the plant and stimulated under LN conditions (Crawford and Forde, 2002; Nacry et al., 2013; Bellegarde et al., 2017; Gent and Forde, 2017). We here show that whatever the N conditions (LN and HN), Col and *sag12* have the same root architecture (**Figure 1**). In addition, no matter which developmental stage was

investigated (vegetative or reproductive), the N uptake by high (HATS) and low (LATS) affinity transporters was similar in Col and *sag12* (**Figure 2**). Taken together, these results invalidated the hypotheses that an increase in N uptake (i) supplemented N allocation to the seeds in the *sag12* plants cultivated under HN conditions or that (ii) N content was lower in the seeds of *sag12* compared to Col when cultivated under LN condition (James et al., 2018). In order to monitor the N remobilization for seed filling, at the final stage of plant development (mature seed 125 DAS) we analyzed the distribution of the ^{15}N provided in a pulse/chase experiment to Col and *sag12* plants cultivated under HN and LN conditions. Under HN, a similar ^{15}N distribution was observed in Col and *sag12* (**Figure 3**), thus suggesting that in *sag12* (SALK_124030), SAG12 depletion did not alter N remobilisation for seed filling when nitrogen was available. These results are in good agreement with the report of James et al. (2018) showing that the cysteine and aspartate proteases increased in *sag12* might support N remobilization during seed filling. Interestingly, growing plants under low N conditions indicated that the proportion of ^{15}N was significantly lower in the seeds of *sag12* in comparison to Col and conversely, significantly higher in the roots of *sag12* compared to the roots of Col (**Figure 3**). No significant difference between Col and *sag12* was found for ^{15}N partitioning in any organs other than the roots and seeds. This then revealed a defect in N remobilization from the roots to the seeds in *sag12* and strongly suggested that the low N content previously observed by James et al. (2018) in the seeds of *sag12* under LN condition was mainly due to the sequestration of N in its roots. Although N remobilization from the root to the seeds is poorly documented, a previous study performed in *Brassica napus* by Rossato et al (2001) showed that more than 11% of the N in seeds came from the remobilization of root N. Moreover, Girondé et al. (2015a) showed that *Brassica napus* genotypes with higher nitrogen remobilization efficiency had a higher contribution of N remobilised from the roots to seeds. Likewise, we observed that the protein concentration was higher in the roots of *sag12* compared to Col, when cultivated under LN, while the amino acid concentrations were unchanged (**Figure 4**). This work performed in *sag12* (SALK_124030) emphasized the role of SAG12 protease in the proteolysis of root proteins that could serve as a nitrogen source for remobilization under low nitrogen conditions.

From this finding, we then decided to investigate whether SAG12 could be expressed in the root tissue, at least under LN conditions, which has never been described before. Indeed, although the expression of SAG12 in leaves during natural and induced senescence was clearly demonstrated by numerous studies performed in various plant species (Lohman et al., 1994; Gan and Amasino, 1997; Desclos et al., 2009; Parrott et al., 2010; Carrión et al., 2013; Singh et al., 2013; Poret et al., 2016; Curci et al., 2017), to our knowledge there was no evidence for SAG12 expression in plant root tissue. In the present work the SAG12 transcripts and proteins were detected in the roots of *Arabidopsis thaliana* especially at the reproductive stage and were much higher in roots of plants cultivated under LN than under HN conditions (**Figure 5**). This makes sense because sink strength is known to be stronger at the reproductive stage due to the maturation of seeds and also stronger under LN conditions. The GUS staining of *promoterSAG12::UIDA* lines at the reproductive stage confirmed that *SAG12* was expressed in the root and especially localized in the stele (**Figure 6**). We noticed that despite higher *SAG12* expression in roots under LN than under HN, GUS staining was weaker in roots of LN plants. This was possibly due to the fact that the stronger protease activity measured under LN may have led to degradation of the b-glucuronidase enzyme, as previously shown in senescent leaf tissues by Noh and Amasino (1999a). Taken together, the expression of SAG12 in roots, and the increase in total protein content in the roots of *sag12* suggests that SAG12 is involved in the proteolysis associated with the root N remobilization, particularly when plants are facing N limitation.

This assumption was verified by measuring the total- and cysteine-protease activities in the roots of Col and *sag12* at the reproductive stage. While the depletion of SAG12 in *sag12* (SALK_124030) did not affect the total protease activity in roots, it decreased significantly the cysteine protease activity of the roots of plants cultivated under LN conditions.

Altogether, the results suggest that the SAG12 protease could plays a major role in the breakdown of root proteins when plants are facing N limitation and is required for efficient N remobilization to the seeds.

CONCLUSION

For the first time, this work shows a clear expression of SAG12 in the stele of the roots. This expression pattern associated with results obtained in *sag12* (SALK_124030) suggest a role of SAG12 for N remobilization from roots to support seed production and seed N content under N limitation. This study open new ways for improving N use efficiency in crops. For example, in *Brassica napus*, the level of SAG12 root expression could have partly explained the contrasting N use efficiency highlighted by Girondé et al. (2015a,b) in different genotypes cultivated under N limiting conditions.

AUTHOR CONTRIBUTIONS

MJ, CM-D, PE, and JT conducted all the experiments, analyzed the data, and wrote the manuscript. PL performed N uptake capacity experiments and wrote the manuscript. DG performed microscopic analysis. MA and AM realized plasmid constructions, transformation and selection of transgenic lines.

ACKNOWLEDGMENTS

The authors would like to thank Dr. Nathalie Nési (INRA, Institut de Génétique, Environnement et Protection des Plantes, Agrocampus Ouest, UMR 1349, Université de Rennes) and Prof. Jean-Christophe Avice (INRA, Ecophysiologie Végétale, Agronomie & Nutritions N.C.S., UCBN 950, UMR, Université de Caen Normandie) for the management of the RAPSODYN

ANR program. They are most grateful to the PLATIN' (Plateau d'Isotopie de Normandie) core facility for elemental analysis, to the "Centre Mondial de l'Innovation" (Groupe Roullier) for amino acid analysis and to Dr. Laurence Cantrill for proofreading and English correction.

SUPPLEMENTARY MATERIAL

The Supplementary Material for this article can be found online at: https://www.frontiersin.org/articles/10.3389/fpls.2018.01998/full#supplementary-material

REFERENCES

Avice, J.-C., and Etienne, P. (2014). Leaf senescence and nitrogen remobilization efficiency in oilseed rape (*Brassica napus* L.). *J. Exp. Bot.* 65, 3813–3824. doi: 10.1093/jxb/eru177

Balazadeh, S., Schildhauer, J., Araújo, W. L., Munné-Bosch, S., Fernie, A. R., Proost, S., et al. (2014). Reversal of senescence by N resupply to N-starved *Arabidopsis thaliana*: transcriptomic and metabolomic consequences. *J. Exp. Bot.* 65, 3975–3992. doi: 10.1093/jxb/eru119

Bellegarde, F., Gojon, A., and Martin, A. (2017). Signals and players in the transcriptional regulation of root responses by local and systemic N signaling in *Arabidopsis thaliana*. *J. Exp. Bot.* 68, 2553–2565. doi: 10.1093/jxb/erx062

Bradford, M. M. (1976). A rapid and sensitive method for the quantitation of microgram quantities of protein utilizing the principle of protein-dye binding. *Anal. Biochem.* 72, 248–254. doi: 10.1016/0003-2697(76)90527-3

Carrión, C. A., Costa, M. L., Martínez, D. E., Mohr, C., Humbeck, K., and Guiamet, J. J. (2013). In vivo inhibition of cysteine proteases provides evidence for the involvement of 'senescence-associated vacuoles' in chloroplast protein degradation during dark-induced senescence of tobacco leaves. *J. Exp. Bot.* 64, 4967–4980. doi: 10.1093/jxb/ert285

Chrobok, D., Law, S. R., Brouwer, B., Lindén, P., Ziolkowska, A., Liebsch, D., et al. (2016). Dissecting the metabolic role of mitochondria during developmental leaf senescence. *Plant Physiol.* 172, 2132–2153. doi: 10.1104/pp.16.01463

Clough, S. J., and Bent, A. F. (1998). Floral dip: a simplified method for *Agrobacterium*-mediated transformation of *Arabidopsis thaliana*. *Plant J. Cell Mol. Biol.* 16, 735–743. doi: 10.1046/j.1365-313x.1998.00343.x

Crawford, N. M., and Forde, B. G. (2002). Molecular and developmental biology of inorganic nitrogen nutrition. *Arabidopsis Book* 1:e0011. doi: 10.1199/tab.0011

Curci, P. L., Aiese Cigliano, R., Zuluaga, D. L., Janni, M., Sanseverino, W., and Sonnante, G. (2017). Transcriptomic response of durum wheat to nitrogen starvation. *Sci. Rep.* 7:1176. doi: 10.1038/s41598-017-01377-0

Desclos, M., Dubousset, L., Etienne, P., Le Caherec, F., Satoh, H., Bonnefoy, J., et al. (2008). A proteomic profiling approach to reveal a novel role of *Brassica napus* drought 22 kD/water-soluble chlorophyll-binding protein in young leaves during nitrogen remobilization induced by stressful conditions. *Plant Physiol.* 147, 1830–1844. doi: 10.1104/pp.108.116905

Desclos, M., Etienne, P., Coquet, L., Jouenne, T., Bonnefoy, J., Segura, R., et al. (2009). A combined 15N tracing/proteomics study in *Brassica napus* reveals the chronology of proteomics events associated with N remobilisation during leaf senescence induced by nitrate limitation or starvation. *Proteomics* 9, 3580–3608. doi: 10.1002/pmic.200800984

Desclos-Théveniau, M., Coquet, L., Jouenne, T., and Etienne, P. (2015). Proteomic analysis of residual proteins in blades and petioles of fallen leaves of *Brassica napus*. *Plant Biol.* 17, 408–418. doi: 10.1111/plb.12241

Gan, S., and Amasino, R. M. (1995). Inhibition of leaf senescence by autoregulated production of cytokinin. *Science* 270, 1986–1988. doi: 10.1126/science.270.5244.1986

Gan, S., and Amasino, R. M. (1997). Making sense of senescence (molecular genetic regulation and manipulation of leaf senescence). *Plant Physiol.* 113, 313–319. doi: 10.1104/pp.113.2.313

Gent, L., and Forde, B. G. (2017). How do plants sense their nitrogen status? *J. Exp. Bot.* 68, 2531–2539. doi: 10.1093/jxb/erx013

Girondé, A., Etienne, P., Trouverie, J., Bouchereau, A., Le Cahérec, F., Leport, L., et al. (2015a). The contrasting N management of two oilseed rape genotypes reveals the mechanisms of proteolysis associated with leaf N remobilization and the respective contributions of leaves and stems to N storage and remobilization during seed filling. *BMC Plant Biol.* 15:59. doi: 10.1186/s12870-015-0437-1

Girondé, A., Poret, M., Etienne, P., Trouverie, J., Bouchereau, A., Le Cahérec, F., et al. (2015b). A profiling approach of the natural variability of foliar N remobilization at the rosette stage gives clues to understand the limiting processes involved in the low N use efficiency of winter oilseed rape. *J. Exp. Bot.* 66, 2461–2473. doi: 10.1093/jxb/erv031

Gregersen, P. L. (2011). "Senescence and nutrient remobilization in crop plants," in *The Molecular and Physiological Basis of Nutrient Use Efficiency in Crops*, eds M. J. Hawkesford and P. Barraclough (Hoboken, NJ: Wiley-Blackwell), 83–102. doi: 10.1002/9780470960707.ch5

Gregersen, P. L., Culetic, A., Boschian, L., and Krupinska, K. (2013). Plant senescence and crop productivity. *Plant Mol. Biol.* 82, 603–622. doi: 10.1007/s11103-013-0013-8

Guo, Y., Cai, Z., and Gan, S. (2004). Transcriptome of Arabidopsis leaf senescence. *Plant Cell Environ.* 27, 521–549. doi: 10.1111/j.1365-3040.2003.01158.x

Hörtensteiner, S., and Feller, U. (2002). Nitrogen metabolism and remobilization during senescence. *J. Exp. Bot.* 53, 927–937. doi: 10.1093/jexbot/53.370.927

James, M., Poret, M., Masclaux-Daubresse, C., Marmagne, A., Coquet, L., Jouenne, T., et al. (2018). SAG12, a major cysteine protease involved in nitrogen mobilization during senescence for seed production in *Arabidopsis thaliana*. *Plant Cell Physiol.* 59, 2052–2063. doi: 10.1093/pcp/pcy125

Jefferson, R. A., Kavanagh, T. A., and Bevan, M. W. (1987). GUS fusions: beta-glucuronidase as a sensitive and versatile gene fusion marker in higher plants. *EMBO J.* 6, 3901–3907. doi: 10.1002/j.1460-2075.1987.tb02730.x

Kim, H., Kim, H. J., Vu, Q. T., Jung, S., Robertson McClung, C., Hong, S., et al. (2018). Circadian control of ORE1 by PRR9 positively regulates leaf senescence in *Arabidopsis*. *PNAS* 115, 8448–8453. doi: 10.1073/pnas.1722407115

Kusaba, M., Tanaka, A., and Tanaka, R. (2013). Stay-green plants: what do they tell us about the molecular mechanism of leaf senescence. *Photosynth. Res.* 117, 221–234. doi: 10.1007/s11120-013-9862-x

Laemmli, U. K. (1970). Cleavage of structural proteins during the assembly of the head of bacteriophage T4. *Nature* 227:680. doi: 10.1038/227680a0

Lainé, P., Ourry, A., Macduff, J., Boucaud, J., and Salette, J. (1993). Kinetic parameters of nitrate uptake by different catch crop species: effects of low temperatures or previous nitrate starvation. *Physiol. Plant.* 88, 85–92. doi: 10.1111/j.1399-3054.1993.tb01764.x

Lim, P. O., Kim, H. J., and Nam, H. G. (2007). Leaf senescence. *Annu. Rev. Plant Biol.* 58, 115–136. doi: 10.1146/annurev.arplant.57.032905.105316

Livak, K. J., and Schmittgen, T. D. (2001). Analysis of relative gene expression data using real-time quantitative PCR and the 2-ΔΔCT method. *Methods* 25, 402–408. doi: 10.1006/meth.2001.1262

Lohman, K. N., Gan, S., John, M. C., and Amasino, R. M. (1994). Molecular analysis of natural leaf senescence in *Arabidopsis thaliana*. *Physiol. Plant.* 92, 322–328. doi: 10.1111/j.1399-3054.1994.tb05343.x

Masclaux, C., Valadier, M.-H., Brugière, N., Morot-Gaudry, J.-F., and Hirel, B. (2000). Characterization of the sink/source transition in tobacco (*Nicotiana tabacum* L.) shoots in relation to nitrogen management and leaf senescence. *Planta. Planta* 211, 510–518. doi: 10.1007/s004250000310

Masclaux-Daubresse, C., Reisdorf-Cren, M., and Orsel, M. (2008). Leaf nitrogen remobilisation for plant development and grain filling. *Plant Biol.* 10(Suppl. 1), 23–36. doi: 10.1111/j.1438-8677.2008.00097.x

Nacry, P., Bouguyon, E., and Gojon, A. (2013). Nitrogen acquisition by roots: physiological and developmental mechanisms ensuring plant adaptation to a fluctuating resource. *Plant Soil* 370, 1–29. doi: 10.1007/s11104-013-1645-9

Noh, Y.-S., and Amasino, R. M. (1999a). Identification of a promoter region responsible for the senescence-specific expression of SAG12. *Plant Mol. Biol.* 41, 181–194. doi: 10.1023/A:1006342412688

Noh, Y. S., and Amasino, R. M. (1999b). Regulation of developmental senescence is conserved between Arabidopsis and *Brassica napus*. *Plant Mol. Biol.* 41, 195–206.

Otegui, M. S., Noh, Y.-S., Martínez, D. E., Vila Petroff, M. G., Andrew Staehelin, L., Amasino, R. M., et al. (2005). Senescence-associated vacuoles with intense

proteolytic activity develop in leaves of Arabidopsis and soybean. *Plant J.* 41, 831–844. doi: 10.1111/j.1365-313X.2005.02346.x

Parrott, D. L., Martin, J. M., and Fischer, A. M. (2010). Analysis of barley (*Hordeum vulgare*) leaf senescence and protease gene expression: a family C1A cysteine protease is specifically induced under conditions characterized by high carbohydrate, but low to moderate nitrogen levels. *New Phytol.* 187, 313–331. doi: 10.1111/j.1469-8137.2010.03278.x

Peoples, M. B., and Dalling, M. J. (1988). "The interplay between proteolysis and amino acid metabolism during senescence and nitrogen reallocation," in *Senescence and Aging in Plants*, eds L. D. Nooden and A. C. Leopold (San Diego, CA: Academic Press), 181–217.

Poret, M., Chandrasekar, B., van der Hoorn, R. A. L., and Avice, J.-C. (2016). Characterization of senescence-associated protease activities involved in the efficient protein remobilization during leaf senescence of winter oilseed rape. *Plant Sci.* 246, 139–153. doi: 10.1016/j.plantsci.2016.02.011

Pružinská, A., Shindo, T., Niessen, S., Kaschani, F., Tóth, R., Millar, A. H., et al. (2017). Major Cys protease activities are not essential for senescence in individually darkened Arabidopsis leaves. *BMC Plant Biol.* 17:4. doi: 10.1186/s12870-016-0955-5

Rossato, L., Lainé, P., and Ourry, A. (2001). Nitrogen storage and remobilization in *Brassica napus* L. during the growth cycle: nitrogen fluxes within the plant and changes in soluble protein patterns. *J. Exp. Bot.* 52, 1655–1663. doi: 10.1093/jexbot/52.361.1655

Singh, S., Giri, M. K., Singh, P. K., Siddiqui, A., and Nandi, A. K. (2013). Down-regulation of OsSAG12-1 results in enhanced senescence and pathogen-induced cell death in transgenic rice plants. *J. Biosci.* 38, 583–592. doi: 10.1007/s12038-013-9334-7

Tegeder, M., and Masclaux-Daubresse, C. (2017). Source and sink mechanisms of nitrogen transport and use. *New Phytol.* 217, 35–53. doi: 10.1111/nph.14876

Tegeder, M., and Rentsch, D. (2010). Uptake and partitioning of amino acids and peptides. *Mol. Plant* 3, 997–1011. doi: 10.1093/mp/ssq047

Wojciechowska, N., Sobieszczuk-Nowicka, E., and Bagniewska-Zadworna, A. (2017). Plant organ senescence - regulation by manifold pathways. *Plant Biol.* 20, 167–181. doi: 10.1111/plb.12672

Conflict of Interest Statement: The authors declare that the research was conducted in the absence of any commercial or financial relationships that could be construed as a potential conflict of interest.

frontiers in Plant Science

ORIGINAL RESEARCH
published: 04 February 2019
doi: 10.3389/fpls.2019.00046

A Genotypic Comparison Reveals That the Improvement in Nitrogen Remobilization Efficiency in Oilseed Rape Leaves Is Related to Specific Patterns of Senescence-Associated Protease Activities and Phytohormones

*Marine Poret[1], Balakumaran Chandrasekar[2,3], Renier A. L. van der Hoorn[2], Sylvain Déchaumet[4], Alain Bouchereau[4], Tae-Hwan Kim[5], Bok-Rye Lee[5], Flavien Macquart[1], Ikuko Hara-Nishimura[6] and Jean-Christophe Avice[1]**

[1] Université de Caen Normandie, UMR INRA–UCBN 950 Ecophysiologie Végétale, Agronomie & Nutritions N.C.S., FED 4277 Normandie Végétal, Caen, France, [2] Plant Chemetics Laboratory, Department of Plant Sciences, University of Oxford, Oxford, United Kingdom, [3] Plant Chemetics Laboratory, Max Planck Institute for Plant Breeding Research, Cologne, Germany, [4] INRA, UMR 1349 Institut de Génétique, Environnement et Protection des Plantes, INRA, Agrocampus Ouest, Université de Rennes 1, Rennes, France, [5] Department of Animal Science, Institute of Agricultural Science and Technology, College of Agriculture and Life Sciences, Chonnam National University, Gwangju, South Korea, [6] Laboratory of Plant Cell Biology, Faculty of Science and Engineering, Konan University Okamoto, Kobe, Japan

OPEN ACCESS

Edited by:
Mercedes Diaz-Mendoza, Centro de Biotecnología y Genómica de Plantas (CBGP), Spain

Reviewed by:
Lyudmila Petrova Simova-Stoilova, Institute of Plant Physiology and Genetics (BAS), Bulgaria
Renu Deswal, University of Delhi, India

***Correspondence:**
Jean-Christophe Avice
jean-christophe.avice@unicaen.fr

Specialty section:
This article was submitted to Plant Proteomics, a section of the journal Frontiers in Plant Science

Received: *31 October 2018*
Accepted: *14 January 2019*
Published: *04 February 2019*

Citation:
Poret M, Chandrasekar B, van der Hoorn RAL, Déchaumet S, Bouchereau A, Kim T-H, Lee B-R, Macquart F, Hara-Nishimura I and Avice J-C (2019) A Genotypic Comparison Reveals That the Improvement in Nitrogen Remobilization Efficiency in Oilseed Rape Leaves Is Related to Specific Patterns of Senescence-Associated Protease Activities and Phytohormones. Front. Plant Sci. 10:46. doi: 10.3389/fpls.2019.00046

Oilseed rape (*Brassica napus* L.) is an oleoproteaginous crop characterized by low N use efficiency (NUE) that is mainly related to a weak Nitrogen Remobilization Efficiency (NRE) during the sequential leaf senescence of the vegetative stages. Based on the hypothesis that proteolysis efficiency is crucial for the improvement of leafNRE, our objective was to characterize key senescence-associated proteolytic mechanisms of two genotypes (Ténor and Samouraï) previously identified with contrasting NREs. To reach this goal, biochemical changes, protease activities and phytohormone patterns were studied in mature leaves undergoing senescence in two genotypes with contrasting NRE cultivated in a greenhouse under limiting or ample nitrate supply. The genotype with the higher NRE (Ténor) possessed enhanced senescence processes in response to nitrate limitation, and this led to greater degradation of soluble proteins compared to the other genotype (Samouraï). This efficient proteolysis is associated with (i) an increase in serine and cysteine protease (CP) activities and (ii) the appearance of new CP activities (RD21-like, SAG12-like, RD19-like, cathepsin-B, XBCP3-like and aleurain-like proteases) during senescence induced by N limitation. Compared to Samouraï, Ténor has a higher hormonal ratio ([salicylic acid] + [abscisic acid])/([cytokinins]) that promotes senescence, particularly under low N conditions, and this is correlated with the stronger protein degradation and serine/CP activities observed during senescence. Short statement: The improvement in N recycling during leaf senescence in a genotype of *Brassica*

napus L. characterized by a high nitrogen remobilization efficiency is related to a high phytohormonal ratio ([salicylic acid] + [abscisic acid])/([cytokinins]) that promotes leaf senescence and is correlated with an increase or the induction of specific serine and cysteine protease activities.

Keywords: *Brassica napus* L., nitrogen remobilization efficiency, senescence, protease activity, regulation, phytohormones

INTRODUCTION

The increase in crop productivity during the last five decades is due particularly to an increase in nitrogen (N) fertilizer inputs (Glass, 2003) in relation to improvements in genetic performance and culture practices. Nevertheless, N fertilizers represent the most costly inputs in crop production (Rothstein, 2007) and their widespread use substantially increases the risk of N pollution. That is why a reduction in N inputs has become a priority for reducing the economic environmental costs in a context of sustainable agriculture (Behrens et al., 2001).

While oilseed rape (*Brassica napus* L.) is the dominant oleoproteaginous crop in northern Europe, it has a high demand for N fertilizers (160–250 kg N ha^{-1} $year^{-1}$) to attain a satisfactory seed yield (Rathke et al., 2005). Despite a considerable capacity to absorb N (Laîné et al., 1993), the N use efficiency (NUE) of winter oilseed rape is lower than other crop plants such as wheat or barley (Sylvester-Bradley and Kindred, 2009). Indeed, only 50% of the N originating from fertilizers is recovered in the seeds while a significant proportion is returned to the environment (Schjoerring et al., 1995) leading to a negative economic and agro-environmental balance for oilseed rape. Several studies have proved that this weak NUE is mainly due to a poor N Remobilization Efficiency (NRE) during the 'sequential' leaf senescence that occurs in the vegetative stages and during the transition between vegetative and reproductive phases of development in oilseed rape (Malagoli et al., 2005a,b; Gombert et al., 2006; Avice and Etienne, 2014). Indeed, a recent screening of NUE, NRE and senescence processes in ten genotypes of oilseed rape defined 4 genotypic profiles with different behaviors during vegetative-stage senescence that were associated with N limitation (Girondé et al., 2015). These authors showed that genotypes with the highest N use efficiency were also characterized by an efficient NRE.

Sequential senescence gradually affects older leaves along the axis of the plant and leads to nutrient remobilization from the source leaves to the young leaves and other sink organs (Guiboileau et al., 2010; Avice and Etienne, 2014). Leaf senescence is tightly linked to global plant productivity and the seed crop yield (Wu et al., 2012; Gregersen et al., 2013), especially in response to low N fertilization. This is a complex process controlled by endogenous and environmental factors (Guo and Gan, 2005; Kusaba et al., 2013). Among the endogenous factors that are able to modulate the progression of senescence, it is well established that leaf senescence can be induced, delayed or suppressed by phytohormones (Jibran et al., 2013; Zhang and Zhou, 2013; Khan et al., 2014). Indeed, cytokinins and gibberellins are known to decelerate senescence processes (Gan and Amasino, 1995 for *Nicotiana tabacum*; Yu et al., 2009 for *Paris polyphylla*) while ethylene, JA, ABA and SA are known to promote and accelerate leaf senescence in *Arabidopsis thaliana* (Morris et al., 2000; He et al., 2001; Jing et al., 2005; Zhang and Gan, 2012). Moreover, some altered senescence phenotypes occur after the alteration of phytohormone signaling. For example, AZF2 encodes for a Cys2/His2 type zinc finger protein and its transcript level was up-regulated by ABA, while a loss-of function of AZF2 delayed natural leaf senescence in *A. thaliana* (Li et al., 2012). It was also recently reported that the overexpression of a cytokinin biosynthesis gene (isopentenyltransferase) in transgenic canola (*B. napus* L.) led to a delay in leaf senescence and improved the seed yield under both rainfed and irrigated conditions (Kant et al., 2015).

Finally, when leaf senescence is initiated, several molecular and physiological events occur such as chloroplast breakdown, as well as oxidation and hydrolysis of macromolecules such as lipids, nucleic acids and proteins (Krupinska et al., 2012; Avice and Etienne, 2014; Kim et al., 2016). The breakdown and particularly the hydrolysis of soluble proteins like RuBisCO (ribulose-1,5-biphosphate carboxylase/oxygenase, EC 4.1.1.39) are the most important degradation processes during leaf senescence. In the context of reducing N fertilizers, this recycling of N compounds from source leaves is crucial to satisfy the N demand of growing organs (Demirevska-Kepova et al., 2005; Thoenen et al., 2007; Diaz et al., 2008). It has been demonstrated that the optimization of NRE in oilseed rape is highly related to soluble protein degradation and the improvement of RuBisCO recycling by proteases during leaf senescence (Desclos-Théveniau et al., 2014; Girondé et al., 2015). Protein degradation during senescence is associated with the activity of several protease classes such as APs, MPs, SPs, CPs and the proteasome (Roberts et al., 2012; Diaz-Mendoza et al., 2016). In oilseed rape leaves, N limitation leads to an increase in AP activity during the first phases of senescence [Desclos et al., 2009 (cv. Capitol); Girondé et al., 2016 (cv. Aviso)]. Moreover, Poret et al. (2016) have demonstrated that AP activities remain stable until the late stages of leaf senescence in oilseed rape (cv. Aviso). MPs and the proteasome have also been implicated in leaf senescence. Indeed, proteomic analyses

Abbreviations: AALP, aleurain-like protease; ABA, abscisic acid; AP, aspartic protease; CP, cysteine protease; CXE, carboxylesterase; HN, high nitrate; IAA, indole acetic acid, auxin; IP, isopentenyladenine; JA, jasmonic acid; LN, low nitrate; MeJA, methyl jasmonate; MES, methylesterase; MP, metalloprotease; N, nitrogen; NPC, no probe control; NRE, nitrogen remobilization efficiency; NUE, nitrogen use efficiency; PAE, pectinacetylesterase; PLCP, papain-like cysteine protease; POPL, prolyloligopeptidase-like protease; RBCL, large subunit of RuBisCO; RuBisCO, ribulose-1,5-biphosphate carboxylase/oxygenase; SA, salicylic acid; SAP, senescence associated protease; SCPL, serine carboxypeptidase-like protein; SP, serine protease; VPE, vacuolar processing enzyme.

showed that a chloroplastic FtsH and the catalytic β1 subunit of the proteasome were induced in oilseed rape during leaf senescence [Desclos et al., 2009 (cv. Capitol)]. Moreover, the global activity of the proteasome remains stable until the end of leaf senescence in oilseed rape [Poret et al., 2016 (cv. Aviso)]. During leaf senescence, the global activity of SPs is also increased in oilseed rape (cv. Aviso) particularly in response to N limitation, and has been associated with several active SPs such as subtilisins (S8) and POPLs (S9) (Poret et al., 2016). As reported for other species (Bhalerao et al., 2003 for *Populus tremula*; Guo et al., 2004 for *A. thaliana*), the CP class corresponds to the most abundant class of up-regulated proteases during leaf senescence and seems to be crucial for the degradation of soluble proteins in oilseed rape. A recent study showed that some PLCPs and VPEs were present in mature leaves and their activity increased during leaf senescence, particularly under low N conditions [Poret et al., 2016 (cv. Aviso)]. In addition, new CP activities were detected during leaf senescence in oilseed rape, especially under nitrate limitation and they corresponded to the activities of RD21-, SAG12-, XBCP3-, and AALPs [Poret et al., 2016 (cv. Aviso)].

As proteolysis efficiency is essential for the improvement of NRE in leaves of oilseed rape, the genotypic variability of leaf NRE observed by Girondé et al. (2015) in response to N limitation could be linked to contrasted protease activities during leaf senescence. Based on this hypothesis, our first goal was to characterize and compare the senescence-associated protease activities of two genotypes (Ténor and Samouraï) previously identified with contrasting NREs (Girondé et al., 2015). Ténor, unlike Samouraï, is able to maintain its leaf biomass production in response to low N supply and this is essentially due to its comparatively greater degradation of soluble proteins in source leaves (Girondé et al., 2015). Moreover, because senescence is tightly controlled by endogenous phytohormones, the putative genotypic differences in protease activities have been hypothesized as being associated with differential regulation of senescence by the phytohormones. In order to verify this assumption, our second objective was to compare the phytohormone contents between the two genotypes during leaf senescence and to correlate the hormonal patterns with the protease activities.

MATERIALS AND METHODS

Chemicals

Ac-YVAD-cmk, diisopropylfluorophosphate (DFP), E-64 and epoxomicin were provided by SIGMA-ALDRICH®. The probes MV201, DCG04, JOPD1, FY01, MVB072, FP-Rh and FP-biotin (Patricelli et al., 2001; Kolodziejek et al., 2011; Richau et al., 2012; Lu et al., 2015) were available in the laboratory. Details are given in **Supplementary Table S1** for correspondence between the classes of proteases, their specific inhibitors and activity-based probes.

Experimental Design

Plants of *B. napus* L. (genotypes Ténor and Samouraï) were cultivated in a greenhouse at the vegetative stage according to previous experiments detailed by Poret et al. (2016). Seedlings were cultivated with 25% Hoagland nutrient solution [1.25 mM $Ca(NO_3)_2.4H_2O$, 1.25 mM KNO_3, 0.5 mM $MgSO_4$, 0.25 mM KH_2PO_4, 0.2 mM EDTA.2NaFe.$3H_2O$, 14 μM H_3BO_3, 5 μM $MnSO_4$, 3 μM $ZnSO_4$, 0.7 μM $(NH_4)_6Mo_7O_{24}$, 0.7 μM $CuSO_4$, 0.1 μM $CoCl_2$] for 6 weeks. Throughout their growth the plants were subjected to a 16 h photoperiod with a mean temperature of 20°C (day)/15°C (night) and received 400 μmoles photon. s^{-1} m^{-2} of photosynthetically active radiation at the canopy. During this experiment, the N remobilization in source leaves was determined precisely using a pulse-chase ^{15}N labeling method. Thus, during the first 6 weeks of culture, plants received nitrate labeled with ^{15}N at 2 atom% excess in order to obtain homogenous labeling throughout the plants. After 6 weeks of growth, corresponding to the beginning of treatments [Day 0 (D0)], the ^{15}N-nitrate labeling was stopped. Plants were separated into two groups and supplied with 25% Hoagland solution containing two different nitrate concentrations: high (HN: 3.75 mM of $CaNO_3$) or low nitrate levels (LN: 0.375 mM $CaNO_3$ with compensation for Ca and K elements by adding 1.25 mM $CaCl_2$,$2H_2O$ and 0.875 mM KCl). Leaves were numbered in order of their date of emergence with leaf rank no. 1 (L1) as the first emerged leaf. At D0, i.e., after 6 weeks of culture, leaf rank no. 12 (L12), a mature leaf becoming senescent during the experiment was chosen on the basis of its leaf area determined with a LI-COR 300 area meter (LI-COR, Lincoln, NE, United States) and chlorophyll content measured with a SPAD meter (Soil Plant Analysis Development; Minolta, SPAD-502 model). This leaf rank (L12) has a mean leaf area value of 57.88 cm^2 ± 1.96% variation and 33.31 cm^2 ± 6.01% variation for Ténor and Samouraï, respectively; mean SPAD value of 54.16 ± 4.55% variation and 55.33 ± 6.65% variation for Ténor and Samouraï, respectively. During the harvests after 0, 16, and 23 days of treatment (D0, D16, and D23), the chlorophyll and anthocyanin levels of L12 were measured by SPAD and an optical sensor system (Multiplex®, Orsay, France; D'Hooghe et al., 2013), respectively. The leaf blade (laminae) of L12 was separated from the petiole and the midrib and was directly frozen at −80°C before further biochemical, proteomic and molecular analyses.

Quantification of N and ^{15}N Contents

The N and ^{15}N contents were quantified at D0, D16, and D23 on L12 of Ténor and Samouraï plants subjected to HN or LN supply. The determination was performed with an elemental analyser (EA3000, EuroVector, Milan, Italy) linked to a continuous flow isotope ratio mass spectrometer (IRMS, IsoPrime GV Instruments, Manchester, United Kingdom).

Profiling of Protease Activities

Soluble proteins were extracted from 200 mg of L12 fresh tissue with 1 mL of water. After centrifugation (5 min, 13,000 *g*, 4°C), concentrations were quantified by protein-dye staining (Bradford, 1976) in equivalent bovine serum albumin (BSA).

The labeling of active proteases was carried out according to Poret et al. (2017). Protein extracts (20 μL; see **Supplementary Table S2** for concentrations of soluble proteins) were incubated in a mix containing 0.5 μM of probe (MV201, FY01, or JOPD1),

50 mM of sodium acetate buffer (NaAc, pH 5.5) and 2 mM DTT (Mix final volume: 200 μL). In parallel, 20 μL of protein extract were incubated in a mix of 50 mM Tris-base buffer (pH 7.5) containing 0.5 μM of MVB072 or 0.25 μM of FP-Rh (200 μL final volume). Because probes have not the same affinity for the active site of the targeted hydrolases, the two different mixtures were incubated for 4 h (MV201, FY01, or JOPD1) or 1 h (MVB072 or FP-Rh) under gentle agitation in the dark for better results. As control, equal volumes of soluble protein extracts of L12 (D0, D16, and D23) treated under HN or LN conditions were combined and 20 μL of each mixture were treated as described above. An equal volume of DMSO was added to the No-Probe-Control (NPC) and competition experiments were carried out by performing a pre-treatment for 30 min with 50 μM of E-64 (competition with MV201 and FY01), ac-YVAD-cmk (competition with JOPD1), epoxomicin (competition with MVB072) or DFP (competition with FP-Rh) before adding probes (see **Supplementary Table S1** for correspondence between the classes of proteases, their specific inhibitors and activity-based probes). Reactions were stopped by adding 1 mL of ice-cold acetone to precipitate the proteins. After centrifugation (15 min, 16,000 *g*, 4°C), the pellet was dissolved in 2X SDS-PAGE gel-loading buffer (140 mM sodium dodecyl sulfate, 200 mM Tris, 20% glycerol, 5% β-mercaptoethanol, 0.3 mM Bromophenol Blue), heated at 90°C for 10 min and separated on 12% SDS-PAGE gels. The fluorescence of labeled proteins was visualized by scanning the gels using a Typhoon 9400 scanner (GE Healthcare Life Science, excitation wavelength: 532 nm; emission wavelength: 580 nm). Signals were quantified by ImageJ software. To control the protein quantity after electrophoresis, gels were stained with Coomassie Brilliant Blue stain [0.5 g CBB G250, 10% acetic acid, 45% methanol in ultra-pure water (v/v)], destained [10% acetic acid, 40% methanol in ultra-pure water (v/v)] and scanned. Finally, specific protease activity was expressed as fluorescence intensity.mg^{-1} protein (see **Supplementary Table S2** for concentrations of soluble proteins).

Identification of Active Proteases

To identify active proteases previously detected on gels as described above, protein extracts were labeled with biotin-tagged probes and a pull-down of biotinylated proteins was performed with a modified protocol from Poret et al. (2016). Briefly, 900 μg of protein was labeled with 10 μM of DCG04 or FP-biotin in labeling buffer [50 mM sodium acetate buffer (NaAc, pH 5.5), 2 mM DTT for DCG04 or 50 mM Tris-buffer, pH 7.5 for FP-biotin]. Samples were incubated under gentle agitation at room temperature for 4 h (for DCG04) or 1 h (for FP-biotin). An additional aliquot was treated as described above but without probes as the control. As described by Chandrasekar et al. (2014), the reaction was stopped and the biotin-proteins were purified using streptavidin beads. Finally, after separation on 12% SDS-PAGE gels, the eluted proteins were stained using the silver staining procedure described by Blum et al. (1987).

Bands of interest were manually excised and were reduced at 50°C for 1 h with 10 mM dithiothreitol (DTT, GE Healthcare) and alkylated for 1 h in the dark with 55 mM iodoacetamide (IAA, Sigma). The gel fragments were washed several times with water and ammonium carbonate, dehydrated with 0.1% acetonitrile and dried. Trypsin digestion was performed overnight with a dedicated automated system (MultiPROBE II, PerkinElmer). The gel fragments were subsequently incubated twice for 15 min in acetonitrile solution to extract peptides from the gel pieces. Peptide extracts were then dried and dissolved in a buffer containing 3% acetonitrile and 0.1% formic acid for chromatographic elution. Peptides were enriched, separated and analyzed using a 6520 Accurate-Mass Q-TOF LC/MS equipped with an HPLC-chip cube interface (Agilent Technologies, Massy, France). The fragmentation data were interpreted using the Mass Hunter software (version B.03.01, Agilent Technologies). For protein identification, MS/MS peak lists were extracted, converted into mzdata.xml format files and compared with the protein database (NCBInr-*Viridiplantae*) using the MASCOT Daemon search engine (version 2.1.3; Matrix Science, London, United Kingdom). The searches were performed with no fixed modification and with variable modifications for oxidation of methionine, and with a maximum of two missed cleavage sites. MS/MS spectra were searched with a mass tolerance of 20 ppm for precursor ions and 0.6 Da for MS/MS fragments. Only peptides matching an individual ion score > 48 were considered. Proteins with two or more unique peptides matching the protein sequence were considered as a positive identification. The assigned protein of best match is provided alongside the UniProt or NCBI/GenBank accession number. Score, queries matched, peptide matches, different peptide matches, experimental mass and theoretical mass are also presented. In addition, other proteins identified in *B. napus* with the same peptides by MASCOT are presented. Protein sequences were matched against sequences of *Brassicacea* proteins using the NCBI BLAST Protein Database (algorithm blastp) and the best BLAST results are presented with the name of the protein, the organism, the UniProt or NCBI/GenBank accession number and the percentage of sequence identity. Finally, PLCPs were classified according to the classification of Richau et al. (2012) while SPs were classified according to the MEROPS database.

Immunodetection of SAG12 and RD21

For immunodetection of the CPs SAG12 and RD21, soluble proteins (30 μg) were first denatured with Laemmli 2X buffer (Laemmli, 1970) containing 5% β-mercaptoethanol (v/v) and separated on a 4–15% gradient in SDS-PAGE precast Stain-free gels (Mini-PROTEAN® TGXTM Stain Free, Bio-Rad, Marne-la-Coquette, France). The gels were scanned under UV light with a Gel Doc™ EZ scanner (Bio-Rad®, Marne-la-Coquette, France) for detection of proteins and the Western blot to the polyvinylidene difluoride (PVDF) membrane was performed as described by Desclos et al. (2008). The immunodetection of SAG12 was made using specific polyclonal antibody from rabbit provided by Agrisera® [1/2000, diluted in Tris buffer saline – Tween 20 (TBST; Tris 10 mM, NaCl 150 mM, pH8, Tween 20 0.15% (v/v)) containing 5% milk (w/v) to avoid non-specific hybridization]. For immunodetection of RD21, specific polyclonal antibody from rabbit kindly provided by Dr. Hara-Nishimura (Yamada et al., 2001) was used (1/1000, diluted in TBST containing 5% milk). The primary antibody was detected

by a secondary antibody from goat coupled with horse-radish peroxidase [(1/10000 and 1/2000 for immunodetection of SAG12 and RD21, respectively) diluted in TBST, Bio-Rad®] and detected by enhanced chemiluminescence (ECL kit, Bio-Rad®) using a ProXPRESS 2D proteomic Imaging System (PerkinElmer, Courtaboeuf, France).

Phytohormone Measurements

Phytohormones were extracted by grinding 200 mg of frozen L12 tissue with 1 mL of extraction buffer (methanol 80%, formic acid 1% in ultra-pure water). After 5 min in an ultrasonic bath at 4°C, samples were agitated for 30 min at room temperature and centrifuged at 12,000 *g* (10 min at 4°C). The resulting supernatant containing phytohormones was collected and a second extraction was performed from the resulting pellet. Both supernatants were mixed and evaporated using a SpeedVac. Finally, the pellet was resuspended in 100 μL of methanol containing 1% of formic acid buffer and then analyzed by UPLC-ESI (+/−) –TQD as described in Pan et al. (2010).

Briefly, the extract obtained is analyzed by ultra-high performance liquid chromatography (UPLC) (Acquity of Waters, Guyancourt, France) on a reverse phase column coupled with a double detection in UV-Visible and by mass spectrometry triple quadrupole (Acquity of Waters, Guyancourt, France), which allows a specificity and sensitivity compatible with the quantification of the phytohormones.

Statistical Analysis

The normality of the data was studied by using the Ryan-Joiner test at 95%. Analysis of variance (ANOVA) and the Newman–Keuls test were performed by using Microsoft® Excel 2010/XLStat® 2014 to compare the means. The non-parametric test of Kruskal–Wallis was carried out if the normality law of the data was not respected. Statistical significance was postulated at $P < 0.05$. Three biological repetitions were analyzed ($n = 3$) for all measurements and all the data are presented as the mean ± standard deviation (SD).

RESULTS AND DISCUSSION

In order to characterize key proteolytic mechanisms capable of distinguishing genotypes with contrasted NRE, our objective was first to identify and compare senescence-associated protease (SAPs) activities of the two genotypes, Ténor (high NRE) and Samouraï (low NRE) (Girondé et al., 2015), and second to associate SAP activities with changes in phytohormonal contents.

Physiological and Biochemical Changes Associated With Senescence for Ténor vs. Samouraï

The two *B. napus* L. genotypes, Ténor and Samouraï, were subjected to ample (HN: 3.75 mM NO_3^-) or low nitrogen supply (LN: 0.375 mM NO_3^-) for 23 days after a pulse-chase labeling treatment with ^{15}N-NO_3^-. Chlorophylls and anthocyanin contents as well as the soluble proteins and the total N and ^{15}N contents were followed in a mature leaf (L12, assumed to commence aging and develop as a source tissue during the time course of the experiment) to study senescence progression during the 23 days of the HN or LN treatments (see section "Materials and Methods").

As previously shown by Poret et al. (2016) in oilseed rape (cv. Aviso), a limitation of nitrate supply accelerated leaf senescence compared to plants subjected to HN conditions in both genotypes (**Figure 1**). Indeed, in agreement with the fact that chlorophyll degradation corresponds to one of the first visible processes of aging (Pan et al., 2010), chlorophyll content decreased significantly after 23 days under LN conditions compared to the HN supply and particularly for Ténor (9.5 ± 3.8 SPAD units) compared to Samouraï (26.9 ± 2.3 SPAD units) (**Figure 1A**). Moreover, the anthocyanin content significantly increased during leaf senescence in the two genotypes and particularly after 23 days under LN supply (**Figure 1B**). This increase in anthocyanin content during leaf senescence was previously shown in oilseed rape (Poret et al., 2016) and corresponds to a stress symptom in oilseed rape (D'Hooghe et al., 2013). It was recently proposed that the photo-protective function of anthocyanins prevents the risk of photooxidation and enables a tightly controlled and efficient chlorophyll breakdown during leaf senescence (Ougham et al., 2005; Diaz et al., 2006; Koeslin-Findeklee et al., 2015).

As proteolysis efficiency is critical for N recycling performance, the quantity of soluble proteins during senescence was compared in Ténor and Samouraï (**Figure 1C**). After 23 days, the quantity of soluble proteins was significantly decreased in L12 and this was particularly acute for Ténor under LN conditions with a degradation of 85% of the initial pool of soluble proteins versus only 70% for Samouraï. Then, because the N requirements of growing organs is significantly fulfilled by the transport of N compounds that originate from the recycling of amino acids and soluble proteins in senescing leaves (Demirevska-Kepova et al., 2005; Thoenen et al., 2007), the total N and ^{15}N contents were studied (**Figures 1D,E**). As expected, the amounts of total N and ^{15}N strongly decreased during leaf senescence, which could correspond to an increase in N remobilization from the old source leaves to the young sink organs. Moreover, Ténor was characterized by a stronger decrease in the total N and ^{15}N contents during the 23 days compared to Samouraï, with a decrease of 70% in ^{15}N for Ténor versus only 50% for Samouraï.

In conclusion, Ténor, which is able to maintain its biomass production under N limitation compared to Samouraï (Girondé et al., 2015), is characterized by a stronger decrease in chlorophyll content, an enhanced degradation of soluble proteins under LN conditions and this leads to a stronger decrease in the ^{15}N and total N quantities under LN conditions compared to Samouraï.

Leaf Senescence-Associated Protease (SAP) Activities for Ténor vs. Samouraï

As shown previously, Ténor is able to strongly degrade soluble proteins compared to Samouraï particularly in plants supplied with LN treatment. From these results, two different hypotheses were postulated: (i) the activities of SAPs may be stronger for Ténor than Samouraï and/or (ii) Ténor may present other SAPs

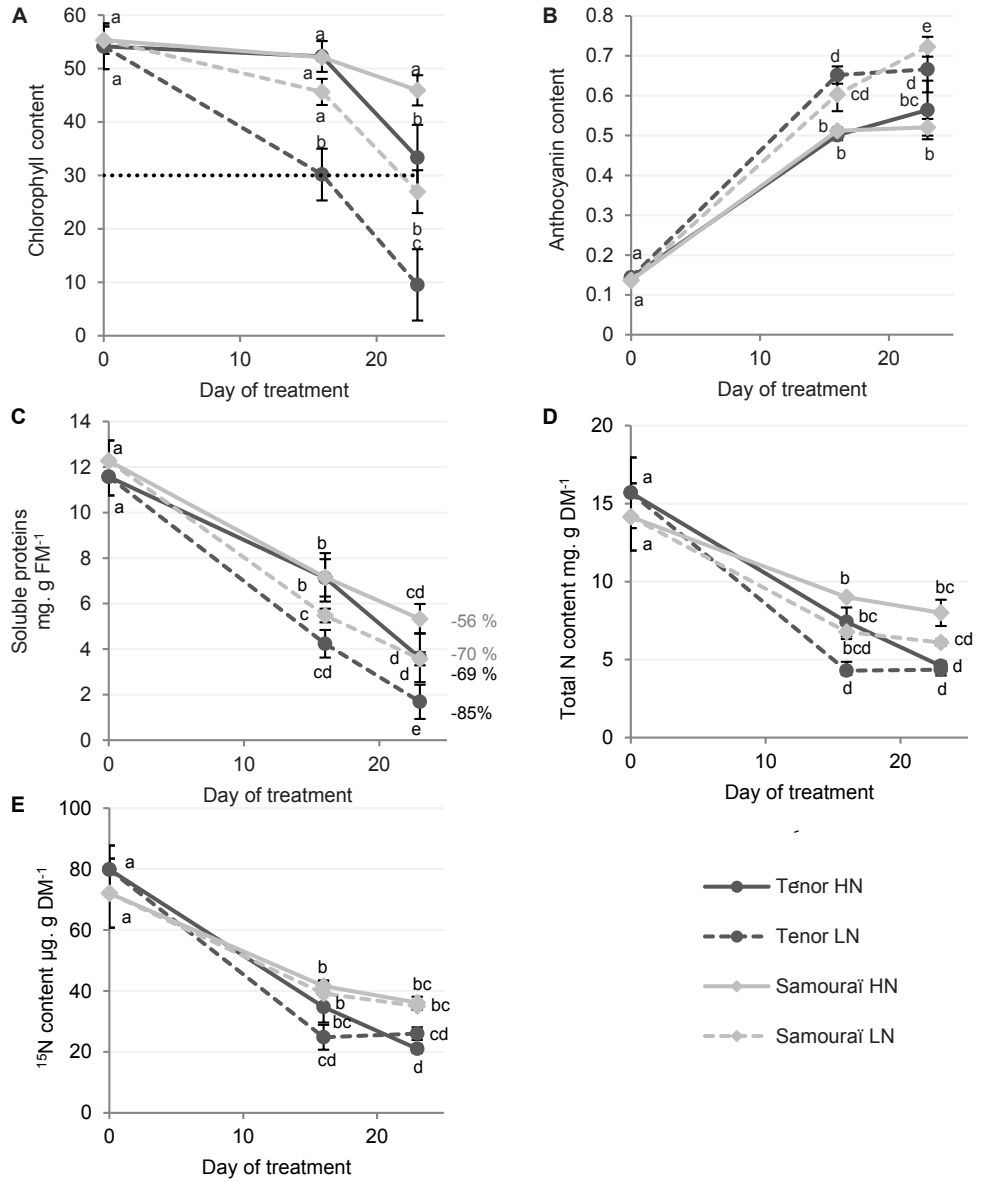

FIGURE 1 | Chlorophyll, anthocyanin, soluble proteins and N and ^{15}N contents in leaf blades during senescence in two genotypes of *Brassica napus* L. supplied with high (HN) or low (LN) nitrate for 23 days. Plants (6 weeks old) of two different genotypes (Ténor and Samouraï) were subjected to ample (HN: 3.75 mM NO_3^-) or low nitrate supply (LN: 0.375 mM NO_3^-) for 23 days. Chlorophyll content of the leaf blades of source leaves (L12) were measured with a SPAD meter **(A)** and were considered as senescent when the chlorophyll content had decreased by at least 40% of the initial value (here the senescence threshold was placed at 30 SPAD units). Anthocyanin content was measured with an optical sensor system (Multiplex) **(B)**. The quantity of soluble proteins was determined after extraction by protein-dye staining **(C)** and the percentages of degradation between D0 and D23 are indicated. The quantity of total nitrogen **(D)** and the quantity of ^{15}N **(E)** were measured by isotope-ratio mass spectrometry (IRMS). Vertical bars indicate ± SD of the mean (n = 3). Statistical differences are represented by letters ($P < 0.05$, ANOVA, Newman–Keuls test).

activities that could be absent in Samouraï. In order to validate or refute these hypotheses, the aim was to address the typology of protease activities associated with leaf senescence for Ténor and Samouraï. To reach this goal, an appropriate method of labeling active proteases was undertaken at pH 5.5 or 7.5 using activity-based probes specific for different protease classes (van der Hoorn and Kaiser, 2012). The following results allowed validation of the two hypotheses postulated above.

Proteasome Activity

The proteasome is physiologically active under neutral pH therefore activity was studied at pH 7.5. In order to study proteasome activity during senescence, a labeling assay using MVB072 (a specific probe of the proteasome) was carried out (**Figure 2**, Kolodziejek et al., 2011). The sum of the activities of the three related catalytic subunits (β1, β2, and β5) of the proteasome showed that the activity increased only after

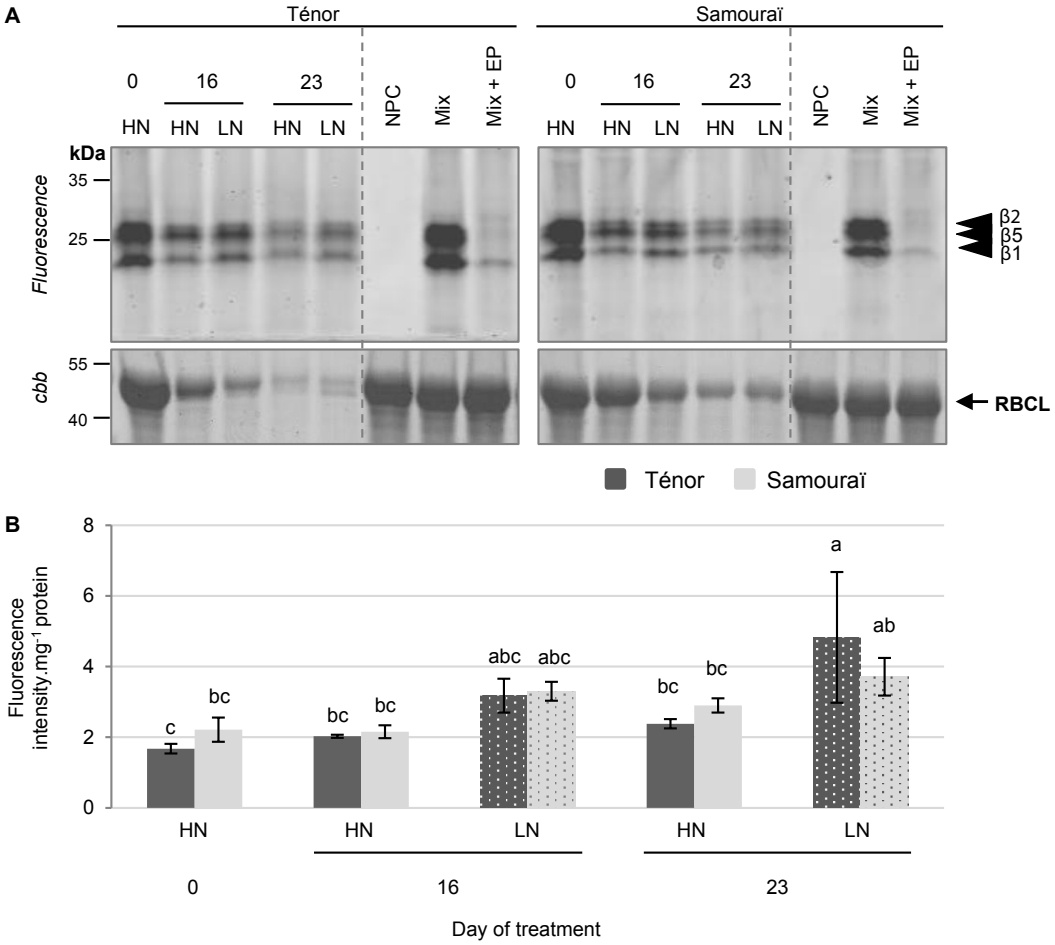

FIGURE 2 | The proteasome activity at pH 7.5 during leaf senescence in two genotypes of *Brassica napus* L. supplied with high (HN) or low (LN) nitrate for 23 days. Soluble proteins were extracted from leaf blade of source leaf (L12) of Ténor or Samouraï plants after 0, 16, and 23 days of HN (3.75 mM NO_3^-) or LN (0.375 mM NO_3^-) treatment. Samples were subjected to a labeling of protease activity with MVB072 (specific fluorescent probe of the proteasome) (pH 7.5; 1 h labeling). The fluorescence was detected by a scanner after separation of samples by SDS-PAGE **(A)**. Mix corresponds to a mixture of the protein extracts obtained at 0, 16, and 23 days for both treatments (HN and LN) in the presence of MVB072. Mix+EP: mix and epoxomicin (specific inhibitor of the proteasome). NPC, no probe control (absence of MVB072). After incubation, the abundance of RuBisCO large subunit (RBLC) was observed after gel staining by coomassie brilliant blue (*cbb*). In each lane, the total amount of loaded proteins corresponds to 20 μL of protein sample. Positions of catalytic subunits of the proteasome (β1, β2, and β5) are represented by black arrowheads. The proteasome activity characterized by the fluorescence intensity was calculated relative to the protein amount **(B)**. The gel is representative of three biological replicates. Vertical bars indicate ± SD of the mean of three biological replicates. Statistical differences are represented by letters ($P < 0.05$, ANOVA, Newman–Keuls test).

23 days of N limitation in Ténor plants (**Figure 2B**). These data suggest that the proteasome plays an important role during leaf senescence with an increase in its activity under LN conditions as previously shown in different genotypes of *B. napus* L. during leaf senescence [Desclos et al., 2009 (cv. Capitol); Poret et al., 2016 (cv. Aviso)]. Indeed, Poret et al. (2016) showed that proteasome activity remains stable until the late stages of senescence, whereas Desclos et al. (2009) showed an accumulation of the β1 subunit in response to nitrate limitation or starvation. Nevertheless, this activity is not significantly stronger in Ténor than Samouraï leaves (**Figure 2B**). These data suggest that the proteasome seems to not be responsible for the enhanced degradation of soluble proteins during the progression of leaf senescence in Ténor compared to Samouraï.

Serine Hydrolase (SH) Including Serine Protease (SP) Activities

In order to study SP activities during senescence, labeling with FP-Rh (a specific probe of SHs including SPs) was performed (**Figure 3**, Patricelli et al., 2001). It was reported that SPs could be located to the vacuole (Parrott et al., 2007) and the chloroplast (Antão and Malcata, 2005), suggesting that SPs could be activated at acidic or neutral pH. In addition, Poret et al. (2016) showed that SH activities at pH 7.5 were strongly activated during leaf senescence in oilseed rape plants. This is why we focused on characterization of the SH activities at pH 7.5. Many of the activities of SPs were detected at 70, 40–50, 38, 35, and 25–30 kDa (**Figure 3A**) in particular. Quantification of the sum of activities indicated that the global activity of SHs increased during

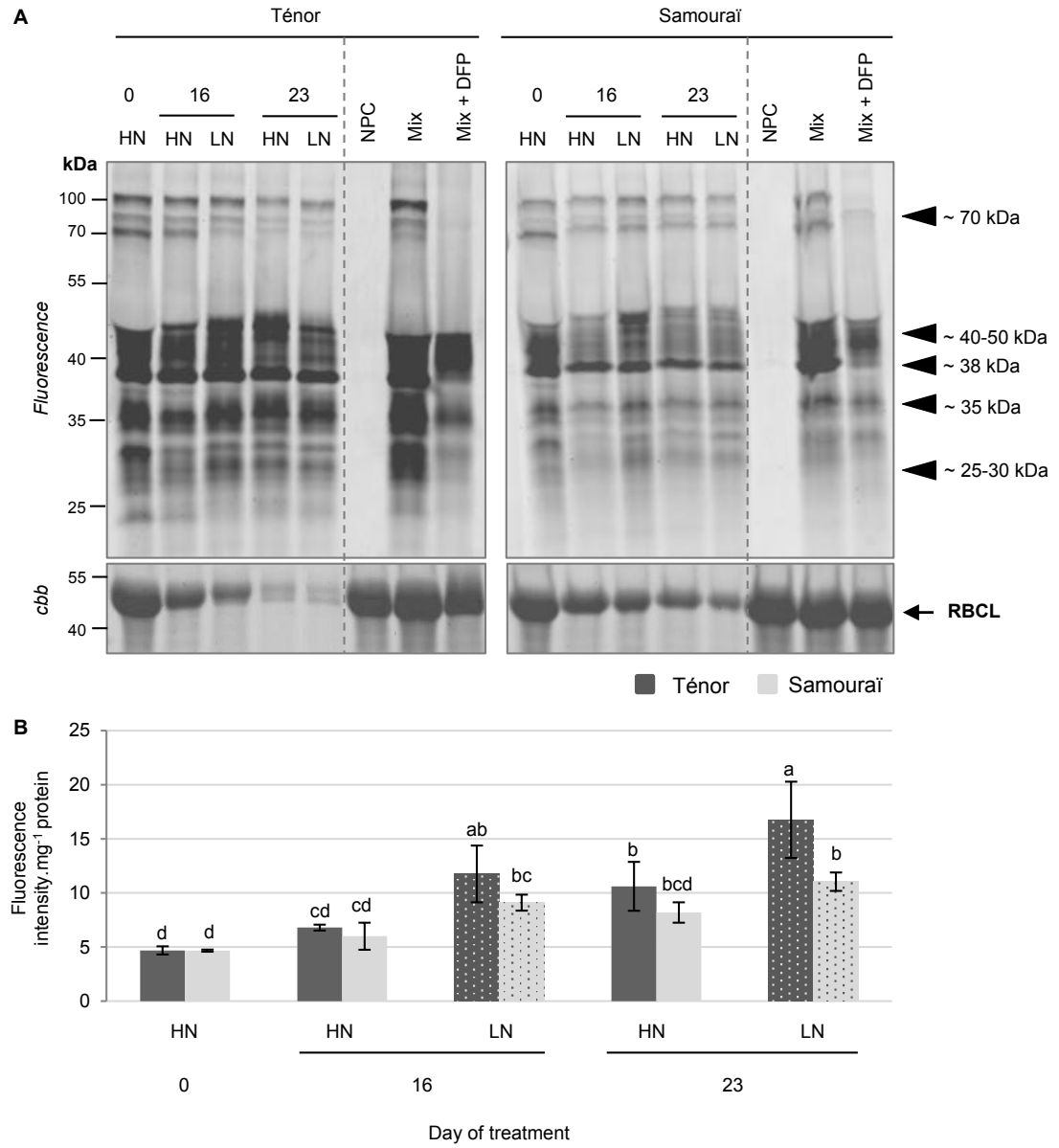

FIGURE 3 | Activity of serine proteases at pH 7.5 during leaf senescence in two genotypes of *Brassica napus* L. supplied with high (HN) or low (LN) nitrate for 23 days. Soluble proteins were extracted from leaf blade of source leaf (L12) of Ténor or Samouraï plants after 0, 16, and 23 days of HN (3.75 mM NO_3^-) or LN (0.375 mM NO_3^-) treatment. Samples were subjected to a labeling of protease activity with FP-Rh (specific fluorescent probe of serine proteases) (pH 7.5; 1 h labeling). The fluorescence was detected by a scanner after separation of samples by SDS-PAGE **(A)**. Mix corresponds to a mixture of the protein extracts obtained at 0, 16, and 23 days for both treatments (HN and LN) in the presence of FP-Rh. Mix+DFP: mix and diisopropylfluorophosphate (specific inhibitor of serine proteases). NPC: no probe control (absence of FP-Rh). After incubation, the abundance of RuBisCO large subunit (RBLC) was observed after gel staining by coomassie brilliant blue (*cbb*). In each lane, the total amount of loaded proteins corresponds to 20 μL of protein sample. Positions of active proteases are represented by black arrowheads. Serine protease global activity characterized by the fluorescence intensity was calculated relative to the protein amount **(B)**. The gel is representative of three biological replicates. Vertical bars indicate ± SD of the mean of three biological replicates. Statistical differences are represented by letters ($P < 0.05$, ANOVA, Newman–Keuls test).

senescence, especially for plants subjected to N limitation for 16 and 23 days for both genotypes (**Figure 3B**). In addition, the global SH activity was stronger for Ténor than Samouraï plants particularly after 23 days under LN conditions and this could be the result of the stronger activities detected at 38, 35, and 25–30 kDa for Ténor compared to Samouraï (**Figure 3B**).

To identify SPs responsible for these activities, labeling of active SHs using a biotin-tagged FP probe (Patricelli et al., 2001) was performed followed by purification of the biotinylated proteins (**Supplementary Figure S1**). This was carried out only for the extract from the senescent leaves of Ténor that was subjected to nitrate limitation over 23 days. Many serine

TABLE 1 | Summary of LC-MS/MS identifications of cysteine and serine proteases labeled with the biotin-tagged probes, DCG04 and FP, respectively, in a senescing leaf of *Brassica napus* L. (cv. Ténor) after 23 days of LN treatment.

Protein accession no [*Brassica napus*]/Uniprot or NCBI accession no.	Classification	Putative location
Cysteine proteases (PLCPs)		
BnaA10g05390D [*Brassica napus*]/CDY06760	RD21-like	Vac
BnaA08g04080D [*Brassica napus*]/A0A078FVG4	RD21-like	Vac
Cysteine proteinase RD21a [*Brassica napus*]/XP_013718810	RD21-like	Vac
BnaA06g36920D [*Brassica napus*]/A0A078G7A3	RD21-like	Vac
Cysteine proteinase RD19a-like [*Brassica napus*]/XP_013701923.1	RD19-like	Vac
Cysteine proteinase RD19a [*Brassica napus*]/XP_013747708.1	RD19-like	Vac
Senescence-specific cysteine protease [*Brassica napus*]/Q9SQH3	SAG12-like	Vac
BnaA06g40240D [*Brassica napus*]/A0A078J304	SAG12-like	Vac
Low-temperature-induced cysteine proteinase-like isoform X2 [*Brassica napus*]/XP_013696759.1	XBCP3-like	Vac
BnaA06g05780D [*Brassica napus*]/CDX93470.1	XBCP3-like	Vac
BnaCnng01440D [*Brassica napus*]/CDY07129.1	Cathepsin-B	Vac
BnaA09g52180D [*Brassica napus*]/A0A078J5J7	Cathepsin-B	Vac
BnaC09g35690D [*Brassica napus*]/CDX80173.1	AALP-like	Vac
BnaC01g26060D [*Brassica napus*]/CDX68528.1	Zingipain	Vac
Serine proteases SPs		
Subtilisin-like protease SBT1.7 [*Brassica napus*]/XP_013654072.1	Subtilisins S8	EC/Vac
BnaCnng41800D [*Brassica napus*]/A0A078JDZ2	Subtilisins S8	EC/Vac
Acylamino-acid-releasing enzyme-like isoform X1 [*Brassica napus*]/XP_013655680.1	POPLs S9	?
BnaA08g30180D [*Brassica napus*]/A0A078IWH3	POPLs S9	?
BnaCnng64630D [*Brassica napus*]/A0A078JVT3	POPLs S9	?
BnaCnng28400D [*Brassica napus*]/A0A078J055	POPLs S9	?
Prolyl endopeptidase-like [*Brassica napus*]/XP_013656097.1	POPLs S9	?
BnaC06g11680D [*Brassica napus*]/CDY06476.1	POPLs S9	?
Acylamino-acid-releasing enzyme-like [*Brassica napus*]/XP_013644416.1	POPLs S9	?
Prolyl endopeptidase-like [*Brassica napus*]/XP_013642253.1	POPLs S9	?
BnaA06g18620D [*Brassica napus*]/CDX99171.1	SCPLs S10	Vac
BnaC01g38630D [*Brassica napus*]/A0A078J0P9	SCPLs S10	Vac
Serine carboxypeptidase-like 35 [*Brassica napus*]/A0A078G963	SCPLs S10	Vac
BnaA04g07190D [*Brassica napus*]/A0A078HQ25	SCPLs S10	Vac
BnaA01g06330D [*Brassica napus*]/A0A078GRW5	SCPLs S10	Vac
Serine carboxypeptidase-like 29 [*Brassica napus*]/A0A078IYZ5	SCPLs S10	Vac
BnaA08g12880D [*Brassica napus*]/A0A078GF58	SCPLs S10	Vac
Lysosomal Pro-X carboxypeptidase-like [*Brassica napus*]/XP_013643207.1	SCPLs S10	Vac
BnaA04g16130D [*Brassica napus*]/A0A078GVN3	SCPLs S10	Vac
BnaA10g23100D [*Brassica napus*]/CDX69961.1	SCPLs S10	Vac
Protease Do-like 1, chloroplastic [*Brassica napus*]/XP_013644609.1	Deg SPs	Chl

Chl, chloroplast; EC, extracellular; Vac, vacuolar compartments. The assigned protein of best match is provided alongside the UniProt or NCBI/GenBank accession number and proteases were classified according to Richau et al. (2012) for CPs or the MEROPS database for SPs. Putative cellular locations of these proteases are given based on the data reported by Roberts et al. (2012) and Diaz-Mendoza et al. (2016).

hydrolases were identified at 70, 50, 45, 37, 35, 30, 27, and 25 kDa (**Table 1**, SHs identifications are detailed in **Supplementary Table S3**). Some of these hydrolases were identified at different molecular weight cutting zones but we identified 8 different POPLs (S9) at 70 kDa in particular, 2 subtilisins (S8) at 70 kDa, 10 carboxypeptidase-like proteins (SCPLs S10) at 50, 45, 37, 35, 30, and 27 kDa, 5 CXEs at 45, 37, 35, 30, and 27 kDa. In addition, 1 PAE at 45 kDa, 1 Deg protease (S1) at 37 kDa, 3 S-formylglutathione hydrolases at 35 and 30 kDa, 2 thiolesterases at 25 kDa and 6 MESs at 25 kDa were identified after LC MS/MS analyses. The majority of the serine hydrolases have not yet been functionally characterized in *A. thaliana* (van der Hoorn et al., 2011) but they seem to be implicated in various biological processes. Poret et al. (2016) also identified active POPLs during leaf senescence after 23 days of LN conditions in *B. napus* L. (cv. Aviso) at 70 kDa and two of these were also found in leaves of Ténor (BnaA08g30180D [*B. napus*]/A0A078IWH3; BnaC06g11680D [*B. napus*]/CDY06476.1). Moreover, several studies have already shown the role of subtilisin-like protease (S8) during senescence in different species (Roberts et al., 2003, 2006, 2011 for wheat; Parrott et al., 2007 for barley; Poret et al., 2016 for oilseed rape). As reported in wheat by Roberts et al. (2003), this type of serine hydrolase is able to degrade *in vitro* soluble proteins such as RuBisCO. Interestingly, the

protease Do-like 1, chloroplastic ([*B. napus*]/XP_013644609.1) was identified at ∼37 kDa. This type of protease is known to play a role in the degradation of protein such as the chloroplastic thylakoid-bound protein D1 of photosystem II (Kato et al., 2015). Finally, many active SHs were identified in the senescing leaves of Ténor after 23 days of nitrate limitation. Many of these active SPs could be responsible for the stronger global activity of SPs in Ténor than in Samouraï. Therefore, additional experiments are required to characterize the function of these different active SHs and SPs between genotypes to determine their role in the proteolysis associated with leaf senescence in oilseed rape.

Cysteine Proteases (CPs): PLCPs and VPEs

Because CPs are located in the vacuole or in senescence-associated vesicles (SAVs) (Otegui et al., 2005; Martínez et al., 2007; Kato et al., 2015; Otegui, 2018), the labeling of CP activities was performed under acidic pH (5.5) according to Poret et al. (2016). The protease activity profiling was undertaken with the fluorescent probes MV201 (specific to papain-like cysteine proteases, PLCPs), FY01 (specific to AALPs and PLCPs) and JOPD1 (a probe specific for vacuolar processing enzymes, VPEs) (**Figures 4–6**).

Many activities of PLCPs were detected using MV201 (**Figure 4A**) particularly at ∼40, ∼35, ∼30, and ∼27 kDa. The sum of the PLCP activities was quantified (**Figure 4B**) and the global activity significantly increased during senescence in leaves of plants subjected to the LN supply during the 23 days. Otherwise, the global PLCP activity was stronger for Ténor than Samouraï after 23 days of LN treatment. This strong PLCP activity was related to the increase in protease activities at ∼40 kDa and particularly due to the appearance of a new activity at ∼27 kDa for Ténor but not for Samouraï (**Figure 4A**).

Moreover, several AALP and PLCP activities were detected using FY01 (**Figure 5A**), particularly at ∼40, ∼35, and ∼27 kDa. The quantification of the sum of these activities (**Figure 5B**) showed that the global activity of the aleurain-like and PLCP proteases was significantly increased during senescence in leaves of Ténor alone in response to a nitrate limitation of 23 days. The AALP and PLCP protease activities were increased particularly at ∼40 and ∼35 kDa while a strong new activity was detected at ∼27 kDa. Because the AALPs are a sub-group of the PLCPs, this strong activity at ∼27 kDa seems to contribute to the new activity for PLCPs at this molecular weight (**Figure 4A**).

Finally, 2 VPE activities were detected after labeling with JOPD1 (**Figure 6A**) at ∼40 and ∼37 kDa. The sum of these activities was quantified (**Figure 6B**) and the global activity of the VPEs increased during senescence particularly in plants subjected to an N limitation, regardless of the genotype. In contrast to the PLCPs and AALPs, VPEs do not seem to be responsible for the contrasted proteolytic processes between Ténor and Samouraï observed in **Figure 1C**.

To identify the PLCPs and AALPs responsible for the increased total CP activity for Ténor compared to Samouraï, labeling with the biotin-tagged DCG04 probe was performed followed by a pull-down of biotinylated proteins (**Supplementary Figure S1**). As for SPs, this was only performed on the extract from senescent leaves of Ténor subjected to LN supply after 23 days of treatment. Many PLCPs were identified at ∼40, ∼35, ∼30, ∼27, and ∼25 kDa (**Table 1**, see detailed data on protein identifications in **Supplementary Table S4**). As for the SPs, some of these PLCPs were identified in different molecular weight zones but we identified 5 different RD21-like proteases, 2 RD19-like proteases, 2 SAG12-like proteases, 2 Cathepsin-B, 2 XBCP3-like proteases, 1 AALP and 1 zingipain.

The CPs are the most up-regulated proteases during leaf senescence [Bhalerao et al. (2003) in *Populus tremula*] and CP activities can represent 44% of the total protease activity in senescent tissues of *B. oleracea* (Coupe et al., 2003). This class of proteases is involved in proteolytic processes during senescence in wheat (Thoenen et al., 2007) and is clearly associated with RuBisCO degradation during sequential leaf senescence in the vegetative stages of *B. napus* L. (Poret et al., 2016). Interestingly, many PLCPs are involved in proteolytic processes during senescence in *A. thaliana*, such as some of the RD21-like proteases, SAG12-like proteases, AALPs, Cathepsin-B proteases or RD19-like proteases (Guo et al., 2004; Otegui et al., 2005; Richau et al., 2012; Ge et al., 2016; James et al., 2018; Otegui, 2018). A recent study also showed that activities of some RD21-like, SAG12-like, and XBCP3-like proteases as well as AALP were especially increased during leaf senescence in *B. napus* L. plants submitted to N limitation [Poret et al., 2016 (cv. Aviso)]. Moreover, BnaA10g05390D [*B. napus*]/CDY06760 (RD21-like protease) and BnaA06g05780D [*B. napus*]/CDX93470.1 (XBCP3-like protease) were also identified as proteases involved in the proteolytic process in the genotype Aviso by Poret et al. (2016).

The main goal of this experiment was to identify proteases responsible for the strong activity that appeared at ∼27 kDa in Ténor but not in Samouraï for PLCPs and AALPs (**Figures 4A,5A**) and which could be associated with the difference in proteolytic performance between the two genotypes. Many proteases were identified at ∼27 and ∼25 kDa (**Table 1** and **Supplementary Table S4**) as 3 different RD21-like proteases, 2 cathepsin-B proteases, 2 SAG12-like proteases, 1 RD19-like protease, 2 XBCP3-like proteases and 1 AALP, which could have been responsible for the strong activity at this molecular weight observed with FY01 labeling (**Figure 5A**). None of these proteases were strongly active during leaf senescence in Samouraï after 23 days of LN treatment compared to Ténor. This is why some of these activities might be associated with the difference in proteolytic performance between the two genotypes.

The *SAG12* gene encodes for a CP and is considered as a senescence-associated gene marker (Lohman et al., 1994). Desclos et al. (2009) have shown an up-regulation of *SAG12* expression and SAG12 protein abundance in senescent leaves of oilseed rape (cv. Capitol) subjected to nitrate limitation. The activity of this type of protease has also been demonstrated in senescing leaves of genotype Aviso subjected to nitrate limitation (Poret et al., 2016). This genotype is able to maintain its leaf biomass production in response to low N supply (Girondé et al., 2015) in a similar way to Ténor. In order to verify that the difference of SAG12 and RD21 activities between both genotypes are related with the abundance of their active forms, the immunodetection of SAG12 and RD21 was carried out in senescent leaves of Ténor or Samouraï plants after 0, 14, 16,

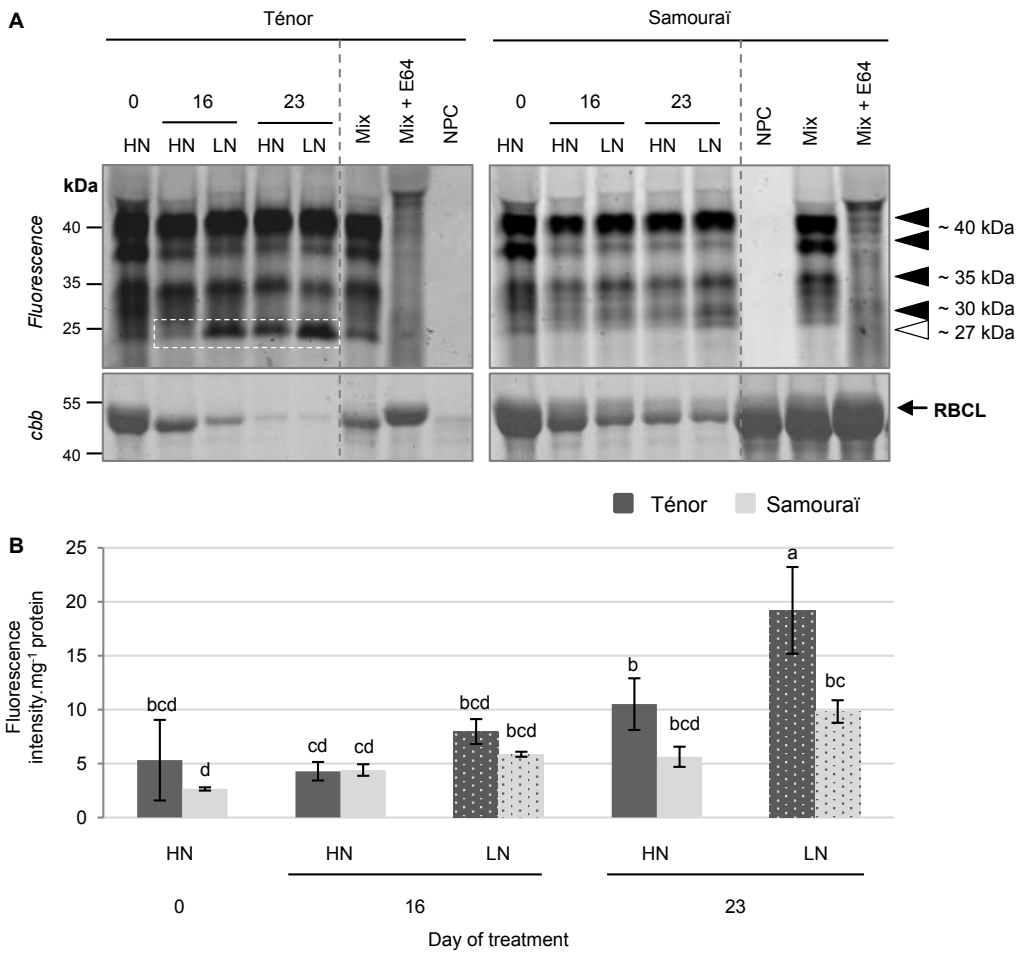

FIGURE 4 | Detection of PLCP activities at pH 5.5 during leaf senescence in two genotypes of *Brassica napus* L. supplied with high (HN) or low (LN) nitrate for 23 days. Soluble proteins were extracted from leaf blade of source leaf (L12) of Ténor or Samouraï plants after 0, 16, and 23 days of HN (3.75 mM NO_3^-) or LN (0.375 mM NO_3^-) treatment. Samples were subjected to a labeling of protease activity with MV201 (specific fluorescent probe of PLCPs) (pH 5.5; 4 h labeling). The fluorescence was detected by a scanner after separation of samples by SDS-PAGE **(A)**. Mix corresponds to a mixture of the protein extracts obtained at 0, 16, and 23 days for both treatments (HN and LN) in the presence of MV201. Mix+E64: mix and E64 (specific inhibitor of cysteine proteases). NPC, no probe control (absence of MV201). After incubation, the abundance of RuBisCO large subunit (RBLC) was observed after gel staining by coomassie brilliant blue (*cbb*). In each lane, the total amount of loaded proteins corresponds to 20 μL of protein sample. Positions of active proteases are represented by black arrowheads while the white arrowhead shows senescence-induced proteases. PLCP global activity characterized by the fluorescence intensity was calculated relative to the protein amount **(B)**. The gel is representative of three biological replicates. Vertical bars indicate ± SD of the mean of three biological replicates. Statistical differences are represented by letters ($P < 0.05$, ANOVA, Newman–Keuls test).

18, and 21 days of HN or LN treatment (**Figure 7**). Compared to Samouraï, the results clearly showed that the abundance of mature form of SAG12 (26–27 kDa) was greater than immature form (40 kDa) in senescing leaves of Ténor plants after 16 days of N limitation or 21 days under HN conditions (**Figure 7A**). In both genotypes, the immature form of RD21 (37 kDa, **Figure 7B**) was detected after 14 days of HN or LN conditions but the abundance is very low. Interestingly, the abundance strongly increased in response of 21 days of N limitation only in senescing leaves of Ténor (**Figure 7B**). These western blot results confirmed that the active forms of RD21 and SAG12 are more abundant in Ténor and are in agreement with the stronger activity of these CPs in Ténor than in Samouraï leaves observed after 23 days under LN conditions (**Figure 4**).

In conclusion, the strong proteolytic performances of Ténor during the leaf senescence associated with N limitation (**Figure 1C**) seem to be closely linked to stronger SP and CP activities, and induction of specific CP activities (SAG12 and RD21) (**Figures 3**–**7** and **Table 1**) than in Samouraï.

Phytohormone Contents During Leaf Senescence in Ténor vs. Samouraï

The senescence process is highly regulated by different endogenous factors that include the phytohormones (Jibran et al., 2013; Khan et al., 2014). Therefore, the difference in leaf-senescence protease activities between Ténor and Samouraï could be associated with differences in the regulation of

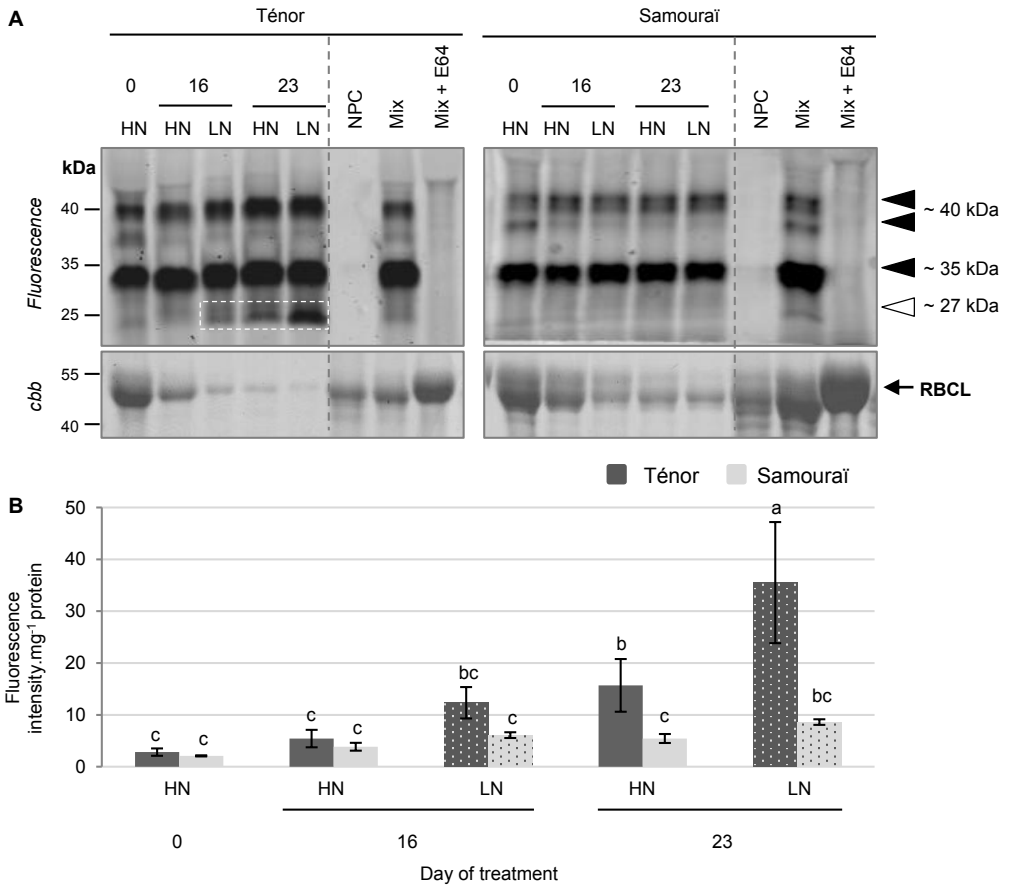

FIGURE 5 | Detection of aleurain-like proteases (AALP) and other PLCP activities at pH 5.5 during leaf senescence in two genotypes of *Brassica napus* L. supplied with high (HN) or low (LN) nitrate for 23 days. Soluble proteins were extracted from leaf blade of source leaf (L12) of Ténor or Samouraï plants after 0, 16, and 23 days of HN (3.75 mM NO_3^-) or LN (0.375 mM NO_3^-) treatment. Samples were subjected to a labeling of protease activity with FY01 (specific fluorescent probe of AALPs and other PLCPs) (pH 5.5; 4 h labeling). The fluorescence was detected by a scanner after separation of samples by SDS-PAGE **(A)**. Mix corresponds to a mixture of the protein extracts obtained at 0, 16, and 23 days for both treatments (HN and LN) in the presence of FY01. Mix+E64: mix and E64 (specific inhibitor of cysteine proteases). NPC: no probe control (absence of FY01). After incubation, the abundance of RuBisCO large subunit (RBLC) was observed after gel staining by coomassie brilliant blue (*cbb*). In each lane, the total amount of loaded proteins corresponds to 20 μL of protein sample. Positions of active proteases are represented by black arrowheads, while the white arrowhead shows senescence-induced proteases. AALP global activity, characterized by the fluorescence intensity, was calculated relative to the protein amount **(B)**. The gel is representative of three biological replicates. Vertical bars indicate ± SD of the mean of three biological replicates. Statistical differences are represented by letters ($P < 0.05$, ANOVA, Newman–Keuls test).

senescence by phytohormones. To validate or refute this hypothesis, our goal was to study and compare phytohormone contents between Ténor and Samouraï during leaf senescence and correlate the hormonal patterns with the protease activities. To reach this goal, several phytohormone contents were measured by UPLC-ESI (+/−) -TQD in plants of Ténor and Samouraï subjected to HN or LN supply for 23 days (**Figure 8**).

Surprisingly, the MeJA content decreased during leaf senescence regardless of the treatment and the genotype (**Figure 8A**) whereas it has been demonstrated that exogenous application of MeJA up-regulates the transcript abundance of genes that are markers of developmental senescence in *A. thaliana* (Jung et al., 2007). Similarly, the JA content decreased during leaf senescence in *B. napus* L. regardless of the nitrate supply or the genotype (**Figure 8B**) while JA biosynthesis is upregulated in senescing leaves of *A. thaliana* (Seltmann et al., 2010). Otherwise, the auxin (IAA) content remained stable during leaf senescence irrespective of the nitrate treatment and the genotype (**Figure 8C**). The role of auxin (IAA) in senescence is not clear. Indeed, it has been demonstrated that the IAA-induced gene, *SAUR36*, was up-regulated during senescence while its dysfunction induced a delay to senescence in *A. thaliana* (Hou et al., 2013). Contrastingly, a senescence repressor role for IAA was demonstrated in *A. thaliana* with the down-regulation of several senescence-associated genes (SAGs), including *SAG12*, by an exogenous application of IAA (Noh and Amasino, 1999; Kim et al., 2011). MeJA, JA and IAA do not seem to be associated with the different behaviors observed during leaf senescence in Ténor and Samouraï because the levels were quite similar, and therefore their roles in senescence processes remain unclear in *B. napus* L.

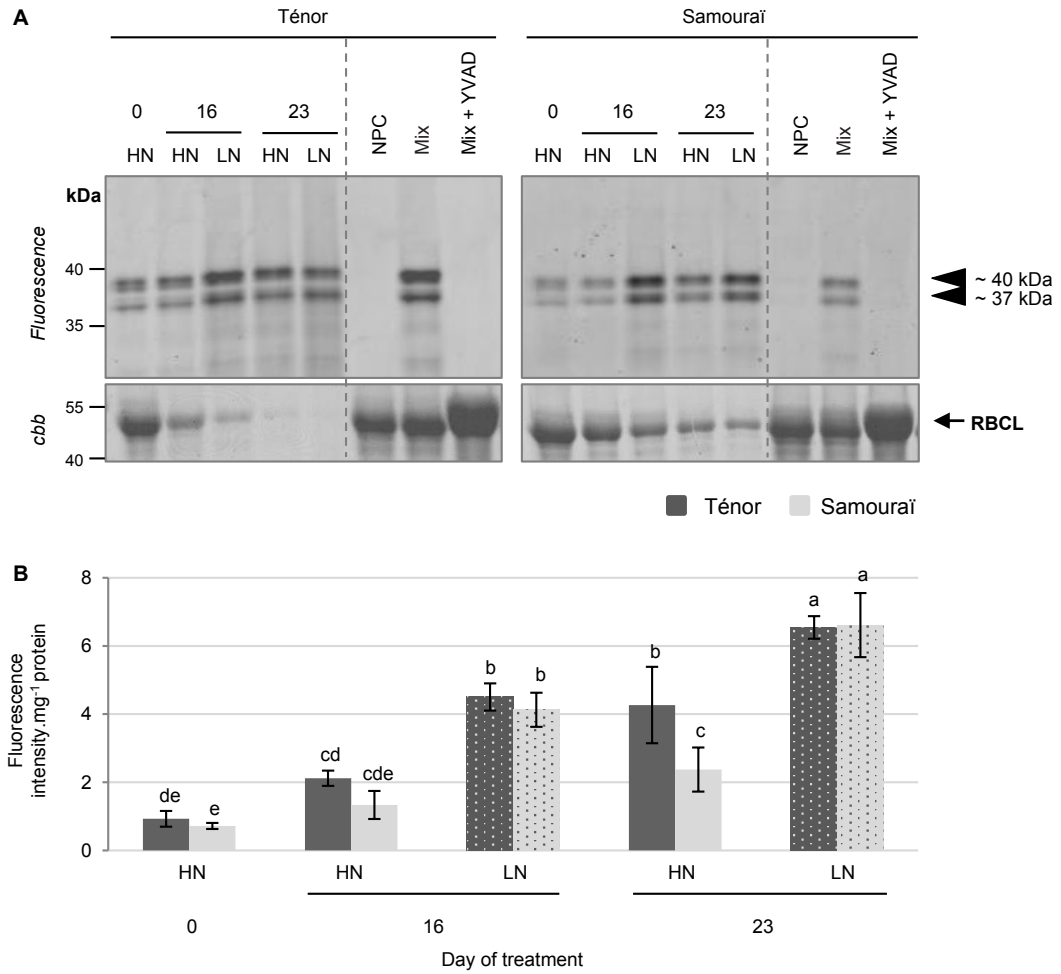

FIGURE 6 | Vacuolar processing enzyme activities at pH 5.5 during leaf senescence in two genotypes of *Brassica napus* L. supplied with high (HN) or low (LN) nitrate for 23 days. Soluble proteins were extracted from leaf blade of source leaf (L12) of Ténor or Samouraï plants after 0, 16, and 23 days of HN (3.75 mM NO_3^-) or LN (0.375 mM NO_3^-) treatment. Samples were subjected to a labeling of protease activity with JOPD1 (specific fluorescent probe of VPEs) (pH 5.5; 4 h labeling). The fluorescence was detected by a scanner after separation of samples by SDS-PAGE **(A)**. Mix corresponds to a mixture of the protein extracts obtained at 0, 16, and 23 days for both treatments (HN and LN) in the presence of JOPD1. Mix+YVAD: mix and YVAD (specific inhibitor of VPEs). NPC, no probe control (absence of JOPD1). After incubation, the abundance of RuBisCO large subunit (RBLC) was observed after gel staining by coomassie brilliant blue (*cbb*). In each lane, the total amount of loaded proteins corresponds to 20 μL of protein sample. Positions of active proteases are represented by black arrowheads. VPE global activity, characterized by the fluorescence intensity, was calculated relative to the protein amount **(B)**. The gel is representative of three biological replicates. Vertical bars indicate ± SD of the mean of three biological replicates. Statistical differences are represented by letters ($P < 0.05$, ANOVA, Newman–Keuls test).

Compared to the initial level (Day 0), the ABA content significantly increased during leaf senescence in Tenor after 23 days under nitrate limitation, while it decreased in Samouraï (**Figure 8D**). A promotive role of ABA has already been demonstrated during senescence in *A. thaliana* with the up-regulation of *SAG113* (a senescence associated gene) linked with an increase in the ABA endogenous content (Zhang et al., 2012). Moreover, endogenous ABA content increases during senescence in many plant species such as *Avena sativa* (Lim et al., 2007) and *A. thaliana* (Zhang et al., 2012).

The SA content increased during leaf senescence in plants subjected to N limitation for 23 days, regardless of the genotype (**Figure 8G**). This is correlated with the fourfold increase in SA levels reported in senescent leaves of *A. thaliana* by Morris et al. (2000). Moreover, these authors have also reported that a dysfunction of SA synthesis in *A. thaliana* leads to a delay in senescence and a down-regulation of *SAG12* expression (Morris et al., 2000).

The contents of two intermediate molecules of cytokinin synthesis, IP and isopentenyladenosine (IPR), decreased during senescence in plants regardless of the N treatment and the genotype (**Figures 8E,F**). This is correlated with the general decrease in cytokinin content observed during leaf senescence in *N. tabacum* while an increase in the endogenous cytokinin level leads to a delay in senescence processes (Yu et al., 2009). Our results are also in agreement with the fact that over-expression of the isopentenyltransferase gene, responsible for cytokinin biosynthesis, generally leads to senescence delay and

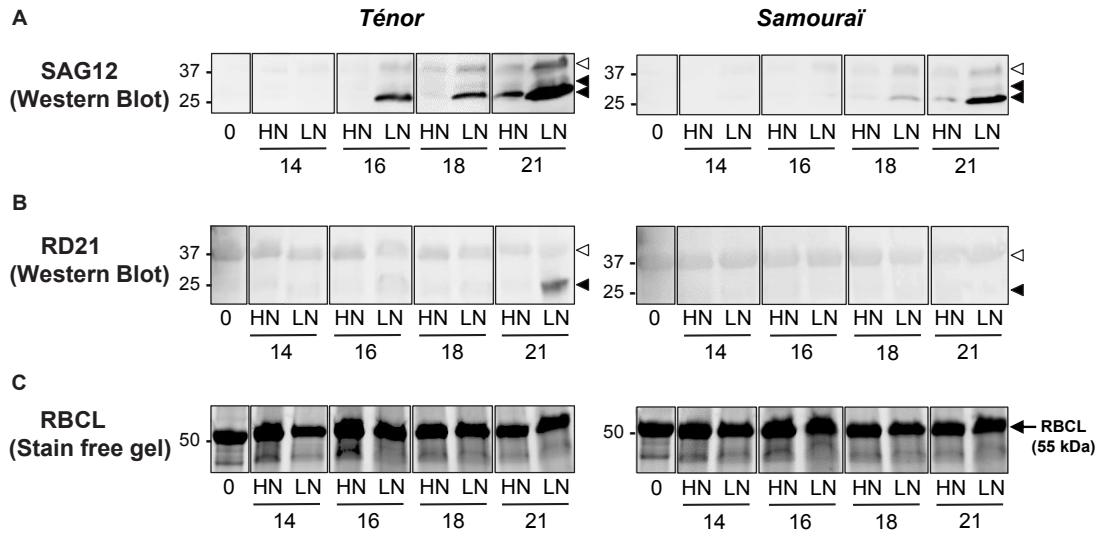

FIGURE 7 | Immunodetection of SAG12 **(A)**, and RD21 **(B)** during leaf senescence in two genotypes of *Brassica napus* L. supplied with high (HN) or low (LN) nitrate during 21 days. Soluble proteins were extracted from leaf blade of source leaf (L12) of Ténor or Samouraï plants after 0, 16, and 23 days of HN (3.75 mM NO_3^-) or LN (0.375 mM NO_3^-) treatment. Thirty μg of soluble proteins per lane were separated on a 4–15% gradient in SDS-PAGE precast Stain-free gels (Bio-Rad) and gels were scanned under UV light to show the total amount of input proteins (as observed for the large subunit of RuBisCO (RBCL) presented in **(C)**. After the transfer to the polyvinylidene difluoride (PVDF) membrane, the immunodetection was realized with an antibody specific of proteins SAG12 and RD21A. White head arrow: immature form, black head arrow: mature form. The gel and Western Blots are representative of three biological replicates (for details see section "Materials and Methods").

stay-green phenotypes in numerous species including *B. napus* (Kant et al., 2015; Zeng and Zhao, 2016). Because ABA, SA and cytokinins seem to be strongly involved in the regulation of leaf senescence in *B. napus* L., we focused our analysis on the content of these phytohormones. The change in the ratio between phytohormones that accelerate leaf senescence, such as ABA and SA, and those that negatively regulate senescence, such as cytokinins was analyzed (**Figure 8H**). The ratio (SA + ABA)/(IP + IPR) increased greatly during leaf senescence in Ténor plants after 23 days of treatment, and particularly after N limitation, whereas it remained stable for Samouraï leaves regardless of the nitrate treatment. This ratio allowed the two genotypes to be distinguished during senescence as well as a clear separation between the N treatments in Ténor during senescence. This ratio was also clearly correlated with the activities of the PLCPs, the AALP and the SPs during senescence with Pearson correlation coefficients of 0.866, 0.932, and 0.905, respectively (p-value < 0.0001, data not shown). These data suggested that different hormonal balances during senescence between Ténor and Samouraï could be associated with stronger PLCP and SP activities and proteolytic performance in Ténor compared to Samouraï during senescence, particularly under N limitation. As already described, phytohormones like ABA and SA are able to up-regulate protease transcripts or protease abundance and dysfunction in SA synthesis during senescence leads to down-regulation of *SAG12* gene expression in *A. thaliana* (Morris et al., 2000). Further, ABA has been shown to enhance RuBisCO degradation in detached leaves of *Oryza sativa* L. floated on a solution containing ABA compared to those on a solution without ABA (Fukayama et al., 2010). This was correlated with an increase in SDS-dependent protease activities (with an optimum pH 5.5 suggesting a vacuolar localization) that significantly increased with ABA treatment. These types of protease activities are also increased during leaf senescence in rice (Fukayama et al., 2010).

In addition to these data, a preliminary study that infiltrated exogenous SA or water in mature leaves of oilseed rape (cv. Aviso) was performed (**Supplementary Figure S2**). The degradation of RuBisCO was followed *in vitro* in the presence or absence of MG132 (an inhibitor of CPs and the proteasome) in these leaves. When leaf tissues were infiltrated with SA, the level of RuBisCO degradation was strongly reduced in the presence of MG132 (with a rate of degradation of 32% versus 60% in the absence of MG132) compared to water infiltration (rate of degradation of 46% versus 59% in the absence of MG132) (**Supplementary Figure S2**). This enhanced inhibition of RuBisCO degradation by MG132 after SA infiltration (inhibition of 46% versus 22% for water infiltration, **Supplementary Figure S2**) suggests that the contribution of CPs and the proteasome activities to proteolysis is more important after SA application and reinforces the assumption that SA is involved in the regulation of CP and proteasome activities in leaves of oilseed rape. According to these results observed during leaf senescence, we have recently demonstrated that the infiltration of ABA and SA in cotyledons of oilseed rape (Ténor) provokes the induction of senescence and several cysteine and SP activities in cotyledons (Poret et al., 2017). Nevertheless, additional experiments will be required to validate the postulate that these phytohormone patterns could regulate PLCP or SP protease activities.

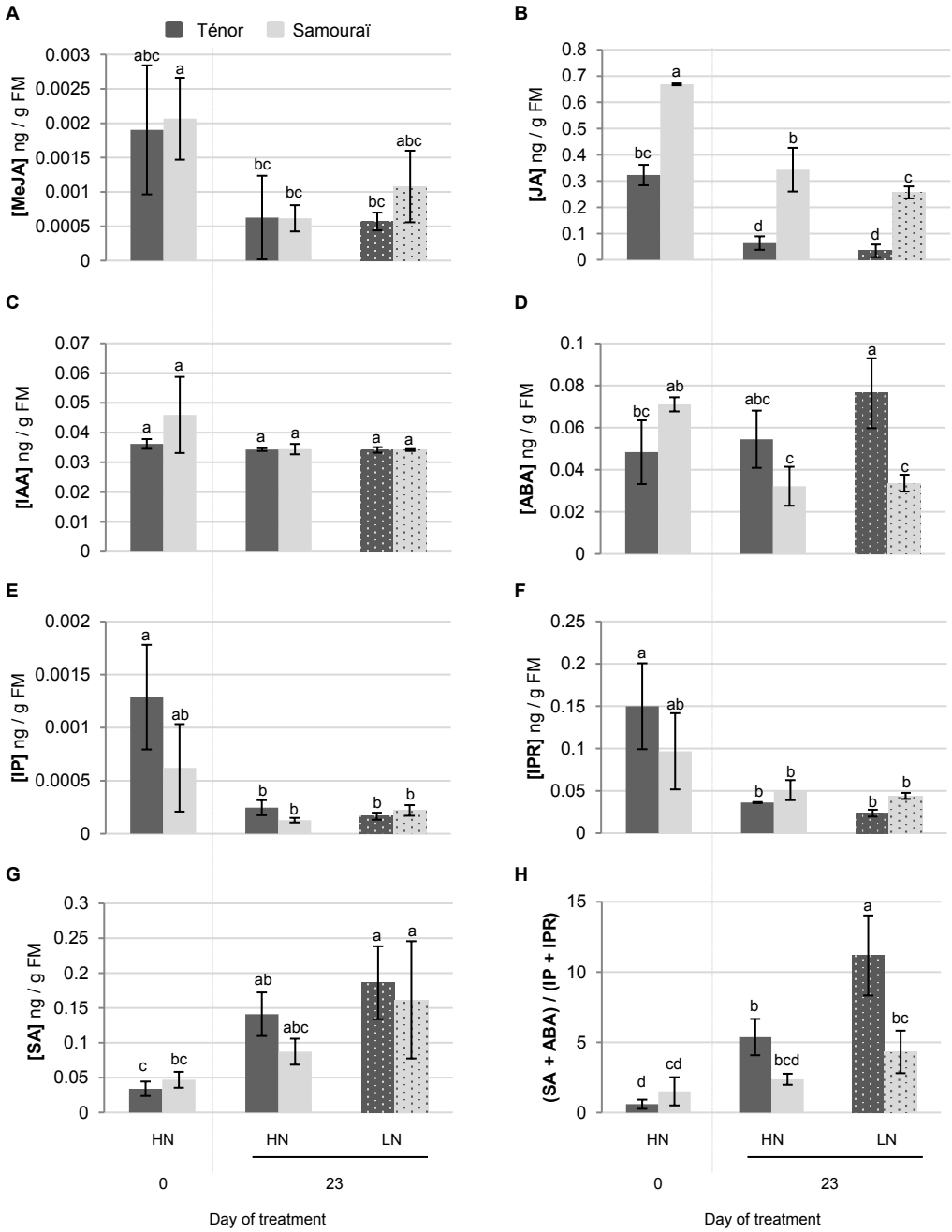

FIGURE 8 | Changes to phytohormone contents during leaf senescence of two genotypes of *Brassica napus* L. supplied with high (HN) or low (LN) nitrate for 23 days. Phytohormones (**A**: MeJA, methyl jasmonate; **B**: JA, jasmonic acid; **C**: IAA, indole acetic acid; **D**: ABA, abscisic acid; **E**: IP, isopentenyladenine; **F**: IPR, isopentenyladenosine and **G**: SA, salicylic acid) were extracted in a methanol/formic acid buffer after 0 and 23 days of HN (3.75 mM NO_3^-) or LN (0.375 mM NO_3^-) for two genotypes of *Brassica napus* L. (Ténor and Samourai) and measured by UPLC-MS (for details see section "Materials and Methods"). The ratio of phytohormone contents (SA+ABA)/(IP+IPR) was calculated at D0 and D23 **(H)**. Vertical bars indicate ± SD of the mean of three biological replicates. Statistical differences are represented by letters ($P < 0.05$, ANOVA, Newman–Keuls test).

CONCLUSION

The genotype Ténor, which unlike Samouraï is temporarily able to maintain its biomass production in response to nitrate limitation (Girondé et al., 2015), demonstrates enhanced senescence processes in response to N restriction including a greater decrease in chlorophyll content, efficient degradation of soluble proteins and a greater decrease in the amount of N in senescing leaves. This efficient proteolytic performance is associated with (i) strong increases in SP and PLCP activities

and (ii) the appearance of new PLCP activities such as RD21 or SAG12, which is absent or very low in Samouraï leaves during senescence. Moreover, in contrast to Samouraï, Ténor is characterized by a hormonal balance (SA + ABA)/(IP + IPR) that promotes senescence. This high ratio between phytohormones positively regulating senescence and phytohormones negatively regulating senescence may be correlated with more efficient protein degradation *via* the induction of PLCP/SP activities for Ténor compared to Samouraï during senescence, particularly under nitrate limitation. More specific investigations will be necessary to validate the phytohormone regulation of protease activities during senescence.

AUTHOR CONTRIBUTIONS

MP and J-CA contributed to the experimental design and tissue sampling. MP carried out the protease activity profiling using activity-dependent fluorescent probes with the help of BC. MP, SD, T-HK, and B-RL carried out the phytohormones extractions, measurements, and chromatograms analyses. MP, FM, IH-N, and J-CA performed other biochemical measurements, proteases analyses, Western Blots, statistical analyses, interpretation of data, and drafting the article. MP, RvdH, AB, T-HK, B-RL, and J-CA were involved in revising the manuscript for important intellectual content.

FUNDING

This work was funded by the French National Research Agency (ANR-11-BTBR-004 RAPSODYN – Investments for the Future: Optimisation of the RAPeSeed Oil content and Yield under low Nitrogen input) and by a Ph.D. grant to MP from the French Ministry of Research and the Ph.D. Doctoral School (EDNBISE, Ecole Doctorale Normande Biologie Intégrative, Santé, Environnement). Further financial support was provided by the ERA-IB project "PRODuCE", the Max Planck Society, COST CM1004 and the University of Oxford.

ACKNOWLEDGMENTS

We would like to thank Dr. Nathalie Nési, INRA (UMR 1349 Institut de Génétique, Environnement et Protection des Plantes, INRA, Agrocampus Ouest, Université de Rennes) who is the leader of this ANR-program, Dr. Jacques Trouverie and Dr. Philippe Etienne for their useful comments on this study, the P2M2 – Metabolic and Metabolomic profiling platform (INRA, UMR 1349 Institut de Génétique, Environnement et Protection des Plantes, INRA, Agrocampus Ouest, Université de Rennes) for phytohormone analysis, Dr. Laurent Coquet for protein identification by ESI LC-MS/MS on the proteomic platform at the University of Rouen Normandie (Pissaro platform, IFR MP 23, Rouen, France) and finally the UMR EVA technical staff for their skilful assistance. We are most grateful to PLATIN' (Plateau d'Isotopie de Normandie) core facility for all element and isotope analysis used in this study. We also wish to acknowledge Dr. Laurence Cantrill for proofreading and English correction.

SUPPLEMENTARY MATERIAL

The Supplementary Material for this article can be found online at: https://www.frontiersin.org/articles/10.3389/fpls.2019.00046/full#supplementary-material

REFERENCES

Antão, C. M., and Malcata, F. X. (2005). Plant serine proteases: biochemical, physiological and molecular features. *Plant Physiol. Biochem.* 43, 637–650. doi: 10.1016/j.plaphy.2005.05.001

Avice, J. C., and Etienne, P. (2014). Leaf senescence and nitrogen remobilization efficiency in oilseed rape (*Brassica napus* L.). *J. Exp. Bot.* 65, 3813–3824. doi: 10.1093/jxb/eru177

Behrens, T., Horst, W. J., and Wiesler, F. (2001). "Effect of rate, timing and form of nitrogen application on yield formation and nitrogen balance in oilseed rape production," in *Plant Nutrition. Developments in Plant and Soil Sciences*, Vol. 92, ed. W. J. Horst (Dordrecht: Springer), 800–801. doi: 10.1007/0-306-47624-X_389

Bhalerao, R., Keskitalo, J., Erlandsson, R., Björkbacka, H., Birve, S. J., Karlsson, J., et al. (2003). Gene expression in autumn leaves. *Plant Physiol.* 131, 430–442. doi: 10.1104/pp.012732

Blum, H., Beier, H., and Gross, H. J. (1987). Improved silver staining of plant proteins, RNA and DNA in polyacrylamide gel. *Electrophoresis* 8, 93–99. doi: 10.1002/elps.1150080203

Bradford, M. M. (1976). A rapid and sensitive method for the quantitation of microgram quantities of protein utilizing the principle of protein-dye binding. *Anal. Biochem.* 72, 248–254. doi: 10.1016/0003-2697(76)90527-3

Chandrasekar, B., Colby, T., Emran Khan Emon, A., Jiang, J., Hong, T. N., Villamor, J. G., et al. (2014). Broad-range glycosidase activity profiling. *Mol. Cell. Proteomics* 13, 2787–2800. doi: 10.1074/mcp.O114.041616

Coupe, S. A., Sinclair, B. K., Watson, L. M., Heyes, J. A., and Eason, J. R. (2003). Identification of dehydration-responsive cysteine proteases during post-harvest senescence of broccoli florets. *J. Exp. Bot.* 54, 1045–1056. doi: 10.1093/jxb/erg105

Demirevska-Kepova, K., Hölzer, R., Simova-Stoilova, L., and Feller, U. (2005). Heat stress effects on ribulose-1,5-bisphosphate carboxylase/oxygenase, Rubisco binding protein and Rubisco activase in wheat leaves. *Biol. Plant.* 49, 521–525. doi: 10.1007/s10535-005-0045-2

Desclos, M., Dubousset, L., Etienne, P., Le Caherec, F., Satoh, H., Bonnefoy, J., et al. (2008). A proteomic profiling approach to reveal a novel role of *Brassica napus* drought 22 kD/water-soluble chlorophyll-binding protein in young leaves during nitrogen remobilization induced by stressful conditions. *Plant Physiol.* 147, 1830–1844. doi: 10.1104/pp.108.116905

Desclos, M., Etienne, P., Coquet, L., Jouenne, T., Bonnefoy, J., Segura, R., et al. (2009). A combined 15N tracing/proteomics study in *Brassica napus* reveals the chronology of proteomics events associated with N remobilisation during leaf senescence induced by nitrate limitation or starvation. *Proteomics* 9, 3580–3608. doi: 10.1002/pmic.200800984

Desclos-Théveniau, M., Coquet, L., Jouenne, T., and Etienne, P. (2014). Proteomic analysis of residual proteins in blades and petioles of fallen leaves of *Brassica napus*. *Plant Biol.* 17, 408–418. doi: 10.1111/plb.12241

D'Hooghe, P., Escamez, S., Trouverie, J., and Avice, J. C. (2013). Sulphur limitation provokes physiological and leaf proteome changes in oilseed rape that lead to perturbation of sulphur, carbon and oxidative metabolisms. *BMC Plant Biol.* 7:23. doi: 10.1186/1471-2229-13-23

Diaz, C., Lemaître, T., Christ, A., Azzopardi, M., Kato, Y., Sato, F., et al. (2008). Nitrogen recycling and remobilization are differentially controlled by leaf

senescence and development stage in Arabidopsis under low nitrogen nutrition. *Plant Physiol.* 147, 1437–1449. doi: 10.1104/pp.108.119040

Diaz, C., Saliba-Colombani, V., Loudet, O., Belluomo, P., Moreau, L., Daniel-Vedele, F., et al. (2006). Leaf yellowing and anthocyanin accumulation are two genetically independent strategies in response to nitrogen limitation in Arabidopsis. *Plant Cell Physiol.* 47, 74–83. doi: 10.1093/pcp/pci225

Diaz-Mendoza, M., Velasco-Arroyo, B., Santamaria, M. E., Gonzalez-Melendi, P., Martinez, M., and Diaz, I. (2016). Plant senescence and proteolysis: two processes with one destiny. *Genet. Mol. Biol.* 39, 329–338. doi: 10.1590/1678-4685-GMB-2016-0015

Fukayama, H., Abe, R., and Uchida, N. (2010). SDS-dependent proteases induced by ABA and its relation to Rubisco and Rubisco activase contents in rice leaves. *Plant Physiol. Biochem.* 48, 808–812. doi: 10.1016/j.plaphy.2010.08.002

Gan, S., and Amasino, R. (1995). Inhibition of leaf senescence by autoregulated production of cytokinin. *Science* 270, 1986–1988. doi: 10.1126/science.270.5244.1986

Ge, Y., Cai, Y. M., Bonneau, L., Rotari, V., Danon, A., McKenzie, E. A., et al. (2016). Inhibition of cathepsin B by caspase-3 inhibitors blocks programmed cell death in Arabidopsis. *Cell Death Diff.* 23, 1493–1501. doi: 10.1038/cdd.2016.34

Girondé, A., Poret, M., Etienne, P., Trouverie, J., Bouchereau, A., Le Cahérec, F., et al. (2015). A profiling approach of the natural variability of foliar N remobilization at the rosette stage gives clues to understand the limiting processes involved in the low N use efficiency of winter oilseed rape. *J. Exp. Bot.* 66, 2461–2474. doi: 10.1093/jxb/erv031

Girondé, A., Poret, M., Etienne, P., Trouverie, J., Bouchereau, A., Le Cahérec, F., et al. (2016). A comparative study of proteolytic mechanisms during leaf senescence of four genotypes of winter oilseed rape highlighted relevant physiological and molecular traits for NRE improvement. *Plants* 5:1. doi: 10.3390/plants5010001

Glass, A. D. (2003). Nitrogen use efficiency of crop plants: physiological constraint upon nitrogen absorption. *Crit. Rev. in Plant Sci.* 22, 453–470. doi: 10.1080/07352680390243512

Gombert, J., Etienne, P., Ourry, A., and Le Dily, F. (2006). The expression patterns of SAG12/Cab genes reveal the spatial and temporal progression of leaf senescence in *Brassica napus* L. with sensitivity to the environment. *J. Exp. Bot.* 57, 1949–1956. doi: 10.1093/jxb/erj142

Gregersen, P. L., Cutelic, A., Boschian, L., and Krupinska, K. (2013). Plant senescence and crop productivity. *Plant Mol. Biol.* 82, 603–622. doi: 10.1007/s11103-013-0013-8

Guiboileau, A., Sormani, R., Meyer, C., and Masclaux-Daubresse, C. (2010). Senescence and death of plant organs: nutrient recycling and developmental regulation. *C. R. Biol.* 333, 382–391. doi: 10.1016/j.crvi.2010.01.016

Guo, Y., Cai, Z., and Gan, S. (2004). Transcriptome of Arabidopsis leaf senescence. *Plant Cell Environ.* 27, 521–549. doi: 10.1111/j.1365-3040.2003.01158.x

Guo, Y., and Gan, S. (2005). Leaf senescence: signals, execution, and regulation. *Curr. Topic Devel. Biol.* 71, 83–112. doi: 10.1016/S0070-2153(05)71003-6

He, Y., Tang, W., Swain, J. D., Green, A. L., Jack, T. P., and Gan, S. (2001). Networking senescence-regulating pathways by using Arabidopsis enhancer trap lines. *Plant Physiol.* 126, 707–716. doi: 10.1104/pp.126.2.707

Hou, K., Wu, W., and Gan, S. (2013). SAUR36, a small auxin up RNA gene, is involved in the promotion of leaf senescence in arabidopsis. *Plant Physiol.* 161, 1002–1009. doi: 10.1104/pp.112.212787

James, M., Poret, M., Masclaux-Daubresse, C., Marmagne, A., Coquet, L., Jouenne, T., et al. (2018). SAG12, a major cysteine protease involved in nitrogen mobilization during senescence for seed production in *Arabidopsis thaliana*. *Plant Cell Physiol.* 59, 2052–2063. doi: 10.1093/pcp/pcy125

Jibran, R., Hunter, D. A., and Dijkwel, P. P. (2013). Hormonal regulation of leaf senescence through integration of developmental and stress signals. *Plant Mol. Biol.* 82, 547–561. doi: 10.1007/s11103-013-0043-2

Jing, H. C., Schippers, J. H., Hille, J., and Dijkwel, P. P. (2005). Ethylene-induced leaf senescence depends on age-related changes and OLD genes in Arabidopsis. *J. Exp. Bot.* 56, 2915–2923. doi: 10.1093/jxb/eri287

Jung, C., Lyou, S. H., Yeu, S., Kim, M. A., Rhee, S., Kim, M., et al. (2007). Microarray-based screening of jasmonate responsive genes in *Arabidopsis thaliana*. *Plant Cell Rep.* 26, 1053–1063. doi: 10.1007/s00299-007-0311-1

Kant, S., Burch, D., Badenhorst, P., Palanisamy, R., Mason, J., and Spangenberg, G. (2015). Regulated expression of a cytokinin biosynthesis gene IPT delays leaf senescence and improves yield under rainfed and irrigated conditions in Canola (*Brassica napus* L.). *PLoS One* 10:e0116349. doi: 10.1371/journal.pone.0116349

Kato, Y., Ozawa, S. I., Takahashi, Y., and Sakamoto, W. (2015). D1 fragmentation in photosystem II repair caused by photo-damage of a two-step model. *Photosynt. Res.* 126, 409–416. doi: 10.1007/s11120-015-0144-7

Khan, M., Rozhon, W., and Poppenberger, P. (2014). The role of hormones in the aging of plants – A mini-review. *Gerontology* 60, 49–55. doi: 10.1159/000354334

Kim, J., Woo, H. R., and Nam, H. G. (2016). Toward systems understanding of leaf senescence: an integrated multi-omics perspective on leaf senescence. *Res. Mol. Plant.* 9, 813–825. doi: 10.1016/j.molp.2016.04.017

Kim, J. I., Murphy, A. S., Baek, D., Lee, S. W., Yun, D. J., Bressan, R. A., et al. (2011). YUCCA6 over-expression demonstrates auxin function in delaying leaf senescence in *Arabidopsis thaliana*. *J. Exp. Bot.* 62, 3981–3992. doi: 10.1093/jxb/err094

Koeslin-Findeklee, F., Rizi, V. S., Becker, M. A., Parra-Londono, S., Arif, M., Balazadeh, S., et al. (2015). Transcriptomic analysis of nitrogen starvation- and cultivar-specific leaf senescence in winter oilseed rape (*Brassica napus* L.). *Plant Sci.* 233, 174–185. doi: 10.1016/j.plantsci.2014.11.018

Kolodziejek, I., Misas-Villamil, J. C., Kaschani, F., Clerc, J., Gu, C., Krahn, D., et al. (2011). Proteasome activity imaging and profiling characterizes bacterial effector Syringolin A. *Plant Physiol.* 155, 477–489. doi: 10.1104/pp.110.163733

Krupinska, K., Mulisch, M., Hollmann, J., Tokarz, K., Zschiesche, W., Kage, H., et al. (2012). An alternative strategy of dismantling of the chloroplasts during senescence observed in a high yield variety of barley. *Physiol. Plant.* 144, 189–200. doi: 10.1111/j.1399-3054.2011.01545.x

Kusaba, M., Tanaka, A., and Tanaka, R. (2013). Stay-green plants: what do they tell us about the molecular mechanism of leaf senescence? *Photosynth. Res.* 117, 221–234. doi: 10.1007/s11120-013-9862-x

Laemmli, U. K. (1970). Cleavage of structural proteins during the heat bacteriophage T4. *Nature* 227, 680–685. doi: 10.1038/227680a0

Laîné, P., Ourry, A., Macduff, J., Boucaud, J., and Salette, J. (1993). Kinetic parameters of nitrate uptake by different catch crop species: effects of low temperatures or previous nitrate starvation. *Physiol. Plant.* 88, 85–92. doi: 10.1111/j.1399-3054.1993.tb01764.x

Li, Z., Peng, J., Wen, X., and Guo, H. (2012). Gene network analysis and functional studies of senescence-associated genes reveal novel regulators of Arabidopsis leaf senescence. *J. Integr. Plant Biol.* 54, 526–539. doi: 10.1111/j.1744-7909.2012.01136.x

Lim, P. O., Kim, H. J., and Nam, H. G. (2007). Leaf senescence. *Annu. Rev. Plant Biol.* 58, 115–136. doi: 10.1146/annurev.arplant.57.032905.105316

Lohman, K. N., Gan, S., John, M. C., and Amasino, R. M. (1994). Molecular analysis of natural leaf senescence in *Arabidopsis thaliana*. *Physiol. Plant.* 92, 322–328. doi: 10.1111/j.1399-3054.1994.tb05343.x

Lu, H., Chandrasekar, B., Oeljeklaus, J., Misas-Villamil, J. C., Wang, Z., Shindo, T., et al. (2015). Subfamily-specific probes for Cys proteases display dynamic protease activities during seed germination. *Plant Physiol.* 168, 1462–1475. doi: 10.1104/pp.114.254466

Malagoli, P., Laine, P., Rossato, L., and Ourry, A. (2005a). Dynamics of nitrogen uptake and mobilization in field-grown winter oilseed rape (*Brassica napus*) from stem extension to harvest: I. Global N flows between vegetative and reproductive tissues in relation to leaf fall and their residual N. *Ann. Bot.* 95, 853–861.

Malagoli, P., Laîné, P., Rossato, L., and Ourry, A. (2005b). Dynamics of nitrogen uptake and mobilization in field-grown winter oilseed rape (*Brassica napus*) from stem extension to harvest. II. An 15N-labelling-based simulation model of N partitioning between vegetative and reproductive tissues. *Ann. Bot.* 95, 1187–1198.

Martínez, D. E., Bartoli, C. G., Grbic, V., and Guiamet, J. J. (2007). Vacuolar cysteine proteases of wheat (*Triticum aestivum* L.) are common to leaf senescence induced by different factors. *J. Exp. Bot.* 58, 1099–1107. doi: 10.1093/jxb/erl270

Morris, K., Mackerness, S. A. H., Page, T., John, C. F., Murphy, A. M., Carr, J. P., et al. (2000). Salicylic acid has a role in regulating gene expression during leaf senescence. *Plant J.* 23, 677–685. doi: 10.1046/j.1365-313x.2000.00836.x

Noh, Y. S., and Amasino, R. M. (1999). Identification of a promoter region responsible for the senescence-specific expression of SAG12. *Plant Mol. Biol.* 41, 181–194. doi: 10.1023/A:1006342412688

Otegui, M., Noh, Y. S., Martinez, D. E., Petroff, M. G. V., Staehelin, L. A., Amasino, R. M., et al. (2005). Senescence-associated vacuoles with intense proteolytic activity develop in leaves of Arabidopsis and soybean. *Plant J.* 41, 831–844. doi: 10.1111/j.1365-313X.2005.02346.x

Otegui, M. S. (2018). Vacuolar degradation of chloroplast components: autophagy and beyond. *J. Exp. Bot.* 69, 741–750. doi: 10.1093/jxb/erx234

Ougham, H. J., Morris, P., and Thomas, H. (2005). The colors of autumn leaves as symptoms of cellular recycling and defenses against environmental stresses. *Curr. Topics Devel. Biol.* 66, 135–160. doi: 10.1016/S0070-2153(05)66004-8

Pan, X., Welti, R., and Wang, X. (2010). Quantitative analysis of major plant hormones in crude plant extracts by high-performance liquid chromatography–mass spectrometry. *Nat. Protoc.* 5, 986–992. doi: 10.1038/nprot.2010.37

Parrott, D. L., McInnerney, K., Feller, U., and Fischer, A. M. (2007). Steam-girdling of barley (Hordeum vulgare) leaves leads to carbohydrate accumulation and accelerated leaf senescence, facilitating transcriptomic analysis of senescence-associated genes. *New Phytol.* 176, 56–59. doi: 10.1111/j.1469-8137.2007.02158.x

Patricelli, M. P., Giang, D. K., Stamp, L. M., and Burbaum, J. J. (2001). Direct visualization of serine hydrolase activities in complex proteomes using fluorescent active site-directed probes. *Proteomics* 1, 1067–1071. doi: 10.1002/1615-9861(200109)1:9<1067::AID-PROT1067>3.0.CO;2-4

Poret, M., Chandrasekar, B., van der Hoorn, R. A. L., and Avice, J. C. (2016). Characterization of senescence-associated protease activities involved in the efficient protein remobilization during leaf senescence of winter oilseed rape. *Plant Sci.* 246, 139–153. doi: 10.1016/j.plantsci.2016.02.011

Poret, M., Chandrasekar, B., van der Hoorn, R. A. L., Coquet, L., Jouenne, T., and Avice, J. C. (2017). Proteomic investigations of proteases involved in cotyledon senescence: a model to explore the genotypic variability of proteolysis machinery associated with nitrogen remobilization efficiency during the leaf senescence of oilseed rape. *Proteomes* 5:29. doi: 10.3390/proteomes5040029

Rathke, G. W., Christen, O., and Diepenbrock, W. (2005). Effects of nitrogen source and rate on productivity and quality of winter oilseed rape (*Brassica napus* L.) grown in different crop rotations. *Field Crops Res.* 94, 103–113. doi: 10.1016/j.fcr.2004.11.010

Richau, K. H., Kaschani, F., Verdoes, M., Pansuriya, T. C., Niessen, S., Stüber, K., et al. (2012). Subclassification and biochemical analysis of plant papain-like cysteine proteases displays subfamily-specific characteristics. *Plant Physiol.* 158, 1583–1599. doi: 10.1104/pp.112.194001

Roberts, I. N., Caputo, C., Criado, M. V., and Funk, C. (2012). Senescence-associated proteases in plants. *Physiol. Plant.* 145, 130–139. doi: 10.1111/j.1399-3054.2012.01574.x

Roberts, I. N., Caputo, C. P., Kade, M., Criado, M. V., and Barneix, A. J. (2011). Subtilisin-like serine proteases involved in N remobilization during grain filling in wheat. *Acta Physiol. Plant.* 33, 1997–2001. doi: 10.1007/s11738-011-0712-1

Roberts, I. N., Murray, P. F., Caputo, C. P., Passeron, S., and Barneix, A. J. (2003). Purification and characterization of a subtilisin-like serine protease induced during the senescence of wheat leaves. *Physiol. Plant.* 118, 483–490. doi: 10.1016/j.phytochem.2013.06.025

Roberts, I. N., Passeron, S., and Barneix, A. J. (2006). The two main endopeptidases present in darkinduced senescent wheat leaves are distinct subtilisin-like proteases. *Planta* 224, 1437–1447. doi: 10.1007/s00425-006-0312-2

Rothstein, S. J. (2007). Returning to our roots: making plant biology research relevant to future challenges in agriculture. *Plant Cell* 19, 2695–2699. doi: 10.1105/tpc.107.053074

Schjoerring, J. K., Bock, J. G. H., Gammelvind, L., Jensen, C. R., and Mogensen, V. O. (1995). Nitrogen incorporation and remobilization in different shoot components of field-grown winter oilseed rape (*Brassica napus* L.) as affected by rate of nitrogen application and irrigation. *Plant Soil* 177, 255–264. doi: 10.1007/BF00010132

Seltmann, M. A., Stingl, N. E., Lautenschlaeger, J. K., Krischke, M., Mueller, M. J., and Berger, S. (2010). Differential impact of lipoxygenase 2 and jasmonates on natural and stress-induced senescence in arabidopsis. *Plant Physiol.* 152, 1940–1950. doi: 10.1104/pp.110.153114

Sylvester-Bradley, R., and Kindred, D. R. (2009). Analysis nitrogen responses of cereals to prioritize routes to the improvement of nitrogen use efficiency. *J. Exp. Bot.* 60, 1939–1951. doi: 10.1093/jxb/erp116

Thoenen, M., Herrmann, B., and Feller, U. (2007). Senescence in wheat leaves: is a cysteine endopeptidase involved in the degradation of the large subunit of Rubisco? *Acta Physiol. Plant.* 29, 339–350. doi: 10.1007/s11738-007-0043-4

van der Hoorn, R. A., and Kaiser, M. (2012). Probes for activity-based profiling of plant proteases. *Physiol. Plant.* 145, 18–27. doi: 10.1111/j.1399-3054.2011.01528.x

van der Hoorn, R. A. L., Colby, T., Nickel, S., Richau, K. H., Schmidt, J., and Kaiser, M. (2011). Mining the active proteome of *Arabidopsis thaliana*. *Front. Plant. Sci.* 2:89. doi: 10.3389/fpls.2011.00089

Wu, X. Y., Kuai, B. K., Jia, J. Z., and Jing, H. C. (2012). Regulation of leaf senescence and crop genetic improvement. *J. Integr. Plant Biol.* 54, 936–952. doi: 10.1111/jipb.12005

Yamada, K., Matsushima, R., Nishimura, M., and Hara-Nishimura, I. (2001). A slow maturation of a cysteine protease with a granulin domain in the vacuoles of senescing Arabidopsis leaves. *Plant Physiol.* 127, 1626–1634. doi: 10.1104/pp.010551

Yu, K., Wei, J., Ma, Q., Yu, D., and Li, J. (2009). Senescence of aerial parts is impeded by exogenous gibberellic acid in herbaceous perennial *Paris polyphylla*. *J. Plant Physiol.* 166, 819–830. doi: 10.1016/j.jplph.2008.11.002

Zeng, X. F., and Zhao, D. G. (2016). Expression of IPT in Asakura-sanshoo (*Zanthoxylum piperitum* (L.) DC. f. inerme Makino) alters tree architecture, delays leaf senescence, and changes leaf essential oil composition. *Plant Mol. Biol. Rep.* 34, 649–658. doi: 10.1007/s11105-015-0948-9

Zhang, H., and Zhou, C. (2013). Signal transduction in leaf senescence. *Plant Mol. Biol.* 82, 539–545. doi: 10.1007/s11103-012-9980-4

Zhang, K., and Gan, S. (2012). An abscisic acid-AtNAP transcription factor-SAG113 protein phosphatase 2C regulatory chain for controlling dehydration in senescing Arabidopsis leaves. *Plant Physiol.* 158, 961–969. doi: 10.1104/pp.111.190876

Zhang, K., Xia, X., Zhang, Y., and Gan, S. (2012). An ABA regulated and Golgi-localized protein phosphatase controls water loss during leaf senescence in Arabidopsis. *Plant J.* 69, 667–678. doi: 10.1111/j.1365-313X.2011.04821.x

Conflict of Interest Statement: The authors declare that the research was conducted in the absence of any commercial or financial relationships that could be construed as a potential conflict of interest.

frontiers in Plant Science

ORIGINAL RESEARCH
published: 14 March 2019
doi: 10.3389/fpls.2019.00293

Phylogenetic Distribution and Diversity of Bacterial Pseudo-Orthocaspases Underline Their Putative Role in Photosynthesis

*Marina Klemenčič[1,2], Johannes Asplund-Samuelsson[3], Marko Dolinar[2] and Christiane Funk[1]**

[1] Department of Chemistry, Umeå University, Umeå, Sweden, [2] Department of Chemistry and Biochemistry, Faculty of Chemistry and Chemical Technology, University of Ljubljana, Ljubljana, Slovenia, [3] Science for Life Laboratory, School of Engineering Sciences in Chemistry, Biotechnology and Health, KTH Royal Institute of Technology, Solna, Sweden

Orthocaspases are prokaryotic caspase homologs – proteases, which cleave their substrates after positively charged residues using a conserved histidine – cysteine (HC) dyad situated in a catalytic p20 domain. However, in orthocaspases pseudo-variants have been identified, which instead of the catalytic HC residues contain tyrosine and serine, respectively. The presence and distribution of these presumably proteolytically inactive p20-containing enzymes has until now escaped attention. We have performed a detailed analysis of orthocaspases in all available prokaryotic genomes, focusing on pseudo-orthocaspases. Surprisingly we identified type I metacaspase homologs in filamentous cyanobacteria. While genes encoding pseudo-orthocaspases seem to be absent in Archaea, our results show conservation of these genes in organisms performing either anoxygenic photosynthesis (orders Rhizobiales, Rhodobacterales, and Rhodospirillales in Alphaproteobacteria) or oxygenic photosynthesis (all sequenced cyanobacteria, except *Gloeobacter*, *Prochlorococcus,* and *Cyanobium*). Contrary to earlier reports, we were able to detect pseudo-orthocaspases in all sequenced strains of the unicellular cyanobacteria *Synechococcus* and *Synechocystis. In silico* comparisons of the primary as well as tertiary structures of pseudo-p20 domains with their presumably proteolytically active homologs suggest that differences in their amino acid sequences have no influence on the overall structures. Mutations therefore affect most likely only the proteolytic activity. Our data provide an insight into diversification of pseudo-orthocaspases in Prokaryotes, their taxa-specific distribution, and allow suggestions on their taxa-specific function.

Keywords: orthocaspase, metacaspase, photosynthesis, pseudo-enzyme, cyanobacteria

OPEN ACCESS

Edited by:
Mercedes Diaz-Mendoza, Centro de Biotecnología y Genómica de Plantas (CBGP), Spain

Reviewed by:
Tanai Cardona, Imperial College London, United Kingdom
Anna Marika Lindahl, Spanish National Research Council (CSIC), Spain

****Correspondence:***
Christiane Funk
Christiane.Funk@umu.se

Specialty section:
This article was submitted to Plant Physiology, a section of the journal Frontiers in Plant Science

Received: *21 December 2018*
Accepted: *22 February 2019*
Published: *14 March 2019*

Citation:
Klemenčič M, Asplund-Samuelsson J, Dolinar M and Funk C (2019) Phylogenetic Distribution and Diversity of Bacterial Pseudo-Orthocaspases Underline Their Putative Role in Photosynthesis. Front. Plant Sci. 10:293. doi: 10.3389/fpls.2019.00293

INTRODUCTION

Metazoan caspases (cysteine-aspartic proteases), playing essential roles in programmed cell death, are synthesized as inactive zymogens, which for activation are cleaved into a catalytic, large (p20) and regulatory, small (p10) subunit (Earnshaw et al., 1999). The family of proteins containing the p20 fold, however, is much broader and contains beside the archetypic caspase proteases (subclass

C14A, reviewed by Shalini et al., 2015) also metacaspases (Minina et al., 2017), paracaspases (Jaworski and Thome, 2016) and orthocaspases (Klemenčič and Funk, 2018a), classified as C14B and found in diverse organisms ranging from plants over slime molds and fungi to bacteria (**Figure 1**). Both subclasses contain active proteases, whose active sites contain catalytic histidine and cysteine residues (HC dyad). Unlike caspases, which cleave their substrates after negatively charged aspartic acid residues, members of the C14B family specifically degrade substrates with basic amino acid residues at position P1 (Vercammen et al., 2004; Hachmann et al., 2012; Klemenčič et al., 2015). Metacaspases represent the largest sub-family of these caspase-homologs and depending on their domain structure they are subdivided into different types (Vercammen et al., 2004). Type I metacaspases contain a proline-rich repeat and a zinc-finger motif in the N-terminal prodomain (Vercammen et al., 2004), whereas type II metacaspases lack these motifs and are hallmarked by the presence of an extended linker region between the p20-like and p10-like domains. Recently, genes encoding a third type of metacaspases (type III metacaspases) have been identified in algae that arose from secondary endosymbiosis (Choi and Berges, 2013), those enzymes harbor the p10 domain N-terminal to the p20 domain. While metacaspases are found in plants, fungi and protists, paracaspases are more similar to caspases and were detected in animals and slime molds. They are classified by lack of a p10 domain, but contain immunoglobulin-like (Ig) domains (Uren et al., 2000).

Since the identification of caspases as the key enzymes in programmed cell death of animals, similar functions were sought for metacaspases of Planta and Protozoa. Although initial reports were focused on portraying direct involvement of metacaspases in processes of programmed cell death (Bozhkov et al., 2005; He et al., 2008; Minina et al., 2013), roles of metacaspases were soon shown to exceed mere functions of cell execution and to function in multiple non-death roles (Lee et al., 2008). Additionally, some protozoan type I metacaspases were discovered to lack the complete catalytic dyad rendering them proteolytically inactive; of the five metacaspases encoded in the genome of *Trypanosoma brucei*, TbMC1 and TbMC4 contain HS and YS substitutions (Szallies et al., 2002). Enzymes lacking functional amino acids in their active sites are very common. They are collectively termed pseudo-enzymes (Eyers and Murphy, 2016) and sometimes also referred to as non-enzymes, dead enzymes, prozymes or 'zombie' proteins (Murphy et al., 2017). These proteins are structurally homologous to their active relatives, but lack catalytic activity due to mutations of critical amino acid residues. Even though they are believed to be catalytically inert, increasing data reveal them being functional, important proteins. Currently best studied and most intensively analyzed are pseudo-kinases (reviewed by Byrne et al., 2017) and pseudo-phosphatases (Reiterer et al., 2014), as well as pseudo-proteases, which are gaining the interest of researchers. Pseudo-variants of orthocaspases were already observed in the first genome-wide analysis of Cyanobacteria (Jiang et al., 2010), and later 16% of all identified prokaryotic p20-containing sequences were found to contain substitutions in the catalytic dyad with YS being the most common one (Asplund-Samuelsson et al., 2012). Interestingly, in the majority of unicellular Cyanobacteria the only orthocaspase encoded in the genome is the pseudo-variant (Klemenčič and Funk, 2018a).

To better understand the distribution of pseudo-orthocaspases, we performed a comprehensive *in silico* analysis on all prokaryotic caspase homologs with focus on variants, which instead of the conserved HC dyad harbor other amino acid residues. We show that these pseudo-enzymes are especially abundant in organisms performing oxygenic and to a lower extent in organisms executing anoxygenic photosynthesis (Cyanobacteria and Alphaproteobacteria, respectively). Their possible function in prokaryotic organisms is discussed.

MATERIALS AND METHODS

Identification of Caspase Homologs

Caspase-homologs including orthocaspases were identified using a p20 domain profile hidden Markov model (HMM) constructed using *hmmbuild* from HMMER v3.1b2[1] and the first 457 columns of the Pfam Peptidase_C14 (PF00656) seed alignment, downloaded from https://pfam.xfam.org/. The p20 HMM was used in an *hmmsearch* versus UniProt release 2018_10 (134,066,004 sequences), downloaded from https://www.uniprot.org/ on 12 November 2018. Hits with a best one domain *E*-value lower than 0.0001 were accepted. Further filtration was then performed by alignment to the p20 HMM using *hmmalign*, followed by removal of sequences with a gap in the His or Cys catalytic dyad positions. Finally, sequences with a p20 domain length not falling within a range of two standard deviations from the mean of the remaining sequences, i.e., 101–200 amino acids, were also removed. For identification of p20-containing proteins in organisms of genera *Synechocystis, Synechococcus*, *Prochlorococcus*, and *Cyanobium* we performed a DELTA-BLAST protein homology search[2] using the previously identified *Synechocystis* sp. PCC 6803 p20 domain (Jiang et al., 2010) as a query.

Classification of Caspase Homologs

The accepted caspase homologs from UniProt were subjected to detailed classification of the catalytic dyad, domain architecture, and taxonomy. The alignment to the p20 HMM was used to extract the amino acid residues corresponding to the His and Cys catalytic dyad positions for each sequence. Next, an *hmmsearch* with four additional HMMs was performed versus the sequence dataset, aiming to identify metacaspases and paracaspases via domain architecture. The p10 domain was identified using a p10 HMM constructed with *hmmbuild* from the last 211 columns of the Pfam Peptidase_C14 seed alignment. Paracaspases were identified by having at least one Pfam Immunoglobulin (Ig) (PF00047), Ig_2 (PF13895), or Ig_3 (PF13927) domain beginning its alignment before the start of the p20 alignment. We applied domain cutoff scores of 30.0 for p10, 21.8 for Ig, 27.0 for Ig_2, and 30.0 for Ig_3. Since a few proteins had multiple p20 domains, a cutoff score was implemented for those as well. First, the maximal

[1]http://hmmer.org/

[2]https://blast.ncbi.nlm.nih.gov/

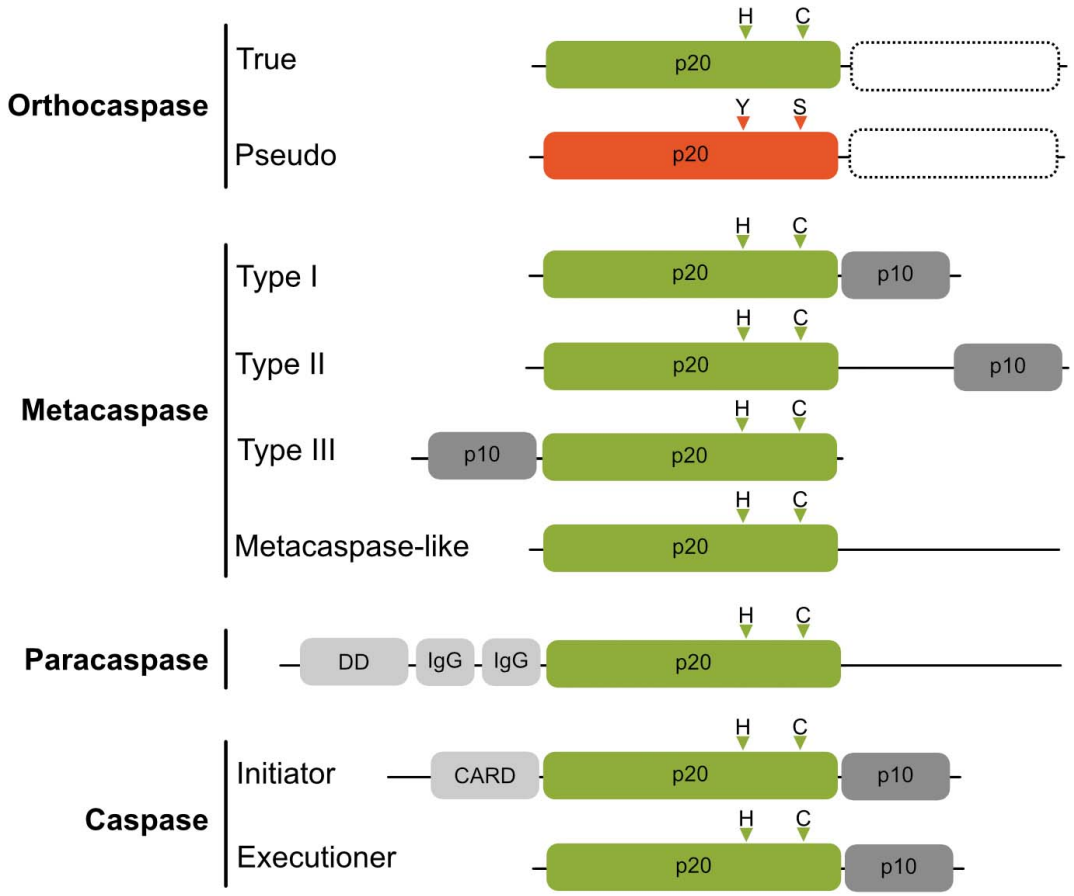

FIGURE 1 | Schematic domain organization of proteins belonging to C14 cysteine proteases. The p20-like domain is colored in green with positions of catalytic His and Cys residues shown as triangles above the domains. Pseudo-orthocaspases are colored in orange, with the most common active site substitution (His to Tyr and Cys to Ser) shown also as orange triangles. True- as well as pseudo-orthocaspases can, but not necessarily do, contain additional domains on the C-terminal (shown as rectangle with a dashed border). The regulatory p10 domain is shown in dark gray and additional domains in light gray (IgG, immunoglobulin-like domain; DD, death domain; CARD, caspase activation and recruitment domain). Figure is not drawn to scale.

p20 score in each sequence was extracted, then the cutoff was set to the minimal value among those maxima, i.e., 35.2. The p20 and p10 domain alignment positions were compiled into a domain architecture. Sequences with a p10 domain starting after the start of the p20 domain were classified as type I metacaspases if the distance between the domains was 66 amino acids or shorter, and otherwise as type II metacaspases. The 66 amino acid limit was based on known interdomain distances (Choi and Berges, 2013) and constitutes the mid-point between the upper limit of a 95% confidence interval (mean plus two standard deviations) for type I metacaspase interdomain distances, and the lower limit of a 95% confidence interval (mean minus two standard deviations) for type II metacaspase interdomain distances. Sequences with a p10 domain ending before the start of a p20 domain were classified as type III metacaspases. If there were more than one p20 or p10 domain, the sequence was classified as ambiguous. Furthermore, the p10 domains were aligned to the p10 HMM using *hmmalign* and the amino acid residues in the conserved Cys and Asp positions (Choi and Berges, 2013; Klemenčič and Funk, 2018b) were extracted to further classify the metacaspases. Finally, each sequence in the dataset was matched to taxonomic data using their NCBI taxonomy IDs and the NCBI taxonomy database, downloaded from https://www.ncbi.nlm.nih.gov/ on 4 October 2018.

Identifying Protein Sequences Motifs

Protein sequence motifs in addition to the p20 domain were identified by submitting FASTA protein sequences to the MOTIF web page[3], which performs a search with a protein query sequence against PROSITE, NCBI-CDD and Pfam motif libraries.

Phylogenetic Tree Construction

In order to trace, visualize, and explore the sequence diversity and evolution, we performed sequence alignments of the p20 domains and phylogenetic tree construction. The p20 domains were extracted from archaeal and bacterial caspase homologs, as well as three metazoan caspases serving as an outgroup

[3]https://www.genome.jp/tools/motif/

(human caspase-3 and caspase-8, and *Caenorhabditis elegans* cell death protein 3; UniProt sequence IDs P42574, Q14790, and P42573), using *hmmalign* versus the p20 HMM with the *--trim* option, followed by gap removal with seqmagick v0.6.2[4]. The p20 domains were aligned using MAFFT v7.271 (Katoh and Standley, 2013), and FastTreeMP v2.1.8 SSE3 (Price et al., 2010) was used for phylogenetic tree construction. Alignment and tree construction was performed for three sequence subsets: All archaeal and bacterial p20 domains, the subset that contained a mutation in the His – Cys catalytic dyad (pseudo-variants), and cyanobacterial p20 domains. Identity of each sequence to each other and to the outgroup sequences was calculated for each of the three alignments as the fraction of matching positions, including internal gaps, unless present in both sequences being compared, and excluding positions with gaps at the ends of the sequences. The phylogenetic trees were visualized using the Interactive Tree of Life (iTOL) v4.1 online service at https://itol.embl.de/ (Letunic and Bork, 2016). To emphasize highly supported clades, branches with a bootstrap support lower than 0.85 were deleted using iTOL.

Sequence Logo Generation

Based on the substitution in the His – Cys catalytic dyad, we recognized two distinct cyanobacterial clades in the phylogenetic tree of mutant p20 domains: YN and YS, labeled by the most prominent catalytic dyad substitutions (see **Supplementary Table S1**). The p20 domains from each clade as well as all cyanobacterial p20 domains with an active dyad (HC) were aligned per sequence group using MAFFT v7.271. The alignments were then transformed to HMMs with *hmmbuild* and submitted to Skylign[5] in order to generate sequence logos based on above background information content, thus illustrating the features in each group of sequences.

RESULTS

Prokaryotes Contain a Rich Pool of Caspase Homologs

According to the MEROPS database of proteolytic enzymes[6], family C14 comprises proteins that contain a characteristic p20 domain with a highly conserved caspase/hemoglobinase fold. This domain accommodates two catalytically crucial residues: a histidine and a cysteine residue (His – Cys, HC), situated on the surface of the domain (Uren et al., 2000; McLuskey and Mottram, 2015). Performing an HMM-search in the most recent UniProt database, which contains 2,936,402 archaeal and 94,326,796 bacterial sequences, representing 4,042 and 94,934 organisms (based on unique taxonomy IDs), respectively, we identified 11,208 protein sequences with homology to the p20 domain in prokaryotic organisms (**Supplementary Table S1**). Among those, only 93 belonged to Archaea, while the rest (11,115) represented bacterial caspase homologs (**Figure 2A**).

In order to distinguish between the structural subtypes of caspase homologs (meta-, para-, orthocaspases), we first tried to identify paracaspases by searching for the presence of immunoglobulin-like (Ig) domains within the identified sequences. Neither Archaea nor Bacteria contained sequences encoding paracaspases, confirming their absence in prokaryotes. The presence of a p10 domain, located either N- or C-terminal to the p20 domain, defines metacaspases. Sequences with high similarity to the p10 domain could be identified in 11 archaeal and 1,121 bacterial sequences, representing 14.9% and 10.1% of all p20-containing sequences, respectively (**Figure 2A**). No type III metacaspases were detected in either of the two prokaryotic superkingdoms. While archaeal sequences were found to contain only type I metacaspases, 10 bacterial metacaspases contained a linker region longer than 66 amino acid residues between the p10 and p20 domain, which would classify them as type II metacaspases. These sequences represented less than 1% of all metacaspase sequences and were not analyzed further. We concluded that bacterial metacaspases generally can be classified as metacaspases of type I.

All remaining sequences lacking the p10 domain were termed orthocaspases. Similar to bacterial orthocaspases (Jiang et al., 2010; Asplund-Samuelsson et al., 2012), also archaeal ones were found to contain additional domains on their N- and C-termini. Among the most prevalent were a C-terminal FGE-sulfatase domain (found in 8 proteins), an EF-hand motif (found in 7 proteins) and an N-terminal Big_7 motif, which is a bacterial Ig-like domain (found in 15 proteins).

Pseudo-Orthocaspases Are Present in Bacteria, but Absent in Archaea

The presence of the HC dyad within the p20 domain is an important prerequisite for proteolytic activity. Analysis of all archaeal meta- as well as orthocaspases revealed the presence of this conserved functional dyad in all 93 sequences (**Figure 2A**). However, some bacterial sequences lacked this catalytic site: 4 out of 1,121 metacaspases and 858 out of 9,994 orthocaspases contained substitutions of either one or both catalytic residues. To distinguish between the presumably active enzymes with conserved catalytic dyad and the presumably inactive ones with substituted/missing active sites, we denoted the sequences "true-" or "pseudo-", respectively, in analogy to the newly established nomenclature for catalytically deficient enzymes (Eyers and Murphy, 2016) (**Figure 2A**).

Since pseudo-metacaspases represented only 0.36% of all bacterial sequences with homology to the p20 domain, they were statistically irrelevant for further analysis. Bacterial pseudo-orthocaspases, however, represented a significant fraction of 8.6% of all bacterial caspase homologs, warranting further analysis. While 90% of all pseudo-orthocaspases were found in organisms belonging to either Alphaproteobacteria (582 sequences) or Cyanobacteria (193 sequences) (**Figure 2B**), only few pseudo-variants were identified in other phyla

[4]https://fhcrc.github.io/seqmagick/

[5]http://skylign.org/

[6]https://www.ebi.ac.uk/merops/

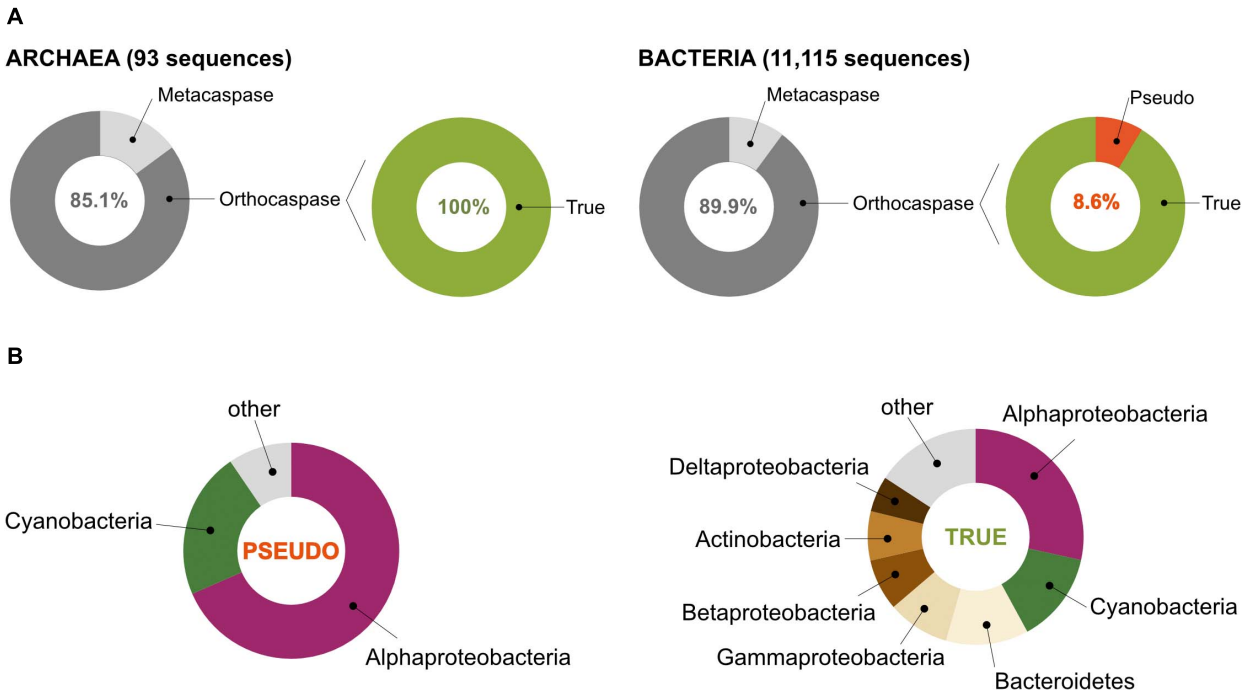

FIGURE 2 | Prokaryotes contain metacaspases and orthocaspases. **(A)** Our study identified 11,208 sequences with homology to the p20 domain. Among these, 93 were found in organisms belonging to Archaea and 11,115 to Bacteria. Sequences homologous to the p10 domain could be identified in 11 archaeal and 1,121 bacterial sequences (metacaspases), the rest represent orthocaspases. Of the bacterial orthocaspases, 8.6% lacked the conserved His – Cys dyad and were termed pseudo-orthocaspases. No pseudo-metacaspases or pseudo-orthocaspases were identified in archaeal organisms. **(B)** Of all pseudo-variants detected, the majority was found in Alphaproteobacteria or Cyanobacteria (left panel), while the true-variants (presumably active enzymes) are distributed among the bacterial groups (phylum; class for Proteobacteria) ranging from Alphaproteobacteria to Deltaproteobacteria (right panel). Only groups containing containing more than 5% of sequences encoding meta- and orthocaspases were named in the chart.

(e.g.,10 out of 1078 sequences in Bacteroidetes, 3 out of 636 sequences in Actinobacteria, and 2 out of 667 sequences in Betaproteobacteria). Notably, this uneven distribution did not reflect the distribution of true-orthocaspases in Bacteria (**Figure 2B**, right panel), where 28.4% of all identified sequences belong to Alphaproteobacteria, and 13.6% to Cyanobacteria, followed by Bacteroidetes (12.4%), Gammaproteobacteria (9.3%), Betaproteobacteria (7.7%), Actinobacteria (7.4%), and Deltaproteobacteria (5.4%). Pseudo-orthocaspases in Alphaproteobacteria and Cyanobacteria therefore seem to have diversified during evolution. To gain a comprehensive overview of the phylogenetic relationships between all prokaryotic caspase homologs, we constructed a phylogenetic tree based on the alignment of their p20 sequences (**Figure 3**). The tree revealed great sequence diversity and a highly mixed contribution from various taxa within subclades, which could be explained by paralogs of potentially diverse function, or extensive horizontal gene transfer. Note, however, that a more detailed analysis is required to attempt to measure the contribution of processes such as horizontal gene transfer. Alphaproteobacterial sequences are placed close to the root, i.e., metazoan caspases, which is in line with the proposed alphaproteobacterial origin of caspases (Aravind and Koonin, 2002). Pseudo-orthocaspases were mainly found clustered in three basal clades and two more distant clades. The presence of such clades suggests conserved functions of those pseudo-orthocaspase variants. Their distribution among true-variants might indicate multiple independent emergences.

Pseudo-Orthocaspases Are a Distinctive Trait of Alphaproteobacteria Performing Anoxygenic Photosynthesis

Although Alphaproteobacteria were found to be rich in metacaspases, 80.4% of alphaproeobacterial sequences containing a p20 domain lacked the p10 domain and were classified as orthocaspases (**Figure 4A**). Among these, 18.9% contained a substitution in the HC dyad, classifying them as pseudo-orthocaspases. Phylogenetically these pseudo-variants seem to be limited to Rhizobiales, Rhodobacterales and Rhodospirillales, the three orders of anaerobic phototrophic purple bacteria. Notably, more than 96% of these pseudo-orthocaspases belonged to organisms of Rhizobiales (561 out of 582), 14 were Rhodobacterial and only two belonged to organisms of Rhodospirillales (**Figure 4B**). Although true-orthocaspases were found to be abundant also in photosynthetic Betaproteobacteria (orders Burkholderiales and Rhodocyclales) and Gammaproteobacteria (order Chromatiales), these organisms lacked pseudo-variants; neither were pseudo-orthocaspases detected in green-sulfur bacteria (Chlorobi). In green-nonsulfur bacteria (Chloroflexi), three sequences

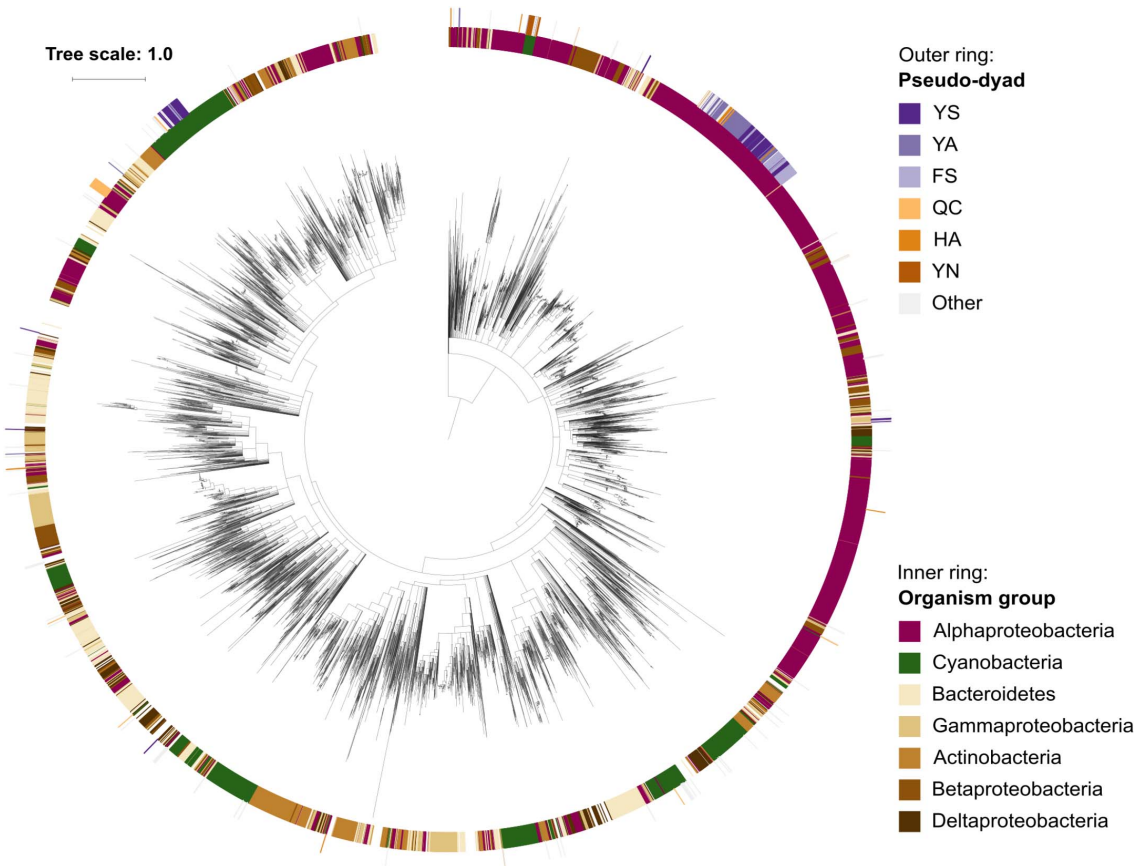

FIGURE 3 | Phylogenetic relationships among prokaryotic caspase homologs. The tree is based on the p20 domain of 11,208 bacterial and archaeal caspase homologs identified in this study, and three metazoan caspases (UniProt IDs P42574, Q14790, and P42573), included as outgroup. The inner ring displays the most abundant organism groups (phylum; class for Proteobacteria), while the outer ring displays the presence and type of substitutions in the catalytic dyad found in pseudo-orthocaspases. Branches with bootstrap support below 0.85 have been deleted. The scale bar shows substitutions per site. The alignment consisted of 2,077 positions and the mean identity to the outgroup sequences was 9.6% (s.d. 2.0%), while 19.0% (s.d. 7.7%) among the prokaryotic sequences. The alignment and a Newick tree are supplied in **Supplementary Data Sheet S1**.

corresponding to pseudo-orthocaspases were found. Two of them were found in the class Ktedonobacteria (species *Ktedonobacter racemifer* DSM 44963 and *Ktedonobacter* sp.), while the third pseudo-orthocaspase was found in the class Anaerolineae (strain *Anaerolineaceae* bacterium 4572_78). Both classes belong to non-phototrophic Chloroflexi.

More detailed analysis of the substitutions of the HC dyad in pseudo-orthocaspases of Rhizobiales showed the most common dyads to be Tyr – Ser (YS), Tyr – Ala (YA) or Phe – Ser (FS). While often both amino acid residues were substituted, also Gln – Cys (QC) and His – Ala (HA) combinations seem to be common. We further observed that each of the substitution variants corresponded to a certain overall protein domain architecture (**Figure 4A**). While p20 domains with YS or YA substitutions contained mostly prolonged C-termini without identifiable domains, those with a FS dyad consistently also contained tetratricopeptide repeats (TPR), which are known scaffolds mediating various protein – protein interactions (Blatch and Lässle, 1999). Moreover, proteins in which the p20 domain contained a QC dyad almost exclusively also contained an N-terminal trypsin-like domain. Examination of this trypsin-like domain identified all three conserved amino acid residues of the catalytic triad of serine proteases (His – Asp – Ser, HDS), suggesting proteolytic activity. At the C-terminus of these proteins a domain of unknown function (DUF4384) was identified, which often co-occurs in proteins with N-terminal kinase domains. This alphaproteobacterial, QC-dyad containing clade seems to be phylogenetically different to other alphaproteobacterial pseudo-orthocaspases, which cluster together in close proximity to the root (**Figure 4B**). Instead, the QC variants appear to be closer related to distal cyanobacterial pseudo-orthocaspase clades.

Cyanobacteria Contain a Rich Pool of Pseudo-Orthocaspases

Although cyanobacteria were thought not to contain metacaspases (Choi and Berges, 2013), we identified 50 protein sequences, which classify as type I metacaspases (**Figure 4C**). All of them belong to genera of filamentous cyanobacteria:

FIGURE 4 | Pseudo-orthocaspases are abundant in Alphaproteobacteria and Cyanobacteria. **(A)** In Alphaproteobacteria we identified 3,826 caspase homologs: 751 metacaspases and 3,075 orthocaspases. 582 enzymes lacked the conserved His – Cys dyad and were termed pseudo-orthocaspases. The most common

(Continued)

FIGURE 4 | Continued
substitutions of the catalytic dyad and their C-terminal domain organizations are shown in the lower panel. Pseudo-enzymes containing FS substitutions consistently had tetratricopeptide repeats C-terminally to the p20 domain (drawn as small gray rectangles). Trypsin denotes the trypsin-like domain, while DUF4843 denotes a well-conserved fold without known function. **(B)** Phylogenetic relationships among bacterial pseudo-orthocaspases. The tree is based on the p20 domain of all 862 bacterial pseudo-orthocaspases identified in this study, and three metazoan caspases (UniProt IDs P42574, Q14790, and P42573), included as the out-group. The inner ring displays Alphaproteobacterial and Cyanobacterial taxonomic orders, while the outer ring displays the amino acids found to substitute the catalytic dyad. Branches with bootstrap support below 0.85 have been deleted. The scale bar shows substitutions per site. The alignment consisted of 360 positions and the mean identity to the outgroup sequences was 11.3% (s.d. 2.5%), while 29.9% (s.d. 18.3%) among the bacterial sequences. The alignment and a Newick tree are supplied in **Supplementary Data Sheet S1**. **(C)** In Cyanobacteria we identified 1,525 caspase homologs: 50 metacaspases and 1,475 orthocaspases. 193 enzymes lacked the conserved His – Cys dyad and were termed pseudo-orthocaspases. The most common substitutions of the catalytic dyad and their C-terminal domain organizations are shown in the lower panel.

Anabaena, *Calothrix*, *Coleofasciculus*, *Lyngbya*, *Moorea,* and *Nostoc*. However, as only few species within these genera contained metacaspases, metacaspases most likely have been acquired via horizontal gene transfer during the evolution of these complex cyanobacteria.

More than 96% of all cyanobacterial p20-containing proteins were found to be orthocaspases. The diversification of true-orthocaspases has been investigated previously (Jiang et al., 2010; Asplund-Samuelsson et al., 2012) and is thus not discussed here. However, 13% of all cyanobacterial orthocaspases were found to lack a functional HC dyad. Unlike in Alphaproteobacteria, where proteins containing pseudo-p20 domains were found to be order-specific, analysis of cyanobacterial genomes revealed the presence of at least one pseudo-orthocaspase in each organism of this phylum, ranging from simple cyanobacteria, such as *Microcystis*, unicellular nitrogen-fixing *Gloeocapsa*, to filamentous nitrogen-fixing *Nostocales*. Their catalytic dyad was most often substituted by YS and no other domains were identified (**Figure 4C**). In rare cases, the catalytic dyad was replaced by YA, FS, or YY. Only in the evolutionary old cyanobacterial genus *Gloeobacter*, i.e., *Gloeobacter violaceus* PCC 7421 and *Gloeobacter kilaueensis* JS1, only true orthocaspases could be found. Additionally, organisms belonging two genera of marine picocyanobacteria were found to lack any p20-containing proteins; *Prochlorococcus*, a simple and heavily streamlined organism (Partensky and Garczarek, 2009) and *Cyanobium*.

Synechococcus and Synechocystis Strains Carry p20-Containing Proteins

Small unicellular organisms, especially strains of freshwater *Synechocystis* and marine *Synechococcus*, have previously been reported to lack orthocaspases (Jiang et al., 2010), and indeed also in our list of p20-domain containing cyanobacteria these organisms seemed to be absent. However, one pseudo-orthocaspase has previously been identified in *Synechocystis* sp. PCC 6803 (Asplund-Samuelsson et al., 2012). To circumvent the rather strict constraints for identification of the p20 domain in our automated search, we performed additional manual analyses within the NCBI database. Proteins with homologous sequences to the p20 domain of *Synechocystis* 6803 were identified in both genera and are listed in **Table 1**; the alignment of their p20 domains is shown in **Supplementary Figure S1**. Surprisingly, each organism identified was found to contain a single gene encoding an orthocaspase and all these p20-domains harbored single- or double substitutions in the HC dyad. YS substitutions were the most common motifs in *Synechococcus* and YG in *Synechocystis*. All identified sequences therefore represent pseudo-orthocaspases.

TABLE 1 | List of manually identified proteins with a p20 domain in the genera of *Synechococcus* and *Synechocystis*.

	NCBI ID	His – Cys conservation	True- or Pseudo-variant
Synechococcus			
PCC 7502	WP_015167715.1	His – Gly	Pseudo
PCC 7003	WP_065712853.1	Tyr – Ser	Pseudo
PCC 8807	WP_065715717.1	Tyr – Ser	Pseudo
PCC 7002	WP_012305740.1	Tyr – Ser	Pseudo
NKBG042902	WP_030006746.1	Tyr – Ser	Pseudo
BDU130192	WP_099239871.1	Tyr – Ser	Pseudo
PCC 73109	WP_062431693.1	Tyr – Ser	Pseudo
PCC 7117	WP_065709860.1	Tyr – Ser	Pseudo
JA-2-3B_a(2-13)	WP_011432265.1	Tyr – Gly	Pseudo
PCC 7336	WP_017327236.1	Tyr – Ser	Pseudo
NIES-970	WP_096415465.1	Tyr – Ser	Pseudo
NKBG15041c	WP_081699644.1	Tyr – Ser	Pseudo
PCC 6312	WP_015123192.1	Tyr – Gly	Pseudo
PCC 7335	WP_006457254.1	His – Gly	Pseudo
Synechocystis			
PCC 6803	WP_010873177.1	Tyr – Gly	Pseudo
PCC 6714	WP_028947383.1	Tyr – Gly	Pseudo
PCC 7509	WP_009633488.1	Tyr – Gly	Pseudo

Only Nitrogen-Fixing Multicellular Cyanobacteria Contain Two Distinct Pseudo-Orthocaspases

Within the set of cyanobacterial pseudo-orthocaspases a large group of sequences contained YS and YN pseudo-catalytic dyads (**Figure 4C**) and lacked any identifiable domain at the C-terminus of the p20-bearing polypeptide chain. We observed that these YS or YN containing p20 domains clustered in two distinct clades, while proteins with other substitutions were scattered throughout the phylogenetic groups (**Figure 5**). Moreover, p20 domains with an YN motif could only be identified in multicellular nitrogen-fixing Cyanobacteria; examples of such genera are: *Leptolyngbya*, *Calothrix*, *Microcoleus*, *Nostoc* as well as *Planktothrix*. As opposed to metacaspases, which were (as previously mentioned)

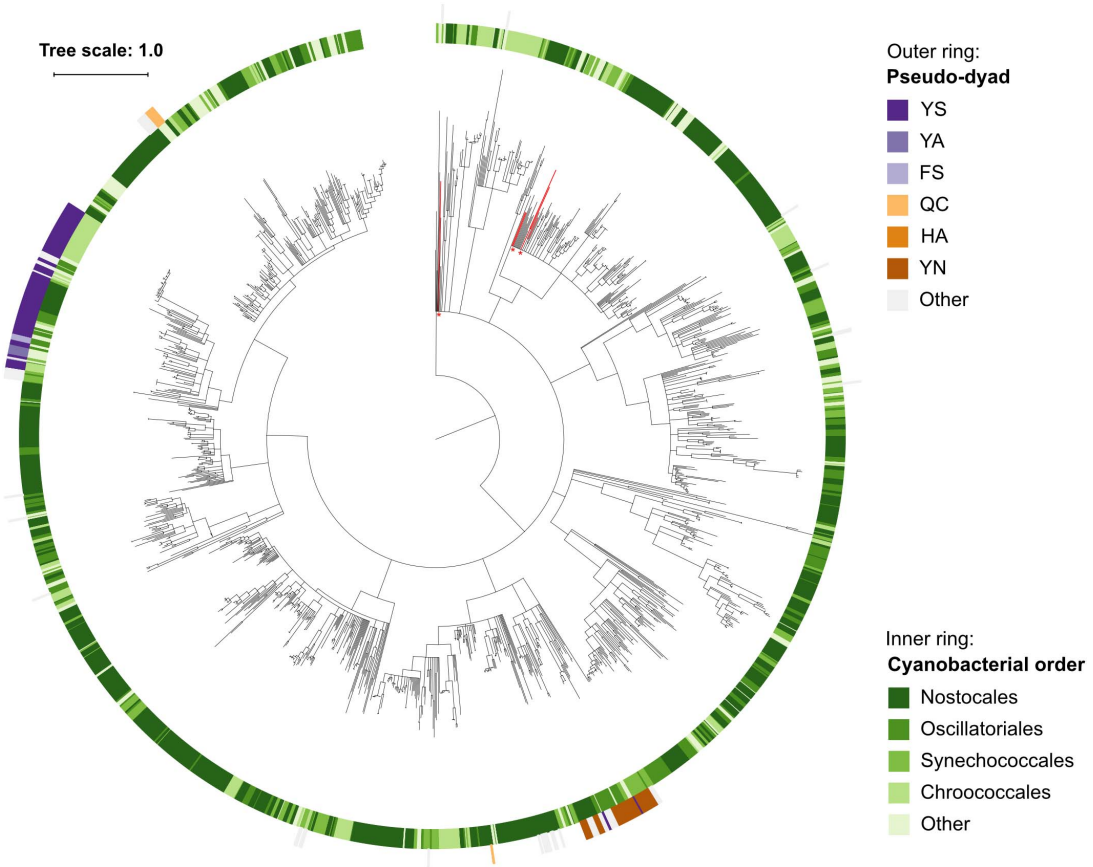

FIGURE 5 | Phylogenetic relationship among Cyanobacterial caspase homologs. The tree is based on the p20 domain of all 1,525 Cyanobacterial caspase homologs identified in this study, and three metazoan caspases (UniProt IDs P42574, Q14790, and P42573) included as the outgroup. The inner ring displays taxonomic orders, while the outer ring displays the presence and catalytic-dyad substitution of pseudo-orthocaspases. The six sequences originating from genus *Gloeobacter* are emphasized in red and with asterisks. Branches with bootstrap support below 0.85 have been deleted. The scale bar shows substitutions per site. The alignment consisted of 668 positions and the mean identity to the outgroup sequences was 9.8% (s.d. 1.8%), while 21.9% (s.d. 11.0%) among the Cyanobacterial sequences. The alignment and a Newick tree are supplied in **Supplementary Data Sheet S1**.

detected only in some filamentous cyanobacterial species, pseudo-orthocaspases with an YN dyad could be found in all analyzed organisms of these genera. It should, however, be noted that YN variants were found to be absent in unicellular nitrogen-fixing Cyanobacteria (e.g., genera: *Cyanothece*, *Gloeocapsa*) as well as filamentous non-heterocystous Cyanobacteria (e.g., *Prochlorothrix hollandica* PCC 9006), thus suggesting specific function of the YN variant in organisms with both properties: multicellularity and nitrogen-fixation. Only multicellular nitrogen-fixing cyanobacteria therefore contain two distinct pseudo-orthocaspase types, one with an YN substitution and the other with an YS substitution.

Acidic Nature of the Specificity Pocket Is Conserved in Cyanobacterial Pseudo-Orthocaspases

Domains C-terminal to the p20 domain, which consistently accompanied certain HC-substitutions have been mentioned earlier. We now investigated if additional amino acid changes in the p20 domain occurred in the pseudo-enzymes. Four amino acid residues have been shown to be crucial for substrate coordination in the p20-domain of type I metacaspase (TbMC2) of *Trypanosoma brucei*: Cys92, Asp95, Ser159 and Asp211 (McLuskey et al., 2012); the two negatively charged amino acid residues were shown to be highly important in accommodating basic residues of substrates. In the p20 domain sequences of prokaryotic pseudo-orthocaspases, these two Asp residues seem to be highly conserved, independent of the substitutions occurring within the catalytic dyad. Sequence logos were constructed for the two most common cyanobacterial substitutions of the HC-dyad, YS and YN, and compared to all cyanobacterial true-variants (**Figure 6A**). Highest conservation was found among those amino acid residues forming the specificity pocket and surrounding the catalytic site, while other residues forming the p20 domain not only differ between pseudo- and true-variants, but also are relatively diverse within each variant. Differences in primary protein structure, however, were not reflected in the tertiary folding (**Figure 6B**), representative models of the p20 domains of three orthocaspases

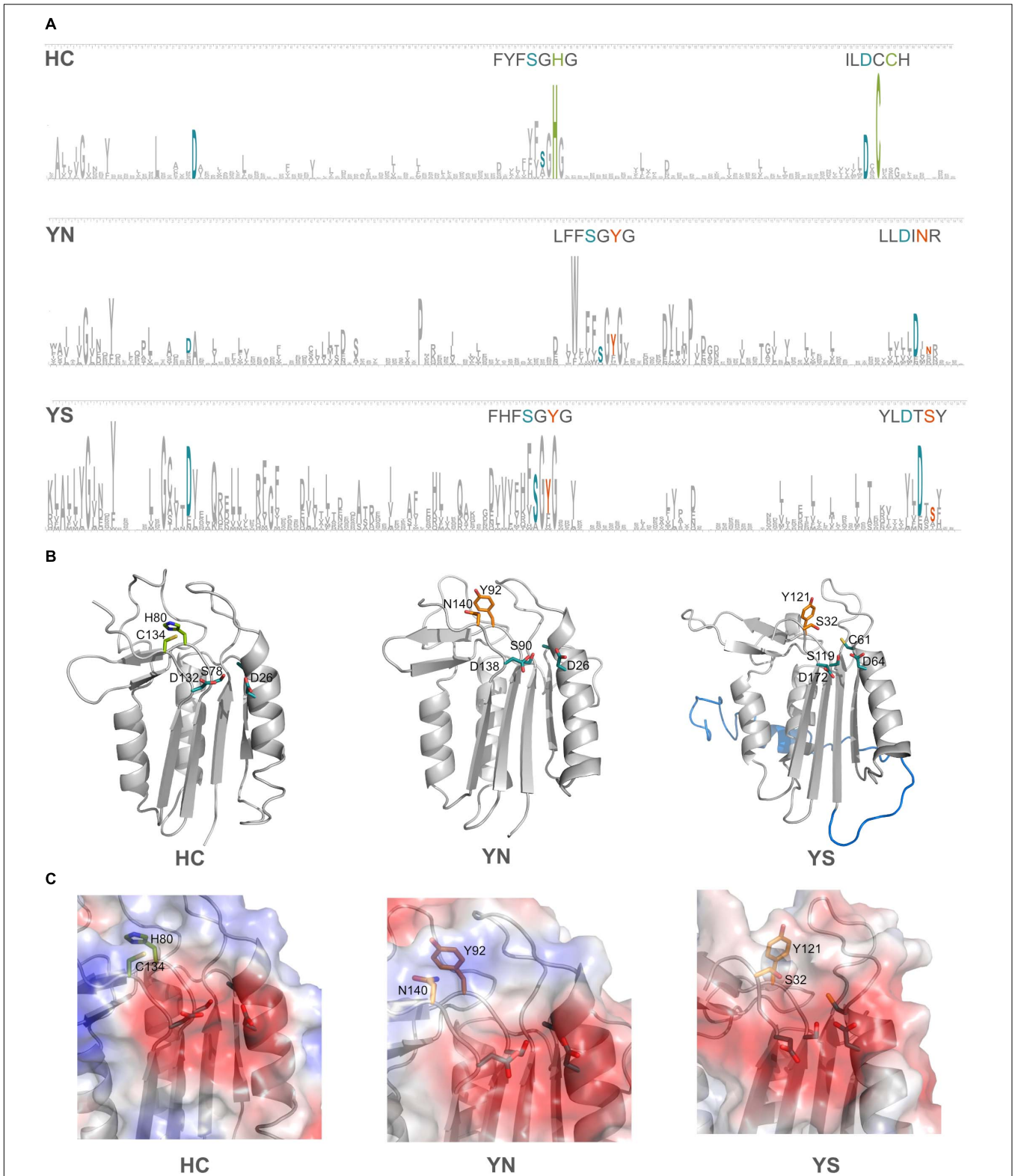

FIGURE 6 | Substitutions in the catalytic dyad of cyanobacterial pseudo-orthocaspases influence the overall folds of neither the p20 domain nor the specificity pocket. **(A)** Sequence logos for positions in the p20 domain are shown for the true- (HC) and two pseudo-variants (YS and YN) in Cyanobacteria. See Methods section "Sequence Logo Generation" for details and **Supplementary Table S1** for the corresponding sequences (121 for YS and 49 for YN). The height of a certain amino acid residue corresponds to its conservation (above background information content). Amino acid residues of the active site are colored according to the

(Continued)

FIGURE 6 | Continued
proteolytic functionality (H and C in green and Y, S, and N in orange). In cyan, residues known to be involved in formation of the specificity pocket are shown. For better visibility of the motifs surrounding the catalytic residues, these stretches are written out above logos. **(B)** Models for each of the three variants are shown in ribbon representation. The p20 domains of three *Nostoc* sp. T09 proteins: HC, A0A252E3G8; YS, A0A252D9J9; YN, A0A252EC77 were submitted to the I-TASSER Suite (https://zhanglab.ccmb.med.umich.edu/I-TASSER/) (Yang et al., 2015) and protein structures were visualized using PyMOL (DeLano Scientific; http://www.pymol.org). All three domains are drawn as ribbons with active site residues and the key amino acid residues involved in substrate coordination as sticks. The N-terminal region, resembling a TAT-signal peptide, is shown in blue in the YS variant. **(C)** Surface potentials of all three specificity pockets are shown in magnified view; blue indicates basic amino acids, red acidic amino acids. Side chains of the amino acids in the catalytic dyad and specificity pocket are shown as sticks.

from *Nostoc sp.* T09 (**Supplementary Figure S2**) contain similar overall folds.

The two well-conserved Asp residues (**Figure 6A**) are located within the substrate binding pocket in the models (**Figure 6C**). Not only do the pseudo-variants contain a well-conserved fold, they can accommodate substrates with basic charge, despite being presumably inactive proteases. Notably different is an extended N-terminal domain of approximately 30 amino acid residues found in the YS variant. In the model this extension forms an alpha-helix (marked in blue color, located behind the p20 domain in **Figure 6B**). This extension seems to be conserved in all identified Synechococcal orthocaspases containing a YS substitution (**Supplementary Figure S1**) and therefore might have a specific function.

DISCUSSION

The caspase-hemoglobinase is one of the most conserved folds, present in proteins of prokaryotic as well as eukaryotic organisms. It is composed of four beta-sheets surrounded by three alpha-helices that form a compact globular domain (Aravind and Koonin, 2002). This fold is the key domain and common denominator of the members of the caspase superfamily, including caspases, metacaspases, paracaspases and orthocaspases. Prokaryotic caspase homologs were first generally termed metacaspases (Asplund-Samuelsson et al., 2012), however, due to the lack of the p10 domain they were renamed to metacaspase-like proteases. Doubts concerning their proteolytic activity (Choi and Berges, 2013) were dispelled, when MaOC1, a cyanobacterial p10-lacking member was shown to be proteolytically active and even to exhibit the highest catalytic efficiency among non-metazoan caspase homologs (Klemenčič et al., 2015). Due to their evolutionary importance and structural as well as functional distinctiveness, these prokaryotic metacaspase-like proteins were termed orthocaspases.

In this study we were able to identify the presence of not only orthocaspases, but also metacaspases in prokaryotes. Although metacaspases were earlier reported to be rather scarce in Alphaproteobacteria and absent in Cyanobacteria (Choi and Berges, 2013), we could identify p10 domain containing enzymes in both groups. With the exception of few metacaspases in Bacteroidetes, all archaeal as well as bacterial metacaspases contain a conserved Asp residue at the N-terminus of the p10 domain (as evident in **Supplementary Table S1**), which was recently shown to be crucial for calcium-binding and activity in eukaryotic type III metacaspases (Klemenčič and Funk, 2018b). A common proteolytic mechanism therefore might be conserved in bacterial and eukaryotic metacaspases.

Additionally, we were able to identify pseudo-proteases among the caspase-homologs, which seem to be restricted to prokaryotic orthocaspases. Substitutions of both catalytic residues were most commonly observed in these pseudo-orthocaspases, similar to the pseudo-metacaspase of *Trypanosoma brucei* TbMC4, in which YS replaces the catalytic dyad (Szallies et al., 2002). This YS variant is also most prevalent among bacterial pseudo-orthocaspases. Beside these substitutions in the active site, the overall folds of the p20-domain or the substrate binding pocket seem not to differ between true- and pseudo-variants as denoted by modeling of cyanobacterial true- and pseudo-variants (**Figure 6**). No protein structures have unfortunately been resolved yet, neither for ortho- nor pseudo-orthocaspases, therefore we cannot exclude larger conformational shifts or the presence of additional amino acid residues, which would sterically hinder substrate binding. In SMIPP-Ss, for example, a multigene family of house dust mite allergen group 3 homologs, which are classified as members of the S1-like family (Wilson et al., 2003), a conserved tyrosine residue at position 200 is predicted to block substrate access to the active site (Fischer et al., 2009). A highly conserved tryptophan residue also can be found in YN pseudo-orthocaspases, located only a few amino acid residues in front of the "catalytic" tyrosine (**Figure 6A**). In our model this residue is predicted to be part of a beta-sheet and positioned adjacent to one of the alpha helices (**Supplementary Figure S3**) and could therefore not directly interfere with coordination of the substrate.

The most striking difference of YS pseudo-orthocaspases compared to the presumably active orthocaspases is the presence of an additional N-terminal domain. Motif prediction software was not able to assign this domain despite its N-terminal double RR and C-terminal A-x-A sequences, specifying cleavage by a signal peptidase (**Supplementary Figures S1, S2**). These two features are characteristic for a TAT (Twin-Arginine Translocation) signal sequence, which in Cyanobacteria translocates proteins that are fully folded either into the periplasm or the thylakoid lumen (Frain et al., 2016). We hypothesize that cyanobacterial YS-pseudo-orthocaspases are involved in photosynthetic processes and/or thylakoid membrane biogenesis in Cyanobacteria, as (i) these enzymes are present in all cyanobacteria except *Gloeobacter* (which lack thylakoid membranes), *Prochlorococcus* and *Cyanobium* and (ii) in *Synechocystis sp.* PCC 6803 as well as in *Microcystis aeruginosa* PCC 7806 genes encoding these pseudo-orthocaspases are strongly light-regulated (Straub et al., 2011; Saha et al., 2016).

Further, we hypothesize that the picocyanobacteria of genera *Prochlorococcus* and *Cyanobium* lost their orthocaspases altogether while adapting to the sparse marine environment, possibly gaining a similarly simplified and pseudo-orthocaspase independent physiology as that of *Gloeobacter*.

Within Alphaproteobacteria, only (anoxygenic) photosynthetic organisms carry pseudo-variants, an observation further supporting our hypothesis that pseudo-orthocaspases are involved in photosynthetic processes in Prokaryotes. However, pseudo-orthocaspases are absent in green- and purple-sulfur bacteria and only three pseudo-orthocaspase sequences within green non-sulfur photosynthetic bacteria (including the phylum Chloroflexi) were detected. The photosynthetic reaction centers (RC) of anoxygenic photosynthetic prokaryotes have a common origin, but diverged in the course of evolution (e.g., Cardona, 2016). RCII of Alphaproteobacteria and Chloroflexi has evolved from the same ancestral RCII, which in oxygenic photosynthetic Cyanobacteria gave rise to Photosystem II. Although this seems to link functions of pseudo-orthocaspases to RCII, absence of pseudo-orthocaspases in phototrophic Chloroflexi and some Cyanobacteria as well as in RCII-bearing Gemmatimonadetes (Zeng et al., 2014) hampers this interpretation.

Pseudo-orthocaspases are presumably proteolytically inactive and based on our data we assume that they evolved from their active relatives: (i) Various pseudo-variants are scattered throughout phylogenetically loosely related organisms (**Figure 3**), suggesting the emergence of pseudo-enzymes to be an example of convergent evolution. Such spontaneous and independent appearance in diverse species is highly reminiscent of the distribution of phototrophy across the bacterial tree, with phototrophic clades dispersed across the tree rather than forming a single clade (Fischer et al., 2016; Ward et al., 2018). (ii) A combination so specific as the HC dyad can be found throughout evolution in all clades (the distant metazoan caspases still retain the catalytic HC dyad throughout millions of years of separated evolution). (iii) Within cyanobacteria, where pseudo-orthocaspases are highly common, the earliest-branching cyanobacterium, *Gloeobacter*, contains only the true variant, appearing to have diverged before the emergence of the distal YS pseudo-orthocaspases (**Figure 5**). Enzymes, which have lost their proteolytic function in comparison to their true-variants have been observed to function as dynamic scaffolds involved in signaling cascades, or can act as competitors, scavenging substrates, which are released under certain circumstances (Reynolds and Fischer, 2015). The pseudo-metacaspase of *T. brucei,* TbMC4, has been shown to be crucial for blood-stage parasite cytokinesis and virulence during mammalian infection. Since it is processed by a true-metacaspase, TbMC3, it is part of the catalytic cascade, thus indirectly regulating the function of its active counterparts (Proto et al., 2011). The pseudo-p20 cFLIP$_L$ variant (cellular FLICE-like inhibitory protein long form), an inactive caspase-8 homolog in humans, has been shown to act as dimerization partner of caspase-8 (Yu et al., 2009). While these well-studied pseudo-variants act in conjunction with their true-relatives, small unicellular Cyanobacteria harbor only a pseudo-variant, suggesting these proteins to have functions independent of active counterparts. Most likely also prokaryotic pseudo-orthocaspases found in organisms, which additionally harbor true-orthocaspases, are not involved in the regulation of their proteolytic activity. It should be noted that genes encoding cyanobacterial pseudo-orthocaspases, especially the YS variant, are highly expressed: metatranscriptomic data from the cyanobacterium *Nodularia spumigena* show consistent and relatively high expression levels in correlation to other genes, suggesting even a "house-keeping" function of the corresponding proteins (Asplund-Samuelsson et al., 2016).

The high conservation of pseudo-orthocaspases in Cyanobacteria and their putative involvement in processes of oxygenic photosynthesis on one hand, with their absence in eukaryotic Chlorophyta and Streptophyta (**Supplementary Table S1**) on the other hand raise many questions regarding their function. Although some functions involving pseudo-caspase homologs have been described for Protista and Metazoa, the loss of pseudo-orthocaspases within the cyanobacterium-plastid transition is intriguing. One also should bear in mind that the presence of the catalytic dyad might not necessarily correspond to proteolytic activity: the role of the type I metacaspase AtMC2 from *Arabidopsis thaliana* was found to be independent of the presence of putative catalytic residues (Coll et al., 2010). Further *in vitro* as well as *in vivo* characterizations are necessary for our understanding of the function of the p20 domain in the various cellular environments they occur: from a simple unicellular bacterium to humans.

DATA AVAILABILITY

All datasets generated for this study are included in the manuscript and/or the **Supplementary Files**.

AUTHOR CONTRIBUTIONS

All authors designed the study. MK and JA-S analyzed the data and drafted the manuscript. All authors revised the manuscript.

FUNDING

This work was funded by the Carl Tryggers Foundation (CTS 17:160; CF)/Umeå University (CF)/Slovenian Research Agency (research core funding no. P1-0179; MK and P1-0048; MD).

ACKNOWLEDGMENTS

We are grateful to Natalie Hendrikse (KTH) for inspiring discussions and to Paul Hudson's lab (KTH) for supplying computational resources.

SUPPLEMENTARY MATERIAL

The Supplementary Material for this article can be found online at: https://www.frontiersin.org/articles/10.3389/fpls.2019.00293/full#supplementary-material

REFERENCES

Aravind, L., and Koonin, E. V. (2002). Classification of the caspase-hemoglobinase fold: detection of new families and implications for the origin of the eukaryotic separins. *Proteins* 46, 355–367. doi: 10.1002/prot.10060

Asplund-Samuelsson, J., Bergman, B., and Larsson, J. (2012). Prokaryotic caspase homologs: phylogenetic patterns and functional characteristics reveal considerable diversity. *PloS One* 7:e49888. doi: 10.1371/journal.pone.0049888

Asplund-Samuelsson, J., Sundh, J., Dupont, C. L., Allen, A. E., McCrow, J. P., Celepli, N. A., et al. (2016). Diversity and expression of bacterial metacaspases in an aquatic ecosystem. *Front. Microbiol.* 7:1043. doi: 10.3389/fmicb.2016.01043

Blatch, G. L., and Lässle, M. (1999). The tetratricopeptide repeat: a structural motif mediating protein-protein interactions. *BioEssays News Rev. Mol. Cell. Dev. Biol.* 21, 932–939.

Bozhkov, P. V., Suarez, M. F., Filonova, L. H., Daniel, G., Zamyatnin, A. A., Rodriguez-Nieto, S., et al. (2005). Cysteine protease mcII-Pa executes programmed cell death during plant embryogenesis. *Proc. Natl. Acad. Sci.* 102, 14463–14468. doi: 10.1073/pnas.0506948102

Byrne, D. P., Foulkes, D. M., and Eyers, P. A. (2017). Pseudokinases: update on their functions and evaluation as new drug targets. *Future Med. Chem.* 9, 245–265. doi: 10.4155/fmc-2016-0207

Cardona, T. (2016). Reconstructing the origin of oxygenic photosynthesis: do assembly and photoactivation recapitulate evolution? *Front. Plant Sci.* 7:257. doi: 10.3389/fpls.2016.00257

Choi, C. J., and Berges, J. A. (2013). New types of metacaspases in phytoplankton reveal diverse origins of cell death proteases. *Cell Death Dis.* 4:e490. doi: 10.1038/cddis.2013.21

Coll, N. S., Vercammen, D., Smidler, A., Clover, C., Breusegem, F. V., Dangl, J. L., et al. (2010). *Arabidopsis* type I metacaspases control cell death. *Science* 330, 1393–1397. doi: 10.1126/science.1194980

Earnshaw, W. C., Martins, L. M., and Kaufmann, S. H. (1999). *Mammalian caspases*: structure, activation, substrates, and functions during apoptosis. *Annu. Rev. Biochem.* 68, 383–424. doi: 10.1146/annurev.biochem.68.1.383

Eyers, P. A., and Murphy, J. M. (2016). The evolving world of pseudoenzymes: proteins, prejudice and zombies. *BMC Biol.* 14:98. doi: 10.1186/s12915-016-0322-x

Fischer, K., Langendorf, C. G., Irving, J. A., Reynolds, S., Willis, C., Beckham, S., et al. (2009). Structural mechanisms of inactivation in scabies mite serine protease paralogues. *J. Mol. Biol.* 390, 635–645. doi: 10.1016/j.jmb.2009.04.082

Fischer, W. W., Hemp, J., and Johnson, J. E. (2016). Evolution of oxygenic photosynthesis. *Annu. Rev. Earth Planet. Sci.* 44, 647–683. doi: 10.1146/annurev-earth-060313-054810

Frain, K. M., Gangl, D., Jones, A., Zedler, J. A. Z., and Robinson, C. (2016). Protein translocation and thylakoid biogenesis in cyanobacteria. *Biochim. Biophys. Acta BBA Bioenerg.* 1857, 266–273. doi: 10.1016/j.bbabio.2015.08.010

Hachmann, J., Snipas, S. J., van Raam, B. J., Cancino, E. M., Houlihan, E. J., Poreba, M., et al. (2012). Mechanism and specificity of the human paracaspase MALT1. *Biochem. J.* 443, 287–295. doi: 10.1042/BJ20120035

He, R., Drury, G. E., Rotari, V. I., Gordon, A., Willer, M., Farzaneh, T., et al. (2008). Metacaspase-8 modulates programmed cell death induced by ultraviolet light and H2O2 in *Arabidopsis*. *J. Biol. Chem.* 283, 774–783. doi: 10.1074/jbc.M704185200

Jaworski, M., and Thome, M. (2016). The paracaspase MALT1: biological function and potential for therapeutic inhibition. *Cell. Mol. Life Sci. CMLS* 73, 459–473. doi: 10.1007/s00018-015-2059-z

Jiang, Q., Qin, S., and Wu, Q. (2010). Genome-wide comparative analysis of metacaspases in unicellular and filamentous cyanobacteria. *BMC Genomics* 11:198. doi: 10.1186/1471-2164-11-198

Katoh, K., and Standley, D. M. (2013). MAFFT multiple sequence alignment software version 7: improvements in performance and usability. *Mol. Biol. Evol.* 30, 772–780. doi: 10.1093/molbev/mst010

Klemenčič, M., and Funk, C. (2018a). Structural and functional diversity of caspase homologues in non-metazoan organisms. *Protoplasma* 255, 387–397. doi: 10.1007/s00709-017-1145-5

Klemenčič, M., and Funk, C. (2018b). Type III metacaspases: calcium-dependent activity proposes new function for the p10 domain. *New Phytol.* 218, 1179–1191. doi: 10.1111/nph.14660

Klemenčič, M., Novinec, M., and Dolinar, M. (2015). Orthocaspases are proteolytically active prokaryotic caspase homologues: the case of *Microcystis aeruginosa*. *Mol. Microbiol.* 98, 142–150. doi: 10.1111/mmi.13110

Lee, R. E. C., Puente, L. G., Kærn, M., and Megeney, L. A. (2008). A non-death role of the yeast metacaspase: yca1p alters cell cycle dynamics. *PLoS One* 3:e2956. doi: 10.1371/journal.pone.0002956

Letunic, I., and Bork, P. (2016). Interactive tree of life (iTOL) v3: an online tool for the display and annotation of phylogenetic and other trees. *Nucleic Acids Res.* 44, W242–W245. doi: 10.1093/nar/gkw290

McLuskey, K., and Mottram, J. C. (2015). Comparative structural analysis of the caspase family with other clan CD cysteine peptidases. *Biochem. J.* 466, 219–232. doi: 10.1042/BJ20141324

McLuskey, K., Rudolf, J., Proto, W. R., Isaacs, N. W., Coombs, G. H., Moss, C. X., et al. (2012). Crystal structure of a *Trypanosoma brucei* metacaspase. *Proc. Natl. Acad. Sci. U.S.A.* 109, 7469–7474. doi: 10.1073/pnas.1200885109

Minina, E. A., Coll, N. S., Tuominen, H., and Bozhkov, P. V. (2017). Metacaspases versus caspases in development and cell fate regulation. *Cell Death Differ.* 24, 1314–1325. doi: 10.1038/cdd.2017.18

Minina, E. A., Filonova, L. H., Fukada, K., Savenkov, E. I., Gogvadze, V., Clapham, D., et al. (2013). Autophagy and metacaspase determine the mode of cell death in plants. *J. Cell Biol.* 203, 917–927. doi: 10.1083/jcb.201307082

Murphy, J. M., Farhan, H., and Eyers, P. A. (2017). Bio-zombie: the rise of pseudoenzymes in biology. *Biochem. Soc. Trans.* 45, 537–544. doi: 10.1042/BST20160400

Partensky, F., and Garczarek, L. (2009). *Prochlorococcus*: advantages and limits of minimalism. *Annu. Rev. Mar. Sci.* 2, 305–331. doi: 10.1146/annurev-marine-120308-081034

Price, M. N., Dehal, P. S., and Arkin, A. P. (2010). FastTree 2 – approximately maximum-likelihood trees for large alignments. *PLoS One* 5:e9490. doi: 10.1371/journal.pone.0009490

Proto, W. R., Castanys-Munoz, E., Black, A., Tetley, L., Moss, C. X., Juliano, L., et al. (2011). *Trypanosoma brucei* metacaspase 4 is a pseudopeptidase and a virulence factor. *J. Biol. Chem.* 286, 39914–39925. doi: 10.1074/jbc.M111.292334

Reiterer, V., Eyers, P. A., and Farhan, H. (2014). Day of the dead: pseudokinases and pseudophosphatases in physiology and disease. *Trends Cell Biol.* 24, 489–505. doi: 10.1016/j.tcb.2014.03.008

Reynolds, S. L., and Fischer, K. (2015). Pseudoproteases: mechanisms and function. *Biochem. J.* 468, 17–24. doi: 10.1042/BJ20141506

Saha, R., Liu, D., Hoynes-O'Connor, A., Liberton, M., Yu, J., Bhattacharyya-Pakrasi, M., et al. (2016). Diurnal regulation of cellular processes in the *Cyanobacterium Synechocystis* sp. Strain PCC 6803: insights from transcriptomic, fluxomic, and physiological analyses. *mBio* 7, e00464–e00516. doi: 10.1128/mBio.00464-16

Shalini, S., Dorstyn, L., Dawar, S., and Kumar, S. (2015). Old, new and emerging functions of caspases. *Cell Death Differ.* 22, 526–539. doi: 10.1038/cdd.2014.216

Straub, C., Quillardet, P., Vergalli, J., de Marsac, N. T., and Humbert, J.-F. (2011). A day in the life of microcystis aeruginosa strain PCC 7806 as revealed by a transcriptomic analysis. *PLoS One* 6:e16208. doi: 10.1371/journal.pone.0016208

Szallies, A., Kubata, B. K., and Duszenko, M. (2002). A metacaspase of *Trypanosoma brucei* causes loss of respiration competence and clonal death in the yeast *Saccharomyces cerevisiae*. *FEBS Lett.* 517, 144–150. doi: 10.1016/S0014-5793(02)02608-X

Uren, A. G., O'Rourke, K., Aravind, L. A., Pisabarro, M. T., Seshagiri, S., Koonin, E. V., et al. (2000). Identification of paracaspases and metacaspases: two ancient families of caspase-like proteins, one of which plays a key role in MALT lymphoma. *Mol. Cell* 6, 961–967. doi: 10.1016/S1097-2765(00)00094-0

Vercammen, D., van de Cotte, B., De Jaeger, G., Eeckhout, D., Casteels, P., Vandepoele, K., et al. (2004). Type II metacaspases Atmc4 and Atmc9 of *Arabidopsis thaliana* cleave substrates after arginine and lysine. *J. Biol. Chem.* 279, 45329–45336. doi: 10.1074/jbc.M406329200

Ward, L. M., Hemp, J., Shih, P. M., McGlynn, S. E., and Fischer, W. W. (2018). Evolution of phototrophy in the chloroflexi phylum driven by horizontal gene transfer. *Front. Microbiol.* 9:260. doi: 10.3389/fmicb.2018.00260

Wilson, P., Slade, R., Currie, B. J., Walton, S. F., Holt, D. C., Fischer, K., et al. (2003). Mechanisms for a novel immune evasion strategy in the scabies mite *Sarcoptes scabiei*: a multigene family of inactivated serine proteases. *J. Invest. Dermatol.* 121, 1419–1424. doi: 10.1046/j.1523-1747.2003.12621.x

Yang, J., Yan, R., Roy, A., Xu, D., Poisson, J., and Zhang, Y. (2015). The I-TASSER Suite: protein structure and function prediction. *Nat. Methods* 12, 7–8. doi: 10.1038/nmeth.3213

Yu, J. W., Jeffrey, P. D., and Shi, Y. (2009). Mechanism of procaspase-8 activation by c-FLIPL. *Proc. Natl. Acad. Sci.* 106, 8169–8174. doi: 10.1073/pnas.0812453106

Zeng, Y., Feng, F., Medová, H., Dean, J., and Koblížek, M. (2014). Functional type 2 photosynthetic reaction centers found in the rare bacterial phylum *Gemmatimonadetes*. *Proc. Natl. Acad. Sci.* 111, 7795–7800. doi: 10.1073/pnas.1400295111

Conflict of Interest Statement: The authors declare that the research was conducted in the absence of any commercial or financial relationships that could be construed as a potential conflict of interest.

frontiers in Plant Science

ORIGINAL RESEARCH
published: 05 April 2019
doi: 10.3389/fpls.2019.00428

The Chloroplast Envelope Protease FTSH11 – Interaction With CPN60 and Identification of Potential Substrates

Zach Adam[1], Elinor Aviv-Sharon[1†], Alona Keren-Paz[1†], Leah Naveh[1], Mor Rozenberg[1†], Alon Savidor[2] and Junping Chen[3]*

[1] The Robert H. Smith Institute of Plant Sciences and Genetics in Agriculture, The Hebrew University of Jerusalem, Rehovot, Israel, [2] de Botton Institute for Protein Profiling, The Nancy and Stephen Grand Israel National Center for Personalized Medicine, Weizmann Institute of Science, Rehovot, Israel, [3] Plant Stress and Germplasm Development Unit, USDA-ARS, Lubbock, TX, United States

FTSH proteases are membrane-bound, ATP-dependent metalloproteases found in bacteria, mitochondria and chloroplasts. The product of one of the 12 genes encoding FTSH proteases in Arabidopsis, FTSH11, has been previously shown to be essential for acquired thermotolerance. However, the substrates of this protease, as well as the mechanism linking it to thermotolerance are largely unknown. To get insight into these, the FTSH11 knockout mutant was complemented with proteolytically active or inactive variants of this protease, tagged with HA-tag, under the control of the native promoter. Using these plants in thermotolerance assay demonstrated that the proteolytic activity, and not only the ATPase one, is essential for conferring thermotolerance. Immunoblot analyses of leaf extracts, isolated organelles and sub-fractionated chloroplast membranes localized FTSH11 mostly to chloroplast envelopes. Affinity purification followed by mass spectrometry analysis revealed interaction between FTSH11 and different components of the CPN60 chaperonin. In affinity enrichment assays, CPN60s as well as a number of envelope, stroma and thylakoid proteins were found associated with proteolytically inactive FTSH11. Comparative proteomic analysis of WT and knockout plants, grown at 20°C or exposed to 30°C for 6 h, revealed a plethora of upregulated chloroplast proteins in the knockout, some of them might be candidate substrates. Among these stood out TIC40, which was stabilized in the knockout line after recovery from heat stress, and three proteins that were found trapped in the affinity enrichment assay: the nucleotide antiporter PAPST2, the fatty acid binding protein FAP1 and the chaperone HSP70. The consistent behavior of these four proteins in different assays suggest that they are potential FTSH11 substrates.

Keywords: FTSH11, chloroplast, envelope, proteolysis, AAA protease, CPN60

OPEN ACCESS

Edited by:
Mercedes Diaz-Mendoza, Centro de Biotecnología y Genómica de Plantas (CBGP), Spain

Reviewed by:
Cornelia Spetea, University of Gothenburg, Sweden
Yusuke Kato, Okayama University, Japan

****Correspondence:***
Zach Adam
zach.adam@mail.huji.ac.il

[†] These authors have contributed equally to this work

Specialty section:
This article was submitted to Plant Physiology, a section of the journal Frontiers in Plant Science

Received: *25 February 2019*
Accepted: *21 March 2019*
Published: *05 April 2019*

Citation:
Adam Z, Aviv-Sharon E, Keren-Paz A, Naveh L, Rozenberg M, Savidor A and Chen J (2019) The Chloroplast Envelope Protease FTSH11 – Interaction With CPN60 and Identification of Potential Substrates. Front. Plant Sci. 10:428. doi: 10.3389/fpls.2019.00428

INTRODUCTION

FTSH proteases are membrane-bound, ATP-dependent metalloproteases, initially identified in *Escherichia coli* (Tomoyasu et al., 1993), and later in all prokaryotes and organelles of prokaryotic origin in eukaryotic cells (Schnall et al., 1994; Lindahl et al., 1996; Sakamoto et al., 2002; Adam et al., 2005; Ito and Akiyama, 2005; Langklotz et al., 2012). FTSH proteases are anchored

to cellular membranes by one or two *trans*-membrane helices (TMs) and form homo- or hetero-hexameric complexes. X-ray crystallography of the cytosolic region of bacterial FTSHs revealed that their active sites are found within a cage-like structure, secluded from the cellular environment (Krzywda et al., 2002; Bieniossek et al., 2006, 2009; Suno et al., 2006), qualifying them as self-compartmentalizing proteases (Lupas et al., 1997). Like all other ATP-dependent proteases, the ATPase function is essential for substrate recognition, its unfolding and translocation to the proteolytic sites (Ito and Akiyama, 2005; Langklotz et al., 2012). Thus, the proteolytic activity of FTSHs is dependent on their ATPase one, but the ATPase can confer chaperone activity that is independent of the proteolytic one. In microbial systems, the usually single FtsH gene-product is essential to their survival at elevated temperatures and is also involved in protection against other environmental stresses (Deuerling et al., 1995; Tomoyasu et al., 1995; Beier et al., 1997; Bourdineaud et al., 2003). It functions as a molecular chaperone and protease and helps organisms to maintain cell homeostasis under optimal and stress conditions (Schumann, 1999; Ito and Akiyama, 2005; Langklotz et al., 2012).

In plants, FTSH proteases are encoded by multiple genes, 12 in the case of Arabidopsis (Adam et al., 2005; Wagner et al., 2012). The best-characterized plant FTSH is that of the hetero-complex found in the thylakoid membrane. It is composed of two types of subunits, A (FTSH1 and FTSH5) and B (FTSH2 and FTSH8). The proteins within a type are redundant, but the presence of both types is essential for the accumulation of a stable complex (Yu et al., 2004; Zaltsman et al., 2005; Adam et al., 2006; Sakamoto, 2006). This complex, designated FTSH1-2-5-8, as well as its homologs in cyanobacteria and algae, is mainly involved in repairing the photosynthetic machinery from damages associated with high-light stress in the context of photoinhibition (Lindahl et al., 2000; Bailey et al., 2002; Kato et al., 2012; Komenda et al., 2012; Malnoe et al., 2014), and also those incurred by heat stress (Yoshioka et al., 2006; Yamamoto et al., 2008). In addition, plant genomes encode proteolytically inactive homologs (FTSHi) (Sokolenko et al., 2002; Wagner et al., 2012), which have their ATPase domain intact but their proteolytic site is mutated. They were suggested to be involved in chloroplast development (Kadirjan-Kalbach et al., 2012; Lu et al., 2014), and recently it was demonstrated that they serve as a motor for protein import into chloroplasts (Kikuchi et al., 2018).

Unlike dozens of publications on the thylakoid FTSH1-2-5-8 complex and its physiological roles, reports on FTSH11 are scarce. FTSH11 was first characterized in Arabidopsis mitochondria, forming a complex together with FTSH4, homologous to the well-known *i*-AAA protease in yeast mitochondria (Urantowka et al., 2005). In that work it was localized to chloroplasts as well. Further confirmation and chloroplast envelope localization were obtained by MS and immunoblot analyses (Knopf et al., 2012; Wagner et al., 2016), but in the latter report FTSH11 could not be detected in purified mitochondria, leaving the question of dual targeting to both organelles ambiguous. Using a genetic approach, an Arabidopsis mutant that was sensitive to moderate heat stress (30°C) and defective in acquired thermotolerance was isolated, and the mutation was mapped to the gene encoding the FTSH11 protease (Chen et al., 2006). Unlike FTSH2 and FTSH5 mutants that are insensitive to heat, the FTSH11 mutant demonstrated reduced photosynthetic activity at elevated temperature (Chen et al., 2018), suggesting that different FTSH proteases have their own roles in response of plants to different stresses.

In the current study, we sought to determine whether the proteolytic or chaperone activities of FTSH11 were responsible for thermotolerance, to revisit the issue of its cellular location, to identify its potential partners and substrates, and to evaluate the proteomic consequences of its loss. We demonstrate here that the proteolytic activity of FTSH11 is indeed essential for growth at elevated temperatures; it is mostly located in chloroplasts; it interacts with the stromal chaperonin CPN60; and we identify a number of potential chloroplast substrates.

RESULTS

The Proteolytic Activity of FTSH11 Is Essential for Thermotolerance

In their original work on FTSH11, Chen et al. (2006) have shown that this protein is essential for survival of Arabidopsis seedlings at elevated temperatures. As the proteolytic activity of FTSH proteases is dependent on their ATPase domain for substrate recognition and unfolding, it raised the question whether thermotolerance was dependent on the proteolytic activity of FTSH, or else, the chaperone-like activity of this domain was sufficient for this function. To answer this question, two different transgenic lines were generated. The first line, designated EE, was FTSH11-knockout mutant, complemented with FTSH11 full-length cDNA, encoding also a HA tag at the C-terminus of the protein, under the control of the endogenous promoter. The second line, designated EQ, was an identical one, with the exception that it contained amino acid substitutions in the proteolytic site. His 620 and Glu621 that are part of the conserved Zn^{2+}-binding site H-E-X-X-H were replaced by Gln. Such mutations are well documented to abolish the proteolytic activity of FTSH proteins in either *E. coli* or yeast mitochondria without affecting their ATPase activity (e.g., Karata et al., 1999; Leonhard et al., 1999). Seedlings of these lines, along with the WT and the FTSH11 knockout lines, were grown on plates at either 22, 27 or 30°C for 3, 6, or 16 days. As shown in **Figure 1A**, all lines grew at 22 and even at 27°C. At 30°C, the knockout lines complemented with the full-length cDNA of FTSH11 grew like WT, reconfirming that the loss of FTSH11 was sufficient to cause thermosensitivity. Moreover, this complementation also confirmed that tagging the protein with the HA tag did not interfere with its physiological activity. Nevertheless, a single amino acid substitution in the proteolytic domain of FTSH11 resulted in a thermosensitive phenotype, similar to the phenotype of the knockout line. Slower growth and a paler phenotype of these lines could be observed even at 22 and 27°C. When mature plants were subjected to heat for 10 days, similar behavior of the different genotypes was observed (**Figure 1B**). These results suggested that the proteolytic activity of FTSH11, and not only its ATPase one, is essential for tolerating elevated temperatures.

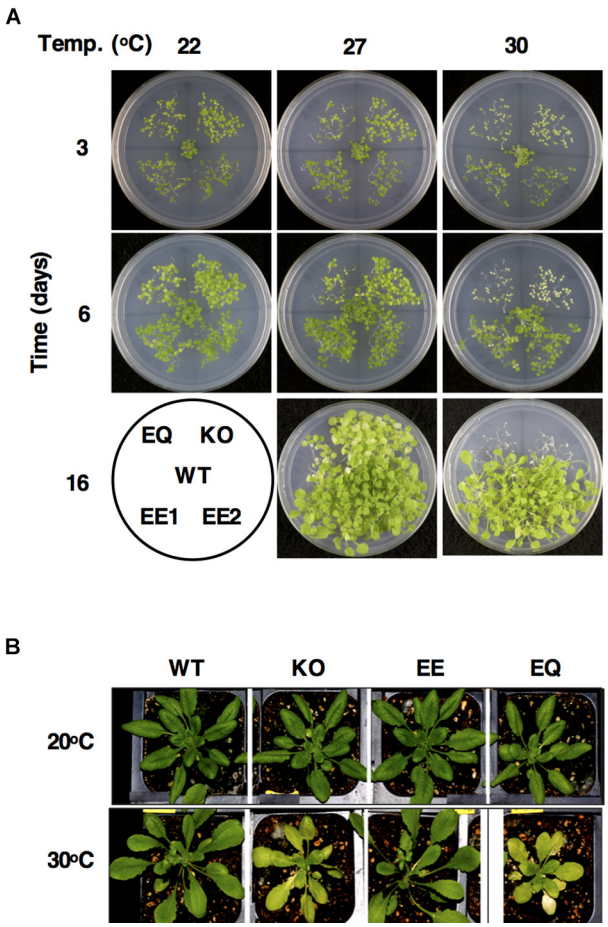

FIGURE 1 | The proteolytic activity of FTSH11 is essential for thermotolerance. **(A)** Different Arabidopsis lines were grown on agar plates for 3, 6, or 16 days at 22, 27, or 30°C. The location of each line on the plate is indicated on the map at the lower left corner of the figure. WT, wild type; KO, FTSH11 knockout; EE1 and 2 – two different lines of FTSH11-HA (active protease); EQ – proteolytically inactive protease. **(B)** The same lines grown on soil at either 20 or 30°C.

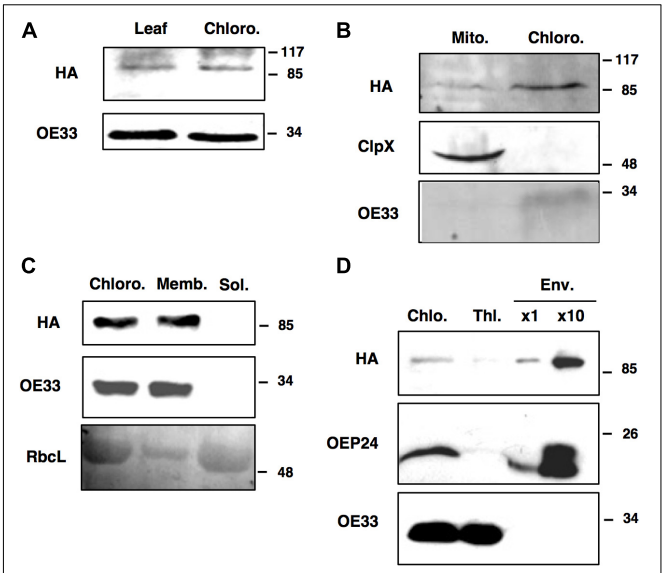

FIGURE 2 | FTSH11 is located in the chloroplast envelope. Different extracts, organelles and fractions, from transgenic plants expressing FTSH11-HA, were subjected to imunoblot analysis with HA and control antibodies. **(A)** Total leaf and isolated chloroplast extracts. **(B)** Isolated mitochondria and chloroplasts. **(C)** Chloroplasts fractionated to membrane and soluble fractions. **(D)** Thylakoid and envelope membranes isolated on the same sucrose gradient. Marker proteins for the different compartments are: OE33 for thylakoids, ClpX for mitochondria, RbcL for stroma and OEP24 for envelopes. Antibodies used are indicated on the left and migration of MW markers (in kDa) are indicated on the right of each blot.

FTSH11 Is Located in the Chloroplast Envelope

Prediction servers such as TargetP suggest that FTSH11 is located in chloroplasts. Using N-terminal signal sequences fused to GFP, Sakamoto and co-workers have concluded that FTSH11 is indeed targeted to chloroplasts (Sakamoto et al., 2003). Another study, making use of immunoblot analysis, suggested that FTSH11 is dually targeted to both chloroplasts and mitochondria (Urantowka et al., 2005). In a mass spectrometry (MS) analysis of chloroplast envelopes, in the context of a study on rhomboid proteases, FTSH11 was identified among 180 other proteins (Knopf et al., 2012). In line with the required multiple lines of evidence to define the subcellular location of plant proteins (Millar et al., 2009), we chose to use the transgenic plants expressing HA-tagged FTSH11 in a knockout background (the aforementioned EE plants) for cellular localization of this protein. This approach eliminated potential cross-reactivity associated with the use of antibodies against proteins belonging to gene families such as FTSH. Comparison of total leaf and chloroplast extracts, in immunoblot analysis with antibodies against the HA tag, loaded on the base of equal chlorophyll, revealed equal signals (**Figure 2A**), suggesting that the signal in the total extract was of chloroplast origin. When equal amounts of protein, extracted from isolated chloroplasts and mitochondria, were compared, chloroplasts displayed a much stronger HA signal (**Figure 2B**). Together, these results suggested that most, if not all of FTSH11 is located in chloroplasts.

When chloroplasts were sub-fractionated to membrane and soluble fractions, all the HA signal was associated with chloroplast membranes (**Figure 2C**). To distinguish between thylakoid and envelope membranes localization, the chloroplast membrane fraction was resolved by density gradient centrifugation on a sucrose gradient. The thylakoid fraction appeared to be somewhat contaminated with envelope proteins, as judged by the faint band of the envelope protein OEP24 in this fraction (**Figure 2D**). However, no trances of the thylakoid protein OE33 were found in the envelope fraction. As for the HA signal, it was associated with the envelope fraction, suggesting that FtsH11 is indeed located in the chloroplast envelope, in agreement with its identification in MS data [e.g., (Knopf et al., 2012; Simm et al., 2013)].

FTSH11 Interacts With CPN60 and Other Chloroplast Proteins

Unlike bacterial FTSH hexamers, which are products of single genes, the thylakoid FTSH hexameric complex comprises of four different subunits, FTSH1, FTSH2, FTSH5, and FTSH8 (Zaltsman et al., 2005; Sakamoto, 2006; Moldavski et al., 2012). This, together with the results of proteomic analyses of chloroplast envelope in which other FTSH proteins were found, raised the possibility that FTSH11 interacts with other FTSH subunits in the envelope. To test this hypothesis, FTSH11 was immuno-precipitated with a HA antibody from the EQ transgenic plants. To increase the stringency of this assay, we used total leaf extracts and washed the precipitates thoroughly prior to elution of the bound proteins with excess of HA peptides. As shown in **Figure 3A**, all of the HA-tagged protein was adsorbed to the matrix, as no signal appeared either in the flow-through or the different washes. Only upon washing the matrix with free HA peptide ("elution" in **Figure 3A**) the HA-tagged protein was released. To test whether other FTSHs, or any other proteins interacted with FTSH11, the eluted material was subjected to MS analysis. As expected, more than 50% of the protein material associated with the anti-HA matrix was identified as FTSH11 (**Figure 3B**). The two other proteins highly represented in the eluted material were CPN60B1 and CPN60A1. Less than 10% of the eluted material was identified as different chloroplast proteins. These same proteins were identified in control immuno-precipitations, performed on either protein extracts from WT plants or transgenic plants expressing HA-tagged rhomboid protease (Knopf et al., 2012). Thus, these proteins were considered as contaminants rather than substrates or components of the FTSH11 complex. Remarkably, unlike the thylakoid FTSH complex, FTSH11 was not associated with any other FTSH protein. Neither FTSH7, FTSH9, FTSH12, nor FTSHi1-4, all residing in the chloroplast envelope, were identified in the immuno-precipitated material.

In light of the results of the MS analysis, the fractions of the immuno-precipitation experiment were further subjected to immuno-blot analysis (**Figure 3A**). The eluted fraction, containing FTSH11, reacted also with a CPN60 antibody, but not with an antibody against the abundant chloroplast protein OE33 of the oxygen-evolving complex. In the mock immuno-precipitation from WT plants, no CPN60 was precipitated, suggesting that the interaction between CPN60 and FTSH11 was indeed specific. The intensity of the CPN60 band in the flow and first wash fractions, compared with that of the load, suggests that only a small fraction of the chloroplast CPN60 associates with FTSH11 (**Figure 3A**).

To further unravel interactions between FtsH11 and potential interactors or substrates, we used the affinity enrichment approach (Keilhauer et al., 2015). Here the immuno-precipitated material, from either the HA-tagged line (EQ) or the reference KO one, is only slightly washed, the proteins associated with the HA beads are not eluted, and the material is subjected to MS analysis, followed by statistical analysis to distinguish true interacting proteins from background ones (**Supplementary Table 1**). The volcano plot presented in **Figure 4A** shows,

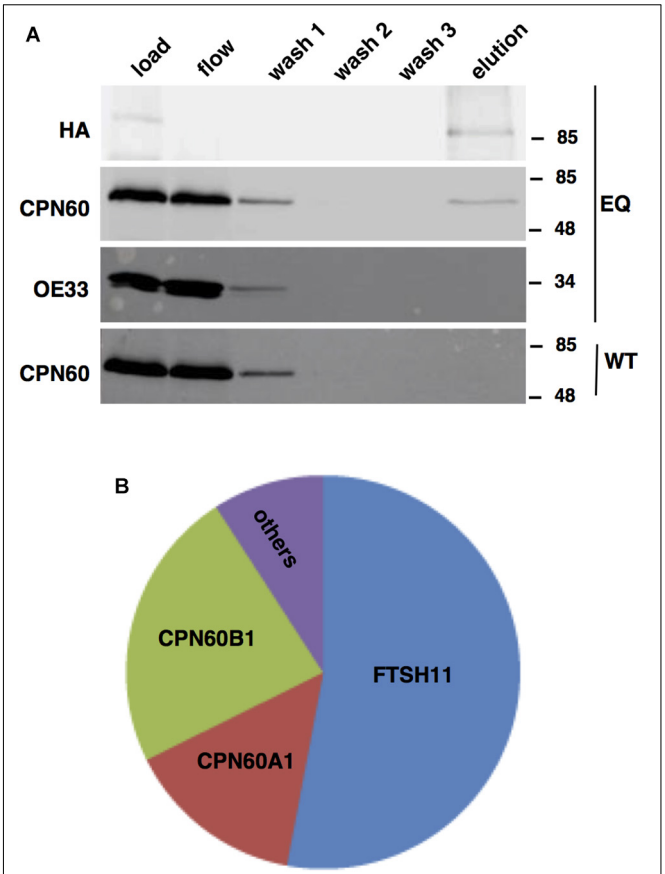

FIGURE 3 | FTSH11-HA associates with CPN60. Total protein extracts from WT and EQ plants were solubilized with β-dodecyl maltoside, loaded on an immobilized anti-HA columns, thoroughly washed, and eluted with HA peptide. Samples from the different steps of the purification procedure were analyzed. **(A)** Immuno-blot analysis with HA, CPN60, and OE33 antibodies. Antibodies used are indicated on the left and migration of MW markers (in kDa) are indicated on the right of each blot. The genotypes of the samples are denoted on the far right of the blots. **(B)** Summary of MS analysis of the eluted fraction. The area of each section in the chart represents the abundance of the identified proteins within the eluted fraction from the EQ plants.

as expected, strong enrichment of FTSH11 in the material precipitated from plants grown at 20°C. Interestingly, none of the other FTSH envelope proteins is found enriched. In agreement with the results of the affinity purification presented in **Figure 3**, CPN60 proteins are also enriched, including CPN60A1, CPN60B1, and CPN60B2, as well as their co-chaperone CPN20.

In addition to CPN60 proteins, other chloroplast proteins were found enriched along with the FTSH11 bait. One protein that co-localizes with FTSH11 is the nucleotide antiporter PAPST2 (Ashykhmina et al., 2019) (also designated EAAC). Proteins residing in the stroma, found associated with FTSH11 include the fatty acid binding protein FAP1, the chaperone HSP70, a hydrolase of unknown function (At1g52510), the ribosomal protein RPS14, the aldolase F12K8 and the glyceraldehyde-3-phosphate dehydrogenase GAPC2 (**Figure 4A**). Thylakoid proteins were also identified among

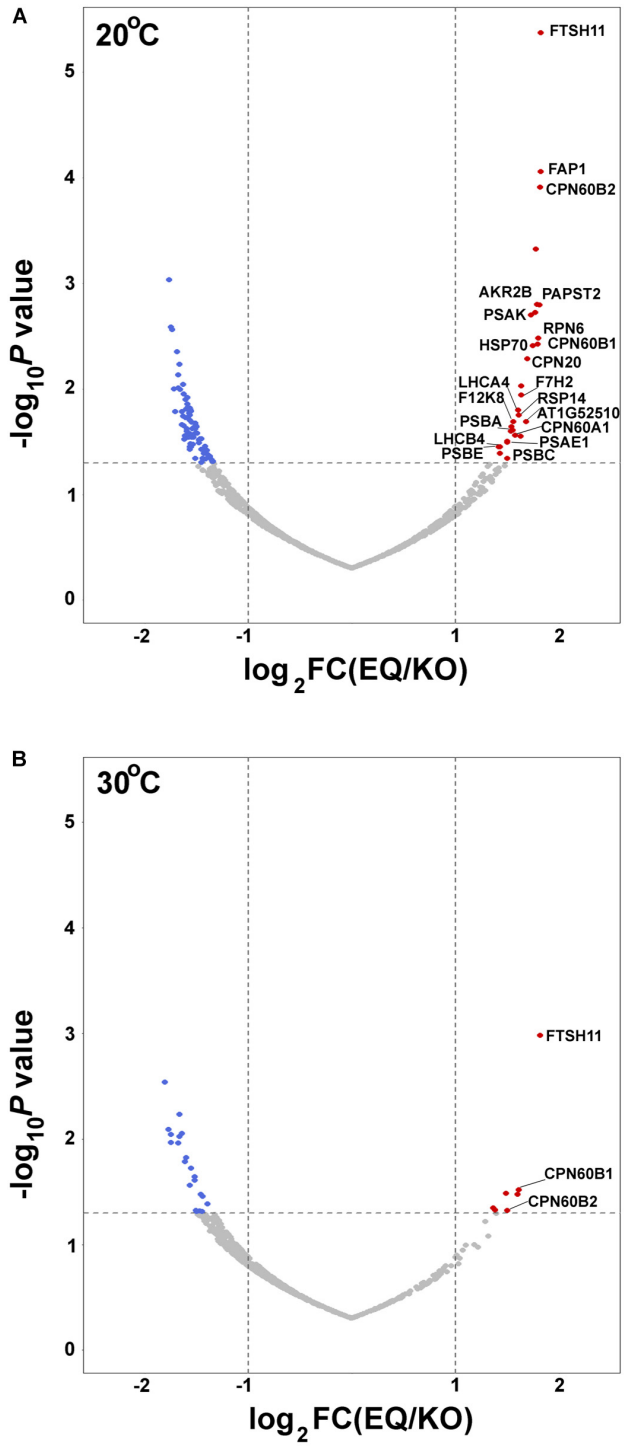

FIGURE 4 | Affinity enrichment of FTSH11-HA. Total protein extracts from EQ and KO plants were solubilized with β-dodecyl maltoside, incubated with immobilized anti-HA beads, and slightly washed. Proteins associated with the beads were then subjected to MS analysis. Volcano plots are presented. Significantly enriched chloroplast proteins interacting with FTSH11 are depicted in red. (De-enriched proteins are in blue, and proteins that were not significantly changed are in gray.) **(A)** Samples from plants grown at 20°C. **(B)** Samples from plants grown at 20°C and then exposed to 30°C for 6 h.

the FTSH11-interacting proteins, including the PSI reaction center proteins PSAE1, PSAK, and their antenna protein LHCA4, the PSII reaction center proteins PSBA, PSBC and PSBE, and their antenna protein LHCB4. As the bait protein was proteolytically inactive, all these might be considered as potential trapped substrates.

This experiment was repeated with the same plants, but prior to the affinity enrichment step, the plants were exposed to 30°C for 6 h. For a reason that is not obvious to us, the only proteins enriched, in addition to FTSH11 itself, were CPN60B1 and CPN60B2 (**Figure 4B**), further highlighting the interaction between CPN60s and FTSH11.

Comparative Proteomics – WT vs. KO, at 20 and 30°C

To gain an insight into the physiological role of FTSH11, a comparative proteomics approach was used on WT and FTSH11 KO plants. Plants were grown for 4 weeks at optimal temperature (20°C) and then remained at the same temperature or exposed to elevated temperatures (30°C) for 6 h. This length of exposure was chosen in order to unravel initial response to heat, before any visual symptoms can be detected. Of the 4,591 proteins identified by LC-MS/MS (**Supplementary Table 2**), 3,390 were identified by more than one peptide, allowing their reliable quantification. Of these, 708 proteins were differentially accumulated in at least one of the comparisons (fold change >2, p-value <0.05). As shown in **Figure 5**, four main characteristic patterns of accumulation could be observed: (1) Proteins downregulated in the KO mutant, regardless of the temperature treatment; (2) Proteins upregulated in the KO regardless of temperature; (3) Proteins upregulated at 30°C, irrespective of the genotype; and (4) Proteins downregulated at 30°C in both genotypes.

As upregulation of proteins in the protease KO mutant may result from their reduced turnover, such proteins can be candidate FTSH11 substrates. We thus took a closer look at all these proteins. Most of them were upregulated in the KO at both temperatures (**Figure 6A**). Noteworthy in this category were four components of the YCF2 inner envelope complex, which serves as a protein import motor (Kikuchi et al., 2018). These included FTSH12, a close homolog of FTSH11, the proteolytically inactive homologs FTSHi2 and FTSHi4, and YCF2 itself. Another component of the YCF2 complex, FTSHi1, accumulated to higher level in the mutant only at 20°C (**Figure 6B**). Moreover, four components of the Tic complex, through which proteins are being imported into the chloroplast (Kovacs-Bogdan et al., 2010; Kikuchi et al., 2013), are also upregulated: TIC214 (YCF1), TIC100, TIC56, and TIC22 (**Figure 6A**). Another protein implicated in precursor import, TIC40 is upregulated at 20°C (**Figure 6B**). Thus, it appears that FTSH11 is involved in regulating the level of the chloroplast import machinery at the inner envelope membrane.

Hints for impairment of the proteolytic capacity in the stroma upon the loss of FTSH11 protease can be seen in the upregulation of stromal chaperones such as two different HSP70s (**Figures 6A,B**) and CLPB3 (**Figure 6C**). Consistent

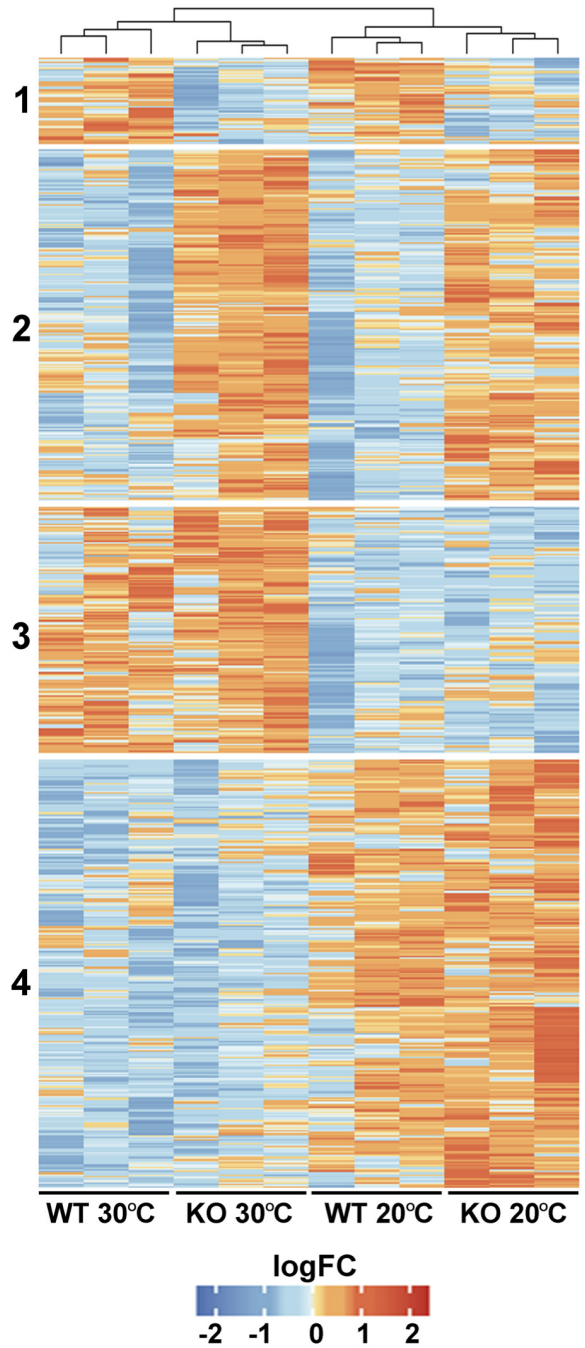

FIGURE 5 | Comparative proteomic analysis of WT and FTSH11 KO mutant. WT and mutant plants were grown at 20°C for 4 weeks and then either exposed or not to 30°C for 6 h. Total protein was extracted from leaves and subjected to label-free quantitative LC-MS/MS analysis. Relative levels of all differentially expressed proteins in the two genotypes and two temperature treatments and their clustering are presented.

with this is the over-accumulation in the mutant of one proteolytic component of the CLP protease (Olinares et al., 2011), CLPP4, and two assembly factors of this protease, CLPT1 and CLPT2 (**Figure 6A**).

Given the essentiality of FTSH11 to thermotolerance, it was interesting to see which chloroplast proteins were upregulated in the KO mutant upon exposure to elevated temperature, as these could be substrates of the protease. Among the numerous such proteins, several were noteworthy. First, two of the four aforementioned CLP proteins, CLPB3 and CLPP4, were found in this list (**Figure 6C**). Second, TIL, which was previously found to be required for thermotolerance (Chi et al., 2009), also over-accumulated in the absence of FTSH11. Consistent with the pale phenotype observed in the mutant at elevated temperatures (**Figure 1**), two protein involved in chlorophyll biosynthesis, CHLH and DVR are upregulated. Another interesting protein in this list is THIC. This stromal protein is involved in thiamine biosynthesis (Coquille et al., 2013), and was found to be one of the 20 most rapidly degrading proteins in Arabidopsis leaves (Li et al., 2017). All these proteins should be considered as candidate substrates of FTSH11 at elevated temperatures in future studies.

Most interesting among the upregulated proteins are three proteins that were found also trapped in the proteolytically inactive FTSH11 (**Figure 4**). These included PAPST2, the nucleotide antiporter located in the chloroplast envelope and mitochondria, the stromal chaperone HSP70, both over-accumulating in the KO mutant at both temperatures (**Figure 6A**), and the fatty acid binding protein FAP1 upregulated in the mutant at 20°C (**Figure 6B**). The identification of these three proteins by two independent experimental approaches strongly suggest that they are physiological substrates of the FTSH11 protease.

Downregulation of TIC40 Upon Recovery From Heat Is Impaired in FTSH11 KO Mutant

As the level of components of the TIC complex appear to regulated by FTSH11 (**Figures 6A,B**), we tested the level of TIC40 in WT and KO plants before and after exposure to high temperature, and following a recovery period at optimal one, by immunoblot analysis. As can be seen in **Figure 7**, after 3 days at 30°C, the level of TIC40 in both WT and KO plants is highly elevated, consistent with the results of the MS analysis after a short exposure to heat (**Figure 6B**). In contrast, the level of CAC3, an unrelated envelope protein, remains quite constant. After transferring the WT plants back to 20°C, the level of TIC40 drops back to its original level whereas the level in the KO plants remains elevated. These results support the notion that the level TIC40 is regulated by FTSH11, probably by proteolytic degradation of excess copies of the protein.

DISCUSSION

When it comes to determining the physiological role of a given FTSH protease, the immediate question that comes to mind is whether this role is dependent on the proteolytic or the ATPase activity of the protease. The relevance of this question is reinforced due to the evolutionary history of FTSH proteins, during which a number of proteolytically inactive

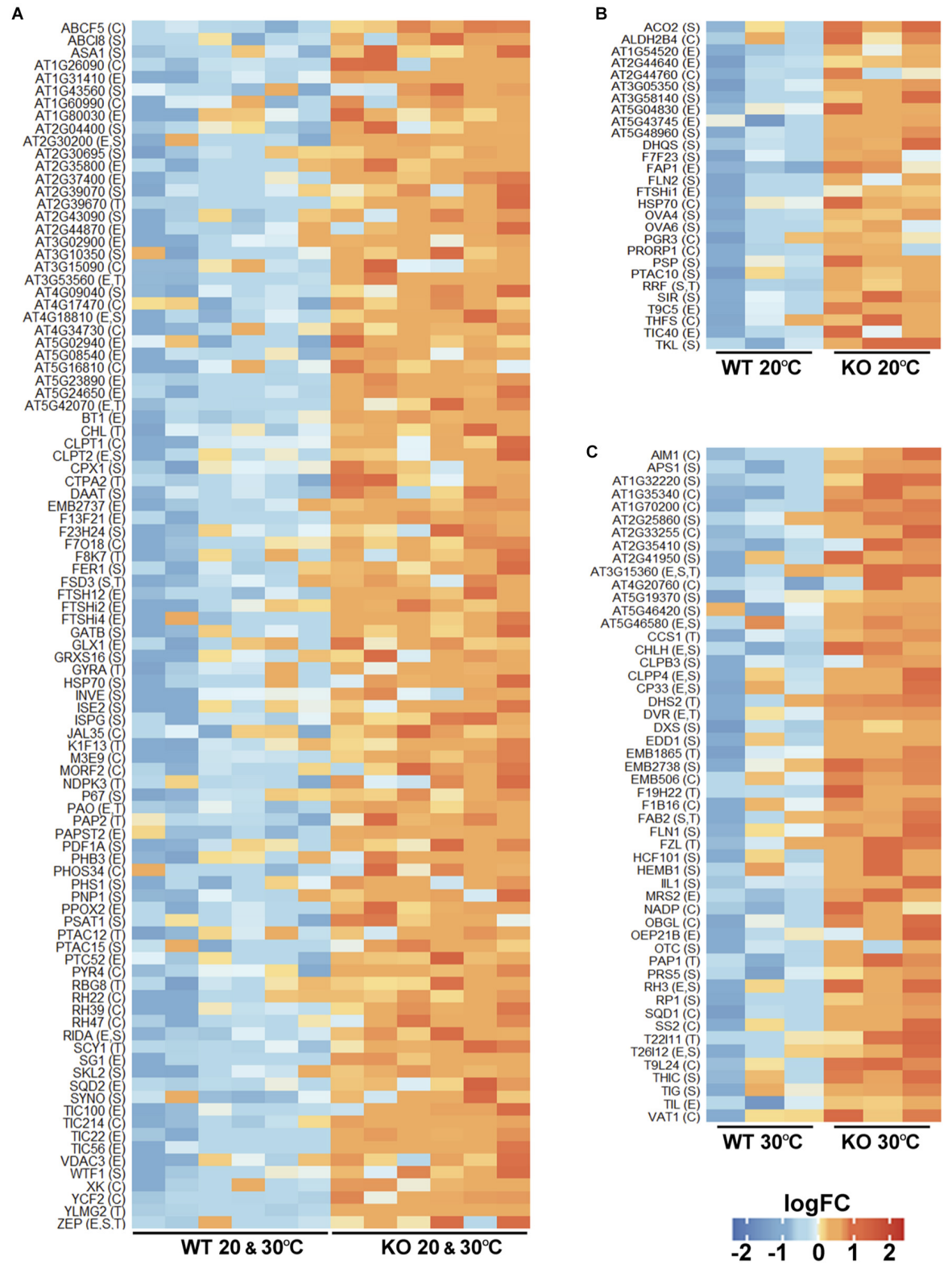

FIGURE 6 | Chloroplast proteins upregulated in the FTSH11 KO mutant. Chloroplasts upregulated proteins were selected from the differentially expressed proteins presented in **Figure 5**. **(A)** Proteins that were upregulated both at 20°C and following exposure to 30°C for 6 h. **(B)** Proteins that were upregulated only at 20°C. **(C)** Proteins upregulated in the mutant only after exposure to 30°C. Protein names are denoted on the left of each panel. Intra-organelle localizations are in parentheses. C, chloroplast; E, envelope; S, stroma; T, thylakoid.

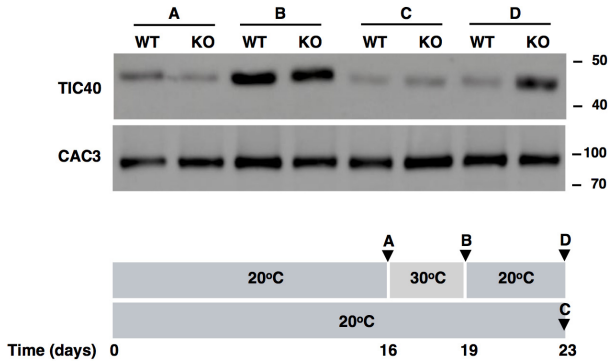

FIGURE 7 | TIC40 is stabilized in the FTSH11 KO mutant upon recovery from heat. Two weeks old seedlings were grown at 20°C for additional 16 days, before being transferred to 30°C for 3 days and then returned to recovery at 20°C for 4 days. A control group was kept at 20°C for the entire duration of the experiment. At the time points indicated (**A–D** in the lower panel), samples were taken, total leaf extracts were made, and subjected to immunoblot analysis (upper panel) with the antibodies indicated in the left of the panel. Antibodies used are indicated on the left and migration of MW markers (in kDa) are indicated on the right of each blot.

FTSHs (designated FTSHi) have been evolved. In the case of Arabidopsis, there are five such proteins, all of them are essential for development and growth (Sokolenko et al., 2002; Wagner et al., 2012; Mishra et al., 2019). Four of these have been recently identified in a large chloroplast complex, together with FTSH12, serving as a motor for protein import into chloroplasts (Kikuchi et al., 2018). Using a complementation assay with proteolytically active and inactive proteins, we found here that the proteolytic activity of FTSH11 is essential for conferring resistance to elevated temperatures (**Figure 1**). This finding is in contrast to the case of FTSH12, whose proteolytic activity is dispensable for its activity in protein import (Kikuchi et al., 2018).

The localization of most if not all of FTSH11 to the chloroplast inner envelope membrane, the same sub-compartment where FTSH12 and the five FTSHi proteins are located, raised the suspicion that it could be a component of a large heteromeric FTSH complex, similar to the one found in the thylakoid, which is composed of four different gene products (Zaltsman et al., 2005). However, we could not find any other FTSH protein associated with FTSH11 in either affinity purification or affinity enrichment assays (**Figures 3**, **4**, respectively), suggesting that it forms a homo-complex. This conclusion is further supported by the aforementioned recent study (Kikuchi et al., 2018), where five envelope FTSH proteins were found in complex, but no FTSH11 was associated with them.

The most surprising finding of this study is probably the association of stromal CPN60 proteins with the FTSH11 complex. This association was observed in both affinity purification and affinity enrichment assays, when proteolytically inactive FTSH11 was used as a bait (**Figures 3**, **4**, respectively). Moreover, CPN60s were associated with FTSH11 when the affinity enrichment assay was carried out after exposure to high temperature as well (**Figure 4B**), where only a few proteins could be identified along with FTSH11. It is also interesting to note that when proteolytically active FTSH11 was used as a bait, we could not observe this interaction (unpublished observation). The functional and physiological significance of the interaction is not clear to us yet. However, it is interesting to note that when similar experiments were carried out on proteolytically inactive FTSH2, located in the thylakoid membrane, whose functional domains are also exposed to the stroma, no CPN60 was associated with it (unpublished observation), so the interaction is likely to be specific to FTSH11. These observations make it tempting to hypothesize that stromal substrates are recruited by CPN60 and delivered to FTSH11 for degradation. The interaction between the two complexes can be observed only when proteolytic degradation is inhibited, in this case, by a mutation in the proteolytic active site. This delivery hypothesis will have to be rigorously tested in the future.

To unravel potential substrates of FTSH11, two independent large-scale approaches were used. The less selective one was comparative proteomics, in which proteomes of total leaf extracts from two genotypes – WT and FTSH11 KO, at optimal and elevated temperatures were compared (**Figures 5**, **6**). Here, potential substrates are expected to be upregulated in the mutant background. Nevertheless, over-accumulation of a given protein in the mutant can represent a pleotropic effect, thus other criteria, such as co-localization, need to applied. A more direct approach is substrate trapping, which is usually done with proteolytically inactive variants, allowing the binding of substrates to the protease, but in the absence of their processing, they can be identified along with the protease trap. Three proteins were identified in both assays: the nucleotide antiporter PAPST2, a stromal HSP70 involved in protein import (Su and Li, 2010), and the envelope fatty acid binding protein FAP1 (Ngaki et al., 2012). The physical proximity between FTSH11 and these proteins, being located in the envelope membrane or the stroma, together with their identification in two different assays, strongly suggest that these three proteins are indeed substrates of the FTSH11 protease who regulates their physiological levels.

Another interesting group of trapped proteins are integral thylakoid membrane proteins of PSI and PSII, seven of them in total (**Figure 4A**). None of these is found among the proteins upregulated in the mutant and they are located in a different membrane than FTSH11. Yet, as thylakoids fill up most of the chloroplast volume, contact between the thylakoid and the envelope membranes is not that scarce. Thus, it could be that an envelope protease participates in degradation of thylakoid membrane proteins. This possibility will have to be tested more directly in future experiments. Similarly, the plethora of envelope and stroma proteins that were found upregulated in the KO mutant, including the rapidly turned over THIC (Li et al., 2017), will have to be further examined as potential substrates of FTSH11.

Using a more targeted approach, we tested the level of a single protein that was found upregulated in FTSH11 KO plants, TIC40 (**Figure 6**), as a representative of the group of TIC proteins that demonstrated a similar behavior. The level of this protein increased at elevated temperatures in both the WT and KO plants (**Figure 7**), and decreased back to normal only in the

WT but not in the KO upon return to normal temperature. This observation suggests that FTSH11, probably by virtue of its proteolytic activity, is responsible for degrading excess copies of TIC40, and probably other TIC components that were found upregulated in the mutant upon exposure to high temperature. This approach will be useful in future attempts to identify and characterize potential substrates of the FTSH11 protease.

MATERIALS AND METHODS

Plant Material

Wild type (WT) and mutant *Arabidopsis thaliana* (ecotype Columbia) plants were grown under controlled conditions of 16 h-light/8 h-dark cycles, with a photon flux density of ∼100 μmol m^{-2} s^{-1}, at 20°C for 4 weeks on moistened Kekkila peat. When needed, plants were transferred to 30°C for additional 6 h. Alternatively, surface sterilized seeds were sown on sterile × 0.5 MS media with 1% sucrose and B5 vitamins, stratified for 2 days at 4°C in the dark, and then grown under long-day conditions for 16 days at either 22, 27 or 30°C.

The FTSH11 knockout (KO) *salk033047* was complemented with either a full length FTSH11 cDNA, encoding also for 3xHA tag at the C-terminus of the protein (EE line), or a similar construct where residues H620 and E621 in the proteolytic active site were replaced by Q (EQ line). The HA tagging and the site-directed mutagenesis were done as previously described (Adam, 1995; Moldavski et al., 2012), respectively. Both constructs contained upstream of the coding region a 2-kb sequence of the FTSH11 native promoter.

Organelle Isolation and Fractionation

Intact chloroplasts and mitochondria were isolated by density gradient centrifugation on Percoll gradients as described in Halperin et al. (2001). Chloroplasts were further fractionated by osmotic shock followed by sonication and centrifugation on sucrose gradients as described (Knopf et al., 2012).

Protein Extraction, Immunoblot Analysis, Affinity Purification and Affinity Enrichment, and MS Analysis

Detailed descriptions of protein extraction, immunoblot analysis and affinity enrichment were recently published (Butenko et al., 2018). The antibodies used were the following: HA (Abcam), CPN60 and TIC40 (from Agrisera), OEP24 and CAC3 from the J. Soll and E. Wurtele labs, respectively. OE33 and ClpX antibodies were described in Itzhaki et al. (1998) and Halperin et al. (2001), respectively. In principle, denatured protein extracts included 8% (w/v) SDS and 5 M urea, whereas non-denatured extracts were solubilized by 1.0% (w/v) n-dodecyl-β-D-maltoside (DDM, Tivan-Biotech). All extractions were done in the presence of Protease Inhibitor Cocktail for plant (Sigma-Aldrich). Both affinity purification and enrichment were done with anti-HA Agarose seven beads (Abcam). In the affinity purification experiments, the bound proteins were eluted by incubating the washed beads with excess of HA peptide, whereas in the affinity enrichment experiments the washed beads were further analyzed as is (thus containing specifically as well as non-specifically bound proteins). All MS analyses were also performed as recently described (Butenko et al., 2018).

Data Processing, Statistical and Bioinformatic Analyses

Mass spectrometry individual intensities were $\log_2$ transformed and *Z*-score normalized. Missing values were imputed using normal distribution, with a mean and standard deviation adjusted to resemble low-abundant proteins signals. Proteins were considered for comparative analysis if a protein was identified in at least two out of three replicates and by a minimum of two peptides. Two-way analysis of variance (ANOVA) was used to identify significant differences across the biological replicates. The criteria used to denote significantly, differentially expressed proteins for further analysis were fold-change >2 and p-value <0.05. The quality of the expressed and differentially expressed data was examined by principal component analysis (PCA). Heat maps were based on K-means clustering, using Pearson correlation coefficient as a distance metric. The optimal number of clusters was computed using the gap statistic method and comprised of 1000 Monte Carlo iterations (Tibshirani et al., 2001). Volcano plots of the CoIP-MS signals were constructed following $\log_2$ transformation, *Z*-score normalization and a pairwise Student's t-test (p-value <0.05). Proteins were annotated using Blast2Go software (Conesa and Gotz, 2008), the AT_CHLORO (Bruley et al., 2012), or PPDB (Sun et al., 2009) databases. Analyses were performed using R/Bioconductor (version R.3.4.2).

DATA AVAILABILITY

All datasets for this study are included in the manuscript and the **Supplementary Files**.

AUTHOR CONTRIBUTIONS

ZA and JC conceived the project and designed the experiments. AK-P, MR, and LN performed the different experiments. AS did all manuscript analyses. EA-S and MR processed all data and did the statistical and bioinformatics analyses. ZA wrote the manuscript and all co-authors read and approved it.

FUNDING

This work was supported by grants from the United States-Israel Binational Agricultural Research and Development Fund (BARD) – No. United States-422-09 to JC and ZA, and from the Israel Science Foundation (ISF) – No. 1167/18 to ZA.

SUPPLEMENTARY MATERIAL

The Supplementary Material for this article can be found online at: https://www.frontiersin.org/articles/10.3389/fpls.2019.00428/full#supplementary-material

REFERENCES

Adam, Z. (1995). A mutation in the small subunit of ribulose-1,5-bisphosphate carboxylase/oxygenase that reduces the rate of its incorporation into holoenzyme. *Photosyn. Res.* 43, 143–147. doi: 10.1007/BF00042971

Adam, Z., Rudella, A., and van Wijk, K. J. (2006). Recent advances in the study of Clp, FtsH and other proteases located in chloroplasts. *Curr. Opin. Plant Biol.* 9, 234–240. doi: 10.1016/j.pbi.2006.03.010

Adam, Z., Zaltsman, A., Sinvany-Villalobo, G., and Sakamoto, W. (2005). FtsH proteases in chloroplasts and cyanobacteria. *Physiol. Plant.* 123, 386–390. doi: 10.1111/j.1399-3054.2004.00436.x

Ashykhmina, N., Lorenz, M., Frerigmann, H., Koprivova, A., Hofsetz, E., Stuhrwohldt, N., et al. (2019). PAPST2 plays critical roles in removing the stress signaling molecule 3′-phosphoadenosine 5′-phosphate from the cytosol and its subsequent degradation in plastids and mitochondria. *Plant Cell* 31, 231–249. doi: 10.1105/tpc.18.00512

Bailey, S., Thompson, E., Nixon, P. J., Horton, P., Mullineaux, C. W., Robinson, C., et al. (2002). A critical role for the Var2 FtsH homologue of *Arabidopsis thaliana* in the photosystem II repair cycle in vivo. *J. Biol. Chem.* 277, 2006–2011. doi: 10.1074/jbc.M105878200

Beier, D., Spohn, G., Rappuoli, R., and Scarlato, V. (1997). Identification and characterization of an operon of *Helicobacter pylori* that is involved in motility and stress adaptation. *J. Bacteriol.* 179, 4676–4683. doi: 10.1128/jb.179.15.4676-4683.1997

Bieniossek, C., Niederhauser, B., and Baumann, U. M. (2009). The crystal structure of apo-FtsH reveals domain movements necessary for substrate unfolding and translocation. *Proc. Natl. Acad. Sci. U.S.A.* 106, 21579–21584. doi: 10.1073/pnas.0910708106

Bieniossek, C., Schalch, T., Bumann, M., Meister, M., Meier, R., and Baumann, U. (2006). The molecular architecture of the metalloprotease FtsH. *Proc. Natl. Acad. Sci. U.S.A.* 103, 3066–3071. doi: 10.1073/pnas.0600031103

Bourdineaud, J. P., Nehme, B., Tesse, S., and Lonvaud-Funel, A. (2003). The ftsH gene of the wine bacterium *Oenococcus oeni* is involved in protection against environmental stress. *Appl. Environ. Microbiol.* 69, 2512–2520. doi: 10.1128/AEM.69.5.2512-2520.2003

Bruley, C., Dupierris, V., Salvi, D., Rolland, N., and Ferro, M. (2012). AT_CHLORO: a chloroplast protein database dedicated to sub-plastidial localization. *Front. Plant Sci.* 3:205. doi: 10.3389/fpls.2012.00205

Butenko, Y., Lin, A., Naveh, L., Kupervaser, M., Levin, Y., Reich, Z., et al. (2018). Differential roles of the thylakoid lumenal Deg protease homologs in chloroplast proteostasis. *Plant Physiol.* 178, 1065–1080. doi: 10.1104/pp.18.00912

Chen, J., Burke, J. J., Velten, J., and Xin, Z. (2006). FtsH11 protease plays a critical role in *Arabidopsis* thermotolerance. *Plant J.* 48, 73–84. doi: 10.1111/j.1365-313X.2006.02855.x

Chen, J., Burke, J. J., and Xin, Z. (2018). Chlorophyll fluorescence analysis revealed essential roles of FtsH11 protease in regulation of the adaptive responses of photosynthetic systems to high temperature. *BMC Plant Biol.* 18:11. doi: 10.1186/s12870-018-1228-2

Chi, W. T., Fung, R. W., Liu, H. C., Hsu, C. C., and Charng, Y. Y. (2009). Temperature-induced lipocalin is required for basal and acquired thermotolerance in *Arabidopsis*. *Plant Cell Environ.* 32, 917–927. doi: 10.1111/j.1365-3040.2009.01972.x

Conesa, A., and Gotz, S. (2008). Blast2GO: a comprehensive suite for functional analysis in plant genomics. *Int. J. Plant Genomics* 2008:619832. doi: 10.1155/2008/619832

Coquille, S., Roux, C., Mehta, A., Begley, T. P., Fitzpatrick, T. B., and Thore, S. (2013). High-resolution crystal structure of the eukaryotic HMP-P synthase (THIC) from *Arabidopsis thaliana*. *J. Struct. Biol.* 184, 438–444. doi: 10.1016/j.jsb.2013.10.005

Deuerling, E., Paeslack, B., and Schumann, W. (1995). The ftsH gene of *Bacillus subtilis* is transiently induced after osmotic and temperature upshift. *J. Bacteriol.* 177, 4105–4112. doi: 10.1128/jb.177.14.4105-4112.1995

Halperin, T., Zheng, B., Itzhaki, H., Clarke, A. K., and Adam, Z. (2001). Plant mitochondria contain proteolytic and regulatory subunits of the ATP-dependent Clp protease. *Plant Mol. Biol.* 45, 461–468. doi: 10.1023/A:1010677220323

Ito, K., and Akiyama, Y. (2005). Cellular functions, mechanism of action, and regulation of FtsH protease. *Annu. Rev. Microbiol.* 59, 211–231. doi: 10.1146/annurev.micro.59.030804.121316

Itzhaki, H., Naveh, L., Lindahl, M., Cook, M., and Adam, Z. (1998). Identification and characterization of DegP, a serine protease associated with the luminal side of the thylakoid membrane. *J. Biol. Chem.* 273, 7094–7098. doi: 10.1074/jbc.273.12.7094

Kadirjan-Kalbach, D. K., Yoder, D. W., Ruckle, M. E., Larkin, R. M., and Osteryoung, K. W. (2012). FtsHi1/ARC1 is an essential gene in *Arabidopsis* that links chloroplast biogenesis and division. *Plant J.* 72, 856–867. doi: 10.1111/tpj.12001

Karata, K., Inagawa, T., Wilkinson, A. J., Tatsuta, T., and Ogura, T. (1999). Dissecting the role of a conserved motif (the second region of homology) in the AAA family of ATPases. Site-directed mutagenesis of the ATP-dependent protease FtsH. *J. Biol. Chem.* 274, 26225–26232. doi: 10.1074/jbc.274.37.26225

Kato, Y., Sun, X., Zhang, L., and Sakamoto, W. (2012). Cooperative D1 degradation in the photosystem II repair mediated by chloroplastic proteases in *Arabidopsis*. *Plant Physiol.* 159, 1428–1439. doi: 10.1104/pp.112.199042

Keilhauer, E. C., Hein, M. Y., and Mann, M. (2015). Accurate protein complex retrieval by affinity enrichment mass spectrometry (AE-MS) rather than affinity purification mass spectrometry (AP-MS). *Mol. Cell. Proteomics* 14, 120–135. doi: 10.1074/mcp.M114.041012

Kikuchi, S., Asakura, Y., Imai, M., Nakahira, Y., Kotani, Y., Hashiguchi, Y., et al. (2018). A Ycf2-FtsHi heteromeric AAA-ATPase complex is required for chloroplast protein import. *Plant Cell* 30, 2677–2703. doi: 10.1105/tpc.18.00357

Kikuchi, S., Bedard, J., Hirano, M., Hirabayashi, Y., Oishi, M., Imai, M., et al. (2013). Uncovering the protein translocon at the chloroplast inner envelope membrane. *Science* 339, 571–574. doi: 10.1126/science.1229262

Knopf, R. R., Feder, A., Mayer, K., Lin, A., Rozenberg, M., Schaller, A., et al. (2012). Rhomboid proteins in the chloroplast envelope affect the level of allene oxide synthase in *Arabidopsis thaliana*. *Plant J.* 72, 559–571. doi: 10.1111/j.1365-313X.2012.05090.x

Komenda, J., Sobotka, R., and Nixon, P. J. (2012). Assembling and maintaining the photosystem II complex in chloroplasts and cyanobacteria. *Curr. Opin. Plant Biol.* 15, 245–251. doi: 10.1016/j.pbi.2012.01.017

Kovacs-Bogdan, E., Soll, J., and Bolter, B. (2010). Protein import into chloroplasts: the Tic complex and its regulation. *Biochim. Biophys. Acta* 1803, 740–747. doi: 10.1016/j.bbamcr.2010.01.015

Krzywda, S., Brzozowski, A. M., Verma, C., Karata, K., Ogura, T., and Wilkinson, A. J. (2002). The crystal structure of the AAA domain of the ATP-dependent protease FtsH of *Escherichia coli* at 1.5 a resolution. *Structure* 10, 1073–1083. doi: 10.1016/S0969-2126(02)00806-7

Langklotz, S., Baumann, U., and Narberhaus, F. (2012). Structure and function of the bacterial AAA protease FtsH. *Biochim. Biophys. Acta* 1823, 40–48. doi: 10.1016/j.bbamcr.2011.08.015

Leonhard, K., Stiegler, A., Neupert, W., and Langer, T. (1999). Chaperone-like activity of the AAA domain of the yeast Yme1 AAA protease. *Nature* 398, 348–351. doi: 10.1038/18704

Li, L., Nelson, C. J., Trosch, J., Castleden, I., Huang, S., and Millar, A. H. (2017). Protein degradation rate in *Arabidopsis thaliana* leaf growth and development. *Plant Cell* 29, 207–228. doi: 10.1105/tpc.16.00768

Lindahl, M., Spetea, C., Hundal, T., Oppenheim, A. B., Adam, Z., and Andersson, B. (2000). The thylakoid FtsH protease plays a role in the light-induced turnover of the photosystem II D1 protein. *Plant Cell* 12, 419–431. doi: 10.1105/tpc.12.3.419

Lindahl, M., Tabak, S., Cseke, L., Pichersky, E., Andersson, B., and Adam, Z. (1996). Identification, characterization, and molecular cloning of a homologue of the bacterial FtsH protease in chloroplasts of higher plants. *J. Biol. Chem.* 271, 29329–29334. doi: 10.1074/jbc.271.46.29329

Lu, X., Zhang, D., Li, S., Su, Y., Liang, Q., Meng, H., et al. (2014). FtsHi4 is essential for embryogenesis due to its influence on chloroplast development in *Arabidopsis*. *PLoS One* 9:e99741. doi: 10.1371/journal.pone.0099741

Lupas, A., Flanagan, J. M., Tamura, T., and Baumeister, W. (1997). Self-compartmentalizing proteases. *Trends Biochem. Sci.* 22, 399–404. doi: 10.1016/S0968-0004(97)01117-1

Malnoe, A., Wang, F., Girard-Bascou, J., Wollman, F. A., and de Vitry, C. (2014). Thylakoid FtsH protease contributes to photosystem II and cytochrome b6f remodeling in *Chlamydomonas reinhardtii* under stress conditions. *Plant Cell* 26, 373–390. doi: 10.1105/tpc.113.120113

Millar, A. H., Carrie, C., Pogson, B., and Whelan, J. (2009). Exploring the function-location nexus: using multiple lines of evidence in defining the subcellular location of plant proteins. *Plant Cell* 21, 1625–1631. doi: 10.1105/tpc.109.066019

Mishra, L. S., Mielke, K., Wagner, R., and Funk, C. (2019). Reduced expression of the proteolytically inactive FtsH members has impacts on the Darwinian fitness of *Arabidopsis thaliana*. *J. Exp. Bot.* doi: 10.1093/jxb/erz004 [Epub ahead of print].

Moldavski, O., Levin-Kravets, O., Ziv, T., Adam, Z., and Prag, G. (2012). The hetero-hexameric nature of a chloroplast AAA+ FtsH protease contributes to its thermodynamic stability. *PLoS One* 7:e36008. doi: 10.1371/journal.pone.0036008

Ngaki, M. N., Louie, G. V., Philippe, R. N., Manning, G., Pojer, F., Bowman, M. E., et al. (2012). Evolution of the chalcone-isomerase fold from fatty-acid binding to stereospecific catalysis. *Nature* 485, 530–533. doi: 10.1038/nature11009

Olinares, P. D., Kim, J., and van Wijk, K. J. (2011). The Clp protease system; a central component of the chloroplast protease network. *Biochim. Biophys. Acta* 1807, 999–1011. doi: 10.1016/j.bbabio.2010.12.003

Sakamoto, W. (2006). Protein degradation machineries in plastids. *Annu. Rev. Plant Biol.* 57, 599–621. doi: 10.1146/annurev.arplant.57.032905.105401

Sakamoto, W., Tamura, T., Hanba-Tomita, Y., Sodmergen, and Murata, M. (2002). The VAR1 locus of *Arabidopsis* encodes a chloroplastic FtsH and is responsible for leaf variegation in the mutant alleles. *Genes Cells* 7, 769–780. doi: 10.1046/j.1365-2443.2002.00558.x

Sakamoto, W., Zaltsman, A., Adam, Z., and Takahashi, Y. (2003). Coordinated regulation and complex formation of YELLOW VARIEGATED1 and YELLOW VARIEGATED2, chloroplastic FtsH metalloproteases involved in the repair cycle of photosystem II in *Arabidopsis* thylakoid membranes. *Plant Cell* 15, 2843–2855. doi: 10.1105/tpc.017319

Schnall, R., Mannhaupt, G., Stucka, R., Tauer, R., Ehnle, E., Schwarzlose, C., et al. (1994). Identification of a set of yeast genes coding for a novel family of putative ATPases with high similarity to constituents of the 26S protease complex. *Yeast* 10, 1141–1155. doi: 10.1002/yea.320100903

Schumann, W. (1999). FtsH - a single-chain charonin? *FEMS Microbiol. Rev.* 23, 1–11.

Simm, S., Papasotiriou, D. G., Ibrahim, M., Leisegang, M. S., Muller, B., Schorge, T., et al. (2013). Defining the core proteome of the chloroplast envelope membranes. *Front. Plant Sci.* 4:11. doi: 10.3389/fpls.2013.00011

Sokolenko, A., Pojidaeva, E., Zinchenko, V., Panichkin, V., Glaser, V. M., Herrmann, R. G., et al. (2002). The gene complement for proteolysis in the cyanobacterium *Synechocystis* sp. PCC 6803 and *Arabidopsis thaliana* chloroplasts. *Curr. Genet.* 41, 291–310. doi: 10.1007/s00294-002-0309-8

Su, P. H., and Li, H. M. (2010). Stromal Hsp70 is important for protein translocation into pea and *Arabidopsis* chloroplasts. *Plant Cell* 22, 1516–1531. doi: 10.1105/tpc.109.071415

Sun, Q., Zybailov, B., Majeran, W., Friso, G., Olinares, P. D., and van Wijk, K. J. (2009). PPDB, the plant proteomics database at cornell. *Nucleic Acids Res.* 37, D969–D974. doi: 10.1093/nar/gkn654

Suno, R., Niwa, H., Tsuchiya, D., Zhang, X., Yoshida, M., and Morikawa, K. (2006). Structure of the whole cytosolic region of ATP-dependent protease FtsH. *Mol. Cell.* 22, 575–585. doi: 10.1016/j.molcel.2006.04.020

Tibshirani, R., Walther, G., and Hastie, T. (2001). Estimating the number of clusters in a data set via the gap statistic. *J. R. Statist. Soc. B* 63, 411–423. doi: 10.1111/1467-9868.00293

Tomoyasu, T., Gamer, J., Bukau, B., Kanemori, M., Mori, H., Rutman, A. J., et al. (1995). *Escherichia coli* FtsH is a membrane-bound, ATP-dependent protease which degrades the heat-shock transcription factor s32. *EMBO J.* 14, 2551–2560. doi: 10.1002/j.1460-2075.1995.tb07253.x

Tomoyasu, T., Yuki, T., Morimura, S., Mori, H., Yamanaka, K., Niki, H., et al. (1993). The *Eschericia coli* FtsH protein is a prokaryotic member of a protein family of putative ATPases involved in membrane functions, cell cycle control, and gene expression. *J. Bacteriol.* 175, 1344–1351. doi: 10.1128/jb.175.5.1344-1351.1993

Urantowka, A., Knorpp, C., Olczak, T., Kolodziejczak, M., and Janska, H. (2005). Plant mitochondria contain at least two i-AAA-like complexes. *Plant Mol. Biol.* 59, 239–252. doi: 10.1007/s11103-005-8766-3

Wagner, R., Aigner, H., and Funk, C. (2012). FtsH proteases located in the plant chloroplast. *Physiol. Plant.* 145, 203–214. doi: 10.1111/j.1399-3054.2011.01548.x

Wagner, R., von Sydow, L., Aigner, H., Netotea, S., Brugiere, S., Sjogren, L., et al. (2016). Deletion of FtsH11 protease has impact on chloroplast structure and function in *Arabidopsis thaliana* when grown under continuous light. *Plant Cell Environ.* 39, 2530–2544. doi: 10.1111/pce.12808

Yamamoto, Y., Aminaka, R., Yoshioka, M., Khatoon, M., Komayama, K., Takenaka, D., et al. (2008). Quality control of photosystem II: impact of light and heat stresses. *Photosynth. Res.* 98, 589–608. doi: 10.1007/s11120-008-9372-4

Yoshioka, M., Uchida, S., Mori, H., Komayama, K., Ohira, S., Morita, N., et al. (2006). Quality control of photosystem II. Cleavage of reaction center D1 protein in spinach thylakoids by FtsH protease under moderate heat stress. *J. Biol. Chem.* 281, 21660–21669. doi: 10.1074/jbc.M602896200

Yu, F., Park, S., and Rodermel, S. R. (2004). The *Arabidopsis* FtsH metalloprotease gene family: interchangeability of subunits in chloroplast oligomeric complexes. *Plant J.* 37, 864–876. doi: 10.1111/j.1365-313X.2003.02014.x

Zaltsman, A., Ori, N., and Adam, Z. (2005). Two types of FtsH protease subunits are required for chloroplast biogenesis and photosystem II repair in *Arabidopsis*. *Plant Cell* 17, 2782–2790. doi: 10.1105/tpc.105.035071

Conflict of Interest Statement: The authors declare that the research was conducted in the absence of any commercial or financial relationships that could be construed as a potential conflict of interest.

frontiers in Plant Science

MINI REVIEW
published: 12 April 2019
doi: 10.3389/fpls.2019.00479

Plant Vacuolar Processing Enzymes

Barend Juan Vorster[1], Christopher A. Cullis[2] and Karl J. Kunert[1]*

[1]Department of Plant and Soil Sciences, Forestry and Agricultural Biotechnology Institute, University of Pretoria, Pretoria, South Africa, [2]Department of Biology, Case Western Reserve University, Cleveland, OH, United States

Plant proteomes contain hundreds of proteases divided into different families based on evolutionary and functional relationship. In particular, plant cysteine proteases of the C1 (papain-like) and C13 (legumain-like) families play key roles in many physiological processes. The legumain-like proteases, also called vacuolar processing enzymes (VPEs), perform a multifunctional role in different plant organs and during different stages of plant development and death. VPEs are similar to animal caspases, and although caspase activity was identified in plants almost 40 years ago, there still remains much research to be done to gain a complete understanding of their various roles and functions in plants. Here we not only summarize the current existing knowledge of plant VPEs, including recent developments in the field, but also highlight the future prospective areas to be investigated to obtain a more detailed understanding of the role of VPEs in plants.

Keywords: vacuolar processing enzyme (VPE), legumain, programmed cell death (PCD), cysteine protease, plant development

OPEN ACCESS

Edited by:
Mercedes Diaz-Mendoza, Centro de Biotecnología y Genómica de Plantas (CBGP), Spain

Reviewed by:
Manuel Martinez, Polytechnic University of Madrid, Spain
Dana Ethel Martinez, Instituto de Fisiología Vegetal (INFIVE), Argentina

****Correspondence:***
Barend Juan Vorster
juan.vorster@up.ac.za

Specialty section:
This article was submitted to Plant Physiology, a section of the journal Frontiers in Plant Science

Received: *11 February 2019*
Accepted: *28 March 2019*
Published: *12 April 2019*

Citation:
Vorster BJ, Cullis CA and Kunert KJ (2019) Plant Vacuolar Processing Enzymes. Front. Plant Sci. 10:479. doi: 10.3389/fpls.2019.00479

INTRODUCTION

Plant vacuolar processing enzymes (VPEs), or legumains, were named because of their role in the proteolytic processing of various vacuolar proteins (Hara-Nishimura and Nishimura, 1987). While they belong to the family of cysteine proteases, they have little sequence similarity to other cysteine proteases apart from the cysteine (Cys) and histidine (His) residues in the active site. VPEs have properties similar to animal caspases and perform limited proteolysis after asparagine (Asn) and aspartic acid (Aps) residues (Abe et al., 1993; Becker et al., 1995; Hiraiwa et al., 1999). They are also able to carry out unlimited proteolysis depending on the protein conformation of the substrate (Müntz et al., 2002). This caspase-like asparagine-specific catalytic activity was first detected in plants almost 10 years before the first successful isolation of VPEs from the cotyledons of *Vicia sativa*, then named Proteinase B (Shutov et al., 1982), and later shown to belong to the legumain family (Becker et al., 1995).

Plant VPEs are not solely expressed in seeds but also in vegetative organs (Hara-Nishimura et al., 1998; Nakaune et al., 2005). Although VPEs have been shown to play a central role in storage protein mobilization (Grudkowska and Zagdanska, 2004; Liu et al., 2018), plant development, and environmental stress responses (Christoff and Rogerio, 2014), detailed research on plant VPEs is still rather limited. To date, only a single review is available specifically focusing on their different functions in plants published 17 years ago (Müntz and Shutov, 2002) and a furthermore recent one on the contribution of a VPE to plant PCD and its role in vacuole-mediated cell death (Hatsugai et al., 2015). Recently, research relating to VPE biology has been increasing and is driven from two largely uncoupled research areas, the mammalian and the plant VPE fields (Dall and Brandstetter, 2016).

In this mini-review, we summarize the current knowledge of plant VPEs, including recent developments in the field, and highlight the future prospective areas to be investigated to obtain a better understanding of the role of VPEs in plants.

CLASSIFICATION AND GENOMICS

Evolutionary VPEs originate from prokaryote pro-legumains descending from Parabasalia and Alveolata before splitting in their separate branches of Chlorophyta and Placozoa (Shutov et al., 2012). Plant VPEs are similar to mammalian caspases, with both involved in regulating programmed cell death (PCD) pathways. In animals, one isoform is encoded and the mature enzymes are located in the cytosol. Plants, however, encode at least four functional isoforms, which are located in the vacuole (Zauner et al., 2018). Plant VPEs have been separated into three subfamilies: a seed type (β-VPE), a vegetative type (α-VPE and γ-VPE), and an uncharacterized type, only found in dicots, called δ-VPE (Müntz et al., 2002; Yamada et al., 2005). The δ-VPE group, which originated early during dicotyledonous diversification, is related to seed coat formation (Nakaune et al., 2005).

The grouping of VPEs into seed and vegetative types is related to the classification of vacuoles as either protein storing or lytic. Protein-storing vacuoles contain large amounts of defensive and storage proteins used during seed germination and growth, while lytic vacuoles contain hydrolytic enzymes (Christoff and Rogerio, 2014). Caution is necessary when using this grouping as there is no substantial sequence difference between the two types of legumains nor is the distinction enough to assign specific roles for each member of this family. This grouping also does not exclude their expression and activity in other tissues or developmental stages (Kinoshita et al., 1995; Gruis et al., 2004; Santos-Silva et al., 2012). In barley, it has been demonstrated that members of both the vegetative and seed types are almost ubiquitous and perform a multifunctional role in different organs (Julián et al., 2013).

The number of VPE genes in various plants seems to differ markedly. Four genes have been described in Arabidopsis (Kuroyanagi et al., 2005), eight in barley (Julián et al., 2013), five in rice (Hatsugai et al., 2015), and 14 in tomato (Wang et al., 2017). Recently, transcriptome sequence information has also permitted the identification of new VPE genes. The detection of additional genes by homology searches has also identified a second class of genes related to the VPEs that have a cyclization function rather than a protease function (Jackson et al., 2018). These genes have a marker of ligase activity (MLA). The MLA represents an easily identifiable marker of asparaginyl endopeptidases (AEPs) capable of post-translational cyclization of ribosomal synthesized peptides. The MLA as a diagnostic tool permits the detection of an asparaginyl endopeptidase ligase from the Violaceae plant family and has identified leads from a selection of non-cyclotide producing plant families. Although six VPE proteins were identified in the flax genome, none had the MLA region, even though flax does produce at least 21 cyclopeptides (Shim et al., 2014). As transcriptomic data have become available, the range of tissues in which a specific gene is expressed has increased, although the expression of some genes is still restricted (Ariizumi et al., 2011). In tomato, *SlVPE1* and *2* were both fruit restricted, but *SlVPE3–5* were also expressed in leaves and flowers (Ariizumi et al., 2011). As the genomic and transcriptomic data are further analyzed, the full range of activities of VPE genes with respect to plant development and response to biotic and abiotic stresses will become clearer.

PROTEIN PROCESSING, ACTIVATION, AND ACTIVITY

In plants, VPE genes code for a pre-prolegumain precursor with an N-terminal signal peptide and a C-terminal extension (**Figure 1**; Müntz and Shutov, 2002) that is moved to the rough endoplasmic reticulum (RER) after translation. Removal of the signal peptide results in the inactive pro-legumains that enter the secretory pathway and are transported to the cell wall (Linnestad et al., 1998) or vacuoles (Schlereth et al., 2001). Due to the autocatalytic removal of the C- and N-terminal, the legumain pro-enzyme becomes active in the acidic pH environments of the cell wall or protein storage vacuoles (Hiraiwa et al., 1999; Müntz and Shutov, 2002). After cleavage, the C-terminal "pro-domain" will confer stability at neutral pH and modulates activity; therefore, the C-terminal "pro-domain" is referred to as the Legumain Stabilization and Activity Modulation (LSAM) domain (Zauner et al., 2018).

Substrate activity of VPEs is specific toward Ans and Asp residues, and although they have limited sequence identity, they possess similar structural and enzymatic properties to mammalian caspase-1 exhibiting YVADase/caspase-1-like cleavage activity (Hatsugai et al., 2006). Their strict cleavage specificity means that they are adapted to perform limited proteolysis of proteins; however, alteration in the substrate protein conformation caused by proteolysis with other proteases can expose additional Asn sites leading to further degradation by VPEs (Chen et al., 1998).

Recombinant γ-VPE recognizes aspartic acid as part of the YVAD sequence (VPE and caspases-1 substrates) but not others such as the DEVD sequence of caspases-3 substrates (Kuroyanagi et al., 2005). However, a VPE from *Papaver rhoeas* pollen (PrVPE1) has been described that can bind and cleave DEVD (Bosch et al., 2010) and NtTPE8 extracted from tobacco seeds, which have the ability to cleave the cathepsin H substrate FVR (Wang et al., 2018a,b) Experiments on Arabidopsis *vpe*-null mutants, which lack all four VPE gene copies, show neither VPE activity nor caspases-1-like activity (Kuroyanagi et al., 2005) and can also decrease papain-like cysteine protease activity (Cilliers et al., 2018). Certain plant VPEs have also been shown to be efficient peptide ligases and cyclases (Yang et al., 2017; Jackson et al., 2018). However, *in vitro* proof for ligase activity of *Arabidopsis thaliana* VPE isoforms is lacking (Zauner et al., 2018). VPEs have also been shown to process mitochondrial proteins in pollen (Bosch et al., 2010). VPEs also activate cysteine proteases by the removal of the I19

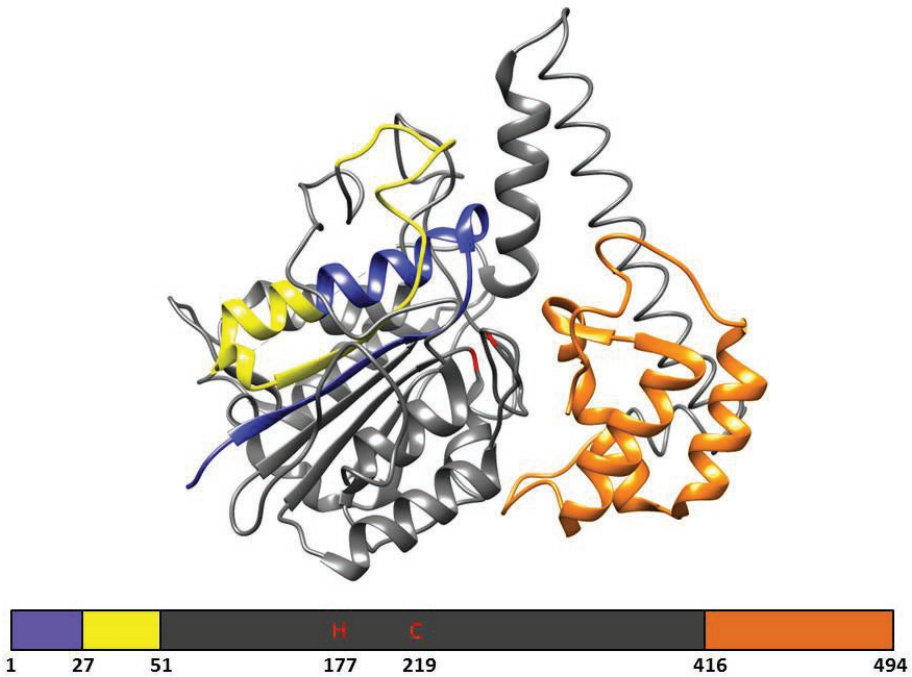

FIGURE 1 | The 3D structure and primary structural organization of Arabidopsis γ-VPE. Showing the pre-prolegumain precursor with an N-terminal signal peptide (blue), the cleavable pro-peptide (yellow), and the C-terminal "pro-domain" is referred to as the Legumain Stabilization and Activity Modulation (LSAM) domain (orange). The mature protein is represented in gray and shows the catalytic histidine (H177) and cysteine (C219) amino acids. The 3D structure is based on the crystal structure (5NIJ) by Zauner et al. (2018).

inhibitory domain of pre-proteases (Roberts et al., 2012). A study in *Vigna mungo* seeds confirmed that a VPE was responsible for the post-translational processing of a cysteine protease (Okamoto and Minamikawa, 1999).

Plant cysteine proteases of the papain family (C1) are inhibited by plant cystatins (Benchabane et al., 2010) and E64. Although VPEs (C13 family) belong to the cysteine protease family, they share very little sequence similarity with other cysteine proteases and are also much less sensitive to inhibition by E64 (Müntz and Shutov, 2002). However, active VPEs are inhibited by a sub-group of cystatins containing a C-terminal extension (Martinez et al., 2007; Santos-Silva et al., 2012). In soybean, only one of the 19 cystatins has this domain (van Wyk et al., 2014); similarly, only one C-terminal extended cystatin has been identified in barley (Julián et al., 2013) and rice (Christoff et al., 2016).

PLANT DEVELOPMENT AND PCD

During germination, VPEs contribute to storage protein degradation and mobilization either due to direct proteolytic degradation or through the activation of other peptidases (Schlereth et al., 2000; Zakharov and Muntz, 2004). The processing function is related to the cleavage of the C-terminal propeptides and activation of papain-like cysteine proteases as well as the N-terminal propeptides from chitinase or the processing of protease inhibitors having Asn-flanked processing sites (Kinoshita et al., 1999). VPEs have been shown to function in regulating PCD in both developmental and defense responses. PCD is a highly regulated physiological process that is essential to the development of eukaryotes. Due to the presence of the cell wall, plant cells, unlike animal cells, are not engulfed by the neighboring cells during PCD. Instead, VPEs are responsible for the collapse of the vacuole membrane resulting in the release of proteases into the cytoplasm (Hara-Nishimura et al., 2005) and initiating a proteolytic cascade leading to PCD (Hatsugai et al., 2015).

During seed development in angiosperms, the seed coat consists of two integuments of maternal tissue consisting of multiple cellular layers. During the early stages of seed development, δ-VPE is expressed in these layers resulting in limited PCD to reduce the thickness of these cell layers and form the seed coat (Nakaune et al., 2005). VPEs of barley have been shown to be involved in the degradation of maternal tissues in the seed of barley including the nucleus and pericarp (Julián et al., 2013; Tran et al., 2014), thereby also influencing seed size (Radchuk et al., 2018). VvβVPE from *Vitis vinifera* has been shown to be essential for ovule maturation and increased germination when overexpressed in Arabidopsis (Gong et al., 2018). A VPE from tobacco, *NtTPE8*, was shown to be exclusively expressed in the integumentary tapetum of tobacco seeds and downregulation of *NtTPE8* induced seed abortion (Wang et al., 2018a,b).

VPEs have also been found to mediate PCD during xylem development (Han et al., 2012) as well as during the breakdown

of apical bud dominance in potato tubers (Teper-Bamnolker et al., 2012), development and senescence of root nodules (van Wyk et al., 2014; Cilliers et al., 2018), leaf and petal senescence (Kinoshita et al., 1999; van Doorn and Woltering, 2008), and pollen development (Hara-Nishimura, 2012). Hybrid lethality in tobacco has also been correlated to VPE activity and the breakdown of the vacuolar membrane (Mino et al., 2007). Two VPEs have been found to be involved in the execution of ethylene-related PCD in leaf pattern development in the lace plant (*Aponogeton madagascariensis* (Mirb.) (Rantong and Gunawardena, 2018).

EXPRESSION UNDER STRESS

VPEs also play a central role in the response to biotic and abiotic stresses and the likely associated change in plant hormone production. The hypersensitive response (HR) is among the known inducers of VPE expression (Zhang et al., 2010). The hypersensitive response is a form of PCD that limits pathogen development in plants and is related to plant immunity to various pathogens. PCD linked to the HR in plants following exposure to bacterial or viral pathogens could be suppressed by inhibiting VPE activity using caspase peptide inhibitors without affecting the induction of other aspects of the HR (del Pozo and Lam, 1998). Similarly, by using gene silencing, VPE deficiency prevented virus-induced HR in tobacco plants (Hatsugai et al., 2004). While the HR response is a defense against pathogen attack, toxin-induced cell death is a strategy used by pathogens during infection where compatible pathogens secrete toxins to induce host cell death and promote their growth. Kuroyanagi et al. (2005) showed that VPEs are essential for mycotoxin-induced cell death in Arabidopsis mediated by a mechanism similar to the resistance response of hypersensitive cell death.

Other known biotic inducers of VPE expression are wounding, aphid infestation, plant hormones associated with biotic stress, such salicylic and jasmonic acid, as well as nitric oxide (Julián et al., 2013; Christoff and Rogerio, 2014). In addition, plant VPEs are further considered as important components of the plant "immune" system because they can also be involved in the generation of cyclic peptides, such as Kalata B1, a peptide from the African plant *Oldenlandia affinis* and an important defense against pathogens (Craik, 2012). In rice, four of the five VPEs are responsive not only to one or several plant hormones but also to abiotic stresses (Wang et al., 2018a,b). Wounding, ethylene, and salicylic acid upregulated the expression of α-VPE and γ-VPE, while jasmonate slightly upregulated the expression of γ-VPE. In barley leaves, *HvLeg-2* (a β- or seed-type VPE) expression in both seed and vegetative tissues responds to both biotic and abiotic stimuli including salicylic and jasmonic acid, nitric oxide, and ABA in vegetative tissue, and it was also induced by gibberellic acid in seeds (Julián et al., 2013).

In general, abiotic stress, such as drought, can induce many forms of cysteine proteases, which might not be expressed during natural senescence (Khanna-Chopra et al., 1999; Martinez and Diaz, 2008; Julián et al., 2013; Cilliers et al., 2018). In our group, we also found evidence that VPEs are involved in the response to drought stress when we investigated the expression of C1 (papain-like) and C13 (VPE) cysteine proteases in soybean nodules exposed to drought conditions (Cilliers et al., 2018). A study of the cysteine protease transcriptome from soybean nodules identified a number of C1 and C13 cysteine proteases that are strongly upregulated under drought conditions. Also, by studying an Arabidopsis α-VPE deficient mutant, we found evidence that soybean α-VPE (Glyma.17G230700) might function in C1 cysteine protease maturation. VPE mutant plants had decreased C1 cysteine protease activity as well as higher biomass and protein levels under stress conditions than wild-type plants. An important role in drought tolerance was also clearly demonstrated in recent Arabidopsis work where *γ-VPE* was found to be strongly expressed in guard cells and involved in water stress response (Albertini et al., 2014). Arabidopsis plants were more drought tolerant when γ-VPE was mutated. These *γ-vpe* knock-out mutants had reduced stomatal opening, suggesting that this type of VPE has a function in the control of stomatal movements. Stomata controls photosynthesis and the water status of the plant (Nadeau, 2008). In rice, it was shown that the suppression of *OsVPE3* enhances salt tolerance by reducing vacuole rupture during PCD as well as by reducing leaf width and stomatal guard cell length (Lu et al., 2016). Stomatal closure can be triggered by pathogens, pathogen-associated molecular patterns (PAMPs), and elicitors, and VPE possibly mediates elicitor-induced stomatal closure by regulating NO accumulation in guard cells (Zhang et al., 2010), thereby playing a role in plant immunity.

FUTURE RESEARCH IN PLANT VPEs

Research on VPEs still lacks behind that on other cysteine proteases in particular the members of the C1 papain-like family. **Figure 2** provides an overview of the processes in which plant VPEs are involved. Despite some recent progress in plant VPE genomics and expression, much remains to be done particularly in elucidating the role and function of VPEs, under stress conditions, and a possible role of VPEs in plant defense signaling. Therefore, more extensive VPE mutant work as well as work to silence different members of the C13 cysteine proteases (VPEs) are, in our opinion, urgently required. However, such work will also require more genomic and transcriptomic data for the identification and characterization of more VPE family members allowing to investigate the full range of activities of VPE genes with respect to plant development and response to biotic and abiotic stresses. In this regard, a better understanding of the exact role of VPEs especially in biotic and abiotic stress resistances is also needed. However, maybe any further mutant and silencing work should also include important crop species, for example, soybean and wheat (van Wyk et al., 2014; Botha et al., 2017), for which a plant transformation system is already available. Lowering VPE expression thereby limiting the maturation of papain-like cysteine proteases might provide a strategy to obtain protection against stress-induced premature senescence

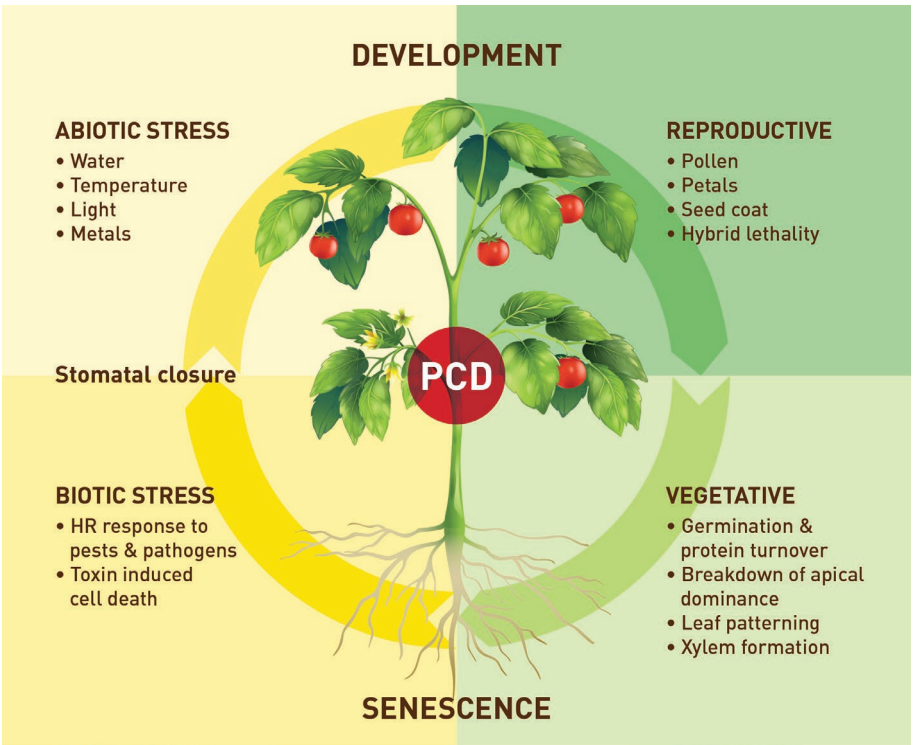

FIGURE 2 | An overview of the processes in which plant VPEs are involved in.

processes involving active papain-like cysteine proteases. It might also result in higher protein content in leaves and seeds due to lowered cysteine protease-induced protein degradation. It has been shown that co-expression of cystatins can increase recombinant protein production in tobacco (Pillay et al., 2012). Given the role that VPEs play in pathogen induced HR there may be scope to target these enzymes to improve plant expression systems for recombinant protein production. Also, the cyclization activities of some of these proteases and the identification of the associated determinants may facilitate in future work the discovery of more ligase-type AEPs and the engineering of AEPs with tailored catalytic properties. These cyclic products may have potential for both human health and pest control. A final interesting aspect to investigate in the future would be what particular role cysteine protease inhibitors play in this interaction between the two C1 (papain-like) and C13 (VPE) proteases. The type of interaction is still a largely unexplored field of study regarding time of expression and specificity of the inhibitor. For instance, the interaction between C1 proteases and their inhibitors (cystatins) is well characterized, and although VPEs have been shown to be inhibited by a cystatin with a C-terminal extension (Julián et al., 2013; Christoff et al., 2016), very little is known about the interaction of VPEs and inhibitors *in situ*.

Therefore, combining various genetic, reverse genetic, and biochemical techniques is important to identify receptors, scaffold proteins, negative regulators, and substrates of VPEs and to target genes that will help us to fully understand these plant development and defense mechanisms.

AUTHOR CONTRIBUTIONS

All authors contributed to the contents of the article. All authors critically reviewed the manuscript and also approved the final manuscript.

FUNDING

Funding to BJV provided by the National Research Foundation, Developmental grant 112144.

REFERENCES

Abe, Y., Shirane, K., Yokosawa, H., Matsushita, H., Mitta, M., Kato, I., et al. (1993). Asparaginyl endopeptidase of jack bean seeds. *Biol. Chem.* 268, 3525–3529.

Albertini, A., Simeoni, F., Galbiati, M., Bauer, H., Tonelli, C., and Cominelli, E. (2014). Involvement of the vacuolar processing enzyme γVPE in response of Arabidopsis thaliana to water stress. *Biol. Plant.* 58, 531–538. doi: 10.1007/s10535-014-0417-6

Ariizumi, T., Higuchi, K., Arakaki, S., Sano, T., Asamizu, E., and Ezura, H. (2011). Genetic suppression analysis in novel vacuolar processing enzymes reveals their roles in controlling sugar accumulation in tomato fruits. *J. Exp. Bot.* 62, 2773–2786. doi: 10.1093/jxb/erq451

Becker, C., Shutov, A. D., Nong, V. H., Senyuk, V. I., Jung, R., Horstmann, C., et al. (1995). Purification, cDNA cloning and characterization of pro-teinase B, an asparagine-specific endopeptidase from germinating vetch (Vicia sativa L.) seeds. *Eur. J. Biochem.* 228, 456–462. doi: 10.1111/j.1432-1033.1995.tb20284.x

Benchabane, M., Schlüter, U., Vorster, J., Goulet, M. C., and Michaud, D. (2010). Plant cystatins. *Biochimie* 92, 1657–1666. doi: 10.1016/j.biochi.2010.06.006

Bosch, M., Poulter, N. S., Perry, R. M., Wilkins, K. A., and Franklin-Tong, V. E. (2010). Characterization of a legumain/vacuolar processing enzyme and YVADase activity in Papaver pollen. *Plant Mol. Biol.* 74, 381–393. doi: 10.1007/s11103-010-9681-9

Botha, A. M., Kunert, K. J., and Cullis, C. A. (2017). Cysteine proteases and wheat (Triticum aestivum L) under drought: a still greatly unexplored association. *Plant Cell Environ.* 40, 1679–1690. doi: 10.1111/pce.12998

Chen, J. M., Rawlings, N. D., Stevens, R. A., and Barrett, A. J. (1998). Identification of the active site of legumain links it to caspases, clostripain and gingipains in a new clan of cysteine endopeptidases. *FEBS Lett.* 441, 361–365.

Christoff, A. P., Passaia, G., Salvati, C., Alves-Ferreira, M., Margis-Pinheiro, M., and Margis, R. (2016). Rice bifunctional phytocystatin is a dual modulator of legumain and papain-like proteases. *Plant Mol. Biol.* 92, 193–207. doi: 10.1007/s11103-016-0504-5

Christoff, A. P., and Rogerio, M. (2014). The diversity of rice phytocystatins. *Mol. Gen. Genomics* 289, 1321–1330. doi: 10.1007/s00438-014-0892-7

Cilliers, M., van Wyk, S. G., van Heerden, P. D. R., Kunert, K. J., and Vorster, B. J. (2018). Identification and changes of the drought-induced cysteine protease transcriptome in soybean (Glycine max) root nodules. *J. Exp. Environ. Bot.* 148, 59–69. doi: 10.1016/j.envexpbot.2017.12.005

Craik, D. J. (2012). Host-defense activities of cyclotides. *Toxins* 4, 139–156. doi: 10.3390/toxins4020139

Dall, E., and Brandstetter, H. (2016). Structure and function of legumain in health and disease. *Biochimie* 122, 126–150. doi: 10.1016/j.biochi.2015.09.022

del Pozo, O., and Lam, E. (1998). Caspases and programmed cell death in the hypersensitive response of plants to pathogens. *Curr. Biol.* 8, 1129–1132. doi: 10.1016/S0960-9822(98)70469-5

Gong, P., Lia, Y., Tanga, Y., Wei, R., Huijun, Z., Wang, Y., et al. (2018). Vacuolar processing enzyme (VvβVPE) from *Vitis vinifera*, processes seed proteins during ovule development, and accelerates seed germination in VvβVPE heterologously over-expressed Arabidopsis. *Plant Sci.* 274, 420–431. doi: 10.1016/j.plantsci.2018.06.023

Grudkowska, M., and Zagdanska, B. (2004). Multifunctional role of plant cysteine proteinases. *Acta Biochim. Pol.* 51, 609–624.

Gruis, D., Schulze, J., and Jung, R. (2004). Storage protein accumulation in the absence of the vacuolar processing enzyme family of cysteine proteases. *Plant Cell* 16, 270–290. doi: 10.1105/tpc.016378

Han, J. J., Lin, W., Oda, Y., Cui, K. M., Fukuda, H., and He, X. Q. (2012). Thepro-teasome is responsible for caspase −3-like activity during xylem development. *Plant J.* 72, 129–141. doi: 10.1111/j.1365-313X.2012.05070.x

Hara-Nishimura, I. (2012). "Plant legumain, asparaginyl endopeptidase, vacuolar processing enzyme" in *Handbook of proteolytic enzymes.* 3rd edn. eds. A. J. Barrett, N. D. Rawlings, and F. J. Woessner (London, UK: Academic Press), 2314–2320.

Hara-Nishimura, I., Hatsugai, N., Nakaune, S., Kuroyanagi, M., and Nishimura, M. (2005). Vacuolar processing enzyme: an executor of plant cell death. *Curr. Opin. Plant Biol.* 8, 404–408. doi: 10.1016/j.pbi.2005.05.016

Hara-Nishimura, I., and Nishimura, M. (1987). Proglobulin processing enzyme in vacuoles isolated from developing pumpkin cotyledons. *Plant Physiol.* 85, 440–445. doi: 10.1104/pp.85.2.440

Hara-Nishimura, I., Shimada, T., Hatano, K., Takeuchi, Y., and Nishimura, M. (1998). Transport of storage proteins to protein storage vacuoles is mediated by large precursor-accumulating vesicles. *Plant Cell* 10, 825–836. doi: 10.1105/tpc.10.5.825

Hatsugai, N., Kuroyanagi, M., Nishimura, M., and Hara-Nishimura, I. (2006). A cellular suicide strategy of plants: vacuole-mediated cell death. *Apoptosis* 11, 905–911. doi: 10.1007/s10495-006-6601-1

Hatsugai, N., Kuroyanagi, M., Yamada, K., Meshi, T., Tsuda, S., Kondo, M., et al. (2004). A plant vacuolar protease, VPE, mediates virus-inducedhypersensitive cell death. *Science* 305, 855–858. doi: 10.1126/science.1099859

Hatsugai, N., Yamada, K., Goto-Yamada, S., and Hara-Nishimura, I. (2015). Vacuolar processing enzyme in plant programmed cell death. *Front. Plant Sci.* 6:234. doi: 10.3389/fpls.2015.00234

Hiraiwa, N., Nishimura, M., and Hara-Nishimura, I. (1999). Vacuolar processing enzyme is self-catalytically activated by sequential removal of the C-terminal and N-terminal propeptides. *FEBS Lett.* 447, 213–216. doi: 10.1016/S0014-5793(99)00286-0

Jackson, M. A., Gilding, E. K., Shafee, T., Harris, K. S., Kaas, Q., Poon, S., et al. (2018). Molecular basis for the production of cyclic peptides by plant asparaginyl endopeptidases. *Nat. Commun.* 9:2411. doi: 10.1038/s41467-018-04669-9

Julián, I., Gandullo, J., Santos-Silva, L. K., Diaz, I., and Martinez, M. (2013). Phylogenetically distant barley legumains have a role in both seed and vegetative tissues. *J. Exp. Bot.* 64, 2929–2941. doi: 10.1093/jxb/ert132

Khanna-Chopra, R., Srivalli, B., and Ahlawat, Y. S. (1999). Drought induces many forms of cysteine proteinases not observed during natural senescence. *Biochem. Biophys. Res. Commun.* 255, 324–327. doi: 10.1006/bbrc.1999.0195

Kinoshita, T., Nishimura, M., and Hara-Nishimura, I. (1995). Homologues of a vacuolar processing enzyme that are expressed in different organs in Arabidopsis thaliana. *Plant Mol. Biol.* 29, 81–89.

Kinoshita, T., Yamada, K., Hiraiwa, N., Kondo, M., Nishimura, M., and Hara-Nishimura, I. (1999). Vacuolar processing enzyme is up-regulated in the lytic vacuoles of vegetative tissues during senescence and under various stressed conditions. *Plant J.* 19, 43–53. doi: 10.1046/j.1365-313X.1999.00497.x

Kuroyanagi, M., Yamada, K., Hatsugai, N., Kondo, M., Nishimura, M., and Hara-Nishimura, I. (2005). Vacuolar processing enzyme is essential for mycotoxin induced cell death in Arabidopsis thaliana. *J. Biol. Chem.* 280, 32914–32920. doi: 10.1074/jbc.M504476200

Linnestad, C., Doan, D. N., Brown, R. C., Lemmon, B. E., Meyer, D. J., Jung, R., et al. (1998). Nucellain, a barley homolog of the dicot vacuolar processing protease, is localized in the nucellar cell wall. *Plant Physiol.* 118, 1169–1180. doi: 10.1104/pp.118.4.1169

Liu, H., Hu, M., Wang, Q., Cheng, L., and Zhang, Z. (2018). Role of papain-like cysteine proteases in plant development. *Front. Plant Sci.* 9:1717. doi: 10.3389/fpls.2018.01717

Lu, W., Deng, M., Guo, F., Wang, M., Zeng, Z., Han, N., et al. (2016). Suppression of $OsVPE_3$ enhances salt tolerance by attenuating vacuole rupture during programmed cell death and affects stomata development in rice. *Rice* 9:65. doi: 10.1186/s12284-016-0138-x

Martinez, M., and Diaz, I. (2008). The origin and evolution of plant cystatins and their target cysteine proteinases indicate a complex functional relationship. *BMC Evol. Biol.* 8:198. doi: 10.1186/1471-2148-8-198

Martinez, M., Diaz-Mendoza, M., Carrillo, L., and Diaz, I. (2007). Carboxy terminal extended phytocystatins are bifunctional inhibitors of papain and legumain cysteine proteinases. *FEBS Lett.* 581, 2914–2918. doi: 10.1016/j.febslet.2007.05.042

Mino, M., Murata, N., Date, S., and Inoue, M. (2007). Cell death in seedlings of the interspecific hybrid of Nicotia nagossei and N. tabacum; possible role of knob-like bodies formed on tonoplast in vacuolar-collapse-mediated cell death. *Plant Cell Rep.* 26, 407–419. doi: 10.1007/s00299-006-0261-z

Müntz, K., Blattner, F. R., and Shuto, A. D. (2002). Legumains: a family of asparagine-specific cysteine endopeptidases involved in propolypeptide processing and protein breakdown in plants. *J. Plant Physiol.* 160, 1281–1293. doi: 10.1078/0176-1617-00853

Müntz, K., and Shutov, A. D. (2002). Legumains and their functions in plants. *Trends Plant Sci.* 7, 340–344. doi: 10.1016/S1360-1385(02)02298-7

Nadeau, J. A. (2008). Stomatal development: new signals and fate determinants. *Curr. Opin. Plant Biol.* 12, 1–7. doi: 10.1016/j.pbi.2008.10.006

Nakaune, S., Yamada, K., Kondo, M., Kato, T., Tabata, S., Nishimura, M., et al. (2005). A vacuolar processing enzyme, deltaVPE, is involved in seed coat formation at the early stage of seed development. *Plant Cell* 17, 876–887. doi: 10.1105/tpc.104.026872

Okamoto, T., and Minamikawa, T. (1999). Molecular cloning and characterization of Vigna mungo processing enzyme 1 (VmPE-1), an asparaginyl endopeptidase possibly involved in post-translational processing of a vacuolar cysteine endopeptidase (SH-EP). *Plant Mol. Biol.* 39, 63–73. doi: 10.1023/A:1006170518002

Pillay, P., Kibido, T., Du Plessis, M., Van der Vyver, C., Beyene, G., Vorster, B. J., et al. (2012). Use of transgenic oryzacystatin-I-expressing plants enhances

recombinant protein production. *Appl. Biochem. Biotechnol.* 168, 1608–1620. doi: 10.1007/s12010-012-9882-6

Radchuk, V., Tran, V., Radchuk, R., Diaz-Mendoza, M., Weier, D., Fuchs, J., et al. (2018). Vacuolar processing enzyme 4 contributes to maternal control of grain size in barley by executing programmed cell death in the pericarp. *New Phytol.* 218, 1127–1142. doi: 10.1111/nph.14729

Rantong, G., and Gunawardena, A. (2018). Vacuolar processing enzymes, AmVPE1 and AmVPE2, as potential executors of ethylene regulated programmed cell death in the lace plant (Aponogeton madagascariensis). *Botany* 96, 235–247. doi: 10.1139/cjb-2017-0184

Roberts, I. N., Caputo, C., Criado, M. V., and Funk, C. (2012). Senescence-associated proteases in plants. *Physiol. Plant.* 145, 130–139. doi: 10.1111/j.1399-3054.2012.01574.x

Santos-Silva, L. K., Soares-Costa, A., Gerald, L. T. S., Meneghin, S. P., and Henrique-Silva, F. (2012). Recombinant expression and biochemical characterization of sugarcane legumain. *Plant Physiol. Biochem.* 57, 181–192. doi: 10.1016/j.plaphy.2012.05.020

Schlereth, A., Becker, C., Horstmann, C., Tiedemann, J., and Müntz, K. (2000). Comparison of globulin mobilization and cysteine proteinases in embryonic axes and cotyledons during germination and seedling growth of vetch (Vicia sativa L.). *J. Exp. Bot.* 51, 1423–1433. doi: 10.1093/jxb/51.349.1423

Schlereth, A., Standhardt, D., Mock, H. P., and Müntz, K. (2001). Stored cysteine proteinases start globulin mobilization in protein bodies of embryonic axes and cotyledons during vetch (Vicia sativa L.) seed germination. *Planta* 212, 718–727. doi: 10.1007/s004250000436

Shim, Y. Y., Gui, B., Arnison, P. G., Wang, Y., and Reaney, J. T. (2014). Flaxseed (Linum usitatissimum L.) bioactive compounds and peptide nomenclature: a review. *Trends Food Sci. Technol.* 38, 5–20. doi: 10.1016/j.tifs.2014.03.011

Shutov, A. D., Blattner, F. R., Kakhovskaya, I. A., and Müntz, K. (2012). New aspects of the molecular evolution of legumains, Asn-specific cysteine proteinases. *J. Plant Physiol.* 169, 319–321. doi: 10.1016/j.jplph.2011.11.005

Shutov, A. D., Do, N. L., and Vaintraub, I. A. (1982). Purification and partial characterization of proteinase B from germinating vetch seeds. *Biokhimija* 47, 814–821.

Teper-Bamnolker, P., Buskila, Y., Lopesco, Y., Ben-Dor, S., Saad, I., Holdengreber, V., et al. (2012). Release of apical dominance in potato tuber is accompanied by programmed cell death in the apical bud meristem. *Plant Physiol.* 158, 2053–2067. doi: 10.1104/pp.112.194076

Tran, V., Weier, D., Radchuk, R., Thiel, J., and Radchuk, V. (2014). Caspase-like activities accompany programmed cell death events in developing barley grains. *PLoS One* 9:109426. doi: 10.1371/journal.pone.0109426

van Doorn, W. G., and Woltering, E. J. (2008). Physiology and molecular biology of petal senescence. *J. Exp. Bot.* 59, 453–480. doi: 10.1093/jxb/erm356

van Wyk, S. G., Du Plessis, M., Cullis, C. A., Kunert, K. J., and Vorster, B. J. (2014). Cysteine protease and cystatin expression and activity during soybean nodule development and senescence. *BMC Plant Biol.* 14:294. http://www.biomedcentral.com/1471-2229/14/294

Wang, W., Cai, J., Wang, P., Tian, S., and Qin, G. (2017). Post-transcriptional regulation of fruit ripening and disease resistance in tomato by the vacuolar protease SlVPE3. *Genome Biol.* 18:47. doi: 10.1186/s13059-017-1178-2

Wang, W., Xiong, H., Lin, R., Zhao, N., Zhao, P., and Sun, M.-X. (2018a). A VPE-like protease NtTPE8 exclusively expresses in the integumentary tapetum and involves in seed development. *J. Integr. Plant Biol.* doi: 10.1111/jipb.12766

Wang, W., Zhou, X., Xiong, H., Mao, W., Zhao, P., and Sun, M. (2018b). Papain-like and legumain-like proteases in rice: genome-wide identification, comprehensive gene feature characterization and expression analysis. *BMC Plant Biol.* 18:87. doi: 10.1186/s12870-018-1298-1

Yamada, K., Shimada, T., Nishimura, M., and Hara-Nishimura, I. (2005). A VPE family sup-porting various vacuolar functions in plants. *Physiol. Plant.* 123, 369–375. doi: 10.1111/j.1399-3054.2005.00464.x

Yang, R., Wong, Y. H., Nguyen, G. K. T., Tam, J. P., Lescar, J., and Wu, B. (2017). Engineering a catalytically efficient recombinant protein ligase. *J. Am. Chem. Soc.* 139, 5351–5358. doi: 10.1021/jacs.6b12637

Zakharov, A., and Muntz, K. (2004). Seed legumains are expressed in stamens and vegetative legumains in seeds of Nicotiana tabacum L. *J. Exp. Bot.* 55, 1593–1595. doi: 10.1093/jxb/erh166

Zauner, F. B., Dall, E., Regl, C., Grassi, L., Huber, C. G., Cabrele, C., et al. (2018). Crystal structure of plant legumain reveals a unique two-chain state with pH-dependent activity regulation. *Plant Cell* 30, 686–699. doi: 10.1105/tpc.17.00963

Zhang, H., Zheng, X., and Zhang, Z. (2010). The role of vacuolar processing enzymes in plant immunity. *Plant Signal. Behav.* 5, 1565–1567. doi: 10.4161/psb.5.12.13809

Conflict of Interest Statement: The authors declare that the research was conducted in the absence of any commercial or financial relationships that could be construed as a potential conflict of interest.

frontiers in Plant Science

ORIGINAL RESEARCH
published: 30 April 2019
doi: 10.3389/fpls.2019.00473

Proteases Underground: Analysis of the Maize Root Apoplast Identifies Organ Specific Papain-Like Cysteine Protease Activity

Jan Schulze Hüynck[1], Farnusch Kaschani[2†], Karina van der Linde[3†], Sebastian Ziemann[1], André N. Müller[3], Thomas Colby[2†], Markus Kaiser[4], Johana C. Misas Villamil[1] and Gunther Doehlemann[1]**

[1] Center of Excellence on Plant Sciences (CEPLAS), Botanical Institute, University of Cologne, Cologne, Germany, [2] Max Planck Institute for Plant Breeding Research, Cologne, Germany, [3] Max Planck Institute for Terrestrial Microbiology, Marburg, Germany, [4] Institute of Chemical Biology, University of Duisburg-Essen, Essen, Germany

Plant proteases are key regulators of plant cell processes such as seed development, immune responses, senescence and programmed cell death (PCD). Apoplastic papain-like cysteine proteases (PL) are hubs in plant-microbe interactions and play an important role during abiotic stresses. The apoplast is a crucial interface for the interaction between plant and microbes. So far, apoplastic maize PL and their function have been mostly described for aerial parts. In this study, we focused on apoplastic PLCPs in the roots of maize plants. We have analyzed the phylogeny of maize PLCPs and investigated their protein abundance after salicylic acid (SA) treatment. Using activity-based protein profiling (ABPP) we have identified a novel root-specific PLCP belonging to the RD21-like subfamily, as well as three SA activated PLCPs. The root specific PLCP CP1C shares sequence and structural similarities to known CP1-like proteases. Biochemical analysis of recombinant CP1C revealed different substrate specificities and inhibitor affinities compared to the related proteases. This study characterized a root-specific PLCP and identifies differences between the SA-dependent activation of PLCPs in roots and leaves.

Keywords: root, apoplast, PLCP, organ specific, salicylic acid

OPEN ACCESS

Edited by:
Mercedes Diaz-Mendoza, Centro de Biotecnología y Genómica de Plantas (CBGP), Spain

Reviewed by:
Junya Mizoi, The University of Tokyo, Japan
Barend Juan Vorster, University of Pretoria, South Africa

***Correspondence:**
Johana C. Misas Villamil
jmisas@uni-koeln.de
Gunther Doehlemann
g.doehlemann@uni-koeln.de

†Present address:
Farnusch Kaschani, Institute of Chemical Biology, University of Duisburg-Essen, Essen, Germany
Karina van der Linde, Cell Biology and Plant Biochemistry, University of Regensburg, Regensburg, Germany
Thomas Colby, Max Planck Institute for Biology of Ageing, Cologne, Germany

Specialty section:
This article was submitted to Plant Proteomics, a section of the journal Frontiers in Plant Science

Received: *15 February 2019*
Accepted: *28 March 2019*
Published: *30 April 2019*

Citation:
Schulze Hüynck J, Kaschani F, van der Linde K, Ziemann S, Müller AN, Colby T, Kaiser M, Misas Villamil JC and Doehlemann G (2019) Proteases Underground: Analysis of the Maize Root Apoplast Identifies Organ Specific Papain-Like Cysteine Protease Activity. Front. Plant Sci. 10:473. doi: 10.3389/fpls.2019.00473

INTRODUCTION

Proteases determine a variety of biological processes ranging from organ maturation, senescence and programmed cell death (PCD) (van der Hoorn and Jones, 2004; van der Hoorn, 2008). They perform cleavage of substrates into small fragments by catalyzing peptide bond hydrolysis. Proteases are classified into four main classes according to their catalytic site: cysteine proteases, serine proteases, aspartic proteases, and metalloproteases (Rawlings et al., 2018). Cysteine proteases are further subdivided into 14 super families, each using the catalytic triad or dyad in a different structural fold, representing convergent evolution of the catalytic mechanism (Rawlings et al., 2018). In this study we are focusing on papain-like cysteine proteases (PLCP). PLCPs are classified into clan CA based on their structural similarity to papain and conserved catalytic residues (Rawlings et al., 2018). They are divided into family C1B (cytosolic) and C1A (apoplastic) and

further subdivided into nine subfamilies based on phylogeny (Richau et al., 2012). PLCPs are known to be involved in growth related senescence (Noh and Amasino, 1999a; McLellan et al., 2009), PCD (Gilroy et al., 2007; Coll et al., 2011; Lampl et al., 2013), predicted to be important for resource acquisition (Adamczyk et al., 2010) and act as hubs in plant immunity, where they are involved in the perception of microbes, initiation of signaling cascades and activation of responses against pathogens (Misas-Villamil and van der Hoorn, 2008; Jashni et al., 2015; Misas-Villamil et al., 2016). Due to their crucial roles in the regulation of various cellular processes, PLCP activity is tightly controlled via autocatalytic posttranslational modifications, as well as by endogenous inhibitors such as cystatins and serpins (Martinez and Diaz, 2008; Ochieng and Chaudhuri, 2010; Martínez et al., 2012; van der Linde et al., 2012a; Lampl et al., 2013). PLCPs carry a signal peptide important for their transport to the apoplast as well as an auto inhibitory prodomain prior to the active C1-protease domain. Some members of the subfamily 1 (RD21) and 4 (XBCP3) contain a granulin domain sharing homology with granulins/epithelin which are growth hormones in animals, released after wounding (Bateman and Bennett, 1998, 2009; Richau et al., 2012). PLCPs contain the conserved catalytic triad Cys, His, Asn. Their general enzymatic activity involves a nucleophilic attack of the thiol-group at the substrate carboxyl-terminus where His acts as a proton acceptor (base) for the catalytic Cys and Asn plays an important role for the orientation of the His (Rawlings et al., 2018).

Maize is one of the most important crop plants. It does not only play an important role for human consumption but also for feeding of livestock and the production of biofuels as an alternative to petrol (FAO, 2012; Ranum et al., 2014). Different models predict that due to climate change the yield of maize might decrease by 2055 up to 10% in some areas like Africa (Jones and Thornton, 2003). This loss has to be compensated by improvements in plant breeding and pest control. To be able to cope with pests we need a better understanding of the interaction between plants and its associated microbes both, in the phyllosphere and the rhizosphere. Maize associates with a variety of microbes, which might lead to either beneficial effects on plant growth such as the interaction with arbuscular mycorrhizal fungi (Subramanian et al., 2013; Bárzana et al., 2014) or to tremendous damage on the plant such as the interaction with the biotrophic fungus *Ustilago maydis* (Brefort et al., 2009) or the necrotrophic pathogen *Fusarium verticillioides* (Duncan and Howard, 2009; Barreau et al., 2010).

Most plants and microbes interact via the apoplast, which contains different types of defense components such as cysteine proteases and toxic metabolites (Ökmen and Doehlemann, 2016). Previously, we have demonstrated the importance of maize apoplastic leaf PLCPs for plant immunity and during *U. maydis* infection. We found an endogenous cystatin to be able to suppress host immunity acting as a compatibility factor (van der Linde et al., 2012a,b), a fungal effector that inhibits apoplastic PLCPs in order to suppress defense responses (Mueller et al., 2013) and an endogenous peptide that requires PLCP activity for its release from the propetide molecule, leading to activation of salicylic acid (SA) defense signaling (Ziemann et al., 2018).

In this study, we investigate apoplastic PLCPs in maize roots. Using a proteomics approach, we have identified different PLCPs activated by SA treatment in roots. Moreover, we have identified and biochemically characterized the novel root specific PLCP, CP1C. In comparison to the well characterized CP1A and CP1B proteases, CP1C shows a distinct substrate specificity and inhibitory profile, albeit their structure and sequence similarities.

RESULTS

Leaf and Root Apoplastic Proteomes Show Differential PLCP Activities

The maize genome encodes 52 PLCP (Rawlings et al., 2018) localized in different compartments such as cytoplasm, vacuoles, vesicles and apoplast. In leaf proteomes, SA has been described to activate apoplastic PLCPs (van der Linde et al., 2012a). Root apoplastic fluids (RAF) of maize seedlings treated with SA were isolated to analyze the effect of SA on the activation of root PLCPs. Fractionation of RAF by ion exchange chromatography followed by an *in vitro* activity assay using the substrate Z-FR-AMC showed one distinct peak corresponding to leaf apoplastic PLCPs (**Figure 1A**) and three distinct peaks representing elevated PLCP activities in roots (**Figure 1B**). Pre-treatment of leaf and root apoplastic proteomes with the specific PLCP inhibitor E-64 abolished this activity (**Figures 1A,B**). Interestingly, the observed activity pattern of the root apoplast significantly differs from the leaf apoplast since the leaf proteome shows 10–20-fold lower activity compared to RAF (**Figures 1A,B**). In a following step, protein fractions corresponding to the three major peaks observed in **Figure 1B** were pooled and active PLCPs were labeled using DCG-04, a probe that binds covalently and irreversible to the active site of PLCPs allowing us to monitor the availability of active sites rather than their abundance (Greenbaum et al., 2000; van der Hoorn et al., 2004). Taking advantage of the biotin tag present in DCG-04, a pull down purification of labeled proteins was performed. Signals corresponding to labeled proteins of different molecular weights, were excised from the gel and subjected to an in – gel digest (IGD) mass spectrometry analysis (**Figure 1C**, position A–C). Five apoplastic PLCPs have been identified (**Figure 1D**). The two CP1-isoforms, CP1A and CP1B, as well as CP2 and XCP2 were detected in roots, correlated to previous identification in the leaf apoplast (van der Linde et al., 2012a). In addition, we found a third CP1-like PLCP, CP1C that has not been previously identified in leaves (**Figure 1D**). CP1C was the only PLCP found in position A and B of peak 1 and it was additionally found in position A of peak 2. In contrast, CP1A and CP1B were not found in peak 1 but in all positions of peak 2 as well as in position B and C of peak 3. The fact that CP1C was fractionated at different volumes than CP1A and CP1B might indicate distinct biochemical properties of CP1C compared to the other two isoforms. All identified unique peptides were located in the predicted protease C1 domain (CD) and confirms the success of the DCG-04 pull down targeting active proteases (**Figure 1E**). Taken together, the comparison of active PLCPs in leaf- and root proteome revealed the presence of the four PLCPs CP1A, CP1B, CP2, and XCP2, previously identified in the leaf apoplast

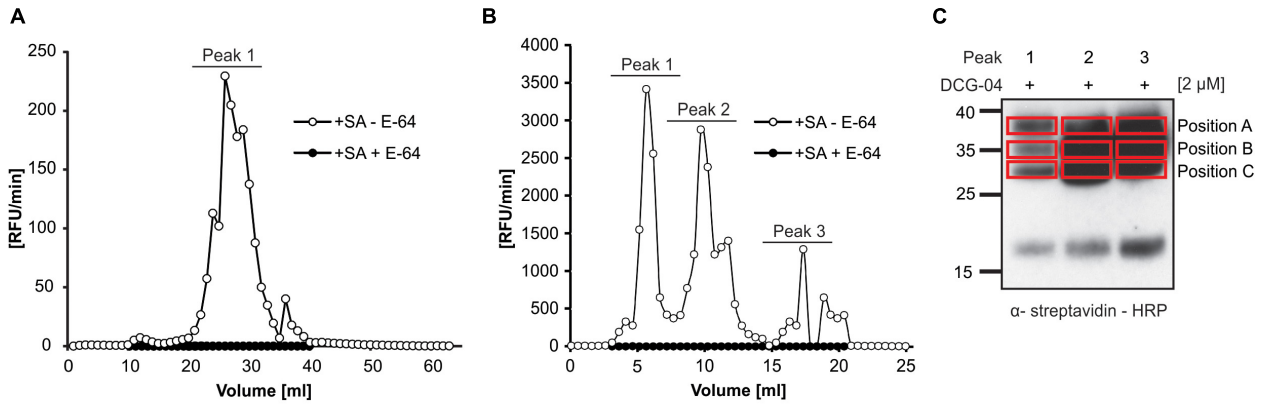

D

Peak	Position	ID	Database entry	Apoplast Leaf*	Apoplast Root
1	A, B	CP1C	GRMZM2G340065	✗	✓
2	A	CP1C	GRMZM2G340065	✗	✓
	A, B, C	CP1A	GRMZM2G166281	✓	✓
	A, B, C	CP1B	GRMZM2G073465	✓	✓
	C	CP2	GRMZM2G038636	✓	✓
3	B, C	CP1A	GRMZM2G166281	✓	✓
	B, C	CP1B	GRMZM2G073465	✓	✓
	B, C	XCP2	GRMZM2G066326	✓	✓

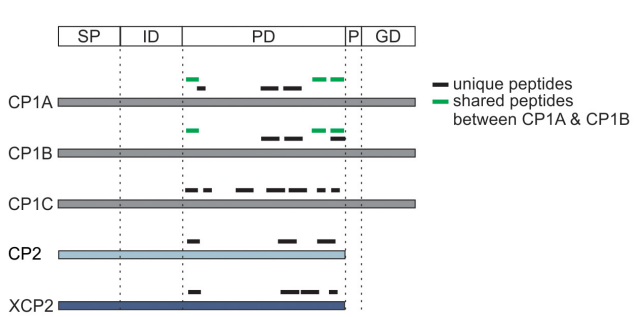

FIGURE 1 | Identification of maize root PLCPs after ion-exchange chromatography. **(A)** Leaf apoplastic fluid (LAF) and **(B)** root apoplastic fluid (RAF) of maize leaves or roots, pre-treated with 2 mM salicylic acid (+SA) were isolated and fractionated using ion exchange chromatography (IEC). Fractions were tested for PLCP activity using 10 µM of the substrate Z-FR-AMC with (+) or without (–) 2 µM E-64. The release of AMC (relative fluorescent unit = RFU) per minute was measured and plotted against fraction volume. Peaks represent fractions of higher PLCP activity that were inhibited when using E-64. **(C)** DCG-04 labeling of fractions corresponding to different peaks **(B)** were pooled and labeled with 2 µM DCG-04 for 2 h. Samples were separated by SDS-PAGE and detection of biotinylated proteins was performed using an α-streptavidin-HRP antibody. Red squares mark samples subjected to in gel digest (IGD) and MS analysis. Peaks 1, 2, and 3 correspond to pooled fractions **(B)** and position A, B, and C mark size separated signals of each peak loaded. **(D)** Identification of apoplastic root PLCPs and comparison with leaf proteome. Apoplastic root-PLCPs identified by MS analysis were compared to PLCPs previously published in leaf apoplastic fluid by van der Linde et al., 2012a (*). Peak and position **(B,C)** of PLCPs identified in this study as well as PLCP presence (✓) or absence (×) is indicated. **(E)** Analysis of peptides found by mass spectrometry. Displayed is a schematic representation of the identified PLCPs and the position of peptides found: SP, signal peptide; ID, autoinhibitory prodomain; PD, protease C1-domain; P, proline-rich domain; GD, granulin domain. Unique peptides are labeled in black and shared peptides are labeled in green.

(van der Linde et al., 2012a), as well as one additional root specific PLCP: CP1C.

We further aimed to characterize the novel root PLCP CP1C and shed light on its role during SA signaling in the root apoplast. We labeled RAF from plants pre-treated with 2 mM SA or mock using DCG-04. Besides an increase in activity, we also noticed a shift into lower molecular weight signals after treatment with SA, suggesting that some PLCPs become less active, while others are activated through SA treatment (**Figure 2A**). To confirm the observed root specificity we also examined the expression pattern of CP1C in comparison to the other four MS-detected PLCPs and Cathepsin B (CathB) which has been previously identified in leaves (van der Linde et al., 2012a). Using publicly available B73 expression data of untreated maize leaves and roots (maizegdb.org), PLCP expression patterns were displayed using a heat map in which root gene expression was normalized to leaves (**Figure 2B**). Overall, apoplastic PLCPs seem to be higher expressed in roots compared to leaves, which correlates with the higher enzyme activity level observed in roots compared to leaves (**Figures 1A,B**). CP1B, CP2, XCP2, and CathB show a slightly higher expression level in roots, whereas CP1A expression is slightly stronger in leaves (**Figure 2B**). CP1C transcripts are detected in leaves, but its expression is about sixfold higher in roots (**Figure 2B**). Remarkably, of all six PLCPs, CP1C shows the strongest differential expression in roots compared to leaves. To understand if the expression levels found for the PLCPs correlate with their abundance and their activity we performed shot-gun analysis together with a DCG-04 pull down. We describe abundance as the total pool of proteins, active or inactive present in the proteome. Roots of maize seedlings were treated with mock or SA. After 2 days root apoplastic fluid was isolated and one part was used for shot-gun analysis and the other part was labeled with DCG-04 (**Figure 2C**). A comparison between protein abundance in mock vs. SA treated samples has been represented using a volcano plot (**Figure 2D**). Several proteins related to the SA pathway such as thioredoxins, shikimate biosynthesis and pathogenesis related PR10 protein increased their abundance in the SA treated samples, confirming a successful SA treatment (**Supplementary Table 1**; Tada et al., 2008; Chen et al., 2010; Dempsey et al., 2011). Interestingly, we found that the abundance

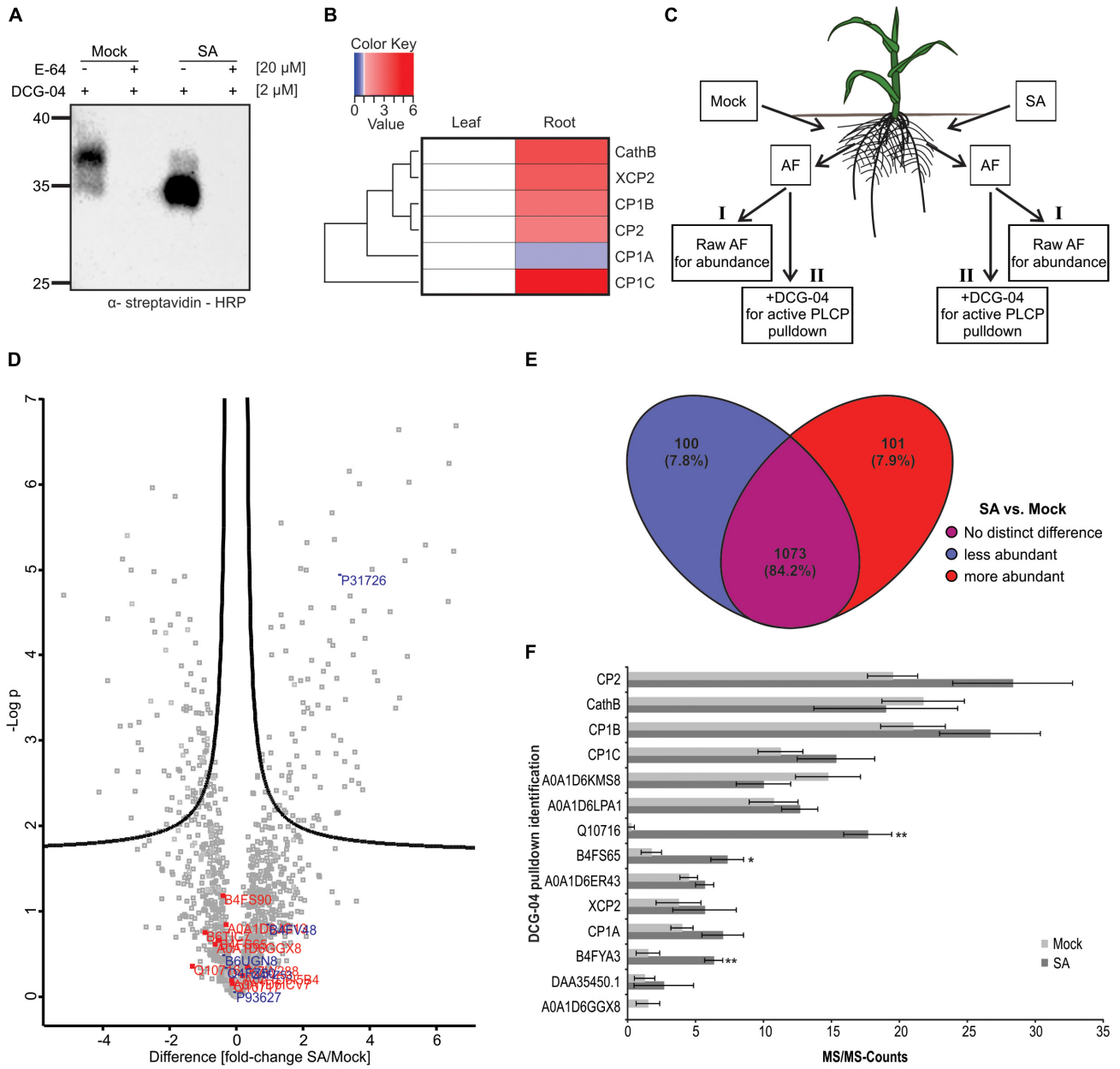

FIGURE 2 | Abundance and activity of root apoplastic PLCPs after SA treatment. **(A)** DCG-04 labeling of root apoplastic fluid (RAF) pre-treated with 2 mM salicylic acid or mock. RAF was preincubated for 30 min either with 20 µM E-64 or DMSO. Then samples were labeled with 2 µM DCG-04 for 2 h and analyzed on a SDS-gel. Biotinylated proteins were detected using an α-streptavidin-HRP antibody. **(B)** Expression pattern of six apoplastic PLCPs. Relative expression of root apoplastic maize PLCPs in untreated B73 based on publicly available data (Winter et al., 2007; Sekhon et al., 2011; Andorf et al., 2016; Stelpflug et al., 2016). Mean expression of leaves and roots at different developmental stages was calculated and normalized to leaf expression for individual PLCPs. The heat map represents a one – to – one comparison for each PLCP. PLCPs were clustered based on their relative expression pattern to leaves. **(C)** Schematic overview of MS experimental setup. Roots of maize plants were treated with 2 mM SA or mock. Apoplastic fluid of four biological replicates was isolated 12 h after treatment. One part of the apoplastic fluid was used for shotgun analysis to investigate protein abundance (I) and the other part was used for a DCG-04 pull down of labeled PLCPs followed by OBD (II). Both, samples I and II, were subjected to mass spectrometry analysis for protein identification and quantification. Modified from Guillaume (2017). **(D)** Protein abundance in roots after SA treatment. A comparison of protein abundance between mock- and SA-treated RAFs is displayed in a volcano plot. Fold change differences between treatments against negative log *p*-value is plotted. Cysteine proteases are labeled in red and cysteine protease inhibitors are labeled in blue. **(E)** Comparison of protein abundance after SA treatment. Changes in protein abundance after SA treatment compared to mock-treated plants were displayed using a Venn diagram. Total numbers of identified proteins and percentages are indicated. Significantly less abundant proteins in SA-treated samples are labeled in blue. No significant differential proteins are labeled in purple and significantly more abundant proteins are shown in red. **(F)** Activation of PLCPs after SA treatment. DCG-04 labeled samples were analyzed and compared between treatments. MS/MS-counts were plotted against identified PLCPs in both treatments. MS/MS-counts of SA treatments are labeled in dark gray and MS/MS-counts of mock-treated samples are labeled in light gray. The experiments were performed using four independent biological replicates. Error bars represent the SEM. *P*-values were calculated with an unpaired *t*-test. $^{*}P < 0.05$; $^{**}P < 0.01$.

of the cystatin P31726, an endogenous cysteine protease inhibitor, was increased almost fourfold after SA treatment whereas the abundance of other cysteine protease inhibitors did not change (**Figure 2D**, blue). Remarkably, the total abundance of PLCPs did not change after SA treatment (**Figure 2D**, red) suggesting a posttranslational activation (**Figure 2A**). The majority of proteins (84.2%) do not change significantly in abundance upon SA treatment but 7.9% show differential behavior being significantly more abundant in the apoplast after SA treatment (**Figure 2E**). To get more insight into the SA-effect on activation of apoplastic PLCPs we performed a DCG-04 pull down of SA treated and mock plant AFs followed by an on bead digest (OBD) and mass spectrometry analysis. MS/MS counts were plotted against identified proteins (**Figure 2F**). The majority of peptides found in this pull down correspond to PLCPs (**Supplementary Table 2**) confirming an enrichment of those proteases after DCG-04 labeling. We found again peptides for CP1A, CP1B, CP1C, CP2, and XCP2 in agreement with the previously described IGD made from samples separated by ion-exchange chromatography (IEC) (**Figures 1E**, **2F**). Additionally, we found CathB, which has so far not been identified in the previous MS analysis made for maize root apoplast (**Figures 1D,E**, **2F**) likely, due to its isoelectric point of 5.49 close to the conditions used for the IEC (pH 6). Remarkably, the activities of the previously characterized PLCPs CP1A, CP1B, CP1C, CP2, XCP2, and CathB and five additionally detected PLCPs do not change significantly after SA treatment compared to mock. In contrast, three other PLCPs were identified with significantly increased activity, up to 70-fold, after SA treatment: B4FS65 belonging to the cysteine protease superfamily, B4FYA3 a xylem bark cysteine peptidase and Q10716 a cysteine proteinase 1 (**Figure 2F** and **Supplementary Figure 1**). With these experiments, we demonstrate the presence of the previously leaf identified PLCPs, CP1A, CP1B, CP1C, CP2, and XCP2 in the root apoplast and additionally, we identify CathB together with other eight PLCPs, which have not been previously found in the IEC root apoplast analysis. Three of the newly identified PLCPs seem to be activated upon SA treatment.

To get insights into the subfamily classification of the newly identified root apoplastic proteases we evaluate the sequence similarity of maize apoplastic PLCPs using phylogeny. A total of 52 maize PLCP sequences from B73 retrieved from the MEROPS database (Rawlings et al., 2018) and our six identified PLCPs from Early Golden Bantam (EGB) were used to generate a phylogenetic tree with the maximum likelihood method. Additionally, for the subfamily classification we included one type member of each PLCP subfamily of *A. thaliana* (Richau et al., 2012). Two serine proteases from *A. thaliana* (AtDGP11 and AtDEGP2) were used as outgroup (Beers et al., 2004; Richau et al., 2012). PLCPs were classified into nine subfamilies: RD21 (1), CEP1 (2), XCP2 (3), XBCP3 (4), THI1 (5), SAG12 (6), RD19A (7), AALP (8), and CTB3 (9). The largest group of maize PLCPs belongs to the RD21 subfamily (12 members), followed by members of the SAG12 subfamily (11 members) and the THI1 subfamily (10 members). Other PLCP subfamilies are represented by few members (**Figure 3**). All identified apoplastic CP1-like PLCPs, CP1A, CP1B, and CP1C carrying a granulin domain, cluster together into the subfamily 1 of RD21, whereas CathB, CP2, and XCP2 grouped into the subfamilies CTB3, AALP, and XCP2, respectively (**Figure 3**). The SA activated PLCP B4FS65 (MER036246) belongs to the THI1 subfamily, whereas Q10716 (MER0001404) was found to be present in the RD19A subfamily (**Figure 3**). Sequence alignment of the SA activated PLCP B4FYA3 (MER0137791) showed high sequence similarity to CP14 belonging to subfamily XBCP3. B4FYA3 is homolog to *Nicotiana benthamiana* and *N. tabaccum* CP14, proteins described to be involved in PCD (Zhao et al., 2013; Paireder et al., 2016).

Altogether, we showed that PLCP expression and activity in root is higher than in leaf apoplast. A comparison of root PLCP abundance vs. activity after SA treatment indicates that PLCP activation likely occurs posttranslationally. Furthermore, we have identified three SA-activated root PLCPs, not previously detected in leaves, suggesting a different mechanisms of SA signaling through PLCPs in different organs.

CP1C Is a Root Specific Apoplastic PLCP

Granulin containing PLCPs of the subfamily 1, such as Mir1 from maize or RD21 from Arabidopsis are known to play crucial roles related to plant defense and senescence (Lopez et al., 2007; Shindo et al., 2012). Here, we have identified CP1C, a root specific granulin containing PLCP closely related to CP1A and CP1B. All three CP1-like proteases are apoplastic localized, consistent with their higher activity at low pH (**Supplementary Figure 4**). Sequence analysis of mature CP1C compared to CP1A and CP1B revealed high similarities, 74% identity, at the amino acid level (**Figure 4A**). All three proteases contain a predicted N-terminal secretion signal, an autoinhibitory prodomain and a C-terminal granulin domain (**Figure 4A**). CP1C catalytic triad consists of three main residues: C179, H316, and N336, as well as Q173, which is believed to stabilize the oxyanion during the catalytic reaction (**Figures 4A,C**). We observed sequence variation between predicted domains, e.g., signal peptide and autoinhibitory prodomain and between autoinhibitory prodomain and protease C1-domain and at the C-terminal granulin domain (**Figure 4A**). To further analyze CP1C at the structural level a three dimensional model was predicted based on caricain (PDB: 1pciA) (Groves et al., 1996; Kelley et al., 2015). An overlay of the models predicted for the mature CP1A and CP1C was performed. The majority of residue changes appeared to be located on the surface of the proteins (**Figure 4B**). Out of 53 different surface residues between CP1A and CP1C 25 were predicted to cause a minor impact for the structure due to similar biochemical properties. Of all changes, only three amino acids were located inside CP1C: D172N, A186S, and K335R. All three amino acids are predicted to be located close to the active site (**Figure 4C**). Interestingly, the catalytic groove seems to be narrower in CP1C compared to CP1A. A different orientation of the basic amino acids K335R close to N336 between CP1A and CP1C might explain the distinct catalytic properties and substrate preferences (**Figure 4C**). Altogether, CP1A and CP1C seem to share similar sequence homology and structure although differences on the surface of CP1C might result into different interaction partners.

To study if CP1C also shares biochemical properties with other apoplastic PLCPs, found in roots and leaves, we analyzed

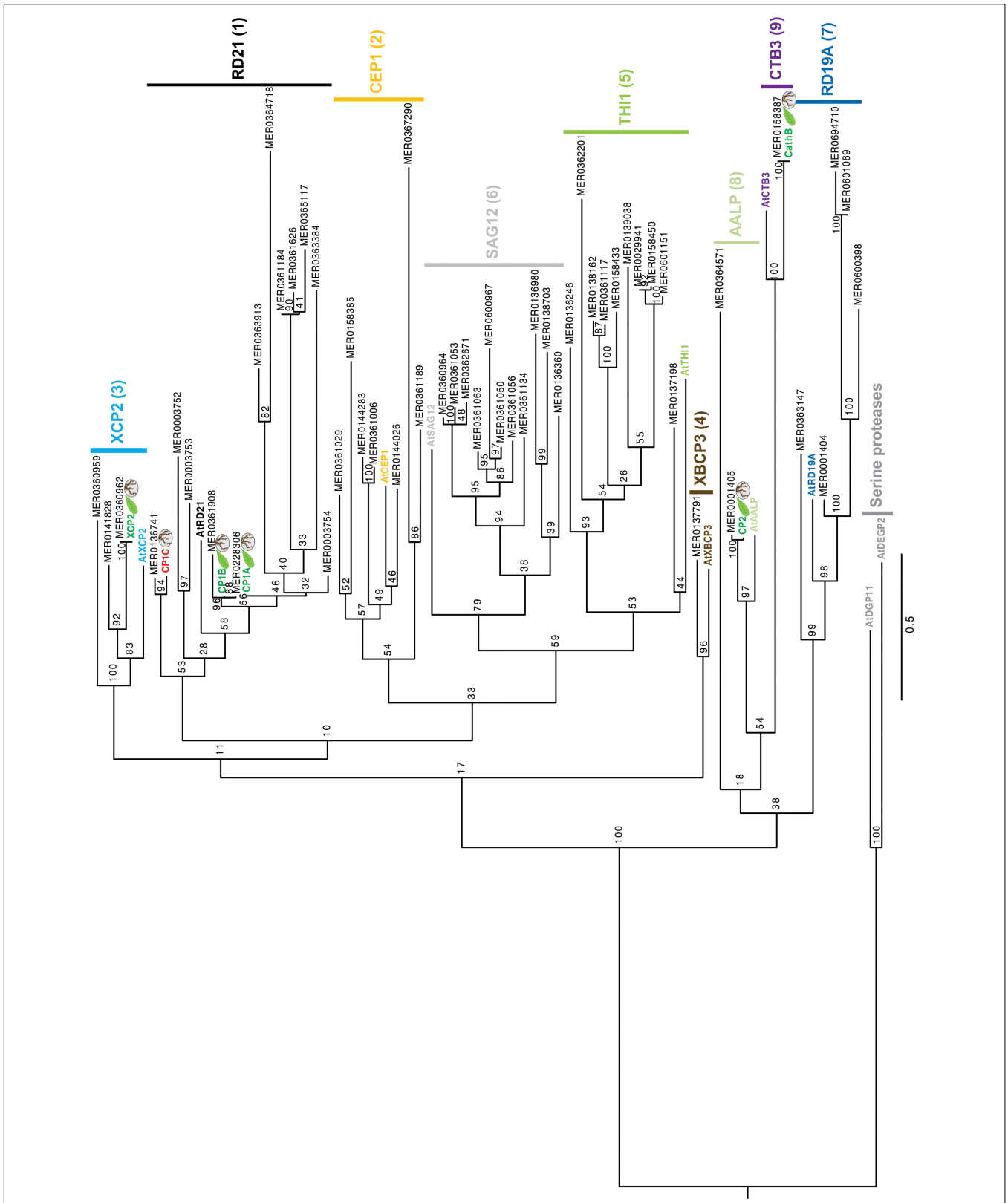

FIGURE 3 | Phylogeny of apoplastic maize-PLCPs. 52 maize PLCP sequences of the line B73 retrieved from the MEROPS database (Rawlings et al., 2018) as well as our six identified PLCPs from Early golden Bantam (EGB) were used to generate a phylogenetic tree.Additionally, we included one type member of each

(Continued)

FIGURE 3 | Continued
PLCP subfamily of *A. thaliana* and two serine proteases DEGP2 and DGP11 from *A. thaliana* as outgroup (Beers et al., 2004; Richau et al., 2012). For the phylogenetical analysis we used full length sequences including signal peptide, prodomain, protease C1-domain and, if present, granulin domain as was described before in Richau et al. (2012). The tree is drawn to scale, with branch lengths measured in the number of substitutions per site. Sequences were aligned using MAFFT (v7.407) (Katoh and Standley, 2013; **Supplementary Table 5**). RAxML with the GTRGAMMA substitution model (v8.2.0) was used for the construction of the tree (Stamatakis, 2014). The robustness was assessed using 100 bootstrap replicates. Apoplastic EGB maize PLCPs were highlighted according to the organs they were found in: leaves (green) roots (red). Numbers indicate the PLCP subfamilies based on Richau et al. (2012).

their substrate specificity. CP1A, CP1B, CP1C, XCP2, CP2, and CathB were transiently overexpressed in *N. benthamiana* using Agrobacterium and after 3 days apoplastic fluids were isolated and tested for their activity using the activity-based probe MV201 (Richau et al., 2012; **Figure 5A**). Additionally, the catalytic inactive mutant of $CP1A^{mut}$ was used as a negative control, as well as overexpressed cytosolic GFP. Both, $CP1A^{mut}$ and GFP allowed us to differentiate the endogenous activity of *N. benthamiana* PLCPs from the overexpressed maize PLCPs (**Figure 5A** and **Supplementary Figure 2**). Apoplastic fluids were tested in a substrate – cleavage assay using 10 μM of four synthetic substrates coupled to a 7-amino-methyl-coumarin (AMC): Phe-Arg-AMC (FR), Phe-Val-Arg-AMC (FVR), Leu-Arg-AMC (LR) and Arg-Arg-AMC (RR). Activity was then normalized to the $CP1A^{mut}$ and the GFP-control. All these substrates differ in their residue at the P2-position which has been previously identified to be crucial for PLCP activity (Turk et al., 1995; Paireder et al., 2016, 2017). PLCP activities were normalized to the highest activity tested (set to 1) and were represented in a heat-map (**Figure 5C**). We observed that all overexpressed PLCPs show a preferred cleavage activity for the substrate LR (**Figures 5B,C**). The basal PLCP activity of *N. benthamiana* also shows LR cleavage preference although with reduced levels in comparison to the overexpressed samples (**Supplementary Figure 2**). CP1A and CP1B also cleave RR, FR, and FVR despite CP1B slightly preference for FR. Strikingly, the root specific CP1C differs in the substrate cleavage preference from CP1A and CP1B. It mostly processes the LR-substrate displaying only trace amounts of activity toward other substrates. This LR unique cleavage preference resembles the cleavage specificities of XCP2 and CathB (**Figures 5B,C**). CP2 shows generally very low cleavage activity toward the tested substrates (**Figure 5B**), although it is active and highly overexpressed in *N. benthamiana* (**Figure 5A**). The low cleavage activity of CP2 indicates distinct substrate specificities for this protease in comparison to the other tested apoplastic PLCPs.

As a second approach to the biochemical characterization of CP1C, we tested the inhibitory profile of apoplastic CP1-like PLCPs toward characterized inhibitors: E-64, a covalent and irreversible PLCP inhibitor (Hanada et al., 1978; Barrett et al., 1982), CC9, an endogenous cystatin (van der Linde et al., 2012a) and cMIP, a conserved microbial inhibitor of proteases shown to inhibit maize PLCPs (Misas-Villamil et al., 2019). To test their inhibitory efficiency toward the CP1-like PLCPs, we performed an inhibitor concentration range using a substrate cleavage assay with Z-LR-AMC. Equal amounts of active PLCPs were used based on signal quantification from MV201 labeled apoplastic fluids (**Supplementary Figure 3**). The cleavage activity of each PLCP in the absence of inhibitors was set to 1 and plotted against Log of inhibitor concentration. E-64 and CC9 show strong inhibition of PLCPs already in the nanomolar-range, with E-64 being a stronger inhibitor for all tested PLCPs than CC9 (**Figures 6A,B**). On the contrary, micromolar concentrations of cMIP were needed to reach inhibition (**Figure 6C**). CP1C is most susceptible toward E-64 compared to CP1A and CP1B (**Figure 6A**) and shows a tendency to be less susceptible toward CC9 (**Figure 6B**). Strikingly, cMIP is least effective for CP1B and most effective for CP1A inhibition. CP1C shows an intermediate susceptibility toward cMIP and at lower inhibitor concentrations, between 30 and 250 nM, CP1C activity seems to be enhanced. On the contrary, CP1A and CP1B show a gradually, dose-dependent reduction in activity with increasing cMIP concentration (**Figure 6C**).

In this work we found that apoplastic PLCP expression and activity differ in leaf and root proteomes and that PLCP activity after SA treatment is likely a posttranslational process. We identified three different SA-activated PLCPs in roots, not detected in leaves, suggesting a divergent mechanism of SA signaling through distinct PLCPs in different organs. Additionally, we identified CP1C, a root specific CP1-like PLCP of the RD21 subfamily. CP1C shows structure and sequence similarities to CP1A but displays different substrate specificity and inhibitor susceptibility. Differences at the surface and in close proximity to the catalytic triad might suggest distinct interaction partners.

DISCUSSION

In this study we characterized changes in protein abundance and activity of RAF of maize seedlings after SA treatment. We specifically focused on the activity of PLCPs which have been described as hubs during plant immunity (Misas-Villamil et al., 2016). We have identified and biochemically characterized CP1C, a novel root specific PLCP sharing sequence homology to the Arabidopsis RD21 subfamily (subfamily 1).

Mass spectrometry analysis of IEC samples identified CP1C mostly present in peak 1 whereas CP1A and CP1B appeared in the second and third peak. The differences in fractionation can be attributed to differential charges. CP1C has a higher isoelectric point (pI: 5.55, without signal peptide and prodomain) compared to CP1A and CP1B (pI: 5.09 and 5.10, without signal peptide and prodomain, respectively). A lower pI corresponds to a stronger negative charge at a specific pH. We have performed IEC at pH 6 which results in a stronger binding to the resin of proteins with lower pI and elution at higher salt concentrations. The differences in elution of CP1A, CP1B, and CP1C are therefore in line with their respective pI of the mature protein. Comparing

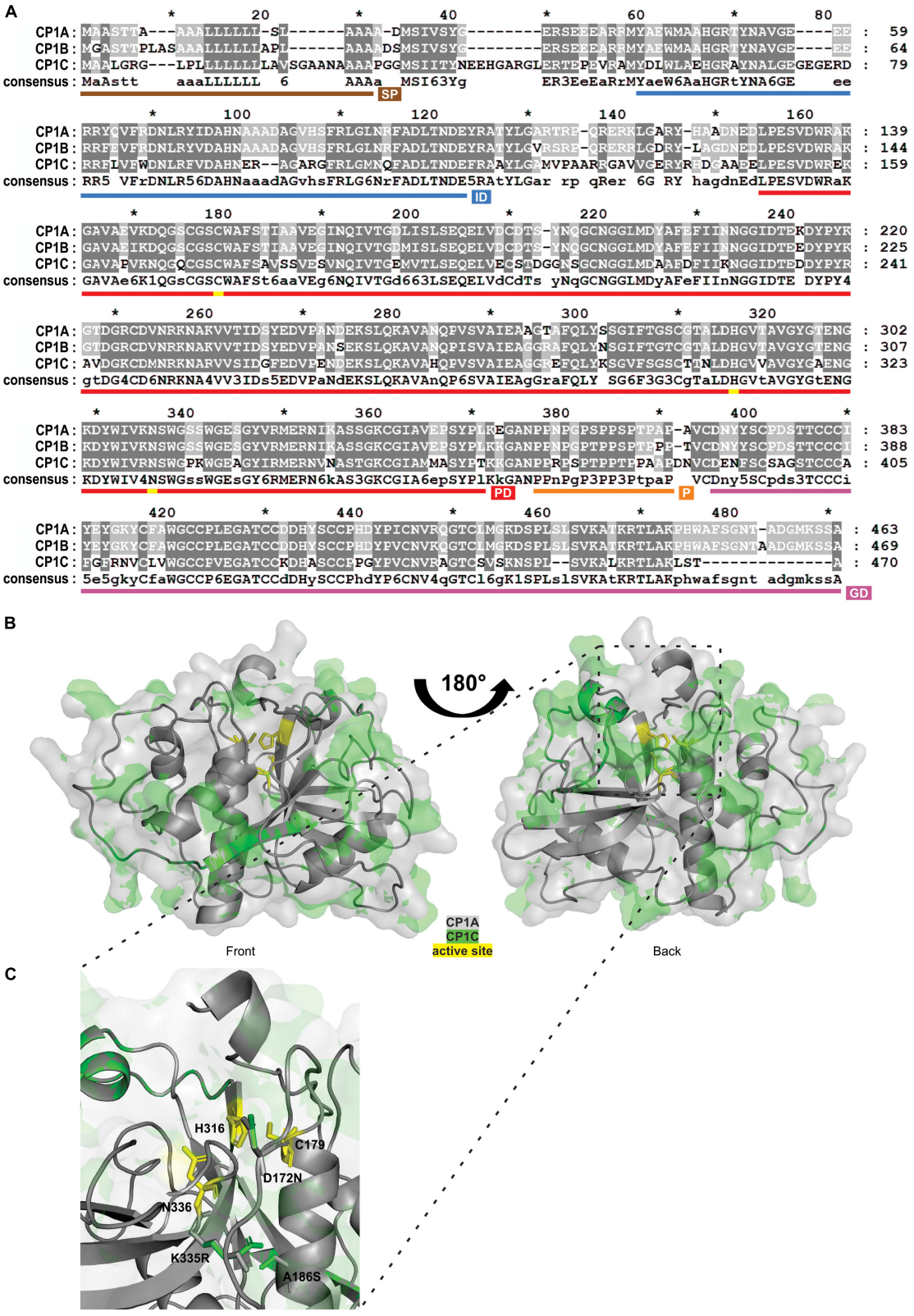

FIGURE 4 | Sequence and structural comparison of maize apoplastic CP1-like PLCPs. **(A)** Sequence homology between CP1-like PLCPs. Amino acid sequences of apoplastic CP1-like PLCPs: CP1A, CP1B, and CP1C of the maize line EGB were aligned to evaluate their sequence conservation. Dark gray background

(Continued)

FIGURE 4 | Continued
indicates conserved amino acids among all three PLCPs, light gray background indicates similar amino acids among two PLCPs and white background indicates different amino acids. Signal peptide (SP, brown), autoinhibitory prodomain (IP, blue), protease C1-domain (PD, red), proline-rich domain (P, orange), and granulin-domain (GD, purple) were predicted. Amino acids forming the catalytic triad C179, H316, N336 are labeled in yellow. **(B)** Structure similarities between CP1A and CP1C. A 3D-model of superimposed mature CP1A and CP1C was generated. CP1A (gray) and CP1C (green) from EGB were modeled without signal peptide, autoinhibitory prodomain and granulin-doman using Phyre2 (Kelley et al., 2015) based on the crystal structure of caricain PDB: 1pciA (Groves et al., 1996). The catalytic triad C179, H316, N336 is indicated in yellow. **(C)** Close-up of the catalytic triad of superimposed CP1A and CP1C. Differences in the catalytic grooves of CP1A and CP1C (B) were examined. The catalytic triad C179, H316, N336 is indicated in yellow. Amino acid differences D172N, A186S, and K335R were modeled from CP1A (gray) to CP1C (green).

PLCP activity of root apoplastic fluid of SA-treated and mock-treated plants, we detected an overall increased activity after SA treatment and also a shift to lower molecular weight (MW) signals (**Figure 2A**). The size shift might be caused by an inactivation of higher MW PLCPs, like CP1C (**Figures 1C,D**) and an activation of other PLCPs with lower MW. Because CP1C was not differentially activated after SA treatment one could assume that this protease is not involved in root SA signaling.

Analysis of the protein abundance after SA treatment showed an increase of proteins associated with SA-signaling like thioredoxins (Tada et al., 2008), shikimate biosynthesis protein (Dempsey et al., 2011) and pathogenesis related PR10 (Chen et al., 2010), confirming the success of the treatment. We also noticed that the abundance of cysteine protease inhibitors did not change after SA treatment except for the cystatin P31726 (Psei1) suggesting a role in closer PLCP regulation after SA treatment (Turk and Bode, 1991). In contrast to CC9, which is highly expressed in leaves, the cystatin P31726 shows sequence similarity to AtCys1, an Arabidopsis cystatin found to be involved in cell death inhibition (Belenghi et al., 2003).

All six apoplastic PLCPs previously identified did not change in abundance upon SA treatment, indicating that the higher activity observed could be due to a posttranslational activation rather than transcriptional regulation. PLCPs can be posttranslational activated through pH shifts, e.g., after translocation into the apoplast (Felle, 1998; Kosegarten et al., 1999; Feliciangeli et al., 2006; Schröder et al., 2010). Posttranslational activation of PLCPs occurs through cleavage of the prodomain from the protease domain (Bryan, 2002). Using DCG-04 labeling we could selectively pull down active PLCPs and compare their activity to their abundance after SA treatment. Surprisingly, we did not observe any of the six previously identified PLCPs, also present in leaves besides CP1C, being more active after SA treatment. Due to the high microbial interaction pressure on roots (Young and Crawford, 2004) compared to aerial parts (Andrews and Harris, 2000; Lindow and Brandl, 2003) the root specific CP1C might be involved in a in a different biological process not directly related to SA signaling. CP1C could be involved in processes such as senescence and apoptosis during the root-development described for other PLCPs such as SAG12 (Lohman et al., 1994; Noh and Amasino, 1999b; Otegui et al., 2005). It could also play a role in nitrogen uptake as shown for other root PLCPs (Godlewski and Adamczyk, 2007; Rentsch et al., 2007; Paungfoo-Lonhienne et al., 2009).

Interestingly, we have identified three PLCPs (B4FS65, B4FYA3, and Q10716) activated after SA treatment. We did not see changes in their abundance indicating that these PLCPs are likely activated via posttranslational modifications. B4FS65 belongs to the THI1 subfamily in which a representative member is the cysteine protease 51 (CP51), an anther-specific cysteine protease, essential for pollen exine formation in *A. thaliana* and potentially involved in PCD (Yang et al., 2014). Q10716 belongs to the Arabidopsis RD19A subfamily of which members are known to be involved in *A. thaliana* defense mechanisms such as RD19 that is targeted by the *Ralstonia* effector PopP2 (Bernoux et al., 2008). B4FYA3 shares high sequence similarity with CP14, containing a granulin domain and belonging to the XBCP3 family. CP14 was described to be involved in programed cell death during plant development (Paireder et al., 2016) where its homolog in *N. benthamiana* NbCP14 was shown to contribute to defense against *Phytophtora infestans* (Kaschani et al., 2010; Bozkurt et al., 2011). Taking together these results show that the leaf characterized PLCPs, CP1A, CP1B, CathB, CP2, and XCP2 as well as the new root PLCP CP1C, might not contribute to the increased PLCP activity after SA treatment in maize roots suggesting that different PLCPs contribute to SA signaling in roots and leaves.

Comparison of maize leaf and root apoplastic PLCPs identified CP1C, a root specific PLCP. Strikingly, CP1C transcripts can be found in leaves. The fact that CP1C has not been previously identified in leaf apoplastic fluids could be explained by its low expression and/or poor activity. Phylogenetic analysis of all maize PLCPs revealed that CP1C groups into the Arabidopsis RD21 subfamily together with previously identified apoplastic PLCPs like CP1A, CP1B and Mir1-3. Due to its high sequence and structural similarities toward CP1A and CP1B it was named CP1C, although CP1C is closer to other maize PLCPs such as Mir1, Mir2 and a pseudotzain whereas CP1A and CP1B are closer to Mir3. The active site of CP1C appears to be narrower than that of CP1A. These structural and biochemical changes might explain the differences in substrate specificity and inhibitor susceptibility in comparison to the other CP1-like PLCPs. The observation that the synthetic substrate AMC-FR, carrying a bulky Phe at the P2-position is preferred by CP1A than by CP1C might also correlate to the narrow grove around the active site in CP1C. Based on the literature, hydrophobic amino acids as well as Arg are predicted to be favored by PLCPs (Niemer et al., 2016; Paireder et al., 2017). We therefore tested three synthetic substrates with different P2-positions. Differential affinities toward the different substrates were observed for CP1-like proteins, which may be explained by unequal substrate accessibility to their active site. Interestingly, the affinities to

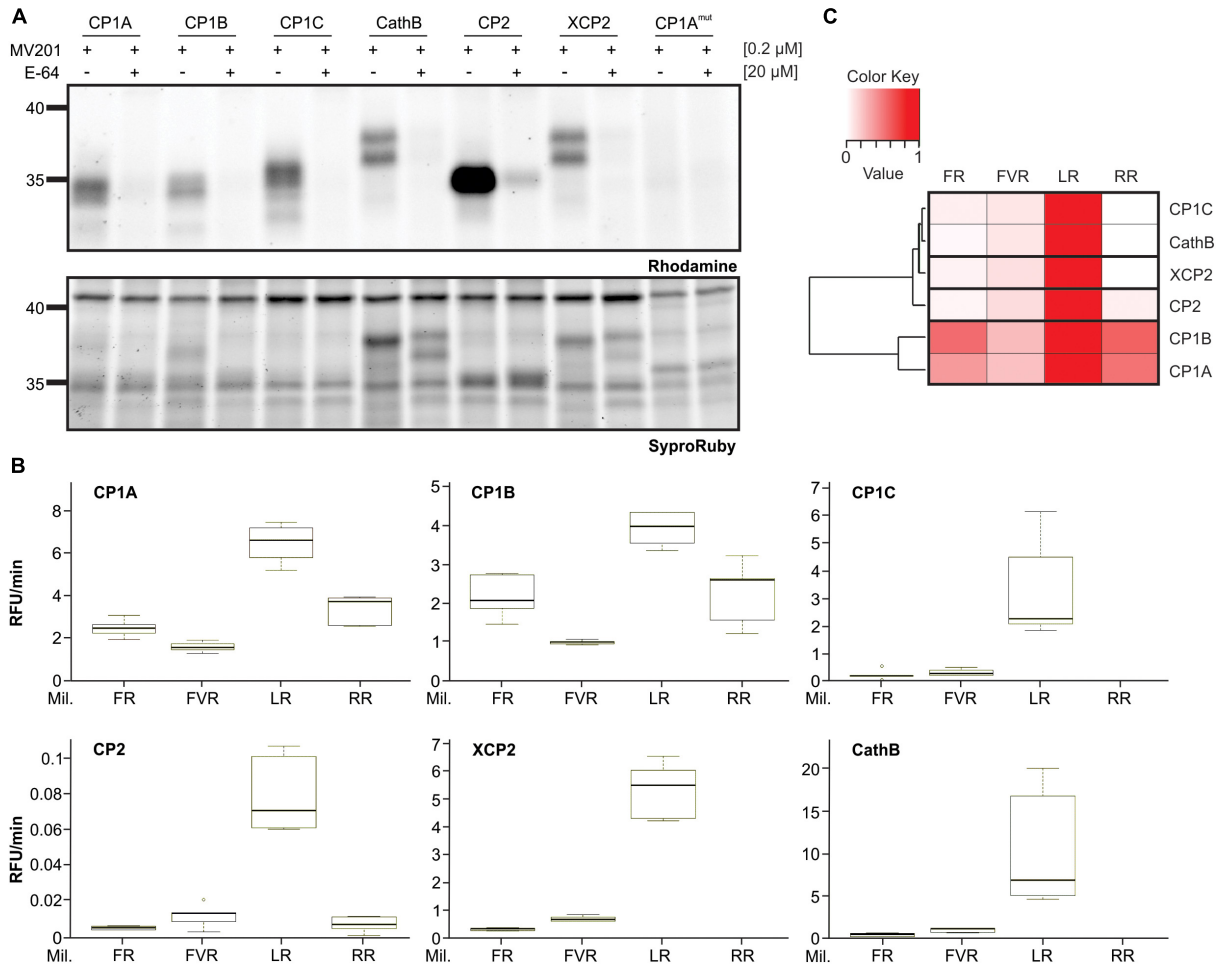

FIGURE 5 | Differential substrate specificities of apoplastic PLCPs. **(A)** Activity of heterologous expressed maize apoplastic PLCPs. Leaf apoplastic fluids of *N. benthamiana* overexpressed PLCPs: CP1A, CP1B, CP1C, Cathepsin B (CathB), CP2, XCP2 and the catalytic inactive CP1A mutant CP1A^{mut} were isolated and labeled with the probe MV201 (Richau et al., 2012). Samples were pre-incubated for 30 min either with 20 µM E-64 (+), a covalent and irreversible PLCP inhibitor (Barrett et al., 1982), or DMSO (–) followed by 2 h labeling with 0.2 µM MV201 (Richau et al., 2012). Labeled PLCPs were visualized by fluorescence scanning (Ex. 532 nm, Em. 580 nm). SyproRuby-stain (Ex. 450 nm, Em. 610 nm) was performed for visualization of sample loading. **(B)** Substrate cleavage assays of PLCPs using different synthetic substrates. Signal quantification from **(A)** was used to normalize for equal amounts of active PLCPs in this assay. Overexpressed PLCPs were tested in substrate cleavage assays using 10 µM of the following substrates: Z-FR-AMC (FR), BZ-FVR-AMC (FVR), Z-LR-AMC (LR), and Z-RR-AMC (RR). The release of AMC (relative fluorescent unit = RFU) per minute was calculated and plotted against each substrate. The box signifies the upper (Q3) and lower (Q1) quartiles, and the median is represented by a short black line within the box for each substrate. Lower and upper whiskers represent Q1−1.5 × IQR and Q3+1.5 × IQR, respectively. This experiment was performed using three independent biological replicates each with technical duplicates. **(C)** Heat-map of relative substrate affinity. PLCP affinity for each substrate used in **(B)** was calculated relative to the strongest activity. The P2-position preference was evaluated relatively to the strongest activity (set to 1, red) to no activity (set to 0, white). PLCPs were clustered based on their relative substrate affinity pattern.

the tested substrates of CP1C are similar to those of XCP2 and CathB which belong to different subfamilies of PLCPs (subfamily 3 and 9, respectively), likely reflecting similar target preferences *in vivo*. Moreover, we did not observe striking inhibitory differences between the CP1-like PLCPs toward CC9, an endogenous cystatin mostly induced in leaves (van der Linde et al., 2012a). It would be interesting to compare the susceptibility of CP1-like proteases against the cystatin P31726 found to be induced after SA treatment. Interestingly, CP1C seems to be more susceptible toward E-64, an inhibitor produced and first isolated from soil *Aspergillus japonicus* (Hanada et al., 1978).

In this study we discovered a novel root specific PLCP that shows sequence and structure similarity to CP1A but differs in substrate specificity. Surprisingly, neither CP1C nor any other of our six previously found apoplastic PLCPs shows higher activity after SA treatment of maize roots. On the contrary, we have identified three additional root apoplastic PLCPs activated after SA treatment indicating a role in SA-signaling and plant immunity. Both, the further characterization of CP1C to elucidate its specific role in the root apoplast and the functional characterization of the three new SA-induced apoplastic PLCPs will provide us with a deeper understanding of the diverse roles of PLCPs in the root apoplast.

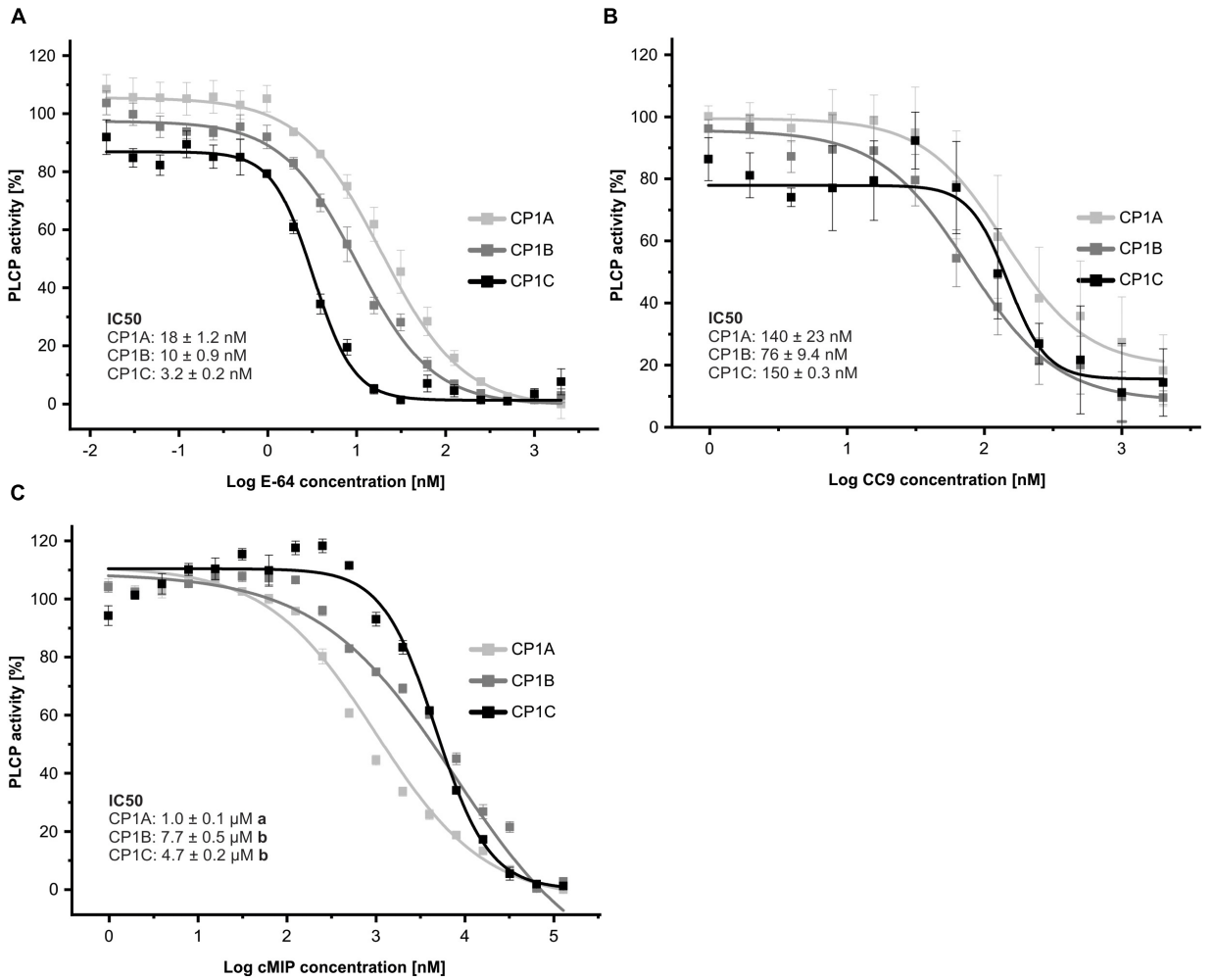

FIGURE 6 | CP1-like proteases show distinct inhibitory profiles. Apoplastic fluids of *N. benthamiana* overexpressed CP1A, CP1B, and CP1C were evaluated for their activity using 10 µM of the substrate Z-LR-AMC (LR). The inhibitory profile for E-64 **(A)**, CC9, an endogenous cystatin **(B)** and cMIP, a conserved microbial inhibitor of proteases **(C)** was tested. We used equal amounts of active PLCPs based on signal quantification from MV201 labeling of apoplastic fluids (**Supplementary Figure 3**). Inhibitor concentrations ranged from 15 pM to 128 µM. Activity was set to 100% in the absence of inhibitor. Normalized values were plotted against Log of inhibitor concentration in nM. The experiment was performed in three independent biological replicates each with technical duplicates. A nonlinear fit based on a dose response function was performed and IC50-values were calculated. Error bars represent the SEM. Significance was calculated using an unpaired *t*-test and differing letters behind the IC50-values indicate significant differences ($\alpha < 0.05$).

MATERIALS AND METHODS

Plant Material

Zea mays variety EGB was grown in phyto-chambers at 28°C on a long day period (16 h light) with 80% humidity. Temperature was decreased to 22°C for 8 h during the night.

Nicotiana benthamiana plants were grown in a greenhouse at 23°C on a long day (16 h light) and at 20°C for 8 h dark period with 30– 40% humidity.

Salicilic Acid (SA) Treatment of Maize Roots and Leaves

Maize plants were sowed in Seramis clay granulat (Sermanis GmbH, Mogendorf, Germany) for root treatment and in soil for leaf treatment and grown for 7–10 days until the three leaf stage. Afterward, 2 mM SA was dissolved in 0.1% ethanol and poured to the maize roots every 12 h for 2 days. As a control mock treated plants were poured with a solution containing 0.1% ethanol. Plants were harvested 60 h after treatment. For leaf treatment same solution were infiltrated into the third leaf using a 1 ml tuberculin-syringe without a hypodermic needle and harvested after 48 h.

Apoplastic Fluid Isolation

For RAF maize plants grown in Seramis were carefully removed from the pots and Seramis clay granulat was removed from the roots using forceps and washes with ddH2O. Roots were separated from the aerial plant parts and put into a beaker filled with ddH2O. A metal-sieve was added on top to prevent roots

from swimming out of the ddH2O. Roots were then vacuum infiltrated 3 times for 15 min at 60 mbar with an interval of 2 min atmospheric pressure. Roots were transferred to syringes hanging in 50 ml falcon tubes and centrifuged at 4°C for 20 min at 3000 g to isolate the apoplastic fluid. Prior to storage at −20°C or direct use in experiments the fluid was passed through a 45 μm syringe filter. Fractionation of apoplastic fluid was performed according to van der Linde et al. (2012a). Apoplastic fluid from maize leaves was prepared as described above except that the leaves were centrifuged at 4°C for 20 min at 2000 g.

Isolation of Apoplastic Fluids From *N. benthamiana* Leaves

Isolation of apoplastic fluids from *N. benthamiana* leaves was performed as described before in Mueller et al. (2013).

Protease Activity Assay Using Fluorogenic Substrates

Root apoplastic fluids as well as apoplstic fluids containing overexpressed PLCPs were tested for its activity using the following substrates: Z-FR-AMC, BZ-FVR-AMC, Z-LR-AMC, Z-RR-AMC (Sigma-Aldrich, St. Louis, MS, United States). For sample measurement 10 μl of apoplastic fluids were mixed with reaction buffer (10 mM sodium phosphate pH 6, 150 mM sodium chloride, 1 mM EDTA and 0.5 mM DTT) and 10 μM substrate. AMC-release was measured over time for 20 min (Excitation: 350 nm, Emission: 460 nm) using a Tecan Infinite 200 Pro plate reader (Tecan Group Ltd., Männendorf, Switzerland). As a control for PLCP activity 2 μM E-64 (Sigma-Aldrich, St. Louis, MS, United States) was added to normalize values. cMIP was obtained as synthetic peptide from GenScript (NJ, United States) and diluted in ddH2O to the needed concentration. CC9 was produced and purified according to van der Linde et al. (2012b). Inhibitors were used as described in the results section and added to the indicated concentrations in the experiments ranging from 15 pM to 128 μM. Relative PLCP activity was calculated to the measured activity without addition of inhibitors.

Activity Based Protein Profiling (ABPP)

Root apoplastic fluid was incubated for 2 h in 50 mM sodium acetate pH 6, 10 mM DTT and 0.2–2 μM of the probe MV201 or DCG-04, respectively (Greenbaum et al., 2000; Richau et al., 2012). As a negative control, one set of samples was pre-incubated for 30 min with 20 μM E-64 (Sigma-Aldrich, St. Louis, MS, United States) prior to labeling. MV201 labeling was performed in darkness. Labeling was stopped by addition of 1xSDS-loading dye (Laemmli, 1970). Samples were heated to 95°C for 5 min and proteins were separated on 12% SDS-gels. For MV201 labeled samples SDS-PAGE was performed in darkness and visualized on gel fluorescent scanning using a ChemiDoc (Biorad, CA, United States) with Rhodamine settings (excitation: 532 nm, emission: 580 nm). The loading control gel was stained with SyproRuby (Invitrogen, Carlsbad, CA, United States) according to the protocol by the manufacturer. Detection of DCG-04 labeled samples was performed using a streptavidin-HRP antibody (Sigma-Aldrich, St. Louis, MS, United States).

PLCP Pulldown Using Streptavidin-Beads

Root apoplastic fluid was incubated for 4 h at room temperature in 50 mM sodium acetate pH 6, 10 mM DTT and 2 μM DCG-04 (Greenbaum et al., 2000) in a total volume of 2.5 ml. As a negative control, one set of samples was pre-incubated for 30 min with 20 μM E-64 (Sigma-Aldrich, St. Louis, MS, United States) prior to labeling. After labeling, samples were transferred and eluted using NaP25 columns (GE healthcare, Chicago, IL, United States) equilibrated with 50 mM Tris-HCl pH 8. Hundred microliter streptavidin sepharose high performance (Sigma-Aldrich, St. Louis, MS, United States), equilibrated with 50 mM Tris-HCl pH 8 and 1 tablet inhibitor cocktail mix (complete™, EDTA-free Protease Inhibitor Cocktail, Roche, Basel, Switzerland) was mixed with the sample and incubated for 1 h at room temperature rotating. Samples were centrifuged for 3 min at 1,400 g and the supernatant was discarded. Sepharose beads were gently re-suspended in 1 ml 50 mM Tris-HCl pH 8 in a new tube. The sepharose beads were washed two times with 1% SDS and two times with 6M Urea. Beads were once washed with 1 ml 50 mM Tris-HCl pH 8 containing 0.1% Tween20 and once with ddH2O. Beads were stored at −20°C until further analysis. Control samples were taken after each step. To confirm the pulldown assay an immunoblot with control samples was performed using streptavidin-HRP antibody (1 μg/ml) (Sigma-Aldrich, St. Louis, MS, United States). The immunoblot was developed using SuperSignal™ West Pico Chemiluminescent Substrate (Thermo Fischer Scientific, Waltham, MA, United States).

Sample Preparation for LC/MS/MS

Samples for LC-MS from proteins labeled with DCG-04 and enriched on streptavidin beads were either prepared by gel electrophoresis and subsequent in-gel digestion (IGD) or the captured proteins were directly digested on the beads (OBD). To identify and cut out gel regions containing DCG-04 targets we employed the "blind-cut"-method (van der Linde et al., 2012a). IGD with trypsin was performed by following a published protocol (Kaschani et al., 2009). Affinity enriched protein samples that were not eluted from the capture resin were on-bead digested (OBD). Briefly, streptavidin beads were washed twice with water to remove SDS. Then bound proteins were reduced with DTT (5 mM) in 50 mM ammonium bicarbonate (ABC) for 30 min at room temperature. Protein reduction was followed by alkylation with iodoacetamide (IAM, 10 mM also in 50 mM ABC, 30 min, room temperature) and quenching of excess IAM with DTT (final concentration DTT 10 mM). Reduction and alkylation was followed by a sequential digestion of proteins with first LysC for 3 h at 37°C followed by a 16 h digestion with trypsin (37°C). The digestion was stopped by adding formic acid (FA) to a final concentration of 0.5%. The supernatant containing the digestion products was passed through home-made glass microfiber StageTips (GE Healthcare; poresize: 1.2 μM; thickness: 0.26 mm).

Cleared tryptic digests were desalted on home-made C18 StageTips as described (Rappsilber et al., 2007). Peptides were passed over a 2 disc StageTip. After elution from the StageTips, samples were dried using a vacuum concentrator (Eppendorf) and the peptides were taken up in 0.1% FA solution (10 µl).

LC/MS/MS

Experiments were performed on an Orbitrap Elite instrument (Thermo Fischer Scientific, Waltham, MA, United States; Michalski et al., 2012) that was coupled to an EASY-nLC 1000 liquid chromatography (LC) system (Thermo Fischer Scientific, Waltham, MA, United States). The LC was operated in the one-column mode. The analytical column was a fused silica capillary (inner diameter 75 µm × 35 cm) with an integrated PicoFrit emitter (New Objective, Woburn, United States) packed in-house with Reprosil-Pur 120 C18-AQ 1.9 µm. The analytical column was encased by a column oven (Sonation, Biberach an der Riß, Germany) and attached to a nanospray flex ion source (Thermo Fischer Scientific, Waltham, MA, United States). The column oven temperature was adjusted to 45°C during data acquisition. The LC was equipped with two mobile phases: solvent A (0.1% formic acid, FA, in water) and solvent B (0.1% FA in acetonitrile, ACN). All solvents were of UHPLC (ultra-high performance LC) grade (Sigma-Aldrich, St. Louis, MS, United States). Peptides were directly loaded onto the analytical column with a maximum flow rate that would not exceed the set pressure limit of 980 bar (usually around 0.5–0.8 µl/min). Peptides were subsequently separated on the analytical column by running a 40 min (ISD) or 140 min (OBD) gradient of solvent A and solvent B [start with 7% B; gradient 7–35% B for 30 min (ISD) or 120 min (OBD); gradient 35–100% B for 5 min (ISD) or 10 min (OBD) and 100% B for 5 min (ISD) or 10 min (OBD)] at a flow rate of 300 nl/min. The mass spectrometer was operated using Xcalibur software (version 2.2 SP1.48). The mass spectrometer was set in the positive ion mode. Precursor ion scanning was performed in the Orbitrap analyzer (FTMS; Fourier Transform Mass Spectrometry) in the scan range of m/z 300–1800 and at a resolution of 60,000 with the internal lock mass option turned on (lock mass was 445.120025 m/z, polysiloxane) (Olsen et al., 2005). Product ion spectra were recorded in a data dependent fashion in the ion trap (ITMS; Ion Trap Mass Spectrometry) in a variable scan range and at a rapid scan rate. The ionization potential (spray voltage) was set to 1.8 kV. Peptides were analyzed using a repeating cycle consisting of a full precursor ion scan [1.0×10^6 ions or 200 ms (IGD) and 3.0×10^6 ions or 50 ms) followed by 10 product ion scans (3.0×10^4 ions or 150 ms (IGD) and 1.0×10^4 ions or 50 ms (OBD)] where peptides are isolated based on their intensity in the full survey scan (threshold of 500 counts) for tandem mass spectrum (MS2) generation that permits peptide sequencing and identification. CID (collision-induced dissociation) collision energy was set to 35% for the generation of MS2 spectra. During MS2 data acquisition dynamic ion exclusion was set to 120 s with a maximum list of excluded ions consisting of 500 members and a repeat count of one. Ion injection time prediction, preview mode for the FTMS, monoisotopic precursor selection and charge state screening were enabled. Only charge states higher than 1 were considered for fragmentation.

Peptide and Protein Identification Using MaxQuant

RAW spectra were submitted to an Andromeda (Cox et al., 2011) search in MaxQuant (version 1.5.3.30) using the default settings (Cox and Mann, 2008). Label-free quantification and match-between-runs was activated (Cox et al., 2014). MS/MS spectra data were searched against the Uniprot *Zea mays* cv B73 database UP000007305_4577.fasta (99369 entries, downloaded 6/4/2018) and the in-house ACE_0229_EGB apoplastic PLCPs AS.fasta database containing Sequences of interest from *Zea mays* cv EGB (7 entries). All searches included a contaminants database (as implemented in MaxQuant, 245 sequences). The contaminants database contains known MS contaminants and was included to estimate the level of contamination. Enzyme specificity was set to "Trypsin/P." The instrument type in Andromeda searches was set to Orbitrap and the precursor mass tolerance was set to ±20 ppm (first search) and ±4.5 ppm (main search). The MS/MS match tolerance was set to ±0.5 Da. The peptide spectrum matches FDR and the protein FDR were set to 0.01 (based on target-decoy approach and decoy mode "revert"). Minimum peptide length was 7 amino acids. Label-free protein quantification was switched on, and unique and razor peptides were considered for quantification with a minimum ratio count of 2. Retention times were recalibrated based on the built-in nonlinear time-rescaling algorithm. MS/MS identifications were transferred between LC-MS/MS runs with the "Match between runs" option in which the maximal match time window was set to 0.7 min and the alignment time window set to 20 min. The quantification is based on the "value at maximum" of the extracted ion current. Modified peptides were allowed for quantification. The minimum score for modified peptides was 40. Further analysis and filtering of the results was done in Perseus v1.5.5.3 (Tyanova et al., 2016). The mass spectrometry proteomics data have been deposited to the ProteomeXchange Consortium via the PRIDE (Vizcaino et al., 2016) partner repository[1] with the dataset identifier PXD013124.

Strain and Plasmid Construction

Golden gate modular cloning system was applied to generate plasmids (Engler et al., 2014). Oligonucleotides that were used for PCR are listed in **Supplementary Table 3**. To obtain pL1M-F1-XCP2-Streptwin::2x35S, pL1M-F1-CathB-Streptwin::2x35S, pL1M-F1-CCP2-Streptwin::2x35S, XCP2 (Maizegdb: GRMZM2G066326), Cathepsin B (Maizegdb: GRMZM2G108849), and CP2 (Maizegdb: GRMZM2G038636) respectively were amplified by PCR from maize cDNA. To obtain pL1M-F1- CP1A_nogran-Streptwin::2x35S, pL1M-F1-CP1B_nogran-Streptwin::2x35S, pL1M-F1-CP1C_nongran-HA::2x35S, CP1A (Maizegdb: GRMZM2G166281), CP1B (Maizegdb: GRMZM2G073465), and CP1C (Maizegdb: GRMZM2G340065) respectively were amplified by PCR from maize cDNA leaving out the DNA sequence coding for the granulin-domains. The amplified sequences were then ligated according to Weber et al. (2011) and Engler et al. (2014), sub-transformed to *E. coli* DH5α competent cells (Thermo Fischer Scientific, Rockfort, United States) and then transformed

[1] https://www.ebi.ac.uk/pride/archive/

to *A. tumefaciens* GV3101 competent cells for overexpression in *N. benthamiana*. To obtain pL1M-F1-CP1A_nogran_mut2-Streptwin::2x35S site directed mutagenesis was performed on pL1M-F1- CP1A_nogran-Streptwin::2x35S according to the instructions of the QuikChange Multi Site-Directed Mutagenesis Kit (Agilent Technologies, Santa Clara, United States) with primers targeting nucleotides of the active site of CP1A. Strains used in this study are listed in **Supplementary Table 4**.

Heterologous Expression of PLCPs in *N. benthamiana* Leaves

Agrobacterium tumefaciens containing the desired constructs were grown in liquid media overnight and diluted in 10 mM magnesium chloride to an OD = 1 with 200 μM acetosyringone (Sigma-Aldrich, Taufkirchen, Germany). After 1 h incubation in the dark cultures were infiltrated into 5–6 weeks old N. benthamiana leaves using a tuberculin-syringe without needle. Three days postinfiltration leaves were harvested and the apoplastic fluid was isolated.

Computational Methods and Statistical Analysis

Heat-maps were performed using the heatmap.2 function of the package gplots (version 3.0.1) in r-studio (R version 3.5.1). Venn diagram was created using the draw.pairwise.venn function of the package Venn diagram (version 1.6.0) in r-studio (R version 3.5.1.). For generation of a phylogenetic tree 52 maize PLCP sequences of the line B73 retrieved from the MEROPS database (Rawlings et al., 2018) and our six identified PLCPs from EGB were used. Additionally, we included one type member of each PLCP subfamily of *A. thaliana* and two serine proteases DEGP2 and DGP11 from *A. thaliana* as outgroup (Beers et al., 2004; Richau et al., 2012). MAFFT (v7.407) (Katoh and Standley, 2013). RAxML with the GTRGAMMA substitution model (v8.2.0) was used for the construction of the tree (Stamatakis, 2014). The tree is drawn to scale, with branch lengths measured in the number of substitutions per site. The robustness was assessed using 100 bootstrap replicates. Quantification of PLCP-signals after ABPP using rhodamine fluorescence signal strength was performed using ImageLab™ software (Bio-Rad, Hercules, CA, United States). Phyre2 (Kelley et al., 2015) was used for modeling of PLCPs based on caricain PDB: 1pciA (Groves et al., 1996). For the inhibitor concentration range plots a nonlinear fit based on the dose response function and calculation of IC50 was performed in Origin 2018 (OriginLab, Northampton, MA, United States).

AUTHOR CONTRIBUTIONS

JS wrote the manuscript with input from all authors. JS, KvdL, GD, and JM designed the experiments. AM, SZ, and KvdL performed IEC in leaves and roots. KvdL and FK did the DCG-04 pull-down of IEC samples. FK, MK, and TC performed MS/MS analysis and protein identification.

FUNDING

This project has been funded by the DFG project DO 1421/5-1 and the UoC Postdoc Grant D72133T.

ACKNOWLEDGMENTS

We would like to thank Svenja Blaskowski for technical assistance in the LC-MS/MS and Jasper Depotter for helping in the analysis of the phylogenetic tree. We also thank Julio Martinez and Friedrich Breidenbach for their technical support in the project. We are very thankful to Bobby Florea and Renier van der Hoorn for providing DCG-04 and MV201, respectively.

SUPPLEMENTARY MATERIAL

The Supplementary Material for this article can be found online at: https://www.frontiersin.org/articles/10.3389/fpls.2019.00473/full#supplementary-material

REFERENCES

Adamczyk, B., Smolander, A., Kitunen, V., and Godlewski, M. (2010). Proteins as nitrogen source for plants: a short story about exudation of proteases by plant roots. *Plant Signal. Behav.* 5, 817–819. doi: 10.4161/psb.5.7.11699

Andorf, C. M., Cannon, E. K., Portwood, J. L. II, Gardiner, J. M., Harper, L. C., Schaeffer, M. L., et al. (2016). MaizeGDB update: new tools, data and interface for the maize model organism database. *Nucleic Acids Res.* 44, D1195–D1201. doi: 10.1093/nar/gkv1007

Andrews, J. H., and Harris, R. F. (2000). The ecology and biogeography of microorganisms on plant surfaces. *Annu. Rev. Phytopathol.* 38, 145–180. doi: 10.1146/annurev.phyto.38.1.145

Barreau, C., Pinson-Gadais, L., Caron, D., Lannou, C., and Richard-Forget, F. (2010). Factors of the fusarium verticillioides-maize environment modulating fumonisin production au - picot, adeline. *Criti. Rev. Microbiol.* 36, 221–231. doi: 10.3109/10408411003720209

Barrett, A. J., Kembhavi, A. A., Brown, M. A., Kirschke, H., Knight, C. G., Tamai, M., et al. (1982). L-trans-epoxysuccinyl-leucylamido(4-guanidino)butane (E-64) and its analogues as inhibitors of cysteine proteinases including cathepsins B, H and L. *Biochem. J.* 201, 189–198. doi: 10.1042/bj2010189

Bárzana, G., Aroca, R., Bienert, G. P., Chaumont, F., and Ruiz-Lozano, J. M. (2014). New insights into the regulation of aquaporins by the arbuscular mycorrhizal symbiosis in maize plants under drought stress and possible implications for plant performance. *Mol. Plant Microbe Interact.* 27, 349–363. doi: 10.1094/MPMI-09-13-0268-R

Bateman, A., and Bennett, H. P. (1998). Granulins: the structure and function of an emerging family of growth factors. *J. Endocrinol.* 158, 145–151. doi: 10.1677/joe.0.1580145

Bateman, A., and Bennett, H. P. (2009). The granulin gene family: from cancer to dementia. *Bioessays* 31, 1245–1254. doi: 10.1002/bies.200900086

Beers, E. P., Jones, A. M., and Dickerman, A. W. (2004). The S8 serine, C1A cysteine and A1 aspartic protease families in Arabidopsis. *Phytochemistry* 65, 43–58. doi: 10.1016/j.phytochem.2003.09.005

Belenghi, B., Acconcia, F., Trovato, M., Perazzolli, M., Bocedi, A., Polticelli, F., et al. (2003). AtCYS1, a cystatin from *Arabidopsis thaliana*, suppresses hypersensitive cell death. *Eur. J. Biochem.* 270, 2593–2604. doi: 10.1046/j.1432-1033.2003.03630.x

Bernoux, M., Timmers, T., Jauneau, A., Brière, C., de Wit, P. J. G. M., Marco, Y., et al. (2008). RD19, an *Arabidopsis* cysteine protease required for RRS1-R-mediated resistance, is relocalized to the nucleus by the *Ralstonia solanacearum* PopP2 effector. *Plant Cell* 20, 2252–2264. doi: 10.1105/tpc.108.058685

Bozkurt, T. O., Schornack, S., Win, J., Shindo, T., Ilyas, M., Oliva, R., et al. (2011). Phytophthora infestans effector AVRblb2 prevents secretion of a plant immune protease at the haustorial interface. *Proc. Natl. Acad. Sci. U.S.A.* 108, 20832–20837. doi: 10.1073/pnas.1112708109

Brefort, T., Doehlemann, G., Mendoza-Mendoza, A., Reissmann, S., Djamei, A., and Kahmann, R. (2009). *Ustilago maydis* as a pathogen. *Annu. Rev. Phytopathol.* 47, 423–445. doi: 10.1146/annurev-phyto-080508-081923

Bryan, P. N. (2002). Prodomains and protein folding catalysis. *Chem. Rev.* 102, 4805–4816. doi: 10.1021/cr010190b

Chen, Z. Y., Brown, R. L., Damann, K. E., and Cleveland, T. E. (2010). PR10 expression in maize and its effect on host resistance against Aspergillus flavus infection and aflatoxin production. *Mol. Plant Pathol.* 11, 69–81. doi: 10.1111/j.1364-3703.2009.00574.x

Coll, N. S., Epple, P., and Dangl, J. L. (2011). Programmed cell death in the plant immune system. *Cell Death Differ.* 18, 1247–1256. doi: 10.1038/cdd.2011.37

Cox, J., Hein, M. Y., Luber, C. A., Paron, I., Nagaraj, N., and Mann, M. (2014). MaxLFQ allows accurate proteome-wide label-free quantification by delayed normalization and maximal peptide ratio extraction, termed MaxLFQ. *Mol. Cell. Proteomics* 13, 2513–2526. doi: 10.1074/mcp.M113.031591

Cox, J., and Mann, M. (2008). MaxQuant enables high peptide identification rates, individualized p.p.*b*.-range mass accuracies and proteome-wide protein quantification. *Nat. Biotechnol.* 26, 1367–1372. doi: 10.1038/nbt.1511

Cox, J., Neuhauser, N., Michalski, A., Scheltema, R. A., Olsen, J. V., and Mann, M. (2011). Andromeda: a peptide search engine integrated into the maxquant environment. *J. Proteome Res.* 10, 1794–1805. doi: 10.1021/pr101065j

Dempsey, D. M. A., Vlot, A. C., Wildermuth, M. C., and Klessig, D. F. (2011). Salicylic acid biosynthesis and metabolism. *Arabidopsis Book* 9:e0156. doi: 10.1199/tab.0156

Duncan, K. E., and Howard, R. J. (2009). Biology of maize kernel infection by *Fusarium verticillioides*. *Mol. Plant Microbe Interact.* 23, 6–16. doi: 10.1094/MPMI-23-1-0006

Engler, C., Youles, M., Gruetzner, R., Ehnert, T. M., Werner, S., Jones, J. D., et al. (2014). A golden gate modular cloning toolbox for plants. *ACS Synth. Biol.* 3, 839–843. doi: 10.1021/sb4001504

FAO (2012). *FAOSTAT Production*. Available at: http://faostat.fao.org/site/567/DesktopDefault.aspx?PageID=567#ancor (accessed October 15, 2012).

Feliciangeli, S. F., Thomas, L., Scott, G. K., Subbian, E., Hung, C.-H., Molloy, S. S., et al. (2006). Identification of a pH sensor in the furin propeptide that regulates enzyme activation. *J. Biol. Chem.* 281, 16108–16116. doi: 10.1074/jbc.M600760200

Felle, H. H. (1998). The apoplastic pH of the Zea mays root cortex as measured with pH-sensitive microelectrodes: aspects of regulation. *J. Exp. Bot.* 49, 987–995. doi: 10.1093/jxb/49.323.987

Gilroy, E. M., Hein, I., van der Hoorn, R., Boevink, P. C., Venter, E., McLellan, H., et al. (2007). Involvement of cathepsin B in the plant disease resistance hypersensitive response. *Plant J.* 52, 1–13. doi: 10.1111/j.1365-313X.2007.03226.x

Godlewski, M., and Adamczyk, B. (2007). The ability of plants to secrete proteases by roots. *Plant Physiol. Biochem.* 45, 657–664. doi: 10.1016/j.plaphy.2007.06.001

Greenbaum, D., Medzihradszky, K. F., Burlingame, A., and Bogyo, M. (2000). Epoxide electrophiles as activity-dependent cysteine protease profiling and discovery tools. *Chem. Biol.* 7, 569–581. doi: 10.1016/S1074-5521(00)00014-4

Groves, M. R., Taylor, M. A., Scott, M., Cummings, N. J., Pickersgill, R. W., and Jenkins, J. A. (1996). The prosequence of procaricain forms an alpha-helical domain that prevents access to the substrate-binding cleft. *Structure* 4, 1193–1203. doi: 10.1016/S0969-2126(96)00127-X

Guillaume, L. (2017). Schematic of a maize plant. doi: 10.6084/m9.figshare.4684996.v1

Hanada, K., Tamai, M., Yamagishi, M., Ohmura, S., Sawada, J., and Tanaka, I. (1978). Isolation and characterization of E–64, a new thiol protease inhibitor. *Agric. Biol. Chem.* 42, 523–528. doi: 10.1080/00021369.1978.10863014

Jashni, M. K., Mehrabi, R., Collemare, J., Mesarich, C. H., and de Wit, P. J. G. M. (2015). The battle in the apoplast: further insights into the roles of proteases and their inhibitors in plant–pathogen interactions. *Front. Plant Sci.* 6:584. doi: 10.3389/fpls.2015.00584

Jones, P. G., and Thornton, P. K. (2003). The potential impacts of climate change on maize production in Africa and Latin America in 2055. *Glob. Environ. Change* 13, 51–59. doi: 10.1016/S0959-3780(02)00090-0

Kaschani, F., Gu, C., Niessen, S., Hoover, H., Cravatt, B. F., and van der Hoorn, R. A. (2009). Diversity of serine hydrolase activities of unchallenged and *Botrytis*-infected *Arabidopsis thaliana*. *Mol. Cell. Proteomics* 8, 1082–1093. doi: 10.1074/mcp.M800494-MCP200

Kaschani, F., Shabab, M., Bozkurt, T., Shindo, T., Schornack, S., Gu, C., et al. (2010). An effector-targeted protease contributes to defense against Phytophthora infestans and is under diversifying selection in natural hosts. *Plant Physiol.* 154, 1794–1804. doi: 10.1104/pp.110.158030

Katoh, K., and Standley, D. M. (2013). MAFFT multiple sequence alignment software version 7: improvements in performance and usability. *Mol. Biol. Evol.* 30, 772–780. doi: 10.1093/molbev/mst010

Kelley, L. A., Mezulis, S., Yates, C. M., Wass, M. N., and Sternberg, M. J. E. (2015). The Phyre2 web portal for protein modeling, prediction and analysis. *Nat. Protoc.* 10, 845–858. doi: 10.1038/nprot.2015.053

Kosegarten, H., Grolig, F., Esch, A., Glüsenkamp, K.-H., and Mengel, K. (1999). Effects of NH4+, NO3− and HCO3− on apoplast pH in the outer cortex of root zones of maize, as measured by the fluorescence ratio of fluorescein boronic acid. *Planta* 209, 444–452. doi: 10.1007/s004250050747

Laemmli, U. K. (1970). Cleavage of structural proteins during the assembly of the head of bacteriophage T4. *Nature* 227, 680–685.

Lampl, N., Alkan, N., Davydov, O., and Fluhr, R. (2013). Set-point control of RD 21 protease activity by A t S erpin1 controls cell death in A rabidopsis. *Plant J.* 74, 498–510. doi: 10.1111/tpj.12141

Lindow, S. E., and Brandl, M. T. (2003). Microbiology of the phyllosphere. *Appl. Environ. Microbiol.* 69, 1875–1883. doi: 10.1128/AEM.69.4.1875-1883.2003

Lohman, K. N., Gan, S., John, M. C., and Amasino, R. M. (1994). Molecular analysis of natural leaf senescence in Arabidopsis thaliana. *Physiol. Plant.* 92, 322–328. doi: 10.1111/j.1399-3054.1994.tb05343.x

Lopez, L., Camas, A., Shivaji, R., Ankala, A., Williams, P., and Luthe, D. (2007). Mir1-CP, a novel defense cysteine protease accumulates in maize vascular tissues in response to herbivory. *Planta* 226, 517–527. doi: 10.1007/s00425-007-0501-7

Martínez, M., Cambra, I., González-Melendi, P., Santamaría, M. E., and Díaz, I. (2012). C1A cysteine-proteases and their inhibitors in plants. *Physiol. Plant.* 145, 85–94. doi: 10.1111/j.1399-3054.2012.01569.x

Martinez, M., and Diaz, I. (2008). The origin and evolution of plant cystatins and their target cysteine proteinases indicate a complex functional relationship. *BMC Evol. Biol.* 8:198. doi: 10.1186/1471-2148-8-198

McLellan, H., Gilroy, E. M., Yun, B. W., Birch, P. R., and Loake, G. J. (2009). Functional redundancy in the *Arabidopsis* cathepsin B gene family contributes to basal defence, the hypersensitive response and senescence. *New Phytol.* 183, 408–418. doi: 10.1111/j.1469-8137.2009.02865.x

Michalski, A., Damoc, E., Lange, O., Denisov, E., Nolting, D., Müller, M., et al. (2012). Ultra high resolution linear ion trap orbitrap mass spectrometer (Orbitrap Elite) facilitates top down LC MS/MS and versatile peptide fragmentation modes. *Mol. Cell. Proteomics* 11:O111.013698. doi: 10.1074/mcp.O111.013698

Misas-Villamil, J. C., Hoorn, R. A. L., and Doehlemann, G. (2016). Papain-like cysteine proteases as hubs in plant immunity. *New Phytol.* 212, 902–907. doi: 10.1111/nph.14117

Misas-Villamil, J. C., Mueller, A. N., Demir, F., Meyer, U., Ökmen, B., Schulze Hüynck, J., et al. (2019). A fungal effector acts as substrate mimicking molecule suppressing plant immunity via an inter-kingdom conserved motif. *Nat. Commun.* 10:1576.

Misas-Villamil, J. C., and van der Hoorn, R. A. (2008). Enzyme-inhibitor interactions at the plant-pathogen interface. *Curr. Opin. Plant Biol.* 11, 380–388. doi: 10.1016/j.pbi.2008.04.007

Mueller, A. N., Ziemann, S., Treitschke, S., Assmann, D., and Doehlemann, G. (2013). Compatibility in the Ustilago maydis-maize interaction requires inhibition of host cysteine proteases by the fungal effector Pit2. *PLoS Pathog.* 9:e1003177. doi: 10.1371/journal.ppat.1003177

Niemer, M., Mehofer, U., Verdianz, M., Porodko, A., Schähs, P., Kracher, D., et al. (2016). Nicotiana benthamiana cathepsin B displays distinct enzymatic features

which differ from its human relative and aleurain-like protease. *Biochimie* 122, 119–125. doi: 10.1016/j.biochi.2015.06.017

Noh, Y.-S., and Amasino, R. M. (1999a). Identification of a promoter region responsible for the senescence-specific expression of SAG12. *Plant Mol. Biol.* 41, 181–194. doi: 10.1023/A:1006342412688

Noh, Y.-S., and Amasino, R. M. (1999b). Regulation of developmental senescence is conserved between Arabidopsis and Brassica napus. *Plant Mol. Biol.* 41, 195–206. doi: 10.1023/a:1006389803990

Ochieng, J., and Chaudhuri, G. (2010). Cystatin superfamily. *J. Health Care Poor Underserved* 21(1 Suppl.), 51–70. doi: 10.1353/hpu.0.0257

Ökmen, B., and Doehlemann, G. (2016). Clash between the borders: spotlight on apoplastic processes in plant–microbe interactions. *New Phytol.* 212, 799–801. doi: 10.1111/nph.14311

Olsen, J. V., de Godoy, L. M., Li, G., Macek, B., Mortensen, P., Pesch, R., et al. (2005). Parts per million mass accuracy on an Orbitrap mass spectrometer via lock mass injection into a C-trap. *Mol. Cell. Proteomics* 4, 2010–2021. doi: 10.1074/mcp.T500030-MCP200

Otegui, M. S., Noh, Y. S., Martinez, D. E., Vila Petroff, M. G., Staehelin, L. A., Amasino, R. M., et al. (2005). Senescence-associated vacuoles with intense proteolytic activity develop in leaves of Arabidopsis and soybean. *Plant J.* 41, 831–844. doi: 10.1111/j.1365-313X.2005.02346.x

Paireder, M., Mehofer, U., Tholen, S., Porodko, A., Schähs, P., Maresch, D., et al. (2016). The death enzyme CP14 is a unique papain-like cysteine proteinase with a pronounced S2 subsite selectivity. *Arch. Biochem. Biophys.* 603, 110–117. doi: 10.1016/j.abb.2016.05.017

Paireder, M., Tholen, S., Porodko, A., Biniossek, M. L., Mayer, B., Novinec, M., et al. (2017). The papain-like cysteine proteinases NbCysP6 and NbCysP7 are highly processive enzymes with substrate specificities complementary to Nicotiana benthamiana cathepsin B. *Biochim. Biophys. Acta Proteins Proteomics* 1865, 444–452. doi: 10.1016/j.bbapap.2017.02.007

Paungfoo-Lonhienne, C., Schenk, P. M., Lonhienne, T. G., Brackin, R., Meier, S., Rentsch, D., et al. (2009). Nitrogen affects cluster root formation and expression of putative peptide transporters. *J. Exp. Bot.* 60, 2665–2676. doi: 10.1093/jxb/erp111

Ranum, P., Peña-Rosas, J. P., and Garcia-Casal, M. N. (2014). Global maize production, utilization, and consumption. *Ann. N. Y. Acad. Sci.* 1312, 105–112. doi: 10.1111/nyas.12396

Rappsilber, J., Mann, M., and Ishihama, Y. (2007). Protocol for micro-purification, enrichment, pre-fractionation and storage of peptides for proteomics using StageTips. *Nat. Protoc.* 2, 1896–1906. doi: 10.1038/nprot.2007.261

Rawlings, N. D., Barrett, A. J., Thomas, P. D., Huang, X., Bateman, A., and Finn, R. D. (2018). The MEROPS database of proteolytic enzymes, their substrates and inhibitors in 2017 and a comparison with peptidases in the PANTHER database. *Nucleic Acids Res.* 46, D624–D632. doi: 10.1093/nar/gkx1134

Rentsch, D., Schmidt, S., and Tegeder, M. (2007). Transporters for uptake and allocation of organic nitrogen compounds in plants. *FEBS Lett.* 581, 2281–2289. doi: 10.1016/j.febslet.2007.04.013

Richau, K. H., Kaschani, F., Verdoes, M., Pansuriya, T. C., Niessen, S., Stüber, K., et al. (2012). Subclassification and biochemical analysis of plant papain-like cysteine proteases displays subfamily-specific characteristics. *Plant Physiol.* 158, 1583–1599. doi: 10.1104/pp.112.194001

Schröder, B. A., Wrocklage, C., Hasilik, A., and Saftig, P. (2010). The proteome of lysosomes. *Proteomics* 10, 4053–4076. doi: 10.1002/pmic.201000196

Sekhon, R. S., Lin, H., Childs, K. L., Hansey, C. N., Buell, C. R., de Leon, N., et al. (2011). Genome-wide atlas of transcription during maize development. *Plant J.* 66, 553–563. doi: 10.1111/j.1365-313X.2011.04527.x

Shindo, T., Misas-Villamil, J. C., Hörger, A. C., Song, J., and van der Hoorn, R. A. L. (2012). A role in immunity for Arabidopsis cysteine protease RD21, the ortholog of the tomato immune protease C14. *PLoS One* 7:e29317. doi: 10.1371/journal.pone.0029317

Stamatakis, A. (2014). RAxML version 8: a tool for phylogenetic analysis and post-analysis of large phylogenies. *Bioinformatics* 30, 1312–1313. doi: 10.1093/bioinformatics/btu033

Stelpflug, S. C., Sekhon, R. S., Vaillancourt, B., Hirsch, C. N., Buell, C. R., de Leon, N., et al. (2016). An expanded maize gene expression atlas based on RNA sequencing and its use to explore root development. *Plant Genome* 9. doi: 10.3835/plantgenome2015.04.0025

Subramanian, K., Balakrishnan, N., and Senthil, N. (2013). Mycorrhizal symbiosis to increase the grain micronutrient content in maize. *Aust. J. Crop Sci.* 7, 900–910.

Tada, Y., Spoel, S. H., Pajerowska-Mukhtar, K., Mou, Z., Song, J., Wang, C., et al. (2008). Plant immunity requires conformational changes of NPR1 via S-nitrosylation and thioredoxins. *Science* 321, 952–956. doi: 10.1126/science.1156970

Turk, D., Podobnik, M., Popovic, T., Katunuma, N., Bode, W., Huber, R., et al. (1995). Crystal structure of cathepsin B inhibited with CA030 at 2.0-A resolution: a basis for the design of specific epoxysuccinyl inhibitors. *Biochemistry* 34, 4791–4797. doi: 10.1021/bi00014a037

Turk, V., and Bode, W. (1991). The cystatins: protein inhibitors of cysteine proteinases. *FEBS Lett.* 285, 213–219. doi: 10.1016/0014-5793(91)80804-C

Tyanova, S., Temu, T., Sinitcyn, P., Carlson, A., Hein, M. Y., Geiger, T., et al. (2016). The perseus computational platform for comprehensive analysis of (prote)omics data. *Nat. Methods* 13, 731–740. doi: 10.1038/nmeth.3901

van der Hoorn, R. A., and Jones, J. D. (2004). The plant proteolytic machinery and its role in defence. *Curr. Opin. Plant Biol.* 7, 400–407. doi: 10.1016/j.pbi.2004.04.003

van der Hoorn, R. A. L. (2008). Plant proteases: from phenotypes to molecular mechanisms. *Annu. Rev. Plant Biol.* 59, 191–223. doi: 10.1146/annurev.arplant.59.032607.092835

van der Hoorn, R. A. L., Leeuwenburgh, M. A., Bogyo, M., Joosten, M. H. A. J., and Peck, S. C. (2004). Activity profiling of papain-like cysteine proteases in plants. *Plant Physiol.* 135, 1170–1178. doi: 10.1104/pp.104.041467

van der Linde, K., Hemetsberger, C., Kastner, C., Kaschani, F., van der Hoorn, R. A., Kumlehn, J., et al. (2012a). A maize cystatin suppresses host immunity by inhibiting apoplastic cysteine proteases. *Plant Cell* 24, 1285–1300. doi: 10.1105/tpc.111.093732

van der Linde, K., Mueller, A., Hemetsberger, C., Kaschani, F., Van der Hoorn, R. A., and Doehlemann, G. (2012b). The maize cystatin CC9 interacts with apoplastic cysteine proteases. *Plant Signal. Behav.* 7, 1397–1401. doi: 10.4161/psb.21902

Vizcaino, J. A., Csordas, A., del-Toro, N., Dianes, J. A., Griss, J., Lavidas, I., et al. (2016). 2016 update of the PRIDE database and its related tools. *Nucleic Acids Res.* 44, D447–D456. doi: 10.1093/nar/gkv1145

Weber, E., Engler, C., Gruetzner, R., Werner, S., and Marillonnet, S. (2011). A modular cloning system for standardized assembly of multigene constructs. *PLoS One* 6:e16765. doi: 10.1371/journal.pone.0016765

Winter, D., Vinegar, B., Nahal, H., Ammar, R., Wilson, G. V., and Provart, N. J. (2007). An "Electronic Fluorescent Pictograph" browser for exploring and analyzing large-scale biological data sets. *PLoS One* 2:e718. doi: 10.1371/journal.pone.0000718

Yang, Y., Dong, C., Yu, J., Shi, L., Tong, C., Li, Z., et al. (2014). Cysteine protease 51 (CP51), an anther-specific cysteine protease gene, is essential for pollen exine formation in Arabidopsis. *Plant Cell Tissue Organ Cult.* 119, 383–397. doi: 10.1007/s11240-014-0542-0

Young, I. M., and Crawford, J. W. (2004). Interactions and self-organization in the soil-microbe complex. *Science* 304, 1634–1637. doi: 10.1126/science.1097394

Zhao, P., Zhou, X.-M., Zhang, L.-Y., Wang, W., Ma, L.-G., Yang, L.-B., et al. (2013). A bipartite molecular module controls cell death activation in the basal cell lineage of plant embryos. *PLoS Biol.* 11:e1001655. doi: 10.1371/journal.pbio.1001655

Ziemann, S., van der Linde, K., Lahrmann, U., Acar, B., Kaschani, F., Colby, T., et al. (2018). An apoplastic peptide activates salicylic acid signalling in maize. *Nat. Plants* 4, 172–180. doi: 10.1038/s41477-018-0116-y

Conflict of Interest Statement: The authors declare that the research was conducted in the absence of any commercial or financial relationships that could be construed as a potential conflict of interest.

frontiers in Plant Science

ORIGINAL RESEARCH
published: 09 May 2019
doi: 10.3389/fpls.2019.00582

Anionic Phospholipids Induce Conformational Changes in Phosphoenolpyruvate Carboxylase to Increase Sensitivity to Cathepsin Proteases

*Jacinto Gandullo[1], José-Antonio Monreal[1], Rosario Álvarez[1], Isabel Díaz[2], Sofía García-Mauriño[1] and Cristina Echevarría[1]**

[1] Departamento de Biología Vegetal, Facultad de Biología, Universidad de Sevilla, Seville, Spain, [2] Centro de Biotecnología y Genómica de Plantas, Universidad Politécnica de Madrid, Campus de Montegancedo, Pozuelo de Alarcón, Madrid, Spain

Phosphoenolpyruvate carboxylase (PEPC) is a cytosolic, homotetrameric enzyme that serves a variety of functions in plants, acting as the primary form of CO_2 fixation in the C_4 photosynthesis pathway (C_4-PEPC). In a previous work we have shown that C_4-PEPC bind anionic phospholipids, resulting in PEPC inactivation. Also, we showed that PEPC can associate with membranes and to be partially proteolyzed. However, the mechanism controlling this remains unknown. Using semi purified-PEPC from sorghum leaf and a panel of PEPC-specific antibodies, we analyzed the conformational changes in PEPC induced by anionic phospholipids to cause the inactivation of the enzyme. Conformational changes observed involved the exposure of the *C*-terminus of PEPC from the native, active enzyme conformation. Investigation of the protease activity associated with PEPC demonstrated that cysteine proteases co-purify with the enzyme, with protease-specific substrates revealing cathepsin B and L as the major protease species present. The anionic phospholipid-induced C-terminal exposed conformation of PEPC appeared highly sensitive to the identified cathepsin protease activity and showed initial proteolysis of the enzyme beginning at the *N*-terminus. Taken together, these data provide the first evidence that anionic phospholipids promote not only the inactivation of the PEPC enzyme, but also its proteolysis.

Keywords: phosphoenolpyruvate carboxylase, phospholipids, phosphatidic acid, proteolysis, conformational changes, cathepsin proteases, sorghum

OPEN ACCESS

Edited by:
Frank Van Breusegem, Ghent University, Belgium

Reviewed by:
Jens Staal, Flanders Institute for Biotechnology, Belgium
R. Glen Uhrig, University of Alberta, Canada

***Correspondence:**
Cristina Echevarría
echeva@us.es

Specialty section:
This article was submitted to Plant Physiology, a section of the journal Frontiers in Plant Science

Received: *05 November 2018*
Accepted: *18 April 2019*
Published: *09 May 2019*

Citation:
Gandullo J, Monreal J-A, Álvarez R, Díaz I, García-Mauriño S and Echevarría C (2019) Anionic Phospholipids Induce Conformational Changes in Phosphoenolpyruvate Carboxylase to Increase Sensitivity to Cathepsin Proteases. Front. Plant Sci. 10:582. doi: 10.3389/fpls.2019.00582

INTRODUCTION

C_4-phosphoenolpyruvate carboxylase (PEPC; EC 4.1.1.31) catalyzes the first carboxylation step in C_4 photosynthesis. Due to the key role that this enzyme plays in the C_4 pathway, the biochemical and signaling mechanisms controlling PEPC activity in the cytosol of leaf mesophyll cells have received significant research attention (Chollet et al., 1996; Echevarria and Vidal, 2003; Izui et al., 2004). In sorghum, PEPC belongs to a multigene family encoding five closely related plant-type PEPCs (PTPC; SbPEPC1-5) and one distantly related bacterial-type PEPC (BTPC)

(Ruiz-Ballesta et al., 2016). Of the PTPCs, one family member, SbPEPC1, is an example of a C_4 photosynthetic PEPC, playing a functional role in C_4 and Crassulacean acid metabolism (CAM)-type photosynthesis, while the remaining four homologs, SbPEPC2-5, are C_3 PEPCs, that perform alternative functions in plants (O'Leary et al., 2011). C_4-PEPC has evolved from an ancestral non-photosynthetic C_3-PEPC. Two important aa determine C_3/C_4-specific function. In the susbtrate-binding center, Ala774 (*Flaveria* numbering) mediates C_3 specificity, while Ser774 determines the increased kinetic efficiency of C_4 PEPC (Paulus et al., 2013). Malate binding in the inhibitory site, is controlled by Arg884 in the C_3 enzyme while, the increased tolerance of C_4-PEPC to the malate inhibitor is mediated by Gly884 (Paulus et al., 2013). All PTPCs are subject to a light-dependent phosphorylation process involving an *N*-terminal regulatory serine that interacts with metabolite effectors, such as the feedback inhibitor L-malate, and the allosteric activator Glucose-6-phosphate (Glc-6P; Echevarria and Vidal, 2003). In addition, C_3-type plant PEPCs have also been shown to be regulated by monoubiquitination (Uhrig et al., 2008; Shane et al., 2013; Ruiz-Ballesta et al., 2014, 2016), though this has not been demonstrated for the photosynthetic C_4-PEPC to date (unpublished results).

C_4-PEPC, Rubisco and pyruvate orthophosphate dikinase are very abundant in plants with C_4-photosynthesis and together account for almost the same amount of protein as observed for Rubisco alone in C_3 plants (Feller et al., 2008). While numerous studies have described Rubisco proteolysis occurring as a consequence of senescence and nutrient reutilization (Otegui, 2018), little is known about the mechanism by which C_4-PEPC may be degraded. Scarce data on the protease(s) involved in determining the C_4-PEPC turnover rate and the amount of protein in the leaf tissue under normal and stress conditions are available. A study by Monreal et al. (2007), showed that a decrease in C_4-PEPC leaf content occurred in response to LiCl treatment and senescence. However, the integrity and activity of the remaining enzyme were unaffected, suggesting reduced catabolism of C_4-PEPC in response to these conditions (Monreal et al., 2007). A variety of proteolytic activities have been proposed for the degradation of other PEPC variants in different plant cell types. It has been hypothesized that the proteolysis of C_3-PEPC in guard cells during their closing phase of action may be dependent on the ubiquitin-proteasome system (Klockenbring et al., 1998). In addition, a C_3-PEPC in castor oil seeds is degraded *in vitro* via a thiol endopeptidase requiring dithiothreitol and salt to remove its *N*-terminus thereby generating a 98 kDa PEPC fragmented form (Crowley et al., 2005; Uhrig et al., 2008). Finally, a bacterial PEPC from castor oil seeds has been shown to be degraded via a cysteine endopeptidase (Gennidakis et al., 2007).

We previously reported that C_4-PEPC, from sorghum, is a phosphatidic acid (PA)-binding protein that shows inhibited activity in presence of PA and other anionic phospholipids (Monreal et al., 2010). In comparison, a study examining tomato and Arabidopsis plants, demonstrated that C_3-PEPC isoenzymes react differently to their C_4-PEPC counterparts, binding PA in cell cultures with increased affinity under conditions of cellular stress (Testerink et al., 2004). However, the molecular basis for this difference in C_4- and C_3-PEPC isoenzymes requires further investigation. Monreal et al. (2010) have shown, via fractionation of sorghum leaf crude extracts, that while the majority of the enzyme is present in the cytosol, a portion of C_4-PEPC is also associated with the cell membranes where it was found to be partially degraded (Monreal et al., 2010). This finding paves the idea that the interaction of PEPC with the membrane phospholipids could indeed lead to its degradation.

In this study we used antibodies to the final 19 C-terminal amino acids of PEPC (C19-IgG) to investigate the effects of the anionic phospholipids PA, phosphatidylinositol 4-P (PI), and lyso-PA (LPA) on PEPC and their potential to induce a conformational change in the enzyme, exposing the *C*-terminus and inactivating the complex. The *C*-terminal domain of PEPC is normally embedded in a hydrophobic region of the protein subunit (Kai et al., 1999; Alvarez et al., 2003), where the carboxyl group of the *C*-terminal residue G960 moves toward the PEP-binding site to allow formation of an ion pair, with the side chain of R647, forming the active enzyme conformation (Kai et al., 2003). The exposure of the *C*-terminus promoted by anionic phospholipids may disrupt the interaction of the ion pair with the R647 side chain, resulting in the inactivation of the enzyme. In addition, this exposed *C*-terminus conformation is highly sensitive to proteolysis by cysteine proteases, which co-purified with PEPC. Here we examine the precise role of PA and anionic phospholipids in PEPC proteolysis and partial characterization of the papain proteases co-purified with PEPC.

MATERIALS AND METHODS

Materials

Polyclonal antibodies against: (i) synthetic peptides corresponding to sorghum C_4-PEPC *C*-terminus [(Y) 942EDTLILTMKGIAAGMQNTG960] and dephosphorylated *N*-terminus [4ERHHSIDAQLRALAPGKVSEE24(YG)], C19-IgG and N24-IgG, respectively, were purchased from NEOSYSTEM S.A. (Strasbourg, France); and (ii) native C_4-PEPC from sorghum leaves (PEPC-IgG) achieved as described in Pacquit et al. (1995).

Phospholipids with varying format and fatty acyl chain composition were all purchased from Avanti Polar Lipids, (Alabaster, AL, United States). Lipids in chloroform stock were dried with gaseous N_2, rehydrated in 0.1 M Tris–HCl buffer (pH 8) and sonicated prior to adding to the assays. Protease inhibitors used were: Chymostatin (cysteine protease, chymotrypsin and elastase inhibitor); phenylmethane sulfonyl fluoride (PMSF; serine protease inhibitor); Aprotinin (serine protease inhibitor); Bestatin (aminopeptidase inhibitor); Leupeptin (serine and cysteine protease inhibitor); E-64 (selective cysteine protease inhibitor, such as cathepsin B and L); and protease inhibitor cocktail (AEBSF; serine proteases inhibitor; Phenanthroline, metalloproteases inhibitor; Pepstatin A, acid proteases inhibitor, Leupeptine, Bestatin and E-64) from Sigma Aldrich code P9599 (St Louis, MO, United States).

Plant Material and Growth Conditions

Sorghum plants (*Sorghum bicolor* (L.) Moench, var. PR87G57; Pioneer Hi-Bred Spain) were grown under controlled environmental conditions in a greenhouse, using a 12 h photoperiod (350 μmol m^{-2} s^{-1}, photosynthetically active radiation), a temperature of 28/20°C (light/dark) and 60% relative humidity, in hydroponic cultures with nitrate-type nutrient solution (Hewitt, 1966).

Preparation of Semi-Purified C_4-PEPC Fraction

All procedures were carried out at 4°C. Dark-adapted (12 h) sorghum leaves (20 g) were homogenized in a Waring blender with 100 mL of extraction buffer containing 0.1 M Tris–HCl pH 7.5, 5 % (v/v) glycerol, 1 mM EDTA, 10 mM $MgCl_2$ and 14 mM β-mercaptoethanol, 1 mM phenylmethysulfonyfluoride (PMSF), 10 μg mL^{-1} chymostatin, 10 μg mL^{-1} leupeptin, 10 mM potassium fluoride, and 2% (w/v) polyvinylpyrrolidone (PVP). The homogenate was filtered through two layers of 80 μm nylon net and centrifuged at 45,000 *g* for 10 min. Proteins in the supernatant were precipitated by polyethylene glycol 8000 (PEG; 8.5% – 15%) and then sedimented by centrifugation (45,000 *g*, 10 min). The pellet was dissolved in 7 mL of buffer A containing 50 mM Hepes/ KOH pH 7.1, 5 mM $MgCl_2$, 1 mM EDTA, 5 mM dithiothreitol (DTT). Econo-Pac CHT-II chromatography cartridges packed with hydroxyapatite (5 mL) from Bio-Rad (Berkeley, CA, United States) were equilibrated with buffer A and anion-exchange chromatography (5 mL, Bio-Rad catalog number 723-4122) was performed according to the procedure of McNaughton et al. (1989), with the exception that chromatography was performed in a Bio-Rad Econo-System at low pressure. The final specific activity of the semi-purified fraction was determined to be 78.5 ± 5 U ml^{-1}. PEPC activity and L-malate sensitivity were determined as described in Echevarria et al. (1994). Soluble protein concentration was measured via a Bradford assay (Bradford et al., 1976), using bovine serum albumin (BSA) as a standard. This final preparation was stored at −20°C, in the presence of 50% glycerol and used as a semipurified-PEPC (sp-PEPC).

Preparation of Crude Extracts From Sorghum Leaves

Protein extracts were obtained by grinding 0.2 g fresh weight of leaf tissue using sand and 1 ml of extraction buffer containing: 0.1 M Tris–HCl buffer (pH 7.5), 20% (v/v) glycerol, 1 mM EDTA, 10 mM $MgCl_2$, 14 mM β-mercaptoethanol, 1 mM PMSF, 10 μg mL^{-1} leupeptin. The homogenate was centrifuged at 12,000 *g* for 2 min. The supernatant was removed and used as a clarified protein extract.

Assessment of Phospholipid Activity on PEPC Activity

Due to the hydrophobic nature of phospholipids difficulties in their solubilization are acknowledged. Consequently, the apparent activity of every preparation was tested prior to its use. An aliquot of sp-PEPC was incubated in the presence or absence of the different lipids for analysis in 50 μl of a medium containing: 0.1 M Tris–HCl buffer (pH 8), 20% glycerol and 0.1 to 0.2 U of PEPC, at 30°C. Aliquots (5 μl) were taken to measure PEPC activity at pH 8.0 and 2.5 mM PEP, at the beginning and following 30 min of incubation. Activity was expressed as a percentage of the initial activity (see **Figure 1C**). Anionic but not neutral phospholipids may completely inactivate the enzyme within 30 min (Monreal et al., 2010).

Proteolytic Assay in Standard Conditions

An aliquot of sp-PEPC containing co-purified protease(s) was incubated in 50 μl of a medium containing 0.1 M Tris–HCl buffer (pH 8) and 20% glycerol, at 30°C, in the presence or absence of the test lipids and/ or protease inhibitors. Aliquots were taken at different times during incubation, analyzed by SDS–PAGE (10% [w/v] acrylamide) and stained with Coomassie Blue or used for immunoblotting.

Assessment of Protease Activity Using Fluorescent Substrates

Protease activity was assessed by measuring the hydrolysis of substrates containing the 7-amino-4-methyl coumarin (AMC) fluorophore in a microtiter plate format, at optimal pH according to the protease of interest. The standard assay volume was 100 μl containing 25 μl of sp-PEPC and the corresponding substrate added to a final concentration of 0.2 mM (Carrillo et al., 2011). Cathepsin B-like (CTB), L-like (CTL) and legumain (LEG) activities were assayed using *N*-Carbobenzoxyloxy-Arg-Arg-7-amido-4-methylcoumarin, (Z-RR-AMC); *N*-Carbobenzoxyloxy-Phe-Arg-7-amido-4-methylcoumarin (Z-FR-AMC) and *N*-Carbobenzoxyloxy-Ala-Ala-Asn-7-amido-4-methylcoumarin (Z-AAN-AMC) substrates, respectively, with a buffer containing 0.1 M citrate pH 6. Trypsin-like (TRY) and elastase-like (ELA) activities were assayed using Z-L-arginine-7-amido-4-methylcoumarin (ZLA-AMC) and MeOSuc-Ala-Ala-Pro-Val-7-amido-4-methylcoumarin (MeOS-AAPV-AMC) substrates, respectively, and a buffer containing 0.1 M glycine-NaOH pH 9.5. The leucine aminopeptidase (LAP) activity was assayed using L-Leu-7-amido-4-methyl coumarin (LL-AMC) substrate in a buffer containing 0.1 M Tris–HCl pH 7.5. All buffers contained 0.15 M NaCl and 5 mM $MgCl_2$ (Carrillo et al., 2011). The reaction was incubated at 30°C for 24 h and fluorescence emitted was quantified with a 365 nm excitation wavelength filter and 465 nm emission wavelength filter in triplicate. Blanks were used to account for spontaneous breakdown of substrates and results were expressed as μmol min^{-1} ml^{-1}. The system was calibrated with known amounts of AMC in a standard reaction mixture.

Assay of PEPC Activity

PEPC activity was measured spectrophotometrically at pH 8.0 using the NAD-malate dehydrogenase-coupled assay at 2.5 mM PEP (Echevarria et al., 1994).

In vitro Phosphorylation and PEPC Phosphorylation State

Aliquots of sp-PEPC were phosphorylated *in vitro* by the catalytic subunit of PKA from bovine heart according to the methods of Alvarez et al. (2003). The phosphorylation state of PEPC was determined using an L-malate test (Echevarria et al., 1994), where the malate inhibition of PEPC activity determined at suboptimal pH of 7.3 is expressed as an IC_{50} value. A high IC_{50} value is correlated to a high degree of PEPC phosphorylation (Echevarria et al., 1994).

Electrophoresis and Immunoblotting

Protein samples were subjected to SDS–PAGE (10% [w/v] acrylamide) according to the method of Laemmli (Laemmli, 1970) at room temperature for 2 h at 100 V in a Mini-Protean ®III-2D cell (Bio-Rad). After electrophoresis, proteins on the gels were stained with Coomassie Blue R-250 or electroblotted onto a nitrocellulose membrane (N-8017, Sigma) at 10 V (5.5 mA cm^{-2}) for 30 min in a semidry transfer blot apparatus (Bio-Rad Laboratories). Membranes were blocked in Tris-buffered saline (20 mM Tris–HCl and 0.15 mM NaCl [pH 7.5]) containing 5% (w/v) powdered milk, and bands were immunochemically labeled by overnight incubation of the membrane at 4°C in 20 ml of Tris-buffered saline containing specific antibodies. Subsequent detection was performed using a horseradish peroxidase conjugated antibody (Bio-Rad) by a peroxidase assay (**Figures 1**, **2**, **3**, **5**) or by a chemiluminescence detection system (Super Signal West Dura Signal; ThermoFisher, Waltham, MA, United States) according to the manufacturer's instructions (**Figures 4**).

Immunoprecipitation

Immunoprecipitation of PEPC polypeptides following different experimental treatments was performed with relevant antibodies, as previously described by Osuna et al. (1999). Immunoprecipitates and supernatants were analyzed by SDS–PAGE and detected by Coomassie blue or immunoblotting.

Statistical Analysis

All data in this report were obtained from at least three independent replicates. Data were analyzed by ANOVA and means were compared using the Duncan's Multiple Range Test or the Dunnett test. A *P*-value of <0.05 was considered to be statistically significant. All statistical analyses were performed using SPSS statistic 34 software (IBM, Armonk, NY, United States).

RESULTS

Phosphatidic Acid Inactivates PEPC Promoting Conformational Change

Sorghum C_4-PEPC is a PA-binding protein that is inhibited in the presence of PA and other anionic phospholipids. The mechanism of this inhibition remains unknown, though it appears to be independent of allosteric regulators, substrate or pH (Monreal et al., 2010). To investigate the potential mechanism by which PA could inhibit C_4-PEPC C19-IgG were utilized. Employing these antibodies allowed analysis of any potential changes in the conformation of the *C*-terminal portion of the protein, which is typically embedded within the protein subunit in the native protein conformation (Kai et al., 2003). To this end, 0.2 U of sp-PEPC were incubated with 0.25 mM PA for 30 min, at 30°C. After incubation 30 μg of C19-IgG were added and incubated 30 min more at room temperature. Finally, protein A (4% [w/v]) was added to the assay to precipitate the immune-complexes and analyzed by SDS–PAGE (**Figure 1A**) or immunoblotted and revealed with PEPC-IgG (**Figure 1B**). C19-IgG failed to immunoprecipitate the majority of native PEPC under standard conditions (**Figures 1A,B**, lane C2). This finding is in agreement with previous studies, demonstrating that the most abundant and active form of PEPC exhibits an embedded *C*-terminus conformation, which would not interact with the C19-IgG used (Alvarez et al., 2003; Kai et al., 2003). However, following incubation of sp-PEPC with PA, immunoprecipitation of PEPC was observed (**Figures 1A,B**, lanes PA). Both the anionic phospholipids PI and LPA have also been previously described as inhibitors of PEPC activity (Monreal et al., 2010), and treatment of sp-PEPC with either of these anionic phospholipids, in this study, similarly, resulted in exposure of the PEPC *C*-terminus to a similar extent as for PA (**Figure 1A**, PI and LPA; **Figure 1B**, LPA). In contrast to the activity of anionic phospholipids on the conformation of PEPC, both the non-anionic phospholipids, phosphatidylcholine (PC) and phosphatidylethanolamine (PE) minimally precipitated the enzyme, suggesting that they have little effect in inducing the conformational change of PEPC promoted by anionic phospholipids (**Figures 1A,B**, lanes PC and PE). Two controls were included in the experiment: an immunoprecipited PEPC with total PEPC-IgG (**Figures 1A,B**, lane C1), and PEPC heated at 60°C, 2 min, to completely expose the *C*-terminus previous to the incubation with C19-IgG (**Figure 1A**, lane 60°C; Alvarez et al., 2003). Finally, **Figure 1C** show the effectiveness of the phospholipids on PEPC activity in absence of C19-IgG. As expected (Monreal et al., 2010), complete inhibition of PEPC activity was observed in the presence of PA, PI or LPA, while PEPC activity was not affected by PC or PE (**Figure 1C**).

These results indicate that anionic phospholipids inactivate C_4-PEPC promoting a conformational change, including exposure of the *C*-terminus. It is known that the carboxyl group of the *C*-terminal residue G960 is directed toward the PEP-binding site in the active conformation of PEPC and forms an ion pair with the side chain of residue R647, which is critical for maximal catalytic activity (Kai et al., 2003).

Glc-6P Reverses the Enzyme Conformation to an Embedded *C*-Terminal State

Many elements have been shown to regulate PEPC activity, including pH, enzyme phosphorylation state, and the presence of specific metabolites. To determine whether any of these factors influence the exposure of the PEPC *C*-terminus, the

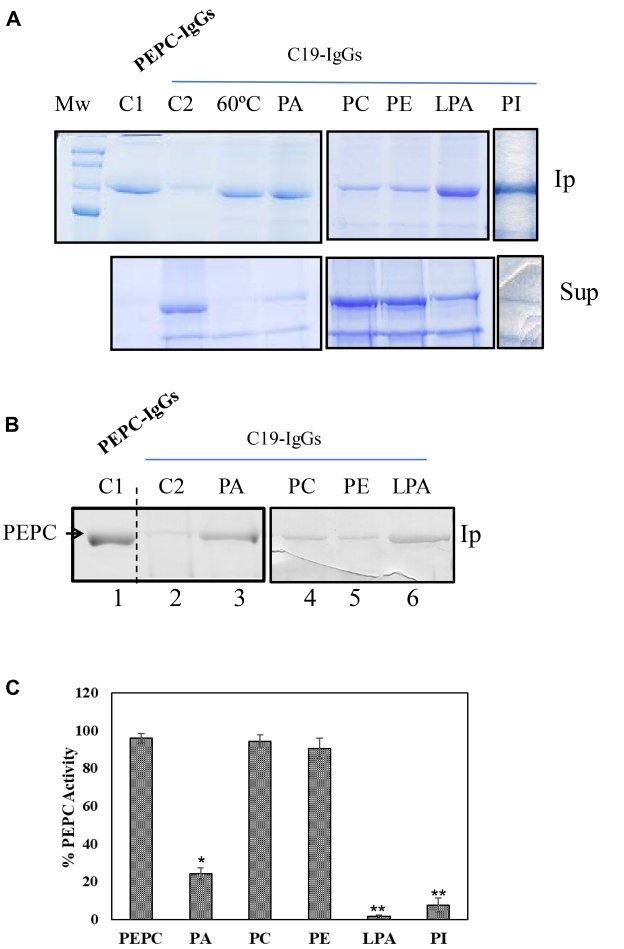

FIGURE 1 | Anionic phospholipids promoted extensive conformational changes in PEPC detected by the exposure of its *C*-terminus. 0.2 U **(A)** or 0.1 U **(B)** of PEPC were incubated in the absence (lanes C1, C2 and 60°C) or presence of 0.25 mM of the phospholipids indicated (lanes PA, PC, PE, LPA, PI). Following 30 min incubation at 30°C, PEPC was immunoprecipitated with PEPC-IgG (lane C1) or C19-IgG (remaining samples). An aliquot of PEPC was heated at 60°C for 2 min to serve as a positive control for C19-IgG (lane 60°C). This treatment completely exposes the *C*-terminus of the protein (Alvarez et al., 2003). **(A)** Immunoprecipitates (Ip) and supernatant (Sup) were analyzed by SDS–PAGE (10%) and stained with Coomassie blue. **(B)** Immunoprecipitates were immunoblotted with PEPC-IgG. The images in **(A)** and **(B)** are representative of at least 3 independent experiments. **(C)** Effect of the different phospholipids on PEPC activity. PA, phosphatidic acid; PC, phosphatidylcholine; PE, phosphatidylethanolamine; LPA, lyso-PA; PI, phosphatidylinositol4-P. Data represent mean ± SE of 3–6 different experiments. Statistically significant difference with respect controls are indicated by (*) at $P < 0.05$, (**) at $P < 0.01$, using the Dunnett test.

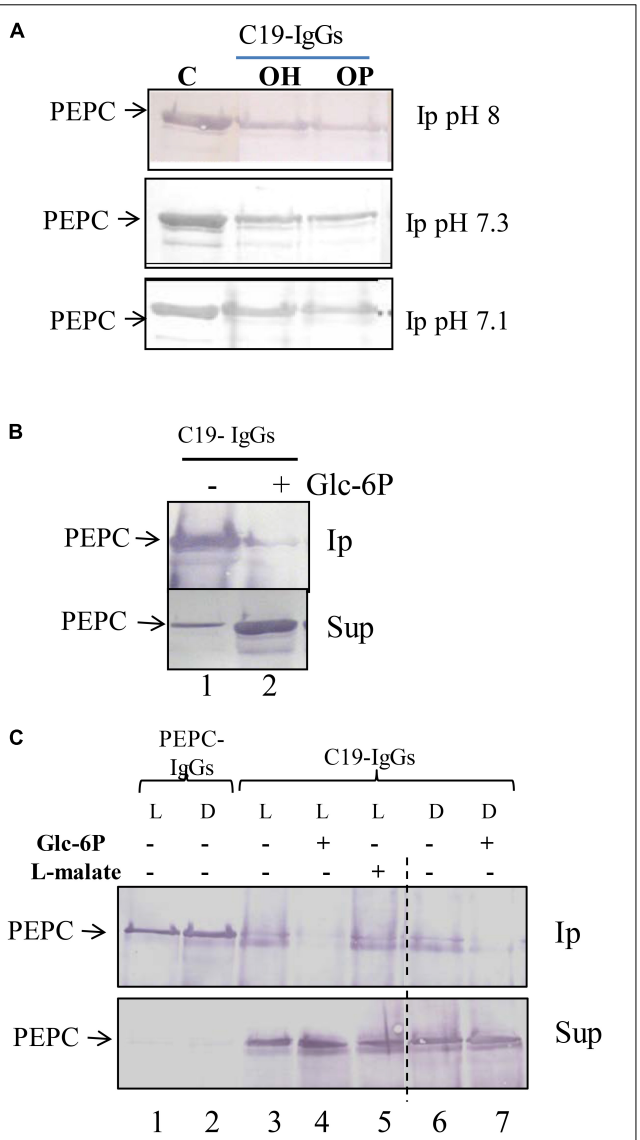

FIGURE 2 | Effect of pH, enzyme phosphorylation state and Glc-6P on the exposure of the *C*-terminus of C_4-PEPC. **(A)** Phosphorylated (OP) or non-phosphorylated (OH) sp-PEPC were incubated in 0.1 M Tris–HCl buffer at different pHs (8, 7,3 or 7,1). Following 30 min at 30°C, PEPC was immunoprecipitated with C19-IgG. Lane C, sp-PEPC prior to immunoprecipitation. Phosphorylated PEPC was obtained by *in vitro* phosphorylation with PKA as described in M&M. **(B)** Non-phosphorylated PEPC incubated with 5 mM Glc-6P for 30 min and then immunoprecipitated with C19-IgG. **(C)** Clarified protein extract from illuminated (L, phosphorylated-PEPC) or dark (D, non-phosphorylated-PEPC) sorghum leaves incubated in the presence of Glc-6P or L-malate and immunoprecipitated with PEPC-IgG (lanes 1, 2) or C19-IgG (lanes 3–7). Protein was detected on immunoblots using PEPC-IgG. Ip, immunoprecipitated; Sup, supernatant. The enzyme phosphorylation state was controlled via the L-malate sensitivity test (**Table 1**).

enzyme conformation was assessed following incubation of sp-PEPC (0.1 U) under a number of different conditions for 1 h at 30°C (**Figure 2**). Post-treatment the PEPC enzyme was immunoprecipitated with C19-IgG, and analyzed by SDS–PAGE and immunoblot. Phosphorylated PEPC was obtained by *in vitro* phosphorylation with PKA and the enzyme phosphorylation state was controlled by use of the L-malate sensitivity test (see Table 1; Echevarria et al., 1994). Neither the phosphorylation state of PEPC nor changes in pH significantly modified the degree of exposure of the *C*-terminus (**Figure 2A**).

Interestingly, treatment of PEPC in which the *C*-terminal was exposed (**Figure 2B**, Ip, lane 1), with Glc-6P appeared to

TABLE 1 | The efficacy of *in vitro* phosphorylation of PEPC with PKA (sp-PEPC), and the *in vivo* phosphorylation state of PEPC in leaves exposed to light (phosphorylated PEPC) or dark (dephosphorylated PEPC) were determined via the L-malate sensitivity test as is described in M & M and Echevarria et al., 1994).

	Phosphorylation state of PEPC (IC_{50} for L-malate)	
sp-PEPC	OH-PEPC	OP-PEPC
	0.64 ± 0.02	0.94 ± 0.07
Leaves Crude Extracts	Dark	Light
	0.31 ± 0.02	0.65 ± 0.03

OH-PEPC, non-phosphorylated PEPC; OP-PEPC, phosphorylated PEPC. Values are mean ± SEM of triplicate assays.

reverse the protein denaturation. In the presence of Glc-6P the C19-IgG failed to precipitate the enzyme (**Figure 2B**, Ip, lane 2) despite its extensive presence in the supernatant (**Figure 2B**, Sup, lane 2). Similar results were obtained by incubating desalted crude extracts from darkened or illuminated leaves with Glc-6P (**Figure 2C**, lanes 4 and 7). Conversely, in the presence of L-malate, a known negative effector of PEPC, (Chollet et al., 1996), the enzyme precipitated to a similar extent as the untreated control (**Figure 2C**, lane 5). Minimal difference in the level of PEPC immunoprecipitation was observed between the crude extracts obtained from illuminated (phosphorylated PEPC) or darkened (dephosphorylated PEPC) leaves (**Figure 2C**, lane 3 and 6). The phosphorylation state of PEPC from illuminated and darkened leaves was determined via the L-malate test (Echevarria et al., 1994) with leaves from illuminated plants showing twice the IC_{50} of those of darkened leaves (**Table 1**).

These results demonstrate that the conformational change promoted by the allosteric activator Glc-6P (Chollet et al., 1996) involves the *C*-terminus moving toward an embedded conformation, to stabilize the enzyme. The embedded and exposed *C*-terminal conformations of PEPC correlate well with high and low C_4-PEPC enzyme activity. This integration of the *C*-terminus into the enzyme structure was seen to be induced in the presence of Glc-6P, and not by changes in the pH or phosphorylation state of the enzyme.

Anionic Phospholipids (PA, PI, and LPA) Increase the Sensitivity of PEPC to Proteolysis

Regulation of PEPC proteolysis has not been extensively studied to date, and consequently little is known about the sensitivity of the different PEPC conformations to proteolysis. The observation that PA, PI, and LAP promoted a conformational change within the PEPC protein, including exposure of the *C*-terminus and inactivation of the enzyme, prompted us to explore whether this conformation was more sensitive to proteolysis.

C_4-PEPC was obtained from dark-adapted sorghum leaves, by means of polyethylene glycol precipitation and chromatography on hydroxyapatite and anion exchange as described in M & M. This PEPC was pure, as shown by Coomassie-staining and SDS–PAGE (**Figure 3**, lanes 3). The preparation appeared stable at −20°C in a medium containing 0.1 M Tris–HCl, pH 7.5, 40% [v/v] glycerol for several weeks (**Figure 3**, lane 4). However, storage for 3 months at −20°C resulted in PEPC appearing to be partially proteolyzed (**Figure 3**, lane 5), providing evidence for the presence of proteases. We termed this fraction containing PEPC and proteases sp-PEPC within this study.

PEPC was shown to be very stable under standard incubation conditions, even for extended time periods of up to 20 h at 30°C (**Figure 4**, lanes C). However, incubation of sp-PEPC in the presence of 0.25 mM PA for 20 h resulted in proteolysis of the enzyme (**Figure 4**, lane PA). Comparable effects were observed for the physiological PA species, C18:1, and the water-soluble short-chain PA, C8:0 (**Supplementary Figure S1**). PA appeared effective in degrading PEPC at concentrations from approximately 0.25–1 mM PA (**Figure 4B**). However, it is difficult to accurately estimate the concentration of PA, as the physiological PA species (C18:1) is highly insoluble. The concentration of PA C8:0 (the water-soluble short-chain variant of PA) necessary to inhibit PEPC activity by 50% (IC_{50}) was previously estimated by Monreal et al. (2010) and shown to be about 65 μM. Incubation of PEPC with the anionic phospholipids PI or LPA, also showed induction of the proteolysis of PEPC (**Figure 4**, lanes PI and LPA). Conversely, in the presence of the neutral phospholipids, PC or PE, PEPC maintained its integrity to a similar extent as the control (**Figure 4**, lanes PC and PE).

Collectively, these results provide evidence that PEPC can be targeted for proteolysis by interaction with anionic phospholipids, such as PA, and that the exposure of the enzyme's *C*-terminus sensitizes the enzyme to this degradation. The contribution of the *C*-terminus of PEPC to the stability of the enzyme has previously referred by Xu et al. (2006). They found that mutagenic deletion of the last 19 residues of C_4-PEPC from sorghum leaf (Leu-942 to G960), resulted in marked reductions in C_4 enzyme accumulation when transformed onto PEPC *E. coli* cells (Xu et al., 2006).

Finally, PEPC activity was not restored following incubation with PA or LPA in the presence of proteases inhibitors (**Supplementary Figure S2**). This result suggests that the inhibition of PEPC activity in the early interaction with anionic

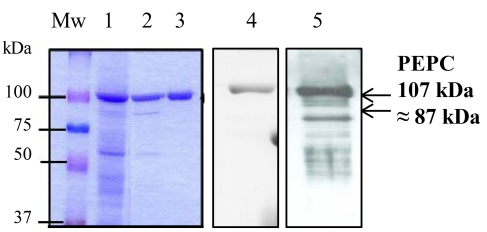

FIGURE 3 | SDS–PAGE analysis of the sp-PEPC fraction during the purification process. PEPC (0.2 U) from the different purification steps were subjected to SDS–PAGE and staining with Commassie blue. Lane 1, clarified protein extract from dark-adapted sorghum leaves; Lanes 2, 3, chromatografhy on Hydroxyapatite and on anion-exchange, respectively. Lane 3 correspond to the final sp-PEPC preparation mainly used in the experiments. Lanes 1–3 contain 0.2 U of PEPC). Lane 4, immunoblot of lane 3 (0.05 U PEPC) detected using PEPC-IgG. Lane 5, immunoblot of sp-PEPC (0.1 U PEPC) following 3 months at –20°C.

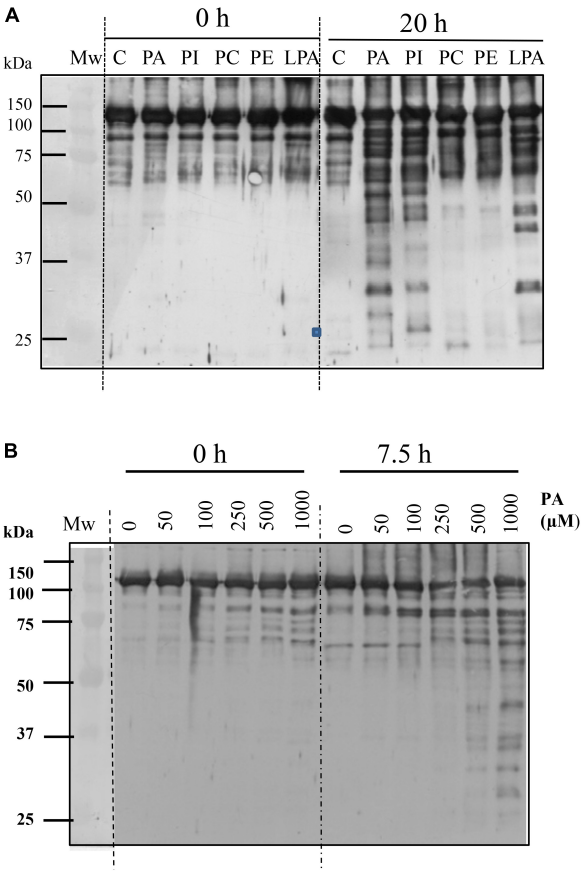

FIGURE 4 | Anionic phospholipids promote proteolysis of C_4-PEPC. **(A)** Sp-PEPC was incubated in the absence (lane C) or in the presence of 0.25 mM of the different phospholipids (lanes PA, PI, PC, PE, LPA) at 30°C as is described in M&M. **(B)** Range of PA concentration promoting PEPC proteolysis. A standard proteolytic assay was performed with increasing concentrations of PA18:1. At the indicated times, 0.05 U PEPC aliquots were removed and subjected to immunoblot. Bands were detected with PEPC-IgG.

phospholipids is due mainly to the conformational changes shown in **Figure 1** and not to its proteolysis.

The PEPC *N*-Terminal Is the Initial Target of PA-Induced Proteolysis

To determine whether the exposed *C*-terminus is an early target for proteolysis sp-PEPC samples were incubated in the presence and absence of 0.25 mM PA during 60 min at 30°C, followed by the addition of C19-IgG for 1.5 h at room temperature. Antibody-bound PEPC complexes were precipitated with protein A and analyzed by SDS–PAGE to reveal that, as expected, PA drives the exposure of the *C*-terminal thus allowing greater precipitation of the protein in the presence of PA. However, SDS–PAGE analysis of the pulled-down PEPC protein showed that a fraction of the protein appeared to be partially proteolyzed (**Figure 5A**, lane 3). As C19-IgG were used to bind the immuno-complexes, it is assumed that the *C*-terminal is present in this PEPC fragment and consequently it is not the target of the early proteolytic activity observed. This was confirmed using specific N24-IgG that recognize the *N*-terminus of the enzyme (the peptide [4ERHHSIDAQLRALAPGKVSEE24(YG)]). PEPC was incubated with PA and subsequently analyzed with the use of PEPC-IgG to show PEPC fragments of different size on immunoblots. However, analysis of these blots using the N24-IgG revealed that the various partially degraded PEPC fragments showed loss of the *N*-terminus at the beginning of the proteolytic process (**Figure 5B**, N24-IgG).

Taken together, these results suggest that the exposed *C*-terminus is not an early target for PA-induced proteolysis in sp-PEPC, rather, a fragment at the *N*-terminal portion of the protein is the initial site of protein degradation.

PEPC Co-purifies With Papain-Like Proteases

In order to identify the types of proteases that co-purified with PEPC as part of the sp-PEPC sample used in this study, a partial characterization of these enzymes was performed. Incubation of PEPC in the presence of PA and a variety of different protease inhibitors allowed identification of the protease activity. The protease activity in the sp-PEPC fraction appeared to be strongly inhibited by the inclusion of chymostatin (65 μM), a Cys/Ser protease type inhibitor (**Figure 6A**, lane 5); by E-64, a specific

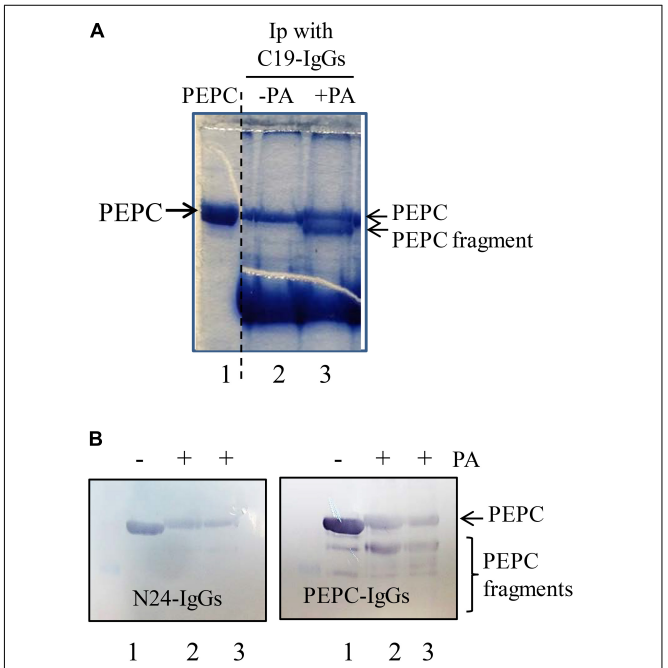

FIGURE 5 | The *N*-terminal of PEPC is the initial target of PA-induced proteolysis. A standard proteolytic assay as is described in M&M was performed in presence or absence of 0.25 mM PA. **(A)** Coomassie blue stained PEPC samples exposed to PA for 60 min at 30°C and immunoprecipitated with C19-IgG. Lane 1, PEPC prior to immunoprecipitation. Lane 2, PEPC without PA. Lane 3, PEPC in presence of PA; **(B)** Immunoblot analysis of PEPC exposed to PA at different times and detected using N24-IgG or PEPC-IgG. Lane 1, PEPC control without PA. Lanes 2 and 3 in B, 5 or 7 h of incubation in presence of PA, respetively.

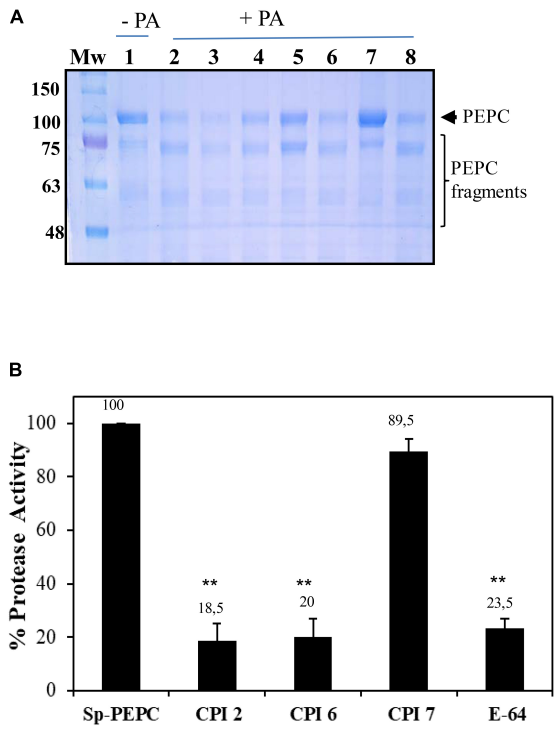

FIGURE 6 | (A) sp-PEPC exposed to PA in the presence of protease inhibitors: sp-PEPC control (lane 1), no protease inhibitors (lane 2), 1 mM Bestatin (lane 3), 0.2 mM Leupeptin (lane 4), 0.065 mM Chymostatin (lane 5), 1 mM PMSF (lane 6), Sigma protease inhibitor cocktail containing AEBSF, 1,10-Phenanthroline, Pepstatin, Leupeptin, Bestatin and E-64 (lane 7) or 0.1 mM Aprotinin (lane 8). Following 20 h of incubation at 30°C, samples were subjected to SDS–PAGE and stained with Commassie Blue. **(B)** Cistatin and E-64 inhibit the protease activity present in sp-PEPC. Aliquots of sp-PEPC (25 μl) were incubated with 1 μM of recombinant purified cystatin (CIP) or E-64 in a 0.1 M citrate buffer (pH 6), 0.15 M NaCl and 5 mM $MgCl_2$ for 10 min at 30°C. Protease activity was assayed by addition of 2 mM of the cathepsin L-specific substrate, Z-FR-AMC. The reaction was developed 5 h at 30°C. Protease activity is expressed as % with respect to the control in absence of inhibitor (sp-PEPC). Date are the mean ± SE of triplicate measurement and statistically significant difference with respect to the control are indicated by (*) at $P < 0.05$, (**) at $P < 0.01$, using the Dunnett test.

inhibitor of cysteine proteases (**Figure 6B**); and also, by the plant protease inhibitor cocktail (**Figure 6A**, lane 7) containing among others E-64. Other inhibitors such as bestatin (1 mM), leupeptine (0.2 mM), PMSF (1 mM) or aprotinin (100 μM), showed no significant inhibition on the protease activity present in sp-PEPC (**Figure 6**, lanes 3, 4, 6 and 8, respectively).

Commercial fluorescent substrates that are commonly used to identify proteases based on their specific activities, were utilized here to further characterize the proteases associated with sp-PEPC. Among the substrates assayed, Z-RR-AMC and Z-FR-AMC, substrates for cathepsin B-like (CTB) and cathepsin L-like (CTL) proteases, respectively, showed a large degree of degradation (**Table 2**). It is well known that the substrate Z-RR-AMC is highly specific for cathepsin B, while Z-FR-AMC is acted upon by cathepsin L, B, and F (Malagón et al., 2010). Proteolytic activity was detected throughout the range pH 5.5-8 in the presence of cathepsin B-like substrates (CTB), (**Supplementary Figure S3**). Cathepsin B-like and Cathepsin L-like proteases are cysteine proteases belonging to the papain-like family C1A (family C1, clan CA). This family is the most extensively studied and the most abundant among plant cysteine peptidases (Martínez and Díaz, 2008). Others substrates, such as LAP (Leucin aminopeptidase substrate), TRY (trypsin-like protease substrate), LEG (legumain protease substrate) and ELA (elastase-like protease substrate) were poorly proteolyzed or showed no proteolysis following incubation with sp-PEPC (**Table 2**).

Cystatin protease inhibitors are small proteins that have the ability to inhibit cysteine proteases from the papain-like family, C1A. These natural inhibitors play an important role in the regulation of endogenous cysteine protease activity (Martínez and Díaz, 2008; Díaz-Mendoza et al., 2014). Cystatin-2 (CPI-2) has been shown to significantly reduce cathepsin L-like and B-like activity in barley protein extracts, while CPI-6 is a specific inhibitor of cathepsin B. CPI-7 is reported to be inactive against a broad spectrum of proteases from barley (Martínez et al., 2009, 2012). Using the substrate with the broadest spectrum for cysteine proteases (Z-FR-AMC), the effect of the three recombinant cystatins (CPI-2, CPI-6, CPI-7) on protease activity in the sp-PEPC fraction was analyzed. Protease activity co-purified with PEPC appeared to be strongly inhibited by both CPI-2 and CPI-6, but not CPI-7 (**Figure 6B**).

Collectively, these results show that cysteine proteases are present in the sp-PEPC fraction and may be responsible for the proteolysis of PEPC in presence of PA. Among them, papain-like protease(s) (cathepsin B and L-like), from the C1A subfamily of the large Cys peptidase family are the major species present.

DISCUSSION

Little is known about the mechanism by which PEPC is proteolyzed. Several proteases have been described as possessing proteolytic activity that may target PEPC *in vitro*, though their *in vivo* activity often remains unexplored. Within this study,

TABLE 2 | Identification of protease activities present in sp-PEPC fraction using specific protease fluorescent substrates.

Protease activity	pH[a]	Activity[c] (μMol/min.ml sp-PEPC)
CTB	6.0	**43,3 ± 0,44 a**
CTL	6.0	**34 ± 3,98 b**
LEG	6.0	0,05 ± 0,02 c
TRY	9.5	2,73 ± 0,89 c
ELA	9.5	0,05 ± 0,02 c
LAP	7.5	5,65 ± 0,97 c

CTB, cathepsin B-like; CTL, cathepsin L-like; LEG, legumain; TRY, trypsin; ELA, elastase; LAP, leucine aminopeptidase. [a]pH measurements were the optimal for the different type of proteases activities [c]. Values are mean ± SEM of triplicate measurements. Different letters denote statistically significant differences according to Duncan's multiple range test, $p < 0.05$.

we describe a relationship between the interaction of C_4-PEPC with anionic phospholipids and the proteolysis of this enzyme. The results presented here demonstrate that PA changes the conformation of the enzyme, resulting in the exposure of the *C*-terminus to allow its precipitation by C19-IgG (**Figure 1**). This conformation was found to be sensitive to proteolysis. Incubation of PEPC in presence of PA increased the proteolysis of the enzyme (**Figure 4**). The conformational changes and the induction of proteolysis were also promoted by other anionic phospholipids, such as PI or LPA, leading the exposure of the *C*-terminus (**Figure 1**) and the inactivation of the enzyme (Monreal et al., 2010, and **Figure 1C**). Neutral phospholipids, such as PC or PE, minimally influenced conformational change in PEPC or any resultant proteolysis. These results represent the first *in vitro* evidence of anionic phospholipids being identified as possible molecules that can trigger the proteolysis of C_4-PEPC. As we have previously described, a portion of intracellular PEPC *in vivo* interacts with the cellular membranes, and this membrane-associated PEPC appears partially proteolyzed (Monreal et al., 2010). Hence, the results presented in this work support the hypothesis that anionic phospholipids could recruit PEPC to the cell membranes for its proteolysis. A previous study by Wu and Wedding (1992), lends weight to this idea, as it discusses the *in vitro* inactivation of maize leaf PEPC by its binding to the outer chloroplast membranes. Association of PEPC with the outer chloroplast membrane has also been observed by additional immunolocalization studies (Perrot-Rechenmann et al., 1982). Furthermore, bacterial- and plant-type PEPC isozymes from developing castor oil seeds have been seen to interact *in vivo* and associate with the outer surface of mitochondria (Park et al., 2012).

Other metabolic enzymes, such as Rubisco, have been reported to travel to the vacuole to be proteolyzed. The proteolysis of Rubisco has been extensively studied and different mechanisms have been described, whereby Rubisco is packed into senescence-associated lytic vacuoles (SAV) that are rich in cysteine proteases, or into Rubisco-containing bodies (RCBs) that drive the enzyme to the vacuole to be digested. Also, Three different autophagic vesicles, in addition to the process of chlorophagy, have also been reported to degrade Rubisco (Ono et al., 2013; for a further revision Otegui, 2018). Rubisco, represents an important source of nitrogen in senescence conditions and is the main target for proteases (Ono et al., 2013). However, in C_4 plants, photosynthetic C_4-PEPC is highly abundant and competes with the Rubisco for nitrogen. PEPC constitutes about a 15% of total soluble protein in C_4 plants (maize). The ratio of phosphoenolpyruvate carboxylase to Rubisco in C_4-plant is about 2:1, whereas it is of 0.1:1 in C_3-plants (O'Leary, 1982). Consequently, in a similar manner as Rubisco, C_4-PEPC may serve as another important target for proteases in senescent leaves. In fact, PEPC is degraded in sorghum plants treated with LiCl and in old leaves of control plants (García-Mauriño et al., 2003; Monreal et al., 2007). Taken together, these results suggest a potential mechanism by which anionic phospholipids are able to inactivate PEPC and target the enzyme for proteolysis. This could be of interest in a physiological context where the degradation of C_4-PEPC is necessary (such as in senescence, stress or photo-damaging radiation) in parallel with other abundant metabolic enzymes such as Rubisco in order to recycle key nutrients. In agreement with this concept, PA transiently accumulates in plant cells within minutes of applying a wide array of stress conditions (O'Leary et al., 2011). Whether the association of C_4-PEPC with cell membranes acts as the initiation of a proteolytic pathway, similar to those operating for Rubisco, or it interact with the membrane of the chloroplast to be engulfed in a chlorophagic process (Otegui, 2018) remains to be investigated. Further experiments will be necessary to study the possible association and/or location of GFP-fused C_4-PEPC in vesicles that are eventually transported into the vacuole for degradation, as occurs with Rubisco (Otegui, 2018). Finally, investigation are need to know how PEPC activity or cellular location is influenced by changes in anionic membranes phospholipids.

Sorghum C_4-PEPC is a PA-binding protein that is inhibited in the presence of anionic phospholipids, PA, PI and LPA. In this work we outlined the mechanism by which PA may inactivate PEPC. This mechanism is based upon the conformational change observed in PEPC that is induced by PA and other anionic phospholipids, in which the C-terminal is exposed. The carboxyl group of the *C*-terminal residue G960 forms part of the active site of PEPC (Kai et al., 2003). Movement of this amino acid impacts on the active conformation of PEPC, driving it to inactivation. Previous reports of the relevance of the *C*-terminus in determining PEPC activity and stability support these findings (Xu et al., 2006).

Glc-6P is a known allosteric activator of PEPC (Chollet et al., 1996). Higher plant PEPCs are generally inhibited by L-malate and activated by Glu-6P. During C_4 photosynthesis PEPC has to fix bicarbonate in the presence of its allosteric inhibitor L-malate. The concentration of L-malate in the mesophyll cell is high enough to block PEPC activity. In this context, PEPC activity is activated *in vivo* by the interplay of Glc-6P and the phosphorylation state of the enzyme (Echevarria et al., 1994). Our findings demonstrate that Glu-6P is able to change the conformation of PEPC to promote the native embedded *C*-terminus conformation (**Figure 2B**) that activates and stabilizes the enzyme against proteolysis. This finding supports the fact that the embedded and exposed conformations of the *C*-terminus correlate well with the active and inactive state of the enzyme, respectively. The influence of the conformational state of PEPC on its proteolysis has been previously demonstrated in maize PEPC with the use of *in vitro* trypsin treatment. For maize PEPC, the activation state of the enzyme during the trypsin attack is dependent upon the presence of a catalytic effector or substrates (PEP+Mg, Glc-6P or L-malate) during the treatment (Maralihalli and Bhagwat, 2001).

Proteolysis of the *N*-terminal of PEPC during purification has been extensively reported. PEPC from maize leaves (C_4-PEPC photosynthetic form) was purified as a double band of 109 and 105 kDa, where the105 kDa species represented a proteolyzed version of the 109 kDa protein in which L-malate sensitivity was lost (McNaughton et al., 1989). The presence of the protease inhibitor chymostatin throughout the enzyme preparation was found to be essential for the maintenance of the L-malate

sensitivity of PEPC during purification. This result suggests that chymostatin acts to protect the enzyme against cleavage of a peptide bond close to the N-terminal domain, which includes the phosphorylation site and sensitivity to malate (McNaughton et al., 1989). Other protease inhibitors, such as Benzamidine and PMSF, failed to prevent this proteolysis. Indeed, similar results were reported by Baur et al. (1992), who demonstrated that when purified in the absence of the protease inhibitor chymostatin, PEPC from *Mesembryanthemum crystallinum* lost an *N*-terminal sequence of 128 amino acids. This proteolyzed enzyme could not be phosphorylated *in vitro*, which is in agreement with the *N*-terminal domain containing the phosphorylation motif (Baur et al., 1992). In both cases the proteolysis of this *N*-terminal fragment affected L-malate sensitivity, but did not impact upon the final specific PEPC activity. Furthermore, it has been reported that the proteolytic cleavage of the 22 amino acids at the *N*-terminal of C_4-PEPC markedly decrease its malate sensitivity (Duff and Chollet, 1995; Chollet et al., 1996). The *N*-terminal proteolysis of the non-photosynthetic PEPC (C_3-PEPC) has also recently been investigated, demonstrating that proteolysis of this C_3-PEPC is performed by an endogenous asparaginyl endopeptidase, which hydrolyzes a polypeptide of approximately 120 amino acids from the *N*-terminus of the castor oil seed PEPC (Crowley et al., 2005). Pioneering studies have shown that the *in vivo* processing of PEPC during the germination of castor oil seeds includes monoubiquitination, with both monoubiquitinated and deubiquitinated subunits being *N*-terminally truncated by 19 amino acids. Moreover, processing of the non-ubiquitinated subunits was induced by truncation of 4 amino acids at the *N*-terminus (Uhrig et al., 2008; O'Leary et al., 2011).

In this study, we have identified and partially characterized a protease activity that co-purified with PEPC. This enzyme showed sensitivity to the Ser/Cys-protease inhibitors, chymostatin and E-64. A more extensive characterization using specific commercial fluorescent substrates, commonly used to identify proteases based on their specific activity, was carried out. Among the substrates assayed, CTB and CTL (substrates for cathepsin B-like and cathepsin L-like proteases, respectively) were efficiently degraded by the proteolytic activity present in the sp-PEPC. Moreover, the protease activity was inhibited by CPI-2 and CPI-6, cystatin inhibitors specific to cathepsin-like proteases L and B, but was not affected by CPI-7 (**Figure 6B**), which has been shown to be inactive against a broad spectrum of proteases in barley plants (Martínez et al., 2009). In agreement with previous studies on the degradation of PEPC, we have shown that proteolysis performed by the identified cysteine protease activity resulted in the initial loss of a fragment from the *N*-terminal of C_4-PEPC (**Figure 5**).

Our results show that cysteine proteases are the main source of protease activity present in the sp-PEPC fraction, with papain-like proteases (cathepsin B and L) representing the majority of co-purified proteases. To gain further information concerning the role of this protease activity, including its physiological relevance to PEPC turnover within the context of C_4-photosynthesis in normal and stressed conditions, it is essential that the protein is purified and the gene identified. Aditionally, bimolecular fluorescence complementation (BiFC) experiments will be necessary to verify the association of the proposed proteases with PEPC *in vivo*.

CONCLUSION

Here we have outlined the mechanism by which PA and other anionic phospholipids inhibit C_4-PEPC activity in sorghum. Large conformational changes in the C_4-PEPC protein complex, evidenced by the exposure of the *C*-terminus, that remains embedded within the protein in the active conformation, are responsible for the inhibition of C_4-PEPC. It has also been demonstrated that the conformational change promoted by anionic phospholipids is very sensitive to proteolysis by proteases that co-purify with C_4-PEPC. These proteases have been partially characterized and found to largely consist of cysteine proteases, with an abundance of cathepsin B and L. Finally, this work represents the first demonstration that anionic phospholipids could trigger one of the different proteolytic pathways operating to degrade C_4-PEPC.

AUTHOR CONTRIBUTIONS

JG, J-AM, CE, SG-M conceived the idea and led the study design. JG, J-AM, RÁ carried out the experiments. ID provided fluorescent substrates of proteases and cystatin for the experiments of proteases characterization which were performed in her laboratory by JG. CE wrote the manuscript.

FUNDING

This work was supported by projects n° BFU2007-61431, AGL2012-35708 and AGL2016-75413-P from "Ministerio de Educación y Ciencia," n° P06-CVI-02186 from "La Junta de Andalucía" and by the "Grupo de Investigación de Fosforilación de Proteínas en Plantas y Metabolismo del Carbono BIO-298" from "La Junta de Andalucía."

ACKNOWLEDGMENTS

We deeply acknowledge Christa Testerink the collaboration that allowed us to start this line of research. We thank Jean Vidal for discussions, advice and his help in writing this manuscript. We also thank Charlesworth Author Services for revised and re-written the manuscript.

SUPPLEMENTARY MATERIAL

The Supplementary Material for this article can be found online at: https://www.frontiersin.org/articles/10.3389/fpls.2019.00582/full#supplementary-material

REFERENCES

Alvarez, R., García-Mauriño, S., Feria, A.-B., Vidal, J., and Echevarría, C. (2003). A conserved 19-amino acid synthetic peptide from the carboxy terminus of phosphoenolpyruvate carboxylase inhibits the in vitro phosphorylation of the enzyme by the calcium-independent phosphoenolpyruvate carboxylase kinase. *Plant Physiol.* 132, 1097–1106. doi: 10.1104/pp.103.023937

Baur, B., Dietz, K. J., and Winter, K. (1992). Regulatory protein phosphorylation of phosphoenolpyruvate carboxylase in the facultative crassulacean-acid-metabolism plant: *Mesembryanthemum crystallinum* L. *Eur. J. Biochem.* 209, 95–101. doi: 10.1111/j.1432-1033.1992.tb17265.x

Bradford, M. M., Dong, Y., Xu, L., Liu, S., Bai, X., Bradford, M., et al. (1976). A rapid and sensitive method for the quantitation of microgram quantities of protein utilizing the principle of protein-dye binding. *Anal. Biochem.* 72, 248–254. doi: 10.1016/0003-2697(76)90527-90523

Carrillo, L., Martínez, M., Ramessar, K., Cambra, I., Castañera, P., Ortego, F., et al. (2011). Expression of a barley cystatin gene in maize enhances resistance against phytophagous mites by altering their cysteine-proteases. *Plant Cell Rep.* 30, 101–112. doi: 10.1007/s00299-010-0948-z

Chollet, R., Vidal, J., and O'Leary, M. H. (1996). Phosphoenolpyruvate carboxylase: a ubiquitous, highly regulated enzyme in plants. *Annu. Rev. Plant Physiol. Plant Mol. Biol.* 47, 273–298. doi: 10.1146/annurev.arplant.47.1.273

Crowley, V., Gennidakis, S., and Plaxton, W. C. (2005). In vitro proteolysis of phosphoenolpyruvate carboxylase from developing castor oil seeds by an endogenous thiol endopeptidase. *Plant Cell Physiol.* 46, 1855–1862. doi: 10.1093/pcp/pci203

Díaz-Mendoza, M., Velasco-Arroyo, B., González-Melendi, P., Martínez, M., and Díaz, I. (2014). C1A cysteine protease-cystatin interactions in leaf senescence. *J. Exp. Bot.* 65, 3825–3833. doi: 10.1093/jxb/eru043

Duff, S., and Chollet, R. (1995). In vivo regulation of wheat-leaf phosphoenolpyruvate carboxylase by reversible phosphorylation. *Plant Physiol.* 107, 775–782.

Echevarria, C., Pacquit, V., Bakrim, N., Osuna, L., Delgado, B., Arrio-dupont, M., et al. (1994). The effect of pH on the covalent and metabolic control of C4 phosphoenolpyruvate carboxylase from *Sorghum* leaf. *Arch. Biochem. Biophys.* 315, 425–430. doi: 10.1006/abbi.1994.1520

Echevarria, C., and Vidal, J. (2003). The unique phosphoenolpyruvate carboxylase kinase. *Plant Physiol. Biochem.* 41, 541–547. doi: 10.1016/S0981-9428(03)00068-68

Feller, U., Anders, I., and Mae, T. (2008). Rubiscolytics: fate of rubisco after its enzymatic function in a cell is terminated. *J. Exp. Bot.* 59, 1615–1624. doi: 10.1093/jxb/eru043

García-Mauriño, S., Monreal, J. A., Alvarez, R., Vidal, J., and Echevarría, C. (2003). Characterization of salt stress-enhanced phosphoenolpyruvate carboxylase kinase activity in leaves of sorghum vulgare: independence from osmotic stress, involvement of ion toxicity and significance of dark phosphorylation. *Planta* 216, 648–655.

Gennidakis, S., Rao, S., Greenham, K., Uhrig, R. G., O'Leary, B., Snedden, W. A., et al. (2007). Bacterial- and plant-type phosphoenolpyruvate carboxylase polypeptides interact in the hetero-oligomeric Class-2 PEPC complex of developing castor oil seeds. *Plant J.* 52, 839–849. doi: 10.1111/j.1365-313X.2007.03274.x

Hewitt, E. J. (1966). Sand and water culture methods used in the study of plant nutrition. *Commonw. Bur. Hortic.* 22:547.

Izui, K., Matsumura, H., Furumoto, T., and Kai, Y. (2004). Phosphoenolpyruvate carboxylase: a new era of structural biology. *Annu. Rev. Plant Biol.* 55, 69–84. doi: 10.1146/annurev.arplant.55.031903.141619

Kai, Y., Matsumura, H., Inoue, T., Terada, K., Nagara, Y., Yoshinaga, T., et al. (1999). Three-dimensional structure of phosphoenolpyruvate carboxylase: a proposed mechanism for allosteric inhibition. *Proc. Natl. Acad. Sci. U.S.A.* 96, 823–828. doi: 10.1073/pnas.96.3.823

Kai, Y., Matsumura, H., and Izui, K. (2003). Phosphoenolpyruvate carboxylase: three-dimensional structure and molecular mechanisms. *Arch. Biochem. Biophys.* 414, 170–179. doi: 10.1016/S0003-9861(03)00170-X

Klockenbring, T., Meinhard, M., and Schnabl, H. (1998). The stomatal phosphoenolpyruvate carboxylase: a potential target for selective proteolysis during stomatal closure? *J. Plant Physiol.* 152, 222–229. doi: 10.1016/S0176-1617(98)80136-80133

Laemmli, U. K. (1970). Cleavage of structural proteins during the assembly of the head of bacteriophage T4. *Nature* 227, 680–685. doi: 10.1038/227680a0

Malagón, D., Díaz-López, M., Benítez, R., and Adroher, F. J. (2010). Cathepsin B- and L-like cysteine protease activities during the in vitro development of *Hysterothylacium aduncum* (Nematoda: Anisakidae), a worldwide fish parasite. *Parasitol. Int.* 59, 89–92. doi: 10.1016/j.parint.2009.11.001

Maralihalli, G. B., and Bhagwat, A. S. (2001). Limited proteolysis by trypsin influences activity of maize phosphoenolpyruvate carboxylase. *Indian J. Biochem. Biophys.* 38, 361–367.

Martínez, M., Cambra, I., Carrillo, L., Díaz-Mendoza, M., and Díaz, I. (2009). Characterization of the entire cystatin gene family in barley and their target cathepsin L-like cysteine-proteases, partners in the hordein mobilization during seed germination. *Plant Physiol.* 151, 1531–1545. doi: 10.1104/pp.109.146019

Martínez, M., Cambra, I., Gonzalez-Melendi, P., Santamaria, M. E., and Díaz, I. (2012). C1A cysteine-proteases and their inhibitors in plants. *Physiol. Plant* 145, 85–94. doi: 10.1111/j.1399-3054.2012.01569.x

Martínez, M., and Díaz, I. (2008). The origin and evolution of plant cystatins and their target cysteine proteinases indicate a complex functional relationship. *BMC Evol. Biol.* 8:198. doi: 10.1186/1471-2148-8-198

McNaughton, G. A., Fewson, C. A., Wilkins, M. B., and Nimmo, H. G. (1989). Purification, oligomerization state and malate sensitivity of maize leaf phosphoenolpyruvate carboxylase. *Biochem. J.* 261, 349–355. doi: 10.1042/bj2610349

Monreal, J. A., López Baena, F. J., Vidal, J., Echevarría, C., and García-Mauriño, S. (2007). Effect of LiCl on phosphoenolpyruvate carboxylase kinase and the phosphorylation of phosphoenolpyruvate carboxylase in leaf disks and leaves of *Sorghum vulgare*. *Planta* 225, 801–812.

Monreal, J. A., McLoughlin, F., Echevarría, C., García-Mauriño, S., and Testerink, C. (2010). Phosphoenolpyruvate carboxylase from C4 leaves is selectively targeted for inhibition by anionic phospholipids. *Plant Physiol.* 152, 634–638. doi: 10.1104/pp.109.150326

O'Leary, B., Park, J., and Plaxton, W. C. (2011). The remarkable diversity of plant PEPC (phosphoenolpyruvate carboxylase): recent insights into the physiological functions and post-translational controls of non-photosynthetic PEPCs. *Biochem. J.* 436, 15–34. doi: 10.1042/BJ20110078

O'Leary, M. (1982). Phosphoenolpyruvate carboxylase: an enzymologist' view. *Ann. Rev. Plant Physiol.* 33, 297–315.

Ono, Y., Wada, S., Izumi, M., Makino, A., and Ishida, H. (2013). Evidence for contribution of autophagy to rubisco degradation during leaf senescence in *Arabidopsis thaliana*. *Plant Cell Environ.* 36, 1147–1159. doi: 10.1111/pce.12049

Osuna, L., Pierre, J.-N., González, M.-C., Álvarez, R., Cejudo, F.-J., Echevarría, C., et al. (1999). Evidence for a slow-turnover form of the Ca^{2+} -independent phosphoenolpyruvate carboxylase kinase in the aleurone-endosperm tissue of germinating barley seeds. (in press).

Otegui, M. S. (2018). Vacuolar degradation of chloroplast components: autophagy and beyond. *J. Exp. Bot.* 69, 741–750. doi: 10.1093/jxb/erx234

Pacquit, V., Giglioli, N., Cretin, C., Pierre, J. N., Vidal, J., and Echevarria, C. (1995). Regulatory phosphorylation of C4 phosphoenolpyruvate carboxylase from sorghum. an immunological study using specific anti-phosphorylation site antibodies. *Photosynth. Res.* 43, 283–288. doi: 10.1007/BF0002994

Park, J., Khuu, N., Howard, A. S. M., Mullen, R. T., and Plaxton, W. C. (2012). Bacterial- and plant-type phosphoenolpyruvate carboxylase isozymes from developing castor oil seeds interact in vivo and associate with the surface of mitochondria. *Plant J.* 71, 251–262. doi: 10.1111/j.1365-313X.2012.04985.x

Paulus, J. K., Schlieper, D., and Groth, G. (2013). Greater efficiency of photosynthetic carbon fixation due to single amino-acid substitution. *Nat. Commun.* 4:1518. doi: 10.1038/ncomms2504

Perrot-Rechenmann, C., Vidal, J., Brulfert, J., Burlet, A., and Gadal, P. (1982). A comparative immunocytochemical localization study of phosphoenolpyruvate carboxylase in leaves of higher plants. *Planta* 155, 24–30. doi: 10.1007/BF00402927

Ruiz-Ballesta, I., Baena, G., Gandullo, J., Wang, L., She, Y. M., Plaxton, W. C., et al. (2016). New insights into the post-translational modification of multiple phosphoenolpyruvate carboxylase isoenzymes by phosphorylation and monoubiquitination during sorghum seed development and germination. *J. Exp. Bot.* 67, 3523–3536. doi: 10.1093/jxb/erw186

Ruiz-Ballesta, I., Feria, A. B., Ni, H., She, Y. M., Plaxton, W. C., and Echevarría, C. (2014). In vivo monoubiquitination of anaplerotic phosphoenolpyruvate carboxylase occurs at Lys624 in germinating sorghum seeds. *J. Exp. Bot.* 65, 443–451. doi: 10.1093/jxb/ert386

Shane, M. W., Fedosejevs, E. T., and Plaxton, W. C. (2013). Reciprocal control of anaplerotic phosphoenolpyruvate carboxylase by in vivo monoubiquitination and phosphorylation in developing proteoid roots of phosphate-deficient *Harsh Hakea*. *Plant Physiol.* 161, 1634–1644. doi: 10.1104/pp.112.213496

Testerink, C., Dekker, H. L., Lim, Z. Y., Johns, M. K., Holmes, A. B., De Koster, C. G., et al. (2004). Isolation and identification of phosphatidic acid targets from plants. *Plant J.* 39, 527–536. doi: 10.1111/j.1365-313X.2004.02152.x

Uhrig, R. G., She, Y. M., Leach, C. A., and Plaxton, W. C. (2008). Regulatory monoubiquitination of phosphoenolpyruvate carboxylase in germinating castor oil seeds. *J. Biol. Chem.* 283, 29650–29657. doi: 10.1074/jbc.M806102200

Wu, M.-X., and Wedding, R. T. (1992). Inactivation of maize leaf phosphoenolpyruvate carboxylase by the binding to chloroplast membranes. *Plant Physiol.* 100, 382–387. doi: 10.1104/pp.100.1.382

Xu, W., Ahmed, S., Moriyama, H., and Chollet, R. (2006). The importance of the strictly conserved, C-terminal glycine residue in phosphoenolpyruvate carboxylase for overall catalysis: mutagenesis and truncation of GLY-961 in the sorghum C4 leaf isoform. *J. Biol. Chem.* 281, 17238–17245. doi: 10.1074/jbc.M602299200

Conflict of Interest Statement: The authors declare that the research was conducted in the absence of any commercial or financial relationships that could be construed as a potential conflict of interest.

frontiers in Plant Science

PERSPECTIVE
published: 29 May 2019
doi: 10.3389/fpls.2019.00721

Plant Proteases: From Key Enzymes in Germination to Allies for Fighting Human Gluten-Related Disorders

*Manuel Martinez[1,2], Sara Gómez-Cabellos[1], María José Giménez[3], Francisco Barro[3], Isabel Diaz[1,2] and Mercedes Diaz-Mendoza[1]**

[1] Centro de Biotecnologia y Genomica de Plantas, Instituto Nacional de Investigacion y Tecnologia Agraria y Alimentaria (INIA), Universidad Politécnica de Madrid (UPM), Campus Montegancedo UPM, Madrid, Spain, [2] Departamento de Biotecnologia-Biologia Vegetal, Escuela Tecnica Superior de Ingenieria Agronomica, Alimentaria y de Biosistemas, Universidad Politécnica de Madrid (UPM), Madrid, Spain, [3] Departamento de Mejora Genética Vegetal, Instituto de Agricultura Sostenible (IAS-CSIC), Córdoba, Spain

Plant proteases play a crucial role in many different biological processes along the plant life cycle. One of the most determinant stages in which proteases are key protagonists is the plant germination through the hydrolysis and mobilization of other proteins accumulated in seeds and cereal grains. The most represented proteases in charge of this are the cysteine proteases group, including the C1A family known as papain-like and the C13 family also called legumains. In cereal species such as wheat, oat or rye, gluten is a very complex mixture of grain storage proteins, which may affect the health of sensitive consumers like celiac patients. Since gluten proteins are suitable targets for plant proteases, the knowledge of the proteases involved in storage protein mobilization could be employed to manipulate the amount of gluten in the grain. Some proteases have been previously found to exhibit promising properties for their application in the degradation of known toxic peptides from gluten. To explore the variability in gluten-degrading capacities, we have now analyzed the degradation of gluten from different wheat cultivars using several cysteine proteases from barley. The wide variability showed highlights the possibility to select the protease with the highest potential to alter grain composition reducing the gluten content. Consequently, new avenues could be explored combining genetic manipulation of proteolytic processes with silencing techniques to be used as biotechnological tools against gluten-related disorders.

Keywords: cysteine protease, germination, proteolysis, gluten, celiac disorders

OPEN ACCESS

Edited by:
Agnieszka Ludwików, Adam Mickiewicz University in Poznań, Poland

Reviewed by:
Barend Juan Vorster, University of Pretoria, South Africa
Philippe Etienne, University of Caen Normandy, France
Jerica Sabotič, Jožef Stefan Institute (IJS), Slovenia

****Correspondence:***
Mercedes Diaz-Mendoza
mercedes.diaz.mendoza@upm.es

Specialty section:
This article was submitted to Plant Biotechnology, a section of the journal Frontiers in Plant Science

Received: *22 February 2019*
Accepted: *16 May 2019*
Published: *29 May 2019*

Citation:
Martinez M, Gómez-Cabellos S, Giménez MJ, Barro F, Diaz I and Diaz-Mendoza M (2019) Plant Proteases: From Key Enzymes in Germination to Allies for Fighting Human Gluten-Related Disorders. Front. Plant Sci. 10:721. doi: 10.3389/fpls.2019.00721

INTRODUCTION

Plant proteases have been described to accomplish multiple roles in different physiological processes along the plant life cycle, such as programmed cell death, senescence, abscission, fruit ripening, plant growth, and N homeostasis (Grudkowska and Zagdańska, 2004; van der Hoorn, 2008; Liu et al., 2018; Tornkvist et al., 2019). In response to abiotic and biotic stresses, proteases are also involved in nutrient remobilization associated with leaf and root proteins degradation to ensure yield (Diaz-Mendoza et al., 2014; Velasco-Arroyo et al., 2016, 2018; Gomez-Sanchez et al., 2019; James et al., 2019), or in triggering the response of the plant to pathogens and phytophagous insects

and acari (van der Hoorn and Jones, 2004; Shindo and van der Hoorn, 2008; Misas-Villamil et al., 2016; Diaz-Mendoza et al., 2017). Moreover, plant proteases play a crucial role in the plant seed germination, through the mobilization of other proteins accumulated in seeds and cereal grains (Grudkowska and Zagdańska, 2004; Cambra et al., 2012; Diaz-Mendoza et al., 2016; Szewinska et al., 2016; Liu et al., 2018; Radchuk et al., 2018).

Cereals grains include proteins with many different functions. Around 80% of these proteins are storage proteins, packed in the endosperm together with starch and lipids (Shewry et al., 1995; Shewry and Halford, 2002). These proteins are synthesized during grain development and maturation, subsequently included as storage proteins, and finally degraded during germination. Several groups of proteases have been implicated in seed germination. The most represented proteases in charge of the mobilization and degradation of storage proteins are the cysteine proteases (CysProt) (Grudkowska and Zagdańska, 2004; Tan-Wilson and Wilson, 2011; Szewinska et al., 2016). Among CysProt, the C1A family known as papain-like and the C13 family also called legumains or vacuolar processing enzymes (VPEs), have been the most studied (Hara-Nishimura et al., 1995, 1998; Kinoshita et al., 1999; Grudkowska and Zagdańska, 2004; Prabucka and Bielawski, 2004; Martínez and Díaz, 2008; Shi and Xu, 2009; Szewinska et al., 2016).

Pharmaceutical, food and beverage, detergent, and biofuel industries have for long time exploited enzyme catalysis in commercial-scale applications, being the use of papain an example of success in food industry over the last four decades (Fernández-Lucas et al., 2017). In recent years, newly identified plant proteases have been found to exhibit promising properties for their application in the food industry (Feijoo-Siota and Villa, 2011). A case of particular interest is the degradation of peptides toxic for celiac patients by proteases involved in the germination of cereals (Hartmann et al., 2006; Kiyosaki et al., 2007; Stenman et al., 2009, 2010). In particular, the 33-mer peptide of gluten is the most immunogenic peptide known so far. It is resistant to human proteases and responsible for eliciting about 90% of the allergic response induced by the full complement of wheat proteins (Tye-Din et al., 2010). The immunogenic peptide can be hydrolyzed by a combination of at least six different peptidases from sourdough lactobacilli and fungal proteases provided as a food supplement (De Angelis et al., 2010). However, the finding and use of plant proteases have several advantages compared to bacterial and fungal peptidases; they are natural components of harmless food and, unlike the fungal proteases, their safety must not be proven with potential benefits for both therapeutics and food processing (Comino et al., 2013). Therefore, the co-administration of exogenous proteases with food is a very appealing therapeutic treatment for celiac patients by facilitating gluten degradation. In particular, the knowledge of the proteases involved in storage protein mobilization could be employed to discover proteases able to degrade gluten efficiently. Several pathologies have been described with gluten intake: celiac disease (CD), an autoimmune disorder with a prevalence of about 0.7–2% in the human population (Rewers, 2005) that has increased in the last fifty years (Rubio-Tapia et al., 2009); and non-celiac wheat sensitivity (NCWS), a new pathology which is estimated to occur in about 6% of the population in western countries (Sapone et al., 2011).

PLANT PROTEASES IN THE GERMINATION PROCESS OF BARLEY

In cereal grains, different proteases have been involved in the germination process (Müntz et al., 2002; Grudkowska and Zagdańska, 2004; Tan-Wilson and Wilson, 2011; Szewinska et al., 2016). In maize, wheat and barley the CysProts are responsible of around 90% of the proteolytic activity (De Barros and Larkins, 1994; Zhang and Jones, 1995; Bottari et al., 1996). Plant CysProts from the papain family (C1A) (Mikkonen et al., 1996; Prabucka and Bielawski, 2004; Shi and Xu, 2009; Cambra et al., 2012; Diaz-Mendoza et al., 2016) and CysProts of the legumain family (C13) (Hara-Nishimura et al., 1998; Radchuk et al., 2011, 2018), are the most representative groups in proteolysis and mobilization of storage proteins in cereal grain. Other proteases have been implicated in the germination process in cereal grains, such as the S10 serine carboxypeptidases (Ser-) (Dal Degan et al., 1994; Washio and Ishikawa, 1994; Dominguez and Cejudo, 1999; Domínguez et al., 2002; Li et al., 2016).

Barley is one of the grain cereals further studied. Proteases, amylases, dextrinases and other hydrolases are crucial for the survival of the seedling until the photosynthesis is finally established (**Figure 1**). In the barley germination, proteases of the papain-like C1A (Koehler and Ho, 1988, 1990a,b; Poulle and Jones, 1988; Zhang and Jones, 1995; Sreenivasulu et al., 2008) and the legumain-like C13 families (Linnestad et al., 1998; Radchuk et al., 2011, 2018) have mainly been identified. Besides, the expression of six serine carboxypeptidases (Ser-CPs) during maturation and germination of the barley grain has been documented (Dal Degan et al., 1994; **Table 1**).

Two cathepsin L-like, EP-A and EP-B, were the first barley CysProts described to participate in the proteolytic degradation of the storage proteins in barley grains (Koehler and Ho, 1988, 1990a,b; Poulle and Jones, 1988; Mikkonen et al., 1996). These CysProts are synthesized in the scutellar epithelium and the aleurone layer and, then, secreted to the endosperm upon germination (Mikkonen et al., 1996; Martínez et al., 2009). An aleurain belonging to the cathepsin H-like group of CysProts has been isolated from aleurone (Rogers et al., 1985; Holwerda and Rogers, 1992) and a cathepsin B-like protein, HvCathB, has been detected in aleurone and developing endosperm (Martínez et al., 2003). Similarly, a member of the cathepsin F-like group, the HvPap-1, has been detected in germinating barley grains (Sreenivasulu et al., 2008). HvPap-1 takes part in the proteolytic mobilization of stored proteins like hordeins, albumins and globulins in the barley endosperm and its activity is modulated by its own propeptide (Cambra et al., 2012). HvPap-1 contributes to barley grain filling and germination since over-expression or silencing of *HvPap-1* gene in barley transgenic plants alters the metabolite composition of the grain, and modifies the germination process by delaying or accelerating it (Diaz-Mendoza et al., 2016). Likewise, the presence of HvPap-4, -6 and -10 in the germinating embryo and aleurone layers has

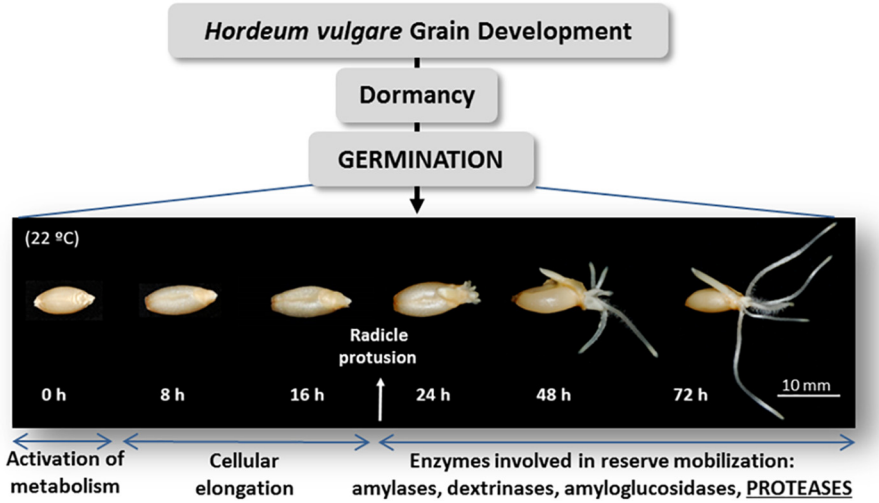

FIGURE 1 | Schematic representation of *Hordeum vulgare* grain germination.

been demonstrated, as well as the capacity of hordein degradation by HvPap-6 and 10 (Martínez et al., 2009). Regarding the barley C13 legumain-like family, their ability to process other CysProts in order to activate them to take part in the proteolytic degradation of the storage proteins it has been also described (Cambra et al., 2010). This is the case of the HvLeg-2 legumain of barley, which is highly expressed during germination and could be involved in the mobilization of storage proteins either by direct proteolytic degradation or by processing and activation of other CysProts (Cambra et al., 2010; Julián et al., 2013). Consequently, for the hydrolysis and mobilization of storage proteins in barley grains the cooperative proteolysis of papain-like CysProt and legumains is essential (Cambra et al., 2010). Overall, the diversity and proteolytic specificity of barley proteases involved in the degradation of storage compounds makes them a starting point to select a potential candidate for further applications.

TABLE 1 | Example of *Hordeum vulgare* proteases involved in germination.

Protease family	*Hordeum vulgare* proteases	References
C1A	Cathepsin L-like (EP-A and EP-B) (HvPap-4, -6 and -16)	Koehler and Ho, 1988, 1990a,b; Poulle and Jones, 1988; Mikkonen et al., 1996; Martínez et al., 2009
	Cathepsin H-like (aleurain)	Rogers et al., 1985; Holwerda and Rogers, 1992
	Cathepsin B-like (HvCathB)	Martínez et al., 2003
	Cathepsin F-like (HvPap-1)	Sreenivasulu et al., 2008; Cambra et al., 2012; Diaz-Mendoza et al., 2016
C13	Legumains-VPEs (HvLeg-2, -3, -7)	Linnestad et al., 1998; Radchuk et al., 2011; Julián et al., 2013
	Legumains-VPEs (HvLeg-5 also called HvVPE4)	Radchuk et al., 2011, 2018
Ser-CP	Six Serine Carboxypeptidases (Ser-CPs)	Dal Degan et al., 1994

POTENTIAL APPLICATION OF BARLEY PROTEASES IN CELIAC DISEASE

From an applied point of view, this wide knowledge on barley proteases acting in the germination process could be employed to manipulate and improve the grain composition not only in barley but also in those cereal species such as wheat, oat, rye and related species and hybrids, in which a number of proteins, known as gluten proteins, affect the health of sensitive consumers.

Celiac disease is the best-characterized pathology associated with gluten consumption and there is a major environmental factor, the ingestion of gluten proteins not only from wheat but also from barley and rye. It has also an important genetic risk factor related to the genes encoding for the human leukocyte antigen (HLA) -DQ2 or -DQ8 (Schuppan, 2000). A lifelong gluten free diet reverses signs and symptoms of celiac disease and NCWS. Nevertheless, this is difficult to follow due to the wide gluten presence in many diet foods. Gluten is a very complex mixture of storage proteins classified into glutenins and gliadins, comprising around 80% of the total grain proteins, with about 30% gliadins and 50% glutenins. Most of the CD related epitopes have been found in the gliadin fraction (Arentz-Hansen et al., 2002). Gliadins are rich in the amino acids proline, and glutamine, which make them resistant to being fully digested in the gastrointestinal tract. This is the case of human proteases, which do not accept proline at their cleavage sites. Partial digestion of gluten generates small peptides which induces a CD4+ T-cell inflammatory response leading to villous atrophy through a two-signal model (Brandtzaeg, 2006). According to this model, a first innate immune response is triggered by certain peptides, such as the 19-mer gliadin peptide, resulting in the production of interleukin 15 (IL-15) by epithelial cells. The

result is the disruption of the epithelial barrier by increasing its permeability. Then, other immune-adaptive peptides, like the 33-mer, can reach the lamina propria and they are deaminated by the tissue transglutaminase (tTG2), providing a strong negative charge to gliadin peptide enhancing their affinity to bind within the HLA-DQ2/8 bound (Bethune and Khosla, 2012).

Different therapeutic alternatives are being developed, as the inhibition of transglutaminase, the antagonism of peptide binding to HLA-DQ2 or HLA-DQ8, the enzymatic detoxification of gluten, or the introduction of natural amino acid substitution to eliminate toxicity (Schuppan et al., 2009; Ruiz-Carnicer et al., 2019). Some other strategies have been developed trying to relieve the negative effect of gluten proteins (Scherf et al., 2018). A promising approach is the down-regulation of genes encoding for gliadins by RNAi technologies, generating transgenic wheat lines with low levels of toxicity for celiacs (Gil-Humanes et al., 2010). Previous investigations have already developed wheat with a down regulation of gliadins expression by hairpin technology. As result, a very low or null T-cells stimulation was proven (Gil-Humanes et al., 2010). The reduced-gliadin breads showed baking and sensory properties, and overall acceptance, similar to those of normal flour, but with up to 97% lower gliadin content (Gil-Humanes et al., 2014). Their results showed that targeting of genes related to celiac disease is feasible and may reduce T-cell epitopes. More recent, low-gluten wheat was engineered with CRISPR/Cas9 technology (Jouanin et al., 2018; Sánchez-León et al., 2018), providing bread and durum with reduced amount of α-gliadins in the seed kernel and a low immunoreactivity for gluten intolerant consumers.

In addition, enzymes able to degrade gliadins have been suggested as hopeful therapeutic agents, as is the barley CysProt EP-B2, which efficiently hydrolyzed a recombinant wheat gluten protein, α2-gliadin, which contains sequences with known immunotoxicity in celiac sprue patients (Bethune et al., 2006). Some prolyl endoproteases from *Aspergillus niger* (AN-PEP) and *Sphingomonas capsulate* (SC-PEP), with also gliadin degradative capacity, have been characterized (Gass et al., 2007). An EP-B2 and SC-PEP combination has been studied as a promising therapeutic tool, being EP-B2 responsible for hydrolyzing gluten proteins into short oligopeptides, which are still toxic, and SC-PEP for breaking down these oligopeptides into non-toxic metabolites (Gass et al., 2007).

WHEAT GLUTEN HYDROLYSIS BY BARLEY CYSPROT

To further explore the enzymatic strategy, we have now analyzed the degradation of six different gliadin fractions from wheat cultivars and breeding lines (Perico, THA1, THA7, THA53, BW2003, and BW208) (Gil-Humanes et al., 2012) by four different CysProt from barley (HvPap-1, -4, -6, and -16) (**Supplementary Material**). These proteases have been previously identified, characterized and purified in *Escherichia coli* (Martínez et al., 2009). With the use of these four CysProt as a representation of different groups of L-like cathepsins and F-like cathepsins, a wide view of their activity on gliadin proteolysis has been achieved. The final goal has been to explore their potential to reduce gliadin content in the wheat gluten or to use them in therapy treatments.

Hydrolysis of the different wheat gliadins by purified barley CysProt was observed by western blot analysis. When gliadins from the six wheat cultivars were treated with HvPap-1, -4, -6, and -16 for 1 and 12 h, different degradation patterns by each CysProt were observed (**Figure 2A**). Degradation in all gliadin samples was appreciated after 1 h of incubation with HvPap-1, -4, -6, and -16 proteases. In most cases, higher bands remained stable while lower molecular weight bands started to disappear after 1 h of treatment. After 12 h of incubation with barley proteases, an increased differential degradation of gliadin bands was observed. Whereas higher molecular weight bands remained stable after HvPap-16 and HvPap-1 treatments (**Figures 2A,A–L)**, degradation was almost complete after HvPap-4 and HvPap-6 action (**Figures 2A,M–X**). To discard any processing or degradation effect due to instability or autohydrolysis, gliadins were incubated for 12 h without proteases (**Figure 2B**). Likewise, as HvPap-1, -4 and -16 were activated by adding pepsin, an analysis of gliadins stability in presence of this commercial peptidase was carried out (**Figure 2B**). Although some smaller bands were hydrolysed by pepsin, in all treatments the band with higher molecular weight remains stable after 12 h incubation, in contrast with the total degradation exerted by HvPap-4 and HvPap-6. These proteases seem to be the most promising gliadin-degrading enzymes. Furthermore, as HvPap-6 does not need to be activated by pepsin, this protease should be selected over HvPap-4 since degradation is only due to its own activity.

PLANT PROTEASES AND CELIAC DISEASE: FUTURE PERSPECTIVES

The potential of plant proteases to alter grain content and the mobilization of stored proteins greatly supports their use as biotechnological tools. As an example, gluten proteins responsible of celiac disease and other gluten-related pathologies are suitable targets for these enzymes. For gluten intolerant patients, the only available treatment is a gluten-free diet, which is extremely difficult to maintain due to gluten ubiquity in human diets. Given the negative impact of quality of life of celiac patients, there is an urgent need to develop food suitable for them. In our research, we have provided new information on the potential of plant CysProt to reduce gliadin content. HvPap-6 CysProt ranks as the best candidate given the encouraging results of this study. The final aim would be the development of transgenic lines of wheat overexpressing this CysProt under endosperm specific promoters to reduce gluten toxicity. This cereal would be used afterward to obtain flour with which to elaborate products suitable for humans with this autoimmune enteropathy. Transgenic wheat lines overexpressing the *HvPap-6* gene from barley would have advantages in comparison of oral enzyme therapy since consumers will not be exposed to harmful gluten. Unwanted reactions in celiac patients probably would decrease by consuming lower or even null levels of toxic gluten from transgenic wheat lines. Administration of hydrolytic

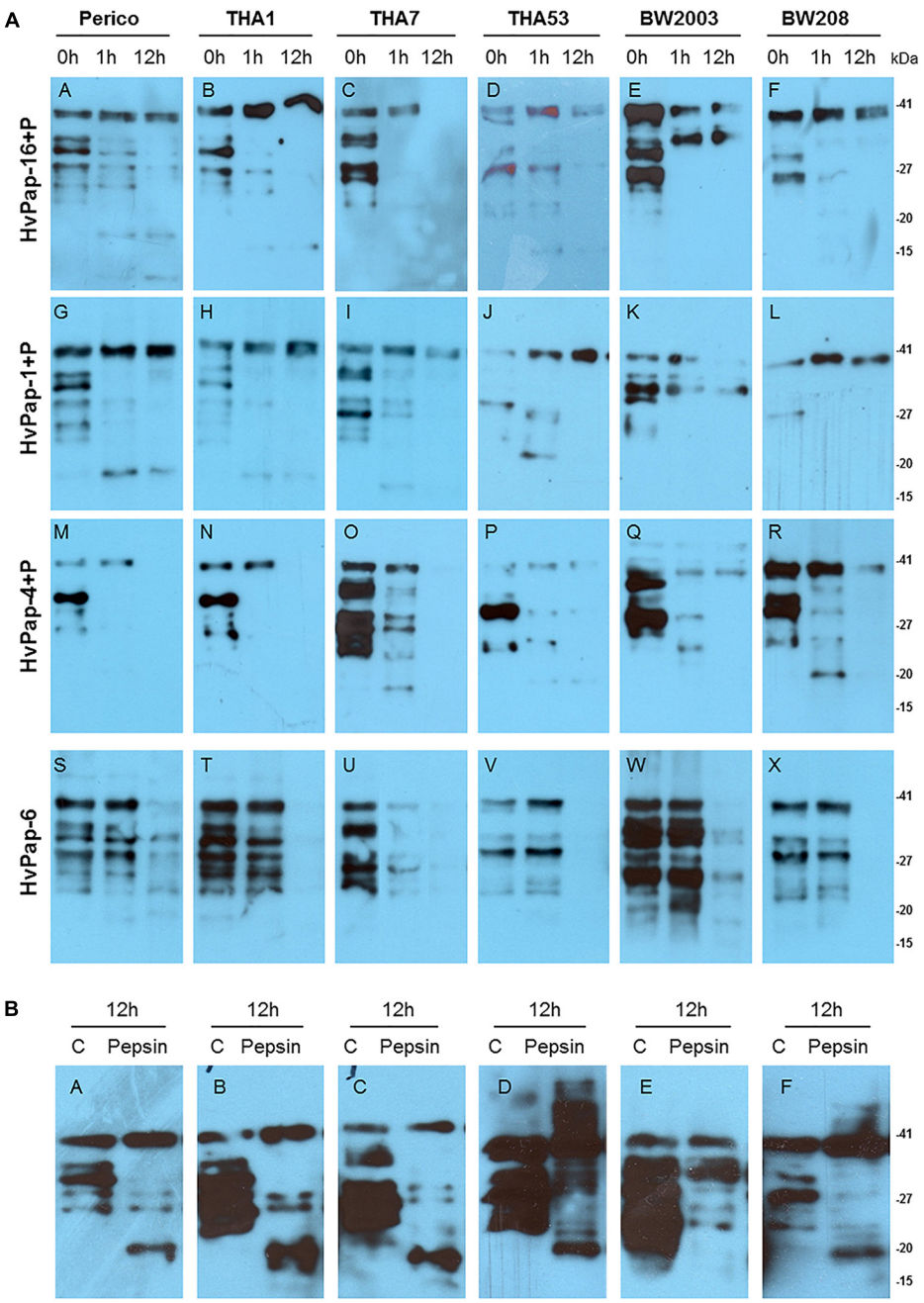

FIGURE 2 | (A) Western blots of 8 μg of gliadins from Perico, THA1, THA7, THA53, BW2003, and BW208 wheat cultivars, incubated with 2 μg of each barley CysProt for 0, 1, and 12 h at 28 °C. Gliadin incubation with HvPap-16+P **(A–F)**; HvPap-1+P **(G–L)**; HvPap-4+P **(M–R)**; HvPap-6 **(S–X)**. **(B)** Gliadins stability assays after 12 h of incubation without pepsin as control and gliadin treatments with 6 μg of pepsin for 12 h **(A–F)**. Immunoblotting was performed with Gluten Tox G12 HRP-conjugate antibody, 200× (Biomedal diagnostics) following the manufacturer instructions. Pepsin (P) and molecular weight in kilo Dalton unit (kDa).

glutenases as food supplement is an alternative to deliver the therapeutic agents directly to the small intestine, for further degradation of wheat gluten. One step beyond would be to produce transgenic wheat lines combining the overexpression of a CysProt with high gliadin-degrading efficiency and the downregulation of the expression of gliadins using genome editing techniques. The next step should be to evaluate the *in vivo* efficiency of selected proteases for degrading wheat gliadins in the endosperm. For that, overexpression of these proteases under the control of endosperm specific promoters, such as those from HMW, gamma or alpha-gliadins would be necessary. A recent publication by Osorio et al. (2019), expressing an endoprotease from barley reinforced our perspective about this approach. These authors overexpressed the barley protease EP-B2,

combined with prolyl endopeptidases from bacterium, under the control of the endosperm specific wheat *1Dy* high-molecular wheat glutenin promoter (pHMWg). A significant reduction (up to 67%) of the amount of the indigestible gluten peptides of all prolamin families was achieved. This approach will contribute, in combination with other strategies like CRISPR/Cas9, to provide wheat varieties suitable for celiac and other gluten intolerance patients. Overall, with new goals, the potential of exploring the properties of plant proteases acting along seed germination will open a great field of research, as a biotechnological alternative to provide new prevention strategies in protein-caused disorders. In conclusion, this is an alternative approach for enzymatic gluten degradation to generate gluten-free wheat to manufacture gluten free products.

DATA AVAILABILITY

All datasets generated for this study are included in the manuscript and/or the **Supplementary Files**.

AUTHOR CONTRIBUTIONS

ID, FB, MM, and MD-M conceived the research. SG-C, MG, and MD-M performed the experimental research. All authors contributed to the final version of the manuscript, and read and approved the final manuscript.

FUNDING

This work was supported by projects from Ministerio de Economia y Competitividad of Spain (project BIO2014-53508-R and AGL2016-80566-P).

SUPPLEMENTARY MATERIAL

The Supplementary Material for this article can be found online at: https://www.frontiersin.org/articles/10.3389/fpls.2019.00721/full#supplementary-material

REFERENCES

Arentz-Hansen, H., Mc Adam, S. N., Molberg, Ø, Fleckenstein, B., Lundin, K. E., Jørgensen, T. J., et al. (2002). Celiac lesion T cells recognize epitopes that cluster in regions of gliadins rich in proline residues. *Gastroenterology* 123, 803–809. doi: 10.1053/gast.2002.35381

Bethune, M. T., and Khosla, C. (2012). Oral enzyme therapy for celiac sprue. *Methods Enzymol.* 502, 241–271. doi: 10.1016/B978-0-12-416039-2.00013-6

Bethune, M. T., Strop, P., Tang, Y., Sollid, L. M., and Khosla, C. (2006). Heterologous expression, purification, refolding and structural-functional characterization of EP-B2, a self-activating barley cysteine endoprotease. *Chem. Biol.* 13, 637–647. doi: 10.1016/j.chembiol.2006.04.008

Bottari, A., Capocchi, A., Galleschi, A., Jopova, A., and Saviozzi, E. (1996). Asparaginyl endopeptidase during maturation and germination of durum wheat. *Physiol. Plant.* 97, 475–480. doi: 10.1111/j.1399-3054.1996.tb00506.x

Brandtzaeg, P. (2006). The changing immunological paradigm in coeliac disease. *Immunol. Lett.* 105, 127–139. doi: 10.1016/j.imlet.2006.03.004

Cambra, I., Garcia, F. J., and Martínez, M. (2010). Clan CD of cysteine peptidases as an example of evolutionary divergences in related protein families across plant clades. *Gene* 449, 59–69. doi: 10.1016/j.gene.2009.09.003

Cambra, I., Martínez, M., Dáder, B., González-Melendi, P., Gandullo, J., Santamaría, M. E., et al. (2012). A cathepsin F-like peptidase involved in barley grain protein mobilization, HvPap-1, is modulated by its own propeptide and by cystatins. *J. Exp. Bot.* 63, 4615–4629. doi: 10.1093/jxb/ers137

Comino, I., Moreno, M., de, L., Real, A., Rodriguez-Herrera, A., Barro, F., et al. (2013). The gluten-free diet: testing alternative cereals tolerated by celiac patients. *Nutrients* 5, 4250–4268. doi: 10.3390/nu5104250

Dal Degan, F., Rocher, A., Cameron-Mills, V., and von Wettstein, D. (1994). The expression of serine carboxypeptidases during maturation and germination of the barley grain. *Proc. Natl. Acad. Sci. U.S.A.* 91, 8209–8213. doi: 10.1073/pnas.91.17.8209

De Angelis, M., Cassone, A., Rizzello, C. G., Gagliardi, F., Minervini, F., Calasso, M., et al. (2010). Mechanism of degradation of immunogenic gluten epitopes from *Triticum turgidum* L. var. durum by sourdough lactobacilli and fungal proteases. *Appl. Environ. Microbiol.* 76, 508–518. doi: 10.1128/AEM.01630-09

De Barros, E. G., and Larkins, B. A. (1994). Cloning of a cDNA encoding a putative cysteine protease gliadin during wheat germination. *Phytochemistry* 43Z, 39–44. doi: 10.1016/0168-9452(94)90176-7

Diaz-Mendoza, M., Dominguez-Figueroa, J. D., Velasco-Arroyo, B., Cambra, I., Gonzalez-Melendi, P., Lopez-Gonzalvez, A., et al. (2016). HvPap-1 C1A protease and HvCPI-2 cystatin contribute to barley grain filling and germination. *Plant Physiol.* 170, 2511–2524. doi: 10.1104/pp.15.01944

Diaz-Mendoza, M., Velasco-Arroyo, B., Gonzalez-Melendi, P., Martinez, M., and Diaz, I. (2014). C1A cysprot-cystatin interactions in leaf senescence. *J. Exp. Bot.* 65, 3825–3833. doi: 10.1093/jxb/eru043

Diaz-Mendoza, M., Velasco-Arroyo, B., Santamaria, M. E., Diaz, I., and Martinez, M. (2017). HvPap-1 C1A protease participates differentially in the barley response to a pathogen and an herbivore. *Front. Plant Sci.* 12:1585. doi: 10.3389/fpls.2017.01585

Dominguez, F., and Cejudo, F. J. (1999). Patterns of starchy endosperm acidification and protease gene expression in wheat grains following germination. *Plant Physiol.* 119, 81–88. doi: 10.1104/pp.119.1.81

Domínguez, F., González, M. C., and Cejudo, F. J. (2002). A germination-related gene encoding a serine carboxypeptidase is expressed during the differentiation of the vascular tissue in wheat grains and seedlings. *Planta* 215, 727–734. doi: 10.1007/s00425-002-0809-2

Feijoo-Siota, L., and Villa, T. G. (2011). Native and biotechnologically engineered plant proteases with industrial applications. *Food Biopro. Technol.* 4, 1066–1088. doi: 10.1007/s11947-010-0431-4

Fernández-Lucas, J., Castañeda, D., and Hormigo, D. (2017). New trends for a classical enzyme: papain, a biotechnological success story in the food industry. *Trends Food Sci. Technol.* 68, 91–101. doi: 10.1016/j.tifs.2017.08.017

Gass, J., Bethune, M. T., Siegel, M., Spencer, A., and Khosla, C. (2007). Combination enzyme therapy for gastric digestion of dietary gluten in patients with celiac sprue. *Gastroenterology* 133, 472–480. doi: 10.1053/j.gastro.2007.05.028

Gil-Humanes, J., Pistón, F., Altamirano-Fortoul, R., Real, A., Comino, I., Sousa, C., et al. (2014). Reduced-gliadin wheat bread: an alternative to the gluten-free diet for consumers suffering gluten-related pathologies. *PLoS One* 9:e90898. doi: 10.1371/journal.pone.0090898

Gil-Humanes, J., Pistón, F., Giménez, M. J., Martín, A., and Barro, F. (2012). The introgression of RNAi silencing of γ-gliadins into commercial lines of bread wheat changes the mixing and technological properties of the dough. *PLoS One* 7:e45937. doi: 10.1371/journal.pone.0045937

Gil-Humanes, J., Pistón, F., Tollefsen, S., Sollid, L. M., and Barro, F. (2010). Effective shutdown in the expression of celiac disease-related wheat gliadin T-cell epitopes by RNA interference. *Proc. Natl. Acad. Sci. U.S.A.* 107, 17023–17028. doi: 10.1073/pnas.1007773107

Gomez-Sanchez, A., Gonzalez-Melendi, P., Santamaria, M. E., Arbona, V., Lopez-Gonzalvez, A., Garcia, A., et al. (2019). Repression of drought-induced cysteine-protease genes alter barley leaf structure and the response to abiotic and biotic stresses. *J. Exp. Bot.* 70, 2143–2155. doi: 10.1093/jxb/ery410

Grudkowska, M., and Zagdańska, B. (2004). Multifunctional role of plant cysteine proteinases. *Acta Biochim. Pol.* 51, 609–624.

Hara-Nishimura, I., Kinoshita, T., Hiraiwa, N., and Nishimura, M. (1998). Vacuolar processing enzymes in protein-storage vacuoles and lytic vacuoles. *J. Plant Physiol.* 152, 668–674. doi: 10.1016/S0176-1617(98)80028-X

Hara-Nishimura, I., Shimada, T., Hiraiwa, N., and Nishimura, M. (1995). Vacuolar processing enzyme responsible for maturation of seed protein. *J. Plant Physiol.* 145, 6412–6417. doi: 10.1016/S0176-1617(11)81275-7

Hartmann, G., Koehler, P., and Wieser, H. (2006). Rapid degradation of gliadin peptides toxic for celiac disease patients by proteases from germinating cereals. *J. Cereal Sci.* 44, 368–371. doi: 10.1016/j.jcs.2006.10.002

Holwerda, B. C., and Rogers, J. C. (1992). Purification and characterization of aleurain: a plant thiol protease functionally homologous to mammalian cathepsin h. *Plant Physiol.* 99, 848–855. doi: 10.1104/pp.99.3.848

James, M., Masclaux-Daubresse, C., Marmagne, A., Azzopardi, M., Laîné, P., Goux, D., et al. (2019). A new role for SAG12 cysteine protease in roots of *Arabidopsis thaliana*. *Front. Plant Sci.* 9:1998. doi: 10.3389/fpls.2018.01998

Jouanin, A., Boyd, L., Visser, R. G. F., and Smulders, M. J. M. (2018). Development of wheat with hypoimmunogenic gluten obstructed by the gene editing policy in Europe. *Front. Plant Sci.* 9:1523. doi: 10.3389/fpls.2018.01523

Julián, I., Gandullo, J., Santos-Silva, L. K., Diaz, I., and Martínez, M. (2013). Phylogenetically distant barley legumains have a role in both seed and vegetative tissues. *J. Exp. Bot.* 64, 2929–2941. doi: 10.1093/jxb/ert132

Kinoshita, T., Yamada, K., Hiraiwa, N., Nishimura, M., and Hara-Nishimura, I. (1999). Vacuolar processing enzyme is up-regulated in the lytic vacuoles of vegetative tissues during senescence and under various stressed conditions. *Plant J.* 19, 43–53. doi: 10.1046/j.1365-313X.1999.00497.x

Kiyosaki, T., Matsumoto, I., Asakura, T., Funaki, J., Kuroda, M., Misaka, T., et al. (2007). Gliadain, a gibberellin-inducible cysteine proteinase occurring in germinating seeds of wheat, *Triticum aestivum* L., specifically digests gliadin and is regulated by intrinsic cystatins. *FEBS J.* 164, 470–477. doi: 10.1111/j.1742-4658.2007.05749.x

Koehler, S. M., and Ho, T. D. (1988). Purification and characterization of gibberelic acid-induced cysteine endoproteases in barley aleurone layers. *Plant Physiol.* 87, 251–258. doi: 10.1104/pp.87.1.95

Koehler, S. M., and Ho, T. D. (1990a). A major gibberellic acid-induced barley aleurone cysteine proteinase which digests hordein. *Plant Physiol.* 94, 251–258. doi: 10.1104/pp.94.1.251

Koehler, S. M., and Ho, T. D. (1990b). Hormonal regulation, processing, and secretion of cysteine proteinases in barley aleurone layers. *Plant Cell* 2, 769–783. doi: 10.1105/tpc.2.8.769

Li, Z., Tang, L., Qiu, J., Zhang, W., Wang, Y., Tong, X., et al. (2016). Serine carboxypeptidase 46 regulates grain filling and seed germination in rice (*Oryza sativa* L.). *PLoS One* 11:e0159737. doi: 10.1371/journal.pone.0159737

Linnestad, C., Doan, D. N. P., Brown, R. C., Lemmon, B. E., Meyer, D. J., Jung, R., et al. (1998). Nucellain, a barley homolog of the dicot vacuolar-processing protease is localized in nucellar cell walls. *Plant Physiol.* 118, 1169–1180. doi: 10.1104/pp.118.4.1169

Liu, H., Hu, M., Wang, Q., Cheng, L., and Zhang, Z. (2018). Role of papain-like cysteine proteases in plant development. *Front. Plant Sci.* 9:1717. doi: 10.3389/fpls.2018.01717

Martínez, M., Cambra, I., Carrillo, L., Diaz-Mendoza, M., and Diaz, I. (2009). Characterization of the entire cystatin gene family in barley and their target cathepsin L-like cysteine proteases, partners in the hordein mobilization during seed germination. *Plant Physiol.* 151, 1531–1545. doi: 10.1104/pp.109.146019

Martínez, M., and Díaz, I. (2008). The origin and evolution of plant cystatins and their target cysteine proteinases indicate a complex functional relationship. *BMC Evol. Biol.* 8:198. doi: 10.1186/1471-2148-8-198

Martínez, M., Rubio-Somoza, I., Carbonero, P., and Diaz, I. (2003). A cathepsin B-like CysProt gene from *Hordeum vulgare* (gene catb) induced by GA in aleurone cells is under circadian control in leaves. *J. Exp. Bot.* 54, 951–959. doi: 10.1093/jxb/erg099

Mikkonen, A., Porali, I., Cercós, M., and Ho, T. D. (1996). Major cysteine proteinase, EPB, in germinating barley seeds: structure of two intronless genes and regulation of expression. *Plant Mol. Biol.* 31, 239–254. doi: 10.1007/BF00021787

Misas-Villamil, J. C., Van Der Hoorn, R. A., and Doehlemann, G. (2016). Papainlike cysteine proteases as hubs in plant immunity. *New Phytol.* 212, 902–907. doi: 10.1111/nph.14117

Müntz, K., Blattner, F. R., and Shutov, A. D. (2002). Legumains – a family of asparagine-specific cysteine endopeptidases involved in propolypeptide processing and protein breakdown in plants. *J. Plant Physiol.* 160, 1281–1293. doi: 10.1078/0176-1617-00853

Osorio, C. E., Wen, N., Mejias, J. H., Liu, B., Reinbothe, S., von Wettstein, D., et al. (2019). Development of wheat genotypes expressing a glutamine-specific endoprotease from barley and a prolyl endopeptidase from *Flavobacterium meningosepticum* or *Pyrococcus furiosus* as a potential remedy to celiac disease. *Funct. Integr. Genomics* 19:123. doi: 10.1007/s10142-018-0632-x

Poulle, M., and Jones, B. L. (1988). A proteinase from germinating barley. Purification and some physical properties. *J. Plant Physiol.* 88, 1454–1460. doi: 10.1104/pp.88.4.1454

Prabucka, B., and Bielawski, W. (2004). Purification and partial characteristic of major gliadin-degrading cysteine endopeptidase from germinating triticale seeds. *Acta Physiol. Plant.* 26, 383–391. doi: 10.1007/s11738-004-0027-6

Radchuk, V., Tran, V., Radchuk, R., Diaz-Mendoza, M., Weier, D., Fuchs, J., et al. (2018). Vacuolar processing enzyme 4 controls grain size in barley by executing programmed cell death in pericarp. *New Phytol.* 218, 1127–1142. doi: 10.1111/nph.14729

Radchuk, V., Weier, D., Radchuk, R., Weschke, W., and Weber, H. (2011). Development of maternal seed tissue in barley is mediated by regulated cell expansion and cell disintegration and coordinated with endosperm growth. *J. Exp. Bot.* 62, 1217–1227. doi: 10.1093/jxb/erq348

Rewers, M. (2005). Epidemiology of celiac disease: what are the prevalence, incidence, and progression of celiac disease? *Gastroenterology* 128, S47–S51. doi: 10.1053/j.gastro.2005.02.030

Rogers, J. C., Dean, D., and Heck, G. R. (1985). Aleurain: a barley thiol protease closely related to mammalian cathepsin H. *Proc. Natl. Acad. Sci. U.S.A.* 82, 6512–6516. doi: 10.1073/pnas.82.19.6512

Rubio-Tapia, A., Kyle, R. A., Kaplan, E. L., Johnson, D. R., Page, W., Erdtmann, F., et al. (2009). Increased prevalence and mortality in undiagnosed celiac disease. *Gastroenterlogy* 137, 88–93. doi: 10.1053/j.gastro.2009.03.059

Ruiz-Carnicer, Á, Comino, I., Segura, V., Ozuna, C. V., Moreno, M. L., López-Casado, M. Á, et al. (2019). Celiac immunogenic potential of α-gliadin epitope variants from *Triticum* and *Aegilops* species. *Nutrients* 22:E220. doi: 10.3390/nu11020220

Sánchez-León, S., Gil-Humanes, J., Ozuna, C. V., Giménez, M. J., Sousa, C., Voytas, D. F., et al. (2018). Low-gluten, nontransgenic wheat engineered with CRISPR/Cas9. *Plant Biotechnol. J.* 16, 902–910. doi: 10.1111/pbi.12837

Sapone, A., Lammers, K. M., Casolaro, V., Cammarota, M., Giuliano, M. T., De Rosa, M., et al. (2011). Divergence of gut permeability and mucosal immune gene expression in two gluten-associated conditions: celiac disease and gluten sensitivity. *BMC Med.* 9:23. doi: 10.1186/1741-7015-9-23

Scherf, K. A., Wieser, H., and Koehler, P. (2018). Novel approaches for enzymatic gluten degradation to create high-quality gluten-free products. *Food Res. Int.* 110, 62–72. doi: 10.1016/j.foodres.2016.11.021

Schuppan, D. (2000). Current concepts of celiac disease pathogenesis. *Gastroenterology* 119, 234–242. doi: 10.1053/gast.2000.8521

Schuppan, D., Junker, Y., and Barisani, D. (2009). Celiac disease: from pathogenesis to novel therapies. *Gastroenterology* 137, 1912–1933. doi: 10.1053/j.gastro.2009.09.008

Shewry, P. R., and Halford, N. G. (2002). Cereal seed storage proteins: structures, properties and role in grain utilization. *J. Exp. Bot.* 53, 947–958. doi: 10.1093/jexbot/53.370.947

Shewry, P. R., Napier, J. A., and Tatham, A. S. (1995). Seed storage proteins: structures and biosynthesis. *Plant Cell* 7, 945–956. doi: 10.1105/tpc.7.7.945

Shi, C., and Xu, L. L. (2009). Characters of cysteine endopeptidases in wheat endosperm during seed germination and subsequent seedling growth. *J. Integr. Plant Biol.* 51, 52–57. doi: 10.1111/j.1744-7909.2008.00778.x

Shindo, T., and van der Hoorn, R. A. L. (2008). Papain-like cysprot: key players at molecular battlefields employed by both plants and their invaders. *Mol. Plant Pathol.* 1, 119–125. doi: 10.1111/j.1364-3703.2007.00439.x

Sreenivasulu, N., Usadel, B., Winter, A., Radchuk, V., Scholz, U., Stein, N., et al. (2008). Barley grain maturation and germination: metabolic pathway and regulatory network commonalities and differences highlighted by new mapman/pageman profiling tools. *Plant Physiol.* 146, 1738–1758. doi: 10.1104/pp.107.111781

Stenman, S. M., Lindfors, K., Venäläinen, J. I., Hautala, A., Männistö, P. T., Garcia-Horsman, J. A., et al. (2010). Degradation of coeliac disease-inducing rye secalin by germinating cereal enzymes: diminishing toxic effects in intestinal epithelial cells. *Clini. Exper. Immunol.* 161, 242–249. doi: 10.1111/j.1365-2249.2010.04119.x

Stenman, S. M., Venäläinen, J. I., Lindfors, K., Auriola, S., Mauriala, T., Kaukovirta-Norja, A., et al. (2009). Enzymatic detoxification of gluten by germinating wheat proteases: implications for new treatment of celiac disease. *Ann. Med.* 41, 390–400. doi: 10.1080/07853890902878138

Szewinska, J., Siminska, J., and Bielawski, W. (2016). The roles of cysteine proteases and phytocystatins in development and germination of cereal seeds. *J. Plant Physiol.* 207, 10–21. doi: 10.1016/j.jplph.2016.09.008

Tan-Wilson, A. L., and Wilson, K. A. (2011). Mobilization of seed protein reserves. *Physiol. Plant.* 145, 140–153. doi: 10.1111/j.1399-3054.2011.01535.x

Tornkvist, A., Liu, C., and Moschou, P. N. (2019). Proteolysis and nitrogen: emerging insights. *J. Exp. Bot.* 70, 2009–2019. doi: 10.1093/jxb/erz024

Tye-Din, J. A., Stewart, J. A., Dromey, J. A., Beissbarth, T., van Heel, D. A., Tatham, A., et al. (2010). Comprehensive, quantitative mapping of T cell epitopes in gluten in celiac disease. *Sci. Transl. Med.* 2, 1–14. doi: 10.1126/scitranslmed.3001012

van der Hoorn, R. A. (2008). Plant proteases: from phenotypes to molecular mechanisms. *Annu. Rev. Plant Biol.* 59, 191–223. doi: 10.1146/annurev.arplant.59.032607.092835

van der Hoorn, R. A. L., and Jones, J. D. G. (2004). The plant proteolytic machinery and its role in defense. *Curr. Opin. Plant Biol.* 7, 400–407. doi: 10.1016/j.pbi.2004.04.003

Velasco-Arroyo, B., Diaz-Mendoza, M., Santamaria, M. E., Gonzalez-Melendi, P., Gomez-Sanchez, A., Arnaiz, A., et al. (2016). Senescence-associated genes in response to abiotic/biotic stresses. *Prog. Bot.* 79, 89–109. doi: 10.1007/124-2017-1

Velasco-Arroyo, B., Martínez, M., Díaz, I., and Diaz-Mendoza, M. (2018). Differential response of silencing HvIcy2 barley plants against *Magnaporthe oryzae* infection and light deprivation. *BMC Plant Biol.* 18:337. doi: 10.1186/s12870-018-1560-6

Washio, K., and Ishikawa, K. (1994). Organ-specific and hormone-dependent expression of genes for serine carboxypeptidases during development and following germination of rice grains. *Plant Physiol.* 105, 1275–1280. doi: 10.1104/pp.105.4.1275

Zhang, N., and Jones, B. L. (1995). Characterization of germinated barley endoproteolytic enzymes by two dimensional gel electrophoresis. *J. Cereal Sci.* 21, 145–153. doi: 10.1016/0733-5210(95)90030-6

Conflict of Interest Statement: The authors declare that the research was conducted in the absence of any commercial or financial relationships that could be construed as a potential conflict of interest.

frontiers in Plant Science

REVIEW
published: 19 June 2019
doi: 10.3389/fpls.2019.00747

Chloroplast Protein Degradation in Senescing Leaves: Proteases and Lytic Compartments

*Agustina Buet, M. Lorenza Costa, Dana E. Martínez and Juan J. Guiamet**

Instituto de Fisiología Vegetal (INFIVE, CONICET-UNLP), La Plata, Argentina

Leaf senescence is characterized by massive degradation of chloroplast proteins, yet the protease(s) involved is(are) not completely known. Increased expression and/or activities of serine, cysteine, aspartic, and metalloproteases were detected in senescing leaves, but these studies have not provided information on the identities of the proteases responsible for chloroplast protein breakdown. Silencing some senescence-associated proteases has delayed progression of senescence symptoms, yet it is still unclear if these proteases are directly involved in chloroplast protein breakdown. At least four cellular pathways involved in the traffic of chloroplast proteins for degradation outside the chloroplast have been described (i.e., "Rubisco-containing bodies," "senescence-associated vacuoles," "ATI1-plastid associated bodies," and "CV-containing vesicles"), which differ in their dependence on the autophagic machinery, and the identity of the proteins transported and/or degraded. Finding out the proteases involved in, for example, the degradation of Rubisco, may require piling up mutations in several senescence-associated proteases. Alternatively, targeting a proteinaceous protein inhibitor to chloroplasts may allow the inhibitor to reach "Rubisco-containing bodies," "senescence-associated vacuoles," "ATI1-plastid associated bodies," and "CV-containing vesicles" in essentially the way as chloroplast-targeted fluorescent proteins re-localize to these vesicular structures. This might help to reduce proteolytic activity, thereby reducing or slowing down plastid protein degradation during senescence.

Keywords: leaf senescence, chloroplast protein degradation, protease, SAG12, vacuole, senescence-associated vacuoles

OPEN ACCESS

Edited by:
Cornelia Spetea,
University of Gothenburg, Sweden

Reviewed by:
Jean-Christophe Avice,
University of Caen Normandy, France
Panagiotis N. Moschou,
Swedish University of Agricultural Sciences, Sweden

***Correspondence:**
Juan J. Guiamet
jguiamet@fcnym.unlp.edu.ar

Specialty section:
This article was submitted to Plant Physiology, a section of the journal Frontiers in Plant Science

Received: *31 January 2019*
Accepted: *21 May 2019*
Published: *19 June 2019*

Citation:
Buet A, Costa ML, Martínez DE and Guiamet JJ (2019) Chloroplast Protein Degradation in Senescing Leaves: Proteases and Lytic Compartments. Front. Plant Sci. 10:747. doi: 10.3389/fpls.2019.00747

INTRODUCTION

The final phase of leaf development, senescence, is a process that precedes cell death, and it is characterized by chloroplast breakdown, with degradation and loss of chloroplast proteins, nucleic acids, pigments, lipids, and polysaccharides (e.g., starch). This deterioration is so extensive that chloroplasts eventually lose all or most of their photosynthetic capacity. Therefore, delaying senescence and thereby extending canopy photosynthesis might be viewed as a plausible goal of crop breeding to increase canopy C gain and grain yield. However, since chloroplasts contain up to 70% of leaf N, the breakdown of leaf proteins and redistribution of released amino acids to other parts of the plant (for example, immature growing seeds) can have a positive impact on the nitrogen use efficiency of crops (Gregersen et al., 2008).

Depending on crop species, growth conditions, or the eventual use of the harvested product (e.g., food with high nutritional value or biofuel), it might be desirable to delay or accelerate senescence in order to increase either C gain or N use efficiency. To manipulate leaf N remobilization, we need a fine understanding of the mechanisms responsible for the regulation and execution of leaf chloroplast protein breakdown, and particularly of the cellular pathways involved and the proteases with a crucial role in this process. This review will focus on proteases associated with senescence and their possible role(s) in chloroplast protein breakdown, as the basis for both decreased photosynthetic capacity of senescing leaves and N redistribution. Since different cellular compartments apparently involved in chloroplast protein breakdown have emerged during the last 15 years, chloroplast protein trafficking for degradation and the cellular compartments possibly involved in the execution of protein degradation will also be discussed.

INCREASED DEGRADATION, NOT REDUCED RATES OF SYNTHESIS, DRIVES THE DECREASE OF CHLOROPLAST PROTEIN LEVELS

The steady-state levels of most photosynthetic proteins decrease markedly during senescence (Krupinska and Humbeck, 2004). Although this might be due to a combination of decreased synthesis plus enhanced degradation rates, the evidence shows clearly that rates of protein synthesis become negligible after complete leaf expansion (Makino et al., 1984; Mae, 2004), and expression of photosynthetic genes typically declines sharply in fully expanded, yet non-senescent leaves (e.g., Krupinska and Humbeck, 2004; Breeze et al., 2011). Chloroplast protein levels are mostly regulated by rates of degradation during senescence (Lamattina et al., 1985; Mae, 2004). An exception is the D1 protein, which is constantly subjected to proteolysis and resynthesis as part of a photodamage repair cycle (Aro et al., 1993; Guiamét et al., 2002); but in spite of its potential impact on photosynthetic rates, breakdown of D1 may not make a large contribution to N redistribution.

EXPRESSION AND ACTIVITY OF PROTEASES DURING SENESCENCE

Given the crucial role of protein degradation in the decline of photosynthetic protein levels, detection of proteases whose activity or expression increases during leaf senescence might contribute to identify putative candidate genes to manipulate senescence. Transcriptomic studies have consistently shown, across a range of different plant species, that some of the genes up-regulated during senescence ("senescence-associated genes," SAGs) are proteases (e.g., Parrott et al., 2007; Breeze et al., 2011; Sekhon et al., 2012; Costa et al., 2013; Zhang et al., 2014). Most proteases associated with senescence are serine and cysteine (Cys) proteases, but some are aspartic proteases and metalloproteases (Roberts et al., 2012; Díaz-Mendoza et al., 2014). Also vacuolar processing enzymes (VPEs) are up-regulated at the mRNA level during senescence (Kinoshita et al., 1999).

The chloroplast seems a logical place to harbor proteases involved in the degradation of photosynthetic proteins. The major chloroplast protease families (Clp, FtsH, DegP) display mostly constitutive expression and seem to be involved in protein quality control and maintenance of homeostasis rather than in massive protein degradation (van Wijk, 2015), although some members of these families can be up-regulated during leaf senescence (Costa et al., 2013). The FtsH6 metalloprotease has been linked to senescence as it was first shown to degrade Lhcb3 *in vitro* (Zelisko et al., 2005), but this result could not be confirmed *in vivo* (Wagner et al., 2011). Another metalloprotease, M58, was shown to localize to plastoglobules (i.e., lipid droplets that accumulate within plastids during senescence), although its function remains unknown (Lundquist et al., 2012).

Several recent studies using *in vitro* protease assays in the presence of class-specific inhibitors, or class-specific substrates, have shown that cysteine proteases are the most active in senescing leaves (i.e, leaves undergoing rapid protein degradation) and that their expression and activity increase substantially during senescence (e.g., Beyenne et al., 2006; Martínez et al., 2007; Carrión et al., 2013; Poret et al., 2016). Most cysteine proteases associated with senescence are located to the central vacuole (Martínez et al., 2007), or other lytic compartments (Costa et al., 2013). Among Cys proteases, cathepsins are highly expressed and active during senescence in *Arabidopsis* (McLellan et al., 2009) and barley (Velasco-Arroyo et al., 2016). RD21 and aleurain are also cysteine proteases associated with senescence in various different species (van der Hoorn et al., 2004; Poret et al., 2016), and they comprise the largest cysteine protease activity of senescing leaves (Pružinská et al., 2017). Several of the proteases associated to senescence are also expressed and/or active in other developmental processes or under different environmental conditions (Martínez et al., 2007). For example, RD21 was initially discovered as a drought-inducible gene (Koizumi et al., 1993). The Cys protease SAG12 was discovered by Lohman et al. (1994) in a search for genes with increased expression during senescence. SAG12 is classified into the cathepsin L-like family, subgroup A (Díaz-Mendoza et al., 2014). Unlike other SAGs, which show a basal level of expression in mature leaves and up-regulation during senescence, SAG12 transcripts are almost undetectable in mature leaves, and SAG12 is expressed exclusively during senescence (Lohman et al., 1994; Grbic, 2002, 2003; Gombert et al., 2006). The senescence-specific responsive element in the SAG12 promoter is located between −603 and −571 bp in the 5′ region (Noh and Amasino, 1999). SAG12 is also expressed in flowers, more specifically in the corolla limb and corolla abscission zone, in anthers and pistils of pollinated flowers (Grbic, 2002), in unfertilized pistils (Carbonell-Bejerano et al., 2011), and in *Arabidopsis* roots (James et al., 2019). The regulated induction of SAG12 has been exploited to use the SAG12 promoter to drive the

senescence-associated expression of IPT, the key gene in cytokinin biosynthesis, to delay senescence in an autoregulated manner (Gan and Amasino, 1995). This approach has been used successfully in various species (e.g., lettuce, McCabe et al., 2001, wheat, Sýkorová et al., 2008, and rice, Liu et al., 2010). Likewise, Liu et al. (2010) described a cysteine protease of rice named SAG39, homologous to AtSAG12, whose expression increases in leaves, roots, culms, and flowers during natural senescence. Vacuolar processing enzymes (VPEs) are a class of Cys proteases likely involved in activation of vacuolar proteases through proteolytic cleavage of inhibitory peptides (Kinoshita et al., 1999). Although VPE mRNAs increase in abundance during senescence, VPE activity may actually decrease in *Arabidopsis* (Pružinská et al., 2017), while in *Brassica napus*, VPE activity increases during senescence to a similar extent in genotypes with different rates of protein breakdown (Poret et al., 2019), casting doubts on VPE involvement in senescence-associated protease activation and protein breakdown.

To strengthen the association of protease activity and/or expression with senescence progression, the rate of senescence can be manipulated through the use of hormonal treatments. Typically, cytokinins delay senescence, while ethylene, abscisic acid (ABA), and salicylic acid (SA) accelerate it (Jibran et al., 2013). Often, hormonal treatments that delay senescence reduce the activity of senescence-associated proteases (e.g., Fukayama et al., 2010; Carrión et al., 2013). Conversely, treatment with ethylene (or its precursor, 1-aminocyclopropane-1-carboxylic-acid), abscisic acid, or salicylic acid increases protease activity/expression concomitantly with accelerated degradation of the photosynthetic machinery (e.g., Chen et al., 2006; Fukayama et al., 2010; Liu et al., 2010; Poret et al., 2017).

KNOCKOUTS, SILENCED OR OVEREXPRESSING LINES, AND *IN VIVO* PHARMACOLOGICAL INHIBITION OF PROTEASES

Increased expression or activity of a protease suggests a role during senescence, but a stronger proof may come from the functional analysis where expression is silenced or knocked down, or where pharmacological approaches are used to decrease protease activity *in vivo*.

In some cases, functional analyses of senescence-associated proteases have shown clearly their involvement in processes other than bulk chloroplast protein degradation and N remobilization. For example, the apoplast-localized subtilisin protease AtSASP (AtSBT1.4) is highly up-regulated at the transcript and activity levels during senescence (Martínez and Guiamet, 2014; Martinez et al., 2015). Knockout *sasp1* plants show no obvious phenotype at juvenile stages, but at the reproductive stage *sasp1* plants develop more branches and siliques, with no significant alteration of leaf senescence (Martinez et al., 2015). Knockout *sasp1* plants are also more sensitive to abscisic acid (ABA) and, therefore, more tolerant to drought (Wang et al., 2018). SASP apparently controls ABA sensitivity by increasing the degradation of Open Stomata 1 (Wang et al., 2018), a positive regulator of ABA-mediated stomatal closure (Acharya et al., 2013). Thus, although SASP is clearly a senescence-associated protease, it is not part of a bulk chloroplast protein degradation and N remobilization pathway, and appears to have a role in diverse regulatory pathways, likely attenuating responses to ABA. It is possible that other senescence-associated proteases function in developmental regulation rather than in direct bulk chloroplast protein breakdown. Expression of the chloroplast-located aspartic protease CND41 increases during senescence, and CND41 degrades partially denatured Rubisco *in vitro* (Kato et al., 2004). CND41 antisense and overexpressing lines of tobacco display retarded and enhanced senescence, respectively, during vegetative growth before anthesis (Kato et al., 2004, 2005), which is in line with its putative involvement in Rubisco degradation. However, the antisense lines where Rubisco degradation is delayed are also deficient in gibberellins and stunted in growth (Nakano et al., 2003); since senescence of a leaf often depends on the correlative influence of younger leaves, slower growth complicates the interpretation of CDN41 results. Testing the impact of protease inactivation in different senescence scenarios (e.g, *in planta* during natural senescence and in excised leaves where effects of N redistribution on whole plant physiology are avoided) may help to ascribe a role for a given protease in chloroplast protein breakdown. These examples illustrate the complexities in assigning roles in chloroplast breakdown to proteases with expression temporally associated with senescence.

The involvement of Cys proteases in Rubisco degradation has been probed using a pharmacological approach with specific inhibitors. Although in recent years, a variety of protease inhibitors have been modified to label proteases and facilitate their detection and isolation, few of these chemicals have been tried *in vivo*, i.e., to block protease activity and examine changes in the stability of specific proteins. E-64 has been broadly used as a diagnostic inhibitor of cysteine proteases *in vitro*, and a few works have extended its application to living tissues. Thoenen et al. (2007) floated wheat leaf segments on 0.1 mM E-64 and found slower degradation of Rubisco large subunit and Rubisco activase, either in leaf segments maintained in darkness for 4 days or after incubation in 25 mM KCl for 7 days under dim light (25 μmol m^{-2} s^{-1} of photosynthetic photon flux density). In a similar approach, tobacco leaf disks pre-treated with ethephon to accelerate senescence were floated on E-64 in darkness for 2 days; E-64 significantly reduced Rubisco loss under these conditions (Carrión et al., 2013). Inhibition of Rubisco degradation closely mirrored the inhibition of cysteine protease activity in these leaves, as determined by microscopic observation of cells stained with a Cys protease fluorescent substrate probe. These studies clearly point to Cys proteases as important in the degradation of Rubisco, but they provide no information on the identity of the protease(s) involved or their specific function.

Reverse genetics approaches provide evidence for the participation of Cys proteases in leaf senescence. Seeβ is a senescence-associated gene coding for a legumain-type Cys protease of maize (Donnison et al., 2007). A screening of a

maize Mutator (Mu) population identified a line with a Mu insertion in Seeβ. Under two N supply regimes, the mutant plants had several characteristics consistent with a role for Seeβ in leaf senescence, including slightly higher and more persistent leaf N contents, which might indicate slower and/or incomplete protein degradation and less N export. Whether the mutation impairs the breakdown of specific leaf proteins was not reported.

Three different genes code for the Cys protease Cathepsin B (CathB) in *Arabidopsis*, and they redundantly function in the development of programmed cell death in response to pathogens. CathB genes are also up-regulated during developmental leaf senescence (McLellan et al., 2009). Interestingly, senescence (monitored as loss of chlorophyll) is delayed in a triple CathB mutant. CathB may act upstream of other senescence-associated proteases regulating their expression, since, for example, SAG12 expression is much reduced in the triple CathB mutant. Although this functional analysis clearly places cathepsins in a pathway regulating senescence, protein targets of CathB are still unknown. A functional analysis of several Papain-like Cysteine proteases (e.g., RD21, SAG12, CTB3, aleurain) failed to detect differences in chlorophyll content between wild type and mutant leaves incubated in darkness for 7 days (Pružinská et al., 2017). However, by counting the number of green vs. yellow leaves per plant, a delay in plant senescence was detected for lines knock-out (KO) for aleurain. Both studies (McLellan et al., 2009; Pružinská et al., 2017) pinpoint proteases with a possible role in the regulation of senescence, but reliance on chlorophyll as the only senescence parameter does not allow to draw conclusions on the role of these proteases in chloroplast protein breakdown. As shown by a number of studies, degradation of pigments and that of proteins appear to be two rather independent processes during senescence of leaves (Thomas and Howarth, 2000; Guiamét et al., 2002).

Cys proteases associated with senescence were studied in barley leaves, and one of them, HvPAP1, was silenced and overexpressed (Velasco-Arroyo et al., 2016). Overexpression of HvPAP1 accelerated the development of senescence symptoms (yellowing), whereas the knockdown lines showed delayed senescence during the reproductive phase. When challenged by stress conditions (i.e., continuous darkness or N deprivation), the decrease in leaf protein content was less marked in the knockdown lines, as expected if HvPAP1 were directly involved in protein remobilization. Inactivation of HvPAP1 also caused some changes in the levels of active/inactive HvPAP16, which uncovers another possible function for HvPAP1, i.e., maturation of other cysteine proteases. Barley Cys proteases (e.g., HvPAP1 and HvPAP19) are up-regulated in response to water deficit, and knockdowns for HvPAP1 and HvPAP19 reduce leaf protein degradation under stress conditions (Gomez-Sanchez et al., 2019).

Otegui et al. (2005) found no visual differences in senescence progression between a wild type and a SAG12 knockout line, but protein degradation was not assessed in that study. James et al. (2018) reported lower harvest index and N harvest index in plants of *Arabidopsis* KO for SAG12 growing under a low nitrogen supply, indicating impaired N redistribution in this mutant. It is noteworthy that the expression of an aspartic protease (the product of At5g10760), and overall activity of the aspartic protease class, increased in the SAG12 KO, possibly reflecting the occurrence of functional protease redundancy during senescence of leaves. Interestingly, inactivation of SAG12 also reduced N redistribution from roots under low nitrogen nutrition (James et al., 2019), suggesting a similar function for SAG12 in such functionally different organs as leaves and roots.

The function of SAG12 in other species is much less clear. In rice, down-regulation of either of two putative orthologs of SAG12 (i.e., OsSAG12-1 and OsSAG12-2) accelerates cell death in response to biotic and abiotic stresses (Singh et al., 2013, 2016). Whether this is due to a different role for SAG12 in different species (e.g., monocots vs. dicots) or to difficulties in uncovering orthologs with SAG12 functions based only on sequence similarities deserves further studies. For example, in order to identify an AtSAG12 ortholog gene in maize (*Zea mays*, B73 inbred line), a phylogenetic tree was constructed including AtSAG12 and ortholog genes reported from other species (i.e., *Brassica napus*, *Nicotiana tabaccum*, *Oryza sativa*, and *Ipomoea batatas*). The resulting tree showed more than 10 maize genes closely related to rice OsSAG39, a putative SAG12 ortholog. All the maize genes analyzed show high percent identity with OsSAG39. However, a search of the expression pattern of five of these genes employing Maize eFP Browser[1] showed that AC225716.2_FG003, AC225716.2_FG006, GRMZM2G028862, GRMZM2G137690, and GRMZM2G165086 show high expression levels in germinating seeds but low expression in senescing leaves, while GRMZM2G095628 shows high expression in germinating seeds and senescing leaves, among other organs (Sekhon et al., 2011). Pinpointing SAG12 orthologs in species other than *Arabidopsis* may require in-depth studies.

Although functional analysis is a robust approach to probe the involvement of specific proteases in chloroplast protein breakdown, pleiotropic effects of proteases may complicate the interpretation of such studies. Reduced growth or development of mutant lines, mentioned before for CND41 (Nakano et al., 2003), or increased cuticle thickness and altered stomatal dimensions in knockdown HvPAP1 and HvPP19 barley lines (Gomez-Sanchez et al., 2019) are good examples of this problem.

ENDOGENOUS PROTEASE INHIBITORS

In addition to changes in protease activity, increased protein degradation during senescence might be related to decreased abundance of endogenous protease inhibitors (Etienne et al., 2007; Martínez et al., 2012; Díaz-Mendoza et al., 2014). Serpins (Fluhr et al., 2012) may be key inhibitors of senescence-associated proteases, such as RD21 (Lampl et al., 2010) and also of metacaspases involved in programmed cell death (Cohen et al., 2019).

[1]http://bar.utoronto.ca/efp_maize/cgi-bin/efpWeb.cgi

Other protease inhibitors likely involved in senescence include the Kunitz-type trypsin inhibitor WSCP, which interacts and inhibits mature RD21 and participates in the control of programmed cell death in the transmitting tract of *Arabidopsis* flowers (Boex-Fontvieille et al., 2015). Given the prevalence of C1A cysteine proteases among senescence-associated proteases, phytocystatins, their specific proteinaceous inhibitors, are of special interest (Díaz-Mendoza et al., 2014). Phytocystatins are encoded by small gene families comprised of seven members in *Arabidopsis* and 12 in rice (Martínez et al., 2005). In some species, levels or expression of cystatins decrease in senescing leaves, presumably allowing for increases in cysteine protease activity (Tajima et al., 2011), whereas in barley cystatin, expression increases under senescence-inducing conditions, e.g., protracted darkness (Díaz-Mendoza et al., 2014). Overexpression of oryzacystatin (OC) in soybean leads to increased branching and delayed senescence; however, both in soybean and *Arabidopsis*, OC-overexpressing lines are slightly delayed in growth (Quain et al., 2014), which might partly explain delayed senescence symptoms. Similar growth effects of overexpression of OC were seen in tobacco (Prins et al., 2008), where cystatin targeted to the cytosol also resulted in delayed degradation of Rubisco and Rubisco activase. It is interesting to note that in this study, OC was localized to the cytosol, whereas Rubisco was located in chloroplasts and in defined non-chloroplastic vesicular structures (i.e., "Rubisco vesicular bodies"). The mechanism for delayed degradation of Rubisco in OC-expressing lines remains to be studied.

CELLULAR PATHWAYS INVOLVED IN CHLOROPLAST PROTEIN BREAKDOWN

In recent years, a number of papers have described protein-trafficking pathways delivering chloroplast proteins to lytic compartments, e.g., the central vacuole or "senescence-associated vacuoles" (Xie et al., 2015). These pathways and lytic compartments might play an important role in the degradation of some of the most abundant chloroplast proteins, e.g., Rubisco (**Figure 1**).

Ishida and co-workers discovered "Rubisco-Containing Bodies" (RCB) in the cytosol of senescing wheat and *Arabidopsis* leaves (Chiba et al., 2003; Ishida et al., 2008). RCBs are spherical vesicles, about 1 μm in diameter, surrounded by a double membrane, and contain Rubisco and glutamine synthetase II. RCBs are eventually internalized into the central vacuole, where their cargo chloroplast proteins are degraded. Both, formation and vacuolar internalization of RCBs depend on the autophagic pathway (Ishida et al., 2008; Wada et al., 2009), implying the involvement of autophagy in chloroplast protein breakdown. Thus, it is intriguing that the phenotype of autophagy mutants includes accelerated senescence and premature loss of chloroplast proteins (e.g., Hanaoka et al., 2002; Thompson et al., 2005; Guiboileau et al., 2013). Accelerated senescence is a typical phenotype for autophagy mutants, and this includes *Arabidopsis* mutants in the autophagy genes

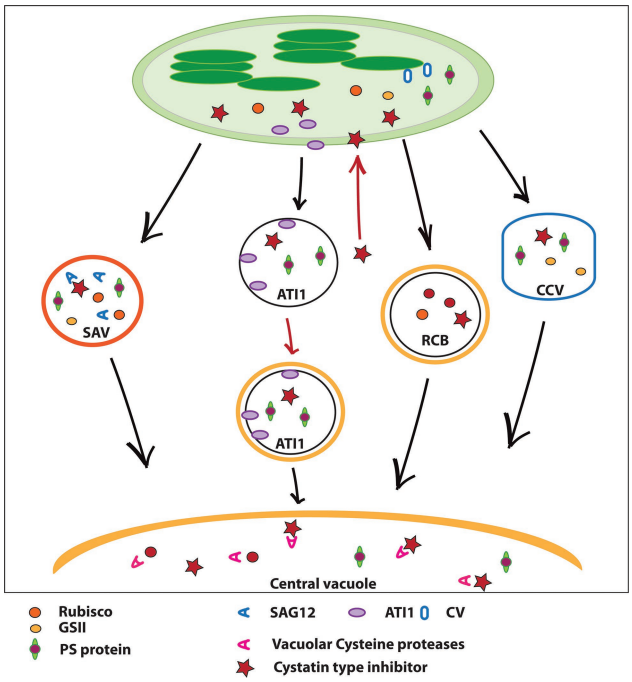

FIGURE 1 | A schematic representation of cellular pathways delivering chloroplast proteins to lytic compartments and a proposed strategy to inhibit plastid protein degradation in crop species. Chloroplast proteins traffic to "senescence-associated vacuoles" (SAVs) and/or to the central vacuole *via* "ATI1-plastid associated bodies" (ATI1-PS), "Rubisco-containing bodies" (RCBs), or "CV-containing vesicles" (CCVs). Each of these vesicles apparently transports specific proteins (Rubisco for SAVs and RCBs, certain thylakoid proteins for ATI1-PS and CCV), which may be degraded by cysteine proteases either in SAVs or the central vacuole. SAVs might also be internalized into the central vacuole, although this is hypothetical. A proposed strategy to reduce/slow down chloroplast protein degradation during senescence in crop plants is the use of targeted protease inhibitors. A proteinaceous protease inhibitor (e.g., a phytocystatin, or a Kunitz-type inhibitor such as WSCP, represented by a red star in the cytosol) fused to a chloroplast transit peptide is expressed under control of a senescence-induced promoter. The chloroplast-located inhibitor would then be redirected to RCBs, ATI1-PS, CCV, and/or SAVs by the same mechanism which directs chloroplast-targeted fluorescent proteins to these vesicular structures. Once in the central vacuole or in SAVs, the inhibitor binds proteases, thus reducing proteolytic activity and preserving protein levels.

ATG7 (Doelling et al., 2002), ATG4 (Hanaoka et al., 2002), ATG5 (Thompson et al., 2005), ATG10 (Phillips et al., 2008), and maize mutant for the ATG12 gene (Li et al., 2015). Accelerated senescence in autophagy mutants involves a salicylic acid-dependent pathway (Yoshimoto et al., 2009), which is reminiscent of SA regulation of normal leaf senescence (Morris et al., 2000). Lack of autophagy seems to be compensated for by increased expression of senescence-associated cysteine proteases, e.g., SAG12 (Havé et al., 2018). This implies some degree of functional redundancy, and exacerbation of separate senescence-associated proteolytic pathways when canonical autophagy is blocked.

Using the senescence-associated protease SAG12 fused to GFP, Otegui et al. (2005) localized SAG12 to small, acidic, proteolytically active "senescence-associated vacuoles" (SAVs),

which are completely absent from mature, non-senescing leaves but appear in substantial numbers during senescence. SAVs are bound by a single membrane, and their diameter ranges from 500 to 800 nm. SAVs were also shown to contain stromal (e.g., Rubisco and Glutamine synthetase II) and thylakoid (e.g., PsaA and Lhcas) proteins, indicating trafficking between the plastid and SAVs in senescing leaves (Martínez et al., 2008; Gomez et al., 2019). Remarkably, SAVs are devoid of PSII components (Gomez et al., 2019). The involvement of SAVs in chloroplast protein degradation was indicated by *in vitro* autodigestion of chloroplast proteins contained within isolated SAVs (Martínez et al., 2008; Gomez et al., 2019), and by *in vivo* experiments where incubation of leaf disks with the cysteine protease inhibitor E-64 completely abolished the protease activity of SAVs and concomitantly reduced Rubisco degradation (Carrión et al., 2013). Since SAVs contain SAG12, the recent finding that leaf N redistribution is impaired in a SAG12-KO line (James et al., 2018) lends support to the idea that SAVs participate in chloroplast protein breakdown. Unlike RCBs, formation of SAVs does not require functional autophagy (Otegui et al., 2005). Their proteolytic activity distinguishes SAVs from all other vesicular pathways associated to senescence described so far.

Two other chloroplast protein-trafficking vesicles are well characterized. ATG8-Interacting Protein 1 (ATI1) participates in vesicular trafficking to the central vacuole from the ER (Honig et al., 2012) and from chloroplasts (Michaeli et al., 2014). ATI1 can be detected within plastids, and also in the cytosol, associated with vesicles (ATI1-plastid associated bodies, ATI1-PS) containing chloroplast-targeted GFP. Formation of ATI1-PS and their release from plastids into the cytosol do not require the autophagic machinery, whereas their internalization in the central vacuole requires the operation of functional autophagy, and it is therefore blocked in ATG5 knockout mutants (Michaeli et al., 2014). ATI1 interacts with several chloroplast proteins, most of them located to the thylakoids, and knocking out ATI1 reduces the degradation of chloroplastic Cys peroxiredoxin, suggesting that Cys peroxiredoxin is broken down through this pathway. Confocal images also show a fluorescent signal corresponding to chlorophyll in ATI1-PS.

The above mentioned pathways require relocation of chloroplast proteins outside the plastid. Recently, the CV (chloroplast vesiculation) gene was identified, and shown to increase in expression during natural and abiotic stress-induced senescence (Wang and Blumwald, 2014). The CV protein localizes to plastids, where it interacts with a number of chloroplast proteins, mainly thylakoid components. CV causes the formation of intra-plastidic vesicles (CV-containing vesicles, CCV) that eventually bud off the plastid and move to the central vacuole, carrying stromal and thylakoid proteins. Overexpression of CV under control of an inducible promoter accelerates senescence, reducing the abundance of PSI and PSII proteins, as well as Glutamine Synthetase II. CCVs are apparently devoid of SAG12, and the CCV pathway remains active in ATG5 knockout mutants, suggesting that this pathway is independent of autophagy.

CONCLUSIONS/OUTLOOK

It is quite possible that chloroplast protein breakdown in senescing leaves is achieved by the coordinated operation of at least several proteases, which might also operate in different lytic compartments, e.g., SAG12 and possibly other proteases within SAVs, or proteases in the central vacuole (e.g., RD21, aleurain, etc.) acting on chloroplast proteins carried there by Rubisco-containing bodies, ATI-PS Bodies, and/or CCVs (**Figure 1**; Costa et al., 2013; Avila-Ospina et al., 2014; Ishida et al., 2014; Michaeli et al., 2014; Wang and Blumwald, 2014; Xie et al., 2015). Such redundancy might explain the relatively small effects of, for example, knocking out one particular protease (e.g., Pružinská et al., 2017). Similarly, the existence of several apparently independent vesicular pathways for chloroplast protein degradation outside the plastid is intriguing. It might be argued that each of these vesicles carries a specific set of chloroplast proteins, affording the cell with the flexibility needed to independently degrade stromal and thylakoid proteins, or PSI vs. PSII components, with different time-courses depending on, for example, environmental conditions. Indeed, pharmacological inhibition of cysteine protease activity in SAVs delayed Rubisco degradation *in vivo* (Carrión et al., 2013), inactivation of ATI1 preserved Cys peroxiredoxin (Michaeli et al., 2014) and overexpression of CV under control of an inducible promoter-accelerated degradation of the thylakoid proteins PsaB, PsbA, and PsbO1 (Wang and Blumwald, 2014). Protein-protein interaction assays also show that ATI1 and CV possibly interact with defined sets of chloroplast proteins (Michaeli et al., 2014; Wang and Blumwald, 2014). While this evidence supports the idea that each pathway might be involved in the breakdown of specific plastid proteins, the fact that all these vesicles are loaded with chloroplast-targeted, fluorescent reporter proteins argues against specificity in their cargo. Thus, whether each of these pathways is specifically involved in the transport and eventual degradation of particular sets of chloroplast proteins is not definitively established. Likewise, each of these structures has so far been probed independently with different fluorescent proteins or activity markers; therefore, examination of senescing cells with combinations of molecular markers for each of these vesicles (e.g., SAG12:GFP plus ATI1:mCherry) would help to establish whether they are truly independent structures or, in some cases, the same vesicles visualized with different tools. To some extent, this has been already done for CCVs (Wang and Blumwald, 2014), but the approach should be extended to the remaining pathways.

If, as presumed, there is redundancy in terms of the proteases and proteolytic pathways involved, manipulation of chloroplast protein degradation to prolong photosynthetic activity in crops might imply piling up several mutations (e.g., through CRISPR editing) in different proteases to decrease proteolytic activity significantly. An alternative approach might be to express protein

inhibitors of cysteine proteases. Work by Thoenen et al. (2007) and Carrión et al. (2013) indicate that cysteine proteases are responsible for a significant part of the degradation of chloroplast proteins. Expressing phytocystatins, for example, might be effective in reducing protein degradation. As already shown for fluorescent proteins, cystatins targeted to plastids might traffic to the intended proteolytic compartments, SAVs, or to the central vacuole *via* RCBs, CCVs, or ATI1-PS (**Figure 1**). To minimize the risk of side-effects, such as slower growth as in the case of constitutive expression of oryzacystatin in the cytosol (Prins et al., 2008), a senescence induced promoter (e.g., pSAG12, Gan and Amasino, 1995) might be used to restrict cystatin expression to senescing leaves. This might represent a feasible approach to reduce cysteine protease activity and partially block protein degradation in senescing leaves of crop plants.

AUTHOR CONTRIBUTIONS

AB, MC, DM, and JG carried out the literature search and wrote the manuscript.

FUNDING

Research in the authors' lab is funded by ANPCYT (PICT 1092).

ACKNOWLEDGMENTS

AB, MC, DM, and JG are researchers of CONICET (Argentina's National Research Council).

REFERENCES

Acharya, B. R., Jeon, B. W., Zhang, W., and Assmann, S. M. (2013). Open Stomata 1 (OST1) is limiting in abscisic acid responses of *Arabidopsis* guard cells. *New Phytol.* 200, 1049–1063. doi: 10.1111/nph.12469

Aro, E. M., Virgin, I., and Andersson, B. (1993). Photoinhibition of photosystem II. Inactivation, protein damage and turnover. *Biochim. Biophys. Acta* 1143, 113–134.

Avila-Ospina, L., Moison, M., Yoshimoto, K., and Masclaux-Daubresse, C. (2014). Autophagy, plant senescence, and nutrient recycling. *J. Exp. Bot.* 65, 3799–3811. doi: 10.1093/jxb/eru039

Beyenne, G., Foyer, C. H., and Kunert, K. J. (2006). Two new cysteine proteinases with specific expression patterns in mature and senescent tobacco (*Nicotiana tabacum* L.) leaves. *J. Exp. Bot.* 57, 1431–1443. doi: 10.1093/jxb/erj123

Boex-Fontvieille, E., Rustgi, S., Reinbothe, S., and Reinbothe, C. (2015). A Kunitz-type protease inhibitor regulates programmed cell death during flower development in *Arabidopsis thaliana*. *J. Exp. Bot.* 66, 6119–6135. doi: 10.1093/jxb/erv327

Breeze, E., Harrison, E., McHattie, S., Hughes, L., Hickman, R., Hill, C., et al. (2011). High resolution temporal profiling of transcripts during *Arabidopsis* leaf senescence reveals a distinct chronology and processes and regulation. *Plant Cell* 23, 873–894. doi: 10.1105/tpc.111.083345

Carbonell-Bejerano, P., Urbez, C., Granell, A., Carbonell, J., and Perez Amador, M. A. (2011). Ethylene is involved in pistil fate by modulating the onset of ovule senescence and the GA-mediated fruit set in *Arabidopsis*. *BMC Plant Biol.* 11:84. doi: 10.1186/1471-2229-11-84

Carrión, C. A., Costa, M. L., Martinez, D. E., Mohr, C., Humbeck, K., and Guiamet, J. J. (2013). *In vivo* inhibition of cysteine proteases provides evidence for the involvement of 'senescence-associated vacuoles' in chloroplast protein degradation during dark-induced senescence of tobacco leaves. *J. Exp. Bot.* 64, 4967–4980. doi: 10.1093/jxb/ert285

Chen, H.-J., Huang, D.-J., Hou, W.-C., Liu, J.-S., and Lin, J.-H. (2006). Molecular cloning and characterization of a granulin-containing cysteine protease SPCP3 from sweet potato (Ipomoea batatas) senescent leaves. *J. Plant Physiol.* 183, 863–876. doi: 10.1016/j.jplph.2005.08.008

Chiba, A., Ishida, H., Nishizawa, N. K., Makino, A., and Mae, T. (2003). Exclusion of ribulose-1,5-bisphosphate carboxylase/oxygenase from chloroplasts by specific bodies in naturally senescing leaves of wheat. *Plant Cell Physiol.* 44, 914–921. doi: 10.1093/pcp/pcg118

Cohen, M., Davydov, O., and Fluhr, R. (2019). Plant serpin protease inhibitors: specificity and duality of function. *J. Exp. Bot.* 70, 2077–2085. doi: 10.1093/jxb/ery460

Costa, M. L., Martínez, D. E., Gomez, F. M., Carrión, C. A., and Guiamet, J. J. (2013). "Chloroplast protein degradation: involvement of senescence-associated vacuoles" in *Advances in photosynthesis and respiration series.* eds. B. Biswal, K. Krupinska, and U. C. Biswal (Dordrecht: Springer Science+Business Media), 417–433.

Díaz-Mendoza, M., Velasco-Arroyo, B., Gonzalez-Melendi, P., Martinez, M., and Diaz, I. (2014). C1A cysteine protease-cystatin interactions in leaf senescence. *J. Exp. Bot.* 65, 3825–3833. doi: 10.1093/jxb/eru043

Doelling, J. H., Walker, J. M., Friedman, E. M., Thompson, A. R., and Vierstra, R. D. (2002). The APG8/12-activating enzyme APG7 is required for proper nutrient recycling and senescence in *Arabidopsis thaliana*. *J. Biol. Chem.* 277, 33105–33114. doi: 10.1074/jbc.M204630200

Donnison, I. S., Gay, A. P., Thomas, H., Edwards, K. J., Edwards, D., James, C. L., et al. (2007). Modification of nitrogen remobilization, grain fill and leaf senescence in maize (*Zea mays*) by transposon insertional mutagenesis in a protease gene. *New Phytol.* 173, 481–494. doi: 10.1111/j.1469-8137.2006.01928.x

Etienne, P., Desclos, M., Le Gou, L., Gombert, J., Bonnefoit, J., Maurel, K., et al. (2007). N-protein mobilisation associated with the leaf senescence process in oilseed rape is concomitant with the disappearanceof trypsin inhibitor activity. *Funct. Plant Biol.* 34, 895–906. doi: 10.1071/FP07088

Fluhr, R., Lampl, N., and Roberts, T. H. (2012). Serpin protease inhibitors in plant biology. *Physiol. Plant.* 145, 95–102. doi: 10.1111/j.1399-3054.2011.01540.x

Fukayama, H., Abe, R., and Uchida, N. (2010). SDS-dependent proteases induced by ABA and its relation to Rubisco and Rubisco activase contents in rice leaves. *Plant Physiol. Biochem.* 48, 808–812. doi: 10.1016/j.plaphy.2010.08.002

Gan, S., and Amasino, R. M. (1995). Inhibition of leaf senescence by autoregulated production of cytokinins. *Science* 270, 1986–1988. doi: 10.1126/science.270.5244.1986

Gombert, J., Etienne, P., Ourry, A., and Le Dily, F. (2006). The expression patterns of SAG12/Cab genes reveal the spatial and temporal progression of leaf senescence in *Brassica napus* L. with sensitivity to the environment. *J. Exp. Bot.* 57, 1949–1956. doi: 10.1093/jxb/erj142

Gomez, F. M., Carrión, C. A., Costa, M. L., Desel, C., Kieselbach, T., Funk, C., et al. (2019). Extra-plastidial degradation of chlorophyll and photosystem I in tobacco leaves involving "senescence-associated vacuoles". *Plant J.* doi: 10.1111/tpj.14337

Gomez-Sanchez, A., Gonzalez-Melendi, P., Santamaria, M. E., Arbona, V., Lopez-Gonzalvez, A., Garcia, A., et al. (2019). Repression of drought-induced cysteine-protease genes alters barley leaf structure and responses to abiotic and biotic stresses. *J. Exp. Bot.* 70, 2143–2155. doi: 10.1093/jxb/ery410

Grbic, V. (2002). Spatial expression pattern of SAG12::GUS transgene in tobacco (*Nicotiana tabacum*). *Physiol. Plant.* 116, 416–422. doi: 10.1034/j.1399-3054.2002.1160318.x

Grbic, V. (2003). SAG2 and SAG12 expression in senescing *Arabidopsis* plants. *Physiol. Plant.* 119, 1–7. doi: 10.1034/j.1399-3054.2003.00168.x

Gregersen, P. L., Holm, P. B., and Krupinska, K. (2008). Leaf senescence and nutrient remobilization in barley and wheat. *Plant Biol.* 10, 37–49. doi: 10.1111/j.1438-8677.2008.00114.x

Guiamét, J. J., Tyystjärvi, E., Tyystjärvi, T., John, I., Kairavuo, M., Pichersky, E., et al. (2002). Photoinhibition and loss of photosystem II reaction center proteins during senescence of soybean leaves. Enhancement of photoinhibition

by the "stay-green" mutation *cytG*. *Physiol. Plant.* 115, 468–478. doi: 10.1034/j.1399-3054.2002.1150317.x

Guiboileau, A., Avila-Ospina, L., Yoshimoto, K., Soulay, F., Azzopardi, M., Marmagne, A., et al. (2013). Physiological and metabolic consequences of autophagy deficiency for the management of nitrogen and protein resources in *Arabidopsis* leaves depending on nitrate availability. *New Phytol.* 199, 683–694. doi: 10.1111/nph.12307

Hanaoka, H., Noda, T., Shirano, Y., Kato, T., Hayashi, H., Shibata, D., et al. (2002). Leaf senescence and starvation-induced chlorosis are accelerated by the disruption of an *Arabidopsis* autophagy gene. *Plant Physiol.* 129, 1181–1193. doi: 10.1104/pp.011024

Havé, M., Balliau, T., Cottyn-Boitte, B., Dérond, E., Cueff, G., Soulay, F., et al. (2018). Increases in activity of proteasome and papain-like cysteine protease in *Arabidopsis* autophagy mutants: back-up compensatory effect or cell-death promoting effect? *J. Exp. Bot.* 69, 1365–1385. doi: 10.1093/jxb/erx482

Honig, A., Avin-Wittenberg, T., Ufaz, S., and Galili, G. (2012). A new type of compartment, defined by plant-specific Atg8-interacting proteins, is induced upon exposure of *Arabidopsis* plants to carbon starvation. *Plant Cell* 24, 288–303. doi: 10.1105/tpc.111.093112

Ishida, H., Izumi, M., Wada, S., and Makino, A. (2014). Roles of autophagy in chloroplast recycling. *Biochim. Biophys. Acta* 1837, 512–521. doi: 10.1016/j.bbabio.2013.11.009

Ishida, H., Yoshimoto, K., Izumi, M., Reisen, D., Yano, Y., Makino, A., et al. (2008). Mobilization of Rubisco and stroma-localized fluorescent proteins of chloroplasts to the vacuole by an ATG gene-dependent autophagic process. *Plant Physiol.* 148, 142–155. doi: 10.1104/pp.108.122770

James, M., Masclaux-Daubresse, C., Marmagne, A., Azzopardi, N., Laîné, P., Goux, D., et al. (2019). A new role for SAG12 protease in roots of *Arabidopsis thaliana*. *Front. Plant Sci.* 9:1998. doi: 10.3389/fpls.2018.01998

James, M., Poret, M., Masclaux-Daubresse, C., Marmagne, A., Coquet, L., Jouenne, T., et al. (2018). SAG12, a major cysteine protease involved in nitrogen allocation during senescence for seed production in *Arabidopsis thaliana*. *Plant Cell Physiol.* 59, 2052–3063. doi: 10.1093/pcp/pcy125

Jibran, R., Hunter, D. A., and Dijkwel, P. P. (2013). Hormonal regulation of leaf senescence through integration of developmental and stress signals. *Plant Mol. Biol.* 82, 547–561. doi: 10.1007/s11103-013-0043-2

Kato, Y., Murakami, S., Yamamoto, Y., Chatani, H., Kondo, Y., Nakano, T., et al. (2004). The DNA-binding protease, CND41, and the degradation of ribulose-1,5-bisphosphate carboxylase/oxygenase in senescent leaves of tobacco. *Planta* 220, 97–104. doi: 10.1007/s00425-004-1328-0

Kato, Y., Yamamoto, Y., Murakami, S., and Sato, F. (2005). Post-translational regulation of CND41 protease activity in senescent tobacco leaves. *Planta* 222, 43–651. doi: 10.1007/s00425-005-0011-4

Kinoshita, T., Yamada, K., Hiraiwa, N., Kondo, M., Nishimura, M., and Hara-Nishimura, I. (1999). Vacuolar processing enzyme is up-regulated in the lytic vacuoles of vegetative tissues during senescence and under various stressed conditions. *Plant J.* 19, 43–53. doi: 10.1046/j.1365-313X.1999.00497.x

Koizumi, M., Yamaguchi-Shinozaki, K., Tsuji, H., and Shinozaki, K. (1993). Structure and expression of two genes that encode distinct drought-inducible cysteine proteinases in *Arabidopsis thaliana*. *Gene* 129, 175–182. doi: 10.1016/0378-1119(93)90266-6

Krupinska, K., and Humbeck, K. (2004). "Photosynthesis and chloroplast breakdown" in *Senescence and programmed cell death in plants*. ed. L. D. Noodén (San Diego, CA: Academic Press), 227–244.

Lamattina, L., Pont-Lezica, R. P., and Conde, R. D. (1985). Protein metabolism in senescing wheat leaves. Determination of synthesis and degradation rates and their effects on protein loss. *Plant Physiol.* 77, 587–590. doi: 10.1104/pp.77.3.587

Lampl, N., Budai-Hadrian, O., Davydov, O., Joss, T. V., Harrop, S. J., Curmi, P. M., et al. (2010). Arabidopsis AtSerpin1: crystal structure and in vivo interaction with its target protease responsive to desiccation-21 (RD21). *J. Biol. Chem.* 285, 13550–13560. doi: 10.1074/jbc.M109.095075

Li, F., Chung, T., Pennington, J. G., Federico, M. L., Kaeppler, H. F., Kaeppler, S. M., et al. (2015). Autophagic recycling plays a central role in maize nitrogen remobilization. *Plant Cell* 27, 1389–1408. doi: 10.1105/tpc.15.00158

Liu, L., Zhou, Y., Szczerba, M., Li, X., and Lin, Y. (2010). Identification and application of a rice, senescence-associated promoter. *Plant Physiol.* 153, 1239–1249. doi: 10.1104/pp.110.157123

Lohman, K. N., Gan, S., John, L. M., and Amasino, R. M. (1994). Molecular analysis of natural leaf senescence in *Arabidopsis thaliana*. *Physiol. Plant.* 92, 322–328. doi: 10.1111/j.1399-3054.1994.tb05343.x

Lundquist, P. K., Poliakov, A., Bhuiyan, N. H., Zybailov, B., Sun, Q., and van Wijk, K. J. (2012). The functional network of the *Arabidopsis* plastoglobule proteome based on quantitative proteomics and genome-wide coexpression analysis. *Plant Physiol.* 158, 1172–1192. doi: 10.1104/pp.111.193144

Mae, T. (2004). "Leaf senescence and nitrogen metabolism" in *Senescence and programmed cell death in plants*. ed. L. D. Noodén (San Diego, CA: Academic Press), 157–168.

Makino, A., Mae, T., and Ohira, K. (1984). Relation between nitrogen and ribulose-1,5-bisphosphate carboxylase in rice leaves from emergence through senescence. *Plant Cell Physiol.* 25, 429–437.

Martínez, M., Abraham, Z., Carbonero, P., and Díaz, I. (2005). Comparative phylogenetic analysis of cystatin gene families from *Arabidopsis*, rice and barley. *Mol. Gen. Genomics*. 273, 423–432. doi: 10.1007/s00438-005-1147-4

Martínez, D., Bartoli, C., Grbic, V., and Guiamet, J. J. (2007). Vacuolar cysteine proteases of wheat (*Triticum aestivum* L.) are common to leaf senescence induced by different factors. *J. Exp. Bot.* 58, 1099–1107. doi: 10.1093/jxb/erl270

Martinez, D. E., Borniego, M. L., Battchikova, N., Aro, E. M., Tyystjärvi, E., and Guiamet, J. J. (2015). SASP, a senescence-associated subtilisin protease, is involved in reproductive development and determination of silique number in *Arabidopsis*. *J. Exp. Bot.* 66, 161–174. doi: 10.1093/jxb/eru409

Martínez, M., Cambra, I., Gonzalez-Melendi, P., Santamaría, M. E., and Días, I. (2012). C1A cysteine proteases and their inhibitors in plants. *Physiol. Plant.* 145, 85–94. doi: 10.1111/j.1399-3054.2012.01569.x

Martínez, D. E., Costa, M. L., Gomez, F. M., Otegui, M. S., and Guiamet, J. J. (2008). "Senescence-associated vacuoles" are involved in the degradation of chloroplasts proteins in tobacco leaves. *Plant J.* 56, 196–206. doi: 10.1111/j.1365-313X.2008.03585.x

Martínez, D. E., and Guiamet, J. J. (2014). Senescence-related changes in the leaf apoplast. *J. Plant Growth Regul.* 33, 44–55. doi: 10.1007/s00344-013-9395-8

McCabe, M. S., Garratt, L. C., Schepers, F., Jordi, W. J. R. M., Stoopen, G. M., Davelaar, E., et al. (2001). Effects of P_{SAG12}-IPT gene expression on development and senescence in transgenic lettuce. *Plant Physiol.* 127, 505–516. doi: 10.1104/pp.010244

McLellan, H., Gilroy, E. M., Yun, B.-W., Birch, P. R. J., and Loake, G. J. (2009). Functional redundancy in the *Arabidopsis Cathepsin* B gene family contributes to basal defence, the hypersensitive response and senescence. *New Phytol.* 183, 408–418. doi: 10.1111/j.1469-8137.2009.02865.x

Michaeli, S., Honig, A., Levanony, H., Peled-Zehavi, H., and Galili, G. (2014). *Arabidopsis* ATG8-Interacting Protein 1 is involved in autophagy-dependent vesicular trafficking of plastid proteins to the vacuole. *Plant Cell* 26, 4084–4101. doi: 10.1105/tpc.114.129999

Morris, K., Mackerness, S. A. H., Page, T., John, C. F., Murphy, A. M., Carr, J. P., et al. (2000). Salicylic acid has a role in regulating gene expression during leaf senescence. *Plant J.* 23, 677–685. doi: 10.1046/j.1365-313x.2000.00836.x

Nakano, T., Nagata, N., Kimura, T., Sekimoto, M., Kawaide, H., Murakami, S., et al. (2003). CND41, a chloroplast nucleoid protein that regulates plastid development, causes reduced gibberellin content and dwarfism in tobacco. *Physiol. Plant.* 117, 130–136. doi: 10.1034/j.1399-3054.2003.1170116.x

Noh, Y.-S., and Amasino, R. M. (1999). Identification of a promoter region responsible for the senescence-specific expression of SAG12. *Plant Mol. Biol.* 41, 181–194. doi: 10.1023/A:1006342412688

Otegui, M. S., Noh, Y.-S., Martinez, D. E., Petroff, A. G. V., Staehelin, L. A., Amasino, R. M., et al. (2005). Senescence-associated vacuoles with intense proteolytic activity develop in leaves of *Arabidopsis* and soybean. *Plant J.* 41, 831–844. doi: 10.1111/j.1365-313X.2005.02346.x

Parrott, D. L., Martin, J. M., and Fischer, A. M. (2007). Analysis of barley (Hordeum vulgare) leaf senescence and protease gene expression: a family C1A cysteine protease is specifically induced under conditions characterized by high carbohydrate, but low to moderate nitrogen levels. *New Phytol.* 1876, 313–331. doi: 10.1111/j.1469-8137.2010.03278.x

Phillips, A., Suttangkakul, A., and Vierstra, R. D. (2008). The ATG12-Conjugating Enzyme ATG10 is essential for autophagic vesicle formation in *Arabidopsis thaliana*. *Genetics* 178, 1339–1353. doi: 10.1534/genetics.107.086199

Poret, M., Chandrasekar, B., van der Hoorn, R. A. L., Coquet, L., Jouenne, T., and Avice, J. C. (2017). Proteomic investigations of proteases involved in cotyledon senescence: a model to explore the genotypic variability of proteolysis machinery associated with nitrogen remobilization efficiency during the leaf senescence of oilseed rape. *Proteomes* 5:29. doi: 10.3390/proteomes5040029

Poret, M., Chandrasekar, B., van der Hoorn, R. A. L., Déchaumet, S., Bouchereau, A., Kim, T.-H., et al. (2019). A genotypic comparison reveals that the improvement in nitrogen remobilization efficiency in oilseed rape leaves is related to specific patterns of senescence-associated protease activities and phytohormones. *Front. Plant Sci.* 10:46. doi: 10.3389/fpls.2019.00046

Poret, M., Chandrasekard, B., van der Hoorn, R. A. L., and Avice, J. C. (2016). Characterization of senescence-associated protease activities involvedin the efficient protein remobilization during leaf senescence of winter oilseed rape. *Plant Sci.* 246, 139–153. doi: 10.1016/j.plantsci.2016.02.011

Prins, A., van Heerden, P. D. R., Olmos, E., Kunert, K. J., and Foyer, C. (2008). Cysteine proteinases regulate chloroplast protein content and composition in tobacco leaves: a model for dynamic interactions with ribulose-1,5-bisphosphate carboxylase/oxygenase (Rubisco) vesicular bodies. *J. Exp. Bot.* 59, 1935–1950. doi: 10.1093/jxb/ern086

Pružinská, A., Shindo, T., Niessen, S., Kaschani, F., Tóth, R., Millar, A. H., et al. (2017). Major Cys protease activities are not essential for senescence in individually darkened *Arabidopsis* leaves. *BMC Plant Biol.* 17:4. doi: 10.1186/s12870-016-0955-5

Quain, M. D., Makgopa, M. E., Márquez-García, B., Comadira, G., Fernandez-García, N., Olmos, E., et al. (2014). Ectopic phytocystatin expression leads to enhanced drought stress tolerance in soybean (Glycine max) and *Arabidopsis thaliana* through effects on strigolactone pathways and can also result in improved seed traits. *Plant Biotechnol. J.* 12, 903–913. doi: 10.1111/pbi.12193

Roberts, I. N., Caputo, C., Criado, M. V., and Funk, C. (2012). Senescence associated proteases in plants. *Physiol. Plant.* 145, 130–139. doi: 10.1111/j.1399-3054.2012.01574.x

Sekhon, R. S., Childs, K. L., Santoro, N., Foster, C. E., Buell, C. R., de Leon, N., et al. (2012). Transcriptional and metabolic analysis of senescence induced by preventing pollination in maize. *Plant Physiol.* 159, 1730–1744. doi: 10.1104/pp.112.199224

Sekhon, R. S., Lin, H., Childs, K. L., Hansey, C. N., Buell, C. R., de Leon, N., et al. (2011). Genome-wide atlas of transcription during maize development. *Plant J.* 66, 553–563. doi: 10.1111/j.1365-313X.2011.04527.x

Singh, S., Giri, M. K., Singh, P. K., Siddiqi, A., and Nandi, A. K. (2013). Down-regulation of OsSAG12-1 results in enhanced senescence and pathogen-induced cell death in transgenic rice plants. *J. Biosci.* 38, 1–10. doi: 10.1007/s12038-013-9334-7

Singh, S., Singh, A., and Nandi, A. K. (2016). The rice OsSAG12-2 gene codes for a functional protease that negatively regulates stress-induced cell death. *J. Biosci.* 41, 445–453. doi: 10.1007/s12038-016-9626-9

Sýkorová, B., Kuresová, G., Daskalova, S., Trcková, M., Hoyerová, K., Raimanová, I., et al. (2008). Senescence-induced extopicc espression of the A. tumefaciens ipt gene in wheat delays leaf senescence, increases cutokinin content nitrate influx and nitrate reductase activity, but does not affect grain yield. *J. Exp. Bot.* 59, 377–387. doi: 10.1093/jxb/erm319

Tajima, T., Yamaguchi, A., Matsushima, S., Satoh, M., Hayasaka, S., Yoshimatsu, K., et al. (2011). Biochemical and molecular characterization of senescence-related cysteine protease-cystatin complex from spinach leaf. *Physiol. Plant.* 141, 97–116. doi: 10.1111/j.1399-3054.2010.01425.x

Thoenen, M., Herrmann, B., and Feller, U. (2007). Senescence in wheat leaves: is a cysteine endopeptidase involved in the degradation of the large subunit of Rubisco? *Acta Physiol. Plant.* 29, 339–350. doi: 10.1007/s11738-007-0043-4

Thomas, H., and Howarth, C. (2000). Five ways to stay green. *J. Exp. Bot.* 51, 329–337. doi: 10.1093/jexbot/51.suppl_1.329

Thompson, A. R., Doelling, J. H., Suttangkakul, A., and Vierstra, R. D. (2005). Autophagic nutrient recycling in *Arabidopsis* directed by the ATG8 and ATG12 conjugation pathways. *Plant Physiol.* 138, 2097–2211. doi: 10.1104/pp.105.060673

van der Hoorn, R. A. L., Leeuwenburgh, M. A., Bogyo, M., Joosten, M. H. A., and Peck, S. C. (2004). Activity profiling of papain-like cysteine proteases in plants. *Plant Physiol.* 135, 1170–1178. doi: 10.1104/pp.104.041467

van Wijk, K. J. (2015). Protein maturation and proteolysis in plant plastids, mitochondria and peroxisomes. *Annu. Rev. Plant Biol.* 66, 75–111. doi: 10.1146/annurev-arplant-043014-115547

Velasco-Arroyo, B., Díaz-Mendoza, M., Gandullo, J., Gonzalez-Melendi, P., Santamaría, M. E., Dominguez-Figueroa, J. D., et al. (2016). HvPAP1 C1A protease actively participates in barley proteolysis mediated by abiotic stresses. *J. Exp. Bot.* 67, 4297–4310. doi: 10.1093/jxb/erw212

Wada, S., Ishida, H., Izumi, M., Yoshimoto, K., Ohsumi, Y., Mae, T., et al. (2009). Autophagy plays a role in chloroplast degradation during senescence in individually darkened leaves. *Plant Physiol.* 149, 885–893. doi: 10.1104/pp.108.130013

Wagner, R., Aigner, H., Pružinská, A., Jänkänpää, H. J., Jansson, S., and Funk, C. (2011). Fitness analysis of *Arabidopsis thaliana* mutants depleted of FtsH metalloproteases and characterization of three FtsH6 deletion mutants exposed to high light stress, senescence and chilling. *New Phytol.* 191, 449–458. doi: 10.1111/j.1469-8137.2011.03684.x

Wang, S., and Blumwald, E. (2014). Stress-induced chloroplast degradation in *Arabidopsis* is regulated via a process independent of autophagy and senescence-associated vacuoles. *Plant Cell.* 26, 4875–4888. doi: 10.1105/tpc.114.133116

Wang, Q., Guo, Q., Guo, Y., Yang, J., Wang, M., Duan, X., et al. (2018). *Arabidopsis* subtilase SASP is involved in the regulation of ABA signaling and drought tolerance by interacting with Open Stomata 1. *J. Exp. Bot.* 69, 4403–4417. doi: 10.1093/jxb/ery205

Xie, Q., Michaeli, S., Peled-Zehavi, H., and Galili, G. (2015). Chloroplast degradation: one organelle, multiple degradation pathways. *Trends Plant Sci.* 20, 264–265. doi: 10.1016/j.tplants.2015.03.013

Yoshimoto, K., Jikumaru, Y., Kamiya, Y., Kusano, M., Consonni, C., Panstruga, R., et al. (2009). Autophagy negatively regulates cell death by controlling NPR1-dependent salicylic acid signaling during senescence and the innate immune response in *Arabidopsis*. *Plant Cell* 21, 2914–2927. doi: 10.1105/tpc.109.068635

Zelisko, A., Garcia-Lorenzo, M., Jackowski, G., Jansson, S., and Funk, C. (2005). AtFtsH6 is involved in the degradation of the light-harvesting complex II during high-light acclimation and senescence. *Proc. Natl. Acad. Sci. USA* 102, 13699–13704. doi: 10.1073/pnas.0503472102

Zhang, W. Y., Xu, Y. C., Li, W. L., Yang, L., Yue, X., Zhang, X. S., et al. (2014). Transcriptional analysis of natural leaf senescence in maize. *PLoS One* 9:e115617. doi: 10.1371/journal.pone.0115617

Conflict of Interest Statement: The authors declare that the research was conducted in the absence of any commercial or financial relationships that could be construed as a potential conflict of interest.

frontiers in Plant Science

ORIGINAL RESEARCH
published: 18 July 2019
doi: 10.3389/fpls.2019.00873

Clathrin-Mediated Endocytosis Delivers Proteolytically Active Phytaspases Into Plant Cells

*Svetlana V. Trusova[1], Anastasia D. Teplova[2], Sergei A. Golyshev[1], Raisa A. Galiullina[1], Ekaterina A. Morozova[2], Nina V. Chichkova[1] and Andrey B. Vartapetian[1]**

[1]Department of Chemistry and Biochemistry of Nucleoproteins, Belozersky Institute of Physico-Chemical Biology, Moscow State University, Moscow, Russia, [2]Faculty of Bioengineering and Bioinformatics, Moscow State University, Moscow, Russia

Phytaspases belong to the family of plant subtilisin-like proteases and are distinct from other family members, as they have strict and rarely occurring aspartate cleavage specificity and unusual localization dynamics. After being secreted into the apoplast of healthy plant tissues, phytaspases are able to return back into cells that have been committed to cell death due to a variety of biotic and abiotic stresses. It was recently discovered that retrograde transport of phytaspases involves clathrin-mediated endocytosis. Here, consequences of phytaspase internalization were studied. Proteolytic activity of phytaspases in the apoplast and intracellular protein fractions obtained from *Nicotiana benthamiana* leaves containing either endogenous phytaspase only or transiently producing *Nicotiana tabacum* phytaspase-EGFP protein (*Nt*Phyt-EGFP) was determined. We demonstrated that triggering phytaspase internalization by antimycin A-induced oxidative stress is accompanied by re-distribution of phytaspase activity from the apoplast to the cell interior. Inhibition of clathrin-mediated endocytosis by co-production of the Hub protein prevented phytaspase internalization and phytaspase activity re-localization. Specificity of endocytic uptake of phytaspases was demonstrated by the co-production of an apoplast-targeted mRFP protein marker, which retained its apoplastic localization when phytaspase internalization was essentially complete. Overproduction of *Nt*Phyt-EGFP, but not of the proteolytically inactive phytaspase mutant, *per se* caused moderate damage in young *Nicotiana benthamiana* seedlings, whereas antimycin A treatment induced a pronounced loss of cell viability independent of the *Nt*Phyt-EGFP overproduction. Interestingly, inhibition of clathrin-mediated endocytosis abrogated cell death symptoms in both cases. In contrast to stress-induced internalization of tobacco phytaspase, *Arabidopsis thaliana* phytaspase-EGFP protein (*At*Phyt-EGFP) was spontaneously internalized when transiently produced in *N. benthamiana* leaves. The *At*Phyt-EGFP uptake was dependent on clathrin-mediated endocytosis as well, the internalized protein being initially visualized within the membranous vesicles. At later time points, the EGFP tag was cleaved off from *At*Phyt, though the elevated level of intracellular *At*Phyt proteolytic activity persisted. Our data, therefore, point to clathrin-mediated endocytosis as a means to deliver proteolytically active phytaspases into plant cells. It would be interesting to learn whether or not phytaspases are unique among the large family of plant subtilisin-like proteases in their ability to utilize retrograde trafficking.

Keywords: plant cell death, clathrin-mediated endocytosis, protein localization, proteolytic activity, subtilisin-like protease, phytaspase

OPEN ACCESS

Edited by:
Mercedes Diaz-Mendoza, Instituto Nacional de Investigación y Tecnología Agraria y Alimentaria, Spain

Reviewed by:
Renier A. L. Van Der Hoorn, University of Oxford, United Kingdom
Juan Guiamet, National University of La Plata, Argentina
Johana Catherine Misas Villamil, University of Cologne, Germany

****Correspondence:***
Andrey B. Vartapetian
varta@genebee.msu.ru

Specialty section:
This article was submitted to Plant Physiology, a section of the journal Frontiers in Plant Science

Received: *09 February 2019*
Accepted: *19 June 2019*
Published: *18 July 2019*

Citation:
Trusova SV, Teplova AD, Golyshev SA, Galiullina RA, Morozova EA, Chichkova NV and Vartapetian AB (2019) Clathrin-Mediated Endocytosis Delivers Proteolytically Active Phytaspases Into Plant Cells. Front. Plant Sci. 10:873. doi: 10.3389/fpls.2019.00873

INTRODUCTION

Phytaspases belong to the vast family of plant subtilisin-like proteases (subtilases), which includes many members in each plant species, e.g., 56 in *Arabidopsis thaliana* (Rautengarten et al., 2005), 63 in rice (*Oryza sativa*, Tripathi and Sowdhamini, 2006), and 82 in grape (*Vitis vinifera*, Cao et al., 2014; Figueiredo et al., 2016) and tomato (*Solanum lycopersicum*, Reichardt et al., 2018). Subtilases are known to be involved in diverse processes, from unselective protein degradation (Yamagata et al., 1994; Hamilton et al., 2003) to precise processing of precursor proteins (Liu et al., 2007; Liu and Howell, 2010; Sénéchal et al., 2014; Ghorbani et al., 2016; Schardon et al., 2016; Beloshistov et al., 2018). However, function of the majority of these proteolytic enzymes remains unknown. Similar to other plant subtilases, phytaspases are synthesized as proteolytically inactive precursor proteins, which possess an N-terminal signal peptide, a prodomain, and a peptidase domain (Chichkova et al., 2010; Schaller et al., 2018). The precursor protein is autocatalytically and constitutively processed, and the mature proteolytically active enzyme is released into the apoplast (Chichkova et al., 2010), which is also typical for plant subtilases. However, phytaspases differ from other subtilases in two ways. First, phytaspases display strict aspartate (Asp) specificity of hydrolysis. The efficiency of hydrolysis after Asp residue strongly depends on the preceding three amino acid-long motif, which confers strong selectivity of phytaspase-mediated protein fragmentation. For native rice phytaspase, the preferred upstream recognition motif is remarkably hydrophobic (Galiullina et al., 2015). Computer-based modeling of the *Nicotiana tabacum* phytaspase with its peptide inhibitor provided an explanation for Asp specificity of phytaspases (Vartapetian et al., 2011). A direct consequence of Asp specificity is observed at the prodomain-peptidase domain junction in the phytaspase precursor protein. The C-terminal residue of prodomain is Asp, which is consistent with the self-processing mode of generation of the mature enzyme. Mutating this junction Asp residue precludes processing/activation of the phytaspase precursor and the release of the mature enzyme into the apoplast (Chichkova et al., 2010). The presence of junction Asp residue may serve as a phytaspase signature within the plant subtilase family, and this sign has been successfully used to identify phytaspase-encoding genes in several plant species. The number of phytaspase genes appears to vary in plant genomes, from a single gene in *A. thaliana* to 12 in *S. lycopersicum* (Chichkova et al., 2018; Reichardt et al., 2018).

The second distinctive characteristic of phytaspases is their dynamic localization. The apoplast is not the end point of phytaspase trafficking. Phytaspases are known to be crucial to the implementation of programmed cell death (PCD) in plants triggered by biotic and abiotic stresses. Increased phytaspase levels were shown to enhance stress-induced and spontaneous plant cell death, whereas down-regulation of phytaspase activity suppressed cell death (Chichkova et al., 2004, 2010; Reichardt et al., 2018). Upon the induction of cell death, phytaspases become physically re-localized from the apoplast toward the cell interior (Chichkova et al., 2010, 2012). This retrograde transport is considered to be unique among plant subtilisin-like proteases. The involvement of clathrin-mediated endocytosis in phytaspase internalization has recently been documented (Trusova et al., 2019), which provokes important questions regarding possible mechanisms and consequences of retrograde phytaspase trafficking.

Here, we examined possible correlations between clathrin-mediated phytaspase re-entry into plant cells and proteolytic activity of phytaspases both outside and inside plant cells. We found that clathrin-mediated endocytosis provides a gateway for delivery of proteolytically active phytaspases into plant cells. Also, results from this study suggest that a specific recognition mechanism for phytaspase internalization may exist. Finally, our study points to the importance of clathrin-mediated endocytosis for the accomplishment of antimycin A-induced and phytaspase overexpression-promoted plant cell death.

MATERIALS AND METHODS

Plant Growth Conditions

Nicotiana benthamiana plants were grown at 25°C in soil in a controlled environment under a 16 h/8 h day/night cycle. Protein transient expression was performed using 6-week-old plants. For evaluation of cell death symptoms, *Nicotiana benthamiana* seedlings were grown on the half-strength Murashige and Skoog medium (pH 5.7) containing 1% glucose and 0.8% agar.

Plasmid Construction

For construction of recombinant *Nt*Phyt-EGFP, *Nt*Phyt-S537A-EGFP, *Nt*Phyt-mRFP, *At*Phyt-EGFP, and *At*Phyt-S553A-EGFP fusion proteins, the downstream GST tag gene in the previously described Phyt-GST constructs within the pLH7000 binary vector backbone (Chichkova et al., 2010, 2018) was substituted with the PCR-amplified EGFP or mRFP gene. To create the SP-mRFP fusion protein, the signal peptide-encoding region of the *Nt*Phyt cDNA was PCR-amplified and ligated upstream of and in frame with the mRFP gene between the *Nco*I and *Sac*I sites of the pLEX7000 expression vector (Beloshistov et al., 2018). The mRFP gene alone was inserted in the same vector in an analogous fashion to serve as a control. To obtain the mRFP-Hub1 fusion protein, a pCambia1300-derived expression vector pCambia1300EX was constructed by inserting the 1,200 bp long *Sal*I-*Eco*RI DNA fragment of pLEX7000 encompassing the dual 35S promoter, a polylinker and a transcription terminator between the *Sal*I and *Eco*RI sites of the pCambia1300 binary vector. cDNA encoding the C-terminal fragment of *A. thaliana* clathrin heavy chain 1was PCR-amplified using primers 5′-CCAGGATCCAAGAAGTTTAACTTAAATGTTCAG-3′ and 5′-GTTGGTACCTTAGTAGCCGCCCATCGGTG-3′. Hub1 cDNA (*c.* 1,870 bp long) was then inserted downstream of and in frame with the mRFP gene between the *Nco*I and *Kpn*I sites of the pCambia1300EX binary vector.

The EGFP-LTI6b-encoding plasmid was a gift from M. Taliansky (The James Hutton Institute, UK).

Agroinfiltration and Protein Fractionation

The obtained plasmid constructs were introduced into *Agrobacterium tumefaciens* C58C1 or GV3101 cells. Transformed agrobacteria were infiltrated into *N. benthamiana* leaves using a blunt syringe or vacuum-infiltrated into seedlings (see below) in combinations described in legends (**Figures 1–7**). Agrobacteria carrying the empty vector (pCambia1300 or pLH7000) were used as a control, and were also added to the infiltration mix in the case of co-expression experiments to equalize plasmid ratio and bacterial load. At the indicated days post-infiltration (p.i.), leaves were examined by confocal fluorescence microscopy. Where indicated, treatment of leaves with antimycin A was performed by vacuum infiltration with water containing 10 μM antimycin A (Sigma, from 20 mM stock solution in ethanol). Control leaves were infiltrated with distilled water supplemented with an equivalent amount of ethanol. After an overnight incubation, confocal microscopy images were taken to determine fluorescence distribution in leaf tissue.

In parallel, leaves were subject to protein fractionation for subsequent determination of phytaspase activity. Apoplastic washes were obtained by low-speed (2,000 *g*) centrifugation of leaves at 4°C for 10 min. The leaf material was re-extracted with 20 mM MES buffer, pH 5.5, containing 100 mM NaCl and 25 μg/ml AEBSF, 2 μg/ml aprotinin, 5 μg/ml E-64 (all from Sigma), and 6 μg/ml leupeptin (MP Biomedicals) protease inhibitors, by vacuum infiltration and centrifugation, and the apoplastic washes were combined. After the separation, the residual leaf material was frozen in liquid nitrogen and disrupted in Minilys homogenizer (Bertin Instruments) using 1.6 mm ceramic beads by two 10 s bursts. An additional 10 s burst was performed after suspending the samples in B1 buffer (20 mM MES, 2 mM dithiothreitol, 0.1% Tween 20, 5% glycerol), pH 5.5, containing 50 mM NaCl and protease inhibitors (225 μl of the buffer per 25 mg of leaves). Debris was eliminated by 10 min centrifugation at 10,000 *g* at 4°C, and the supernatants (as well as the apoplastic washes) were taken for phytaspase activity determination. Leaves without prior separation of the apoplastic liquid were processed in an analogous fashion to obtain "total protein" samples. For western blot analysis and for glucose 6-phosphate dehydrogenase (G6PDH) activity determination, leaves were infiltrated with 20 mM MES buffer, pH 5.5, containing 100 mM NaCl and protease inhibitors. After separating the apoplastic protein fraction, the remaining leaf material (as well as the total/unwashed tissue) was ground in liquid nitrogen and extracted with 10 mM Tris-HCl buffer, pH 9.0, containing 0.2 M KCl, 30 mM $MgCl_2$, 0.2 M sucrose, 10 mM 2-mercaptoethanol, and protease inhibitors. Western blot analysis of the EGFP- and mRFP-fused proteins was performed using monoclonal anti-EGFP 3A9 antibody (Sukhacheva et al., 2002) and polyclonal anti-mRFP antibodies (Abcam) as described (Chichkova et al., 2010).

For G6PDH activity determination (Yang et al., 2019), the intracellular protein and apoplastic fractions obtained from approximately 12 mg of leaf tissues were diluted 10- to 100-fold with 33 mM HEPES buffer, pH 7.5, containing 5 mM $MgCl_2$, and 5 mM glucose 6-phosphate. As the protein fractions were obtained in different buffers, to equalize buffer conditions, the reaction mixtures were supplemented with the corresponding amounts of the complementary buffer prior to starting the reaction by the addition of NADP to a final concentration of 0.5 mM. G6PDH activity was determined spectrophotometrically, by measuring change in absorbance at 340 nm.

Phytaspase Activity Quantification

Proteolytic activity of phytaspases in apoplastic washes, intracellular protein fractions, and in total *N. benthamiana* leaf extracts was determined using either the Ac-VEID-AFC [AFC, 7-amino-4-(trifluoromethyl) coumarin] fluorogenic peptide substrate (for *Nt*Phyt and for endogenous *N. benthamiana* phytaspase), or for *At*Phyt, the Ac-YVAD-AFC substrate (both from California Peptide). Fluorogenic peptide substrates Ac-VAD-AFC, Ac-VDVAD-AFC, Ac-LEHD-AFC, Ac-WEHD-AFC, Ac-DEVD-AFC (all from Calbiochem), Ac-VNLD-AFC (California Peptide), Ac-STATD-AFC (Bachem), and Ac-IETD-AFC (Anaspec) were used to assess cleavage specificity. Peptide substrates were used at a final concentration of 30 μM. Protein samples were 10- to 15-fold diluted before activity measurements. Kinetic measurements of relative fluorescence increase were performed in B1 buffer, pH 5.5 (for tobacco phytaspases) or pH 6.5 (for *At*Phyt), containing 0.5 M NaCl and protease inhibitors at 28°C. Where indicated, N-ethylmaleimide (Sigma) was added to the reaction mixtures to a final concentration of 2 mM. The Fluoroskan Ascent reader (Thermo Fisher Scientific) equipped with 390 nm excitation and 510 emission filters was used to quantitate fluorescence intensities. Data are presented as means ± SD from three independent experiments. Statistical significance was analyzed using Student's *t*-test. $p < 0.01$ were considered significant.

Treatment of *N. benthamiana* Seedlings

Seven-day-old sterile *N. benthamiana* seedlings grown in solid growth medium (2.17 g/L Murashige and Skoog basal salt mixture, 0.5 g/L MES, 10 g/L glucose, 0.8% agar, pH 5.7) were vacuum infiltrated with transformed agrobacteria. Three days after infiltration, seedlings were detached and submerged in water containing 10 μM antimycin A for 3 h. Control seedlings were submerged in water supplemented with an equivalent amount of ethanol. After that, seedlings were stained with Evans Blue (Sigma) according to Minina et al., 2013. Briefly, detached seedlings were vacuum infiltrated with fresh aqueous solution of 0.5% Evans Blue and incubated for 15 min at room temperature, then washed three times for 15 min with water, slightly shaking to remove unbound dye. Chlorophyll was removed by incubating samples in 96% ethanol for 10 min at room temperature twice, then ethanol was removed by washing with 70, 50, 20% ethanol and water, consequently.

Confocal Fluorescence Microscopy

Samples were studied using Nikon C2+ confocal microscope based on Nikon Eclipse Ti (Nikon, Japan) inverted body equipped with 60× NA 1.2 plan-apochromat water immersion lens with the working distance of 300 μm and 402, 488, and 562 nm lasers used for excitation of DAPI, EGFP, and mRFP fluorescence, respectively. Fluorescence was detected using 560 nm dichroic mirror and 525/50 and 595/40 nm blocking filters for EGFP and mRFP-tagged proteins, respectively. FM4-64 fluorescence was also recorded using 595/40 nm filter. The same pinhole diameter setting of 60 μm was used for both channels, resulting in optical sectioning of 650 nm for green and red channels. Deconvolution was performed using Richardson-Lucy algorithm implemented in the microscope controlling software Nis Elements AR (Nikon, Japan). FM4-64 (Molecular Probes) was infiltrated into leaves at a 5 μM concentration in water. Images were taken 4 h p.i. Data were reproducible over at least three independent experiments.

RESULTS

Stress-Induced Internalization of *N. tabacum* Phytaspase Depends on Clathrin-Mediated Endocytosis and Is Specific

N. tabacum phytaspase (*Nt*Phyt) is known to accumulate in the apoplast of healthy leaves and to re-localize toward the cell interior in response to PCD-inducing triggers (Chichkova et al., 2010). To follow *Nt*Phyt trafficking, the *Nt*Phyt-EGFP protein was transiently produced in *N. benthamiana* leaves by agroinfiltration. Fluorescence microscopy examination of the infiltrated leaves confirmed the production of the target protein, with no fluorescence occurring in the cell interior (**Figure 1A**). Triggering oxidative stress-induced cell death in these leaves by treatment with 10 μM antimycin A resulted in the re-distribution of *Nt*Phyt-EGFP, visible as the formation of multiple small dots within the cell (**Figure 1B**). Western blot analysis of protein samples from control (mock-treated) and antimycin A-treated leaves did not reveal degradation of the *Nt*Phyt-EGFP protein in response to antimycin A treatment (**Figure 1C**). To verify the initial apoplastic localization of *Nt*Phyt, a plasma membrane protein marker EGFP-LTI6b (Cutler et al., 2000) was transiently produced together with *Nt*Phyt-mRFP in *N. benthamiana* leaves (**Figure 1D**). In plasmolysed leaf samples, the *Nt*Phyt-mRFP red fluorescence was visualized in the space between two plasma membranes (green) of the adjacent epidermal cells (**Figures 1E–G**). This observation was also supported by measuring fluorescence intensities across the boundaries of the two adjacent plant cells (**Figure 1H**). The *Nt*Phyt-mRFP protein responded to treatment with antimycin A similarly to the *Nt*Phyt-EGFP fusion, i.e., by forming small dots within the cell (**Figures 1I,J**).

To verify the involvement of clathrin-mediated endocytosis in the observed antimycin A-induced re-localization of *Nt*Phyt, mRFP-Hub1 was produced together with *Nt*Phyt-EGFP in *N. benthamiana* leaves. Hub1 represents the C-terminal fragment of *A. thaliana* clathrin heavy chain 1, which acts, upon over-production in *A. thaliana* and *N. benthamiana*, in a dominant negative fashion to specifically inhibit clathrin-mediated endocytosis (Liu et al., 1995; Dhonukshe et al., 2007; Kitakura et al., 2011; Li and Pan, 2017). In the presence of mRFP-Hub1, no stress-induced re-localization of *Nt*Phyt-EGFP was observed (**Figures 1K–P**). Thus, similar to results from previous studies (Chichkova et al., 2010; Trusova et al., 2019), oxidative stress-induced PCD caused retrograde transport of *Nt*Phyt-EGFP from the apoplast to the cell interior, which could be efficiently blocked by inhibiting clathrin-mediated endocytosis.

One could imagine that internalization of *Nt*Phyt by means of clathrin-mediated endocytosis could be achieved either through specific recognition of the cargo or non-specific capturing of the apoplastic fluid by the newly forming clathrin-coated pits. Availability of an inert soluble apoplastic protein marker would be helpful to distinguish between these possibilities. To construct such a marker, we fused the *Nt*Phyt signal peptide (SP, amino acid residues 1–24) to the N-terminus of the mRFP protein to drive secretion of the fluorescent protein into the apoplast and produced the resultant SP-mRFP protein in *N. benthamiana* leaves by agroinfiltration. **Figure 2A** shows that mRFP fluorescence was detectable at the cell borders in the infiltrated leaves. After separating the proteins into apoplastic and intracellular fractions, mRFP was visualized as an apoplastic protein by western blot analysis (**Figure 2B**). This was in sharp contrast to the behavior of free mRFP (without signal peptide) produced in *N. benthamiana* leaves. While mRFP fluorescence was located to the cell periphery and the nucleus (**Figure 2C**), separating the proteins into apoplastic and intracellular fractions expectedly revealed free mRFP as an intracellular protein by western blot analysis (**Figure 2D**). Of note also, the results of western blot analyses (**Figures 2B,D**) demonstrate the absence of appreciable cross-contamination between apoplastic and intracellular fractions. To further confirm this notion, enzymatic activity of glucose 6-phosphate dehydrogenase (G6PDH), an intracellular protein (Debnam and Emes, 1999), was quantified in both fractions. **Figure 2E** shows that the majority of the G6PDH activity was present in the intracellular fraction, with less than 5% of the total activity observed in the apoplastic fraction.

As production of SP-mRFP was found to generate a reliable and soluble apoplastic protein marker, we aimed to use it to assess specificity of phytaspase internalization. Co-production of *Nt*Phyt-EGFP and SP-mRFP in *N. benthamiana* leaves resulted in co-localization of both proteins in the apoplast under non-stressed conditions (**Figures 2F,H,J**). Antimycin A-induced cell death caused the expected shift of the *Nt*Phyt-EGFP fluorescence toward the cell interior (**Figure 2G**). In contrast, mRFP fluorescence retained its extracellular localization (**Figures 2I,K**).

We concluded that clathrin-mediated endocytosis of phytaspase proceeds through a specific recognition step, most likely involving a phytaspase receptor at the plasma membrane of plant cells, rather than by a non-specific fluid-phase uptake.

Internalized Phytaspase Retains Proteolytic Activity

To determine if phytaspase retains its proteolytic activity upon PCD-induced internalization, we analyzed the behavior of

endogenous *N. benthamiana* phytaspase (*Nb*Phyt) first. Apoplastic washes were obtained from *N. benthamiana* leaves containing endogenous phytaspase only (in the absence of *Nt*Phyt-EGFP production) and from leaves producing mRFP-Hub1, either treated with antimycin A or untreated. Phytaspase activity was quantified in these apoplastic washes ("apoplast"), as well as

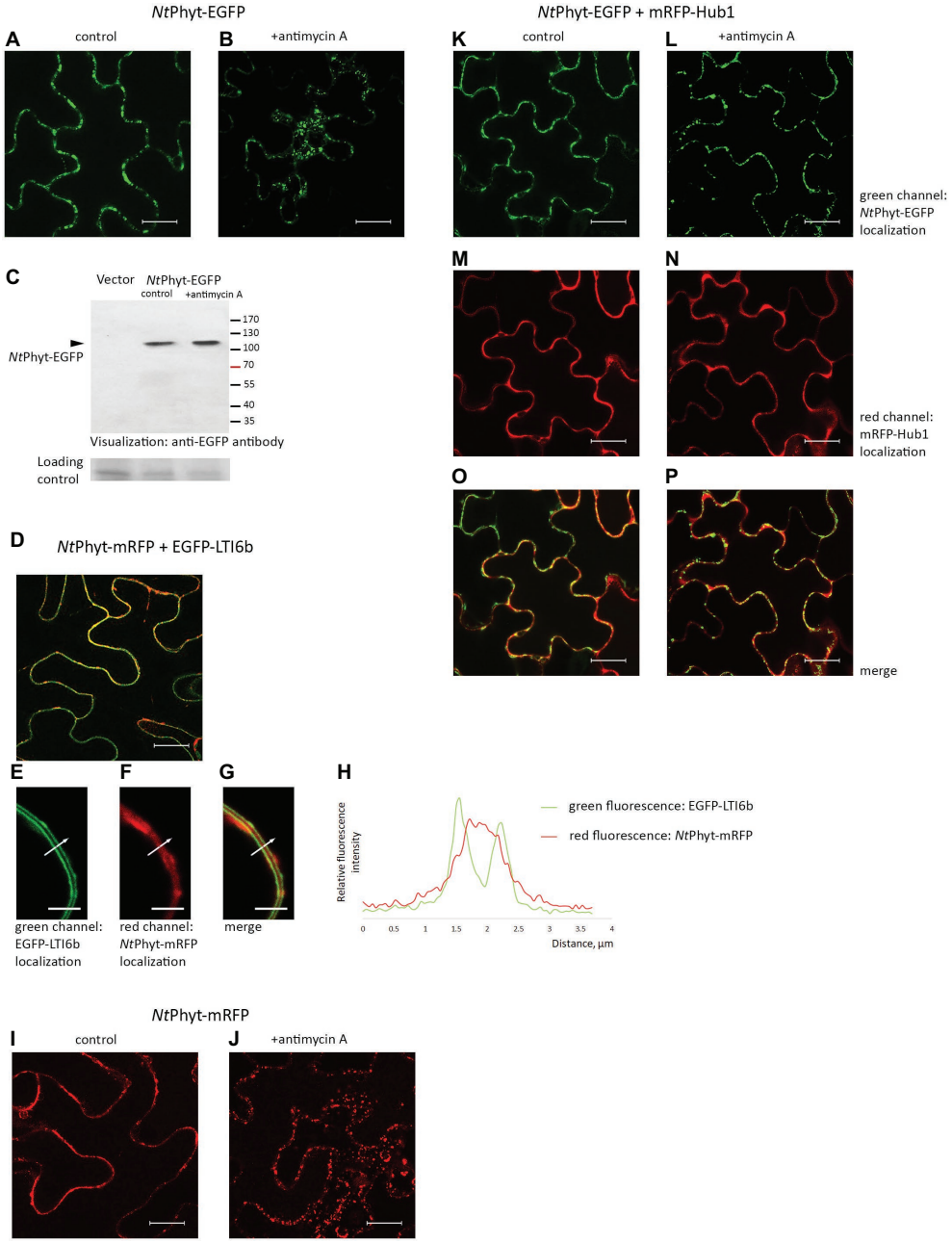

FIGURE 1 | Re-localization of the *Nt*Phyt-EGFP protein in *N. benthamiana* leaves upon induction of oxidative stress depends on clathrin-mediated endocytosis. Confocal microscopy visualization of the *Nt*Phyt-EGFP protein in non-stressed leaves **(A)** and in antimycin A-treated leaves (10 µM antimycin A for 14 h, **B**). **(C)** The *Nt*Phyt-EGFP protein (~110 kDa) is not degraded in response to antimycin A treatment. Western blot analysis of protein extracts obtained from mock-treated (control) and antimycin-treated leaves (+antimycin A) using anti-EGFP antibody. "Vector," the empty vector control from leaves without *Nt*Phyt-EGFP production. The lower panel, the loading control depicting the Coomassie blue-stained Rubisco band. **(D)** Co-production of *Nt*Phyt-mRFP and EGFP-LTI6b visualizes both proteins at the cell borders. In **(D–G)**, the agro-infiltrated tissues were plasmolysed with 0.5 M mannitol, 15 min before confocal analysis, to demonstrate largely apoplastic fluorescence of *Nt*Phyt-mRFP versus the plasma membrane-localized fluorescence of EGFP-LTI6b. Bar, 5 µm for **(E–G)**. **(H)** Measuring green (EGFP-LTI6b) and red (*Nt*Phyt-mRFP) fluorescence intensities across the boundaries of the adjacent cells (shown by the arrow in **E–G**), which shows that red fluorescence is peaking between the plasma membranes. **(I,J)** The *Nt*Phyt-mRFP protein is localized similarly to *Nt*Phyt-EGFP both before **(I)** and after **(J)** overnight treatment with 10 µM antimycin A. **(K–P)** Co-production of *Nt*Phyt-EGFP together with mRFP-Hub1 prevents *Nt*Phyt-EGFP internalization in response to antimycin A treatment. Of note, no discernible signal was detected in **(A)** and **(B)** in the red channel with the current settings in the absence of mRFP production. Bar, 20 µm for images **(A,B,D,I–P)**.

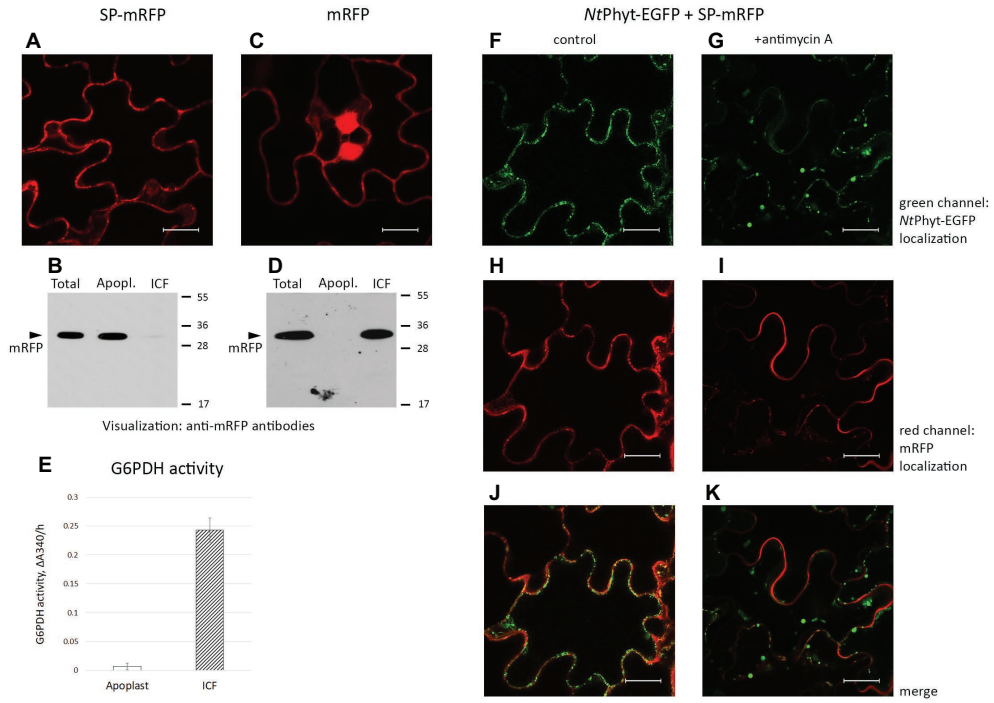

FIGURE 2 | Signal peptide-mRFP (SP-mRFP) as a soluble apoplastic protein marker. **(A)** Confocal fluorescence microscopy of *N. benthamiana* leaves producing SP-mRFP visualizes mRFP fluorescence at the cell borders. **(B)** Western blot analysis of mRFP (~30 kDa) distribution between the apoplastic ("Apopl.") and intracellular ("ICF") protein fractions. "Total" represents the leaf extract without fractionation. Anti-mRFP antibodies were used for protein detection. Positions of molecular weight protein markers are indicated on the right. **(C)** Fluorescence microscopy localization of free mRFP synthesized in *N. benthamiana* leaves. Bar in **(A)** and **(C)**, 20 μm. **(D)** Western blot analysis demonstrating intracellular localization of free mRFP. Designations as in **(B)**. **(E)** Determination of glucose 6-phosphate dehydrogenase (G6PDH) activity in the apoplastic ("Apoplast") and intracellular ("ICF") protein fractions. The activity was determined spectrophotometrically, by measuring change in absorbance at 340 nm/h (ΔA340/h). Average ± SD for three independent experiments with two replicates in each. **(F–K)** Using SP-mRFP as a marker to assess specificity of *Nt*Phyt-EGFP internalization. Confocal fluorescence microscopy of *N. benthamiana* leaves co-producing *Nt*Phyt-EGFP and SP-mRFP. The left column shows non-stressed leaves and the right column shows leaves treated with 10 μM antimycin A for 14 h. Bar, 20 μm.

in residual leaf tissue ("intracellular fraction") and in the total (unwashed) tissues ("total"). The preferred fluorogenic peptide substrate of *Nt*Phyt, Ac-VEID-AFC (Chichkova et al., 2010), was used for proteolytic activity measurements. In the "endogenous *Nb*Phyt only" leaves in the absence of stress, the majority of phytaspase activity was detected in the apoplast. Antimycin A-induced oxidative stress resulted in a dramatic re-localization of the phytaspase proteolytic activity to inside the cell (**Figure 3A**, upper panel). Production of mRFP-Hub1 did not have an appreciable effect on the level and distribution of phytaspase activity in healthy *N. benthamiana* tissues. However, upon the induction of oxidative stress, the inhibition of clathrin-mediated endocytosis precluded the accumulation of phytaspase activity inside the cells (**Figure 3A**, lower panel).

Analogous fractionation and proteolytic activity measurements were then performed for *N. benthamiana* leaves transiently producing *Nt*Phyt-EGFP, leaves producing *Nt*Phyt-EGFP together with mRFP-Hub1, either treated with antimycin A or not. The distribution of proteolytic activity of the ectopically produced *Nt*Phyt-EGFP was found to be similar to that of endogenous enzyme in regards to the stress-induced re-localization to inside the cells (**Figure 3B**, upper panel) and the dependence of this retrograde trafficking on clathrin-mediated endocytosis (**Figure 3B**, lower panel). The only variance was the apparently less pronounced difference between the proteolytic activity levels in the apoplast versus the intracellular protein fractions observed upon the *Nt*Phyt-EGFP overproduction.

An increase in the phytaspase-specific proteolytic activity observed upon *Nt*Phyt-EGFP overproduction suggests that this activity belongs to *Nt*Phyt-EGFP. To further verify this assumption, total extracts were prepared from leaves infiltrated with agrobacteria carrying either the wild type *Nt*Phyt-EGFP – encoding plasmid, or the *Nt*Phyt-S537A-EGFP – encoding plasmid driving production of catalytically inactive phytaspase mutant (Chichkova et al., 2010), or the empty vector. Determination of the Ac-VEID-AFC – hydrolyzing activities in total extracts demonstrated a marked increase of the proteolytic activity in the case of wild type *Nt*Phyt-EGFP production, relative to the empty vector control (**Figure 3C**). Production of the inactive *Nt*Phyt-S537A-EGFP protein, on the other hand, failed to increase proteolytic activity over the background level, although both proteins were overproduced to a similar level judging by western blot analysis of the extracts (**Figure 3D**) and fluorescence intensities of infiltrated leaves (**Figures 3E,F**).

Based on the results obtained both with the endogenous and ectopically produced phytaspases, we conclude that induction

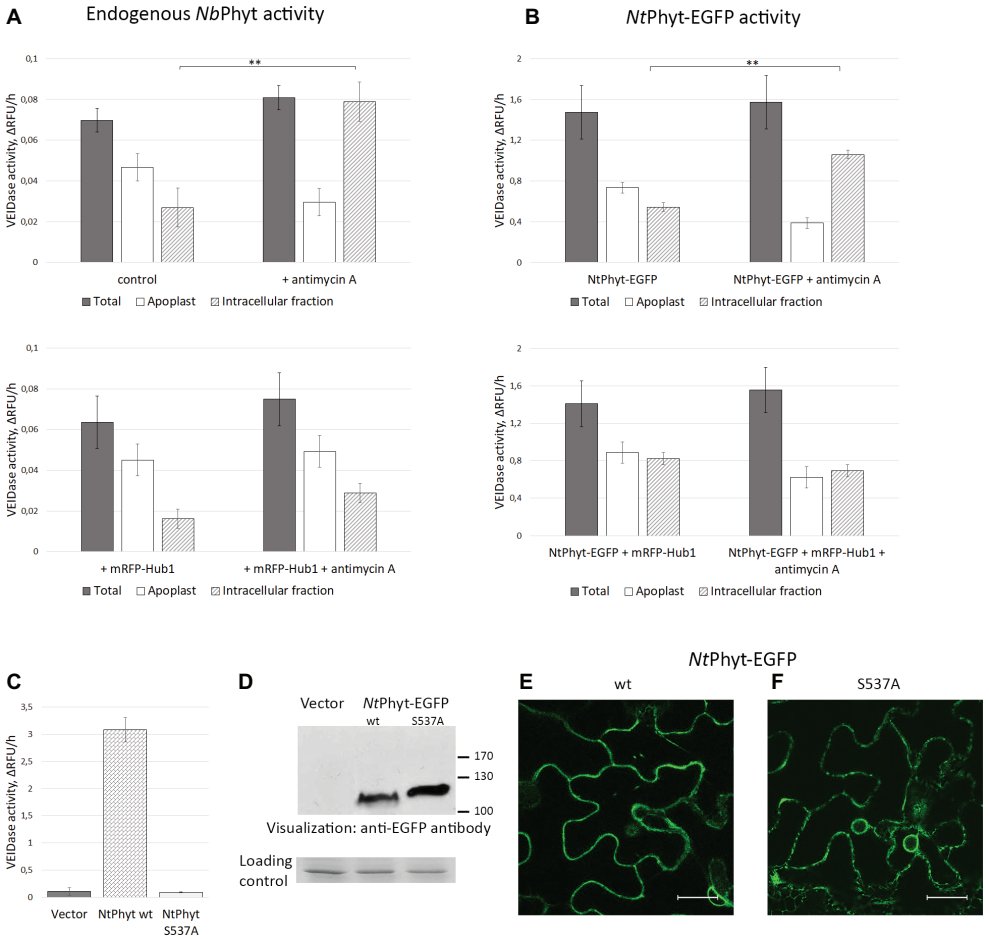

FIGURE 3 | The internalized *Nt*Phyt-EGFP and endogenous *N. benthamiana* phytaspases are proteolytically active. Endogenous *Nb*Phyt **(A)** and ectopic (*Nt*Phyt-EGFP, **B**) phytaspase activity in the extracellular ("Apoplast") and intracellular fractions obtained from non-stressed leaves and from antimycin A-treated leaves that either produce mRFP-Hub1 (lower panels) or do not produce mRFP-Hub1 (upper panels). "Total" represents the leaf extract without fractionation. +antimycin A, samples from antimycin A-treated leaves (10 μM antimycin A for 14 h). Control, samples from water-infiltrated leaves. Phytaspase activity was analyzed using 30 μM Ac-VEID-AFC fluorogenic peptide as a substrate. Relative rates of hydrolysis were determined as an increase of relative fluorescence units per hour (ΔRFU/h). Data represent the mean of three experiments ±SD. Significant differences are shown as $^{**}p < 0.01$ (Student's *t*-test). Samples in **(A)** and **(B)** were prepared in an identical fashion. Note that 'total' activity values in **(B)** are approximately 20-fold higher than in **(A)** due to *Nt*Phyt-EGFP production. **(C)**, production of *Nt*Phyt-EGFP in *N. benthamiana* leaves results in a significant increase of the Ac-VEID-AFC-hydrolyzing activity observed in total protein extracts, whereas production of the catalytically inactive phytaspase mutant (*Nt*PhytS537A-EGFP) does not. "Vector" sample from leaves infiltrated with agrobacteria carrying empty vector. Proteolytic activity was determined as in **(A)** and **(B)**. Data represent the mean of three independent experiments ±SD. **(D)** Western blot analysis of extracts used in **(C)** with anti-EGFP antibody to confirm comparable levels of production and accumulation of the *Nt*Phyt-EGFP (wt, ~ 110 kDa) and *Nt*Phyt-S537A-EGFP (S537A, ~ 120 kDa) proteins. The lower panel, the loading control depicting the Coomassie blue-stained Rubisco band. **(E,F)** Confocal microscopy images of *N. benthamiana* cells producing *Nt*Phyt-EGFP (wt) and *Nt*PhytS537A-EGFP (S537A). Bar, 20 μm.

of cell death does not markedly change the overall level of phytaspase activity in plant tissues. Rather, it causes the re-distribution of proteolytically active phytaspase from the apoplast to inside the cells through the retrograde trafficking step that is critically dependent on clathrin-mediated endocytosis.

Correlating *Nt*Phyt Activity and Trafficking With Plant Cell Death

Previously, by using transgenic tobacco plants with up- and down-regulated phytaspase activity, *Nt*Phyt has been demonstrated to promote plant cell death induced by biotic and abiotic stresses, with concomitant retrograde transport of the enzyme (Chichkova et al., 2010). We, therefore, strived to evaluate whether transient *Nt*Phyt overproduction and/or inhibition of *Nt*Phyt internalization could affect plant cell viability. To address these issues, seven-days-old *N. benthamiana* seedlings were vacuum-infiltrated with agrobacteria carrying either empty vector, or the *Nt*Phyt-EGFP – encoding plasmid, or the mRFP-Hub1 – encoding plasmid, or a combination thereof, or the *Nt*Phyt-S537A-EGFP – encoding plasmid. Cell death in the cotyledons was examined by staining with Evans Blue both with and without treatment of seedlings with antimycin A. As shown in **Figure 4**, antimycin A-induced oxidative stress caused extensive cell death (**A,B**), as expected.

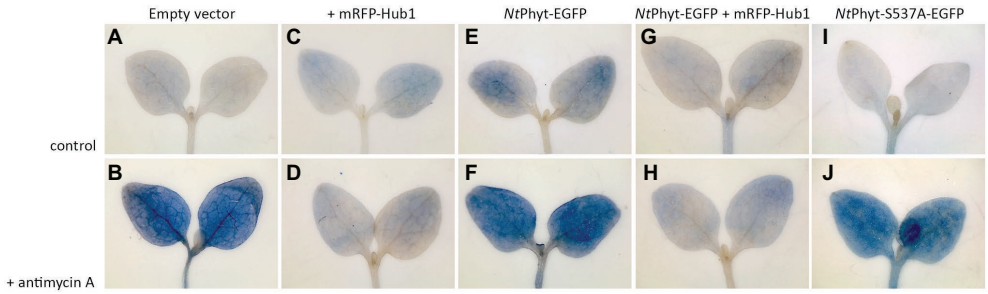

FIGURE 4 | Inhibition of clathrin-mediated endocytosis in *N. benthamiana* seedlings by mRFP-Hub1 production opposes cell death. Seven-day-old seedlings were agroinfiltrated to produce mRFP-Hub1 **(C,D)**, *Nt*Phyt-EGFP **(E,F)**, both proteins together **(G,H)**, or neither of them (empty vector, **A** and **B**), and *Nt*Phyt-S537A-EGFP **(I,J)**. Three days after agroinfiltration, the seedlings were treated with 10 μM antimycin A for 3 h (the lower row) or mock-treated (buffer only control, the upper row). Subsequent staining with Evans Blue revealed marked cell death in the cotyledons upon antimycin A treatment **(B,F,J)**, which was prevented by the mRFP-Hub1 production **(D,H)**. Overproduction of *Nt*Phyt-EGFP caused moderate damage by itself **(E)** and again, co-expression of mRFP-Hub1 nullified this effect **(G)**. Overproduction of proteolytically inactive *Nt*Phyt-S537A-EGFP mutant failed to cause cell death in the absence of antimycin A treatment **(I)**. Data were reproducible over three independent experiments.

On the other hand, transient production of *Nt*Phyt-EGFP predisposed cells to death even in the absence of antimycin A treatment (**Figure 4**, compare images **A** and **E**), whereas the proteolytically inactive phytaspase mutant failed to do so (**Figure 4**, compare images **E** and **I**). The pro-death effect of *Nt*Phyt-EGFP production was further enhanced by the subsequently applied oxidative stress (**Figure 4F**). Notably in the presence of mRFP-Hub1, both the antimycin A-induced and *Nt*Phyt-EGFP-promoted cell death was attenuated (**Figures 4D,G,H**). These results are in line with pro-death proteolytic activity of *Nt*Phyt, and furthermore they highlight the importance of clathrin-mediated endocytosis for accomplishment of stress-induced and *Nt*Phyt-promoted death of plant cells.

Clathrin-Mediated Internalization of *A. thaliana* Phytaspase in a Model System

The *A. thaliana* phytaspase (*At*Phyt) is distinct from the characterized phytaspases in other plant species in a number of ways (Chichkova et al., 2018). In particular, Trusova et al., 2019 recently documented the unexpected mobility of *At*Phyt-EGFP produced in *N. benthamiana* leaves. The recombinant protein expressed in *N. benthamiana* epidermal cells by agroinfiltration initially localizes along cell borders. However after 2 days post infiltration (p.i.), *At*Phyt-EGFP was spontaneously (in the absence of any additional treatment) re-imported into *N. benthamiana* cells (**Figures 5A,B**). This differs significantly from the behavior of the same protein in *A. thaliana* epidermal cells and of *Nt*Phyt-EGFP protein in the non-stressed *N. benthamiana* cells. Notably, EGFP fluorescence in tissues rapidly declined on days 4 and 5 p.i. (**Figures 5C,D**). Spontaneous *At*Phyt-EGFP internalization in this system occurred in the absence of death symptoms in leaf tissue (Trusova et al., 2019) and was critically dependent on clathrin-mediated endocytosis (**Figures 5E–P**). When clathrin-mediated endocytosis was suppressed by co-production of the mRFP-Hub1 inhibitor, no internalization of the enzyme occurred at days 3 and 4 (**Figures 5F,G**), and apoplastically "arrested" *At*Phyt-EGFP persisted outside the cells at day 5 p.i. (**Figures 5E–H**).

Co-production of the SP-mRFP protein together with *At*Phyt-EGFP in *N. benthamiana* leaves revealed that the secreted mRFP retained its apoplastic localization when the internalization of *At*Phyt-EGFP was essentially complete (**Figures 5Q–T**). This indicates that the spontaneous internalization of *At*Phyt-EGFP occurs specifically, similar to the stress-induced internalization of *Nt*Phyt-EGFP described above.

To determine whether the internalized *At*Phyt-EGFP protein retains its proteolytic activity, intracellular proteins were obtained from the *At*Phyt-EGFP-producing leaves on different days following infiltration. *At*Phyt proteolytic activity was quantified using the preferred *At*Phyt fluorogenic peptide substrate Ac-YVAD-AFC (Chichkova et al., 2018), which is also a sub-optimal substrate for the tobacco phytaspase. Internalization of *At*Phyt-EGFP occurring at days 3 and 4 p.i. was followed by an increase of *At*Phyt activity inside the cells (**Figure 6A**). At day 5 p.i. this intracellular proteolytic activity was still clearly detectable, although somewhat decreased.

Western blot analysis with an anti-EGFP antibody of the total protein extracts obtained from the *At*Phyt-EGFP-producing leaves on different days following infiltration revealed the accumulation of the *At*Phyt-EGFP protein at days 2 and 3 p.i., which was followed by a sharp decline of the protein level at days 4 and 5 p.i. (**Figure 6B**). Concomitantly with the *At*Phyt-EGFP disappearance, a protein of approximately 28 kDa was accumulated during days 3–5 p.i. The absence of EGFP fluorescence in leaf tissues at day 5 p.i. (**Figure 5D**) may indicate that this newly formed product corresponds to a non-fluorescent EGFP fragment. Meanwhile, the presence of the YVADase activity in the 5 day p.i. sample suggests that either active *At*Phyt survives after the EGFP detachment, or the observed proteolytic activity does not belong to *At*Phyt.

To clarify this issue, a panel of 10 synthetic fluorogenic peptide substrates used previously to characterize *At*Phyt cleavage specificity (Chichkova et al., 2018) was employed. In full agreement with the established *At*Phyt specificity, protein samples obtained at days 3, 4, and 5 following infiltration hydrolyzed Ac-YVAD-AFC and Ac-IETD-AFC

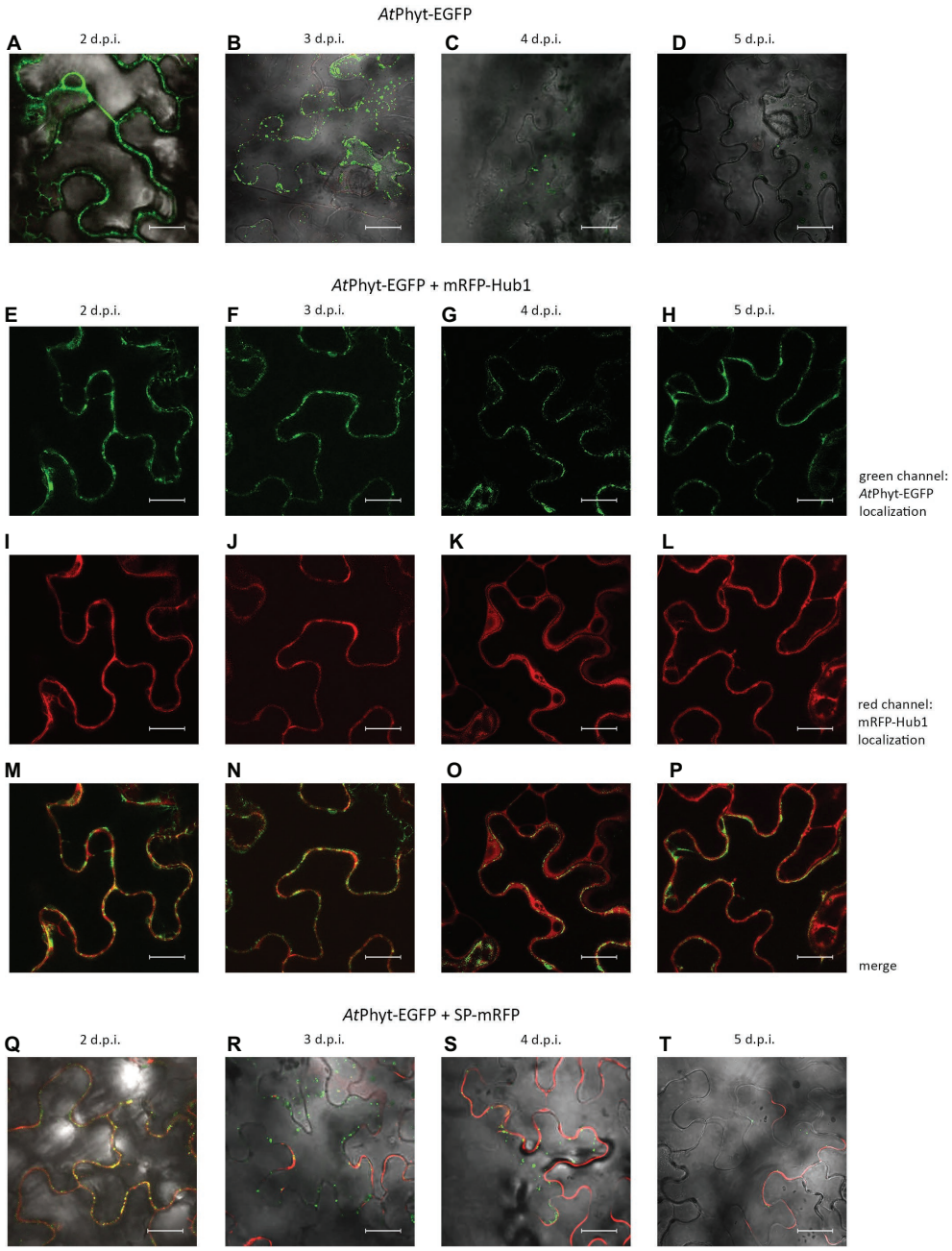

FIGURE 5 | Localization dynamics of *At*Phyt-EGFP in *N. benthamiana* leaves: confocal microscopy examination. The upper row **(A–D)** shows leaves producing only *At*Phyt-EGFP at different days post-infiltration (d.p.i., indicated at the top). Internalization of *At*Phyt-EGFP is most clearly visible at day 3 p.i. **(B)**, after which the signal intensity drops dramatically. **(E–P)** show leaves co-producing *At*Phyt-EGFP and mRFP-Hub1 at different d.p.i. Note that no spontaneous internalization of *At*Phyt-EGFP occurred in the presence of Hub1 at any time point. **(Q–T)** show leaves co-producing *At*Phyt-EGFP and SP-mRFP at different d.p.i., demonstrating specificity of *At*Phyt-EGFP internalization. For **(A–D)** and **(Q–T)**, signals in red channel, green channel, and bright field were merged. Bar, 20 μm.

substrates most efficiently (**Figure 6C**), whereas low level of cleavage or no hydrolysis at all was observed with other fluorogenic peptides.

As an alternative, the YVADase activity in the intracellular protein extracts could belong to vacuolar processing enzyme (VPE), a cysteine-dependent proteinase known to recognize YVAD-based substrates and inhibitors (Hatsugai et al., 2004; Rojo et al., 2004). However, hydrolysis of the Ac-YVAD-AFC substrate by protein extracts was not affected by the presence of 2 mM N-ethylmaleimide, a VPE inhibitor (Hiraiwa et al., 1999) (**Figure 6D**). Finally, when the catalytically inactive *At*PhytS553A-EGFP mutant was transiently produced in *N.*

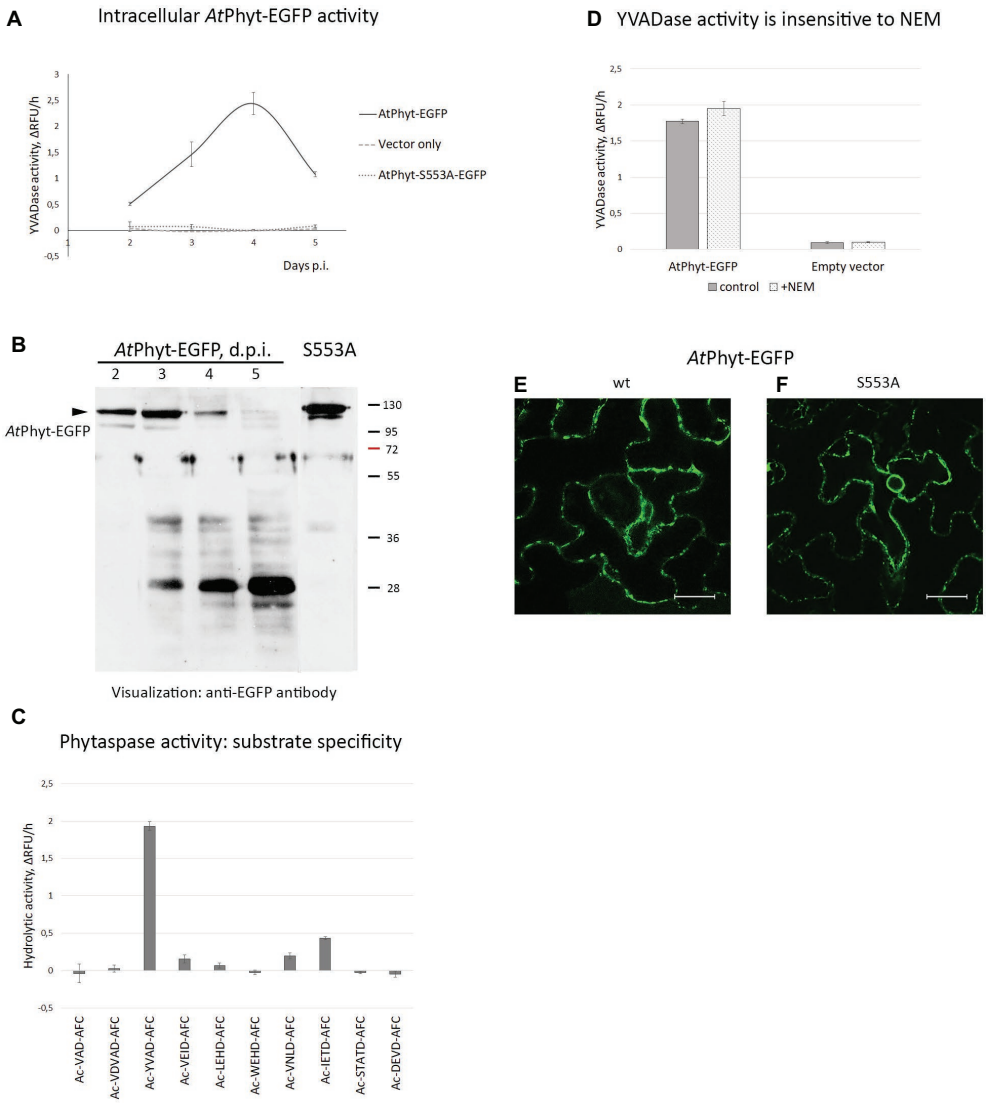

FIGURE 6 | Origin of phytaspase activity in *At*Phyt-EGFP producing *N. benthamiana* leaves. **(A)** Determination of phytaspase activity in intracellular protein fractions obtained at various days p.i. from leaves producing *At*Phyt-EGFP (bold line). Intracellular protein fractions from *N. benthamiana* leaves infiltrated with *Agrobacterium* cells carrying the empty vector (pCambia1300, dashed line) and total protein fractions from leaves producing the inactive *At*Phyt-S553A-EGFP mutant (dotted line) served as controls. Fluorogenic peptide substrate Ac-YVAD-AFC was used at 30 μM to quantify the phytaspase activity. Relative rates of hydrolysis were determined as an increase of relative fluorescence units per hour (ΔRFU/h). Data represent the mean of three experiments ±SD. **(B)** Western blot analysis of *At*Phyt-EGFP in total extracts from *N. benthamiana* leaves producing the *At*Phyt-EGFP protein at various days p.i. The arrowhead points to position of full-length protein (~120 kDa). S553A, sample from leaves producing catalytically inactive *At*PhytS553A-EGFP protein at 3 d.p.i. Monoclonal anti-EGFP antibody was used for protein detection. Positions of molecular weight markers are indicated on the right. **(C)** Cleavage specificity of the proteolytic activity under study corresponds to that of *At*Phyt. Total protein extract obtained at day 4 p.i. was incubated with a panel of fluorogenic peptide substrates (30 μM). Ac-YVAD-AFC and Ac-IETD-AFC are the preferred *At*Phyt substrates (Chichkova et al., 2018). Relative rates of hydrolysis were determined as in **(A)**. Data represent the mean of three experiments ±SD. Specificity profiles with protein samples obtained at day 3 and 5 p.i. were similar to this one. **(D)** N-ethylmaleimide (2 mM), an inhibitor of VPE protease, does not interfere with hydrolysis of Ac-YVAD-AFC by total protein extracts obtained at day 4 p.i. from *At*Phyt-EGFP producing (*At*Phyt-EGFP) and non-producing (Empty vector) leaves. Relative rates of hydrolysis were determined as in **(A)**. Data represent the mean of two experiments ±SD. Similar results were obtained with a 3 d.p.i. sample. **(E,F)** The *At*Phyt-EGFP protein (wt, **E**) and its catalytically inactive mutant *At*PhytS553A-EGFP (S553A, **F**) are produced with similar efficiency in *N. benthamiana* leaves. Images were obtained at day 2 post-infiltration. Bar, 20 μm.

benthamiana leaves (see **Figure 6B** for the relative level of production), no proteolytic activity above the background level was observed with the Ac-YVAD-AFC substrate using total leaf extracts obtained at any time point (**Figure 6A**). Fluorescence microscopy examination of agroinfiltrated tissues confirmed efficient production of both proteins as well (**Figures 6E,F**).

Taken together, these results suggest that the enhanced intracellular YVAD-AFC-hydrolyzing proteolytic activity belongs

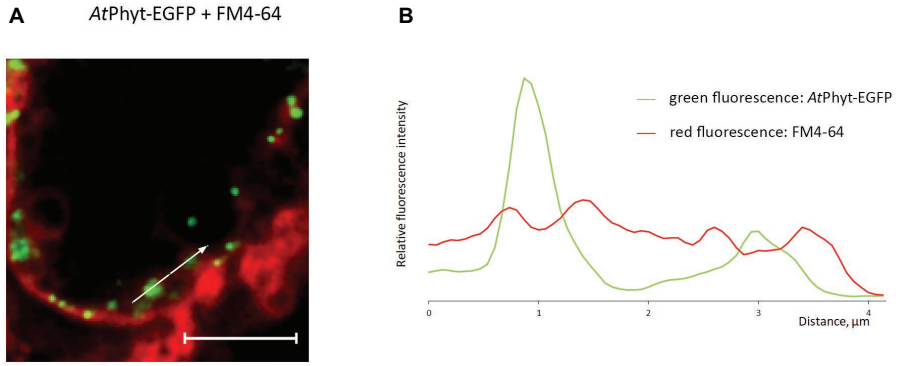

FIGURE 7 | Vesicular membrane trafficking of *At*Phyt-EGFP in the course of internalization. **(A)** *At*Phyt-EGFP-producing *N. benthamiana* leaves were treated at day 3 p.i. with the FM4-64 fluorescent membrane-staining dye for 4 h and examined by confocal fluorescence microscopy. Bar, 5 µm. **(B)** Plotting fluorescence intensity for *At*Phyt-EGFP (green) and FM4-64 (red) along the line drawn through phytaspase-positive dots (shown by the arrow in **A**) demonstrates phytaspase encirclement with membranous structures.

to the transiently produced *At*Phyt, and that the activity survives within the cell for several days.

To further examine the retrograde vesicular membrane trafficking of phytaspase at the healthy cell background, *At*Phyt-EGFP-producing *N. benthamiana* leaves at 3 days p.i. (when the *At*Phyt-EGFP protein was largely intact) were treated with FM4-64 fluorescent membrane-staining dye. Prolonged incubation with FM4-64 allowed the dye to become endocytosed and stain intracellular membranous compartments (Jelínková et al., 2010), whereas *At*Phyt-EGFP was visualized as intracellular green dots (**Figure 7A**). Measuring green and red fluorescence intensities along the line drawn through phytaspase-positive dots (direction is shown by the arrow in **Figure 7A**) revealed that the internalized *At*Phyt-EGFP (green) is entrapped within the membranous (FM4-64-positive, red) structures (**Figure 7B**). This is consistent with the vesicular membrane mechanism of delivery of active phytaspase into plant cells.

DISCUSSION

Clathrin-mediated endocytosis was recently shown to drive PCD-induced retrograde transport of phytaspases, plant cell death-related proteases, from the apoplast into the plant cells (Trusova et al., 2019), raising new important questions regarding mechanisms and functional consequences of this unanticipated trafficking pathway. What happens to the proteolytic activity of the enzyme upon internalization? Is the uptake of phytaspases specific, or any soluble apoplastic protein will become internalized upon induction of cell death? Will interference with the phytaspase uptake compromise cell death? Here, we addressed these questions using *N. benthamiana* leaves either containing endogenous phytaspase only, or overproducing *Nt*Phyt tagged with EGFP or mRFP that allowed to follow phytaspase re-distribution with the aid of fluorescence microscopy in parallel with the determination of a peculiar Asp-specific activity of phytaspases. *N. benthamiana* leaves either treated with antimycin A to trigger oxidative stress-induced PCD and phytaspase internalization, or mock-treated were used in these studies.

By separating proteins into apoplastic and intracellular fractions and by quantifying phytaspase proteolytic activity using fluorogenic peptide substrates of phytaspases, we showed that retrograde transport of phytaspases is accompanied by the shift of phytaspase activity toward the cell interior. When internalization of phytaspases was blocked by co-production of Hub, the inhibitor of clathrin-mediated endocytosis, phytaspase proteolytic activity was retained within the apoplast. It is important to note that the overall level of phytaspase activity in leaf tissues was not diminished after phytaspase internalization. Efficient degradation within the vacuole is a frequent outcome for endocytosed proteins (Kleine-Vehn et al., 2008; Korbei and Luschnig, 2013; Claus et al., 2018; Reynolds et al., 2018). However, the internalized phytaspases are evidently able to deviate from the degradation pathway.

Therefore, our results indicate that clathrin-mediated endocytosis accomplishes the delivery of active phytaspases inside the plant cell. The process of phytaspase internalization appears to be specific, as the apoplastic mRFP protein (originating from the signal peptide-mRFP precursor) retained its extracellular localization both before and after the induction of cell death. This suggests that a receptor for phytaspases exists in the plant cell plasma membrane. Indeed, clathrin-mediated endocytosis targets proteins that localize at the plasma membrane and possess cytoplasmic domains, to which clathrin is recruited with the aid of adapter proteins (Traub, 2009; Jackson et al., 2010; Chen et al., 2011; Traub and Bonifacino, 2013; Paez Valencia et al., 2016). Phytaspases, however, are soluble proteins that can be easily obtained in apoplastic wash. Therefore, an interface between phytaspases and clathrin endocytic machinery appears to be necessary. Identification of such a receptor would be an interesting task for the future.

The known involvement of phytaspases in the accomplishment of stress-induced plant cell death (Chichkova et al., 2004, 2010; Reichardt et al., 2018) has pushed us to explore whether prevention of phytaspase internalization would promote cell

viability under the unfavorable conditions. We found that interruption of phytaspase uptake through inhibition of clathrin-mediated endocytosis correlated with alleviation of cell death induced by oxidative stress (antimycin A treatment) and by *Nt*Phyt overproduction. These findings appear to provide the first indication of the importance of clathrin-mediated endocytosis for stress-induced death of plant cells. Also, inability of the catalytically inactive *Nt*Phyt mutant, in contrast to the wild type enzyme, to cause cell damage further emphasizes the importance of the *Nt*Phyt proteolytic activity for promoting plant cell death. However, although the obtained data are in line with the current model of phytaspase participation in plant PCD (Vartapetian et al., 2011; Chichkova et al., 2012; Trusova et al., 2019), further efforts are obviously required for detailed characterization of the underlying mechanisms.

The second experimental system used in this study, the "*At*Phyt-EGFP in *N. benthamiana*" model, can of course be regarded as artificial and results obtained with this system should be interpreted with some caution. Indeed, we do not yet understand why internalization of the *At*Phyt-EGFP protein begins spontaneously in *N. benthamiana* epidermal cells after a 2-day lag period. A requirement for high level pre-accumulation of the *At*Phyt-EGFP protein within the apoplast to drive internalization could possibly account for the observed phenomenon. Also, what is the difference between *At*Phyt-EGFP and *Nt*Phyt-EGFP that allows the former to enter cells spontaneously, while the latter requires a PCD-inducing stimulus for internalization?

Despite these open questions, the behaviors of *Nt*Phyt and *At*Phyt in *N. benthamiana* leaves share a number of features, as shown by the employment of clathrin-mediated endocytosis for their specific internalization. As spontaneous uptake of *At*Phyt-EGFP does not appear to be associated with *N. benthamiana* cell death (Trusova et al., 2019), the *At*Phyt-EGFP model may offer an opportunity to address details of phytaspase internalization in live plant cells, in the absence of major complicating perturbations occurring in dying cells. With this approach, co-localization of the internalized *At*Phyt-EGFP protein with intracellular membranous vesicles was observed, which is consistent with the endocytic entry pathway for phytaspases.

The described localization dynamics of phytaspases is atypical for plant subtilisin-like proteases, for which secretion into the apoplast was considered to be the end point of their trafficking. In this regard, it would be interesting to learn whether phytaspases represent a rare exception in their retrograde vesicular trafficking, or perhaps other plant subtilases behave in a similar manner under certain conditions.

DATA AVAILABILITY

The raw data supporting the conclusions of this manuscript will be made available by the authors, without undue reservation, to any qualified researcher.

AUTHOR CONTRIBUTIONS

AV, NC, and ST designed the study and directed the research. ST, AT, SG, EM, RG, and NC performed experiments. NC, ST, AT, SG, EM, RG, and AV analyzed and interpreted the data. AV wrote the manuscript with contribution from NC. All the authors read and approved the manuscript.

FUNDING

This work was supported by the Russian Science Foundation (grant nos. 16-14-10043 and 19-14-00010).

ACKNOWLEDGMENTS

We thank M. Taliansky (The James Hutton Institute, UK) for providing the EGFP-LTI6b construct. We are grateful to the reviewers for their helpful comments and suggestions.

REFERENCES

Beloshistov, R. E., Dreizler, K., Galiullina, R. A., Tuzhikov, A. I., Serebryakova, M. V., Reichardt, S., et al. (2018). Phytaspase-mediated precursor processing and maturation of the wound hormone systemin. *New Phytol.* 218, 1167–1178. doi: 10.1111/nph.14568

Cao, J., Han, X., Zhang, T., Yang, Y., Huang, J., and Hu, X. (2014). Genome-wide and molecular evolution analysis of the subtilase gene family in *Vitis vinifera*. *BMC Genomics* 15:1116. doi: 10.1186/1471-2164-15-1116

Chen, X., Irani, N. G., and Friml, J. (2011). Clathrin-mediated endocytosis: the gateway into plant cells. *Curr. Opin. Plant Biol.* 14, 674–682. doi: 10.1016/j.pbi.2011.08.006

Chichkova, N. V., Galiullina, R. A., Mochalova, L. V., Trusova, S. V., Sobri, Z. M., Gallois, P., et al. (2018). *Arabidopsis thaliana* phytaspase: identification and peculiar properties. *Funct. Plant Biol.* 45, 171–179. doi: 10.1071/FP16321

Chichkova, N. V., Kim, S. H., Titova, E. S., Kalkum, M., Morozov, V. S., Rubtsov, Y. P., et al. (2004). A plant caspase-like protease activated during the hypersensitive response. *Plant Cell* 16, 157–171. doi: 10.1105/tpc.017889

Chichkova, N. V., Shaw, J., Galiullina, R. A., Drury, G. E., Tuzhikov, A. I., Kim, S. H., et al. (2010). Phytaspase, a relocalisable cell death promoting plant protease with caspase specificity. *EMBO J.* 29, 1149–1161. doi: 10.1038/emboj.2010.1

Chichkova, N. V., Tuzhikov, A. I., Taliansky, M., and Vartapetian, A. B. (2012). Plant phytaspases and animal caspases: structurally unrelated death proteases with a common role and specificity. *Physiol. Plant.* 145, 77–84. doi: 10.1111/j.1399-3054.2011.01560.x

Claus, L. A. N., Savatin, D. V., and Russinova, E. (2018). The crossroads of receptor-mediated signaling and endocytosis in plants. *J. Integr. Plant Biol.* 60, 827–840. doi: 10.1111/jipb.12672

Cutler, S. R., Ehrhardt, D. W., Griffitts, J. S., and Somerville, C. R. (2000). Random GFP::cDNA fusions enable visualization of subcellular structures in cells of Arabidopsis at a high frequency. *Proc. Natl. Acad. Sci. USA* 97, 3718–3723. doi: 10.1073/pnas.97.7.3718

Debnam, P. M., and Emes, M. J. (1999). Subcellular distribution of enzymes of the oxidative pentose phosphate pathway in root and leaf tissues. *J. Exp. Bot.* 50, 1653–1661. doi: 10.1093/jxb/50.340.1653

Dhonukshe, P., Aniento, F., Hwang, I., Robinson, D. G., Mravec, J., Stierhof, Y. D., et al. (2007). Clathrin-mediated constitutive endocytosis of PIN auxin efflux carriers in Arabidopsis. *Curr. Biol.* 17, 520–527. doi: 10.1016/j.cub.2007.01.052

Figueiredo, J., Costa, G. J., Maia, M., Paulo, O. S., Malhó, R., Sousa Silva, M., et al. (2016). Revisiting *Vitis vinifera* subtilase gene family: a possible role in grapevine resistance against *Plasmopara viticola*. *Front. Plant Sci.* 7:1783. doi: 10.3389/fpls.2016.01783

Galiullina, R. A., Kasperkiewicz, P., Chichkova, N. V., Szalek, A., Serebryakova, M. V., Poreba, M., et al. (2015). Substrate specificity and possible heterologous targets of phytaspase, a plant cell death protease. *J. Biol. Chem.* 290, 24806–24815. doi: 10.1074/jbc.M115.675819

Ghorbani, S., Hoogewijs, K., Pečenková, T., Fernandez, A., Inzé, A., Eeckhout, D., et al. (2016). The SBT6.1 subtilase processes the GOLVEN1 peptide controlling cell elongation. *J. Exp. Bot.* 67, 4877–4887. doi: 10.1093/jxb/erw241

Hamilton, J. M., Simpson, D. J., Hyman, S. C., Ndimba, B. K., and Slabas, A. R. (2003). Ara12 subtilisin-like protease from *Arabidopsis thaliana*: purification, substrate specificity and tissue localization. *Biochem. J.* 370, 57–67. doi: 10.1042/BJ20021125

Hatsugai, N., Kuroyanagi, M., Yamada, K., Meshi, T., Tsuda, S., Kondo, M., et al. (2004). A plant vacuolar protease, VPE, mediates virus-induced hypersensitive cell death. *Science* 305, 855–858. doi: 10.1126/science.1099859

Hiraiwa, N., Nishimura, M., and Hara-Nishimura, I. (1999). Vacuolar processing enzyme is self-catalytically activated by sequential removal of the C-terminal and N-terminal propeptides. *FEBS Lett.* 447, 213–216. doi: 10.1016/S0014-5793(99)00286-0

Jackson, L. P., Kelly, B. T., McCoy, A. J., Gaffry, T., James, L. C., Collins, B. M., et al. (2010). A large-scale conformational change couples membrane recruitment to cargo binding in the AP2 clathrin adaptor complex. *Cell* 141, 1220–1229. doi: 10.1016/j.cell.2010.05.006

Jelínková, A., Malínská, K., Simon, S., Kleine-Vehn, J., Parezová, M., Pejchar, P., et al. (2010). Probing plant membranes with FM dyes: tracking, dragging or blocking? *Plant J.* 61, 883–892. doi: 10.1111/j.1365-313X.2009.04102.x

Kitakura, S., Vanneste, S., Robert, S., Löfke, C., Teichmann, T., Tanaka, H., et al. (2011). Clathrin mediates endocytosis and polar distribution of PIN auxin transporters in Arabidopsis. *Plant Cell* 23, 1920–1931. doi: 10.1105/tpc.111.083030

Kleine-Vehn, J., Leitner, J., Zwiewka, M., Sauer, M., Abas, L., Luschnig, C., et al. (2008). Differential degradation of PIN2 auxin efflux carrier by retromer-dependent vacuolar targeting. *Proc. Natl. Acad. Sci. USA* 105, 17812–17817. doi: 10.1073/pnas.0808073105

Korbei, B., and Luschnig, C. (2013). Plasma membrane protein ubiquitylation and degradationas determinants of positional growth in plants. *J. Integr. Plant Biol.* 55, 809–823. doi: 10.1111/jipb.12059

Li, X., and Pan, S. Q. (2017). Agrobacterium delivers VirE2 protein into host cells via clathrin-mediated endocytosis. *Sci. Adv.* 3:e1601528. doi: 10.1126/sciadv.1601528

Liu, J. X., and Howell, S. H. (2010). Endoplasmic reticulum protein quality control and its relationship to environmental stress responses in plants. *Plant Cell* 22, 2930–2942. doi: 10.1105/tpc.110.078154

Liu, J. X., Srivastava, R., Che, P., and Howell, S. H. (2007). An endoplasmic reticulum stress response in Arabidopsis is mediated by proteolytic processing and nuclear relocation of a membrane-associated transcription factor, bZIP28. *Plant Cell* 19, 4111–4119. doi: 10.1105/tpc.106.050021

Liu, S. H., Wong, M. L., Craik, C. S., and Brodsky, F. M. (1995). Regulation of clathrin assembly and trimerization defined using recombinant triskelion hubs. *Cell* 83, 257–267. doi: 10.1016/0092-8674(95)90167-1

Minina, E. A., Filonova, L. H., Sanchez-Vera, V., Suarez, M. F., Daniel, G., and Bozhkov, P. V. (2013). Detection and measurement of necrosis in plants. *Methods Mol. Biol.* 1004, 229–248. doi: 10.1007/978-1-62703-383-1_17

Paez Valencia, J., Goodman, K., and Otegui, M. S. (2016). Endocytosis and endosomal trafficking in plants. *Annu. Rev. Plant Biol.* 67, 309–335. doi: 10.1146/annurev-arplant-043015-112242

Rautengarten, C., Steinhauser, D., Büssis, D., Stintzi, A., Schaller, A., Kopka, J., et al. (2005). Inferring hypotheses on functional relationships of genes: analysis of the *Arabidopsis thaliana* subtilase gene family. *PLoS Comput. Biol.* 1:e40. doi: 10.1371/journal.pcbi.0010040

Reichardt, S., Repper, D., Tuzhikov, A. I., Galiullina, R. A., Planas-Marques, M., Chichkova, N. V., et al. (2018). The tomato subtilase family includes several cell death-related proteinases with caspase specificity. *Sci. Rep.* 8:10531. doi: 10.1038/s41598-018-28769-0

Reynolds, G. D., Wang, C., Pan, J., and Bednarek, S. Y. (2018). Inroads into internalization: five years of endocytic exploration. *Plant Physiol.* 176, 208–218. doi: 10.1104/pp.17.01117

Rojo, E., Martín, R., Carter, C., Zouhar, J., Pan, S., Plotnikova, J., et al. (2004). VPEgamma exhibits a caspase-like activity that contributes to defense against pathogens. *Curr. Biol.* 14, 1897–1906. doi: 10.1016/j.cub.2004.09.056

Schaller, A., Stintzi, A., Rivas, S., Serrano, I., Chichkova, N. V., Vartapetian, A. B., et al. (2018). From structure to function – a family portrait of plant subtilases. *New Phytol.* 218, 901–915. doi: 10.1111/nph.14582

Schardon, K., Hohl, M., Graff, L., Pfannstiel, J., Schulze, W., Stintzi, A., et al. (2016). Precursor processing for plant peptide hormone maturation by subtilisin-like serine proteinases. *Science* 354, 1594–1597. doi: 10.1126/science.aai8550

Sénéchal, F., Graff, L., Surcouf, O., Marcelo, P., Rayon, C., Bouton, S., et al. (2014). Arabidopsis PECTIN METHYLESTERASE17 is co-expressed with and processed by SBT3.5, a subtilisin-like serine protease. *Ann. Bot.* 114, 1161–1175. doi: 10.1093/aob/mcu035

Sukhacheva, E. A., Evstafieva, A. G., Fateeva, T. V., Shakulov, V. R., Efimova, N. A., Karapetian, R. N., et al. (2002). Sensing prothymosin alpha origin, mutations and conformation with monoclonal antibodies. *J. Immunol. Methods* 266, 185–196. doi: 10.1016/S0022-1759(02)00098-4

Traub, L. M. (2009). Tickets to ride: selecting cargo for clathrin-regulated internalization. *Nat. Rev. Mol. Cell Biol.* 10, 583–596. doi: 10.1038/nrm2751

Traub, L. M., and Bonifacino, J. S. (2013). Cargo recognition in clathrin-mediated endocytosis. *Cold Spring Harbor Persp. Biol.* 5:a016790. doi: 10.1101/cshperspect.a016790

Tripathi, L. P., and Sowdhamini, R. (2006). Cross genome comparisons of serine proteases in *Arabidopsis* and rice. *BMC Genomics* 7:200. doi: 10.1186/1471-2164-7-200

Trusova, S. V., Golyshev, S. A., Chichkova, N. V., and Vartapetian, A. B. (2019). Sometimes they come back: endocytosis provides localization dynamics of a subtilase in cells committed to cell death. *J. Exp. Bot.* 70, 2003–2007. doi: 10.1093/jxb/erz014

Vartapetian, A. B., Tuzhikov, A. I., Chichkova, N. V., Taliansky, M., and Wolpert, T. J. (2011). A plant alternative to animal caspases: subtilisin-like proteases. *Cell Death Differ.* 18, 1289–1297. doi: 10.1038/cdd.2011.49

Yamagata, H., Masuzawa, T., Nagaoka, Y., Ohnishi, T., and Iwasaki, T. (1994). Cucumisin, a serine protease from melon fruits, shares structural homology with subtilisin and is generated from a large precursor. *J. Biol. Chem.* 269, 32725–32731.

Yang, L., Wang, X., Chang, N., Nan, W., Wang, S., Ruan, M., et al. (2019). Cytosolic glucose-6-phosphate dehydrogenase is involved in seed germination and root growth under salinity in Arabidopsis. *Front. Plant Sci.* 10:182. doi: 10.3389/fpls.2019.00182

Conflict of Interest Statement: The authors declare that the research was conducted in the absence of any commercial or financial relationships that could be construed as a potential conflict of interest.

frontiers in Plant Science

ORIGINAL RESEARCH
published: 10 September 2019
doi: 10.3389/fpls.2019.01080

Phosphorylation of the Chloroplastic Metalloprotease FtsH in *Arabidopsis* Characterized by Phos-Tag SDS-PAGE

*Yusuke Kato and Wataru Sakamoto**

Institute of Plant Science and Resources (IPSR), Okayama University, Kurashiki, Japan

FtsH is an essential ATP-dependent metalloprotease for protein quality control in the thylakoid membrane of *Arabidopsis thaliana* chloroplasts. It is required for chloroplast development during leaf growth, and particularly for the specific degradation of photo-damaged D1 protein in the photosystem II (PSII) complex to maintain photosynthesis activity. In the thylakoid membrane, the reversible phosphorylation of proteins is known to control the activity and remodeling of photosynthetic complexes, and previous studies implicate that FtsH is also phosphorylated. We therefore assessed the phosphorylation status of FtsH and its possible role in the regulatory mechanism in this study. The phosphorylation level of FtsHs that compose the FtsH heterohexameric complex was investigated by phosphate-affinity gel electrophoresis using a Phos-Tag molecule. Phos-tag SDS-PAGE of thylakoid proteins and subsequent immunoblot analysis showed that both type A (FtsH1/5) and type B (FtsH2/8) subunits were separable into phosphorylated and non-phosphorylated forms. Neither different light conditions nor the lack of two major thylakoid kinases, STN7 and STN8, resulted in any clear difference in FtsH phosphorylation, suggesting that this process is independent of the light-dependent regulation of photosynthesis-related proteins. Site-directed mutagenesis of putatively phosphorylated Ser or Thr residues into Ala demonstrated that Ser-212 may play a role in FtsH stability in the thylakoid membranes. Different phosphorylation status of FtsH oligomers analyzed by two-dimensional clear-native/Phos-tag SDS-PAGE implied that phosphorylation partially affects FtsH complex formation or its stability.

Keywords: FtsH, thylakoid, chloroplast, protein phosphorylation, protease, photosynthesis

OPEN ACCESS

Edited by:
Mercedes Diaz-Mendoza, National Institute of Agricultural and Food Research and Technology, Spain

Reviewed by:
Zach Adam, Hebrew University of Jerusalem, Israel
Christiane Funk, Umeå University, Sweden

***Correspondence:**
Wataru Sakamoto
saka@okayama-u.ac.jp

Specialty section:
This article was submitted to Plant Physiology, a section of the journal Frontiers in Plant Science

Received: *22 May 2019*
Accepted: *08 August 2019*
Published: *10 September 2019*

Citation:
Kato Y and Sakamoto W (2019) Phosphorylation of the Chloroplastic Metalloprotease FtsH in Arabidopsis Characterized by Phos-Tag SDS-PAGE. Front. Plant Sci. 10:1080. doi: 10.3389/fpls.2019.01080

INTRODUCTION

FtsH is an ATP-dependent zinc metalloprotease with a transmembrane domain. The N-terminal transmembrane domain anchors FtsH to cellular membranes with their ATPase domain facing the membranes. Thus, FtsH protease pulls their substrates out of membranes in an ATP-dependent manner and degrades them to small peptides in the proteolytic chamber (Ito and Akiyama, 2005; Nishimura et al., 2016). FtsH protease is originally identified in a temperature-sensitive phenotype of *Escherichia coli*. FtsH protein homologues have been found in other prokaryotes as well as in organelles of bacterial origin, such as mitochondria and chloroplasts. The fundamental function of FtsH protease is the quality control of membrane proteins, but its contribution to stress responses

is also suggested (reviewed by Janska et al., 2013; van Wijk, 2015; Kato and Sakamoto, 2018).

In the *Arabidopsis thaliana* genome, 12 genes encoding members of the FtsH family have been identified. Nine of these proteins (FtsH1, 2, 5, 6, 7, 8, 9, 11, and 12) are located in the chloroplast (Sakamoto et al., 2003). Additionally, the *Arabidopsis* genome encodes five proteolytically inactive homologues (FtsHi) (Wagner et al., 2012); four of them (FtsHi1, 2, 4, and 5) form a complex with Ycf2 and FtsH12 at the chloroplast inner envelope membrane (Kikuchi et al., 2018; Schreier et al., 2018). This AAA-ATPase complex associates with the chloroplast TIC complex (Nakai, 2018), and participates in the translocation of chloroplast-targeted proteins as the import motor (Kikuchi et al., 2018). Much effort has been devoted to identify and characterize the FtsH protease in the thylakoid membranes. Five FtsH homologues (FtsH1, 2, 5, 6, and 8) function in the thylakoid membrane (Sakamoto et al., 2003; Yu et al., 2004; Yu et al., 2005; Wagner et al., 2011; Zaltsman et al., 2005a). Of them, four FtsH (FtsH1, 2, 5, and 8) form a heterohexameric complex (hereafter simply called FtsH complex) in the thylakoid membrane; these homologues are divided into two types, type A (FtsH1/FtsH5) and type B (FtsH2/FtsH8) (Sakamoto et al., 2003; Yu et al., 2004; Yu et al., 2005; Zaltsman et al., 2005b). Mutants lacking FtsH5 and FtsH2 are known as *yellow variegated1* (*var1*) and *var2*; these mutants show weak and strong leaf-variegated phenotype, respectively, whereas mutants lacking FtsH1 and FtsH8 do not show the leaf-variegated phenotype (Chen et al., 2000; Takechi et al., 2000; Sakamoto et al., 2002). Both types of subunits are essential for the active FtsH complex in the thylakoid membranes and the severity of the mutant phenotype depends on the level of FtsH complex in thylakoid membranes (Chen et al., 2000; Takechi et al., 2000; Yu et al., 2004; Zaltsman et al., 2005b; Miura et al., 2007; Kato et al., 2012a). Mass spectrometry analyses suggested that *Arabidopsis* FtsH complex contains two type-A subunits and four type-B subunits in a hexameric complex (Moldavski et al., 2012), but a study in cyanobacteria (Boehm et al., 2012) and a recent research of our group (Kato et al., 2018) suggested that the ratio between type A and type B subunits in the hexameric complex is 3:3.

Another relevant phenotype which characterizes mutants lacking FtsH is photosensitivity, with higher accumulation of reactive oxygen species (ROS) in the chloroplasts due to impairment of the repairing-capacity of photosystem II (PSII) from light-induced damage (Lindahl et al., 2000; Bailey et al., 2002; Sakamoto et al., 2002; Sakamoto et al., 2003; Kato et al., 2009). Thylakoid FtsH mediates the degradation of the damaged D1 protein, which is part of the PSII reaction center (Kato et al., 2009; Kato et al., 2012b). The removal of damaged D1 protein is essential for the PSII repair cycle, which is required for the recovery of photosynthetic efficiency reduced by photoinhibition (reviewed by Nixon et al., 2010; Järvi et al., 2015). A possible regulation mechanism of FtsH activity by prohibitin-like proteins, which form a megacomplex with FtsH hexamers, was suggested in *E. coli* (Kihara et al., 1996; Saikawa et al., 2004). The interaction between prohibitin-like proteins and FtsH has been observed in cyanobacteria (Boehm et al., 2012). However, such prohibitin-like proteins have not been reported in chloroplasts, suggesting that thylakoid FtsH may have acquired other regulatory mechanisms along the endosymbiotic process.

Recent studies suggest that an increased turnover rate of FtsH during light irradiation is important for FtsH-mediated protein homeostasis in chloroplasts (Zaltsman et al., 2005a; Li et al., 2017; Wang et al., 2017; Kato et al., 2018). In the chloroplast of seed plants, thylakoid FtsH complex is rather unstable, and FtsH seems to exist in smaller complexes such as dimers (Yoshioka et al., 2010; Kato et al., 2018). The higher turnover rate of FtsH with flexible oligomerization seems to be required for the quality control of itself to access the damaged PSII complex, where ROS might generate at a high rate. On the other hand, disulfide bonds of FtsH controlled by the redox state are involved in the regulation of FtsH oligomerization and its proteolytic activity in *Chlamydomonas reinhardtii* (Wang et al., 2017).

Protein phosphorylation is one of the most important post-translational modifications (PTMs) in thylakoid membranes (Grieco et al., 2016). For example, phosphorylation of PSII core proteins and light-harvesting antenna proteins (LHCII), which are the best-characterized phosphorylated proteins in the thylakoid membrane, undergoes light-dependent regulation. These proteins are dephosphorylated in dark condition and rapidly phosphorylated under low to moderate light irradiation. Under a high light condition, the phosphorylation of PSII core proteins shows a light-dependent increase, whereas LHCII phosphorylation drastically decreases (Rintamäki et al., 1997; Tikkanen et al., 2006). The phosphorylation of these photosynthetic proteins contributes to the fine-tuning of the photosynthetic apparatus to achieve rapid photosynthetic acclimation. The phosphorylation of LHCII, which needs for state transition, is regulated by the STN7 kinase and PPH1 phosphatase pair (Bellafiore et al., 2005; Bonardi et al., 2005; Pribil et al., 2010; Shapiguzov et al., 2010). On the other hand, the reversible phosphorylation of PSII core proteins is regulated by the STN8 kinase–PBCP phosphatase system, being responsible for both positive and negative modulation of D1 degradation (Bonardi et al., 2005; Tikkanen et al., 2008; Samol et al., 2012; Kato and Sakamoto, 2014; Puthiyaveetil et al., 2014a). Recent studies reported the potential phosphorylation of FtsH proteases in the chloroplasts (Stael et al., 2012 and PhosPhAt 4.0 database). In contrast to extensive studies related to the involvement of PSII core proteins in PSII repair, the role of FtsH phosphorylation in that process, however, has been scarcely addressed and remains unclear.

In this study, we attempted to assess the effect of FtsH phosphorylation on this metalloprotease function. Aiming at that goal, we investigated the potential phosphorylation in FtsH by phosphate-affinity gel electrophoresis using a Phos-Tag molecule (Phos-tag SDS-PAGE) followed by immunoblot analysis. Both types of FtsH subunits were separated into phosphorylated and non-phosphorylated forms. We found that phosphorylation of thylakoid FtsH was neither dependent on light exposure nor the presence of the major thylakoid protein kinases, STN7 and STN8. Instead, we found that the phosphorylation status of FtsH varied with FtsH oligomerization degree. Furthermore, the leaf-variegated

phenotype of *var2* was not rescued by expressing a mutated FtsH2 protein, harboring an amino acid substitution in the predicted phosphorylation site. These results imply that FtsH phosphorylation does not regulate FtsH function but FtsH complex formation or its stability.

MATERIALS AND METHODS

Plant Materials and Growth Conditions

Arabidopsis (*Arabidopsis thaliana*) Columbia ecotype was used as wild type. The mutant lines used in this study, *stn7-1*, *stn8-1*, and *var2-1*, were described previously (Bellafiore et al., 2005; Bonardi et al., 2005; Vainonen et al., 2005; Kato and Sakamoto, 2014). Plants were germinated and grown on 0.7% (w/v) agar plates containing Murashige and Skoog medium supplemented with Gamborg's vitamins (Sigma-Aldrich Corp.) and 1.5% (w/v) sucrose under 12-h light (approximately 100 µmol photons m^{-2} s^{-1}), at a constant temperature of 22°C. The potential phosphorylation sites in FtsH2 were searched in the *Arabidopsis* Protein Phosphorylation Site Database (PhosPhAt 4.0; http://phosphat.mpimp-golm.mpg.de/).

For creating transgenic plants expressing mutated FtsHs under *var2-1* background, vector constructions were prepared as follows, using the primers shown in **Supplementary Table S1**. Amino acid substitutions in FtsH2 at the putative phosphorylation sites, S292A, T337A, S380A, and S393A, were introduced into the corresponding *VAR2* cDNA by PCR-based site-directed mutagenesis, using the appropriate set of primers (e.g. VAR2 Infusion-Fw/VAR2 S212A-Rv and VAR2 S212A-Fw/VAR2 Infusion-Rv, for S212A). The resulting PCR fragments were cloned into the BamHI-SacI site of a binary vector pBI121 using the In-fusion HD cloning kit (Takara Bio, USA). Final constructs were each subjected to sequencing, to confirm the accurate mutations inserted in the corresponding region. The constructs were transformed into *Agrobacterium tumefaciens* strain LBA4404 cells, and the positive LBA4404 strains were used to transform *var2-1* plants. Transgenic plants were selected by kanamycin resistance, and confirmed by PCR analysis (**Supplementary Figure S5**). At least three independent lines were obtained.

Sample Preparation and Phos-Tag SDS-PAGE

Isolated thylakoid membranes were used for Phos-tag SDS-PAGE. Harvested 4-week-old seedlings were ground in a blender with ice-cold homogenization buffer (0.35 M sucrose, 50 mM HEPES, pH 7.0, 5 mM $MgCl_2$, 10 mM NaCl, 10 mM NaF) containing EDTA-free complete protease inhibitor (Roche). Homogenates filtered through miracloth (Merck Millipore) were centrifuged at 2,380 × *g* for 10 min. The pellet was resuspended in the same buffer and centrifuged at 300 × *g* for 1 min. The supernatant was again centrifuged at 2,380 × *g* for 10 min. The pellet was resuspended in 1 x SDS-PAGE sample buffer and used for Phos-tag SDS-PAGE analyses. For phosphatase treatment, the thylakoid membranes were resuspended in 1 x Takara buffer for CIAP (supplied with CIAP) with cOmplete™ EDTA-free protease inhibitor (Merck) to a final chlorophyll concentration of 1 µg/µl. Resuspended thylakoid membranes were incubated with or without CIAP phosphatase for 2 h at 37°C. Phosphorylation of thylakoid membrane proteins was analyzed by Phos-tag SDS-PAGE. Phos-Tag™ was purchased from FUJIFILM Wako Pure Chemical Corporation and used according to the manufacturer's protocol. In brief, gels for Phos-tag SDS-PAGE consisted of a separating gel [10% (w/v) acrylamide, 350 mM Bis-Tris, pH 6.8, 25 µM Phos-tag acrylamide, 100 µM $ZnCl_2$, 0.1% (v/v) N,N,N',N'-tetramethylethylenediamine (TEMED), and 0.05% (w/v) ammonium persulfate (APS)] and a stacking gel [4.5% (w/v) acrylamide, 350 mM Bis–Tris, pH 6.8, 0.1% (v/v) TEMED, and 0.05% (w/v) APS]. Electrophoresis was performed at a constant current of ≤20 mA/gel with the running buffer [100 mM Tris, 100 mM MOPS, and 0.1% (w/v) SDS], to which 5 mM of sodium bisulfite was added. For immunoblot analysis, gels were washed in wash buffer [25 mM Tris, 192 mM glycine, 0.1% (v/v) SDS, 10 mM EDTA] for 10 min three times to remove metal ions, followed by one wash in transfer buffer [25 mM Tris, 192 mM glycine, 0.1% (v/v) SDS, 20% methanol] for 10 min. Then, the proteins were electroblotted to the polyvinylidene difluoride (PVDF) membrane (ATTO Corporation).

Two Dimensional (2D) Phos-Tag SDS PAGE

Purified thylakoid membranes were used for two-dimensional Phos-tag SDS-PAGE. Purified thylakoid membranes were resuspended in buffer [25 mM Bis–Tris, 20% (w/v) glycerol, pH 7.5] to a concentration of 2 mg/ml chlorophyll. To solubilize thylakoid membranes, an equal volume of n-dodecyl ß-D-maltoside was added to a final concentration of 1% (w/v). After centrifugation at 14,000 × *g* for 5 min, NativePAGE™ 5% G-250 Sample Additive (Thermo Fisher Scientific Inc.) was added to the supernatant according to the manufacturer's instructions, and samples were loaded onto a NativePAGE™ 4–16% Bis–Tris Protein gel (Thermo Fisher Scientific Inc.) Electrophoresis was performed at 4°C overnight at 50 V. The gel lane was then excised from the gel and incubated in equilibration buffer [50 mM Tris–HCl, 6 M urea, 2% (w/v) SDS, 0.05% (w/v) BPB, 10 mM dithiothreitol] for 30 min at 37°C. Then proteins were separated using Phos-tag SDS-PAGE or conventional SDS-PAGE.

Immunoblot Analysis

Prior to immunoreaction, transferred membranes were blocked with 1% (w/v) bovine serum albumin (BSA) in 50 mM sodium phosphate buffer, pH 7.5, containing 155 mM NaCl and 0.05% (v/v) Tween 20 (PBST buffer) for 1 h. The membranes were then incubated with anti-D1 (dilution 1:5,000), anti-VAR2 (dilution 1:5,000), anti-VAR1 (dilution 1:5,000), anti-CP43 (Agrisera; dilution, 1:5,000), anti-CP47 (Agrisera; dilution, 1:5,000), and anti-Lhcb1 (Agrisera; dilution, 1:5,000). After two washes with PBST buffer, the membranes were incubated with secondary antibodies Amersham ECL Rabbit IgG, HRP-linked F(ab)2 fragment from donkey (GE Healthcare; dilution, 1:10,000 in PBST). Luminata Forte Western HRP Substrate (EMD Millipore Corp.) was used to develop blots,

and chemiluminescence was detected on ChemiDoc XRS+ System (Bio Rad Laboratories, Inc.).

Fluorescence Measurements

Chlorophyll fluorescence was measured in mature leaves of 6-week-old plants using FluorCam800MF (Photon Systems Instruments). To induce photodamage, leaves were incubated for 4 h under high-light conditions (White LED light; 1,200 μmol photons m^{-2} s^{-1}). Before measurement, leaves were dark-adapted for 10 min to oxidize plastoquinone. Initial fluorescence yield of PSII (F_o) and maximal fluorescence yield of PSII (F_M) were measured. Maximal PSII quantum yield (F_V/F_M) was calculated as $(F_M–F_o)/F_M$.

RESULTS

Detection of Phosphorylated FtsH in Thylakoid Membranes

To evaluate potential phosphorylation in FtsH, we employed a phosphate-affinity gel electrophoresis system using a Phos-Tag molecule and subsequent immunoblot analysis. We first tested Phos-tag SDS-PAGE with Mn^{2+} as a chelating divalent cation using purified thylakoid membranes. The detected signals by immunoblotting using anti-VAR1 and VAR2 specific antibodies, which recognize type A and type B subunits, respectively, showed blurred signals of FtsH proteins, whereas phosphorylated PSII core proteins (D1 and CP43) and a light-harvesting antenna protein (Lhcb1) were properly resolved and separated from their unphosphorylated forms (**Figure 1A**). To improve the mobility shift of FtsH proteins, we next tested the Phos-tag SDS-PAGE procedure using Zn^{2+} instead of Mn^{2+}, with a neutral pH buffer system (Kinoshita and Kinoshita-Kikuta, 2011). The result shown in **Figure 1A** indicated that the improved Phos-tag method successfully enabled us to detect both the phosphorylated and non-phosphorylated forms of FtsH proteins. A majority of the signals detected by anti-VAR1 antibodies (corresponding to type A FtsH) was observed in the up-shifted band, suggesting that type A subunits are extensively phosphorylated. Meanwhile, the phosphorylated form of type B FtsH detected by anti-VAR2 antibodies was less than half respect to total immunoblot signals (**Figure 1A**). These results are consistent with the different susceptibility of recombinant FtsH5 and FtsH2 found in calcium-dependent phosphorylation assays in a previous report (Stael et al., 2012). In contrast, a non-phosphorylated PSII core protein CP47 did not show any mobility shift in both electrophoresis conditions. The mobility shifts of FtsH proteins were substantially reduced after treatment with calf intestine alkaline phosphatase (CIAP), suggesting that the up-shifted band in the gel indeed resulted from phosphorylation (**Figure 1B**). Additionally, we found unexpectedly that FtsH levels were decreased in phosphatase-treated samples as compared to untreated samples. Since the levels of the non-phosphorylated form of FtsH were not significantly altered after phosphatase treatment, the decrease in FtsH total content seemed to reflect degradation of dephosphorylated-FtsH.

Phosphorylation of FtsH Under Various Light Conditions and in the Kinase Mutants

Since FtsH is involved in the PSII repair resulting from light-dependent photo-damage (Lindahl et al., 2000; Bailey et al., 2002; Sakamoto et al., 2002; Sakamoto et al., 2003; Kato et al., 2009), we assessed whether the phosphorylated state of FtsH was affected by light conditions. Thylakoid proteins obtained from 4-week-old seedlings preincubated in the dark overnight and exposed to low- (5 μmol photons m^{-2} s^{-1}), growth- (100 μmol photons m^{-2} s^{-1}), or high-light (800 μmol photons m^{-2} s^{-1}) for 2 h were subjected to Phos-tag SDS-PAGE and immunoblotting analysis. The results demonstrated that the phosphorylation level of PSII core protein CP43 increased in a light-dependent manner (**Figure 2**). On the other hand, Lhcb1 had few detectable phosphorylations in the dark incubation; the phosphorylation form increased upon low-light illumination, whereas diminished in the high-light irradiation. These results were consistent with those obtained in the previous studies (Rintamäki et al., 1997; Vener et al., 1998; Tikkanen et al., 2006). However, no obvious change in the phosphorylation state of FtsH proteins could be detected (**Figure 2**), suggesting that phosphorylation of FtsH is independent of the light-dependent regulation of photosynthesis-related proteins.

To clarify the relationship between the phosphorylation state of FtsH and light-dependent kinase activities in thylakoid membranes, we further evaluated the effect of two major thylakoid kinases, STN7 and STN8, on FtsH phosphorylation. STN7 is a thylakoid-associated kinase responsible for LHCII phosphorylation, which is required for state transition (Bellafiore et al., 2005; Bonardi et al., 2005). On the other hand, the phosphorylation of PSII core proteins is mainly regulated by STN8 kinase, but some degree of PSII core proteins phosphorylation is observed in the *stn8* knockout mutant due to an overlap in substrate specificity of STN7 and STN8 (Bonardi et al., 2005; Vainonen et al., 2005). In 4-week-old seedlings exposed to growth light (100 μmol photons m^{-2} s^{-1}), the major phosphorylation band of Lhcb1 in *stn7*-mutant thylakoids was drastically decreased below the detection level (**Figure 3**), while minor phosphorylation band of Lhcb1 in a lower position was not affected in *stn7* mutant. A previous study reported that there is STN7 independent phosphorylation of a serine residue in Lhcb1; the serine residue corresponds to Ser-48 in Lhcb1.1 protein (Ingelsson and Vener, 2012). It seems that Phos-tag SDS-PAGE allows for detection of serine phosphorylation in Lhcb1. On the other hand, the phosphorylation level of FtsH proteins was comparable with that detected in control samples. Additionally, the band intensity of phosphorylated FtsH proteins obtained from *stn8*-mutant seedlings showed no difference compared with that of control seedlings under growth-light condition (100 μmol photons m^{-2} s^{-1}). Phosphorylation of the PSII core protein D1 was still observed in this experimental condition, suggesting that the aforementioned phenomenon of overlapping activity of these two major thylakoid kinases effectively operated under this light intensity. However, under high-light condition (800 μmol photons m^{-2} s^{-1}), the phosphorylation level of D1

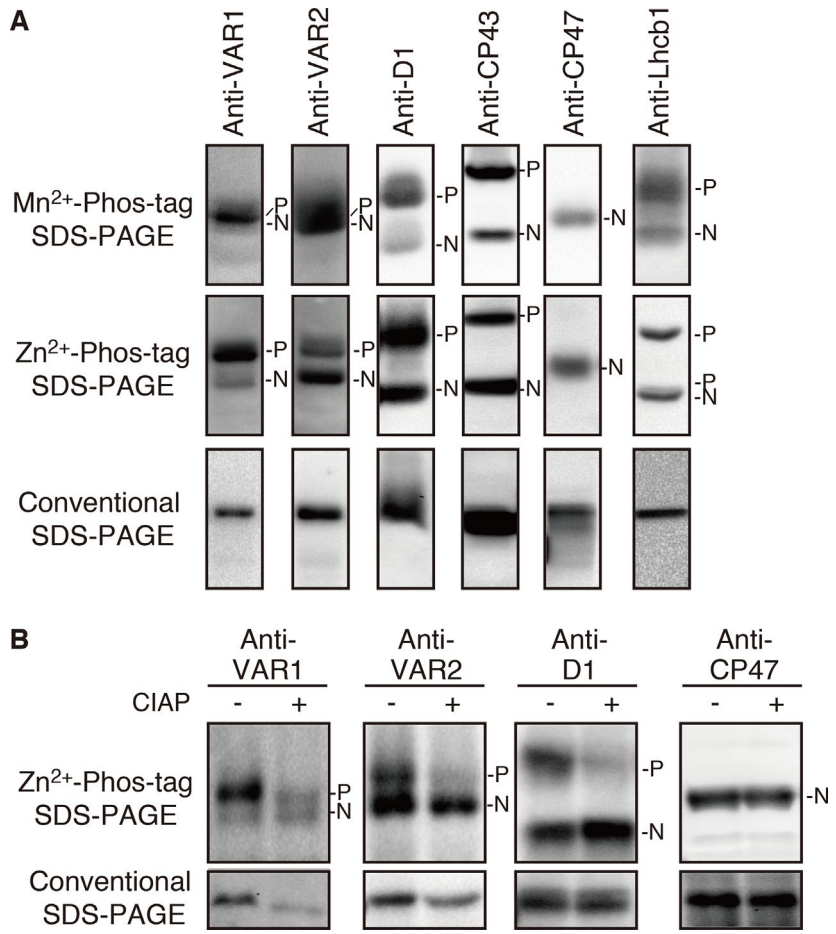

FIGURE 1 | Mobility shift detection of phosphorylated and non-phosphorylated thylakoid proteins. **(A)** Thylakoid membrane proteins were isolated from 4-week-old seedlings and subjected to Mn^{2+}–Phos-tag, Zn^{2+}–Phos-tag, and conventional (Phos-tag-free) SDS–PAGE analyses. Immunoblot analyses were performed using anti-VAR1, anti-VAR2, anti-D1, anti-CP43, anti-CP47, and anti-Lhcb1 antibodies. **(B)** Purified thylakoid membranes were incubated with or without calf intestinal alkaline phosphatase (CIAP) and then subjected to Zn^{2+}–Phos-tag SDS–PAGE and conventional SDS–PAGE analyses. Immunoblot analyses were performed using anti-VAR1, anti-VAR2, anti-D1, and anti-CP47 antibodies. The phosphorylated form (P) and non-phosphorylated form (N) are indicated. Proteins were loaded equally based on total chlorophyll content. The band density was measured with the ImageJ and showed in **Supplemental Figure S1**.

proteins in the *stn8*-mutant was remarkably reduced (**Figure 3**), indicating that the phosphorylation of photosynthetic proteins was predominantly mediated by STN8 kinase in this irradiance situation. Nevertheless, the phosphorylation state of FtsH in *stn8*-mutant thylakoids showed no difference compared with that in control samples. These results suggested that STN8 is not involved in phosphorylation of FtsH.

Phosphorylation State and FtsH Oligomerization

Unlike bacterial FtsH megacomplexes, the FtsH hexamer complex in *Arabidopsis* chloroplasts was considered to be unstable, giving rise to smaller oligomers detected in a native PAGE (Li et al., 2017; Kato et al., 2018). To investigate the relation, if any, between phosphorylation and the oligomerization of FtsH, thylakoid membrane preparations solubilized in 1% n-dodecyl-β-D-maltoside were subjected to two-dimensional (2D) gel electrophoresis. Protein complexes were separated by clear-native (CN) PAGE in the first dimension and further separated by Zn^{2+}-Phos-tag SDS-PAGE or conventional SDS-PAGE in the second dimension. The migration of FtsH proteins was resolved by immunoblotting using anti-VAR2 (for Type B) and anti-VAR1 (for Type A) antibodies. Conventional 2D-CN-SDS-PAGE showed that FtsH proteins migrated broadly from the higher molecular weight position, that was around PSII dimer, approximately 650 kDa, to the lower molecular weight size in a range of less than 140 kDa, estimated by the size of LHCII trimer complex (**Figures 4A**, **B**). Since the predicted molecular mass of FtsH monomer is about 70 kDa, the immunoblot signal at the smallest molecular size and that around LHCII trimer seemed to be the monomer and the dimer of FtsH, respectively. On the other hand, the phosphorylation pattern obtained after 2D electrophoresis using Phos-tag showed a noticeable change, particularly in the ratio of non-phosphorylated forms to phosphorylated forms

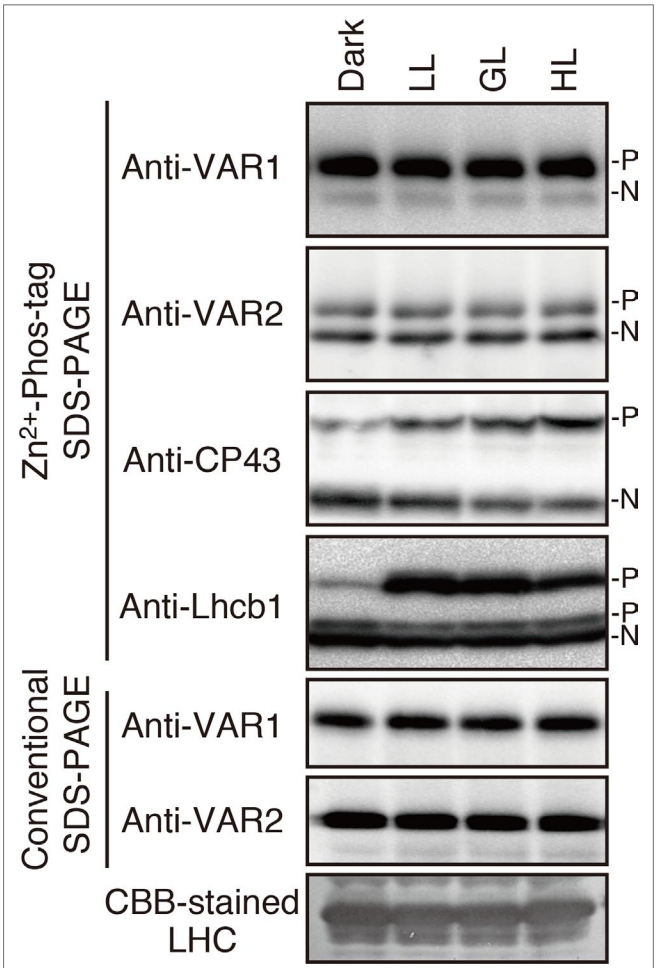

FIGURE 2 | Phosphorylation of thylakoid proteins under various light conditions. Thylakoid membrane proteins were isolated from dark-adapted seedlings or seedlings exposed for 2 h to low (5 μmol photons m^{-2} s^{-1}) (LL), growth (100 μmol photons m^{-2} s^{-1}) (GL), or high (800 μmol photons m^{-2} s^{-1}) (HL) light. Proteins were separated by Zn^{2+}–Phos-tag SDS-PAGE and immunoblotted with anti-VAR1, anti-VAR2, anti-CP43, and anti-Lhcb1 antibodies. Conventional (Phos-tag-free) SDS–PAGE analysis was also carried out. The phosphorylated form (P) and non-phosphorylated form (N) are indicated. Proteins were loaded equally based on total chlorophyll content. (A Coomassie Brilliant Blue-stained gel of the same samples is shown at the bottom; LHC: light harvest complex). The band density was measured with the ImageJ and showed in **Supplemental Figure S2**.

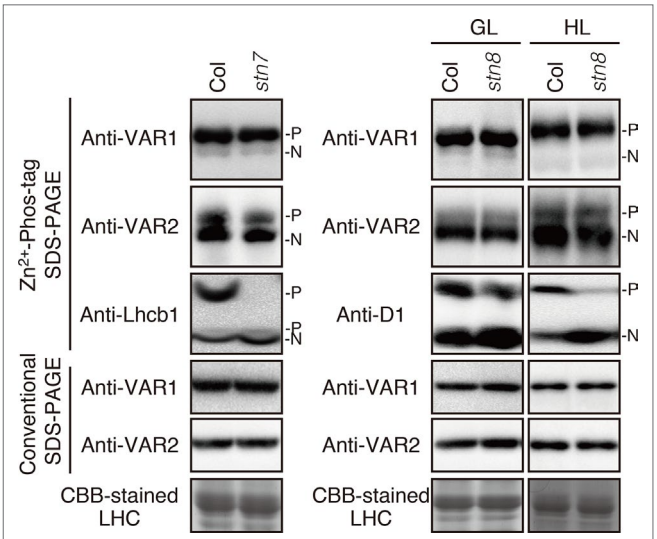

FIGURE 3 | Phosphorylation of FtsH proteins in the kinase mutants. Thylakoid proteins were isolated from 4-week-old seedlings of wild-type (Col) and mutants lacking either STN7 (*stn7*) or STN8 (*stn8*). For additional analysis of protein phosphorylation in the *stn8* mutant, seedlings were exposed for 2 h to high-light (800 μmol photons m^{-2} s^{-1}). The proteins were separated by Zn^{2+}–Phos-tag SDS-PAGE and immunoblotted with anti-VAR1, anti-VAR2, anti-Lhcb1, and anti-D1 antibodies. Proteins were loaded equally based on total chlorophyll content. The phosphorylated form (P) and non-phosphorylated form (N) are indicated. The band density was measured with the ImageJ and showed in **Supplemental Figure S3**.

in the Type B FtsH oligomers (**Figure 4A**). The immunoblot bands in the 2D CN PAGE showed that the phosphorylated form of FtsH migrated broadly, whereas high accumulation of the non-phosphorylated form of Type B FtsH was observed in the higher molecular weight and monomer positions. In addition, a portion of FtsH in the position corresponding to the dimeric and monomeric forms showed further retarded migration. Distribution of Type A FtsH assessed by anti-VAR1 antibodies showed the similar pattern to that of Type B FtsH, indicating that various oligomeric forms are detected in out 2D gel system (**Figure 4B**). In contrast to Type B, however, the non-phosphorylated forms strongly accumulated in the hexameric and monomeric regions were not noticeably observed. We reasoned that Type A FtsHs are extensively phosphorylated (**Figures 1** and **3**) and are not detectable in our gel system.

Amino Acid Substitution of Potential Phosphorylated Residues in FtsH2

In the database of *Arabidopsis* large-scale phosphoproteomic studies (PhosPhAt 4.0) (Heazlewood et al., 2008; Durek et al., 2010), four Ser or Thr residues at position Ser-212, Thr-337, Ser-380, and Ser-393 were reported to be phosphorylated in the FtsH2 mature protein (**Table 1**). Amino acid alignment is shown in **Supplementary Figure S4**. To evaluate whether these potential phosphorylated residues in FtsH2 influence FtsH function, we performed site-directed mutagenesis to create an amino acid substitution. As shown in **Figure 5A**, we made *FtsH2* constructs (driven by CaMV *35S* promoter) in which the sequences corresponding to each Ser or Thr residue were replaced with Ala, and the mutanted FtsHs. The resulting constructs were introduced into a FtsH2-knockout mutant *var2-1*. Transgenic lines were designated as *var2* (S212A), *var2* (T337A), *var2* (S380A), and *var2* (S393A), respectively. Our previous work indicated that overexpression of FtsH2 restores leaf variegation successfully and accumulates FtsH levels comparable to the wild type (Zhang et al., 2010), suggesting post-translational control of FtsH heterocompex accumulation. As shown in **Figure 6A**, 4-week-old plants indicated that three of these transgenic

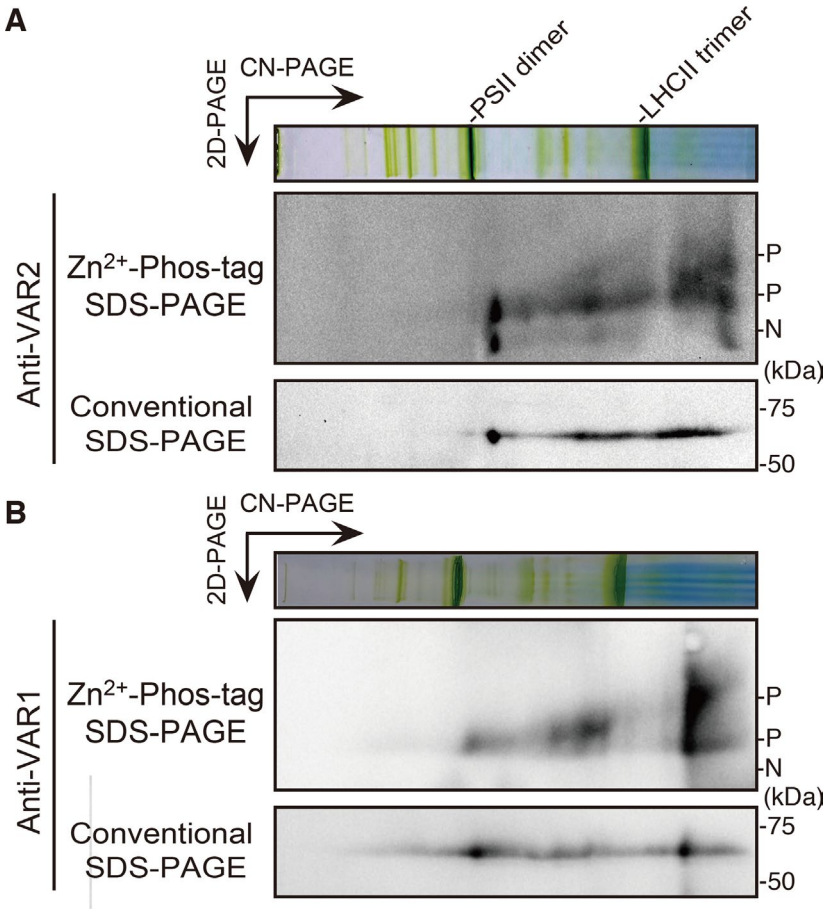

FIGURE 4 | FtsH phosphorylation in different oligomeric complexes. Thylakoid membrane proteins were isolated from 4-week-old seedlings and solubilized with 1% n-dodecyl ß-D-maltoside. Solubilized protein complexes were subjected to clear-native (CN) PAGE at the first dimension. The gel lane was then subjected to Zn^{2+}–Phos-tag and conventional SDS–PAGE analyses at the second dimension. Immunoblot analyses were performed using anti-VAR2 **(A)** and anti-VAR1 **(B)** antibodies. PSII dimer and LHCII trimer protein complexes positions are indicated at the CN-PAGE. The phosphorylated form (P) and non-phosphorylated form (N) are indicated. Representative results from three biological replicates (anti-VAR2) and two biological replicates (anti-VAR1) are shown.

lines, *var2* (T337A), *var2* (S380A), and *var2* (S393S), rescued leaf variegated phenotype in *var2-1*, demonstrating that the corresponding amino-acid substitutions are tolerated to restore the defective activity of FtsH. However, we found that leaf variegation persisted in *var2* (S212A), suggesting that Ser-212 is important to maintain its activity (**Figure 6A**).

To examine if mutated FtsH2 proteins accumulated in the transgenic lines, thylakoid membrane proteins from 4-week-old seedlings were subjected to immunoblot analysis (**Figure 6B**). FtsHs accumulated to a similar extent in control, *var2* (T337A), *var2* (S380A), and *var2* (S393A) lines. By contrast, accumulation of FtsH in *var2* (S212A) was reduced considerably, whose levels appeared to be comparable to those in the original *var2* mutant. Since anti-VAR2 antibodies recognize type B FtsH, the remaining bands in *var2* samples were assumed to correspond to another type B protein, FtsH8. Therefore, it is likely that the lack of recovery from variegation in *var2* (S212A) was due to the impaired accumulation of FtsH2 in this line. On the other hand, Phos-tag SDS-PAGE demonstrated phosphorylation of FtsH in the three transgenic lines, *var2* (T337A), *var2* (S380A), and *var2* (S393S); their phosphorylation levels were comparable to that of control. To further evaluate whether these amino-acid substitutions affected FtsH activity in the thylakoid membrane, high-light sensitivity of PSII activity was measured using chlorophyll fluorescence analysis. As expected, an increased PSII photosensitivity was observed in *var2* (S212A), similar to that of *var2* mutant (**Figure 6C**). The F_V/F_M values in *var2* (T337A), *var2* (S380A), and *var2* (S393S) lines slightly decreased with respect to that of the wild type during high-light irradiation, but these differences were not statistically significant. These results using transgenic plants were thus unable to confirm that phosphorylation of the predicted target residues plays a critical role in FtsH phosphorylation. Nevertheless, our data demonstrated that S212, localized at the stromal edge of transmembrane domain connecting the ATPase domain, is important for FtsH stability.

DISCUSSION

Protein phosphorylation of FtsH has been observed in large-scale comparative phosphoproteomics studies in *Arabidopsis* (**Table 1**).

TABLE 1 | Putative phosphorylation sites of thylakoid FtsH proteins in *Arabidopsis thaliana* and *Chlamydomonas reinhardtii*.

Gene	Protein	Peptide	No. pSTY	Putative phospho-site(s)	References
AT5G42270	AtFtsH5(VAR1)	SKFQEVPETGVTFGDVAGADQAK	1	S237, T245, T248	Reiland et al., 2009; Reiland et al., 2011
		SKSKFQEVPETGVTFGDVAGADQAK	1	S235, S237, T245, T248	
		QVTVDRPDVAGR	1	T416	Roitinger et al., 2015
AT1G50250	AtFtsH1	MASNSLLR	1	S5	Engelsberger and Schulze, 2012
		QVTVDRPDVAGR	1	T428	Roitinger et al., 2015
AT2G30950	AtFtsH2(VAR2)	AASSACLVGNGLSVNTTTKQR	3	S5, S14, T17	Mithoe et al., 2012
		QTSFSSVIR	1	S33	Roitinger et al., 2015
		SGGGMGGPGGPGNPLQFGQSK	1	S212	
		GTGIGGGNDER	1	T337	
		QRGTGIGGGNDER	1	T337	
		ADILDSALLRPGR	1	S380	
		QVSVDVPDVK	1	S393	
AT1G06430	AtFtsH8	SSGGMGGPGGPGFPLQIGQSKAK	1	S205	
		GTGIGGGNDER	1	T330	Roitinger et al., 2015
		QRGTGIGGGNDER	1	T330	
		ADILDSALLRPGR	1	S373	
		QVSVDVPDVK	1	S386	Roitinger et al., 2015; Bhaskara et al., 2017
		IVAGMEGTVMTDGK	1	T467	Bhaskara et al., 2017
Cre17.g720050	CrFtsH2	QVSVDLPDQK	1	S382	Wang et al., 2014
		GGAELVAAATRMEL	1	T685	
		KGGAELVAAATRMEL	1	T685	

In addition, previous studies reported the phosphorylation of FtsH in isolated chloroplasts of pea and *Arabidopsis* (Stael et al., 2012), and also in *Chlamydomonas* (Wang et al., 2014; Szyszka-Mroz et al., 2015). Although several reports suggested the potential phosphorylation of FtsH in thylakoid membranes, its regulatory role remains to be elucidated. Over the past decades, phosphorylation of thylakoid proteins has been characterized as one of the most important regulatory mechanisms of photosynthesis. However, characterization of phosphorylated proteins, focusing on the particular protein target in thylakoid membrane by using immunoblot analysis, appears to have several limitations; for example, conventional immunoblot approaches using anti-phosphothreonine antibodies exclusively detect major phosphorylated proteins such as PSII core proteins and LHCII, which hampers detection of minor phosphorylation. To overcome this drawback, we attempted to evaluate FtsH phosphorylation based on a Phos-tag approach. In PAGE gels containing Phos-tag molecules (Phos-tag SDS-PAGE), Phos-tag interferes with the migration of phosphorylated proteins, thereby exhibiting them as a retarded band, in addition to its non-phosphorylated forms. We found that the use of Zn^{2+} as divalent cation enabled us to identify the phosphorylated form of FtsH in thylakoid membranes successfully (**Figure 1**).

Since photodamage of D1 in the PSII complex increases with higher light intensity, we may predict the existence of light-induced regulation that governs the proteolytic machinery for an efficient quality control of PSII activity. One of the lumenal serine-type Deg proteases, Deg1, which facilitates the effective D1 degradation by FtsH in photoinhibitory conditions, has a regulation mechanism dependent on thylakoid lumen acidification (Kley et al., 2011). However, our characterization under various light conditions showed that the phosphorylation state of FtsH in the thylakoid membranes did not undergo light-dependent regulation (**Figure 2**), suggesting that phosphorylation of FtsH is not important to increase proteolysis under high-light intensity. This idea was further supported by the finding that FtsH phosphorylation was not directly regulated by two major thylakoid kinases (**Figure 3**). FtsH phosphorylation is likely mediated by other ill-defined protein kinases localized in chloroplasts. Of note is that in several experiments, bands corresponding to phosphorylated-FtsH proteins from thylakoids of *stn7*-mutant seedlings slightly decreased than those observed in control seedlings; nevertheless, the reproducibility of this result was limited. Given that the loss of STN7 kinase affects both short and long-term photosynthetic acclimation (Pesaresi et al., 2009), we cannot exclude the possibility that indirect effects caused by the loss of STN7 influenced the phosphorylation state of FtsH.

It is unclear as to how FtsH function is regulated by light in the chloroplasts of *Arabidopsis*, apart from the light-induced transcription of FtsH8, which is likely to compensate for the rapid FtsH degradation caused by high-light (Sinvany-Villalobo et al., 2004; Zaltsman et al., 2005a; Wang et al., 2017; Kato et al., 2018). Previous studies demonstrated that FtsH selectively degrades D1 even in dark condition (Lindahl et al., 2000; Krynická et al., 2015), suggesting that light is not always a decisive factor for FtsH protease activity per se; rather, accessibility to their substrates may be crucial for FtsH-mediated protein degradation (Krynická et al., 2015). Together with our results, these observations raise the possibility that the structural change around D1 in the damaged PSII complex is probably more important for the increased proteolysis expected under high-light intensity than light-dependent induction of protease activity in FtsH (Lindahl et al., 2000; Krynická et al., 2015). This possibility well fits with the observation that

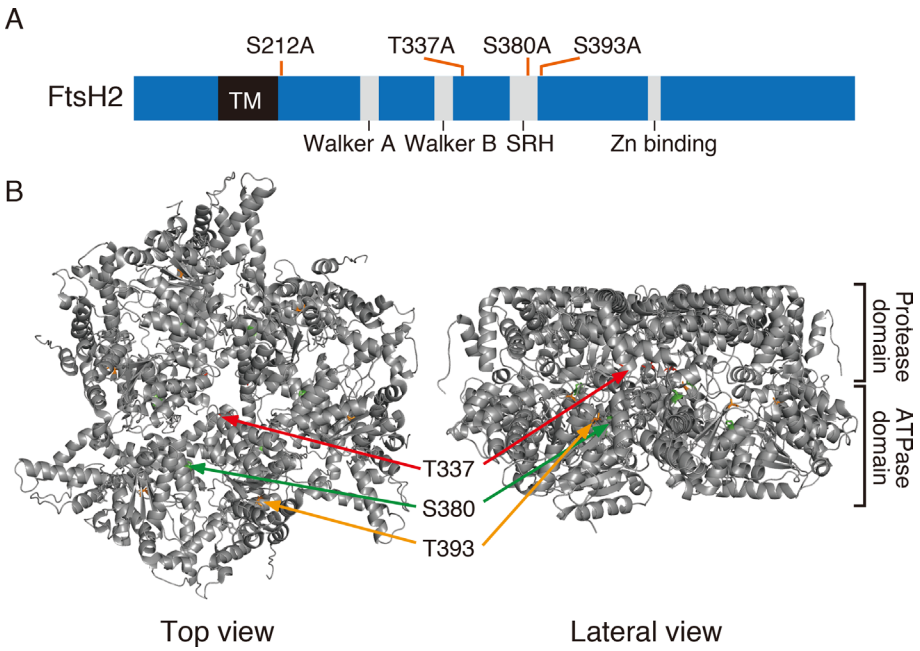

FIGURE 5 | FtsH2 protein and possible phosphorylation sites. **(A)** Schematic representation of *Arabidopsis* FtsH2 protein as a horizontal bar, with its transmembrane domain (TM), their conserved motifs in the ATPase domain (Walker A, Walker B, and SRH), and the catalytic domain of Zn metalloprotease (Zn-binding site). Putative phosphorylated amino acids previously reported for FtsH2 (PhosPhAt Database) and assessed in this study are indicated above the bar. **(B)** Structure of FtsH hexamer in *Thermus thermophilus*, lacking the transmembrane domain. The positions corresponding to amino acids Thr-337, Ser-380, and Ser-393 of *Arabidopsis* FtsH are indicated (Thr-337 in red, Ser-380 in green, and Ser-393 in orange).

light-induced unstacking of the grana expands the grana margin region in the thylakoid membrane; the expansion of grana margin seems to increase the accessibility of photodamaged D1 to FtsH (Puthiyaveetil et al., 2014b; Yoshioka-Nishimura et al., 2014). The alternative possibility may be the redox regulation of FtsH mediated by the formation of Cys disulfide bonding, as suggested in *Chlamydomonas* under high-light irradiation (Wang et al., 2017). Further investigation is necessary to study post-translational regulation of FtsH in *Arabidopsis* chloroplasts.

Amino acid substitutions carried out in FtsH2, based on information provided at the *Arabidopsis* Protein Phosphorylation Site Database (PhosPhAt 4.0), showed that Ser-212 is important for FtsH accumulation, whereas these residues did not critically affect the phosphorylation state of FtsH assessed by Phos-tag analysis (**Figure 6**). The N-terminal Ser-212 residue was found to be conserved between type A and type B subunits among photosynthetic organisms, whereas the Ser-380 in the second region of homology (SRH) motifs of ATPase domain is conserved between type A and type B subunits, but it is not found in FtsH proteins of other photosynthetic organisms (**Supplementary Figure S4**). Besides, Thr-337 and Ser-393 in the ATPase domain are conserved in the type B subunit of FtsH protein between *Arabidopsis* and *Chlamydomonas*, in contrast to type A subunit. The structural model of FtsH hexamer lacks the surrounding transmembrane domain including the position corresponding to Ser-212 (**Figure 5B**). Given the sequence homology among FtsH proteases, Ser-212 would locate between the transmembrane domain and the first alpha-helix in the ATPase domain. This connecting area would be sandwiched between thylakoid membranes and the stromal region of FtsH and seems to be important for substrate translocation and recognition. The phosphorylation of this region was also observed in FtsH5, although it remained unclear which amino acid residue was phosphorylated (**Table 1**). The finding of decreased accumulation of thylakoid FtsH after phosphatase treatment (**Figure 1B**) suggests the possible effect of phosphorylation on FtsH stability in the thylakoid membranes. However, the possibility that in the transgenic line *var2* (S212A), designed for Ser-212 amino acid substitution, this condition itself could have influenced the translation process or the stability of FtsH protein, cannot be ruled out.

In thylakoid membranes, the FtsH functional complex is likely a temporary complex formed when the proteolysis is executed in the grana margin region (Yoshioka et al., 2010; Kato et al., 2018). Thus, FtsH in thylakoid membranes probably does not form a megacomplex with other proteins but is mainly present as smaller complexes. This flexible oligomerization capability of FtsH in the chloroplasts might contribute to the turnover of FtsH itself to maintain its activity under high-light condition (Wang et al., 2017; Kato et al., 2018). Interestingly, our two-dimensional PAGE approach showed different phosphorylation states among FtsH oligomers (**Figure 4**): greater phosphorylation degree of FtsH seems to be found in smaller oligomers, suggesting that FtsH phosphorylation was somehow related to the stability of its monomeric and dimeric forms in the thylakoid membranes.

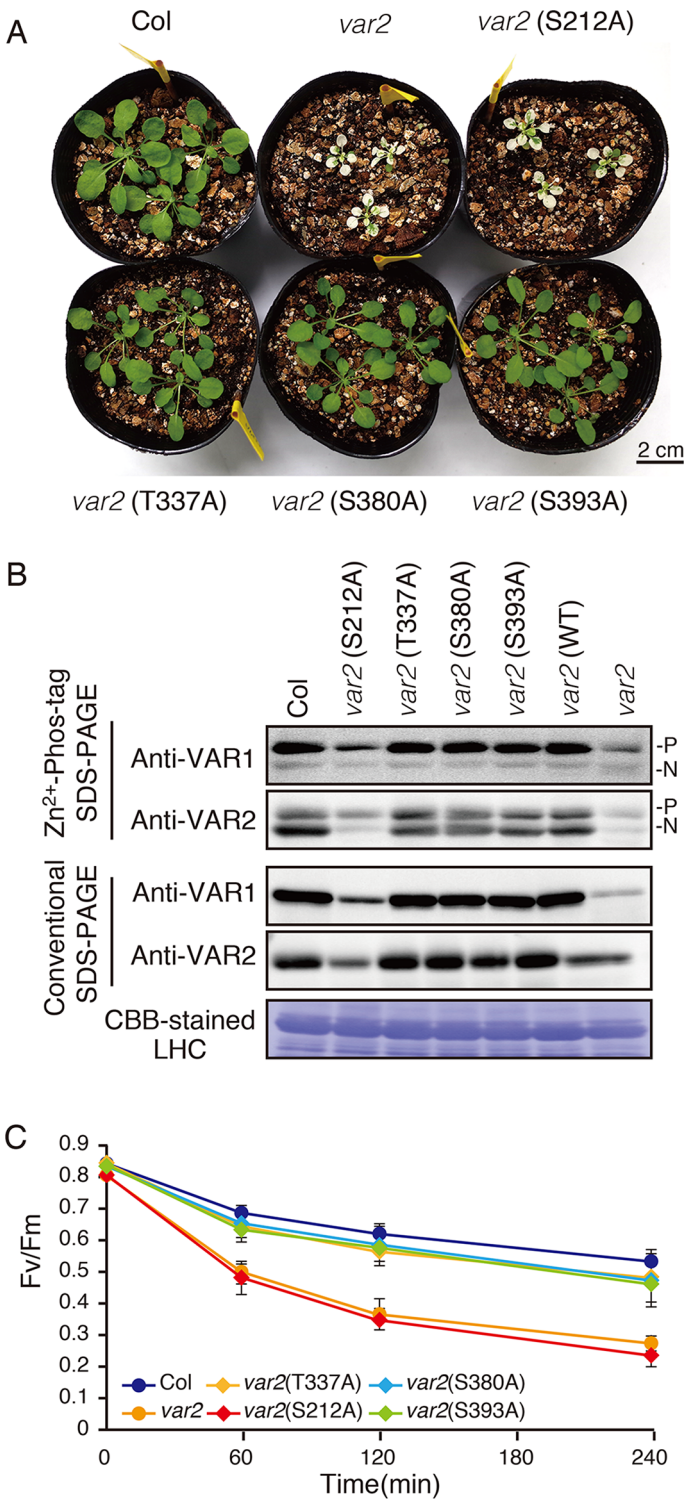

FIGURE 6 | Complementation analyses of *var2* with mutated FtsH2 plants. **(A)** Photographs of 4-week-old Col, *var2-1*, *var2* (S212A), *var2* (T337A), *var2* (S380A), and *var2* (S393A) seedlings. Bars = 2 cm. **(B)** Accumulation and phosphorylation state of FtsH proteins. Thylakoid membrane proteins were isolated from 4-week-old seedlings and subjected to Zn^{2+}–Phos-tag and conventional SDS–PAGE analyses. Immunoblot analyses were performed using anti-VAR1 and anti-VAR2 antibodies. Proteins were loaded equally based on total chlorophyll content. The phosphorylated form (P) and non-phosphorylated form (N) are indicated. A Coomassie Brilliant Blue-stained gel of the samples is shown at the bottom. **(C)** PSII photosensitivity during high light irradiation. Leaf discs obtained from mature leaves of Col, *var2-1*, *var2* (S212A), *var2* (T337A), *var2* (S380A), and *var2* (S393A) seedlings were exposed to high light (1,200 μmol photons m^{-2} s^{-1}) and maximal fluorescence yields of PSII (F_M) at 0, 60, 120, and 240 min after irradiation were determined. F_V/F_M values were calculated as indicated in *Materials and Methods* (Data were obtained from six replicates; means ± SD are shown).

However, the possibility that the phosphorylation state of FtsH affects the solubilization process of the FtsH complexes could not be excluded. On the other hand, it is still unclear how calcium-dependent phosphorylation of FtsH, reported in a previous study (Stael et al., 2012), influences FtsH complex formation and function.

DATA AVAILABILITY

All datasets generated for this study are included in the manuscript/ **Supplementary Files**.

AUTHOR CONTRIBUTIONS

YK and WS conceived the study and wrote the manuscript. YK performed the experiments. All authors reviewed the results and approved the final version of the manuscript.

FUNDING

This work was supported by KAKENHI grants from Japan Society for the Promotion of Science (16H06554 and 17H03699 to WS; 18K06290 to YK) and from the Oohara Foundation (to WS and YK).

ACKNOWLEDGMENTS

We would like to thank Rie Hijiya and Kenji Nishimura for technical assistance.

SUPPLEMENTARY MATERIAL

The Supplementary Material for this article can be found online at: https://www.frontiersin.org/articles/10.3389/fpls.2019.01080/full#supplementary-material

REFERENCES

Bailey, S., Thompson, E., Nixon, P. J., Horton, P., Mullineaux, C. W., Robinson, C., et al. (2002). A critical role for the Var2 FtsH homologue of *Arabidopsis thaliana* in the photosystem II repair cycle *in vivo*. *J. Biol. Chem.* 277, 2006–2011. doi: 10.1074/jbc.M105878200

Bellafiore, S., Barneche, F., Peltier, G., and Rochaix, J. D. (2005). State transitions and light adaptation require chloroplast thylakoid protein kinase STN7. *Nature* 433, 892–895. doi: 10.1038/nature03286

Bhaskara, G. B., Wen, T. N., Nguyen, T. T., and Verslues, P. E. (2017). Protein phosphatase 2Cs and microtubule-associated stress protein 1 control microtubule stability, plant growth, and drought response. *Plant Cell* 29, 169–191. doi: 10.1105/tpc.16.00847

Boehm, M., Yu, J., Krynicka, V., Barker, M., Tichy, M., Komenda, J., et al. (2012). Subunit organization of a *Synechocystis* hetero-oligomeric thylakoid FtsH complex involved in photosystem II repair. *Plant Cell* 24, 3669–3683. doi: 10.1105/tpc.112.100891

Bonardi, V., Pesaresi, P., Becker, T., Schleiff, E., Wagner, R., Pfannschmidt, T., et al. (2005). Photosystem II core phosphorylation and photosynthetic acclimation require two different protein kinases. *Nature* 437, 1179–1182. doi: 10.1038/nature04016

Chen, M., Choi, Y., Voytas, D. F., and Rodermel, S. (2000). Mutations in the *Arabidopsis VAR2* locus cause leaf variegation due to the loss of a chloroplast FtsH protease. *Plant J.* 22, 303–313. doi: 10.1046/j.1365-313x.2000.00738.x

Durek, P., Schmidt, R., Heazlewood, J. L., Jones, A., MacLean, D., Nagel, A., et al. (2010). PhosPhAt: the *Arabidopsis thaliana* phosphorylation site database. An update. *Nucleic Acids Res.* 38, D828–D834. doi: 10.1093/nar/gkp810

Engelsberger, W. R., and Schulze, W. X. (2012). Nitrate and ammonium lead to distinct global dynamic phosphorylation patterns when resupplied to nitrogen-starved *Arabidopsis* seedlings. *Plant J.* 69, 978–995. doi: 10.1111/j.1365-313X.2011.04848.x

Grieco, M., Jain, A., Ebersberger, I., and Teige, M. (2016). An evolutionary view on thylakoid protein phosphorylation uncovers novel phosphorylation hotspots with potential functional implications. *J. Exp. Bot.* 67, 3883–3896. doi: 10.1093/jxb/erw164

Heazlewood, J. L., Durek, P., Hummel, J., Selbig, J., Weckwerth, W., Walther, D., et al. (2008). *PhosPhAt*: a database of phosphorylation sites in *Arabidopsis thaliana* and a plant-specific phosphorylation site predictor. *Nucleic Acids Res.* 36, D1015–D1021. doi: 10.1093/nar/gkm812

Ingelsson, B., and Vener, A. V. (2012). Phosphoproteomics of *Arabidopsis* chloroplasts reveals involvement of the STN7 kinase in phosphorylation of nucleoid protein pTAC16. *FEBS Lett.* 586, 1265–1271. doi: 10.1016/j.febslet.2012.03.061

Ito, K., and Akiyama, Y. (2005). Cellular functions, mechanism of action, and regulation of FtsH protease. *Annu. Rev. Microbiol.* 59, 211–231. doi: 10.1146/annurev.micro.59.030804.121316

Janska, H., Kwasniak, M., and Szczepanowska, J. (2013). Protein quality control in organelles — AAA/FtsH story. *Biochim. Biophys. Acta - Mol. Cell Res.* 1833, 381–387. doi: 10.1016/j.bbamcr.2012.03.016

Järvi, S., Suorsa, M., and Aro, E. M. (2015). Photosystem II repair in plant chloroplasts—regulation, assisting proteins and shared components with photosystem II biogenesis. *Biochim. Biophys. Acta - Bioenergetics.* 1847, 900–909. doi: 10.1016/j.bbabio.2015.01.006

Kato, Y., and Sakamoto, W. (2014). Phosphorylation of photosystem II core proteins prevents undesirable cleavage of D1 and contributes to the fine-tuned repair of photosystem II. *Plant J.* 79, 312–321. doi: 10.1111/tpj.12562

Kato, Y., and Sakamoto, W. (2018). FtsH protease in the thylakoid membrane: physiological functions and the regulation of protease activity. *Front. Plant. Sci.* 9, 855. doi: 10.3389/fpls.2018.00855

Kato, Y., Hyodo, K., and Sakamoto, W. (2018). The photosystem II repair cycle requires FtsH turnover through the EngA GTPase. *Plant Physiol.* 178, 596–611. doi: 10.1104/pp.18.00652

Kato, Y., Kouso, T., and Sakamoto, W. (2012a). Variegated tobacco leaves generated by chloroplast FtsH suppression: implication of FtsH function in the maintenance of thylakoid membranes. *Plant Cell Physiol.* 53, 391–404. doi: 10.1093/pcp/pcr189

Kato, Y., Miura, E., Ido, K., Ifuku, K., and Sakamoto, W. (2009). The variegated mutants lacking chloroplastic FtsHs are defective in D1 degradation and accumulate reactive oxygen species. *Plant Physiol.* 151, 1790–1801. doi: 10.1104/pp.109.146589

Kato, Y., Sun, X., Zhang, L., and Sakamoto, W. (2012b). Cooperative D1 degradation in the photosystem II repair mediated by chloroplastic proteases in *Arabidopsis*. *Plant Physiol.* 159, 1428–1439. doi: 10.1104/pp.112.199042

Kihara, A., Akiyama, Y., and Ito, K. (1996). A protease complex in the *Escherichia coli* plasma membrane: HflKC (HflA) forms a complex with FtsH (HflB), regulating its proteolytic activity against SecY. *EMBO J.* 15, 6122–6131. doi: 10.1002/j.1460-2075.1996.tb01000.x

Kikuchi, S., Asakura, Y., Imai, M., Nakahira, Y., Kotani, Y., Hashiguchi, Y., et al. (2018). A Ycf2-FtsHi heteromeric AAA-ATPase complex is required for chloroplast protein import. *Plant Cell* 30, 2677–2703. doi: 10.1105/tpc.18.00357

Kinoshita, E., and Kinoshita-Kikuta, E. (2011). Improved Phos-tag SDS-PAGE under neutral pH conditions for advanced protein phosphorylation profiling. *Proteomics* 11, 319–323. doi: 10.1002/pmic.201000472

Kley, J., Schmidt, B., Boyanov, B., Stolt-Bergner, P. C., Kirk, R., Ehrmann, M., et al. (2011). Structural adaptation of the plant protease Deg1 to repair photosystem II during light exposure. *Nat. Struct. Mol. Biol.* 18, 728–731. doi: 10.1038/nsmb.2055

Krynická, V., Shao, S., Nixon, P. J., and Komenda, J. (2015). Accessibility controls selective degradation of photosystem II subunits by FtsH protease. *Nat. Plants* 1, 15168. doi: 10.1038/nplants.2015.168

Li, L., Nelson, C. J., Trösch, J., Castleden, I., Huang, S., and Millar, A. H. (2017). Protein degradation rate in *Arabidopsis thaliana* leaf growth and development. *Plant Cell* 29, 207–228. doi: 10.1105/tpc.16.00768

Lindahl, M., Spetea, C., Hundal, T., Oppenheim, A. B., Adam, Z., and Andersson, B. (2000). The thylakoid FtsH protease plays a role in the light-induced turnover of the photosystem II D1 protein. *Plant Cell* 12, 419–432. doi: 10.1105/tpc.12.3.419

Mithoe, S. C., Boersema, P. J., Berke, L., Snel, B., Heck, A. J., and Menke, F. L. (2012). Targeted quantitative phosphoproteomics approach for the detection of phosphotyrosine signaling in plants. *J. Proteome Res.* 11, 438–448. doi: 10.1021/pr200893k

Miura, E., Kato, Y., Matsushima, R., Albrecht, V., Laalami, S., and Sakamoto, W. (2007). The balance between protein synthesis and degradation in chloroplasts determines leaf variegation in *Arabidopsis yellow variegated* mutants. *Plant Cell* 19, 1313–1328. doi: 10.1105/tpc.106.049270

Moldavski, O., Levin-Kravets, O., Ziv, T., Adam, Z., and Prag, G. (2012). The hetero-hexameric nature of a chloroplast AAA+ FtsH protease contributes to its thermodynamic stability. *PLoS One* 7, e36008. doi: 10.1371/journal.pone.0036008

Nakai, M. (2018). New perspectives on chloroplast protein import. *Plant Cell Physiol.* 59, 1111–1119. doi: 10.1093/pcp/pcy083

Nishimura, K., Kato, Y., and Sakamoto, W. (2016). Chloroplast proteases: updates on proteolysis within and across suborganellar compartments. *Plant Physiol.* 171, 2280–2293. doi: 10.1104/pp.16.00330

Nixon, P. J., Michoux, F., Yu, J., Boehm, M., and Komenda, J. (2010). Recent advances in understanding the assembly and repair of photosystem II. *Ann. Bot.* 106, 1–16. doi: 10.1093/aob/mcq059

Pesaresi, P., Hertle, A., Pribil, M., Kleine, T., Wagner, R., Strissel, H., et al. (2009). *Arabidopsis* STN7 kinase provides a link between short- and long-term photosynthetic acclimation. *Plant Cell* 21, 2402–2423. doi: 10.1105/tpc.108.064964

Pribil, M., Pesaresi, P., Hertle, A., Barbato, R., and Leister, D. (2010). Role of plastid protein phosphatase TAP38 in LHCII dephosphorylation and thylakoid electron flow. *PLoS Biol.* 26, e1000288. doi: 10.1371/journal.pbio.1000288

Puthiyaveetil, S., Tsabari, O., Lowry, T., Lenhert, S., Lewis, R. R., Reich, Z., et al. (2014a). Compartmentalization of the protein repair machinery in photosynthetic membranes. *Proc. Natl. Acad. Sci. U.S.A.* 111, 15839–15844. doi: 10.1073/pnas.1413739111

Puthiyaveetil, S., Woodiwiss, T., Knoerdel, R., Zia, A., Wood, M., Hoehner, R., et al. (2014b). Significance of the photosystem II core phosphatase PBCP for plant viability and protein repair in thylakoid membranes. *Plant Cell Physiol.* 55, 1245–1254. doi: 10.1093/pcp/pcu062

Reiland, S., Finazzi, G., Endler, A., Willig, A., Baerenfaller, K., Grossmann, J., et al. (2011). Comparative phosphoproteome profiling reveals a function of the STN8 kinase in fine-tuning of cyclic electron flow (CEF). *Proc. Natl. Acad. Sci. U. S. A.* 108, 12955–12960. doi: 10.1073/pnas.1104734108

Reiland, S., Messerli, G., Baerenfaller, K., Gerrits, B., Endler, A., Grossmann, J., et al. (2009). Large-scale *Arabidopsis* phosphoproteome profiling reveals novel chloroplast kinase substrates and phosphorylation networks. *Plant Physiol.* 150, 889–903. doi: 10.1104/pp.109.138677

Rintamäki, E., Salonen, M., Suoranta, U. M., Carlberg, I., Andersson, B., and Ar, E. M. (1997). Phosphorylation of light-harvesting complex II and photosystem II core proteins shows different irradiance-dependent regulation *in vivo.* Application of phosphothreonine antibodies to analysis of thylakoid phosphoproteins. *J. Biol. Chem.* 272, 30476–30482. doi: 10.1074/jbc.272.48.30476

Roitinger, E., Hofer, M., Köcher, T., Pichler, P., Novatchkova, M., Yang, J., et al. (2015). Quantitative phosphoproteomics of the ataxia telangiectasia-mutated (ATM) and ataxia telangiectasia-mutated and rad3-related (ATR) dependent DNA damage response in *Arabidopsis thaliana. Mol. Cell Proteomics* 14, 556–571. doi: 10.1074/mcp.M114.040352

Saikawa, N., Akiyama, Y., and Ito, K. (2004). FtsH exists as an exceptionally large complex containing HflKC in the plasma membrane of *Escherichia coli. J. Struct. Biol.* 146, 123–129. doi: 10.1016/j.jsb.2003.09.020

Sakamoto, W., Tamura, T., Hanba-Tomita, Y., Sodmergen, and Murata, M. (2002). The *VAR1* locus of *Arabidopis* encodes a choloroplastic FtsH and is responsible for leaf variegation in the mutant alleles. *Genes Cells* 7, 769–780. doi: 10.1046/j.1365-2443.2002.00558.x

Sakamoto, W., Zaltsman, A., Adam, Z., and Takahashi, Y. (2003). Coordinated regulation and complex formation of YELLOW VARIEGATED1 and YELLOW VARIEGATED2, chloroplastic FtsH metalloproteases involved in the repair cycle of photosystem II in *Arabidopsis* thylakoid membranes. *Plant Cell* 15, 2843–2855. doi: 10.1105/tpc.017319

Samol, I., Shapiguzov, A., Ingelsson, B., Fucile, G., Crèvecoeur, M., Vener, A. V., et al. (2012). Identification of a photosystem II phosphatase involved in light acclimation in *Arabidopsis. Plant Cell* 24, 2596–2609. doi: 10.1105/tpc.112.095703

Schreier, T. B., Cléry, A., Schläfli, M., Galbier, F., Stadler, M., Demarsy, E., et al. (2018). Plastidial NAD-dependent malate dehydrogenase: a moonlighting protein involved in early chloroplast development through its interaction with an FtsH12-FtsHi protease complex. *Plant Cell* 30, 1745–1769. doi: 10.1105/tpc.18.00121

Shapiguzov, A., Ingelsson, B., Samol, I., Andres, C., Kessler, F., Rochaix, J. D., et al. (2010). The PPH1 phosphatase is specifically involved in LHCII dephosphorylation and state transitions in *Arabidopsis. Proc. Natl. Acad. Sci. U. S. A.* 107, 4782–4787. doi: 10.1073/pnas.0913810107

Sinvany-Villalobo, G., Davydov, O., Ben-Ari, G., Zaltsman, A., Raskind, A., and Adam, Z. (2004). Expression in multigene families. Analysis of chloroplast and mitochondrial proteases. *Plant Physiol.* 135, 1336–1345. doi: 10.1104/pp.104.043299

Stael, S., Rocha, A. G., Wimberger, T., Anrather, D., Vothknecht, U. C., and Teige, M. (2012). Cross-talk between calcium signalling and protein phosphorylation at the thylakoid. *J. Exp. Bot.* 63, 1725–1733. doi: 10.1093/jxb/err403

Szyszka-Mroz, B., Pittock, P., Ivanov, A. G., Lajoie, G., and Huner, N. P. (2015). The Antarctic psychrophile, *Chlamydomonas* sp. UWO 241, preferentially phosphorylates a PSI-cytochrome *b6/f* supercomplex. *Plant Physiol.* 169, 717–736. doi: 10.1104/pp.15.00625

Takechi, K., Sodmergen, Murata, M., Motoyoshi, F., and Sakamoto, W. (2000). The *YELLOW VARIEGATED* (*VAR2*) locus encodes a homologue of FtsH, an ATP-dependent protease in *Arabidopsis. Plant Cell Physiol.* 41, 1334–1346. doi: 10.1093/pcp/pcd067

Tikkanen, M., Nurmi, M., Kangasjärvi, S., and Aro, E. M. (2008). Core protein phosphorylation facilitates the repair of photodamaged photosystem II at high light. *Biochim. Biophys. Acta - Bioenergetics* 1777, 1432–1437. doi: 10.1016/j. bbabio.2008.08.004

Tikkanen, M., Piippo, M., Suorsa, M., Sirpiö, S., Mulo, P., Vainonen, J., et al. (2006). State transitions revisited—a buffering system for dynamic low light acclimation of *Arabidopsis. Plant Mol. Biol.* 62, 779–793. doi: 10.1007/s11103-006-9044-8

Vainonen, J. P., Hansson, M., and Vener, A. V. (2005). STN8 protein kinase in *Arabidopsis thaliana is* specific in phosphorylation of photosystem II core proteins. *J. Biol. Chem.* 280, 33679–33686. doi: 10.1074/jbc.M505729200

van Wijk, K. J. (2015). Protein maturation and proteolysis in plant plastids, mitochondria, and peroxisomes. *Annu. Rev. Plant. Biol.* 66, 75–111. doi: 10.1146/annurev-arplant-043014-115547

Vener, A. V., Ohad, I., and Andersson, B. (1998). Protein phosphorylation and redox sensing in chloroplast thylakoids. *Curr. Opin. Plant Biol.* 1, 217–223.

Wagner, R., Aigner, H., and Fun, C. (2012). FtsH proteases located in the plant chloroplast. *Physiol. Plant.* 145, 203–214. doi: 10.1111/j.1399-3054.2011.01548.x

Wagner, R., Aigner, H., Pružinská, A., Jänkänpää, H. J., Jansson, S., and Funk, C. (2011). Fitness analyses of *Arabidopsis thaliana* mutants depleted of FtsH metalloproteases and characterization of three FtsH6 deletion mutants exposed to high light stress, senescence and chilling. *New Phytol.* 191, 449–458. doi: 10.1111/j.1469-8137.2011.03684.x

Wang, F., Qi, Y., Malnoë, A., Choquet, Y., Wollman, F. A., and de Vitry, C. (2017). The high light response and redox control of thylakoid FtsH protease in *Chlamydomonas reinhardtii. Mol. Plant* 10, 99–114. doi: 10.1016/j.molp.2016.09.012

Wang, H., Gau, B., Slade, W. O., Juergens, M., Li, P., and Hicks, L. M. (2014). The global phosphoproteome of *Chlamydomonas reinhardtii* reveals complex organellar phosphorylation in the flagella and thylakoid membrane. *Mol. Cell. Proteomics* 13, 2337–2353. doi: 10.1074/mcp.M114.038281

Yoshioka-Nishimura, M., Nanba, D., Takaki, T., Ohba, C., Tsumura, N., Morita, N., et al. (2014). Quality control of photosystem II: direct imaging of the changes in the thylakoid structure and distribution of FtsH proteases in spinach chloroplasts under light stress. *Plant Cell Physiol.* 55, 1255–1265. doi: 10.1093/pcp/pcu079

Yoshioka, M., Nakayama, Y., Yoshida, M., Ohashi, K., Morita, N., Kobayashi, H., et al. (2010). Quality control of photosystem II: FtsH hexamers are localized

near photosystem II at grana for the swift repair of damage. *J. Biol. Chem.* 285, 41972–41981. doi: 10.1074/jbc.M110.117432

Yu, F., Park, S., and Rodermel, S. R. (2004). The *Arabidopsis* FtsH metalloprotease gene family: interchangeability of subunits in chloroplast oligomeric complexes. *Plant J.* 37, 864–876. doi: 10.1111/j.1365-313X.2003.02014.x

Yu, F., Park, S., and Rodermel, S. R. (2005). Functional redundancy of AtFtsH metalloproteases in thylakoid membrane complexes. *Plant Physiol.* 138, 1957–1966. doi: 10.1104/pp.105.061234

Zaltsman, A., Feder, A., and Adam, Z. (2005a). Developmental and light effects on the accumulation of FtsH protease in *Arabidopsis* chloroplasts—implications for thylakoid formation and photosystem II maintenance. *Plant J.* 42, 609–617. doi: 10.1111/j.1365-313X.2005.02401.x

Zaltsman, A., Ori, N., and Adam, Z. (2005b). Two types of FtsH protease subunits are required for chloroplast biogenesis and photosystem II repair in *Arabidopsis*. *Plant Cell* 17, 2782–2790. doi: 10.1105/tpc.105.035071

Zhang, D., Kato, Y., Zhang, L., Fujimoto, M., Tsutsumi, N., Sodmergen, et al. (2010). The FtsH protease heterocomplex in *Arabidopsis*: dispensability of type-B protease activity for proper chloroplast development. *Plant Cell* 22, 3710–3725. doi: 10.1105/tpc.110.079202

Conflict of Interest Statement: The authors declare that the research was conducted in the absence of any commercial or financial relationships that could be construed as a potential conflict of interest.

frontiers in Plant Science

REVIEW
published: 18 September 2019
doi: 10.3389/fpls.2019.01122

Dealing With Stress: A Review of Plant SUMO Proteases

*Rebecca Morrell and Ari Sadanandom**

Department of Biosciences, Durham University, Durham, United Kingdom

The SUMO system is a rapid dynamic post-translational mechanism employed by eukaryotic cells to respond to stress. Plant cells experience hyperSUMOylation of substrates in response to stresses such as heat, ethanol, and drought. Many SUMOylated proteins are located in the nucleus, SUMOylation altering many nuclear processes. The SUMO proteases play two key functions in the SUMO cycle by generating free SUMO; they have an important role in regulating the SUMO cycle, and by cleaving SUMO off SUMOylated proteins, they provide specificity to which proteins become SUMOylated. This review summarizes the broad literature of plant SUMO proteases describing their catalytic activity, domains and structure, evolution, localization, and response to stress and highlighting potential new areas of research in the future.

Keywords: SUMO protease, SUMO cycle, Ubiquitin-like, Cysteine protease, Post-translational modification, Stress

OPEN ACCESS

Edited by:
Mercedes Diaz-Mendoza, National Institute of Agricultural and Food Research and Technology, Spain

Reviewed by:
Andreas Bachmair, University of Vienna, Austria
Anna-Maria Botha-Oberholster, Stellenbosch University, South Africa

***Correspondence:**
Ari Sadanandom
ari.sadanandom@durham.ac.uk

Specialty section:
This article was submitted to Plant Physiology, a section of the journal Frontiers in Plant Science

Received: *03 June 2019*
Accepted: *14 August 2019*
Published: *18 September 2019*

Citation:
Morrell R and Sadanandom A (2019) Dealing With Stress: A Review of Plant SUMO Proteases. Front. Plant Sci. 10:1122. doi: 10.3389/fpls.2019.01122

INTRODUCTION

SUMO (small ubiquitin-like modifier) proteins are critical for the normal function of eukaryotic cells; the protein is found in all eukaryotes from single-celled yeast *Saccharomyces cerevisiae* to all mammals and plants species. Deleting the only SUMO isoform, SMT3, from a yeast cell, causes a loss of cell viability (Meluh and Koshland, 1995; Giaever et al., 2002) and deletion in *Arabidopsis thaliana* of *sumo1sumo2-1* is embryonic lethal (Saracco et al., 2007; van den Burg et al., 2010), highlighting the critical role of SUMO in cell biology.

SUMO is an 11-kDa protein with one isoform in yeast and eight isoforms currently identified in *A. thaliana* through computational analysis (Novatchkova et al., 2004). In *Arabidopsis*, SUMO1, 2, 3, and 5 are expressed (Benlloch and Lois, 2018), but only SUMO1 and 2 are expressed at high levels (Castaño-Miquel et al., 2011). AtSUMO1 and 2 share 83% amino acid sequence identity and are orthologs of human SUMO2/3, based on sequence similarity. AtSUMO1/2 and human SUMO2/3 also have similar functions and are influenced by stress conditions. Conversely, AtSUMO3/5 are weakly expressed non-conserved isoforms. They are more distantly related to AtSUMO1/2 containing approximately 35% sequence similarity to AtSUMO1/2 (Castaño-Miquel et al., 2011).

SUMOylation is induced by heat, ethanol, drought stress, and oxidative stress; this is conserved in many species from *Arabidopsis, Drosophila,* and *Caenorhabditis elegans* to humans (Saitoh and Hinchey, 2000; Kurepa et al., 2003; Augustine et al., 2016). Indeed, there are many evolutionarily conserved SUMO targets and processes that SUMO is involved in throughout different species. Global proteomic studies in *C. elegans* have identified over 800 SUMO targets; based on these targets, *Arabidopsis* is predicted to have 5660 SUMOylated proteins. The breadth of SUMOylation is on par with other major PTMs (post-translational modifications) like phosphorylation and ubiquitylation (Drabikowski et al., 2018; Millar et al., 2019).

In addition to responding to stress, SUMO is also implicated in many essential cellular processes (Hannoun et al., 2010). Drabikowski et al. (2018) undertook a comprehensive analysis

of all the proteins SUMOylated in *C. elegans*. They identified SUMOylated protein targets including proteins involved in genome stability, cell cycle progression, chromatin maintenance and modification, transcription, translation RNA splicing, and ribosome biogenesis. Many identified proteins were non-nuclear localizing in the mitochondria or extracellular matrix. Cytosolic proteins include proteasomal, ribosomal, metabolism, signaling, cell morphology, and motility (cytoskeleton, microtubules, intermediate filaments, and proteins connecting the cytoskeleton to the plasma membrane) proteins. In addition, transport and vesicular transport proteins were identified. The group predicted that at least 15–20% of the eukaryotic proteome can be SUMOylated and suggested that SUMO functions in three main areas: regulation of activity of individual proteins, biogenesis of macromolecular complexes, and SUMO-directed proteasomal degradation (Drabikowski et al., 2018).

A similar study was carried out by Rytz et al. (2018) looking into SUMOylated proteins in *Arabidopsis* found over 1000 SUMOylated targets; many of which were nuclear targeted. The proteins identified included major transcription factors, coactivators/repressors, and chromatin modifiers connected to abiotic and biotic stress defense (Rytz et al., 2018).

The SUMO cycle is likened to ubiquitin due to the similarities in the biochemical steps that catalyze SUMO conjugation and deconjugation of protein substrates (Kerscher et al., 2006). SUMO has a similar 3D structure to ubiquitin, adopting the signature β-grasp fold (characterized by β-sheet with five anti-parallel β-strands and a single helical element between strands β-4 and β-5) but only shares 20% sequence similarity with ubiquitin. SUMO is longer than ubiquitin and has a longer disordered C-terminal tail, which requires processing (Bayer et al., 1998). Like ubiquitin, SUMO can form polySUMO chains of multiple SUMO moieties attached to one lysine or a single-SUMO molecule can be attached to a single lysine residue.

Ubiquitin conjugation to substrate proteins targets them for degradation; conjugation of SUMO can aid the substrate protein for degradation through STUbLs (SUMO-targeted ubiquitin ligases). STUbLs are a novel class of ubiquitin E4 ligases that target proteins with polySUMO chains, ubiquitinating the proteins resulting in degradation. STUbLs have been identified in plants but await biochemical analyses (Elrouby et al., 2013). However, unlike ubiquitin, SUMOylation can have numerous other effects on target proteins, protecting a protein from degradation by protecting lysine residues prone to ubiquitylation, changing its localization, or altering the protein–protein interaction or protein–DNA interactions (Johnson, 2004); the effects of SUMOylation are summarized in **Figure 1**. The protein–protein interaction can occur *via* a non-covalent bond that forms with proteins harboring SIM sites (SUMO-interacting motifs). SIMs are characterized by hydrophobic residues flanked by acidic residues or residues that can be phosphorylated. Alternatively, SUMO can prevent interactions by masking partner-binding sites.

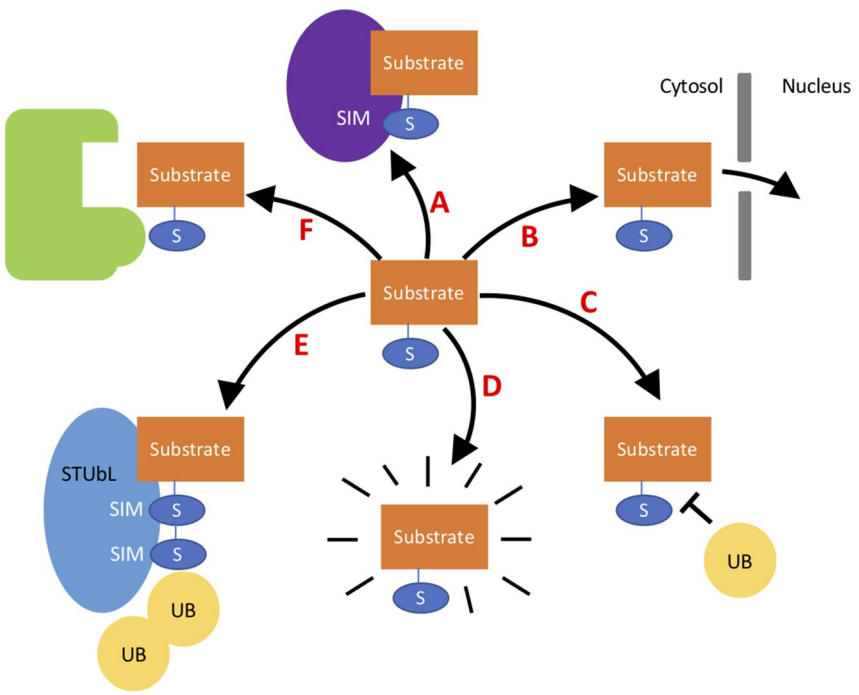

FIGURE 1 | A variety of the different effects SUMO can have on a target substrate. A- SUMO can aid interaction with proteins containing a SIM site. B- SUMO can change the cellular localization of a protein—for example, directing the protein to the nucleus. C- SUMO can protect substrates from degradation by blocking lysine residues in substrates that may be ubiquitinated. D- SUMO binding to a protein can alter its structure activating the protein. E- SUMOylated proteins can signal to STuBL proteins to target for degradation *via* ubiquitination. F- SUMO can block interaction with proteins by blocking binding sites.

The outcome of SUMOylation is largely target dependent and altered by the location and number of SUMO substrates on a target. Indeed, target protein substrates can have single SUMO monomers covalently attached to a lysine, multiple SUMO monomers attached to multiple lysines, or a polySUMO chain from one lysine. This results in a high complexity of different SUMO patterns that can form on one protein altering the molecular consequences of the SUMOylation. For example, the SUMOylation at one site may stabilize the protein by protecting the lysine from ubiquitination, and the SUMOylation at a second site may promote interaction with a protein harboring a SIM site that usually the substrate does not interact with. Despite the complexity of SUMO modification target proteins can experience, it has been observed that, commonly, only a small percentage of target proteins are SUMO modified at a given time entitled the "SUMO enigma" by Hay (2005).

SUMO CYCLE

SUMOylation is a highly dynamic cyclical process with SUMO changing between conjugated and non-conjugated free SUMO forms. SUMO conjugates are dynamic, changing during the cell cycle and in response to stimuli. The SUMO system accomplishes accurate, rapid, specific responses to stimuli. It has a series of biochemical steps, which are similar to ubiquitination, and involves activation, conjugation, and ligation (**Figure 2**).

Firstly, mature SUMO is generated by a SUMO peptidase cleaving 10 amino acids, exposing a carboxyl-terminal diglycine motif (Johnson, 2004). SUMO is activated by an E1 activation heterodimer of SAE1/2 (SUMO-activating enzyme). SAE1 has two isoforms SAE1a and SAE1b; either can be used to create the E1 heterodimer with SAE2, using ATP the complex forms SUMO-AMP. The AMP is released from the SUMO-AMP resulting in the formation of a high-energy thioester bond, between the sulfhydryl group of the catalytic cysteine residue in SAE2 and the carboxyl group of glycine in SUMO.

Activated SUMO is transferred from the SAE2 to a cysteine residue in SCE1 (SUMO conjugating enzyme), an E2 conjugation enzyme, in a transesterification reaction to form SUMO-SCE1 thioester complex. This complex catalyzes the reaction of SUMOylation onto a lysine in the target substrate *via* an isopeptide bond between the SUMO carboxyl terminal glycine and the ε-amino group of lysine (K). The lysine, typically, is part of the SUMOylation consensus motif ψKXE/D; ψ denotes a large hydrophobic residue, K the acceptor lysine, X any amino acid, and E/D glutamate or aspartate.

SUMO E3 ligases are SCE1-interacting proteins that also help aid the transfer of SUMO from SCE1 to the target substrate. There are two identified E3 ligases in *Arabidopsis* SIZ1 (SAP and MIZ1) and HPY2 (high ploidy2), these complex proteins require a number of domains including nuclear localization and SUMO-interacting domains. However, SUMOylation of a target residue can occur without the presence of E3 ligases; it is as yet unclear how essential E3 ligases are.

An additional catalytic step has been identified involving E4 ligases. These ligases form SUMO chains; two E4 ligases have been identified in *Arabidopsis* PIAL1 and 2 (protein inhibitor of activated STAT-like 1/2).

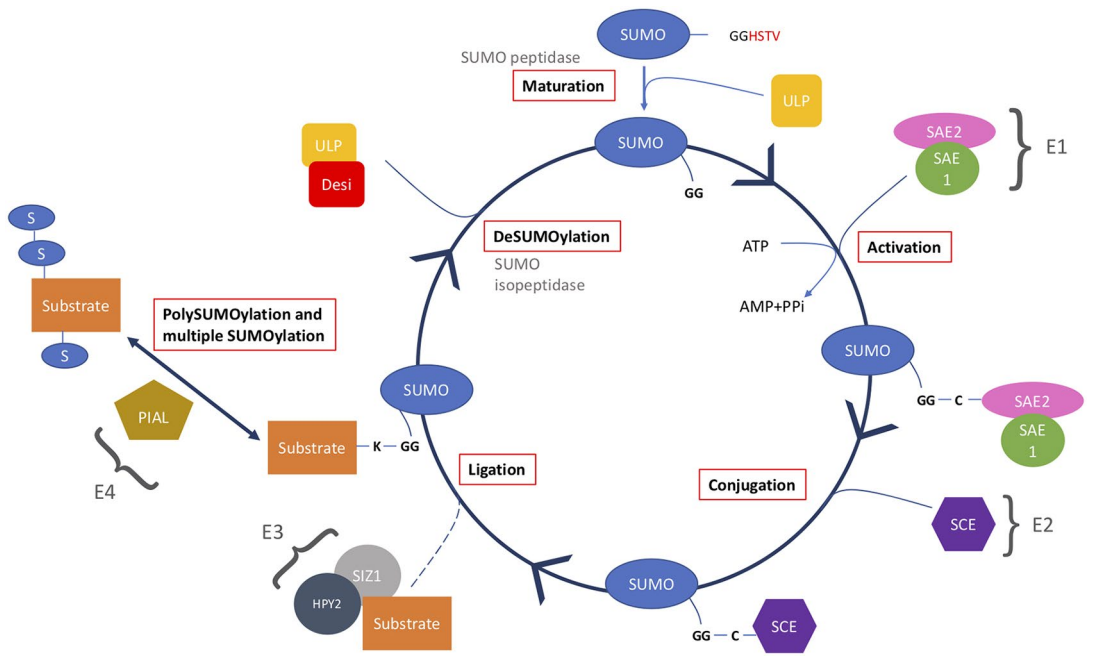

FIGURE 2 | The SUMO cycle starts with maturation of immature SUMO by cleaving off the C-terminus using a SUMO peptidase. Mature SUMO is then activated using ATP and a heterodimer of SAE1 and SAE2. The SUMO is then passed to SCE in a conjugation step, and using a SUMO ligase is ligated onto the substrate. This substrate can then be SUMOylated at more than one SUMO site or form a polySUMO chain. Lastly, in the deSUMOylation step, SUMO is removed from the substrate using a SUMO isopeptidase to generate free SUMO.

Finally, SUMOylation is a cyclical process due to SUMO proteases, which carry out two main functions in the SUMO system. First, they cleave SUMO from target substrates, providing a pool of free SUMO, making SUMO a reversible modification (isopeptidase activity). Secondly, they mature newly synthesized SUMO by cleaving a c-terminal peptide from the immature SUMO (hydrolase/peptidase activity). These sources of SUMO are believed to be critical in the SUMO cycle as the cellular pools of unconjugated SUMO are very low (Johnson, 2004). In yeast, there are two SUMO proteases ULP1 and 2 (ubiquitin-like protease 1/2); the *ulp1-1* mutant is lethal, demonstrating the critical role of SUMO proteases in cell function.

In the ubiquitin system, it is assumed that the ubiquitin E3 ligases provide the specificity in the system due to the large number of E3 ligases. However, in the SUMO system, few SUMO E3 ligases have been identified. Conversely, a relatively larger number of SUMO proteases have been identified, which display specificity to the target proteins suggesting that they may provide specificity in the SUMO system (Chosed et al., 2006; Colby et al., 2006; Yates et al., 2016; Benlloch and Lois, 2018).

CYSTEINE PROTEASES

There are four major classes of proteases in plants, described in the MEROPS database: cysteine-, serine-, aspartate-, and metallo-proteases, with the protease superfamily comprising 2% of coding genes in plants (Hou et al., 2018). All identified SUMO proteases are cysteine proteases. Cysteine proteases are named after the cysteine residue in their active site which is used as a nucleophile for the formation of an acyl intermediate during proteolytic cleavage (Rawlings et al., 2008). Cysteine proteases are often specialized proteases and are widespread in eukaryotes and in plants, with most species having many types of cysteine proteases. The cysteine proteases are important in plants due to their functions in many processes from seed germination to plant senescence. Environmental cues trigger changes in the proteases enabling the plant to react to stimuli including in response to biotic and abiotic stresses. In plants, cysteine proteases are typically found in lytic vacuoles (Roberts et al., 2012). The superfamily of cysteine proteases is highly conserved and has diversified greatly (Gillies and Hochstrasser, 2012).

SUMO Proteases Belong to Different Classes of Cysteine Proteases

Previously, the SUMO proteases have belonged to the same protein superfamily, the ULP superfamily, identified due to their similarity to yeast ULP1/2 proteases. Currently, eight ULPs have been predicted in *Arabidopsis*; six have been characterized as SUMO proteases. The active site has a characteristic papain-like fold found in all ubiquitin-specific and UBL (ubiquitin-like)-specific cysteine proteases (Mukhopadhyay and Dasso, 2007; Hickey et al., 2012).

However, two new classes of SUMO proteases have since been identified. Shin et al. (2012) identified a novel type of SUMO protease in mouse; the two proteins were named DeSI1 (deSUMOylating isopeptidase1) and DeSI2, which lacked sequence similarity to ULP enzymes. Orosa et al. (2018) identified eight putative DeSI proteases in *Arabidopsis* based on sequence similarity to human DeSI1/2 and functionally characterized one protein, DeSI3a. Another SUMO protease recently identified in humans is called USPL1 (ubiquitin-specific protease-like1) (Schulz et al., 2012); currently, however, no homologues have been identified in *Arabidopsis*.

The three families of SUMO proteases identified are cysteine proteases. The cysteine proteolytic enzymes all contain a cysteine residue that acts as a nucleophile at the heart of the catalytic site triad or dyad capable of breaking the thioester bond between the SUMO and target protein. Also present in the active site in addition to the catalytic cysteine is a histidine that functions as a general base, and additionally, in some cases, there is an extra base that is required for stability. The orientation of the cystine, histidine, and stabilizing amino acid can differ. The SUMO proteases identified in yeast and *Arabidopsis* are listed in **Table 1**.

Surprisingly, the three families of SUMO proteases currently identified (ULP, DeSI, and USLP1) are all members of different clans, which show evolutionary relationships between a broad number of proteases, despite all being SUMO proteases. The different clan classifications are due to the different amino acids and the order of the amino acids required for the active site. Within the clan, the proteases are further characterized into families which shows a statistically significant relationship in amino acid sequence to at least one other family member. The ULP proteases are members of the CE cysteine clan, further characterized into the C48 cysteine protease family. The CE clan is characterized as having catalytic triad with residues in the order histidine, glutamine (or asparagine), and then cysteine. The DeSI proteases are from the CP clan in the C97 cysteine protease family. The CP clan has a catalytic dyad composed of histidine and cysteine: in the DeSI active site, no third residue is required to orientate the histidine ring (Suh et al., 2012).The third type of SUMO protease USPL1 is a clan CA C98 cysteine protease family member (Rawlings et al., 2018). The CA clan is characterized as having the catalytic triad in the opposite orientation to that of CE clan with the residues cysteine, histidine, and asparagine (or Aspartic acid). However, all the proteases contain a papain fold, which characterizes all ubiquitin-specific and UBL-specific cysteine proteases characterized so far (Gillies and Hochstrasser, 2012).

Proteolytic Mechanism of Cysteine Proteases

Cysteine proteases are characterized by containing a nucleophilic cysteine thiol that is responsible for the peptide bond attack providing the mechanism of proteolytic activity. The adjacent histidine, which acts as a general base, donates a proton to the cysteine residue to enhance the nucleophilicity. The cysteine's anionic sulfur attacks the carbonyl carbon of the substrate, producing the first tetrahedral thioester intermediate in the reaction, releasing an amine or amino terminus fragment from the substrate. Additionally, the histidine residue in the catalytic triad is restored to its deprotonated form, and an intermediate is formed. The thioester bond is hydrolyzed, to produce a carboxylic

TABLE 1 | List of currently identified SUMO proteases in yeast and *Arabidopsis*, giving all their known names, TAIR accession number, cysteine protease classification, and tissue expression.

Species	Name	Cysteine protease clan	Cysteine protease family	TAIR accession	Tissue expression
Saccharomyces cerevisiae	ULP1	CE	C48	NA	NA
	ULP2	CE	C48	NA	NA
Arabidopsis thaliana	OTS1 (ULP1d)	CE	C48	At1g60220	Root tissue, shoot vasculature of seedlings, developing flowers, wounding sites
	OTS2 (ULP1c)	CE	C48	At1g10570	Root tissue, shoot vasculature of seedlings, petioles, filaments, wounding sites
	ESD4	CE	C48	At4g15880	Seedlings, leaves, shoots, flowers and roots
	ELS1 (ULP1a)	CE	C48	At3g06910	Ubiquitously high levels in root vasculature tissue and flowers
	ELS2 (ULP1b)	CE	C48	At4g00690	Uncharacterized
	FUG1	CE	C48	AT3G48480	Uncharacterized
	SPF1/ASP1/ULP2like2	CE	C48	At1g09730	Ubiquitous in seedlings newly developing leaves and the tips of the roots. Also present in embryo sacs, inflorescences, anthers, and developing seed with intermediate expression levels in stems and rosette leaves
	SPF2/ULP2like1	CE	C48	At4g33620	Leaves, vasculature, inflorescences and maternal floral tissues, stems, cauline leaves, rosette leaves, and middle-length siliques
	Desi 1	CP	C97	At3g07090	Uncharacterized
	Desi 2A	CP	C97	At4g25660	Uncharacterized
	Desi 2B	CP	C97	At4g25680	Uncharacterized
	Desi 3A	CP	C97	At1g47740	Not known
	Desi 3B	CP	C97	At2g25190	Uncharacterized
	Desi 3C	CP	C97	At5g25170	Uncharacterized
	Desi 4A	CP	C97	At4g17486	Uncharacterized
	Desi 4B	CP	C97	At5g47310	Uncharacterized

acid moiety from the remaining substrate fragment helping form the oxyanion hole.

The catalytic action of the protease depends on the clan. In the CA clan, including USPL1, catalysis is caused by an acyl-enzyme intermediate, a glutamine amino acid that helps form the oxyanion hole that contains an electrophilic center. The electrophilic center helps stabilize the tetrahedral intermediate, and asparagine orientates the imidazolium ring of the catalytic histidine.

Whereas the ULP proteases are clan CE, the catalysis uses glutamine that, as in clan CA, helps form the oxyanion hole and glutamine that has a similar role to asparagine in CA clan of orientating the imidazolium ring of histidine. Additionally, an asparagine helps stabilize the histidine in the catalytic dyad. Many of the CE proteases show a preference for cleaving diglycine which may be due to a tryptophan following the catalytic histidine (Golubtsov et al., 2006). The tertiary structure for some of the CE proteases has been solved showing the active site is located between two structural subdomains, one being the beta barrel and the second a helical bundle.

In contrast, the DeSI proteases are the only yet identified members of the CP clan, which was identified when the crystal structure was solved (Suh et al., 2012). Unlike clan CA and CE proteases, there is no third active residue to orient the histidine ring; asparagine has been identified as a structurally important amino acid, but it has been shown to not interact with the catalytic histidine. The DeSI1 proteins forms a homodimer; this provides a prominent surface groove between the two monomers, similar to clan CA with the active site being located between a helix and a beta barrel, with the active sites directed toward the groove (Suh et al., 2012).

IDENTIFICATION OF THE SUMO PROTEASES IN PLANTS

ULP1 (ubiquitin like protease 1) was the first isolated SUMO protease in an activity-based screen of yeast *S. cerevisiae* (Li and Hochstrasser, 1999). ULP1 has an essential role in the G2/M phase of the yeast cell cycle. It was identified by expressing yeast enzymes from a genomic DNA library in *Escherichia coli*. The transformed *E. coli* was also transformed to express a substrate composed of histidine-tagged ubiquitin fused to HA-tagged SMT3. Running the bacterial extracts on SDS-PAGE gels could

determine if cleavage after the diglycine motif had occurred between the SMT3 and ubiquitin.

ESD4 (early in short days4) was the first characterized SUMO protease in *Arabidopsis*, firstly identified by Reeves et al. (2002) by conducting a general mutagenesis study. ESD4 was found due to its early flowering phenotype and the reduced mRNA abundance of floral repressor FLC (floral locus C). However, it was not identified as a SUMO protease until Murtas et al. (2003) sequenced ESD4 and searched databases for proteins with similar sequence homology. The search identified similar proteins including human SENP1 (sentrin-specific protease 1), yeast ULP1, and mouse SMT3IP1. The protein similarity was approximately 200 amino acids in the C-terminus forming the active site of a cysteine protease. To confirm ESD4 as a SUMO protease, ESD4 was purified and its peptidase activity monitored *in vitro*. Furthermore, the activity of ESD4 was blocked by thiol reagent (cysteine protease inhibitor) *N*-ethylmaleimide (NEM), which is also inhibited yeast ULP1. However, ESD4 was not inhibited by ubiquitin aldehyde which inhibits deubiquitinating protease. Additionally, a mutant of ESD4, with the catalytic cysteine in the catalytic triad mutated to a serine, was assayed for deSUMOylation activity and was found to be inactive. Finally, the double glycine motif at the C-terminus of the SUMO that linked to FLC was mutated to two alanine residues. No cleavage was detected by ESD4 between the SUMO and FLC. *Arabidopsis esd4-1* mutants also have reduced levels of free SUMO and an increased abundance of SUMO conjugates.

Kurepa et al. (2003) identified *A. thaliana* SUMO proteases by their sequence similarity to yeast ULP1. The study used BLAST to identify *Arabidopsis* proteins with sequence similarity to animal and yeast ULP1 catalytic domains. The catalytic domain is a conserved region of 200 amino acids, which surrounds a triad of histidine, aspartate, and cysteine residues. The search found 12 genes which were further classified into three subfamilies, with two subfamilies more related to yeast ULP1 and the third more similar to yeast ULP2. Of the SUMO proteases identified by Kurepa et al. (2003), they noted on the lack of similarity in the proteins outside of the ULP1 catalytic domain; hypothesizing this may provide substrate specificity.

ELS1 (ESD4-like SUMO protease1) (which was identified by Kurepa et al. (2003) and named ULP1a) was characterized due to its sequence similarity to ESD4. ELS1 contains the same ULP1-catalytic domain as in ESD4 and ULP1. The SUMO activity was also assayed *in vitro* in the same assay as ESD4, using purified ESL1 to cleave SUMO from an extension. As with ESD4, the SUMO protease activity was blocked with NEM and when the catalytic cysteine was mutated to serine. Despite the sequence homology between ESD4 and ELS1, they do not show functional redundancy (Hermkes et al., 2011).

ELS2 was identified in the initial blast search performed by Kurepa et al. (2003) that also identified ELS1, named ULP1b. FUG1 (fourth ULP gene) was identified by Lois (2010) using human SENP1 and was shown to have an expressed sequence tag. It was classified to fourth ULP gene class due to its different phylogeny. Both proteases have been identified *via* bioinformatic techniques but are yet to be functionally addressed.

OTS1 and 2 (overly tolerant to salt 1/2) were initially identified in *Arabidopsis* in the screen by Kurepa et al. (2003) and named ULP1d and ULP1c, respectively. Chosed et al. (2006) and Colby et al. (2006) demonstrated that OTS1 and OTS2 had *in vitro* SUMO protease activity. Chosed et al. (2006) designed an assay with SUMO with an HA (hemagglutinin) tag fused to the diglycine residues and incubated this substrate with purified SUMO proteases. If the SUMO-HA is cleaved, the product runs faster on an SDS/PAGE gel and can be identified. The assay demonstrated that OTS1 and OTS2 can cleave SUMO1 and SUMO2 to produce mature SUMO. They then tested for isopeptidase activity by purifying RanGAP (RanGAP [GTPase-activating protein]) substrate modified by various recombinant GST-SUMO proteins. Both OTS1 and OTS2 were capable of cleaving various SUMO variants from RanGAP. In a similar approach, Colby et al. (2006) also expressed purified OTS1 and OTS2 and assayed for isopeptidase activity using *in vitro* SUMOylation. Initially, they tested AtSUMO1, 2, and 3 conjugated to ScPCNA (proliferating cell nuclear antigen). OTS1 and OTS2 cleaved SUMO1 and SUMO2 from ScPCNA. Colby et al. (2006) also used a similar assay to determine that OTS1 and OTS2 in addition to possessing isopeptidase activity also possess peptidase activity capable of maturing SUMO. Conti et al. (2008) demonstrated that *ots1ots2-1* mutants had increased levels of SUMO conjugates.

SPF1 and SPF2 (SUMO protease related to fertility 1/2) were initially identified by Novatchkova et al. (2004) and called ULP2-like-2 and ULP2-like-1, respectively. They were identified by searching the *Arabidopsis* genome for a protein that was most similar to the yeast query protein, ULP2. The proteins identified however were not characterized as a SUMO proteases until 2017. Two groups characterized the proteins: Liu et al. (2017a) renamed the proteins SPF1 and SPF2, Kong et al. (2017) renamed the ULP2-like-2 ASP1 (*Arabidopsis* SUMO protease1). Kong et al. (2017) confirmed *in vitro* that SPF1 has endopeptidase activity by incubating purified SPF1 with SUMOylated FLC and demonstrating that SUMO was cleaved by WT (wild-type) SPF1 but not by a mutation to the cysteine catalytic site or when NEM was added to the incubation. Additionally, they showed that both SPF1 and SPF2 can process immature SUMO to the mature form, and both single and double mutant knockouts have higher levels of SUMO conjugates. Kong et al. (2017) showed that the number of SUMO conjugates remain higher after heat shock in the *spf1-1* mutant.

Unlike the ULP proteins, DeSI1 was not identified from yeast as it does not contain a homologue. Originally, the DeSI proteins were identified as PPPDE (peptidase-permuted papain fold peptidases) of dsRNA (double-stranded RNA) viruses and eukaryotes. The DeSI proteins were identified in mice by Shin et al. (2012) using BZEL (BTB-ZF protein expressed in effector lymphocytes) in a yeast two-hybrid screen as bait. It was predicted to function as a deubiquitinating peptidase, but no activity had been reported. DeSI1 was unable to deubiquitinate ubiquitinated BZEL but was capable of deSUMOylating SUMOylated BZEL; additionally, DeSI1 was capable of cleaving polymeric SUMO2/3 from targets in mouse. Mutating the catalytic cysteine in DeSI1 abolished the deSUMOylation capabilities of DeSI-1. However,

the DeSIs do not have SUMO-processing peptidase activity (Shin et al., 2012, Suh et al., 2012).

Orosa et al. (2018) searched for *Arabidopsis* homologues using the mammalian DeSI1 active site as a search criteria identifying eight putative *Arabidopsis* DeSI proteins. One protein, named DeSI3a, was purified and assayed *in vitro* for deSUMOylation activity, compared to the same protein with the catalytic cysteine mutation to serine, which was incapable of deSUMOylation. DeSI3a WT (wild type) showed cleavage of the isopeptide-linked SUMO; the mutated DeSI3a did not show activity. Additionally, DeSI3a was shown to specifically reduce higher molecular weight SUMO-conjugated isoforms of the kinase domain of FLS2 (flagellin-sensitive2), which the mutated form of DeSI3a was unable to (Orosa et al., 2018).

Schulz et al. (2012) were encouraged to search for novel SUMO proteases due to the low number of identified SUMO proteases and the small number of different families of SUMO proteases compared to ubiquitin proteases. They used an activity-based search with suicide substrates that irreversibly cross-link with SUMO proteases. This technique has been used for the identification of ubiquitin proteases; they purified HA-tagged SUMO ligated to vinylmethylester and incubated the SUMO with human cell lysates. The HA-tagged proteins were immunopurified from the lysate and analyzed with mass spectrometry. This led to the identification of USPL1, which, when the catalytic cysteine was mutated to the serine, USPL1 was no longer capable of binding to the SUMO. USPL1 was shown to interact with SUMO2, but not ubiquitin, to have some peptidase activity, and it shows some chain editing activity. Fluorescence-tagged USPL1 was found exclusively in Cajal bodies which are in the nucleus, associated with mRNA processing, and are highly dynamic, changing in number, size, and composition during cell cycle, development, and stress (Cioce and Lamond, 2005; Nizami et al., 2010). Interestingly, RNAi-mediated knockdown of USPL1 affected proliferation and COILIN localization; however, the phenotype was rescued by both USPL1 and the mutated form of USPL1, suggesting it has other functions (Schulz et al., 2012; Hutten et al., 2014). USPL1 highlights the importance of characterization of proteases, as USPL1 was originally misannotated as an ubiquitin protease due to sequence similarity.

Following previously outlined techniques to identify SUMO proteases in *Arabidopsis,* the catalytic site of USPL1 was blasted into the *Arabidopsis* genome. Two proteases were identified as potential matches: UBP6 and UBP7 (ubiquitin-specific protease6/7) shown in **Figure 3**. Both these proteases have already been identified as ubiquitin proteases through bioinformatic techniques. Moon et al. (2005) identified the protease as an interacting partner with CAM2 (Calmodulin2). However, they were unable to demonstrate in *E. coli* that UBP6 was capable of cleaving ubiquitin from substrates. It can only be speculated that UBP6 and its close homologue UBP7 are SUMO proteases currently. It will require functional characterization to prove their SUMO proteolytic activity. If, however, it is shown that UBP6/7 are SUMO proteases, it will be the third identified cysteine protease family present in *Arabidopsis*; there may be more yet.

DOMAINS AND STRUCTURES OF SUMO PROTEASES

The domains and structures of plant SUMO proteases have not been well studied; they are largely based on similarity to yeast SUMO proteases. The ULP proteases typically have a 200–amino acid catalytic domain at the C-terminus of the protein (see **Figure 4**). The N-terminus of the protein is typically highly variable and is presumed to be responsible for specificity of SUMO protein–conjugate recognition and modulation of enzymatic activity and directing subcellular localization (Li and Hochstrasser, 2003; Gong and Yeh, 2006; Mukhopadhyay et al., 2006; Kroetz et al., 2009). The N terminal domain is also thought to contain SIM (SUMO-interacting motif) sites which may increase enzyme affinity for SUMOylated substrates; alternatively, they may help aid orientation of the SUMOylated proteins in the catalytic site (Hickey et al., 2012).

However, as can be seen in **Figure 4**, the structure of the ULP proteases varies between the proteases, helping to provide their

```
UBP6_A_thaliana     AT--NLGYSAGLVNLGNTCYMNSTVQCLKSVPELKSALSNYSLAARSNDVDQTSHMLTVA      154
UBP7_A_thaliana     AA--NLGYSAGLVNLGNTCYMNSTMQCLISVPELKSELSNYQS-ARTKDVDQTSHMLTVA      208
USPL1_H_sapien      CTSFPQALCVQWKNAYALCWLDCILSALVHSEELKNTVTG--------------------      257
USPL1_D_rerio       SELVPVHSELFWKNEENMCWLDAMLVMLVHCRTIRGTPCRG--------IKLSD------      391
                    .           *    *:::. :  *     ::.

UBP6_A_thaliana     DAEASANGSGESSTVNPQEGTSSEKETHMTG-IYDLVAVLTHKGRSADSGHYVAWVKQES      439
UBP7_A_thaliana     DAEGSSNQSGESSTGDQQEGA----SPHMTG-IYDLVSVLTHKGRSADSGHYVAWVKQES      489
USPL1_H_sapien      LEKVSPIFMLHFVEGLPQNDLQH-YAFHFEGCLYQITSV---IQYRA-NNHFITWILDAD      465
USPL1_D_rerio       LEKLSSVFALHFVEGLPRKDLTK-YGFTFQGFQYSVSTI---IQYNKHLQHFVTWVRQSN      601
                      : *     .      ::.        : *  *.: ::           *:::*: : .

UBP6_A_thaliana     GKWIQYDDDNPSMQREEDITKLSGGGDWHMAYITMYKARFVSM------------------      482
UBP7_A_thaliana     GKWVQYDDANTSLQRGEDIIKLSGGGDWHMAYIVMYKARLISM------------------      532
USPL1_H_sapien      GSWLECDDLKGPCSERHKKFEVPA-SEIHIV---IWERKISQVTDKEAACLPLKKTNDQH      521
USPL1_D_rerio       GFWLELDDLKHPYSPTHKRLPFPS-SEFHIL---FWETDSFKE-EHSEVCLPTAPPEVPN      656
                    * *:: ** :   .  ..   . . .: *:    :::    .
```

FIGURE 3 | *Arabidopsis* UBP6 and UBP7 may be a distant USPL1 homologue. Alignment of human USPL1, zebrafish USPL1, *Arabidopsis* UBP6, and *Arabidopsis* UBP7. The red boxes highlighting the conserved residues indicate the catalytic triad.

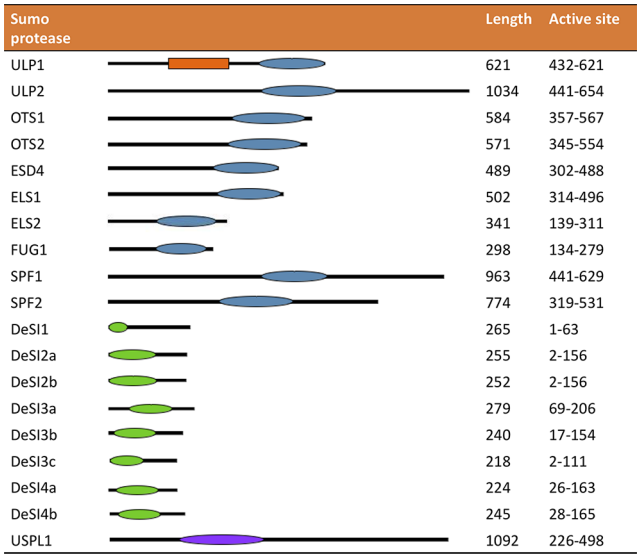

FIGURE 4 | The location of the active site and length of several different SUMO proteases. The orange box denotes the SIM site in ULP1. The blue oval depicts the location of the C48 active site, the green oval the C97 active site, and the purple oval the C98 active site.

individual specificity. The catalytic domain in ELS2 is closer to the N-terminus, and the catalytic domains in SPF1 and SPF2 are located in the center of the protein and form much larger proteins than the other ULP proteases. Chosed et al. (2006) examined the effect of truncating the OTS1, OTS2, ELS1, and ESD4, expressing just the catalytic domain *in vitro*. Truncated ESL1 and ESD4 were unable to function as SUMO proteases requiring the full length of the gene. Conversely, the truncated form of OTS2 was able to cleave more forms of SUMO than when the N-terminus of the protein was intact; the truncated form of OTS2 was able to cleave yeast and mammalian and tomato SUMO; this activity was not present in the full length of OTS2 (Chosed et al., 2006).

Additionally, the *Arabidopsis* ULP proteases have not had the crystal structure solved. It is assumed, however, that the structure will be similar to yeast ULP1. The crystal structure of yeast ULP1 catalytic domain interacting with SUMO has revealed a tight but shallow VDW tunnel that recognizes the Gly–Gly motif, stably orienting substrates to come into close interaction with the active site. The structure showed that side chains of residues other than glycine would sterically clash with the narrow tunnel, providing specificity (Mossessova and Lima, 2000). When the substrate is positioned in the VDW tunnel, the scissile bond after the double glycine is converted from a trans to a cis bond causing a kink in the SUMO C-terminal tail (Shen et al., 2006). This configuration is thought to be rare in proteins and is induced to destabilize the bond and promote cleavage (Hickey et al., 2012). The active site in ULP1 is in a narrow cleft structured to enable both large SUMO conjugates and single-SUMO molecules to access it (Mossessova and Lima, 2000). The active site is between two structural subdomains, one subdomain is a beta-barrel carrying the active site histidine and glutamine (or aspartic acid), and the second subdomain consists of a helical bundle, with one helix carrying the catalytic cysteine.

Compared to the ULPs, the DeSI proteins are smaller proteins with a larger component of their size comprising the active site (**Figure 4**), which is around 140 amino acids; the active site is also closer to the N terminus. As with the ULP proteases, the DeSI proteases have putative SIM sites (Hickey et al., 2012). The crystal structure for the DeSI proteases in *Arabidopsis* has not been solved but can be assumed to be similar to the solved structure of human DeSI1. It revealed the protein forms as a homodimer forming a papain groove between the two subunits forming the active site with the catalytic dyad. In the DeSI protein, the proteolytic groove forms between the cysteine at the N-terminal end of a helix, and the histidine on a strand that is part of a beta-barrel. Surprisingly, the C-terminal tails of DeSI1 were shown to fold into the groove, seemingly blocking access to the active site. However, activity assays with a truncated C-terminal tail show no effect compared to WT, suggesting the structure may be an effect of crystallization (Suh et al., 2012).

The domains and structure of USPL1 have not currently been characterized but can be hypothesized to have similar functions to that of the ULP proteases containing SIM site signals for cellular localization and providing substrate specificity.

EVOLUTION AND DIVERSIFICATION OF SUMO PROTEASES IN PLANTS

The ULP SUMO proteases are evolutionarily distinct from the DeSI SUMO proteases (**Figure 5**). The ULP SUMO proteases have a phylogenetic origin that can be traced to green algae and other eukaryotes including yeast ULP1 and ULP2 (Castro et al., 2018a). The evolutionary classification of the proteases has proved difficult due to the high amino acid sequence divergence. Initially, OTS1 and OTS2 were classified in a group that was more closely related to ESD4/ELS1/ELS2 believed to be related to *Sc*ULP1 due

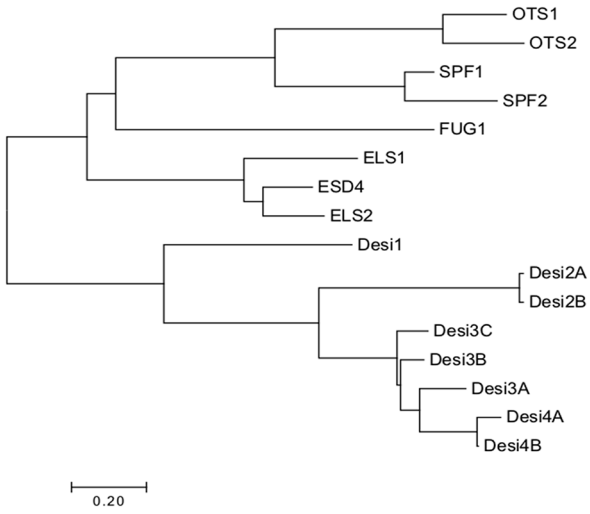

FIGURE 5 | Phylogenetic tree of currently identified SUMO proteases in *Arabidopsis*. The proteases cluster according to their catalytic triad. Alignments were made using ClustalX and visualized in Jalview. Bootstrap neighbor-Joining trees were made using ClustalX and visualized using MEGA7.

to the active site being located at the C-terminus of the protein like *Sc*ULP1 (Novatchkova et al., 2004; Lois, 2010). However, based on amino acid conservation, they are more similar to *Sc*ULP2 (Castro et al., 2016). The current classification in use was carried out by Novatchkova et al. (2012), who conducted an in-depth phylogenetic analysis, including *Arabidopsis*, tomato, grapevine, and poplar genomes. They generated a novel grouping of the ULP proteases into four groups in *Arabidopsis*, namely, A, B1, B2, and C (Novatchkova et al., 2012). Benlloch and Lois (2018) suggested using the same classification system classing the ULP proteases on sequence similarity and organization of the ULP domain; however, they suggested classing the proteases independently of their similarity to yeast ULPs. Conversely, Castro et al. (2018a) used the classification system to divide the ULP proteases into evolution from ScULP1 and ScULP2; however, the naming system was changed and is being used in this review. Class I ELS type of homologues is believed to have evolved from ScULP1 including ESD4, ELS1, and ELS2. Three different subdivisions have evolved from ScULP2 including class II OTS-type homologues including OTS1 and OTS2 class III SPF-type homologues, including SPF1 and SPF2 and class IV FUG type that is yet to be characterized as a SUMO protease. However, the relationship of FUG1 to the other SUMO protease groups strongly suggests that it has the same activity (Novatchkova et al., 2012). FUG1 may be a relatively newer protease as it appears to be absent from early plant taxa, being present in flowering plants (Castro et al., 2018a).

The DeSI proteins are not as well studied evolutionarily due to their very recent identification in *Arabidopsis*; however, due to the similarities in some of their sequences, it can be hypothesized that they may share functional redundancy (Orosa et al., 2018), but this is yet to be determined.

If USPL1 homologues are found in *Arabidopsis*, it is likely that they will share more evolutionary similarity with the ULP proteases as clan CE proteases are hypothesized to share sequence similarity with clan CA proteases.

LOCALIZATION OF SUMO PROTEASES IN THE CELL AND PLANT TISSUE

The subcellular localization of the SUMO proteases is thought to provide specificity to the SUMOylation machinery (Chosed et al., 2006). Li and Hochstrasser (2003) expressed in yeast cells lacking *Sc*ULP2 a truncated form of *Sc*ULP1 with just the catalytic domain expressed; this mutant was capable of suppressing defects of cells lacking ULP2, whereas full length *Sc*ULP1 was unable to. This suggests that the N-terminal region of ULP1 restricted activity of the protease; this may have been its cellular location to enable proteolytic activity. The known subcellular localization of the *Arabidopsis* SUMO proteases are summarized in **Figure 6**. The cellular localization is largely based on the N-terminal sequence; deletion of the localization domain alters the targets that are deSUMOylated (Li and Hochstrasser, 2003; Gong and Yeh, 2006; Mukhopadhyay et al., 2006; Kroetz et al., 2009). Yeast ULPs all localize to the nucleus, *Sc*ULP1 localizes to the nuclear pore complexes in the nuclear envelope (Panse et al., 2003), and *Sc*ULP2 localizes to the nucleoplasm (Li and Hochstrasser, 2000).

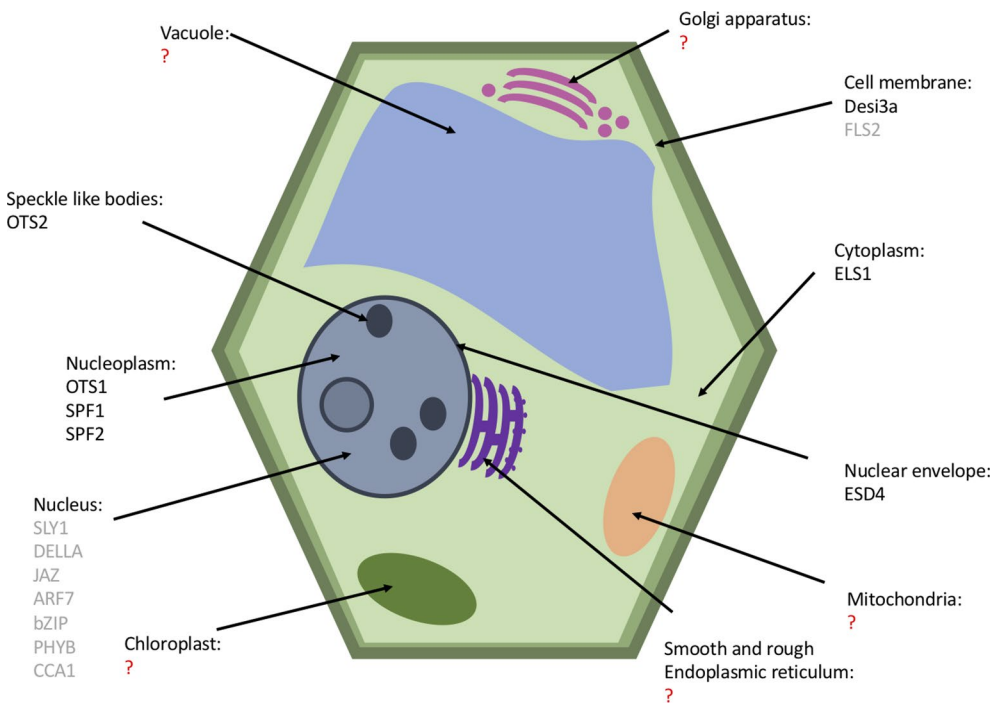

FIGURE 6 | A plant cell featuring the known cellular location of SUMO proteases (black) and their substrates (gray). Organelles with a question mark (red) have no known SUMO proteases or substrates but may have undiscovered SUMO proteases.

The ULP proteases largely all localize to the nucleus; ESD4 predominantly localizes to the periphery of the nucleus at the nuclear periphery and envelope (Murtas et al., 2003; Xu et al., 2007). Surprisingly, unlike the other ULP proteases, the closest homologue of ESD4, ELS1, is present in the cytosol (Hermkes et al., 2011). OTS1 and OTS2 localize to the nucleus, and OST2 is also found in nuclear foci (Conti et al., 2008). Additionally, the recent characterization of SPF1 and SPF2 showed that they are nuclear proteases (Kong et al., 2017; Liu et al., 2017a).

The DeSI1 proteases identified in human cells have been found to be located at both inside and outside the nucleus, localizing predominately in the cytoplasm, whereas DeSI2 localizes exclusively in the cytoplasm (Shin et al., 2012, Suh et al., 2012). The only DeSI currently characterized in *Arabidopsis*; DeSI3a was found to localize in the cell membrane by expressing mCherry-DeSI3a in *Nicotiana benthamiana*. Ultracentrifugation which separated the cytoplasmic nuclear and membrane fractions identified DeSI3a in the membrane fraction (Orosa et al., 2018).

The SUMO proteases are localized in all tissues in the plant; generally, their localization correlates with their phenotypes when knocked out. The highest concentration of ESD4 mRNA was detected in the inflorescence and flowers; however, it was also detected at lower concentrations in the seedlings, leaves, shoots, and roots of wild-type plants and was found to be constantly present throughout the 24-hour cycle (Murtas et al., 2003). An ELS1 promoter–GUS fusion showed that ELS1 is expressed ubiquitously in the plant with a higher accumulation in the vasculature and roots. RT-PCR demonstrated that there is also high expression in flowers and low levels of expression in the siliques and leaves (Hermkes et al., 2011).

Both OTS1 and OTS2 have a similar expression pattern as observed through GUS staining, both present from the early developmental stages, with high expression levels in vascular tissue in the root and shoot of seedlings and in the petioles. In mature plants, expression in the leaves was reduced, compared to the seedlings. The proteases were also identified in the flowers and siliques with OTS2 expression stronger than OTS1; for most other tissues, OTS1 expression was stronger (Castro et al., 2016).

The GUS reporter system for SPF1 expression found ubiquitous expression in 2-day-old seedlings; 4-day-old SPF1 was detected in the hypocotyl, cotyledons, and shoot and root apices of the seedlings. In older seedlings, it is present in newly developing leaves, shoot apex and root tips (Kong et al., 2017; Liu et al., 2017a). SPF1 and SPF2 strongest gene activity was detected in the reproductive organs, specifically localizing to embryo sacs, inflorescences, anthers, and developing seeds (Kong et al., 2017; Liu et al., 2017a). Despite SPF1 and SPF2 being expressed in the same tissues, both have different expression patterns in the respective tissues. Tissue-specific PCR revealed that SPF1 transcription is highest in inflorescences and cauline leaves, with intermediate expression levels in stems and rosette leaves. SPF2 transcription was seen to be at its highest in stems, cauline leaves, rosette leaves, and middle-length siliques, and interestingly, no expression of SPF2 was detected in root tissue (Liu et al., 2017a).

SUMO PROTEASE SPECIFICITY

The SUMO proteases provide specificity in the SUMO targets they cleave. This can include specificity in the SUMO isoform they cleave, whether they mature the SUMO isoform, and the target protein they cleave SUMO from. The specificity the SUMO proteases exhibit is summarized in **Table 2**.

ELS1 is hypothesized to be more likely to be involved in SUMO maturation than in deconjugation. This is due in part to the observations that the loss of yeast ULP1 (the hypothesized SUMO maturase in yeast) can be rescued through ELS1 expression, and that *Arabidopsis els1-1* mutants show only slightly increased accumulation of high molecular weight SUMO conjugates, suggesting a limited role in SUMO regulation (Hermkes et al., 2011). Chosed et al. (2006) also found ELS1 to have greater SUMO peptidase than isopeptidase activity. ELS1 was shown to cleave SUMO1, 2, and 3 to generate mature SUMO. They also demonstrated that ELS1 can deconjugate SUMO1 and SUMO2 from target proteins; however, these studies were carried out *in vitro (*Chosed et al., 2006).

Surprisingly, given the high sequence similarity between ELS1 and ESD4, ESD4 was not capable of suppressing the yeast *ulp1* phenotype. In contrast, ESD4 was capable of complementing the *ulp2* yeast mutant temperature sensitivity. Yeast ULP2 predominantly cleaves polymeric SUMO chains on target proteins (Li and Hochstrasser, 1999; Schwienhorst et al., 2000; Bylebyl et al., 2003; Hermkes et al., 2011). This suggests that ESD4 may play a role in SUMO chain editing. ESD4 is capable of deconjugating SUMO1 and SUMO2 from target proteins, but not SUMO3. ESD4 also displays SUMO endopeptidase activity toward SUMO1 and SUMO2, but not SUMO3 (Chosed et al., 2006; Colby et al., 2006).

SPF1 has the weakest capabilities of cleaving SUMO1 from target proteins (Kong et al., 2017). Both SPF1 and SPF2 have SUMO peptidase activity toward SUMO1 but are unable to mature SUMO2 or SUMO3 (Liu et al., 2017a). SPF1 and SPF2 have SUMO deconjugase activity particularly in inflorescences; in *Arabidopsis spf-1* and *spf1-1 spf2-1* mutants, there was a greater number of higher molecular weight SUMO conjugates in inflorescences compared to WT and compared to seedlings (Liu et al., 2017a).

TABLE 2 | Summary of known specificity of SUMO proteases against the different SUMO isoforms in *Arabidopsis*. SUMO 5 is not included in the table as there is no currently identified protease for SUMO 5. M, matures SUMO; D, deconjugates SUMO; NT, not tested.

	SUMO 1		SUMO 2		SUMO 3	
	M	D	M	D	M	D
ESD4	High	High	High	High	–	–
ELS1	High	High	High	High	Low	–
OTS1	High	High	High	High	–	–
OTS2	High	High	High	High	–	–
SPF1	Medium	Low	–	NT	–	NT
SPF2	Medium	NT	–	NT	–	NT
Desi3a	NT	High	NT	NT	NT	NT

OTS1 and OTS2 are capable of deconjugating SUMO1 and SUMO2 from target proteins, but not SUMO3. OTS1 and OTS2 also display SUMO endopeptidase activity toward SUMO1 and SUMO2, but not SUMO3 (Colby et al., 2006; Conti et al., 2008).

In mouse, the DeSI proteins do not possess SUMO maturation activity; so far, they have only been involved with deconjugating SUMO and chain editing (Mukhopadhyay and Dasso, 2007; Shin et al., 2012; Suh et al., 2012). DeSI3a, the only currently characterized DeSI in plants was shown to cleave isopeptide-linked poly-SUMO chains (Orosa et al., 2018); however, SUMO peptidase activity was not tested.

PHYSIOLOGICAL EFFECT OF SUMO PROTEASES

SUMOylation has pleiotropic effects on cell dynamics, and currently over 1,000 proteins have been identified as SUMO targets (See Elrouby and Coupland, 2010; Miller et al., 2010; Rytz et al., 2018). Due to the importance of the SUMO proteases in regulating the SUMOylation in plants, alterations in SUMO protease expression levels can alter the development and physiology of the plant. The different physiological phenotypes of the SUMO proteases can provide an insight into the role of the individual SUMO proteases and their targets. The physiological phenotypes the SUMO proteases alter is summarized in **Figure 7**.

ESD4 was initially phenotyped by Reeves et al. (2002); Murtas et al. (2003) identified ESD4 as a SUMO protease. Reeves et al. (2002) identified the *esd4-1* mutant as having an early flowering phenotype, which was most obvious under short photoperiods. Additional phenotypes observed of the *esd4-1* mutant included premature termination of the shoot and an alteration of phyllotaxy along the stem, giving a dwarf stature and deformed siliques, irregularly positioned along the stem (Reeves et al., 2002). The early flowering was determined to be in part due to the level of the floral repressor FLC mRNA being reduced in *esd4-1* mutants; however, it was also suggested that ESD4 also promotes flowering independently of FLC (Reeves et al., 2002). Furthermore, the phenotype was enhanced when SUMO1, 2, and 3 were overexpressed in the *esd4-1* mutant (Murtas et al., 2003).

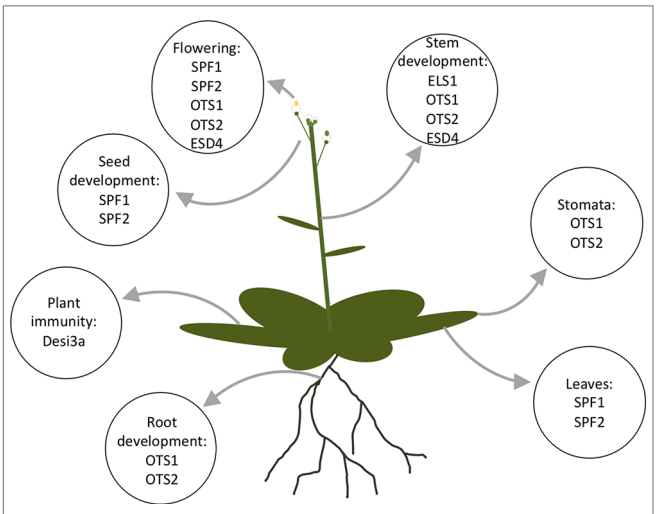

FIGURE 7 | An *Arabidopsis* plant with labeled organs listing the proteases that are known to be present in the organ or effect the organ development.

Els1-1 mutants appear similar to wild type except for slightly reduced growth and thinner stems (Hermkes et al., 2011). *Els1-1* knockout mutants were analyzed for difference in flowering time, due to ELS1 close homologue ESD4 having such an obvious phenotype; however, *els1-1* mutants showed no strong statistically significant difference between WT and *els1*-1 (Hermkes et al., 2011).

The SPF single and double mutants do not display a severe phenotype in early stages of development (Castro et al., 2018b). At the flowering stage, however, the *spf1-1* mutant has a late flowering phenotype, which is more pronounced under long days (Kong et al., 2017). *Spf2-1* mutants exhibit no clear phenotype, and the *spf1-1 spf2-1* double mutant has a greater flowering delay than the single mutants (Castro et al., 2018b). In addition to the timing of flowering, *spf1-1* has shorter siliques and abnormal seeds; this was not observed in the *spf2-1* mutants (Liu et al., 2017a). In the *spf1-1 spf2-1* double mutants, overall seed production was reduced with the mutants producing larger seeds (Liu et al., 2017a; Castro et al., 2018b). As has been observed with the other phenotypes, *spf2-1* did not show a difference in flowers compared to WT; however, *spf1-1* and *spf1-1 spf2-1* mutants had two thirds of flowers with abnormally long styles, which causes a physical fertility barrier (Liu et al., 2017a). Additionally, the *spf1-1* and *spf1-1 spf2-1* mutant flowers had fewer pollen grains. The reduced fertility in the *spf1-1* and *spf1-1 spf2-1* mutants was partially due to abnormal microgametophytes. Many pollen grains were shown to be non-viable with abnormal shapes and reduced cytoplasmic content, implicating SPF1 and SPF2 in pollen grain development (Liu et al., 2017a). Ovule development was also analyzed; abnormal ovules were only observed in the *spf1-1 spf2-1* double mutant, showing arrested embryo sacs and degeneration of embryo sacs which may be due to the regulation of callose degradation (Liu et al., 2017a). Particularly in the *spf1-1 spf2-1* double mutant, abnormal embryos were detected with irregular morphologies (Liu et al., 2017a). The physiological observations of abnormal fertility organs were further supported genetically as fertility gene expression was also abnormal in the *spf1-1* and *spf1-1 spf2-1* mutant plants compared to WT. Finally, *spf1-1* and *spf1-1 spf2-1* mutants displayed altered leaf morphology showing elongated darker leaves due to an accumulation of chlorophyll, carotenoids, and anthocyanins (Castro et al., 2018b). Microarray analysis demonstrated that differentially expressed genes were involved in cell wall and secondary metabolism including genes pertaining biosynthesis of phenylpropanoids, glucosinolates, and lipids (Castro et al., 2018b).

Double mutants of *ots1-1 ots2-1* have a small stature and early onset flowering; this phenotype was not observed in the single mutants. Additionally, the *ots1-1 ots2-1* double mutant, but not the single mutant, show reduced shoot weight, rosette radius, number of leaves, and late germination (Castro et al., 2016). The observed developmental defects were further supported by microarray analysis of *ots1-1 ots2-1* showing overrepresentation of genes related to shoot development including organ morphogenesis (Castro et al., 2016).

The *ots1-1 ots2-1* double mutants also produce a lower number of seeds and have a significantly reduced filament length. Some of the observed phenotypes in *ots1-1 ots2-1* double mutant are reversed to WT conditions if either a DELLA protein is also knocked out from the mutant such as RGA (repressor of ga1-3) or GAI (gibberellin-insensitive), or if GA (gibberellins) or JA (jasmonic acid) is applied (Campananaro et al., 2016). This suggests that the fertility phenotype of *ots1-1 ots2-1* is controlled through the DELLA proteins (Campananaro et al., 2016). It has been demonstrated that the DELLA proteins are SUMOylated, with SUMO stabilizing the DELLA proteins and OTS1/2 are the proteases that cleave SUMO from the DELLAs (Conti et al., 2014). In the *ots1-1 ots2-1* double mutant, there are increased levels of DELLAs, due to the SUMOylated DELLAs being stabilized (Conti et al., 2014). The higher accumulation of DELLAs in the *ots1-1 ots2-1* mutant results in reduced fertility in the plants; this phenotype is reversed in a triple mutant of *ots1-1 ots2-1 della* mutant (Campananaro et al., 2016). Finally, *ots1-1 ots2-1* double mutant also has an increased stomatal aperture compared to WT (Castro et al., 2016).

The knockout mutant of *desi3a* does not have differences in global SUMOylation immunoblots, compared to WT. Additionally, no obvious physiological phenotype was reported in Orosa et al., 2018; it was hypothesized due to DeSI3a having a narrow range of targets (Orosa et al., 2018).

ROLE OF SUMO PROTEASES IN PLANT HORMONAL PATHWAYS

SUMO may provide a key point of cross talk between the different PTMs as SUMOylation can act as a signal for ubiquitination of proteins (Elrouby et al., 2013) and can also regulate kinases and phosphatases (Crozet et al., 2014). This enables SUMO to act as a central regulator of signaling and enables the PTMs to coordinate complex molecular responses (Garrido et al., 2018). This may enable the SUMO system to exert control over hormonal responses in plants. **Table 3** summarizes the currently identified SUMO proteases that have been shown to have roles in the hormonal pathways.

Esd4-1 mutants accumulate elevated levels of SA (salicylic acid). The *esd4-1* phenotype is partially alleviated by mutation of salicylic acid biosynthesis gene ICS1 (isochorisate synthase1). Double *esd4-1 ics1-1* mutants are larger and flower later than *esd4-1* mutants and accumulate less SA. They also accumulate fewer SUMO conjugates, with levels falling back to wild type or slightly above wild type depending on the background (Villajuana-Bonequi et al., 2014). This last observation implies that the increase in SUMO conjugates visible in *esd4-1* mutants may be caused in part by an increase in SUMOylation rather than by a decrease in deSUMOylation. While, the inactivation of ICS1 reduces the levels of SUMO conjugates in *esd4-1* mutants, it does not increase the levels of free SUMO1/2 (Villajuana-Bonequi et al., 2014) as would be expected in the case of increased deconjugation. However, the exact relationship between SA and free SUMO is still unknown. A variety of SUMO-related mutants, including *esd4-1*, *ots1-1 ots2-1*, *siz1-1,* and *sum1-amiR sum2*, and SUMO overexpression lines show hallmarks of an increased SA response (van den Burg et al., 2010; Villajuana-Bonequi et al., 2014; Bailey et al., 2016).

Microarray analysis of *spf1-1 spf2-1* observed upregulation of genes associated with auxin, brassinosteroid, cytokinin, gibberellin, jasmonate, and salicylic acid hormones. It was observed that *spf1-1* and *spf2-2* mutants are less sensitive to ABA (abscisic acid) treatment; the induction of ABA response genes was reduced in *spf1-1* mutant plants compared to WT. It was demonstrated that SPF1 is capable of regulating ABI5 (ABA-insensitive5) and MYB30 (MYB domain protein30); these proteins regulate ABA signaling during early seedling development. In *spf1-1*, mutant plants ABI5 and MYB30 accumulate to greater levels than in WT. SPF1 transcription increases in ABA treated seeds, but not in seedlings (Wang et al., 2018).

OTS1/2 also shows an ABA phenotype, *ots1-1 ots2-1* double mutants have a lower germination success rate, and this physiological trait can be a marker of ABA. The root length of *ots1-1 ots2-1* is shorter on ABA, compared to WT, and germination is delayed in *ots1-1 ots2-1* grown on ABA. Additionally, the stomatal size of *ots1-1 ots2-1* is greater than WT when ABA is added (Castro et al., 2016).

The double mutant *ots1-1 ots2-1* is less sensitive to JA (jasmonic acid), than WT (Srivastava et al., 2018). This is believed to be due to JAZ6 (jasmonate-ZIM-domain protein6) and JAZ1 (jasmonate-ZIM-domain protein1), JA repressor proteins, being SUMOylated and deSUMOlyated by OTS1/2. SUMOylation of the JAZ repressors stabilizes the proteins; SUMOylated JAZ6 is less capable of interacting with the JA receptor COI1 (coronatine-insensitive1). Stimulated by JA, COI1 binds to JAZ6 mediating the degradation of JAZ6 *via* the ubiquitin pathway. The *ots1-1 ots2-1* mutants display JA insensitivity as the JAZ proteins are more SUMOylated in the *ots1-1 ots2-1* background and thus are more stable; due to

TABLE 3 | Table of known hormones in plants and identified SUMO proteases that have a role in the hormone pathway, highlighting the hormone pathways where SUMO proteases have not currently been identified to have a role, which may be a research opportunity.

Hormone	Role of hormone	SUMO protease
Gibberellin	Plant growth, floral development, fruit growth	OTS1, OTS2, ESD4
Auxin	Apical dominance, tropism, branching, lateral roots	
Cytokinin	Releases lateral buds from apical dominance, delays senescence	
Ethylene	Flowering/fruit ripening, stress response, seed germination	
Abscisic acid	Stomatal closure, drought response, seed maturation, germination, root shoot growth	OTS1, OTS2, SPF1, SPF2
Jasmonic acid	Plant defense from insects, necrotrophy pathogen response, root growth	OTS1, OTS2
Salicylic acid	System acquired resistance to pathogens, biotrophic pathogen	OTS1, OTS2, ESD4
Brassinosteriods	Cell division/elongation in stem/roots, photomorphogenesis, reproductive development, leaf senescence	OTS1, OTS2
Strigolactone	Branching, leaf senescence, root development, plant microbe interaction	

less interaction with COI1, the JAZ6 repressors block downstream signaling of JA (Srivastava et al., 2018).

OTS1/2 have also been shown to play a role in the SA pathway. The *ots1-1 ots2-1* double mutant has more SA signaling genes upregulated. This may be due to SA biosynthesis genes also being upregulated in the *ots1-1 ots2-1* mutant including ICS1, an SA biosynthesis gene, which is further increased when the plants are subjected to SA or an SA functional analogue. The mutants may lack restrictive regulation of ICS1 gene transcription. Furthermore, OTS1/2 are degraded in SA suggesting that they negatively regulate SA signaling and provide a feedback mechanism. In high levels of SA, OTS1 and OTS2 are degraded; when OTS1 and OTS2 are more abundant, they lower SA levels by reducing ICS1 levels, and this may be *via* deSUMOylation of a transcription factor that has not yet been identified (Bailey et al., 2016).

SUMOylation also determines the interaction of GA (gibberellins) receptors with DELLA proteins. GA is a growth promoting hormone, stimulating the degradation of growth-repressor DELLA proteins. SUMOylated DELLA proteins are stabilized and therefore accumulate and act to inhibit growth through DNA binding. DeSUMOylation of DELLA proteins by OTS1 allows these proteins to interact with the GA receptors GID1 (gibberellin-insensitive dwarf1), resulting in their degradation and therefore repression of the DELLA inhibitory pathway, thus allowing plant growth. The double mutant *ots1-1 ots2-1* has increased levels of DELLA due to higher levels of SUMOylation and therefore stabilization of the protein. When SUMO is conjugated to DELLA, it changes the conformation of GID1 (the GA receptor that promotes degradation of DELLA *via* the ubiquitin pathway) through a SIM site in GID1, preventing GID1 from promoting degradation of DELLA (Conti et al., 2014).

Most studies of the posttranslational control of the GA pathway focus on the DELLA proteins, the repressor proteins of the hormonal pathway. The DELLA proteins interact with and control the stability of SLY1 (sleepy1) which forms the Skp, CULLIN, F-box (SCF), and complex of E3 ubiquitin ligases that polyubiquitinate and degrades the DELLA proteins. SLY1 encodes an F-box protein that provides substrate specificity of the SCF complex recognizing and binding the DELLA proteins. SLY1 is SUMOylated by SIZ1, a SUMO E3 ligase, upon SUMOylation SLY1 is stabilized and activated. A non-SUMOylatable mutated SLY1 protein has the same dwarf phenotype as a *sly1-1* knockout plants. The SUMO protease ESD4 was identified as the SUMO protease cleaves SUMO from SLY1. In *esd4-1* mutant plants, there were higher levels of SLY1 protein, due to higher levels of SLY1 SUMOylation resulting in stability and activation of SLY1, degrading more DELLA proteins resulting in more GA signaling (Kim et al., 2015).

RESPONSES TO BIOTIC ENVIRONMENT

The role of SUMO proteases in immunity has been speculated for some time as plant pathogens including *Xanthomonas campestris, Ralstonia solanacearum*, *Pseudomonas syringae*, *Erwinia pyrifoliae*, and *Rhizobium* spp. utilize effector proteins, which are injected into plants to overcome the host defense, which have sequence homology to ULP SUMO proteases and display efficient isopeptidase activity to SUMO1/2 and SUMO3 (Orth et al., 1999; Orth et al., 2000; Deslandes et al., 2003; Hotson et al., 2003; Hotson and Mudgett, 2004; Roden et al., 2004; Bartetzko et al., 2009; Kim et al., 2013). The bacteria that causes bacterial spot (*X. campestris* pv. *vesicatoria [X.c.v.])* does not possess an endogenous SUMOylation system; however, it injects an effector into host cells that is capable of deSUMOylating protein targets in host cells and prevent hypersensitive response (Orth et al., 2000). This highlights the important role of SUMO proteases in plant immunity and how modulating SUMO protease activity can play a critical role in pathogen resistance. Understanding the SUMOylated proteins the effector proteases are targeting may help provide information on important SUMOylated substrates in plant pathogen defense.

DeSI3a is a cell membrane–bound SUMO protease that plays a role in PAMP (pathogen-associated molecular patterns) detection. Upon detection of flagellin, FLS2 is SUMOylated triggering the release of BIK1 (Botrytis-induced kinase1), a cytoplasmic kinase resulting in downstream signaling in innate immunity. When flagellin is perceived, DeSI3a is degraded which enhances FLS2 SUMOylation, triggering BIK1 dissociation and downstream intracellular immune signaling. Mutant *desi3a-1* plants do not have different global SUMO levels compared to WT, suggesting that DeSI3a acts on a narrow range of targets; however, it did exhibit increased transcript levels of key defense genes upon treatment with flg22 (flagellin22). Additionally, FLS2 in the *desi3a-1* background exhibited hyper SUMOylation compared to FLS2 in the WT background, this in turn resulted in a greater release of BIK1 in the *desi3a-1* background due to greater ROS (reactive oxygen species) burst levels and MAPK (mitogen-activated protein kinases) activation in this background (Orosa et al., 2018).

OTS1 and OTS2 have been implicated in having a role in pathogen defense; the *ots1-1 ots2-1* double mutant has increased resistance to *Pst* DC3000 (*P. syringae* pv. *tomato*). This may be due to the increased expression of PR1 and PR2 (pathogenesis-related 1/2) (pathogen defense genes) and higher levels of SA, caused by higher expression of SA biosynthesis genes such as ICS1. SA binds in plants to pathogen-related proteins that interact with transcription factors activating SA-mediated defense and enabling hypersensitive cell death response (Halim et al., 2006).

While *esd4-1* mutants have not been phenotyped for pathogen resistance, it can be hypothesized that it may have increased pathogen resistance. This is because the *esd4-1* mutant exhibit increased levels of SA which provides resistance to pathogens. Additionally, the *esd4-1* mutant has increased expression of PR1, a pathogen defense gene (Villajuana-Bonequi et al., 2014).

The *ots1-1 ots2-1* double mutant is more susceptible to *Botrytis cinerea* necrotrophs, having larger nectrophic lesions than WT likely due to *ots1-1 ots2-1* double mutants being less sensitive to JA. With some exceptions, JA usually activates defense against necrotrophic pathogens and herbivorous insects, whereas SA is often used in response to biotrophic pathogens (Glazebrook, 2005; Howe and Jander, 2008). As has already been described, in the *ots1-1 ots2-1* mutants, JAZ6 and JAZ1 are SUMOylated and stable. During *B. cinerea* infection, JAZ6 SUMOylation is enhanced and OTS1 degradation occurs. This results in *ots1-1 ots2-1* plants exhibiting more sensitivity to *B. cinerea* pathogens, as JAZ6 is more SUMOylated and is more stable and less able to interact with COI1, blocking the JA signaling cascade (Srivastava et al., 2018).

RESPONSES TO ABIOTIC ENVIRONMENT

Due to the SUMO proteases playing a key role in responding to stress, alterations in SUMO protease protein levels may not provide a clear phenotype under healthy conditions. The phenotypes may only be observed when a plant is stressed.

OTS has been shown to influence many responses to the environment. Initially, OTS1 was identified due to high salt sensitivity; *ots1-1 ots2-1* root growth is significantly inhibited when grown on high salt. In high salt environments, OTS1/OTS2 is degraded while gene transcription remains unchanged (Conti et al., 2008). Similar to salt stress, OTS1/OTS2 have also been identified with having a role in osmotic stress. These two proteases have been identified as the proteases that removes SUMO from ARF7 (auxin response factor7), a transcription factor that induces expression of its target genes in an asymmetric manner in lateral root founder cells, providing roots with hydropatterning. When the root is in a wet environment, e.g., surface contact with an agar plate, ARF7 is deSUMOylated by OTS1/2 resulting in transcription of AF7 target genes and lateral roots formation in the direction of the water. When the root is in a dry environment e.g., the part of the root above the agar, ARF7 remains SUMOylated enabling interaction with IAA3 (indole-3-acetic acid inducible3), a repressor protein with a SIM site, preventing downstream transcription of ARF7 target genes. This prevents lateral roots growing in dry environments (Orosa-Puente et al., 2018). Placing *ots1-1 ots2-1* seedlings on media containing PEG (polyethylene glycol) or mannitol demonstrated that the double mutant is hypersensitive to osmotic stress, which may demonstrate that the proteases promote resistance to osmotic stress and not the ionic component of salt stress. This may be due to *ots1-1 ots2-1* having increased stomatal aperture (Castro et al., 2016). In rice, knocking out OTS1/2 promotes drought tolerance; rice OTS1-RNAi lines are much more sensitive to ABA and survive better in drought conditions losing less water. *Os*OTS1 interacts with *Os*bZIP (basic leucine zipper domain), a transcription factor that regulates ABA and drought responses. In the *Os*OTS1 RNAi lines, *Os*bZIP23 has higher levels of SUMOylation and is stabilized, leading to the transcription of more drought tolerant genes. *Os*OTS1 is degraded by exposure to desiccation, mannitol, and ABA, working as a feedback loop to stabilize *Os*bZIP23 under drought conditions (Srivastava et al., 2017). Srivastava et al. (2016a), also identified that rice *Os*OTS1 RNAi lines have a lower germination success rate; this physiological trait can be a marker of ABA (Srivastava et al., 2016a; Srivastava et al., 2016b). Castro (2013) reported a single mutant phenotype that *ots1-1* single mutants have an increased drought tolerance, while *ots2-1* mutants exhibit the same level of phenotypic drought tolerance as WT controls (Castro, 2013).

Another abiotic stress the OTS SUMO proteases have a role in is light. PHYB (phytochrome B) is a light absorbing photoreceptor that cycles between active and inactive states and switches to regulate photomorphogenesis. PHYB interacts with PIF (phytochrome-interacting factor) in low light levels which blocks photomorphogenesis. PHYB is SUMOylated in response to light; in low light levels, PHYB has low levels of SUMOylation; in high light, the levels of SUMOylated PHYB largely increase. When PHYB is SUMOylated, it blocks the interaction of PHYB with PIF5, inhibiting elongation and promoting growth. SUMOylation desensitizes PHYB signaling. OTS1/2 regulate PHYB action by deconjugating SUMO from PHYB. OTS1 therefore controls fundamental processes in plants such as inhibition of transcription factors and photomorphogenesis (Sadanandom et al., 2015).

OTS1 has also been implicated in copper tolerance; high levels of copper in the soil can cause plant toxicity. *Ots1-2* knockout mutant exhibited increased sensitivity to excess copper. Under excess copper, OTS1 regulates photosynthetic activity and ROS accumulation. When WT plants are subjected to a high dose of copper, the levels of SUMOylated proteins in a WT plant risesteadily, then fall with time. However, *ots1-2* plants have a constantly high level of SUMOylated proteins that does not show much of a response to the high levels of copper. OTS1 was shown to function in copper uptake and distribution; in the *ots1-2* mutant, more copper was detected in seedlings shoots and roots compared to WT; additionally, these knockout plants had greater expression of genes responding to high copper when placed on excess copper media than WT (Zhan et al., 2018).

Lastly, OTS1 and OTS2 also have a role in controlling the plants biological clock. CCA1 (circadian clock-associated1) is a novel regulator of key clock proteins and is SUMOylated at the end of the night/dawn phase. When CCA1 is SUMOylated, DNA binding affinity is reduced, which was seen in the *ots1-1 ots2-1* double mutant. The results demonstrate that SUMOylation also plays a role in regulating the biological clock in plants; CCA1 binds to over 1,500 gene promoters; imbalances in SUMOylation of CCA1 could have wide consequences for the growth and health of plants (Hansen et al., 2018).

FUTURE RESEARCH

Analyses of SUMO proteases using gain-of-function and loss-of-function studies have shown involvement in various cellular processes such as hormone signaling, plant defense, abiotic stress, enzyme activity, cell cycle progression, and plant development (Melchior, 2000; Lois et al., 2003; Murtas et al., 2003; Conti et al., 2008; Budhiraja et al., 2009; Hickey et al., 2012; Conti et al., 2014; Nelis et al., 2015; Sadanandom et al., 2015; Bailey et al., 2016). The SUMO proteases have been demonstrated to be important molecules in controlling these processes. However, there still remain some important questions that have yet to be answered on SUMO proteases which the last section will highlight.

Unidentified SUMO Proteases

Currently, there are many SUMO proteases that have been identified through bioinformatic techniques but have not yet been functionally characterized using genetic, physiological, and biochemical approaches. These uncharacterized proteases include all but one of the DeSI proteases and two ULP proteases, FUG1 and ELS2, as have been earlier highlighted. Characterizing these proteases and understanding their molecular targets and localization may spread more light on the many pathways SUMO has a role in.

Despite this, however, among the SUMO machinery, the SUMO proteases are the most numerous family members, and they also show substrate specificity. Due to a small fraction of proteins being SUMOylated at a given time, SUMO proteases may play an important regulatory role in SUMOylation (Chosed et al., 2006; Colby et al., 2006; Yates et al., 2016; Benlloch and Lois, 2018). A large number of SUMO proteases may be required as SUMOylation specificity comes from spatiotemporal determinants, and thus, such a large number of proteins are required (Psakhye and Jentsch, 2012). Additionally, there is a large variation in the N-terminal domain of the SUMO proteases, which may provide specificity for the proteases. Some PTMs confer specificity by providing modifiers to protein complexes. In deubiquitinating enzymes (DUBs), additional levels of regulation are applied to the enzymes by forming protein complexes with "modifier" proteins. Scaffold proteins ensure DUBs with low affinity, but good catalytic capability for ubiquitin has substrates in close proximity. Adaptor proteins can bind to the DUB/scaffold protein and target protein to bring the ubiquitin into close proximity. These additional proteins ensure the correct protein substrate, and DUBs are in the right place at the right time; these types of proteins have not been identified in the SUMO system yet. Instead, the large variety in the N-terminal domains in the SUMO proteases may confer the role of these additional modifiers to the SUMO proteases, thus requiring a large number of differing SUMO proteases.

However, compared to the ubiquitin system, there is a much smaller number of SUMO proteases compared to ubiquitin proteases. To date, there are almost 100 different ubiquitin proteases belonging to five different protease families (Komander et al., 2009; Reyes-Turcu et al., 2009). It is likely that there are many other SUMO proteases to be identified. Some proteases that have currently, *via* bioinformatic techniques, been identified as a ubiquitin protease but have not yet been characterized may in fact be a SUMO protease, as was the case for USPL1 (Schulz et al., 2012).

Using predictive bioinformatic tools on already existing data may enable the identification of novel SUMO proteases. It is helpful that there are some known missing SUMO proteases, and this enables targeted searching. Some known missing SUMO proteases are proteases capable of maturing and deconjugating SUMO5, and deconjugating SUMO3 isoforms remain to be identified (Chosed et al., 2006; Colby et al., 2006). Furthermore, SUMO proteases may also play a role in additional modern techniques that could be utilized particularly to understand the proteases substrate specificity using molecular modeling and molecular dynamics methods. Additionally, it is likely that the SUMO proteases act in a complex web with some acting redundantly. Deciphering the role of individual SUMO proteases may require complex systems biology.

In addition to identifying more plant endogenous SUMO proteases, more research is also required into the pathogen effector molecules injected into plants that have SUMO protease activity. Plant pathogens infect plants with effector molecules that help dismantle host perception machinery and degrade host defense structures. As has earlier been discussed SUMO proteases have already been identified as playing a role in plant pathogen defense; effector molecules from various pathogens have been shown to have ULP protease homology and capable of deSUMOylation. There is a wide variety of pathogens and hosts, and each may have a different novel action of SUMO proteolytic activity. Additionally, understanding the SUMOylated substrates, the SUMO proteases target may help provide more information in pathogen disease progression and provide molecular targets to combat the disease. Currently of the identified pathogen effector molecules that have been identified most of the host target molecules are unknown.

In addition to SUMO proteases having a critical role in plant-pathogen interactions, the other major biotic stress plants can respond to is herbivorous attack. The role of SUMO proteases has not yet been explored. Due to the importance of SUMO proteases in responding to stress, it is likely that they will play a role in herbivore defense. A better understanding of these mechanisms may provide breeding targets in crop species to better protect crops against herbivore attack.

Research in Crops

SUMO has been proven to have a critical role in stress responses (Kurepa et al., 2003; Miura et al., 2007; Saracco et al., 2007; Golebiowski et al., 2009), and it has been hypothesized that the SUMO proteases provide the SUMO system with specificity (Yates et al., 2016). This has led to the hypothesis that the crop species may have a greater number of SUMO proteases due to the selection pressures that have been applied to domesticated plants and bred in for stress tolerance (Augustine et al., 2016; Garrido et al., 2018). Generally, this has been observed in maize, with nine proteases identified based on sequence similarity to *Arabidopsis* ESD4 and OTS1 and 2 (Augustine et al., 2016). The crop *Brassica* species (maize, rice and sorghum) were all found to have many more sequences that matched ULP protease domain than four other members of non-domesticated *Brassicas* that were examined, suggesting that crop domestication may result in diversification of the SUMO proteases (Garrido et al., 2018).

However, there has, currently, been limited research into the SUMO system in crops. Many components of the SUMO system have been identified by bioinformatic techniques for rice, wheat, maize, and soybean (Yates et al., 2016; Li et al., 2017), and the maize SUMO system has been reconstituted (Augustine et al., 2016). Of the limited research carried out on crops, mainly knockout and overexpression lines of SUMO proteases, they have shown phenotypes demonstrating their importance in crops. Rice SUMO protease knockout lines with sequence homology to *Arabidopsis* ELS1 and FUG1 have been generated and examined with the plants showing dwarf phenotype, defects in fertility, seed weight, and flowering timing (Rosa et al., 2018). Additionally, rice knockout lines of *Os*OTS1 have shown reduced germination rate and reduced primary root growth (Srivastava et al., 2016a). RNAi rice lines of *Arabidopsis* OTS1 and OTS2 show salt hypersensitivity (Srivastava et al., 2016b; Srivastava et al., 2017), much like the *Arabidopsis ots1-1 ots2-1* double mutant (Conti et al., 2008). Furthermore, over expressing *Arabidopsis* OTS1 in wheat led to improved plant growth under water stress in addition to higher moisture content, photosynthesis rate, and chlorophyll content (le Roux et al., 2019).

From limited research into the crop SUMO proteases, they are already proving to be vital to crop stress survival. Further studies into a wider variety of crops will likely provide greater insights into their important role in stress survival and may prove useful targets for breeders.

Regulation of Proteases

Understanding the regulation of the SUMO proteases can help explain how they are controlled and how they exert specificity to the SUMO system. The SUMO proteases are hypothesized in part to provide specificity by their specific expression, localization, regulation, sequestration, and degradation, although not many of these aspects are known for the SUMO proteases. Improving sophistication of cellular and molecular imaging may help shed light on how plants regulate the spatiotemporal location of the SUMO proteases.

A number of experiments have shown that the SUMO proteases are degraded by the ubiquitin protease system. During stress SUMO conjugates accumulate (Kurepa et al., 2003), which protects the plants, these conjugates may accumulate due to degradation of SUMO proteases by PTMs. OTS1 and OTS2 are degraded in high SA levels (Bailey et al., 2016), and DeSI3a is degraded by high flagellin levels (Orosa et al., 2018).

Transcription of the SUMO proteases may also react to stimulus—for example, SPF1 transcript levels increase in response to ABA (Wang et al., 2018). However, largely the transcriptional regulation and post translational modification of these proteins are not well understood. Elucidating the regulation of the proteases may help explain the role the proteases play in the SUMO system.

Role of SUMO Protease in a Dynamic Cell

When analysis of the *Arabidopsis* SUMOylome was carried out, many SUMOylated targets were found to be present in the nucleus (Miller et al., 2013). Many proteins were known to be involved with histones, chromatin remodeling, transcription activators, co-repressors, and DNA repair (Miller et al., 2013), and substrates related to chromatin and RNA-dependent processes in *Arabidopsis* are SUMOylated (Budhiraja et al., 2009). These substrates are involved in processes that include regulation of chromatin structure, splicing, translation, DNA endoreduplication, and DNA repair. This has been supported by similar studies in animal and yeast cells (Psakhye and Jentsch, 2012; Seifert et al., 2015). As the vast collection of proteins SUMO targets involve DNA, RNA, and proteins that interact with these biomolecules such as transcription factors, coactivators and repressors, and chromatin modifiers, it suggests that stress-induced SUMOylation targets these components, potentially rewiring the chromatin and changing the transcriptional environment, enabling plant survival (Saracco et al., 2007; Miller et al., 2013; Augustine and Vierstra, 2018; Rytz et al., 2018). This is further supported by SUMO pathway loss-of-function mutants, in particular SUMO protease mutants, showing stress sensitive response in *Arabidopsis* and rice (Miura et al., 2007; Conti et al., 2008; Srivastava et al., 2016b; Srivastava et al., 2017). It is already known that OTS1 is required for maintaining gene silencing, and SUMO E3 ligase, SIZ1, is also involved in silencing regulation (Liu et al., 2017b). However, little research has been carried out yet specifically examining the role of *Arabidopsis* SUMO mutants on the nucleus.

Additionally, when a cell is stressed, many nuclear-associated proteins are SUMOylated; when the stress is removed, the proteins become deSUMOylated again, returning to normal levels, enabling rapid reversible response to differing environmental stimuli. This SUMO response is also capable of displaying memory; if a second stress is induced immediately following, a stress the stress-induced SUMOylation pattern is suppressed (Kurepa et al., 2003; Miller et al., 2013). However, it is not yet understood how the SUMO system is capable of displaying memory, and this requires additional research.

However, with advances in knowledge and technology, the ability to extract and identify SUMOylated proteins may show that SUMO has a role in many aspects of the cell and is not as limited to the nucleus. Indeed, some SUMO proteases may specifically localize to other organelles in the cell.

CONCLUDING REMARKS

Since its discovery over 20 years ago, the role of SUMO in many different processes in plants has been uncovered. The role of SUMO in so many important aspects of plant biology, from hormonal processes, to abiotic responses to disease responses has demonstrated that SUMO is a critical post-translational modification in plants. In particular, the role of SUMO proteases has suggested that they play a vital role in regulating the SUMO cycle, making their role in plants highly critical. It is likely that more SUMO proteases will be identified with roles in numerous other pathways and in other components of the plant cell. With the identification of more SUMO proteases, it may help answer the big question in SUMO: how the SUMO system identifies targets and provides the specificity in SUMOylation. The specificity in the SUMO system may come from SUMO proteases providing specificity in deSUMOylation. With research continually uncovering important SUMOylated proteins in plants, further research is still required to understand how the SUMO proteases, through their combined action help regulate and maintain the plant SUMOylome to ensure proper growth, development, and appropriate stress responses.

AUTHOR CONTRIBUTIONS

RM and AS designed and wrote the article.

ACKNOWLEDGMENTS

We would like to acknowledge Catherine Gough for help proof-reading the manuscript.

ABBREVIATIONS

PTM, post translational modification; STUbL, SUMO-targeted ubiquitin ligases; SIM, SUMO-interacting motif; SAE1/2, SUMO-activating enzyme 1/2 ; SCE1, SUMO-conjugating enzyme 1;

SIZ1, SAP and MIZ1; HPY2, high ploidy 2; PIAL1, protein inhibitor of activated STAT-like 1; ULP1, ubiquitin-like protease 1; UBL, ubiquitin like; DeSI, DeSUMOylating isopeptidase; USPL1, ubiquitin-specific protease-like 1; ESD4, early in short days 4; FLC, flowering locus C; SENP1, sentrin-specific protease 1; NEM, N-ethylmaleimide; ELS1/2, ESD4-like SUMO protease 1/2; FUG1, fourth ULP gene 1; OTS1/2, overly tolerant to salt 1/2; RanGAP, Ran GTPase-activating protein; ScPCNA, proliferating cell nuclear agent; SPF1, SUMO protease related to fertility 1; ASP1, Arabidopsis SUMO protease 1; WT, wild type; PPPDE, peptidases-permuted papain fold peptidases; dsRNA, double stranded RNA; BZEL, BTB-ZF protein expressed in effector lymphocytes; FLS2, flagellin sensitive 2; UBP6, ubiquitin-specific protease 6; CAM, Calmodulin2; RGA, repressor of ga1-3; GAI, gibberellin-insensitive; GA, gibberellins; JA, jasmonic acid; SA, salicylic acid; ICS1, isochorisate synthase 1; ABA, abscisic acid; ABI5, ABA-insensitive 5; MYB30, MYB domain protein 30; JAZ6, jasmonate-ZIM-domain protein 6; COI1, coronatine-insensitive 1; GID1, gibberellin-insensitive dwarf 1; SLY1, sleepy 1; SCF, Skp, CULLIN, F-box; X.c.v., X. campestris pv. Vesicatoria; PAMP, pathogen-associated molecular patterns; BIK1, botrytis-induced kinase 1; Flg22, flagellin22; ROS, reactive oxygen species; MAPK, mitogen-activated protein kinases; Pst DC3000, Pseudomonas syringae pv. Tomato; PR1, pathogenesis-related 1; ARF7, auxin response factor 7; IAA3, indole-3-acetic acid inducible3; PEG, polyethylene glycol; OsbZIP, basic leucine zipper domain; PHYB, phytochrome B; PIF, phytochrome-interacting factor; CCA1, circadian clock-associated 1; DUBs, deubiquitinating enzymes.

REFERENCES

Augustine, R. C., and Vierstra, R. D. (2018). SUMOylation: re-wiring the plant nucleus during stress and development. *Curr. Opin. Plant Biol.* 45, 143–154. doi: 10.1016/j.pbi.2018.06.006

Augustine, R. C., York, S. L., Rytz, T. C., and Vierstra, R. D. (2016). Defining the SUMO system in maize: SUMOylation is up-regulated during endosperm development and rapidly induced by stress. *Plant Physiol.* 171 (3), 2191–2210. doi: 10.1104/pp.16.00353

Bailey, M., Srivastava, A., Conti, L., Nelis, S., Zhang, C., Florance, H., et al. (2016). Stability of small ubiquitin-like modifier (SUMO) proteases OVERLY TOLERANT TO SALT1 and -2 modulates salicylic acid signalling and SUMO1/2 conjugation in Arabidopsis thaliana. *J. Exp. Bot.* 67, 353–363. doi: 10.1093/jxb/erv468

Bartetzko, V., Sonnewald, S., Vogel, F., Hartner, K., Stadler, R., Hammes, U. Z., et al. (2009). The Xanthomonas campestris pv. vesicatoria type III effector protein XopJ inhibits protein secretion: evidence for interference with cell wall-associated defense responses. *Mol. Plant Microbe Interact.* 22 (6), 655–664. doi: 10.1094/MPMI-22-6-0655

Bayer, P., Arndt, A., Metzger, S., Mahajan, R., Melchior, F., Jaenicke, R., et al. (1998). Structure determination of the small ubiquitin related modifier SUMO-1. *J. Mol. Biol.* 280, 275–286. doi: 10.1006/jmbi.1998.1839

Benlloch, R., and Lois, L. M. (2018). Sumoylation in plants: mechanistic insights and its role in drought stress. *J. Exp. Bot.* 69, 4539–4554. doi: 10.1093/jxb/ery233

Budhiraja, R., Hermkes, R., Müller, S., Schmidt, J., Colby, T., Coupland, G., et al. (2009). Substrates related to chromatin and to RNA-dependent processes are modified by Arabidopsis SUMO isoforms that differ in a conserved residue with influence on de-sumoylation. *Plant Physiol.* 149, 1529–1540. doi: 10.1104/pp.108.135053

Bylebyl, G. R., Belichenko, I., and Johnson, E. S. (2003). The SUMO isopeptidase Ulp2 prevents accumulation of SUMO chains in yeast. *J. Biol. Chem.* 45, 44113–44120. doi: 10.1074/jbc.M308357200

Campananaro, A., Battaglia, R., Galbiati, M., Sadanandom, A., Tonelli, C., and Conti, L. (2016). SUMO proteases OTS1 and 2 control filament elongation through a DELLA-dependent mechanism. *Plant Reprod.* 29 (4), 287–290. doi: 10.1007/s00497-016-0292-8

Castaño-Miquel, L., Seguí, J., and Lois, L. M. (2011). Distinctive properties of Arabidopsis SUMO paralogues support the in vivo predominant role of AtSUMO1/2 isoforms. *Biochem. J.* 436:581–590. doi: 10.1042/BJ20101446

Castro, P. H., Bachmair, A., Bejarano, E. R., Coupland, G., Lois, L. M., Sadanandom, A., et al. (2018a). Revised nomenclature and functional overview of the ULP gene family of plant deSUMOylating proteases. *J. Exp. Bot.* 69 (19), 4505–4509. doi: 10.1093/jxb/ery301

Castro, P. H., Santos, M. A., Freitas, S., Cana-Quijada, P., Lourenco, T., Rodrigues, M. A. A., et al. (2018b). Arabidopsis thaliana SPF1 and SPF2 are nuclear-located ULP2-like SUMO proteases that act downstream of SIZ1 in plant development. *J. Exp. Bot.* 69 (19), 4633–4649. doi: 10.1093/jxb/ery265

Castro, P. H., Couto, D., Freitas, S., Verde, N., Macho, A. P., Huguet, S., et al. (2016). SUMO proteases ULP1c and ULP1d are required for development and osmotic stress responses in Arabidopsis thaliana. *Plant Mol. Biol.* 92, 143–159. doi: 10.1007/s11103-016-0500-9

Castro, P. H. A. R. F. (2013). *Functional analysis of the SUMO conjugation/deconjugation system during the development and stress response of Arabidopsis thaliana*. Universidade do Minho.

Catala, R., Ouyang, J., Abreu, I. A., Hu, Y., Seo, H., Zhang, X., et al. (2007). The Arabidopsis E3 SUMO ligase SIZ1 regulates plant growth and drought responses. *Plant Cell* 19, 2952–2966. doi: 10.1105/tpc.106.049981

Chosed, R., Mukherjee, S., Lois, L. M., and Orth, K. (2006). Evolution of a signalling system that incorporates both redundancy and diversity: Arabidopsis SUMOylation. *Biochem. J.* 398, 521–529. doi: 10.1042/BJ20060426

Cioce, M., and Lamond, A. I. (2005). Cajal bodies: a long history of discovery. *Annu. Rev. Cell Dev. Biol.* 21, 105–131. doi: 10.1146/annurev.cellbio.20.010403.103738

Colby, T., Matthäi, A., Boeckelmann, A., and Stuible, H. P. (2006). SUMO-conjugating and SUMO-deconjugating enzymes from Arabidopsis. *Plant Physiol.* 142 (1), 318–332. doi: 10.1104/pp.106.085415

Conti, L., Nelis, S., Zhang, C., Woodcock, A., Swarup, R., Galbiati, M., et al. (2014). Small ubiquitin-like modifier protein SUMO enables plants to control growth independently of the phytohormone gibberellin. *Dev. Cell* 28, 102–110. doi: 10.1016/j.devcel.2013.12.004

Conti, L., Price, G., O'Donnell, E., Schwessinger, B., Dominy, P., and Sadanandom, A. (2008). Small ubiquitin-like modifier proteases OVERLY TOLERANT TO SALT1 and -2 regulate salt stress responses in Arabidopsis. *Plant Cell* 20 (10), 2894–2908. doi: 10.1105/tpc.108.058669

Crozet, P., Margalha, L., Confraria, A., Rodrigues, A., Martinho, C., Adamo, M., et al. (2014). Mechanisms of regulation of SNF1/AMPK/SnRK1 protein kinases. *Front. Plant Sci* 5, 190. doi: 10.3389/fpls.2014.00190

Deslandes, L., Olivier, J., Peeters, N., Feng, D. X., Khounlotham, M., Boucher, C., et al. (2003). Physical interaction between RRS1-R, a protein conferring resistance to bacterial wilt, and PopP2, a type III effector targeted to the plant nucleus. *Proc. Natl. Acad. Sci.* 100, 8024–8029. doi: 10.1073/pnas.1230660100

Drabikowski, K., Ferralli, J., Kistowski, M., Oledzki, J., Dadlez, M., and Chiquet-Ehrismann, R. (2018). Comprehensive list of SUMO targets in Caenorhabditis elegans and its implication for evolutionary conservation of SUMO signaling. *Sci. Rep.* 8 (1), 1139. doi: 10.1038/s41598-018-19424-9

Elrouby, N., and Coupland, G. (2010) Proteome-wide screens for small ubiquitin-like modifier (SUMO) substrates identify Arabidopsis proteins implicated in diverse biological processes. *PNAS* 107 (40) 17415-17420. doi: 10.1073/pnas.1005452107

Elrouby, N., Bonequi, M. V., Porri, A., and Coupland, G. (2013). Identification of Arabidopsis SUMO-interacting proteins that regulate chromatin activity and developmental transitions. *Proc. Natl. Acad. Sci.* 110, 19956–19961. doi: 10.1073/pnas.1319985110

Garrido, E., Srivastava, A. K., and Sadanandom, A. (2018). Exploiting protein modification systems to boost crop productivity: SUMO proteases in focus. *J. Exp. Bot.* 69 (19), 4625–4632. doi: 10.1093/jxb/ery222

Giaever, G., Chu, A. M., Ni, L., Connelly, C., Riles, L., Veronneau, S., et al. (2002). Functional profiling of the Saccharomyces cerevisiae genome. *Nature* 418, 387–391. doi: 10.1038/nature00935

Gillies, J., and Hochstrasser, M. A. (2012). New class of SUMO proteases. *EMBO Rep.* 13, 284–285. doi: 10.1038/embor.2012.34

Glazebrook, J. (2005). Contrasting mechanisms of defense against biotrophic and necrotrophic pathogens. *Annu. Rev. Phytopathol.* 43, 205–227. doi: 10.1146/annurev.phyto.43.040204.135923

Golebiowski, F., Matic, I., Tatham, M. H., Cole, C., Yin, Y., Nakamura, A., et al. (2009). System-wide changes to SUMO modifications in response to heat shock. *Sci. Signal.* 2 (72), ra24. doi: 10.1126/scisignal.2000282

Golubtsov, A., Kääriäinen, L., and Caldentey, J. (2006). Characterization of the cysteine protease domain of Semliki Forest virus replicase protein nsP2 by *in vitro* mutagenesis. *FEBS Lett.* 580 (5), 1502–1508. doi: 10.1016/j.febslet.2006.01.071

Gong, L., and Yeh, E. T. (2006). Characterization of a family of nucleolar SUMO-specific proteases with preference for SUMO-2 or SUMO-3. *J. Biol. Chem.* 281, 15869–15877. doi: 10.1074/jbc.M511658200

Halim, V. A., Vess, A., Scheel, D., and Rosahl, S. (2006). The role of salicylic acid and jasmonic acid in pathogen defence. *Plant Biol. (Stuttg.)* 8 (3), 307–313. doi: 10.1055/s-2006-924025

Hannoun, Z., Greenhough, S., Jaffray, E., Hay, R. T., and Hay, D. C. (2010). Post-translational modification by SUMO. *Toxicology* 278, 288–293. doi: 10.1016/j.tox.2010.07.013

Hansen, L. L., Imrie, L., Le Bihan, T., van den Burg, H. A., and van Ooijen, G. (2017). Sumoylation of the plant clock transcription factor CCA1 suppresses DNA binding. *J. Biol. Rhythms* 32 (6), 570–582. doi: 10.1177/0748730417737695

Hay, R. T. (2005). SUMO: a history of modification. *Mol. Cell* 18, 1–12. doi: 10.1016/j.molcel.2005.03.012

Hermkes, R., Fu, Y. F., Nürrenberg, K., Budhiraja, R., Schmelzer, E., Elrouby, N., et al. (2011). Distinct roles for Arabidopsis SUMO protease ESD4 and its closest homolog ELS1. *Planta* 233 (1), 63–73. doi: 10.1007/s00425-010-1281-z

Hickey, C. M., Wilson, N. R., and Hochstrasser, M. (2012). Function and regulation of SUMO proteases. *Nat. Rev. Mol. Cell Biol.* 13, 755–766. doi: 10.1038/nrm3478

Hotson, A., and Mudgett, M. B. (2004). Cysteine proteases in phytopathogenic bacteria: identification of plant targets and activation of innate immunity. *Curr. Opin. Plant Biol.* 7, 384–390. doi: 10.1016/j.pbi.2004.05.003

Hotson, A., Chosed, R., Shu, H., Orth, K., and Mudgett, M. B. (2003). Xanthomonas type III effector XopD targets SUMO-conjugated proteins in planta. *Mol. Microbiol.* 50, 377–389. doi: 10.1046/j.1365-2958.2003.03730.x

Hou, S., Jamieson, P., and He, P. (2018). The cloak, dagger and shield: proteases in plant-pathogen interactions. *Biochem. J.* 475, 2491–2509. doi: 10.1042/BCJ20170781

Howe, G. A., and Jander, G. (2008). Plant immunity to insect herbivores. *Annu. Rev. Plant Biol.* 59, 41–66. doi: 10.1146/annurev.arplant.59.032607.092825

Hutten, S., Chachami, G., Winter, U., Melchior, F., and Lamond, A. I. (2014). A role for the Cajalbody-associated SUMO isopeptidase USPL1 in snRNA transcription mediated by RNA polymerase II. *J. Cell Sci.* 127, 1065–1078. doi: 10.1242/jcs.141788

Johnson, E. S. (2004). Protein modification by SUMO. *Annu. Rev. Biochem.* 73, 355–382. doi: 10.1146/annurev.biochem.73.011303.074118

Kerscher, O., Felberbaum, R., and Hochstrasser, M. (2006). Modification of proteins by ubiquitin and ubiquitin-like proteins. *Annu. Rev. Cell Dev. Biol.* 22, 159–180. doi: 10.1146/annurev.cellbio.22.010605.093503

Kim, S. I., Park, B. S., Kim, D. Y., Yeu, S. Y., Song, S. I., Song, J. T., et al. (2015). E3 SUMO ligase AtSIZ1 positively regulates SLY1-mediated GA signalling and plant development. *Biochem. J.* 469, 299–314. doi: 10.1042/BJ20141302

Kim, J. G., Stork, W., and Mudgett, M. B. (2013). Xanthomonas type III effector XopD desumoylates tomato transcription factor SlERF4 to suppress ethylene responses and promote pathogen growth. *Cell Host Microbe* 13, 143–154. doi: 10.1016/j.chom.2013.01.006

Komander, D., Clague, M. J., and Urbe, S. (2009). Breaking the chains: structure and function of the deubiquitinases. *Nat. Rev. Mol. Cell Biol.* 10 (8), 550–563. doi: 10.1038/nrm2731

Kong, X., Luo, X., Qu, G. P., Liu, P., and Jin, J. B. (2017). Arabidopsis SUMO protease ASP1 positively regulates flowering time partially through regulating FLC stability. *J. Integr. Plant Biol.* 59, 15–29. doi: 10.1111/jipb.12509

Kroetz, M. B., Su, D., and Hochstrasser, M. (2009). Essential role of nuclear localization for yeast Ulp2 SUMO protease function. *Mol. Biol. Cell* 20, 2196–2206. doi: 10.1091/mbc.e08-10-1090

Kurepa, J., Walker, J. M., Smalle, J., Gosink, M. M., Davis, S. J., Durham, T. L., et al. (2003). The small ubiquitn-like modifier (SUMO) protein modification system in Arabidopsis. *J. Biol. Chem.* 278, 6862–6872. doi: 10.1074/jbc.M209694200

le Roux, M. L., Kunert, K. J., van der Vyver, C., Cullis, C. A., and Botha, A.-M. (2019). Expression of a small ubiquitin-like modifier protease increases drought tolerance in wheat (Triticum aestivum L.). *Front. Plant Sci.* 10, 266 eCollection. doi: 10.3389/fpls.2019.00266

Li, S.-J., and Hochstrasser, M. (1999). A new protease required for cell-cycle progression in yeast. *Nature* 398, 246–251. doi: 10.1038/18457

Li, S.-J., and Hochstrasser, M. (2003). The Ulp1 SUMO isopeptidase: distinct domains required for viability, nuclear envelope localization, and substrate specificity. *J. Cell Biol.* 160, 1069–1081. doi: 10.1083/jcb.200212052

Li, S.-J., and Hochstrasser, M. (2000). The yeast ULP2 (SMT4) gene encodes a novel protease specific for the ubiquitin-like Smt3 protein. *Mol. Cell. Biol.* 20, 2367–2377. doi: 10.1128/MCB.20.7.2367-2377.2000

Li, Y., Wang, G., Xu, Z., Li, J., Sun, M., Guo, J., et al. (2017). Organisation and regulation of soybean SUMOylation system under abiotic stress conditions. *Front. Plant Sci* 8, 1458. doi: 10.3389/fpls.2017.01458

Liu, L., Jiang, Y., Zhang, X., Wang, X., Wang, Y., Han, Y., et al. (2017a). Two SUMO proteases SUMO PROTEASE RELATED TO FERTILITY1 and 2 are required for fertility in Arabidopsis. *Plant Physiol.* 175 (4), 1703–1719. doi: 10.1104/pp.17.00021

Liu, L., Yan, X., Kong, X., Zhao, Y., Gong, Z., Jin, J. B., et al. (2017b). Transcriptional gene silencing maintained by OTS1 SUMO protease requires a DNA-dependent polymerase V-dependent pathway. *Plant Physiol.* 173, 655–667. doi: 10.1104/pp.16.01365

Lois, L. M. (2010). Diversity of the SUMOylation machinery in plants. *Biochem. Soc. Trans.* 38, 60–64. doi: 10.1042/BST0380060

Lois, L. M., Lima, C. D., and Chua, N. H. (2003). Small ubiquitin-like modifier modulates abscisic acid signaling in Arabidopsis. *Plant Cell* 15, 1347–1359. doi: 10.1105/tpc.009902

Melchior, F. (2000). SUMO–nonclassical ubiquitin. *Annu. Rev. Cell Dev. Biol.* 16, 591–626. doi: 10.1146/annurev.cellbio.16.1.591

Meluh, P. B., and Koshland, D. (1995). Evidence that the MIF2 gene of Saccharomyces cerevisiae encodes a centromere protein with homology to the mammalian centromere protein CENP-C. *Mol. Biol. Cell* 6, 793–807. doi: 10.1091/mbc.6.7.793

Miller, M. J., Barrett-Wilt, G. A., Hua, Z., and Vierstra, R. D. (2010). Proteomic analyses identify a diverse array of nuclear processes affected by small ubiquitin-like modifier conjugation in Arabidopsis. *Proc. Natl. Acad. Sci. U.S.A.* 107, 16512–16517. doi: 10.1073/pnas.1004181107

Miller, M. J., Scalf, T. C., Rytz, S. L., Hubler, L. M., and Vierstra, R. D. (2013). Quantitative proteomics reveals factors regulating RNA biology as dynamic targets of stress-induced SUMOylation in Arabidopsis. *Mol. Cell Proteomics* 12, 449–463. doi: 10.1074/mcp.M112.025056

Millar, A. H., Heazlewood, J. L., Giglione, C., Holdsworth, M. J., Bachmair, A., and Schulze, W. X. (2019). The scope, functions, and dynamics of posttranslational protein modifications. *Annu. Rev. Plant Biol.* 70, 119–151. doi: 10.1146/annurev-arplant-050718-100211

Miura, K., Jin, J. B., Lee, J., Yoo, C. Y., Stirm, V., Miura, T., et al. (2007). SIZ1-mediated sumoylation of ICE1 controls CBF3/DREB1A expression and freezing tolerance in *Arabidopsis. Plant Cell* 19, 1403–1414. doi: 10.1105/tpc.106.048397

Moon, B. C., Choi, M. S., Kang, Y. H., Kim, M. C., Cheong, M. S., Park, C. Y., et al. (2005). Arabidopsis ubiquitin-specific protease 6 (AtUBP6) interacts with calmodulin. *FEBS Lett.* 579, 3885–3890. doi: 10.1016/j.febslet.2005.05.080

Mossessova, E., and Lima, C. D. (2000). Ulp1-SUMO crystal structure and genetic analysis reveal conserved interactions and a regulatory element essential for cell growth in yeast. *Mol. Cell* 5, 865–876. doi: 10.1016/S1097-2765(00)80326-3

Mukhopadhyay, D., and Dasso, M. (2007). Modification in reverse: the SUMO proteases. *Trends Biochem. Sci.* 32, 286–295. doi: 10.1016/j.tibs.2007.05.002

Mukhopadhyay, D., Ayaydin, F., Kolli, N., Tan, S. H., Anan, T., Kametaka, A., et al. (2006). SUSP1 antagonizes formation of highly SUMO2/3-conjugated species. *J. Cell Biol.* 174, 939–949. doi: 10.1083/jcb.200510103

Murtas, G., Reeves, P. H., Fu, Y.-F., Bancroft, I., Dean, C., and Coupland, G. (2003). A nuclear protease required for flowering-time regulation in Arabidopsis reduces the abundance of SMALL UBIQUITIN-RELATED MODIFIER conjugates. *Plant Cell* 15 (10), 2308–2319. doi: 10.1105/tpc.015487

Nelis, S., Conti, L., Zhang, C., and Sadanandom, A. (2015). A functional small ubiquitin-like modifier (SUMO) interacting motif (SIM) in the gibberellin hormone receptor GID1 is conserved in cereal crops and disrupting this motif does not abolish hormone dependency of the DELLA-GID1 interaction. *Plant Signal. Behav.* 10 (2), e987528. doi: 10.4161/15592324.2014.987528

Nie, M., Xie, Y., Loo, J. A., and Courey, A. J. (2009). Genetic and proteomic evidence for roles of Drosophila SUMO in cell cycle control, Ras signaling, and early pattern formation. *PLoS One* 4 (6), e5905. doi: 10.1371/journal.pone.0005905

Nizami, Z., Deryusheva, S., and Gall, J. G. (2010). The Cajal body and histone locus body. *Cold Spring Harb. Perspect. Biol.* 2 (7), a000653. doi: 10.1101/cshperspect.a000653

Novatchkova, M., Budhiraja, R., Coupland, G., Eisenhaber, F., and Bachmair, A. (2004). SUMO conjugation in plants. *Planta* 220, 1–8. doi: 10.1007/s00425-004-1370-y

Novatchkova, M., Tomanov, K., Hofmann, K., Stuible, H. P., and Bachmair, A. (2012). Update on sumoylation: defining core components of the plant SUMO conjugation system by phylogenetic comparison. *New Phytol.* 195, 23–31. doi: 10.1111/j.1469-8137.2012.04135.x

Orosa, B., Yates, G., Verma, V., Srivastava, A. K., Srivastava, M., Campanaro, A., et al. (2018). SUMO conjugation to the pattern recognition receptor FLS2 triggers intracellular signalling in plant innate immunity. *Nat. Commun.* 9 (1), 5185. doi: 10.1038/s41467-018-07696-8

Orosa-Puente, B., Leftley, N., von Wangenheim, D., Banda, J., Srivastava, A. K., Hill, K., et al. (2018). Root branching toward water involves posttranslational modification of transcription factor ARF7. *Science* 362 (6421), 1407–1410. doi: 10.1126/science.aau3956

Orth, K., Palmer, L. E., Bao, Z. Q., Stewart, S., Rudolph, A. E., Bliska, J. B., et al. (1999). Inhibition of the mitogen-activated protein kinase kinase superfamily by a Yersinia effector. *Science* 285 (5435), 1920–1923. doi: 10.1126/science.285.5435.1920

Orth, K., Xu, Z., Mudgett, M. B., Bao, Z. Q., Palmer, L. E., Bliska, J. B., et al. (2000). Disruption of signaling by Yersinia effector YopJ, a ubiquitin-like protein protease. *Science* 290, 1594–1597. doi: 10.1126/science.290.5496.1594

Panse, V. G., Kuster, B., Gerstberger, T., and Hurt, E. (2003). Unconventional tethering of Ulp1 to the transport channel of the nuclear pore complex by karyopherins. *Nat. Cell Biol.* 5, 21–27. doi: 10.1038/ncb893

Psakhye, I., and Jentsch, S. (2012). Protein group modification and synergy in the SUMO pathway as exemplified in DNA repair. *Cell* 151, 807–820. doi: 10.1016/j.cell.2012.10.021

Rawlings, N. D., Barrett, A. J., Thomas, P. D., Huang, X., Bateman, A., and Finn, R. D. (2018). The MEROPS database of proteolytic enzymes, their substrates and inhibitors in 2017 and a comparison with peptidases in the PANTHER database. *Nucleic Acids Res.* 46, D624–D632. doi: 10.1093/nar/gkx1134

Rawlings, N. D., Morton, F. R., Kok, C. Y., Kong, J., and Barrett, A. J. (2008). MEROPS: the peptidase database. *Nucleic Acids Res.* 36, D320–D325. doi: 10.1093/nar/gkm954

Reeves, P. H., Murtas, G., Dash, S., and Coupland, G. (2002). early in short days 4, a mutation in Arabidopsis that causes early flowering and reduces the mRNA abundance of the floral repressor FLC. *Development* 129, 5349–5361. doi: 10.1242/dev.00113

Reyes-Turcu, F. E., Ventii, K. H., and Wilkinson, K. D. (2009). Regulation and cellular roles of ubiquitin-specific deubiquitinating enzymes. *Annu. Rev. Biochem.* 78, 363–397. doi: 10.1146/annurev.biochem.78.082307.091526

Roberts, I. N., Caputo, C., Criado, M. V., and Funk, C. (2012). Senescence-associated proteases in plants. *Physiol. Plant.* 145, 130–139. doi: 10.1111/j.1399-3054.2012.01574.x

Roden, J., Eardley, L., Hotson, A., Cao, Y., and Mudgett, M. B. (2004). Characterization of the Xanthomonas AvrXv4 effector, a SUMO protease translocated into plant cells. *Mol. Plant Microbe Interact.* 17, 633–643. doi: 10.1094/MPMI.2004.17.6.633

Rosa, M. T. G., Almeida, D. M., Pires, I. S., da Rosa Farias, D., Martins, A. G., da Maia, L. C., et al. (2018). Insights into the transcriptional and post-transcriptional regulation of the rice SUMOylation machinery and into the role of two rice SUMO proteases. *BMC Plant Biol.* 18 (1), 349. doi: 10.1186/s12870-018-1547-3

Rytz, T. C., Miller, M. J., McLoughlin, F., Augustine, R. C., Marshall, R. S., Juan, Y.-T., et al. (2018). SUMOylome profiling reveals a diverse array of nuclear targets modified by the SUMO ligase SIZ1 during heat stress. *Plant Cell* 30, 1077–1099. doi: 10.1105/tpc.17.00993

Sadanandom, A., Adam, E., Orosa, B., Viczian, A., Klose, C., Zhang, C., et al. (2015). SUMOylation of phytochrome-B negatively regulates light-induced signaling in Arabidopsis thaliana. *Proc. Natl. Acad. Sci. U.S.A.* 112, 11108–11113. doi: 10.1073/pnas.1415260112

Saitoh, H., and Hinchey, J. (2000). Functional heterogeneity of small ubiquitin-related protein modifier SUMO-1 versus SUMO-2/3. *J. Biol. Chem.* 275, 6252–6258. doi: 10.1074/jbc.275.9.6252

Saracco, S. A., Miller, M. J., Kurepa, J., and Vierstra, R. D. (2007). Genetic analysis of sumoylation in Arabidopsis: Heat-induced conjugation of SUMO1 and 2 is essential. *Plant Physiol.* 145 (1), 119–134. doi: 10.1104/pp.107.102285

Schulz, S., Chachami, G., Kozaczkiewicz, L., Winter, U., Stankovic-Valentin, N., Haas, P., et al. (2012). Ubiquitin-specific protease-like 1 (USPL1) is a SUMO isopeptidase with essential, non-catalytic functions. *EMBO Rep.* 13, 930–938. doi: 10.1038/embor.2012.125

Schwienhorst., Johnson ES, and Dohmen, R. J. (2000). SUMO conjugation and deconjugation. *Mol. Gen. Genet.* 263, 771–786. doi: 10.1007/s004380000254

Seifert, A., Schofield, P., Barton, G. J., and Hay, R. T. (2015). Proteotoxic stress reprograms the chromatin landscape of SUMO modification. *Sci. Signal.* 8, rs7. doi: 10.1126/scisignal.aaa2213

Shen, T. H., Lin, H.-K., Scaglion, P. P., Yung, T. M., and Pandolfi, P. P. (2006). The mechanisms of PML-nuclear body formation. *Mol. Cell* 24, 331–339. doi: 10.1016/j.molcel.2006.09.013

Shin, E. J., Shin, H. M., Nam, E., Kim, W. S., Kim, J. H., Oh, B. H., et al. (2012). DeSUMOylating isopeptidase: a second class of SUMO protease. *EMBO Rep.* 13, 339–346. doi: 10.1038/embor.2012.3

Srivastava, A., Orosa, B., Singh, P., et al. (2018). SUMO Suppresses the Activity of the Jasmonic Acid Receptor CORONATINE INSENSITIVE 1. *Plant Cell.* 30 (9), 2099–2115. doi: 10.1105/tpc.18.00036

Srivastava, A. K., Zhang, C., Caine, R. S., Gray, J., and Sadanandom, A. (2017). Rice SUMO protease Overly Tolerant to Salt 1 targets the transcription factor, OsbZIP23 to promote drought tolerance in rice. *Plant J.* 92, 1031–1043. doi: 10.1111/tpj.13739

Srivastava, A. K., Zhang, C., and Sadanandom, A. (2016a). Rice OVERLY TOLERANT TO SALT 1 (OTS1) SUMO protease is a positive regulator of seed germination and root development. *Plant Signal. Behav.* 11 (5), e1173301. doi: 10.1080/15592324.2016.1173301

Srivastava, A. K., Zhang, C., Yates, G., Bailey, M., Brown, A., and Sadanandom, A. (2016b). SUMO is a critical regulator of salt stress responses in rice. *Plant Physiol.* 170 (4), 2378–2391. doi: 10.1104/pp.15.01530

Suh, H. Y., Kim, J. H., Woo, J. S., Ku, B., Shin, E. J., Yun, Y., et al. (2012). Crystal structure of DeSI-1, a novel deSUMOylase belonging to a putative isopeptidase superfamily. *Proteins* 80, 2099–2104. doi: 10.1002/prot.24093

van den Burg, H. A., Kini, R. K., Schuurink, R. C., and Takken, F. L. (2010). Arabidopsis small ubiquitin-like modifier paralogs have distinct functions in development and defense. *Plant Cell* 22, 1998–2016. doi: 10.1105/tpc.109.070961

Villajuana-Bonequi, M., Elrouby, N., Nordström, K., Griebel, T., Bachmair, A., and Coupland, G. (2014). Elevated salicylic acid levels conferred by increased expression of ISOCHORISMATE SYNTHASE 1 contribute to hyperaccumulation of SUMO1 conjugates in the Arabidopsis mutant early in short days 4. *Plant J.* 79, 206–219. doi: 10.1111/tpj.12549

Wang, Q., Qu, G. P., Kong, X., Yan, Y., Li, J., and Jin, J. B. (2018). Arabidopsis SUMO protease ASP1 positively regulates ABA signaling during early seedling development. *J. Integr. Plant Biol.* 60 (10), 924–937. doi: 10.1111/jipb.12669

Xu, X. M., Rose, A., Muthuswamy, S., Jeong, S. Y., Venkatakrishnan, S., Zhao, Q., et al. (2007). The Arabidopsis homolog of Tpr/Mlp1/Mlp2/Megator, is involve in mRNA export and SUMO homeostasis and affects diverse aspects of plant development. *Plant Cell* 19, 1537–1548. doi: 10.1105/tpc.106.049239

Yates, G., Srivastava, A. K., and Sadanandom, A. (2016). SUMO proteases: Uncovering the roles of deSUMOylation in plants. *J. Exp. Bot.* 67 (9), 2541–2548. doi: 10.1093/jxb/erw092

Zhan, E., Zhou, H., Li, S., Liu, L., Tan, T., and Lin, H. (2018). OTS1-dependent deSUMOylation increases tolerance to high copper levels in Arabidopsis. *J. Integr. Plant Biol.* 60 (4), 310–322. doi: 10.1111/jipb.12618

Conflict of Interest Statement: The authors declare that the research was conducted in the absence of any commercial or financial relationships that could be construed as a potential conflict of interest.

Advantages of publishing in Frontiers

OPEN ACCESS
Articles are free to read for greatest visibility and readership

FAST PUBLICATION
Around 90 days from submission to decision

HIGH QUALITY PEER-REVIEW
Rigorous, collaborative, and constructive peer-review

TRANSPARENT PEER-REVIEW
Editors and reviewers acknowledged by name on published articles

Frontiers
Avenue du Tribunal-Fédéral 34
1005 Lausanne | Switzerland

Visit us: www.frontiersin.org
Contact us: info@frontiersin.org | +41 21 510 17 00

REPRODUCIBILITY OF RESEARCH
Support open data and methods to enhance research reproducibility

DIGITAL PUBLISHING
Articles designed for optimal readership across devices

FOLLOW US
@frontiersin

IMPACT METRICS
Advanced article metrics track visibility across digital media

EXTENSIVE PROMOTION
Marketing and promotion of impactful research

LOOP RESEARCH NETWORK
Our network increases your article's readership